Sustainable Conversion of Biomass Oxygenates: Ab Initio Based Model Simulation

Duurzame omzetting van zuurstofhoudende verbindingen uit biomassa: ab initio gebaseerde modelsimulatie

Paschalis Paraskevas

Promotors: Prof. M.-F. Reyniers, PhD, Prof. G. B. Marin, PhD, Prof. N. G. Papayannakos, PhD
Doctoral thesis submitted in order to obtain the academic degrees of
Doctor of Chemical Engineering (Ghent University) and
Doctor of Engineer (National Technical University of Athens)

Department of Chemical Engineering and Technical Chemistry
Head of Department: Prof. G. B. Marin, PhD
Faculty of Engineering and Architecture

School of Chemical Engineering
Dean of the School: Prof. A. Boudouvis, PhD
National Technical University of Athens

Academic year 2015 - 2016

ISBN 978-90-8578-841-6
NUR 952
Wettelijk depot: D/2015/10.500/85

Promotoren

Prof. dr. ir. Guy B. Marin

Prof. dr. Marie-Françoise Reyniers

Universiteit Gent
Vakgroep Chemische proceskunde en Technische Chemie (EA12)
Laboratorium voor Chemische Technologie
Technologiepark 914
9052 Gent
België

Decaan: Prof. dr. ir. Rik Van de Walle

Rector: Prof. dr. Anne De Paepe

Promotor

Prof. dr. ir. Nikolaos G. Papayannakos

National Technical University of Athens
Department of Chemical Engineering and Technology
Chemical Reaction Engineering Laboratory
Heroon Polytechniou 9
15780 Zografos, Athens
Greece

Dean: Prof. dr. ir. Andreas G. Boudouvis

Rector: Prof. dr. ir. Ioannis K. Golias

Acknowledgements

I would like to express my appreciation and special thanks to my advisors, Professors Guy B. Marin, Marie-Françoise Reyniers and Nikos G. Papayannakos for giving me the opportunity to do my PhD research in the University of Ghent jointly with the National Technical University of Athens. It has been an honor for me to have you as my teachers. Thank you very much for encouraging me and inspiring me throughout this experience.

Many thanks to my committee members for their significant contribution to my PhD dissertation, for their brilliant comments and suggestions.

I would like to specially thank my friend and excellent scientist Maarten Sabbe, he was always there to teach me, to give me ideas and explaining things to me. Maarten, you have been a tremendous mentor for me. Thank you for all this devoted work, knowledge and dedicated time you generously offered to me.

I would also like to thank all my friends in LCT, who made my moments there more interesting. Kostas, Panos, Maria, Gonzalo, Hans, Andres, Marco, Jelena, Mike, Aäron, Stamatis, Stavros, Gils, Petra, Sarah, Ruben vdB, Alper, Georges, Ruben vdV, Ezgi and all the other people there, thank you very much.

I want to thanks also my parents, my brother and friends for all their support and encouragement to me to follow this difficult path of knowledge. And last but not least, my wife Sofia, for being always there, being so patient with my long-hour studying intervals, supporting me and encouraging me to walk this road till the end…

Paschalis D. Paraskevas
Gent 2015

This work was supported by the European Research Council under the European Union's Seventh Framework Program FP7/2007-2013 (ERC grant agreement no 290793) and by the Long Term Structural Methusalem Funding by the Flemish Government. It was carried out using the Stevin Supercomputer Infrastructure at Ghent University.

EXAMENCOMMISSIE

Leescommissie

Prof. dr. Marie-Françoise Reyniers [promotor]
Vakgroep Chemische proceskunde en Technische Chemie
Faculteit Ingenieurswetenschappen en Architectuur (EA12)
Universiteit Gent

Dr. ir. Pierre-Alexandre Glaude
Laboratoire Réactions et Génie des Procédés
National Polytechnic Institute of Lorraine

Prof. dr. ir. Bart Merci
Vakgroep Mechanica van Stroming, Warmte en Verbranding
Faculteit Ingenieurswetenschappen en Architectuur (EA03)
Universiteit Gent

Prof. dr. ir. Maarten K. Sabbe [secretary]
Vakgroep Chemische proceskunde en Technische Chemie
Faculteit Ingenieurswetenschappen en Architectuur (EA12)
Universiteit Gent

Andere leden van de examencommissie

Prof. dr. ir. Gert de Cooman [chairman]
Vakgroep Elektronica en Informatiesystemen (SYSTeMS)
Faculteit Ingenieurswetenschappen en Architectuur (EA06)
Universiteit Gent

Prof. dr. ir. Guy B. Marin [promotor]
Vakgroep Chemische proceskunde en Technische Chemie
Faculteit Ingenieurswetenschappen en Architectuur (EA12)
Universiteit Gent

Prof. dr. ir. Nikolaos G. Papayannakos [promotor]
Department of Chemical Engineering and Technology
School of Chemical Engineering
National Technical University of Athens

Prof. dr. ir. Kevin van Geem
Vakgroep Chemische proceskunde en Technische Chemie
Faculteit Ingenieurswetenschappen en Architectuur (EA12)
Universiteit Gent

Contents

Notation

Roman Symbols

A	pre-exponential factor	m^3 $kmol^{-1}$ s^{-1} or s^{-1}
$\tilde{A}$	single-event pre-exponential factor	m^3 $kmol^{-1}$ s^{-1} or s^{-1}
$\tilde{A}_{ref}$	single-event pre-exponential factor of the reference reaction	m^3 mol^{-1} s^{-1} or s^{-1}
$C_p°$	standard heat capacity	J mol^{-1} K^{-1}
E	energy	kJ mol^{-1}
ΔE(0 K)	activation barrier at 0 K including ZPVE	kJ mol^{-1}
ΔE_0	electronic activation barrier (excluding ZPVE)	kJ mol^{-1}
E_a	activation energy	kJ mol^{-1}
E_a^o	intrinsic activation energy (Evans-Polanyi correlation)	kJ mol^{-1}
$E_{a,ref}$	activation energy of reference reaction	kJ mol^{-1}
E_{el}	electronic energy	kJ mol^{-1}
F	significance of regression	-
F_0	initial total mass flow	kg s^{-1}
F_j	molar flow rate of component j	mol s^{-1}
G	Gibbs energy	kJ mol^{-1}
$\Delta^{\ddagger}G$	Gibbs activation energy	kJ mol^{-1}
$\Delta_r G°$	standard reaction Gibbs energy	kJ mol^{-1}
$\overline{\mathrm{GAV}}$	estimation vector of group additive values	
h	Planck constant	6.62 10^{-34} J s
$\Delta^{\ddagger}H$	activation enthalpy	kJ mol^{-1}
$\Delta_a H°$	standard atomization enthalpy	kJ mol^{-1}
$\Delta_f H°$	standard enthalpy of formation	kJ mol^{-1}
$\Delta_r H$	reaction enthalpy	kJ mol^{-1}

k	reaction rate coefficient	m^3 mol^{-1} s^{-1} or s^{-1}
$\tilde{k}$	single event rate coefficient	m^3 mol^{-1} s^{-1} or s^{-1}
K	equilibrium coefficient	m^3 mol^{-1} or -
k_B	Boltzmann constant	1.38 10^{-23} J K^{-1}
n_e	number of single events	-
n_{opt}	number of optical isomers	-
p	pressure	Pa
q	molecular partition function	-
Q	canonical partition function	-
R	universal gas constant	8.314 J mol^{-1} K^{-1}
r_k	rate of reaction k	mol m^{-3} s^{-1}
$S°$	standard entropy	J $mol^{-1}K^{-1}$
$\Delta^{\ddagger}S$	activation entropy	J $mol^{-1}K^{-1}$
$\Delta_r S°$	standard reaction entropy	J mol^{-1} K^{-1}
S_{int}	intrinsic entropy	J $mol^{-1}K^{-1}$
T	temperature	K
$V(\varphi)$	potential energy profile for internal rotation	kJ mol^{-1}
V_{p}	parameter within the Blowers and Masel relationship, related to the intrinsic activation energy E_a^o	kJ mol^{-1}
w	bond dissociation energy	kJ mol^{-1}

Greek Symbols

γ_p	transfer coefficient (Evans-Polanyi)	-
κ	Tunneling coefficient	-
ν	frequency	cm^{-1} or s^{-1}
ν_{kj}	stoichiometric coefficient of component j in reaction k	-
ρ	factor of deviation between rate coefficients, $k_{\mathrm{max}}/k_{\mathrm{min}}$	-
σ	symmetry number	-
ψ	wave function	

Sub- and superscripts

‡	transition state
atom	atomization
calc	calculated
eq	equilibrium
exp	experimental
ref	reference
opt	optical isomers
res	resonance
•	radical
int	internal
ext	external
tot	total

Acronyms

1D-HR	uncoupled (one-dimensional) Hindered Rotation
AI	Ab Initio
BDE	Bond Dissociation Energy
CBS	Complete Basis Set
C_d	double-bonded carbon atom
C_t	triple-bonded carbon atom
CTST	Canonical Transition State Theory
DFT	Density Functional Theory
GAV	Group Additive Value
HBI	Hydrogen Bond Increment
HF	Hartee Fock
HO	Harmonic Oscillator
HR	Hindered Rotation treatment of rotation about forming/breaking bond in transition state and product radical
IRC	Intrinsic Reaction Coordinate
MAD	Mean Absolute Deviation
MAX	Maximum deviation
MB	Methyl butanoate
NNI	Non-nearest Neighbor Interaction
PES	Potential Energy Surface
RMG	Reaction Mechanism Generator
RMS	Root Mean Square deviation
RRKM	Rice-Ramsperger-Kassel-Marcus theory
TS	Transition State
TST	Transition State Theory
VTST	Variational Transition State Theory
ZPVE	Zero Point Vibrational Energy

Samenvatting

Biomassa kan, als bron van hernieuwbare energie, een belangrijke bijdrage leveren aan het inperken van de wereldwijde klimaatverandering en de effecten hiervan op de mensheid. Door de aandacht voor duurzame ontwikkeling en het streven naar milieuvriendelijker producten zal de omzetting van biomassa in vloeibare brandstoffen, energie en fijnchemicaliën in de komende jaren wellicht aan belang winnen. Veel van de omzettingsprocessen van biomassa, zoals verbranding, pyrolyse en gasificatie, zijn gebaseerd op radicaalchemie. Een grondige optimalisering van deze processen vereist de ontwikkeling van fundamentele kinetische modellen, die typisch duizenden reacties bevatten. De bepaling van de thermodynamische en kinetische parameters voor al deze reacties is één van de grote uitdagingen in kinetische modellering.

Door de reactieve aard van de intermediaire radicalen is het onmogelijk om al deze parameters rechtstreeks uit experimenten te bepalen. Computationele chemie kan hier een betrouwbare, complementaire bijdrage leveren aan experimentele data, waarbij deze methode accurate thermodynamische en kinetische parameters voor een breed bereik aan chemische verbindingen kan aanreiken. Voor grotere moleculen is een haalbaarder alternatief deze data te verkrijgen via groepencontributiemethodes, wat structuur-eigenschap relaties zijn die de waarde van een eigenschap linken aan de structurele functionele bouwstenen in de molecule. De parameters voor

deze groepencontributiemethodes kunnen bepaald worden met computationele chemie voor kleinere moleculen.

Doelstelling Het doel van dit onderzoek is om consistente en accurate modellen te ontwikkelen voor de inschatting van de thermodynamische parameters van zuurstofbevattende koolwaterstoffen, evenals de Arrheniusparameters en snelheidscoëfficiënten voor de belangrijkste reactiefamilies die betrokken zijn bij de thermische decompositie van zuurstofhoudende koolwaterstoffen. De toepasbaarheid van de verkregen groepsadditieve modellen voor thermodynamische en kinetische data zal geïllustreerd worden in de simulatie van de pyrolyse van methylbutanoaat, een veelgebruikte modelmolecule voor biodiesel.

Thermochemie Accurate thermodynamische parameters zijn onontbeerlijk bij de ontwikkeling van reactienetwerken voor de bepaling van reactie-evenwichten en reactie-enthalpieën. In dit werk werd de accurate CBS-QB3 methode gebruikt met correcties voor eendimensionale rotatie (1D-HR) voor de bepaling van thermodynamische parameters (standaardvormingsenthalpie $\Delta_f H^o$, standaardentropie S^o, en warmtecapaciteiten C_p) van 450 zuurstofhoudende koolwaterstoffen en radicalen. Op basis van deze data werden 157 Benson groepsadditieve waarden (GAVs) voor zuurstofhoudende koolwaterstoffen en radicalen bepaald. Daarnaast werden, om de accuratesse van het model te verbeteren, 26 correcties voor niet-gebonden interacties (NNI) geïntroduceerd. Het grootste deel van deze waarden is nooit eerder bepaald geworden. Voor de methode van de waterstofbindingsincrementen (HBI), een interessant alternatief voor de groepsadditieve methode voor de bepaling van de standaardvormingsenthalpie van radicalen, werden 77 nieuwe HBI structuren geïntroduceerd. Vergelijking van groepsadditief berekende waarden met experimentele en ab initio berekende waarden resulteert in gemiddelde absolute afwijkingen kleiner dan 4 kJ mol^{-1} voor standaardvormingsenthalpieën, en kleiner dan 4 J mol^{-1} K^{-1} voor standaardentropieën en warmtecapaciteiten.

Kinetiek In dit werk worden twee types reacties bestudeerd: waterstofabstractiereacties tussen zuurstofhoudende koolwaterstoffen en radicaaladdities/β-scissies tussen dit type moleculen. Snelheidscoëfficiënten zijn bepaald met behulp van conventionele transitietoestandstheorie (CTST) op basis van ab initio berekeningen met de CBS-QB3 methode met correcties voor eendimensionale gehinderde rotaties rond de zich vormende/brekende binding in de transitietoestand. Voor waterstofabstractiereacties zijn ook correcties voor tunneling doorheen de reactiebarrière in rekening gebracht met behulp van de Eckart methode.

De modellering van de kinetische parameters gebeurde op basis van de groepsadditieve methode voor kinetiek, zoals ontwikkeld aan het Laboratorium voor Chemische Technologie (LCT). In deze methode worden Arrheniusparameters van een reactie berekend door perturbatietermen bij te tellen bij de overeenkomstige parameters van een referentiereactie. Deze perturbaties weerspiegelen de structurele verschillen tussen de transitietoestand van de beschouwde en de referentiereactie, en kunnen afgeleid worden op basis van groepsadditiviteit voor enthalpie en entropie. In deze studie werd aangetoond dat het gebruik van secundaire contributies noodzakelijk is om de accuratesse van het model te kunnen garanderen. Voor waterstofabstractiereacties werden ook correcties geïntroduceerd die het effect van resonantiestabilisatie op de transitietoestand in rekening brengen. In totaal werden in dit werk vier groepsadditieve modellen voor kinetiek opgebouwd, die hierna kort besproken worden.

Waterstofabstractiereacties van zuurstofhoudende koolwaterstoffen door koolstofradicalen: Ab initio snelheidscoëfficiënten en Arrheniusparameters werden berekend voor 103 waterstofabstractiereacties van zuurstofhoudende koolwaterstoffen door koolstofradicalen. Op basis van deze data werden 15 groepsadditieve waarden (ΔGAV^{o}) afgeleid voor de voorwaartse en terugwaartse reactie, waaronder zowel primaire als secundaire contributies, en daarnaast ook negen correcties voor resonantiestabilisatie in de transitietoestand. Het resulterende groepsadditieve model is gevalideerd aan de hand van een reeks ab initio snelheidscoëfficiënten, waarbij de gemiddelde absolute afwijking op de pre-exponentiële factoren en activeringsenergieën resp. 0.250 log(m^3 mol^{-1} s^{-1}) en 1.5 kJ mol^{-1} is bij 300 K. Daarnaast komen de groepsadditief berekende snelheidscoëfficiënten goed overeen met experimenteel bepaalde snelheidscoëfficiënten, met een gemiddelde afwijking van een factor 2.2 op een reeks van 33 reacties.

Waterstofabstractiereacties van zuurstofhoudende koolwaterstoffen door waterstofatomen Dezelfde aanpak als voor abstractie door koolstofradicalen wordt toegepast voor abstracties door waterstofradicalen, waarbij van kinetische parameters voor 60 reacties in totaal 15 groepsadditieve waarden (ΔGAV^o) bepaald werden voor de voorwaartse en terugwaartse reactie. Vergelijking van groepsadditief berekende snelheidscoëfficiënten met ab initio en experimentele waarden levert een gemiddelde afwijking op van resp. een factor twee en drie.

Waterstofabstractiereacties van zuurstofhoudende koolwaterstoffen door zuurstofradicalen In deze reactiefamilie werden twee types transitietoestand bestudeerd: de abstractie door een zuurstofradicaal van een waterstofatoom gebonden aan een koolstofatoom, en dat van een H-atoom gebonden aan een zuurstofatoom, wat schematisch overeenstemt met transitietoestanden van de types O--H--C en O--H--O. Op basis ab initio kinetische parameters voor 118 reacties werden 43 ΔGAV^os bepaald voor primaire en secundaire contributies, en 37 correcties voor resonantiestabilisatie in de transitietoestand. De ontwikkelde groepsadditieve modellen presteren goed in vergelijking met ab initio berekende snelheidscoëfficiënten voor 25 reacties, en een experimentele set van 61 reacties, met een gemiddelde afwijking van een factor 3 voor beide.

Koolstofradicaaladdities aan zuurstofbevattende koolwaterstoffen en de omgekeerde β-scissiereacties Op basis van ab initio Arrheniusparameters voor 66 radicaaladdities aan zuurstofhoudende koolwaterstoffen werden 32 groepsadditieve waarden bepaald voor primaire en secundaire contributies. Voor zover gekend zijn er nooit groepsadditieve waarden voor deze reactiefamilie gerapporteerd, terwijl experimentele data voor deze reactiefamilie uiterst zeldzaam zijn. Bij gebrek aan experimentele data in de wetenschappelijke literatuur werd de accuratesse van het groepsadditief model geverifieerd door groepsadditief berekende snelheidscoëfficiënten vergelijken met ab initio berekende waarden, resulterend in een gemiddelde afwijking van een factor drie.

Simulatie van de pyrolyse van methylbutanoaat (MB) Het programma Genesys, ontwikkeld aan het Laboratorium voor Chemische Technologie van de UGent, laat automatische generering toe van reactienetwerken voor de ontbinding van organische verbindingen. De berekende ab initio data en opgebouwde groepsadditieve modellen voor thermochemie en kinetiek zijn geïmplementeerd in Genesys' databanken. Met Genesys werd vervolgens een reactienetwerk gegenereerd voor de pyrolyse van methylbutanoaat, met de kinetische parameters op basis van ab initio gebaseerde groepsadditiviteit voor de reacties tussen grotere moleculen, en op basis van experimentele data voor de decompositiereacties van de kleinere moleculen. De gesimuleerde conversie van methylbutanoaat en de meeste productopbrengsten komen goed overeen met experimentele waarden verkregen binnen het LCT, wat het nut van de geconstrueerde groepsadditieve modellen voor gebruik in grote reactienetwerken aantoont.

Conclusie Op basis van ab initio berekende snelheidscoëfficiënten werden in dit werk accurate groepsadditieve modellen ontwikkeld die de thermodynamica en kinetiek beschrijven van reacties tussen zuurstofbevattende koolwaterstoffen. Het aan het LCT ontwikkelde programma Genesys is succesvol gebruikt om een reactienetwerk te genereren voor de pyrolyse van methylbutanoaat. De goede overeenkomst van de gesimuleerde conversie van methylbutanoaat en de meeste productopbrengsten met experimentele resultaten tonen het nut en de accuratesse aan van de ontwikkelde groepsadditieve modellen voor de simulatie van de thermische ontbinding van zuurstofbevattende koolwaterstoffen.

Περίληψη

Η βιομάζα, ως μία πηγή ανανεώσιμης ενέργειας, μπορεί να συνεισφέρει σημαντικά στην αντιμετώπιση της παγκόσμιας κλιματικής αλλαγής και την επίδρασής της στην ανθρωπότητα. Η δυνατότητα μετατροπής της βιομάζας σε καύσιμα, ενέργεια, χημικά και βιομηχανικά προϊόντα αναμένεται να αυξήσει την αξία της τα επόμενα χρόνια, εξαιτίας της επιτακτικής ανάγκης για βιώσιμη ανάπτυξη και για δημιουργία περιβαλλοντικά φιλικών προϊόντων. Πολλές από τις βασικές μεθόδους μετατροπής της βιομάζας, όπως η καύση, η αεριοποίηση και η πυρόλυση, βασίζονται στη χημεία των ελευθέρων ριζών. Η βελτιστοποίηση των διεργασιών αυτών απαιτεί την ανάπτυξη θεμελιωδών κινητικών μοντέλων που περιέχουν χιλιάδες αντιδράσεις. Και η ανάπτυξη των μοντέλων αυτών καθιστά απαραίτητη τη γνώση όλων των θερμοδυναμικών και κινητικών παραμέτρων των εμπλεκόμενων ενώσεων και αντιδράσεων.

Η απόκτηση όλων των αναγκαίων δεδομένων μέσω πειραμάτων είναι αδύνατη, κυρίως λόγω της υψηλής δραστικότητας των ενδιαμέσων σχηματιζόμενων ριζών. Η Υπολογιστική Χημεία προσφέρει ένα αξιόπιστο, συμπληρωματικό στα πειραματικά δεδομένα, εργαλείο, συμβάλλοντας στην απόκτηση θερμοδυναμικών και κινητικών δεδομένων μεγάλης ακρίβειας για ένα ευρύ φάσμα χημικών ενώσεων. Το βασικό της μειονέκτημα είναι το αυξανόμενο υπολογιστικό κόστος καθώς αυξάνει το μέγεθος των υπό μελέτη ενώσεων. Εναλλακτικά, ακριβή δεδομένα για μεγαλύτερες ενώσεις μπορούν να προκύψουν από τη χρήση μεθόδων προσθετικών ιδιοτήτων κατά ομάδες που βασίζονται σε σχέσεις δομής-ιδιοτήτων και οι οποίες συσχετίζουν παραμέτρους με τις αντίστοιχες λειτουργικές μονάδες στη δομή μία ένωσης. Αυτές οι

παράμετροι για μεγαλύτερες ενώσεις μπορούν να προκύψουν χρησιμοποιώντας μεθόδους υπολογιστικής χημείας για μικρότερα μόρια.

Αντικειμενικός Σκοπός Ο αντικειμενικός σκοπός της παρούσας εργασίας είναι η ανάπτυξη μοντέλων μεγάλης ακρίβειας για τον προσδιορισμό θερμοδυναμικών ιδιοτήτων οξυγονούχων οργανικών ενώσεων και τον προσδιορισμό των παραμέτρων της εξίσωσης Arrhenius και των κινητικών αντιδράσεων για μερικούς από τους σημαντικότερους τύπους αντιδράσεων που συμμετέχουν στη θερμική αποδόμηση οξυγονούχων οργανικών ενώσεων. Οι θερμοδυναμικές παράμετροι και τα κινητικά δεδομένα που θα προκύψουν υπολογιστικά θα χρησιμοποιηθούν, σε συνδυασμό με τα μοντέλα θερμοδυναμικών ιδιοτήτων που θα αναπτυχθούν στο πλαίσιο της εργασίας αυτής, για την προσομοίωση της πυρόλυσης του μεθυλεστέρα βουτυρικού οξέος, μίας ένωσης που προσομοιάζει τις βασικές ιδιότητες του βιοντήζελ.

Θερμοδυναμικές Ιδιότητες Θερμοδυναμικά δεδομένα μεγάλης ακρίβειας είναι απαραίτητα για την ανάπτυξη δικτύων αντιδράσεων, καθώς τα δεδομένα αυτά χρησιμοποιούνται για τον υπολογισμό της ενθαλπίας της αντίδρασης και της σταθεράς χημικής ισορροπίας, βάσει των οποίων υπολογίζονται οι ταχύτητες των χημικών αντιδράσεων. Στην παρούσα εργασία χρησιμοποιήθηκε η ab initio μέθοδος CBS-QB3, με χρήση διορθώσεων για μονοδιάστατη παρεμποδιζόμενη περιστροφή, με σκοπό τον προσδιορισμό θερμοδυναμικών παραμέτρων (πρότυπη ενθαλπία σχηματισμού, $\Delta_f H^o$, πρότυπη εντροπία, S^o, και θερμοχωρητικότητα, C_p) για 450 οξυγονούχες οργανικές ενώσεις. Από αυτή τη βάση δεδομένων υπολογίσθηκαν, χρησιμοποιώντας τη μέθοδο του Benson, 157 τιμές προσθετικών ιδιοτήτων κατά ομάδες (group additive values, GAVs) που αφορούν οξυγονούχες οργανικές ενώσεις. Για να επιτύχουμε μεγαλύτερη ακρίβεια στο μοντέλο που αναπτύχθηκε, εισήχθησαν 26 διορθώσεις για αλληλεπιδράσεις μεταξύ μη άμεσα γειτονικών ατόμων (non-nearest-neighbor-interactions, NNIs). Η πλειονότητα των τιμών που υπολογίσθηκαν στο πλαίσιο της μελέτης αυτής δεν έχει υπολογισθεί ποτέ στο παρελθόν. Εναλλακτικά της μεθόδου προσθετικών ιδιοτήτων για τις ρίζες, μπορεί να χρησιμοποιηθεί η μέθοδος της προσθήκης δεσμού υδρογόνου (hydrogen bond increment method, HBI). Προσδιορίσθηκαν 77 τιμές για προσθήκες δεσμών υδρογόνου για τον προσδιορισμό θερμοδυναμικών ιδιοτήτων ριζών οξυγονούχων οργανικών ενώσεων. Η αξιοπιστία του μοντέλου προσθετικών ιδιοτήτων που αναπτύχθηκε πιστοποιήθηκε με σύγκριση των προβλέψεων του μοντέλου με πειραματικά δεδομένα καθώς επίσης και με ab initio υπολογισμένες τιμές. Η μέση απόλυτη τιμή της απόκλισης που προέκυψε από τη σύγκριση αυτή ήταν κάτω από 4 kJ mol^{-1} για την πρότυπη ενθαλπία σχηματισμού, και κάτω από 4 J mol^{-1} K^{-1} για την πρότυπη εντροπία και θερμοχωρητικότητα.

Κινητικές Αντιδράσεων Δύο τύποι αντιδράσεων μελετήθηκαν στη Διατριβή αυτή, οι αντιδράσεις απόσπασης υδρογόνου και οι αντιδράσεις προσθήκης ριζών άνθρακα (με αντίστροφη αντίδραση τη σχάση σε *β* θέση) που αφορούν οξυγονούχες οργανικές ενώσεις. Οι ταχύτητες αντιδράσεων υπολογίσθηκαν με τη χρήση της συμβατικής θεωρίας επιπέδου μετάβασης κατά την εξέλιξη της αντίδρασης από τα αντιδρώντα στα προϊόντα (conventional transition state theory, CTST). Οι ab initio υπολογισμοί έγιναν με τη χρήση της μεθοδολογίας CBS-QB3, συμπεριλαμβάνοντας διορθώσεις για μονοδιάστατη παρεμποδιζόμενη περιστροφή γύρω από τον σχηματιζόμενο/αποδομούμενο δεσμό στο επίπεδο ματάβασης της αντίδρασης. Επιπλέον, μόνο για τις αντιδράσεις απόσπασης υδρογόνου, συμπεριλήφθησαν διορθώσεις για το φαινόμενο σήραγγας όπως αυτές καθορίσθηκαν από τον Eckart (Eckart’s zero curvature tunneling corrections).

Για τη μοντελοποίηση των κινητικών αντιδράσεων χρησιμοποιήθηκε η μεθοδος προσθετικών ιδιοτήτων κατά ομάδες που αναπτύχθηκε στο Εργαστήριο Χημικής Τεχνολογίας της Γάνδης (Laboratory for Chemical Technology of the University of Ghent, LCT). Σύμφωνα με τη μέθοδο αυτή, οι παράμετροι της εξίσωσης Arrhenius για την υπό μελέτη αντίδραση μπορούν να υπολογισθούν προσθέτωντας «διαταράξεις» στις αντίστοιχες παραμέτρους μια αντίδρασης αναφοράς. Οι «διαταράξεις» αυτές αναφέρονται σε διαφορές στη δομή της υπό μελέτη αντίδρασης σε σχέση με την αντίδραση αναφοράς και βασίζονται στις προσθετικές ιδιότητες παραμέτρων όπως η ενθαλπία και η εντροπία. Στη μελέτη αυτή κρίθηκε αναγκαίο, για να αυξηθεί η ακρίβεια του μοντέλου, να συμπεριληφθεί και η συνεισφορά των δευτερευουσών ομάδων ατόμων. Επιπλεον, για τις αντιδράσεις απόσπασης υδρογόνου, χρησιμοποιήθηκαν επίσης διορθώσεις που αφορούν φαινόμενα συντονισμού από αλληλεπιδράσεις χαρακτηριστικών ομάδων εκατέρωθεν του επιπέδου μετάβασης κατά την εξέλιξη της αντίδρασης. Στο πλαίσιο της διατριβής αυτής αναπτύχθηκαν τέσσερα μοντέλα προσθετικών ιδιοτήτων τα οποία θα αναλυθούν με λεπτομέρειες παρακάτω.

Αντιδράσεις απόσπασης υδρογόνου από οξυγονούχες οργανικές ενώσεις μέσω ριζών με ενεργό κέντρο άνθρακα. Δημιουργήθηκε μια βάση δεδομένων με παραμέτρους της εξίσωσης Arrhenius και ταχύτητες αντιδράσεων για 103 αντιδράσεις απόσπασης υδρογόνου από οξυγονούχες οργανικές ενώσεις μέσω ριζών με ενεργό κέντρο άνθρακα. Από τα δεδομένα αυτά 15 τιμές προσθετικών ιδιοτήτων κατά ομάδες (ΔGAV^os) υπολογίσθηκαν για πρωταρχικές και δευτερεύουσες ομάδες, καθώς επίσης και 9 παράγοντες διόρθωσης για φαινόμενα συντονισμού εκατέρωθεν του επιπέδου μετάβασης κατά την εξέλιξη μιας αντίδρασης. Η αξιοπιστία του μοντέλου που προέκυψε πιστοποιήθηκε με σύγκριση των προβλέψεων του μοντέλου με ab initio υπολογισμένες τιμές (μέση απόλυτη τιμή της απόκλισης 0.250 log(m^3 mol^{-1} s^{-1}) και 1.5 kJ mol^{-1} για τον προεκθετικό παράγοντα και την ενέργεια ενεργοποίησης, αντίστοιχα, στους 300 K). Συγκρίνοντας την πρόβλεψη του μοντέλου για τις ταχύτητες των αντιδράσεων με 33 πειραματικές ταχύτητες, η μέση απόλυτη τιμή της απόκλισης ήταν μόνο 2.2.

Αντιδράσεις απόσπασης υδρογόνου από οξυγονούχες οργανικές ενώσεις μέσω ρίζας υδρογόνου. Η ίδια προσέγγιση χρησιμοποιήθηκε επίσης για 60 αντιδράσεις απόσπασης υδρογόνου από οξυγονούχες οργανικές ενώσεις μέσω ρίζας υδρογόνου. Από τις αντιδράσεις αυτές υπολογίσθηκαν 15 τιμές προσθετικών ιδιοτήτων κατά ομάδες για πρωταρχικές και δευτερεύουσες ομάδες. Η αξιοπιστία του μοντέλου που προέκυψε πιστοποιήθηκε με σύγκριση των προβλέψεων του μοντέλου με ab initio υπολογισμένες τιμές και με πειραματικά δεδομένα με μέση απόλυτη απόκλιση 2.0 και 3.0 αντίστοιχα.

Αντιδράσεις απόσπασης υδρογόνου από οξυγονούχες οργανικές ενώσεις μέσω ριζών με ενεργό κέντρο οξυγόνο. Αυτή η κατηγορία αντιδράσεων περιλαμβάνει δύο τύπους επιπέδων μετάβασης από τα αντιδρώντα στα προϊόντα, και συγκεκριμένα αποσπάσεις υδρογόνου από άτομο συνδεδεμένο με άτομο άνθρακα ή με άτομο οξυγόνου, που αντιστοιχούν σε επίπεδα μετάβασης της μορφής O--H--C και O--H--O αντίστοιχα. 118 αντιδράσεις μελετήθηκαν και κινητικές παράμετροι υπολογίσθηκαν με ab initio μεθόδους για θερμοκρασιακό εύρος 300-2500 K. Από τα δεδομένα αυτά υπολογίσθηκαν 43 ΔGAV^os για πρωταρχικές και δευτερεύουσες ομάδες και 37 παράγοντες διόρθωσης για φαινόμενα συντονισμού εκατέρωθεν του επιπέδου μετάβασης κατά την εξέλιξη μιας αντίδρασης. Η πιστοποίηση της αξιοπιστίας του μοντέλου στην πρόβλεψη κινητικών αντιδράσεων υλοποιήθηκε με τη χρήση ενός σετ 25 αντιδράσεων με ab initio υπολογισμένες παραμέτρους και ενός σετ 61 πειραματικών ταχυτήτων αντιδράσεων με αποκλίσεις περίπου 3.0 και για τα δύο σετ αντιδράσεων.

Αντιδράσεις προσθήκης ρίζας με ενεργό κέντρο άνθρακα σε οξυγονούχες οργανικές ενώσεις και αντιδράσεις β σχάσης από οξυγονούχες οργανικές ενώσεις. Δημιουργήθηκε μια βάση δεδομένων με παραμέτρους της εξίσωσης Arrhenius και ταχύτητες αντιδράσεων για 66 αντιδράσεις προσθήκης ρίζας με ενεργό κέντρο άνθρακα σε οξυγονούχες ενώσεις και αντιδράσεις *β* σχάσης από οξυγονούχες οργανικές ενώσεις σε θερμοκρασίες 300-2500 K. Από τα δεδομένα αυτά υπολογίσθηκαν 32 ΔGAV^os για πρωταρχικές και δευτερεύουσες ομάδες προσθετικών ιδιοτήτων. Εξαιτίας της έλλειψης πειραματικών δεδομένων η πιστοποίηση της αξιοπιστίας του μοντέλου που αναπτύχθηκε έγινε με σύγκριση των προβλέψεων του μοντέλου με ab initio υπολογισμένες παραμέτρους για αντιδράσεις αυτού του τύπου οδηγώντας σε αποκλίσεις περίπου 3.0 και για τις δύο κατευθύνσεις της αντίδρασης. Από όσο γνωρίζουμε για την κατηγορία των αντιδράσεων προσθήκης των ενώσεων αυτών δεν έχουν καθορισθεί ομάδες προσθέτικών ιδιοτήτων ποτέ στο παρελθόν, ενώ τα πειραματικά δεδομένα για τις ενώσεις αυτές είναι πολύ σπάνια.

Προσομοίωση της πυρόλυσης του μεθυλεστέρα του βουτυρικού οξέος (methyl butanoate, MB) Το λογισμικό με το όνομα Genesys που αναπτύχθηκε στο LCT επιτρέπει την αυτοματοποιημένη ανάπτυξη δικτύων αντιδράσεων για υδρογονάνθρακες, οξυγονούχες και άλλων τύπων οργανικές ενώσεις. Τα ab initio υπολογισμένα δεδομένα και οι τιμές των ομάδων προσθετικών ιδιοτήτων που προέκυψαν στα προηγούμενα στάδια της παρούσας Διατριβής ενσωματώθηκαν στις βάσεις δεδομένων του λογισμικού του Genesys. Στη συνέχεια δημιουργήθηκε ένα δίκτυο αντιδράσεων με τη χρήση του Genesys για τη μελέτη της θερμικής αποδόμησης μεγαλων αλυσίδων οξυγονούχων οργανικών ενώσεων. Συγκεκριμένα έγινε προσομοίωση της πυρόλυσης του MB με χρήση ab initio δεδομένων σε συνδυασμό με έναν μηχανισμό πυρόλυσης βασισμένο σε πειραματικά δεδομένα για την περιγραφή της θερμικής αποδόμησης μικρότερων οργανικών ενώσεων. Τα αποτελέσματα της προσομοίωσης αυτής για τη χημική μετατροπή του MB συμφωνούν με τα αντίστοιχα πειραματικά δεδομένα διαθέσιμα από το LCT, ενώ όσον αφορά τις αποδόσεις στα προϊόντα της πυρόλυσης υπήρχε συμφωνία στην πλειοψηφία των προϊόντων αυτών. Τα αποτελέσματα αυτά καταδεικνύουν τη χρησιμότητα των μοντέλων προσθετικών ιδιοτήτων κατά ομάδες για χρήση στην ανάπτυξη μεγάλων δικτύων χημικών αντιδράσεων.

Συμπεράσματα Στο πλαίσιο της παρούσας μελέτης αναπτύχθηκαν μοντέλα προσθετικών ιδιοτήτων κατά ομάδες ατόμων για τον προσδιορισμό θερμοδυναμικών ιδιοτήτων οξυγονούχων οργανικών ενώσεων και τον προσδιορισμό κινητικών παραμέτρων που αφορούν αντιδράσεις μεταξύ οξυγονούχων οργανικών ενώσεων. Το πρόγραμμα Genesys που αναπτύχθηκε στο LCT χρησιμοποιήθηκε για τη δημιουργία ενός δικτύου αντιδράσεων για τη περιγραφή της πυρόλυσης του MB. Η συμφωνία κατά τη σύγκριση των αποτελεσμάτων της προσομοίωσης με διαθέσιμα πειραματικά δεδομένα από το LCT, ενισχύει τη χρησιμότητα των μοντέλων προσθετικών ιδιοτήτων κατά ομάδες ατόμων στην προσομοίωση χημικών διεργασιών όπως της θερμικής αποδόμησης οξυγονούχων οργανικών ενώσεων.

Summary

Biomass, as an abundant source for renewable energy, can provide a considerable contribution to facing the global climate change and its impacts on humanity. The conversion of biomass into fuels, energy, specialty chemicals and industrial products is expected to increase in importance the coming years due to the concern for sustainable development and environmentally friendlier products. Many of the most important biomass conversion processes, such as combustion, gasification and pyrolysis are based on free-radical chemistry. The optimization of such processes requires the development of fundamental kinetic models that contain thousands of reactions. Thermodynamic and kinetic parameters for all compounds involved are necessary and the determination of all these parameters is a major challenge in kinetic modeling.

It is impossible to acquire all these parameters needed from experimental data only, due to the reactive nature of radical intermediates. Computational chemistry offers a reliable and complementary tool to experiment, allowing to obtain accurate thermodynamic and kinetic parameters for a variety of compounds. Its main drawback is the increasing computational cost for larger compounds. Alternatively, accurate data for larger compounds can be obtained by using group contribution methods based on structure-property relations that link the

corresponding parameter to structural functional subunits. These parameters can be derived using computational chemistry methods for smaller compounds.

Objective: The objective of this research is to develop consistent and accurate models for the prediction of the thermochemistry of oxygenate compounds and of the Arrhenius parameters and the rate coefficients for some of the most important reaction families involved in the thermal decomposition of oxygenates. The acquired thermodynamic and kinetic data and the group additive models developed will be applied in simulating the pyrolysis of methyl butanoate, a commonly used biodiesel model compound.

Thermochemistry: Accurate thermodynamic parameters are necessary when developing reaction networks since they can be used for the determination of reaction enthalpies and reaction equilibria. In this work the accurate CBS-QB3 ab initio method was employed, with corrections for one-dimensional hindered rotation (1D-HR), to determine thermodynamic parameters (standard enthalpy of formation, $\Delta_f H^o$, standard entropy, S^o, and heat capacities, C_p) for 450 oxygenate molecules and radicals. From this dataset 157 group additive values (GAVs) for oxygenate molecules and radicals have been determined within Benson's group additivity method. To improve the accuracy, 26 corrections for non-nearest-neighbor interactions are introduced for oxygenate molecules and radicals. The vast majority of these values have never been determined before. As an alternative to the group additive method for radicals, the hydrogen bond increment method (HBI) is used to introduce 77 new HBI structures and to calculate their thermodynamic parameters. The developed group additive model was validated by comparing model predictions with both experimentally obtained and ab initio calculated data, resulting in mean absolute deviations below 4 kJ mol^{-1} for standard enthalpies of formation and below 4 J mol^{-1} K^{-1} for standard entropies and heat capacities.

Kinetics: Two types of reactions have been studied in this work, hydrogen abstraction reactions and carbon radical additions with their reverse β-scissions involving oxygenates. Rate coefficients in this study are determined using the conventional transition state theory (CTST). Ab initio calculations are performed by the CBS-QB3 method including corrections for one-dimensional hindered rotation around the forming/breaking bond in the transition state. For hydrogen abstraction reactions also zero curvature tunneling corrections according to the Eckart scheme are included.

For the modeling of kinetics, the group additive method developed at the Laboratory for Chemical Technology (LCT) of Ghent University was used. With this method, Arrhenius parameters of a target reaction can be determined by adding perturbations to the corresponding parameters of a reference reaction. These perturbation terms refer to structural differences between the transition states of the studied and the reference reaction, and are based upon group additivity for enthalpy and entropy. In this study it was shown that the inclusion of secondary contributions is necessary to obtain an accurate model. For hydrogen abstractions, corrections accounting for the effect of resonance stabilization around the transition state were shown to be necessary for increasing the accuracy of the model. Four group additive models have been developed in the framework of this work, which will be discussed hereafter.

Hydrogen abstractions from oxygenates by carbon-centered radicals: A dataset has been developed consisting of ab initio calculated Arrhenius parameters and rate coefficients for 103 hydrogen abstraction reactions from oxygenates by carbon-centered radicals. Based on these data fifteen group additive values (ΔGAV^os) are obtained for the forward and the reverse direction of the reaction accounting for primary and secondary contributions and also nine corrections for cross-resonance stabilization of the transition state. The resulting group additive model has been validated upon an ab initio dataset showing mean absolute deviation smaller than 0.250 log(m^3 mol^{-1} s^{-1}) and 1.5 kJ mol^{-1} for pre-exponential factors and activation energies, respectively, for the forward direction of the reaction at 300 K. Comparing the group additive predictions with a set of 33 experimental rate coefficients shows that the mean factor of deviation between group additively predicted and experimentally obtained rate coefficients is only 2.2.

Hydrogen abstractions from oxygenates by hydrogen atom: The same approach is adopted for hydrogen abstractions by hydrogen atoms, and kinetic parameters for 60 reactions have been determined. From this set of reactions, fifteen group additive values for Arrhenius parameters for the forward and the reverse reaction have been obtained; these ΔGAV^{o}s account for primary and secondary contributions. The accuracy of the model was validated upon an ab initio and an experimental validation set, showing that rate coefficients can be predicted with a mean deviation factor of 2 and 3, respectively.

Hydrogen abstractions from oxygenates by oxygen-centered radicals: This reaction family involves two types of transition states, that is, the abstraction of a hydrogen atom linked to a carbon or an oxygen atom by an oxygen-centered radical, which correspond to transition states of the O--H--C and O--H--O types, respectively. A total set of 118 reactions was studied and kinetic parameters have been obtained by ab initio calculations at temperatures 300-2500 K. Based on this set of reactions, 43 ΔGAV^{o}s are determined for primary and secondary contributions, along with 37 corrections accounting for cross-resonance effects in the transition state. The developed group additive model has been validated upon an ab initio validation set including 25 reactions and an experimental validation set of 61 rate coefficients with a mean factor of deviation of ~3 both for the two validation sets.

Carbon-centered radical additions to oxygenates and β-scissions of oxygenates: A database of Arrhenius parameters and rate coefficients for 66 carbon radical additions to oxygenates and their reverse β-scissions of oxygenates was developed covering temperatures from 300 to 2500 K. Based on these data, 32 group additive values are determined accounting for primary and secondary contributions. In the absence of experimental data in literature, an ab initio validation set is used to compare with the corresponding group additively predicted values, resulting in a mean factor of deviation of 3 both for the radical addition and the β-scission reactions. To the best of our knowledge ΔGAV^os for these reaction families have never been determined before, whereas experimental data for this type of reactions are very scarce.

Simulation of methyl butanoate (MB) pyrolysis: The program Genesys, developed at the LCT, allows an automated construction of reaction networks for hydrocarbons, oxygenates and several other compounds. The calculated ab initio data and the group additive values determined for thermochemistry and kinetics have been implemented in the corresponding Genesys databases. The reaction network generated by Genesys allows to study the thermal decomposition of large oxygenate compounds. In this study the pyrolysis of methyl butanoate was simulated using ab initio based group additivity for the reactions between larger compounds combined with an experiment-based seed mechanism for the thermal decomposition reactions of the smaller compounds. The results of this simulation for MB conversion and the majority of the product yields agree well with the corresponding available experimental values, which shows the usefulness of the constructed group additive models for use in large reaction networks.

Conclusion: In this study group additive models have been developed for an accurate prediction of thermodynamic parameters for oxygenate compounds and kinetic parameters for reactions between oxygenates. The Genesys software, developed at the LCT, was successfully used to generate a reaction network for the pyrolysis of methyl butanoate. Based on the agreement in the MB conversion and the majority of the product yields to experimental data, the usefulness and accuracy of the developed group additive models for the simulation of the thermal decomposition of oxygenate compounds has been shown.

Chapter 1

Introduction

Energy demand worldwide has increased the past decades and is expected to continue to grow rapidly in the foreseeable future. In covering this ever increasing energy demand, fossil resources will still play an important role, however, the need for sustainable development makes it progressively imperative to allocate fossil fuels more wisely, develop ways to diminish existing dependencies, and search for alternative sources. Biomass is an abundant and relatively cheap feedstock for bio-based energy and chemicals production. It is also renewable and environmentally cleaner than fossil-based feedstock and, hence, it can significantly contribute to a more sustainable economy and environmentally friendlier products.

Bio-based feedstock mainly consists of lingo-cellulosic biomass, a high-oxygen content organic material, the processing of which can reduce the impact on our environment, such as the climate change and the related global warming. Hence, it becomes increasingly important to optimize current technologies and introduce new processes in order to mitigate the climate change and its impacts on humanity. There are a number of technological options available to use biomass as a renewable resource for energy, commodities or specialty chemicals [1]. Biomass conversion processes can be categorized into biochemical or enzymatic and chemical, such as catalytic and thermal processes. Among the latter, combustion, gasification or pyrolysis are the main thermal biomass conversion processes [2]. The evaluation of the industrial feasibility of these processes and their optimization requires the development of fundamental kinetic models that can contain up to thousands of elementary reactions, and hence, their contribution in predicting the behavior of thermal biomass conversion processes over a broad range of temperatures and pressures is of major importance.

The limited number of experimental data available, which contrasts to the large amount of data needed even for the most simple kinetic models, prohibits the use of experimental rate coefficients only, and makes it imperative to turn to faster and more efficient methods than experimental methods. The recent advances in computer science, combined with the development of computational tools within the rapidly emerging field of computational chemistry, enable first principles determination of the required rate coefficients. Computational chemistry packages, such as Gaussian [3], allow the determination of electronic energies by solving the basic equations of quantum mechanics. In a next step, the calculated data can be used for the determination of rate coefficients using statistical mechanics and transition state theory [4-6].

However, the number of reactions involved in fundamental kinetic models increases exponentially with the carbon chain length of the reactant compounds, which makes it impossible and rather complicated to acquire all these data by means of computational chemistry. Moreover, ab initio calculations, despite their increased accuracy, are computationally too demanding for larger compounds. Therefore, a variety of faster methods has been developed for the prediction of accurate thermochemical and kinetic data. Among the most important and widely used methods is the group contribution method developed by

Benson and co-workers [7-9]. In the framework of this method, thermodynamic parameters can be obtained by using additive structure-property relations that link the corresponding thermodynamic parameter to structural functional subunits. These models and data, can be implemented in automated reaction mechanism generator software packages like PRIM [10], RMG [11] and GENESYS [12], leading to accurate kinetic modeling of several processes.

In this work group additive models are developed for an accurate prediction of the thermochemistry and kinetics for the radical gas phase chemistry of oxygenate compounds based on a consistent set of ab initio calculated data for the most important types of reactions and reaction families involved. The main advantage of using group additivity is the combination of a fast yet accurate prediction of the thermodynamic and kinetic parameters even for larger species, for which accurate quantum chemical calculations are computationally too expensive. Group additive models have been used successfully to model thermodynamics and kinetics for hydrocarbons [13-17], organosulfur [18-21] and silicon compounds [22, 23]. Thermodynamic and kinetic parameters reported in this work have been determined over a wide temperature range, 300-2500 K, covering the most important radical processes involving oxygenates.

Two main types of reactions are studied in the framework of this research, i.e., hydrogen abstractions and radical addition reactions along with their reverse β-scissions involving oxygenate compounds. Hydrogen abstraction reactions involve the simultaneous formation and cleavage of a hydrogen bond, with a hydrogen atom transferred from one molecule to another:

$$R_1^{\bullet} + R_2{-}H \rightleftharpoons R_1{-}H + R_2^{\bullet}$$

Reactions of this type play a prominent role in thermal biomass conversion processes and hence, kinetic data for this reaction type are indispensable for reaction network generation of such processes. They can be further categorized into hydrogen abstractions by carbon- or oxygen-centered radicals or by hydrogen atoms and involve the simultaneous formation and cleavage of a carbon-, oxygen- or hydrogen-hydrogen bond.

Radical addition reactions refer to the addition of a radical into an unsaturated carbon atom with the corresponding formation of a radical adduct. The reverse reaction of a radical addition is the *β*-scission reaction, a unimolecular reaction, in which a radical decomposes by the scission of a C−C or a C−H bond, in *β* position of the radical site, into a radical and an unsaturated molecule.

$$R_3^{\bullet} + R_2{=}R_1 \rightleftharpoons R_3{-}R_2{-}R_1^{\bullet}$$

During biomass thermal decomposition processes the monomolecular *β*-scissions govern the decomposition of large oxygenate compounds, whereas radical addition reactions to smaller olefins play a significant role in the final products of these processes. Normally, at temperatures lower than about 900-1000 K, the forward addition reaction is thermodynamically favored, while at higher temperatures the reverse *β*-scission reaction is dominant.

In the remainder of this chapter an overview of the biomass thermal conversion processes is provided. It is followed by a brief discussion on the ab initio methods applied for calculating thermochemistry and kinetics and the procedure used in this work to develop the aforementioned group additive models. Finally, the objectives of this study are formulated.

1.1 Thermal Processes

There are plenty of technological options available to convert the energy stored in biomass to more useful forms such as fuels, chemicals and power [2]. Among them there are processes in which heat is the dominant mechanism to convert the biomass into other chemicals; these processes are widely known as thermal processes. They can be classified into three principal methods depending on the extent to which oxygen is admitted to the conversion process usually in the form of air: combustion in excess air, gasification in a limited amount of air and pyrolysis in the absence of air [24].

Combustion [2] is the technologically most mature method among thermal processes; it can be further categorized into full and partial combustion. During that process biomass is burnt in excess air (full combustion) and the main product of this process is heat, which can be partially converted into power. The first stage of combustion involves the evolution of combustible vapors from biomass, which can be burned as flames. The derived heat can be used in a steam generator, and the produced steam can be expanded through a conventional turbo-alternator to produce electricity or other types of energy. In case there is no excess air, such as in partial combustion, the main residual products are energy carriers such as charcoal, oil or gas which can be further used to produce heat in a second stage or in co-combustion with biomass or fossil fuels. The current research into combustion [2, 24] is focused towards reducing emissions, ash deposition and carbon conversion through incomplete combustion. Finding a more environmentally sound and affordable manner for processing combustion co-products and emissions would be a step forward to the sustainable development of our society.

Biomass gasification [2, 25] is the second thermal biomass conversion process, which takes place with a restricted supply of oxygen. It occurs through the removal of the biomass moisture content, commonly referred to as drying, followed by the volatilization of the dry solid biomass and (partial) combustion of the volatile material to produce char and a fuel gas rich in hydrogen and carbon monoxide. This fuel gas is widely known as synthesis gas or syngas and has lower caloric value than natural gas. The main applications of gasification technology are in electricity generation, in transportation fuels, in hydrogen production, as well as in various industrial applications. Gasification generally occurs at lower temperatures than combustion and air emissions are generally lower.

The third promising biomass thermal conversion process is pyrolysis [1, 2], a process that occurs in the absence of oxygen or steam and at lower temperatures, compared to the other thermal conversion processes. During pyrolysis, biomass is heated to the point at which it is converted into a combination of solid char, gas and a liquid bio-oil. The proportion of these products are highly dependent on the reaction time. Hence, pyrolysis technologies can be further categorized into “slow” or “fast” pyrolysis and their products can be widely used as a feedstock for gasification or as a co-firing inlet for heat or power generation.

Although pyrolysis is a less mature technology compared to combustion or gasification, it is generally accepted that pyrolysis of biomass proceeds according to a radical mechanism. Due to the reactive nature of the radical intermediates, these mechanisms can include up to thousands of reactions between hundreds of different species, depending on the carbon chain number of the feedstock.

The main categories of the reactions involved are summarized hereafter. (a) Unimolecular bond scissions and their reverse radical recombination reactions: they are among the most important reactions in biomass pyrolysis processes, since they provide the initiation steps of that processes and determine the total radical concentration. (b) Bimolecular hydrogen abstraction reactions: these reactions involve the simultaneous breaking and formation of a hydrogen bond, migrating a hydrogen atom from one molecule to another. (c) Radical addition reactions to unsaturated compounds and their reverse β-scission reactions. In addition to these reaction families also some other radical reactions are involved, such as isomerization reactions and other side reactions that lead to the CO, CO_2, and coke formation, on the reactor wall.

1.2 Ab Initio Methods

The term “ab initio” in quantum chemistry indicates that the calculation is derived from first principles and does not rely on empirical data, assumptions or experimental data. Special effort is directed towards unraveling the chemistry of different compounds by calculating the electronic state of a system consisting of the nuclei and the electrons. This can be achieved by integrating the time-independent Schrödinger equation (eq (1-1)).

$$H\Psi=E\Psi \tag{1-1}$$

with H the total Hamiltonian operator acting on the wave function Ψ, and E the energy eigenvalue of the state Ψ. Eq (1-1) can be solved exactly only for the hydrogen atom and similar one-electron systems. For the rest of the systems it can only be solved by making assumptions, one of which is that the wave function Ψ can be written as a Slater determinant of one-electron wave functions [4]. In general, the higher the number of basis functions, the higher the accuracy by which the wave function Ψ can be reproduced, but the longer the calculation takes. Hence, the number of basis functions that should be used comes down to a trade-off between the desired accuracy and the computational efficiency.

The two main categories of methods used for obtaining electronic energies are the molecular orbital (MO) methods [26], also called Hartee-Fock (HF) based methods, and the density functional theory (DFT) methods [5]. The essence of the HF methods is that electron-electron interactions can be approximated as interactions between an electron and the mean field generated by other electrons, whereas the remaining electron correlations are only averaged. According to the HF method it is assumed that the calculated energy will always be higher than the exact solution of the Schrödinger equation, and that the electronic wave function can be written as a single Slater determinant [4]. Post-HF methods, such as perturbation [27] and couple-cluster [28] methods, express the wave function as a sum of Slater determinants and include electron correlation effects in the electronic structure calculations to render these calculations more accurate.

DFT methods [29] are considered to be an alternative to the HF based methods, as they replace the wave function used in HF based methods by the electron density function. Within the DFT formalism, the energy, *E*, of the ground state can be expressed as a unique functional of the electron density, as it is expressed in eq (1-2).

$$E[\rho] = -\frac{1}{2}\sum_{i=1}^{n}\int \Phi_i^*(r_1)\nabla^2\Phi_i(r_1)dr_1 - \sum_{x=1}^{N}\int \frac{Z_x}{r_{xi}}\rho(r_1)dr_1 + \frac{1}{2}\iint \frac{\rho(r_1)\rho(r_2)}{r_{12}}dr_1dr_2 + E^{XC}[\rho] \quad (1\text{-}2)$$

In eq (1-2) Φ_i are the Kohn-Sham orbitals. The first term corresponds to the kinetic energy of the non-interacting electrons, the second term represents the nuclear-electron attractions, whereas the third term describes the Coulomb repulsion between the total charge distributions at the points r_1 and r_2 in space. The fourth term is the exchange-correlation functional, which accounts for the correction for the kinetic energy arising from the interaction between the electrons and all the non-classical corrections to the electron-electron energy. Among the most commonly used DFT methods in this work are the B3LYP [30] and the BMK [31] method. However, there are modern functionals, such as the Minnesota density functionals, and especially the MO6 family [32-34], which were shown to have improved performance compared to the B3LYP functional [35, 36]. This improved performance can be mainly attributed to the improved treatment of medium-range correlation energy, which includes overlap dispersion interactions [37, 38].

Composite methods combine results for different levels of theory extrapolated to the complete-basis-set limit and full electron correlation. Among the most widely used composite methods are the complete basis set (CBS) methods developed by Petersson and co-workers [39, 40], the Gaussian methods developed by Curtiss et al. [41-44] and the Weizmann methods of Martin et al. [31, 45, 46]. The CBS-QB3 method of Montgomery et al. [39] is applied in this work, consistent with previous group additive models construction [13-15, 17, 47].

1.2.1 Thermochemistry

Accurate thermodynamic parameters are of major importance in developing reaction networks. These parameters are indispensable for the calculation of reaction equilibria and heat management in reactors. To deal with collections of molecules, usually denoted as ensembles, in statistical mechanics, it is important that certain macroscopic conditions are held constant and are not influenced by any external factor. This can be achieved by introducing the canonical partition function, Q, for a canonical ensemble of constant number of particles, N, volume, V, and temperature, T. Using the ideal gas assumption for this ensemble the problem is then transferred to the determination of the molecular partition functions, q [4].

Using molecular partition functions, q, the thermodynamic parameters of an ideal gas (internal energy, U, entropy, S, enthalpy, H, and Gibbs free energy, G) can be expressed by the eq (1-3)−(1-6).

$$U = k_B T^2 \left(\frac{\partial \ln q}{\partial T} \right)_V \tag{1-3}$$

$$S = k_B T \left(\frac{\partial \ln q}{\partial T} \right)_V + k_B \ln q \tag{1-4}$$

$$H = U + pV = U + RT \tag{1-5}$$

$$G = H - TS \tag{1-6}$$

Next to that, the equilibrium coefficient can be determined on the basis of thermodynamic parameters as indicated in eq (1-7).

$$K = \exp\left(-\frac{\Delta_r G^o}{RT} \right) \tag{1-7}$$

The standard enthalpy of formation, $\Delta_f H^o$, in this work is calculated by using the atomization enthalpy method. According to this method the standard enthalpy of formation of a compound is obtained as the difference between the ab initio calculated atomization enthalpy of the compound and the experimentally determined standard enthalpies of formation of the gas phase atoms of which the molecule consists. The approach for calculating the standard enthalpy of formation for oxygenate compounds is presented in Figure 1-1.

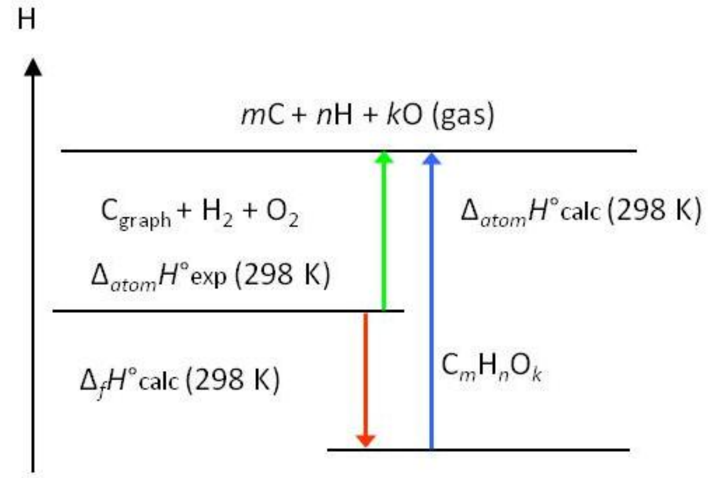

Figure 1-1: Enthalpy scheme illustrating the atomization enthalpy method for the ab initio calculation of the standard enthalpy of formation ($\Delta_f H°$) of an oxygenate compound ($C_mH_nO_k$). [$\Delta_{atom}H^o{}_{exp} = m\Delta_f H°_{exp}(C) + n\Delta_f H°_{exp}(H) + k\Delta_f H°_{exp}(O)$ and $\Delta_{atom}H^o{}_{calc} = mH°_{AI}(C) + nH°_{AI}(H) + kH°_{AI}(O) - H°_{AI}(C_mH_nO_k)$]

The equation that corresponds to Figure 1-1 and provides the standard enthalpy of formation of oxygenates using the atomization enthalpy method is the eq (1-8):

$$\Delta_f H°_{calc}(C_mH_nO_k) = m\Delta_f H°_{exp}(C) + n\Delta_f H°_{exp}(H) + k\Delta_f H°_{exp}(O) - [mH°_{AI}(C) + nH°_{AI}(H) + kH°_{AI}(O) - H°_{AI}(C_mH_nO_k)] = \Delta_{atom}H^o{}_{exp} - \Delta_{atom}H^o{}_{calc} \quad (1\text{-}8)$$

in which $\Delta_f H°_{exp}(C)$=716.68 kJ mol^{-1}, $\Delta_f H°_{exp}(H)$=218.0 kJ mol^{-1} and $\Delta_f H°_{exp}(O)$=249.18 kJ mol^{-1} at 298 K [48].

In this work the CBS-QB3 composite method is used for the ab initio calculation of standard enthalpies of formation since it was shown [49] to accurately reproduce experimental reaction enthalpies for hydrocarbons. Moreover, this method was shown [50] to be accurate yet computationally cost-effective in a benchmark study comparing results with advanced methods such as the G3B3 [42] composite method, and the MPW1PW91 [51] and BMK [52] density functional theory (DFT) methods with experimental data.

However, the agreement between the results for standard enthalpy of formation used in ab initio calculations and the experimental enthalpies of formation can be significantly improved by introducing spin-orbit (SO) corrections [53]. SO corrections account for the coupling of the spin magnetic moment of the electron with the magnetic moment induced by the motion of the electron around the nucleus.

A further improvement can be achieved by implementing bond additive corrections (BAC) [14, 54]. BACs are empirical systematic additive corrections linked to the atomic bonds present in the studied compound. These correction factors are used to compensate for the systematic errors in the electronic energy obtained by the CBS-QB3 ab initio method.

The calculation of the entropy requires the geometry and the vibrational frequencies of the species studied. The standard harmonic oscillator (HO) approximation usually performs poorly when compared to the true system, since even at very short distances beyond the equilibrium bond length, the true potential energy of the bond stretch curve is lower than that predicted by the parabolic potential of the HO approximation. Alternatively to the HO approximation, the one-dimensional hindered rotor (1D-HR) approach of Vansteenkiste and co-workers [55-57] can be applied for introducing hindered rotor corrections, assuming decoupled internal rotations. This method was chosen for the determination of standard entropies in this work since it was shown by Sabbe et al. [47] to significantly improve the accuracy of the calculated entropies and heat capacities. Alternative methods such as the multidimensional hindered rotation approximation [55], the treatment of all large amplitude motions [58] or the coupling between large amplitude motions [59, 60], can provide even more accurate results but at a significant additional computational cost. Therefore, in this study the one-dimensional hindered rotor approach was implemented.

Finally, molar heat capacities (C_p) can be calculated, using partition functions, by the eq (1-9).

$$C_P = k_B + 2k_B T \frac{\partial \ln q}{\partial T} + k_B T^2 \frac{\partial^2 \ln q}{\partial T^2} \tag{1-9}$$

1.2.2 Kinetics

Rate coefficients in this work are calculated using the conventional transition state theory (CTST) [61]. Within this theory the reactive system is assumed to move from reactants to products over the potential energy surface (PES), which is defined as a hyper-surface of the electronic energy of a collection of atoms as function of the atomic coordinates. The motion of the nuclei on the PES can then be solved within quantum chemistry by solving the Schrödinger equation. The transition state (TS) is a first-order saddle point on the PES, which corresponds to a maximum in the reaction coordinate direction and a minimum along all other directions. The easiest path from one minimum to another, is along the minimum energy path. A schematic representation of a reaction path is provided in Figure 1-2 [4].

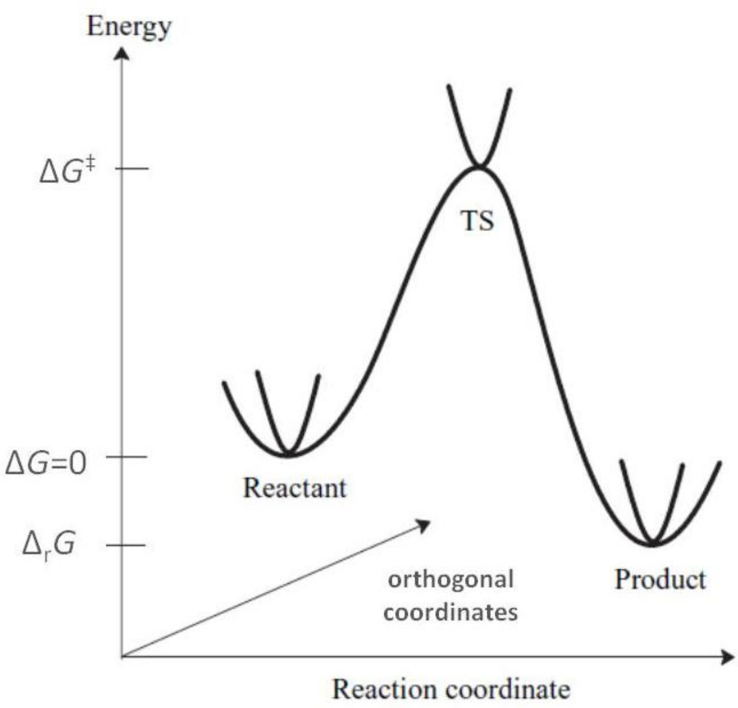

Figure 1-2: Schematic illustration of a reaction path [4].

In the assumption that quasi-equilibrium is achieved between the reactants and the transition state structure, and the transition state directly relaxes to the products, the rate coefficient can be expressed as in the eq (1-10):

$$k(T) = \frac{k_B T}{h} e^{\frac{-\Delta G^{\ddagger}}{RT}} \tag{1-10}$$

In eq (1-10), $\Delta G^{\ddagger}$ is the Gibbs activation barrier, that is the Gibbs free energy difference between the TS and the reactants. Based on this equation the rate coefficient of a particular reaction in the framework of the TS theory can be determined by the Gibbs energy of the TS structure relative to the reactants. However, since Gibbs activation barrier accounts only for enthalpic and entropic effects in the transition state, it is made clear that no tunneling effects are considered. This is the main limitation of this approach; it does not include neither recrossing nor tunneling/non-classical reflection effects. Within the CTST all molecules passing through the dividing surface go on to form the products and no re-crossing occurs. Tunneling and non-classical reflection effects can be taken into account by introducing a tunneling coefficient calculated using one of the tunneling methods available, such as the Eckart [62], Wigner [63], or Skodje and Truhlar [64] method. Tunneling coefficients can significantly increase the accuracy of the method. Tunneling effects are particularly important when the motion along the reaction coordinate mainly involves displacement of light atoms and at low temperatures. Non-classical reflection effects are more important at high temperatures (see Figure 1-3).

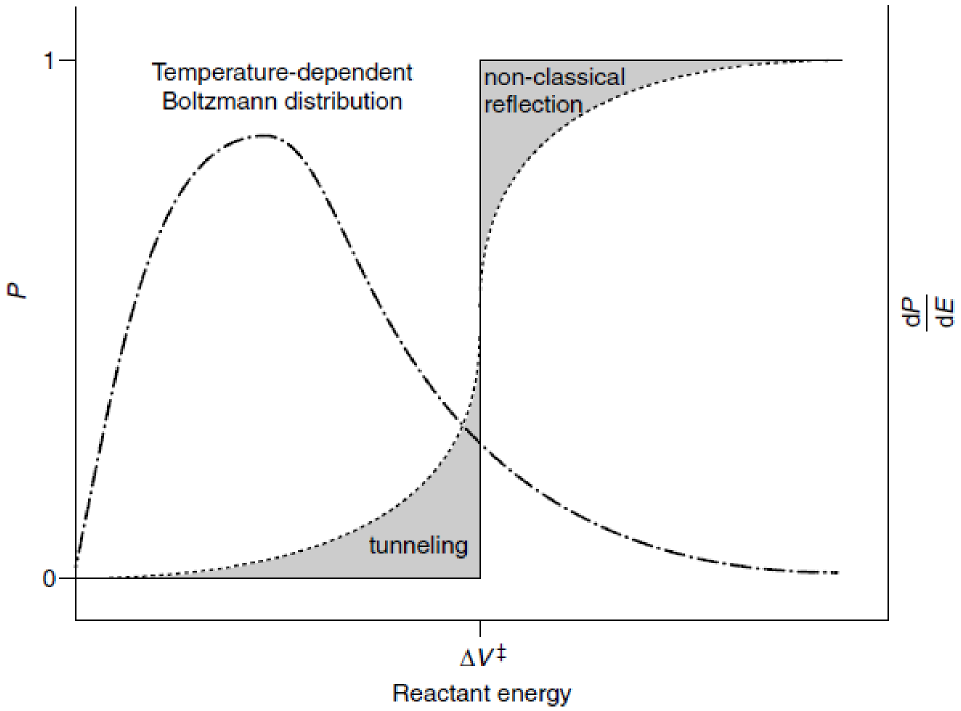

Figure 1-3: Probability of reaction (P) for systems moving towards a parabolic barrier for a reaction with a zero-point-including potential energy of activation, ΔV‡. The full line indicates classical systems, the dotted line indicates quantum systems (left axis). The dashed line indicates a typical Boltzmann distribution of the energy of a reacting system (right axis) [5].

Eq (1-10) can be reformulated, using statistical thermodynamics and including tunneling effects, to eq (1-11) for bimolecular reactions:

$$k(T) = \kappa_{\mathrm{Eckart}}(T)\frac{k_{\mathrm{B}}T}{h}\frac{q_{\ddagger}}{q_{\mathrm{A}}q_{\mathrm{B}}}e^{-\frac{\Delta E(0\,\mathrm{K})}{RT}} \tag{1-11}$$

with q the molecular partition function per unit volume, for reactant A and B (q_{A} and q_{B}, respectively) and the transition state ($q_{\ddagger}$).

A significant limitation of the CTST method is that the TS is assumed to be at the saddle point of the potential energy surface, which is not guaranteed to be also the maximum of the Gibbs free energy surface. To overcome this limitation, a more accurate approach for obtaining rate coefficients is the variational transition state approach (VTST) [65-67] in which the dividing surface is shifted along the reaction path to minimize possible recrossing effects and also maximizing the Gibbs free energy, which consequently minimizes the calculated rate coefficient. VTST does still not account for tunneling and it is computationally extremely demanding, but its implementation is imperative for reactions with very low reaction barriers such as recombination reactions [4].

Another limitation of the CTST method is the fact that fast energy exchange is assumed with the surroundings, meaning that thermal equilibrium is assumed between the reacting molecule and the environment. This assumption may not hold especially for gas-phase association and/or dissociation reactions at low pressures. In such cases microcanonical variational TST (μ-VTST) [68-70] is applied assuming a constant-energy system. A method representative of μ-VTST methods is the Rice-Ramsperger-Kassel-Marcus (RRKM) method [70, 71]. Within this method pressure dependence can be determined, but at the cost of information about the transition state, the potential energy surface, the vibration modes and the internal rotations [72]. Due to the significant computational cost required by these methods, pressure dependencies have not been implemented into the calculated rate coefficients in the present work. For pyrolysis conditions, about 1 bar and 1000 K, pressure dependence can typically be neglected but for the very smallest reactants [73].

In this work the accurate composite method CBS-QB3 of Montgomery et al. [39] is used to provide Arrhenius parameters (activation energies and pre-exponential factors) for the type of reactions studied, i.e., hydrogen abstractions and radical additions along with their reverse β-scissions. Only for a few cases of hydrogen abstractions by oxygen-centered radicals, in which the standard B3LYP geometry optimization procedure of the CBS-QB3 method failed to determine TS geometries, the BMK DFT method [31] was used for the geometry and the frequency optimization step.

1.3 Group Additivity Methods

1.3.1 Thermochemistry

Thermodynamic parameters of species involved in a reaction network are among the most important parameters, because they determine the reaction equilibrium coefficients, and hence the equilibrium composition of the reaction mixture. In literature only a limited number of thermodynamic parameters is available due to financial and instrumental limitations, because experimental equipment usually only covers a narrow range of conditions, and experiments are always subject to time limitations. This holds a fortiori for radicals due to their instable nature. Moreover, despite the significant progress in ab initio calculations, determining accurate thermodynamic and kinetic parameters for all species and reactions involved, is computationally too demanding especially for larger species. The need to surpass all these limitations lead to the development of additive structure-property relations that link the thermochemical values to structural molecular subunits, regardless of their location in a certain molecular structure.

Benson's group additivity (GA) method [7, 8] is the most widely applied method of this type. In the framework of this method, a group is defined as "a polyvalent atom together with all of its ligands" and it is denoted as $X{-}(A)_i(B)_j(C)_k(D)_l$ with X the central atom surrounded by *i* A ligands, *j* B ligands, *k* C ligands and *l* D ligands. The central atom is defined as an atom that has at least two ligands, and in special cases the central atom can also be a polyatomic group, that is, in this work, the carbonylic C=O group. In this work, different types of carbon atoms are distinguished and notated distinctly: C stands for a single-bond carbon atom with sp^3 hybrid orbitals, C_d for a double-bond carbon atom with sp^2 hybridization and C_t for a triple-bond carbon atom with sp hybrid orbitals, whereas $C^\bullet$ stands for a carbon radical.

From the definition of a Benson's group it can be easily concluded that these groups cannot account for non-local effects. Thus, many resonance effects, hyperconjugative effects and steric interactions cannot be accounted for by Benson's groups and their absence can lead to significant deviations compared to the experimental thermodynamic parameters of the compound studied. To overcome this deficiency of the method, contributions need to be defined that account for non-local effects, such as the interactions between parts of a molecule that are not directly bonded. These interactions are called non-nearest-neighbor interactions (NNI) and their inclusion contributes significantly to the accuracy of the method. In oxygenate compounds typical NNIs include hydrogen bonds, gauche and *cis* interactions.

Benson's GA method for determining thermodynamic parameters can be used not only for molecular but also for radical compounds. The main drawback of the method in case of radicals is that the number of group additive values (GAVs) needed increases significantly because of the necessity of determining radical-centered and radical-adjacent groups. An alternative method is the hydrogen atom bond increment (HBI) method developed by Lay et al. [74]. Within this method thermodynamic properties of a radical, $R^{\bullet}$, are determined by adding a hydrogen atom bond increment to the corresponding parameter of the parent molecule RH. Although this method was shown to be less accurate than the GA method for oxygenate radicals (Chapter 2), it uses a reduced number of parameters and, additionally, can account for resonance effects that extend beyond the group region, meaning that with the HBI method the inclusion of NNIs is not required.

As an example of the application of the two aforementioned methods, the standard enthalpy of formation ($\Delta_f H^o$) for the 2-methoxypropan-2-yl radical (see Figure 1-4) is calculated using (i) Benson's GA method and (ii) HBIs method.

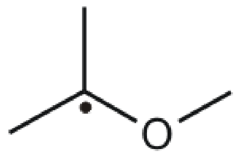

Figure 1-4: 2-methoxypropan-2-yl radical.

The following groups can be identified for the particular radical from left to right: C-(C$^{\bullet}$)(H)$_3$, C$^{\bullet}$-(C)$_2$(O), C-(C$^{\bullet}$)(H)$_3$, O-(C$^{\bullet}$)(C) and C-(O)(H)$_3$. Within the HBI method the GAV^{o}s for the parent molecule from left to right are: C-(C)(H)$_3$, C-(C)$_2$(O)(H), C-(C)(H)$_3$, O-(C)$_2$ and C-(O)(H)$_3$ and the HBI [CCJ(C)O]. In HBI notation J represents a radical on the preceding carbon or oxygen atom, following the nomenclature proposed by Lay et al. [74].

The standard enthalpy of formation for the particular radical can be calculated as follows by the Benson's GA method [eq (1-12)] and by the HBI method [eq (1-13)]:

$$\Delta_f H^o = 2\ \text{GAV}[\text{C-(C}^{\bullet})(\text{H})_3] + \text{GAV}[\text{C}^{\bullet}\text{-(C)}_2(\text{O})] + \text{GAV}[\text{O-(C}^{\bullet})(\text{C})] + \text{GAV}[\text{C-(O)(H)}_3] \quad (1\text{-}11)$$

$$\Delta_f H^o = 2\ \text{GAV}[\text{C-(C)(H)}_3] + \text{GAV}[\text{C-(C)}_2(\text{O})(\text{H})] + \text{GAV}[\text{O-(C}^{\bullet})(\text{C})] + \text{GAV}[\text{C-(O)(H)}_3] + \\ + \text{HBI}[\text{CCJ(C)O}] \quad (1\text{-}12)$$

1.3.2 Kinetics

Kinetic modeling and reaction network generation plays an important and decisive role in the in-depth understanding and optimization of chemical reactors. Accurately predicting the behavior of complex chemical reaction mechanisms requires a tremendous amount of thermodynamic and kinetic data that increases exponentially with the size of the reactant(s). Acquiring all these data by experiment is not possible due to practical restrictions. Alternatively, kinetic parameters for a wide range of reaction types and reaction families can be obtained by means of correlation methods and group additive models that can be used for the development of accurate kinetic models.

Early steps towards this direction are kinetic correlation methods, such as Evans−Polanyi [75, 76] correlations, the Blowers and Masel [77] model or the intersecting parabolas method developed by Denisov [78]. According to the Evans−Polanyi correlation, the activation energy, E_a, for reactions within a reaction family can be obtained from a linear correlation with the standard reaction enthalpy [eq (1-14)]:

$$E_a = E_a^o + \gamma_p \Delta_r H^o \tag{1-14}$$

in which E_a is the activation energy of the reaction studied, $\Delta_r H^o$ is the reaction enthalpy, E_a^o is the intrinsic barrier and γ_p is the transfer coefficient.

A refined variation on the Evans-Polanyi correlation is the reaction class approach to determine rate coefficients for hydrogen abstractions as developed by Truong et al. [79, 80]. The main assumption of this method is that reactions that belong to the same class have the same reactive moiety and thus, they are expected to have similarities in their potential energy surfaces. Hence, difference in rate coefficients between the reference and a target reaction can be expressed as a product of different components, accounting for symmetry number (f_σ), for quantum effects (f_κ), for effects caused by changing partition functions (f_Q), for the effect caused by the potential energy barrier (f_V), and for hindered rotation (f_{HR}) factor as presented in eq (1-15).

$$\frac{k_{\mathrm{target}}}{k_{ref}} = f_\sigma \, f_\kappa \, f_Q \, f_V \, f_{HR} \tag{1-15}$$

The most detailed methods with wide application range are those based on the structure of the transition state. In the structural contribution method developed by Willems and Froment [81, 82] the main assumption is that frequency factors and activation energies can be calculated by adding contributions to the corresponding parameters of a reference reaction. These parameters account for the structural differences between the target and the reference reaction. The introduction of the term “supergroup” is attributed to Sumathi et al. [83-85], with a supergroup defined to encompass the reactive moiety of the transition state structure. Due to this assumption a supergroup can account for contributions originating from interactions from non-adjacent groups, but the number of parameters needed increases combinatorially when different abstracting radicals are considered.

The method used in this work for obtaining accurate Arrhenius parameters and rate coefficients is the group contribution method introduced by Saeys et al. [13, 86] for the calculation of activation energies, E_a, for radical additions and hydrogen-abstraction reactions involving hydrocarbons and further refined by Sabbe et al. [15, 17] to include also pre-exponential factors, log$A$, for the studied reaction families. This method is in fact an extension of Benson’s group additivity scheme for transition states. According to this method, group additivity can be used in terms of differences between the transition state (TS) and the reactants to calculate accurate activation energies, E_a, and pre-exponential factors, log$A$ for a wide range of reaction types. This method was successfully used for several types of reactions, such as hydrogen abstractions [17, 19, 21], radical additions [15, 16], β-scissions and homolytic substitutions [20]. An additional advantage of this method is that the temperature dependence of the calculated group additivity (GA) values for the Arrhenius parameters can be incorporated in the corresponding parameters of a well-chosen reference reaction for each reaction family studied. Within this method there is the option to apply higher level computational methods in order to determine the kinetics for the reference reaction. Although this is not applied in the current study, it is expected that this can improve the accuracy of the aforementioned GA method.

Kinetic modeling and reaction network generation for pyrolysis of oxygenate compounds, as investigated in this study, requires kinetic parameters for several reaction families. Among the most important types of reactions are the hydrogen abstraction reactions and radical additions along with their reverse β-scission reactions involving oxygenate compounds. Hence, in the framework of this study group additivity models were developed for the following reaction types: 1) Hydrogen-abstraction reactions from oxygenates by carbon-centered radicals, with transition states of the C--H--C type. 2) Hydrogen-abstraction reactions from oxygenates by hydrogen atom, with transition states of the H--H--C type. 3) Hydrogen-abstraction reactions from oxygenates by oxygen-centered radicals, with transition states of the O--H--C and the O--H--O type. 4) Carbon-carbon radical additions to oxygenates and their reverse β-scissions of oxygenates, with transition states of the C--C--C type. In Figure 1-5 a schematic representation of the TS structure of hydrogen abstractions and radical additions studied in this work is provided.

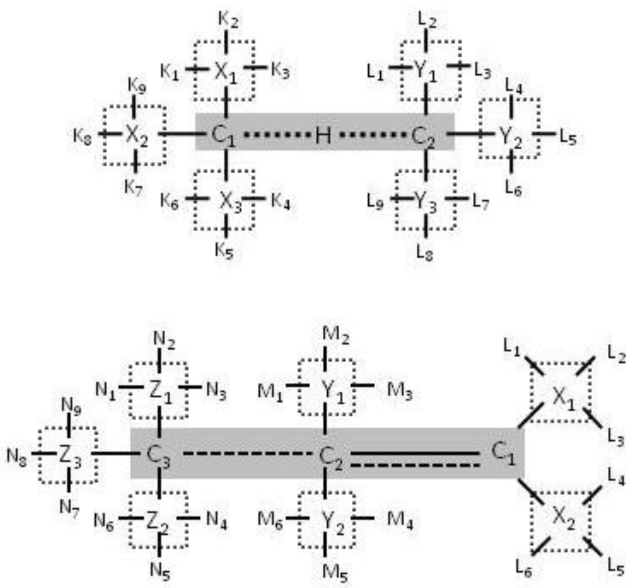

Figure 1-5: Schematic representation of the TS of 1) a hydrogen abstraction (upper scheme) and 2) a carbon radical addition/β-scission reaction (lower scheme). The grey zone indicates the central atoms of the primary contributions. The dotted line encompasses the central atoms of the secondary contributions.

During a hydrogen abstraction a hydrogen atom migrates from the group on C_2 to the group on C_1 (Figure 1-5, upper scheme), while during the addition of C_3 radical (Figure 1-5, lower scheme) to the C_2–C_1 double bond, C_1 changes from double-bonded carbon atom into carbon radical, C_2 changes from double-bonded carbon atom into single-bonded carbon atom and C_3 changes from carbon radical into single-bonded carbon atom. The major contributions to the Arrhenius parameters (primary contributions) stem from the atoms between which the hydrogen is abstracted (C_1 and C_2) for hydrogen abstractions and from the atoms that are involved in the addition reaction (C_1, C_2 and C_3). Secondary contributions refer to those arising from groups adjacent to the central atoms of the transition state, whereas tertiary contributions refer to non-nearest-neighbor interactions (NNI). In addition to that, also cross-resonance stabilization and hyperconjugative effects may contribute significantly to the kinetic parameters of a given reaction and should be accounted for.

By using the group contribution method previously discussed the Arrhenius parameters of a target reaction belonging to hydrogen abstraction reactions can be obtained by the eq (1-16) and (1-17).

$$\begin{aligned} E_{\mathrm{a}}(T) = E_{\mathrm{a,ref}}\,(T) + \sum_{i=1}^{2} \Delta\mathrm{GAV}^{\mathrm{o}}_{\mathrm{E_a}}(C_i) + \sum_{i=1}^{3} \Delta\mathrm{GAV}^{\mathrm{o}}_{\mathrm{E_a}}(X_i) + \\ + \sum_{i=1}^{3} \Delta\mathrm{GAV}^{\mathrm{o}}_{\mathrm{E_a}}(Y_i) + \sum_{i} NNI_i^{o} + \Delta\mathrm{E}^{\mathrm{o}}_{\mathrm{E_{a,res}}} \end{aligned} \tag{1-16}$$

$$\begin{aligned} \log \tilde{A}(T) = \log \tilde{A}_{ref}\,(T) + \sum_{i=1}^{2} \Delta\mathrm{GAV}^{\mathrm{o}}_{\log\tilde{\mathrm{A}}}(C_i) + \sum_{i=1}^{3} \Delta\mathrm{GAV}^{\mathrm{o}}_{\log\tilde{\mathrm{A}}}(X_i) + \\ + \sum_{i=1}^{3} \Delta\mathrm{GAV}^{\mathrm{o}}_{\log\tilde{\mathrm{A}}}(Y_i) + \sum_{i} NNI_i^{o} + \Delta \log \tilde{A}^{o}_{res} \end{aligned} \tag{1-17}$$

In eq (1-16) and (1-17) the first term refers to the Arrhenius parameter of the reference reaction, whereas the remaining terms account for the structural differences between the transition state of the target reaction and the reference reaction and can be categorized into primary, secondary, tertiary contributions and cross-resonance stabilization and/or hyperconjugative effects. Secondary and tertiary contributions were shown to be negligible for carbon radical additions and their reverse *β*-scissions involving hydrocarbons [15] and for hydrogen abstraction reactions between hydrocarbons [17]. However, for hydrogen abstractions from sulfides [19] one secondary contribution was shown to be significant. In this work secondary contributions were shown to be of major importance for all types of reactions investigated, while tertiary contributions are negligible. Corrections for cross-resonance and/or hyperconjugative effects are only included for hydrogen abstractions, since their contribution to the kinetic parameters of the studied reactions was significant.

The Arrhenius parameters obtained by using the eq (1-16) and (1-17) can be implemented in the eq (1-18) to determine the rate coefficients for a particular reaction.

$$k = \kappa n_{\mathrm{e}} k_{\mathrm{GA}} = \kappa n_{\mathrm{e}} \tilde{A} e^{-\frac{E_{\mathrm{a}}}{RT}} \tag{1-18}$$

In eq (1-18) κ stands for the tunneling coefficient, n_{e} is the reaction path degeneracy or number of single events, $\tilde{A}$ is the single-event pre-exponential factor obtained from eq (1-17) and E_{a} is the activation energy derived from eq (1-16). In this work, for the study of hydrogen abstractions involving oxygenates, Eckart's [62] tunneling model is used to determine tunneling coefficients, because it was shown that this method gives more accurate results for the reaction families studied [87] in a benchmark study with other methods [63, 64]. However, tunneling effects were shown to be negligible in the GA model for the carbon radical additions to oxygenates and their reverse *β*-scissions of oxygenates. The number of single events, n_e, is analogue to the reaction path degeneracy and is given by the eq (1-19), as it was proposed by Pollak and Pechukas [88] and Coulson [89]:

$$n_e = \frac{n_{\mathrm{opt},\ddagger}}{n_{\mathrm{opt,A}} n_{\mathrm{opt,B}}} \frac{\sigma_{\mathrm{A}} \sigma_{\mathrm{B}}}{\sigma_{\ddagger}} \tag{1-19}$$

In eq (1-19) σ represents the global symmetry number of the reactants A and B, σ_A and σ_B, and the transition state, $\sigma_{\ddagger}$, and n_{opt} is the number of optical isomers.

The application of the developed group additivity models is illustrated by the following examples of a hydrogen abstraction and a carbon radical addition reaction. As a first example the hydrogen abstraction from methanol by vinyloxy radical (CH_2=$CHO^{\bullet}$) was chosen.

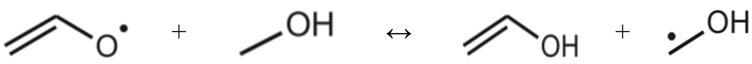

In this hydrogen abstraction reaction with transition state of the O--H--C type, the following ΔGAV^{o}s should be used for the calculation of its activation energy:

Primary Contributions: O_1−(C_d) and C_2−(O)$(H)_2$. (subscripts 1 and 2 in the central atoms of the hydrogen abstraction denote the forward and reverse direction of the reaction, respectively: “1” is the radical that abstracts a hydrogen bond to “2”)

Secondary Contributions: C_d−(O_1)(H) and O−(C_2)(H)

Resonance Corrections: $\pi_{C=C}$O−Cp$_{aO}$, which corresponds to the resonance interaction between a double bond π-conjugating system on the oxygen side and an α oxygen atom on the carbon side of the transition state. On the basis of the above mentioned groups the activation energy for the example reaction can be calculated by the eq (1-20):

$$E_{\mathrm{a}}\,(T) = E_{\mathrm{a,ref}}\,(T) + \Delta\mathrm{GAV}_{Ea}{}^{\mathrm{o}}[\mathrm{O_1{-}(C_d)}] + \Delta\mathrm{GAV}_{Ea}{}^{\mathrm{o}}[\mathrm{C_2{-}(O)(H)_2}] + \Delta\mathrm{GAV}_{Ea}{}^{\mathrm{o}}[\mathrm{C_d{-}(O_1)(H)}] + \\ + \Delta\mathrm{GAV}_{Ea}{}^{\mathrm{o}}[\mathrm{O{-}(C_2)(H)}] + \Delta E_{\mathrm{a,res}}[\pi_{\mathrm{C=C}}\mathrm{O{-}Cp_{aO}}] \tag{1-20}$$

T refers to the studied temperature in K.

The second example illustrates the carbon-carbon radical addition of 2-oxopropyl ($^{\bullet}CH_2COCH_3$) to but-1-ene ($CH_2{=}CHCH_2CH_3$) producing 6-oxoheptan-2-yl ($CH_3COCH_2CH_2{}^{\bullet}CHCH_2CH_3$).

For the calculation of the pre-exponential factor for this carbon-carbon radical addition the following ΔGAV^os needed:

Primary Contributions: $C_2{-}(C)(H)$ and $C_3{-}(CO)(H)_2$

Secondary Contributions: $CO{-}(C_3)(C)$

Using these ΔGAV^os for this carbon radical addition the pre-exponential factor can be calculated by the eq (1-21):

$$\log A\,(T) = \log\tilde{A}_{ref}\,(T) + \Delta GAV_{\log\tilde{A}}^{o}[C_2\text{-}(C)(H)] + \Delta GAV_{\log\tilde{A}}^{o}[C_3\text{-}(CO)(H)_2] +$$

$$+ \Delta GAV_{\log\tilde{A}}^{o}[CO\text{-}(C_3)(O)] + \log(n_e) \tag{1-21}$$

The number of single events, n_e, should be calculated by using eq (1-19), whereas T refers to the studied temperature in K.

1.4 Objective

The aim of this research is to develop an accurate and consistent model for the prediction of the thermodynamic parameters of oxygenate compounds and the prediction of the kinetic parameters of some of the most important reaction types that govern the thermal decomposition of oxygenates. The combination of the obtained data can be used for the simulation of the thermal decomposition of methyl butanoate, one of the widely used biodiesel surrogates.

To this end, Benson's [7-9] group contribution method is applied for the determination of standard enthalpy of formation ($\Delta_f H^o$) and entropy (S^o) at 298 K and heat capacities (C_p) at various temperatures (300-1500 K) of oxygenate compounds. These values derived from an extensive database of accurate thermodynamic parameters obtained from CBS-QB3 ab initio calculations, including hindered rotor corrections for all internal rotors.

Moreover, a database of accurate Arrhenius kinetic parameters and reaction rates for hydrogen abstractions, carbon-centered radical additions and their reverse β-scissions involving a wide range of oxygenate species at temperatures ranging from 300 K to 2500 K was constructed. Group additive values (ΔGAV^{o}s) for the Arrhenius parameters of the aforementioned reaction types studied, determined on the basis of the group additive method developed by Saeys et al. [13, 86] for activation energies and extended by Sabbe et al. [15-17] to include also pre-exponential factors for reactions involving hydrocarbons. All these models were validated by comparison of the predicted values with (a) ab initio obtained values, (b) experimental values from literature [90-93] and (c) the predictions of other models [77, 78]. The ultimate validation of the group additive thermodynamic and kinetic data obtained in this study is performed by comparing the results of the simulation of pyrolysis of methyl butanoate with bench-scale experimental data obtained from the LCT. The reaction network for methyl butanoate pyrolysis is constructed using the Genesys [12] software package developed at the LCT.

This PhD dissertation consists of a compilation of journal papers published within this research, and the manuscripts that are to be submitted for publication in the near future. In Chapter 2 the group additive modeling for the gas-phase standard enthalpies of formation, entropies and heat capacities of oxygenates is presented, providing an accurate and consistent set of ab initio determined thermodynamic parameters from which group additive values for oxygenate molecules and radicals along with hydrogen bond increments for oxygenate radicals are determined.

Chapter 3 provides a kinetic model for the hydrogen abstraction reactions from unsaturated and saturated oxygenate compounds by carbon-centered radicals. Chapter 4 is dedicated to the kinetic model for the hydrogen abstractions from unsaturated and saturated oxygenate compounds by hydrogen atoms. The kinetic model concerning the reaction type of hydrogen abstractions from oxygenate compounds by oxygen-centered radicals is discussed in Chapter 5. These kinetic models allow the prediction of kinetic parameters of the reaction families mentioned previously over a temperature range of 300-2500 K. Chapter 6 discusses another reaction type, the carbon-centered radical additions to oxygenates and their reverse β-scissions of oxygenates at temperatures ranging from 300 to 2500 K. Finally, the data obtained from the previous chapters were applied in the simulation of the thermal decomposition of methyl butanoate using the software package of Genesys [12] (Chapter 7) to develop the corresponding reaction network. Conclusions and prospects for future work are given in the final chapter (Chapter 8) of this dissertation.

1.5 References

1. Ulber, R., D. Sell, and T. Hirth, eds. *Renewable Raw Materials: New Feedstocks for the Chemical Industry*. 2011, Wiley-VCH Verlag GmbH & Co: Weinheim, Germany.

2. Brown, R.C., ed. *Thermochemical Processing of Biomass: Conversion into Fuels, Chemicals and Power*. ed. C.V. Stevens. 2011, John Wiley & Sons, Ltd: Chichester, UK. .

3. Frisch, M.J., G.W. Trucks, H.B. Schlegel, G.E. Scuseria, M.A. Robb, J.R. Cheeseman, G. Scalmani, V. Barone, B. Mennucci, et al., *Gaussian 09, Revision D.01*, 2009, Gaussian, Inc.: Wallingford CT.

4. Jensen, F., *Introduction to computational chemistry*. 1999, Chichester: Wiley.

5. Cramer, C.J., *Essentials of computational chemistry: theories and models*. 2005, Chichester: Wiley. 596.

6. Ramachandran, K.I., G. Deepa, and K. Namboori, eds. *Computational Chemistry and Molecular Modeling: Principles and Applications*. 2008, Springer: Springer. 398.

7. Benson, S.W. and J.H. Buss, *Additivity Rules for the Estimation of Molecular Properties. Thermodynamic Properties.* J Chem Phys, 1958. **29**(9): p. 546-561.

8. Benson, S.W., *Thermochemical Kinetics*. 1968, New York: John Wiley & Sons Ltd.

9. Benson, S.W., F.R. Cruickshank, D.M. Golden, G.R. Haugen, H.E. O'Neal, A.S. Rodgers, R. Shaw, and R. Walsh, *Additivity Rules for the Estimation of Thermochemical Properties.* Chem Rev, 1969. **69**: p. 279-324.

10. Clymans, P.J. and G.F. Froment, *Computer-Generation of Reaction Paths and Rate-Equations in the Thermal-Cracking of Normal and Branched Paraffins.* Computers & Chemical Engineering, 1984. **8**(2): p. 137-142.

11. William H. Green, Joshua W. Allen, Beat A. Buesser, Robert W. Ashcraft, Gregory J. Beran, Caleb A. Class, Connie Gao, C. Franklin Goldsmith, Michael R. Harper, et al., *RMG - Reaction Mechanism Generator v4.0.1*, 2013.

12. Vandewiele, N.M., K.M. Van Geem, M.F. Reyniers, and G.B. Marin, *Genesys: Kinetic Model Construction Using Chemo-Informatics.* Chem Eng J, 2012. **207**: p. 526-538.

13. Saeys, M., M.F. Reyniers, G.B. Marin, V. Van Speybroeck, and M. Waroquier, *Ab Initio Group Contribution Method for Activation Energies for Radical Additions.* Aiche J, 2004. **50**(2): p. 426-444.

14. Sabbe, M.K., M. Saeys, M.F. Reyniers, G.B. Marin, V. Van Speybroeck, and M. Waroquier, *Group additive values for the gas phase standard enthalpy of formation of hydrocarbons and hydrocarbon radicals.* J Phys Chem A, 2005. **109**(33): p. 7466-7480.

15. Sabbe, M.K., M.F. Reyniers, V. Van Speybroeck, M. Waroquier, and G.B. Marin, *Carbon-centered Radical Addition and Beta-Scission Reactions: Modeling of Activation Energies and Pre-Exponential Factors.* Chem Phys Chem, 2008. **9**(1): p. 124-140.

16. Sabbe, M.K., M.F. Reyniers, M. Waroquier, and G.B. Marin, *Hydrogen Radical Additions to Unsaturated Hydrocarbons and the Reverse beta-Scission Reactions: Modeling of Activation Energies and Pre-Exponential Factors.* Chem Phys Chem, 2010. **11**(1): p. 195-210.

17. Sabbe, M.K., A.G. Vandeputte, M.F. Reyniers, M. Waroquier, and G.B. Marin, *Modeling the Influence of Resonance Stabilization on the Kinetics of Hydrogen Abstractions.* Phys Chem Chem Phys, 2010. **12**(6): p. 1278-1298.

18. Vandeputte, A.G., M.K. Sabbe, M.F. Reyniers, and G.B. Marin, *Modeling the Gas-Phase Thermochemistry of Organosulfur Compounds.* Chem-Eur J, 2011. **17**(27): p. 7656-7673.

19. Vandeputte, A.G., M.K. Sabbe, M.F. Reyniers, and G.B. Marin, *Kinetics of Alpha Hydrogen Abstractions from Thiols, Sulfides and Thiocarbonyl Compounds.* Phys Chem Chem Phys, 2012. **14**(37): p. 12773-12793.

20. Vandeputte, A.G., M.F. Reyniers, and G.B. Marin, *Kinetics of Homolytic Substitutions by Hydrogen Atoms at Thiols and Sulfides.* Chem Phys Chem, 2013. **14**(8): p. 1703-1722.

21. Vandeputte, A.G., M.F. Reyniers, and G.B. Marin, *Kinetic Modeling of Hydrogen Abstractions Involving Sulfur Radicals.* Chem Phys Chem, 2013. **14**(16): p. 3751-3771.

22. Adamczyk, A.J., M.F. Reyniers, G.B. Marin, and L.J. Broadbelt, *Kinetic Correlations for H2 Addition and Elimination Reaction Mechanisms During Silicon Hydride Pyrolysis.* Phys Chem Chem Phys, 2010. **12**(39): p. 12676-12696.

23. Adamczyk, A.J., M.F. Reyniers, G.B. Marin, and L.J. Broadbelt, *Kinetics of Substituted Silylene Addition and Elimination in Silicon Nanocluster Growth Captured by Group Additivity.* Chem Phys Chem, 2010. **11**(9): p. 1978-1994.

24. Dahlquist, E., ed. *Technologies for Converting Biomass to Useful Energy*. 2013, CRC Press: USA.

25. Basu, P., ed. *Biomass Gasification, Pyrolysis and Torrefaction: Practical Design and Theory* 2013, Elsevier Inc.: USA.

26. Hehre, W.J., L. Radom, P.v.R. Schleyer, and P.J. A., eds. *Ab Initio Molecular Orbital Theory*. ed. K.B. Wiberg. 1986, John Wiley: New York. 548.

27. Pople, J.A., *Molecular Orbital Perturbation Theory .1. A Perturbation Method Based on Self-Consistent Orbitals.* Proc R Soc Lon Ser-A, 1955. **233**(1193): p. 233-241.

28. Crawford, T.D. and H.F. Schaefer, *An introduction to coupled cluster theory for computational chemists.* Rev Comput Chem, 2000. **14**: p. 33-136.

29. Koch, W. and M.C. Holthausen, eds. *A Chemist's Guide to Density Functional Theory*. 2001, Wiley-VCH Verlag GmbH: New York.

30. Becke, A.D., *A New Mixing of Hartree-Fock and Local Density-Functional Theories.* J Chem Phys, 1993. **98**(2): p. 1372-1377.

31. Boese, A.D. and J.M.L. Martin, *Development of density functionals for thermochemical kinetics.* J Chem Phys, 2004. **121**(8): p. 3405-3416.

32. Zhao, Y. and D.G. Truhlar, *Density functional for spectroscopy: No long-range self-interaction error, good performance for Rydberg and charge-transfer states, and better performance on average than B3LYP for ground states.* J Phys Chem A, 2006. **110**(49): p. 13126-13130.

33. Zhao, Y. and D.G. Truhlar, *A new local density functional for main-group thermochemistry, transition metal bonding, thermochemical kinetics, and noncovalent interactions.* J Chem Phys, 2006. **125**(19).

34. Zhao, Y. and D.G. Truhlar, *The M06 suite of density functionals for main group thermochemistry, thermochemical kinetics, noncovalent interactions, excited states, and transition elements: two new functionals and systematic testing of four M06-class functionals and 12 other functionals.* Theor Chem Acc, 2008. **120**(1-3): p. 215-241.

35. Zhao, Y. and D.G. Truhlar, *A density functional that accounts for medium-range correlation energies in organic chemistry.* Org Lett, 2006. **8**(25): p. 5753-5755.

36. Rokob, T.A., A. Hamza, and I. Papai, *Computing reliable energetics for conjugate addition reactions.* Org Lett, 2007. **9**(21): p. 4279-4282.

37. Steinmann, S.N., M.D. Wodrich, and C. Corminboeuf, *Overcoming systematic DFT errors for hydrocarbon reaction energies.* Theor Chem Acc, 2010. **127**(5-6): p. 429-442.

38. Zhao, Y. and D.G. Truhlar, *Applications and validations of the Minnesota density functionals.* Chem Phys Lett, 2011. **502**(1-3): p. 1-13.

39. Montgomery, J.A., M.J. Frisch, J.W. Ochterski, and G.A. Petersson, *A Complete Basis Set Model Chemistry. VI. Use of Density Functional Geometries and Frequencies.* J Chem Phys, 1999. **110**(6): p. 2822-2827.

40. Montgomery, J.A., M.J. Frisch, J.W. Ochterski, and G.A. Petersson, *A complete basis set model chemistry. VII. Use of the minimum population localization method.* J Chem Phys, 2000. **112**(15): p. 6532-6542.

41. Curtiss, L.A., K. Raghavachari, G.W. Trucks, and J.A. Pople, *Gaussian-2 Theory for Molecular-Energies of 1St-Row and 2Nd-Row Compounds.* J Chem Phys, 1991. **94**(11): p. 7221-7230.

42. Curtiss, L.A., K. Raghavachari, P.C. Redfern, V. Rassolov, and J.A. Pople, *Gaussian-3 (G3) theory for molecules containing first and second-row atoms.* J Chem Phys, 1998. **109**(18): p. 7764-7776.

43. Baboul, A.G., L.A. Curtiss, P.C. Redfern, and K. Raghavachari, *Gaussian-3 theory using density functional geometries and zero-point energies.* J Chem Phys, 1999. **110**(16): p. 7650-7657.

44. Curtiss, L.A., P.C. Redfern, K. Raghavachari, and J.A. Pople, *Gaussian-3X (G3X) theory using coupled cluster and Brueckner energies.* Chem Phys Lett, 2002. **359**(5-6): p. 390-396.

45. Martin, J.M.L. and G. de Oliveira, *Towards standard methods for benchmark quality ab initio thermochemistry - W1 and W2 theory.* J Chem Phys, 1999. **111**(5): p. 1843-1856.

46. Karton, A., E. Rabinovich, J.M.L. Martin, and B. Ruscic, *W4 theory for computational thermochemistry: In pursuit of confident sub-kJ/mol predictions.* J Chem Phys, 2006. **125**(14).

47. Sabbe, M.K., F. De Vleeschouwer, M.F. Reyniers, M. Waroquier, and G.B. Marin, *First Principles Based Group Additive Values for the Gas Phase Standard Entropy and Heat Capacity of Hydrocarbons and Hydrocarbon Radicals.* J Phys Chem A, 2008. **112**(47): p. 12235-12251.

48. Afeefy, H.Y., J.F. Liebman, S.E. Stein, P.J. Lindstrom, and W.G. Mallard, *Neutral Thermochemical Data*, in *NIST Chemistry WebBook, NIST Standard Reference Database Number 69*, 2005, National Institute of Standards and Technology: Gaithersburg MD.

49. Saeys, M., M.F. Reyniers, G.B. Marin, V. Van Speybroeck, and M. Waroquier, *Ab Initio Calculations for Hydrocarbons: Enthalpy of Formation, Transition State Geometry, and Activation Energy for Radical Reactions.* J Phys Chem A, 2003. **107**(43): p. 9147-9159.

50. Vandeputte, A.G., M.F. Reyniers, and G.B. Marin, *A theoretical study of the thermodynamics and kinetics of small organosulfur compounds.* Theor Chem Acc, 2009(123): p. 391-412.

51. Lynch, B.J., P.L. Fast, M. Harris, and D.G. Truhlar, *Adiabatic connection for kinetics.* J Phys Chem A, 2000. **104**(21): p. 4811-4815.

52. Boese, A.D., M. Oren, O. Atasoylu, J.M.L. Martin, M. Kallay, and J. Gauss, *W3 theory: Robust computational thermochemistry in the kJ/mol accuracy range.* J Chem Phys, 2004. **120**(9): p. 4129-4141.

53. Curtiss, L.A., K. Raghavachari, P.C. Redfern, and J.A. Pople, *Assessment of Gaussian-2 and density functional theories for the computation of enthalpies of formation.* J Chem Phys, 1997. **106**(3): p. 1063-1079.

54. Montgomery, J.A., A.M.J. Frisch, J.W. Ochterski, G.A. Petersson, K. Raghavachari, and V.G. Zakrzewski, *Comment on "Assessment of complete basis set methods for calculation of enthalpies of formation" [J. Chem. Phys. 188, 692 (1998)].* J Chem Phys, 1998. **109**(15): p. 6505-6506.

55. Van Speybroeck, V., P. Vansteenkiste, D. Van Neck, and M. Waroquier, *Why Does the Uncoupled Hindered Rotor Model Work Well for the Thermodynamics of n-Alkanes?* Chem Phys Lett, 2005. **402**(4-6): p. 479-484.

56. Vansteenkiste, P., D. Van Neck, V. Van Speybroeck, and M. Waroquier, *An extended hindered-rotor model with incorporation of Coriolis and vibrational-rotational coupling for calculating partition functions and derived quantities.* J Chem Phys, 2006. **124**(4): p. 044314.

57. Vansteenkiste, P., V. Van Speybroeck, G.B. Marin, and M. Waroquier, *Ab Initio Calculation of Entropy and Heat Capacity of Gas-Phase n-Alkanes Using Internal Rotations.* J Phys Chem A, 2003. **107**(17): p. 3139-3145.

58. Katzer, G. and A.F. Sax, *Identification and thermodynamic treatment of several types of large-amplitude motions.* Journal of Computational Chemistry, 2005. **26**(14): p. 1438-1451.

59. Wong, B.M. and W.H. Green, *Effects of large-amplitude torsions on partition functions: beyond the conventional separability assumption.* Molecular Physics, 2005. **103**(6-8): p. 1027-1034.

60. Vansteenkiste, P., D. Van Neck, V. Van Speybroeck, and M. Waroquier, *An extended hindered-rotor model with incorporation of Coriolis and vibrational-rotational coupling for calculating partition functions and derived quantities (vol 124, pg 044314, 2006).* J Chem Phys, 2006. **125**(4): p. Art. No. 049902.

61. Eyring, H., *The Activated Complex in Chemical Reactions.* J Chem Phys, 1935. **3**: p. 107-115.

62. Eckart, C., *The Penetration of a Potential Barrier by Electrons.* Phys Rev, 1930. **35**: p. 1303-1309.

63. Wigner, E., *Calculation of the Rate of Elementary Association Reactions.* J Chem Phys, 1937. **5**: p. 720-725.

64. Skodje, R.T., D.G. Truhlar, and B.C. Garrett, *A General Small-Curvature Approximation for Transition-State-Theory Transmission Coefficients.* J Phys Chem-Us, 1981. **85**(21): p. 3019-3023.

65. Truhlar, D.G. and B.C. Garrett, *Variational Transition-State Theory.* Accounts Chem Res, 1980. **13**(12): p. 440-448.

66. Truhlar, D.G. and B.C. Garrett, *Variational Transition-State Theory.* Annu Rev Phys Chem, 1984. **35**: p. 159-189.

67. Hu, W.P., Y.P. Liu, and D.G. Truhlar, *Variational Transition-State Theory and Semiclassical Tunneling Calculations with Interpolated Corrections - a New Approach to Interfacing Electronic-Structure Theory and Dynamics for Organic-Reactions.* J Chem Soc Faraday T, 1994. **90**(12): p. 1715-1725.

68. Smith, S.C., *Microscopic Rate Coefficients in Reactions with Flexible Transition-States - Analysis of the Transitional-Mode Sum of States.* J Chem Phys, 1991. **95**(5): p. 3404-3430.

69. Smith, S.C., *Angular-Momentum Resolution in Transitional-Mode State Counting for Loose Transition-States.* J Chem Phys, 1992. **97**(4): p. 2406-2416.

70. Smith, S.C., *Flux Factors in Variational Transition-State Theory.* J Phys Chem-Us, 1994. **98**(26): p. 6496-6504.

71. Smith, S.C., *Rapid Algorithms for Microcanonical Variational Rice-Ramsperger-Kassel-Marcus Theory.* J Phys Chem-Us, 1993. **97**(27): p. 7034-7039.

72. Wong, B.M., D.M. Matheu, and W.H. Green, *Temperature and molecular size dependence of the high-pressure limit.* J Phys Chem A, 2003. **107**(32): p. 6206-6211.

73. Sabbe, M.K., K.M. Van Geem, M.F. Reyniers, and G.B. Marin, *First Principle-Based Simulation of Ethane Steam Cracking.* Aiche J, 2011. **57**(2): p. 482-496.

74. Lay, T.H., J.W. Bozzelli, A.M. Dean, and E.R. Ritter, *Hydrogen-Atom Bond Increments for Calculation of Thermodynamic Properties of Hydrocarbon Radical Species.* J Phys Chem-Us, 1995. **99**(39): p. 14514-14527.

75. Evans, M.G. and M. Polanyi, *Further Considerations on the Thermodynamics of Chemical Equilibria and Reaction Rates.* Proc. Roy. Soc. A, 1936. **154**: p. 1333-1360.

76. Evans, M.G. and M. Polanyi, *Inertia and Driving Force of Chemical Reactions.* Trans. Faraday Soc., 1938. **1938**(34): p. 11-29.

77. Blowers, P. and R. Masel, *Engineering Approximations for Activation Energies in Hydrogen Transfer Reactions.* Aiche J, 2000. **46**(10): p. 2041-2052.

78. Denisov, E.T., *New Empirical Models of Free Radical Abstraction Reactions.* Usp Khim+, 1997. **66**(10): p. 953-971.

79. Truong, T.N., *Reaction Class Transition State Theory: Hydrogen Abstraction Reactions by Hydrogen Atoms as Test Cases.* J Chem Phys, 2000. **113**(12): p. 4957-4964.

80. Truong, T.N., W.T. Duncan, and M. Tirtowidjojo, *A Reaction Class Approach for Modeling Gas Phase Reaction Rates.* Phys Chem Chem Phys, 1999. **1**(6): p. 1061-1065.

81. Willems, P.A. and G.F. Froment, *Kinetic Modeling of the Thermal-Cracking of Hydrocarbons .1. Calculation of Frequency Factors.* Ind Eng Chem Res, 1988. **27**(11): p. 1959-1966.

82. Willems, P.A. and G.F. Froment, *Kinetic Modeling of the Thermal-Cracking of Hydrocarbons .2. Calculation of Activation-Energies.* Ind Eng Chem Res, 1988. **27**(11): p. 1966-1971.

83. Sumathi, R., H.H. Carstensen, and W.H. Green, *Reaction Rate Prediction via Group Additivity Part 1: H Abstraction from Alkanes by H and CH3.* J Phys Chem A, 2001. **105**(28): p. 6910-6925.

84. Sumathi, R., H.H. Carstensen, and W.H. Green, *Reaction Rate Prediction via Group Additivity, Part 2: H-Abstraction from Alkenes, Alkynes, Alcohols, Aldehydes and Acids by H Atoms.* J Phys Chem A, 2001. **105**(39): p. 8969-8984.

85. Sumathi, R. and W.H. Green, *Oxygenate, Oxyalkyl and Alkoxycarbonyl Thermochemistry and Rates for Hydrogen Abstraction from Oxygenates.* Phys Chem Chem Phys, 2003. **5**(16): p. 3402-3417.

86. Saeys, M., M.F. Reyniers, V. Van Speybroeck, M. Waroquier, and G.B. Marin, *Ab Initio Group Contribution Method for Activation Energies of Hydrogen Abstraction Reactions.* Chem Phys Chem, 2006. **7**(1): p. 188-199.

87. Vandeputte, A.G., M.K. Sabbe, M.F. Reyniers, V. Van Speybroeck, M. Waroquier, and G.B. Marin, *Theoretical Study of the Thermodynamics and Kinetics of Hydrogen Abstractions from Hydrocarbons.* J Phys Chem A, 2007. **111**(46): p. 11771-11786.

88. Pollak, E.L.I. and P. Pechukas, *Symmetry Numbers, Not Statistical Factors, Should be Used in Absolute Rate Theory and in Bronsted Relations.* J Am Chem Soc, 1978. **100**(10): p. 2984-2991.

89. Coulson, D.R., *Statistical Factors in Reaction-Rate Theories.* J Am Chem Soc, 1978. **100**(10): p. 2992-2996.

90. *NIST Standard Reference Database Number 69, http://webbook.nist.gov/chemistry/.* 2009: NIST.

91. *Chemical Kinetics Database, NIST Standard Reference Database 17, Version 7.0 (Web Version), Release 1.6.7, Data Version 2013*, 2013.

92. Atkinson, R., D.L. Baulch, R.A. Cox, J.N. Crowley, R.F. Hampson, R.G. Hynes, M.E. Jenkin, M.J. Rossi, and J. Troe, *Evaluated Kinetic and Photochemical Data for Atmospheric Chemistry: Volume I - Gas Phase Reactions of Ox, HOx, NOx, and SOx, Species.* Atmos Chem Phys, 2004. **4**(4): p. 1461-1738.

93. Atkinson, R., D.L. Baulch, R.A. Cox, J.N. Crowley, R.F. Hampson, R.G. Hynes, M.E. Jenkin, M.J. Rossi, and J. Troe, *Evaluated Kinetic and Photochemical Data for Atmospheric Chemistry: Volume II - Gas Phase Reactions of Organic Species.* Atmos Chem Phys, 2006. **6**(6): p. 3625-4055.

Chapter 2

Group Additive Values for the Gas-Phase Standard Enthalpy of Formation, Entropy and Heat Capacity of Oxygenates

This chapter includes the following paper:

Paraskevas, P. D.; Sabbe, M. K.; Reyniers, M. F.; Papayannakos, N.; G.B. Marin, Group Additive Values for the Gas Phase Standard Enthalpy of Formation, Entropy and Heat Capacity of Oxygenates. *Chemistry - A European Journal* **2013**, *19*, 16431-16452.

2.1 Abstract

A complete and consistent set of 60 Benson group additive values (GAVs) for oxygenate molecules and 97 GAVs for oxygenate radicals is provided, which allow to describe their standard enthalpies of formation, entropies and heat capacities. Approximately half of the GAVs for oxygenate molecules and the majority of the GAVs for oxygenate radicals have not been reported before. The values are derived from an extensive and accurate database of ab initio obtained thermochemical data calculated at the CBS-QB3 level of theory for 202 molecules and 248 radicals. These compounds include saturated and unsaturated, α- and β-branched, mono- and bifunctional oxygenates. Internal rotations were accounted for using one-dimensional hindered rotor corrections. The accuracy of the database was further improved by adding bond additive corrections to the CBS-QB3 standard enthalpies of formation. Furthermore, 14 corrections for non-nearest-neighbor interactions (NNI) were introduced for molecules and 12 for radicals. The validity of the constructed group additive model was established by comparing the predicted values with both ab initio calculated values and experimental data for oxygenates and oxygenate radicals. The group additive method predicts standard enthalpies of formation, entropies and heat capacities with chemical accuracy, respectively within 4 kJ mol^{-1} and 4 J mol^{-1} K^{-1}, for both ab initio calculated and experimental values. As an alternative, the hydrogen bond increment (HBI) method developed by Lay et. al. (T. H. Lay, J. W. Bozzelli, A. M. Dean, E. R. Ritter, *J. Phys. Chem.* **1995**, *99*, 14514) was used to introduce 77 new HBI structures and to calculate their thermodynamic parameters ($\Delta_f H°$, $S°$, $C_p°$). The GAVs reported in this work can be reliably used for the prediction of thermochemical data for large oxygenate compounds, combining rapid prediction with wide-ranging application.

2.2 Introduction

In the face of global climate change, the need for sustainable development requires us to optimize current technologies, design new processes and explore the use of alternative renewable raw material to replace fossil feeds. Biomass is invaluable as an intermediate and relatively cheap energy resource to provide the initial feedstock for the development of a large bio-energy industry, offering an environmentally acceptable way of disposing of unwanted and sometimes polluting waste. It is mainly composed of organic oxygenate compounds and its use as a substitute for fossil fuels, rather than solely for carbon sequestration, will enable biomass to play a much greater role in coping with greenhouse effect and its impacts on humanity. To assess the economic feasibility of the processing of this type of renewable feedstock, kinetic simulations are necessary. The required themodynamical data for oxygenates are largely lacking and their experimental determination is practically infeasible because the majority of species involved are radicals, which are very instable.

Another possible solution to acquiring the necessary data is the use of ab initio methods. Ab initio calculations, despite their increased accuracy, are computationally too demanding for larger compounds. The group additivity method introduced by Benson [1-3] provides a powerful tool for obtaining accurate thermodynamic data for larger compounds belonging to different classes of molecules based on a limited set of parameters, the so-called group additivity values (GAVs). Benson's GAVs can be determined either by using a training set of ab initio calculated data or by using experimentally obtained data.

Several studies have used experimental data and data obtained by ab initio methods to provide reliable group additivity models. Based on experimental data Cohen [4] provided a simultaneous compilation and evaluation of data for all three phases (gas, liquid and solid) of carbon-hydrogen and carbon-hydrogen-oxygen compounds. The distinctive feature of this particular work was the extension and the revision of Benson's group additivity method for similar compounds and the definition of a new ketene group family (>C=C=O). One of the largest compilations of group additivity values based on experimental data for hydrocarbons, oxygenates and nitrogen- or sulfur-containing compounds has been provided by Poling et al. [5] Luo [6] has presented a large set of experimental-based GAVs for the enthalpy of formation of radicals in the gas phase.

Recent progress in the application of group additivity procedures has been based on ab initio methods. Sabbe and co-workers [7, 8] created a group additive model for the calculation of standard enthalpies of formation, entropies and heat capacities for hydrocarbon compounds such as alkanes, alkenes, cycloalkanes, cycloalkenes, alkynes, monocyclic aromatics and their corresponding radicals. A consistent set of GAVs is derived from CBS-QB3 calculated values. Sumathi and Green [9] provided a group additivity model based on ab initio calculations for ketenes. A set of 20 GAVs and 3 non-nearest-neighbor interactions (NNIs) based on alkylketenes, oxygenated ketenes, 1,3-bisketenes and ketene-substitute alcohols was determined based on CBS-Q calculations. A recent study that is relevant to atmospheric chemistry and particularly to compounds that contain carbon, oxygen, nitrogen, and hydrogen was performed by Khan and Broadbelt [10] using Gaussian-3 (G3), a high-level composite method similar to the CBS-QB3 method, with geometries based on density functional theory (DFT) calculations using the B3LYP functional.

In addition to the determination of GAVs by using ab initio methods, experimental data are still used to extend group additivity methods. Recently, Bhattacharya and Shivalkar [11] used experimental data to estimate the GAVs for the standard enthalpy of formation of free radicals of hydrocarbons and oxygenates. In addition, the Benson GAV terms for the estimation of standard enthalpies of formation for a wide variety of carbon-, hydrogen-, oxygen-, nitrogen-, and sulfur-containing molecules have been revised and extended by Holmes and Aubry [12, 13].

Perusal of the literature shows that the group additive values for many oxygenate compounds and mostly for radicals have remained undetermined, and that those that exist are largely limited to standard enthalpies of formation, completely neglecting entropy effects and temperature dependence. The aim of this study was to develop an integrated, consistent group additive model for the thermochemistry of oxygenates, describing the standard enthalpies of formation, entropies and heat capacities. In this study we have established a set of GAVs based on calculations at the CBS-QB3 level for 202 molecules and 248 radicals of oxygenates. The species considered were alcohols, ethers, esters, aldehydes, ketones, acids and ketenes, saturated and unsaturated, α- and β-branched, mono- and bifunctional compounds and their corresponding radicals. To develop the model, a database was compiled of accurate enthalpies of formation, entropies and heat capacities for oxygenates molecules and radicals calculated at the CBS-QB3 level including hindered rotor corrections for all internal rotations. The need for additional NNIs was evaluated by examining the deviations between the ab initio values and group additive predicted values. The GA model was validated by comparing the GA predictions with ab initio values for a validation set consisting of 22 oxygenate compounds and also with experimental values obtained in the literature [14].

Finally, the hydrogen bond increment (HBI) method, as established by Lay et al. [15] was used as an alternative to the Benson's group additive method to determine the thermodynamic properties of oxygenate radicals. The HBI method is particularly interesting for resonance-stabilized radicals, but HBI data are scarce and to the best of our knowledge only bond dissociation energies have previously been calculated by Sun and Bozzelli [16, 17] for ethanol, α-monoethanol and 2-propanol radicals, by Sebbar et al. [18] for unsaturated radicals, and by Hudzik and Bozzelli [19] for ketone radicals. Based on the training set of the 248 radicals 75 HBIs were determined and validated by comparison with the corresponding data available in the literature [16-19].

2.3 Computational Methods

In this work all electronic structure calculations have been performed with the Gaussian-03 program [20], by using an approach consistent with previous work [7, 21]. For every compound contained in the current set, the lowest-energy conformer at the B3LYP/6-311G(d,p) level was determined by screening the possible conformers. The CBS-QB3 composite method was used to determine the electronic energy and corrections for hindered rotation for all internal rotors were included, based on B3LYP/6-31G(d) DFT energy profiles for internal rotation.

The internal rotations were automatically identified based on the topology of the molecule. The one-dimensional (1D-HR) approach of Vansteenkiste and co-workers [22-24] was applied for the hindered rotor corrections, assuming decoupled internal rotations. In the applied method, as described by Vansteenkiste [22-24], the resulting rotational partition function replaced the harmonic contribution derived from the same potential energy profile.

For rotational modes with barriers to internal rotation of less than 1 kJ mol^{-1}, the energy profile for internal rotation was often scattered or discontinuous. Therefore, for these loose rotations, the free rotor approximation was used to determine the partition function for internal rotation. This free rotor contribution replaced the vibrational contribution from the harmonic frequency analysis. Standard enthalpies of formation were calculated by using the atomization energy method. According to this method the standard enthalpy of formation is determined as the difference between the ab initio (AI) calculated atomization enthalpy of a compound and the experimentally determined enthalpy of formation of the gaseous atoms [14]. The agreement between ab initio calculated and experimental enthalpies of formation was improved by using spin-orbit (SO) corrections and empirical bond additive corrections (BAC) [8, 25].

Various group additivity methods are available for estimating thermochemical data of chemical compounds [26, 27], but the method developed by Benson [1-3] is the most widely used and the method used in this work. According to this method a group is defined as "a polyvalent atom together with all of its ligands" and is denoted as $X{-}(A)_i(B)_j(C)_k(D)_l$ with X the central atom surrounded by *i* ligands A, *j* ligands B and so on. Different types of carbon atoms are distinguished and notated distinctly: sp^3 C represents a single-bonded carbon atom, sp^2 C_d a double-bonded carbon atom, sp C_t a triple-bonded carbon atom, C_b represents an aromatic sp^2 carbon atom in a benzene ring, and $C^\bullet$ represents a carbon radical. In this work only C, C_d and $C^\bullet$ types of carbon atoms were examined. The oxygen-related groups studied in this work involve oxygen-centered, >C=O (carbonyl) and >C=C=O (ketene) groups, as well as their corresponding radicals. According to Benson's group additivity method [1-3], a central atom is defined as an atom that has at least two ligands. In the aforementioned >C=O and >C=C=O groups, the oxygen is not considered as a central atom because it only has one double-bonded carbon atom as a ligand.

In general the group additive values obtained by Benson's method cannot account for all interactions present in a molecule. There are interactions that can be implicitly accounted for by a specific group, for example, the interaction between the ligands of a central atom is accounted for by the specific group, but there also exist interactions that should be explicitly accounted for. These are interactions between the ligands of neighboring atoms in a molecule or radical that exist without these particular atoms having a direct bond between them. These so-called non-nearest neighbor interactions (NNI) are accounted for by adding NNI corrections.

The group additive values and corrections for non-nearest neighbor interactions (NNI) are determined simultaneously by unweighed least-squares analysis, minimizing the following objective function (2-1):

$$SSQ = \sum_{i}^{n} \left(y_i - \hat{y}_i \right)^2 \qquad (2\text{-}1)$$

In this function y_i is the ab initio calculated enthalpy of formation ($\Delta_f H^o$), the intrinsic entropy ($S°_{int}$) or heat capacity ($C_p°$) of molecule i and $\hat{y}_i$ is the group additively calculated value. This results in the usual eq (2-2)

$$\overline{\mathrm{GAV}} = \left(\mathrm{X}^{\mathrm{T}} \mathrm{X} \right)^{-1} \mathrm{X}^{\mathrm{T}} \mathrm{y} \qquad (2\text{-}2)$$

in which $\overline{\mathrm{GAV}}$ is the estimated vector of the group additive values and X the matrix in which the elements X_{ij} specify the number of occurrences of group j in molecule i, and y is the vector containing ab initio calculated thermodynamic values to which the group additive values (GAVs) are regressed. Each of the columns of the matrix of independent variables X corresponds to a group whereas each row corresponds to a molecule. As a result of the definition of a group, each group contains information about the neighboring groups, and therefore the columns in X are linearly dependent for each class of molecules except for alkanes. Linear dependent subsets were identified and for this work 16 GAVs were set equal to structurally similar groups. The linear dependent subsets identified are provided in Table S1 in Appendix A.

To assess the reliability of the group additivity approximation, a statistical analysis is performed. The reported significance F of the regression, mean absolute deviation (MAD), root mean square deviation (RMS) and maximum deviation (MAX) correspond to the differences between the thermochemical data predicted by the ab initio group additivity method and the values obtained by CBS-QB3 ab initio method. The reported significance (F) of the regression is calculated by eq (2-3)

$$F = \frac{\sum_{i=1}^{n} \hat{y}_i^2 \Big/ p}{\sum_{i=1}^{n} \left(\hat{y}_i - y_i\right)^2 \Big/ (n-p)} \tag{2-3}$$

in which y is the CBS-QB3-BAC ab initio enthalpy of formation, $\hat{y}$ the enthalpy of formation predicted by our ab initio group additivity method, n is the number of molecules in the regression and p is the number of parameters, that is, the number of estimated GAVs. Furthermore, 97.5% confidence intervals on the estimated GAVs are determined by using the standard deviation between the predicted group additive and CBS-QB3 values.

Another method that can be used to predict the thermodynamic properties of radicals is the hydrogen bond increment (HBI) method introduced by Lay et al. [15]. Compared with Benson's [1-3] group additive (GA) method, the HBI method uses a reduced number of parameters and moreover can account for resonance effects that extend beyond the group region.

The HBI for the standard enthalpy of formation ($\Delta_f H^o$), intrinsic entropy ($S°_{int}$) and heat capacities ($C_p°$) of a radical are calculated by subtracting the thermodynamic property ($\Delta_f H^o$, $S°_{int}$, $C_p°$) of the corresponding parent molecule from the corresponding thermodynamic parameter of the particular radical. In particular, for the reaction $R{-}H \leftrightarrow R^{\bullet} + H^{\bullet}$, in which R is an oxygenate compound, the HBIs for $\Delta_f H^o$, $S°_{int}$ and $C_p°$ are calculated according to equations (2-4)-(2-6):

$$\mathrm{HBI}(\Delta_f H^o) = \Delta_f H^o_{AI}(\mathrm{R}^\bullet) - \Delta_f H^o_{GA}(\mathrm{RH}) \tag{2-4}$$

$$\mathrm{HBI}(S^\circ_{int}) = S^\circ_{int}(\mathrm{R}^\bullet) - S^\circ_{int}(\mathrm{RH}) \tag{2-5}$$

$$\mathrm{HBI}(C_p^\circ) = C_p^\circ(\mathrm{R}^\bullet) - C_p^\circ(\mathrm{RH}) \tag{2-6}$$

For radicals, ab initio calculated values are used, whereas for their parent molecules, values are obtained by using the group additivity method developed in this work. This is preferable because in the practical application of the HBI method the thermodynamic properties for parent molecules usually stem from GA methods because experimental or ab initio data are scarce, especially for oxygenate compounds.

Because there is a direct relationship between the HBIs for the standard enthalpy of formation and the bond dissociation enthalpy [BDE; eq. (2-7)], experimental BDEs for C−H and O−H bonds in oxygenate compounds can be used to validate the calculated HBIs for the standard enthalpies of formation.

$$\mathrm{HBI}(\Delta_f H^o) = \Delta_f H^o_{AI}(\mathrm{R}^\bullet) - \Delta_f H^o_{GA}(\mathrm{RH}) = \mathrm{BDE}(\mathrm{R{-}H}) - \Delta_f H^o(\mathrm{H}^\bullet) \tag{2-7}$$

2.4 Results and Discussion

To evaluate the effect of 1D-HR corrections, the thermochemical data calculated with the CBS-QB3 HO approximation and the CBS-QB3 1D-HR approximation were compared with experimental data obtained from the NIST databank for standard enthalpies of formation, entropies and heat capacities at 298 K [14]. The results of these comparisons are provided in Tables S2−S4 in Appendix A for enthalpies, entropies, and heat capacities, respectively, and an overview of the statistics used for these comparisons is provided in Table 2-1.

The 1D-HR approximation greatly improves the agreement between calculated values and experiment, particularly for entropies and heat capacities, resulting in mean absolute deviations (MADs) of 0.85 J mol^{-1} K^{-1} for entropies and 1 J mol^{-1} K^{-1} for heat capacities at

298 K. Therefore the 1D-HR approximation was chosen for all internal rotations present. The agreement for the standard enthalpy of formation is initially poor with a MAD of 3.43 kJ mol^{-1} and a mean deviation (MD) of 1.53 kJ mol^{-1}. This systematic overestimation can be removed by using isodesmic bond additive corrections (BACs), a procedure similar to isodesmic reactions described by Petersson et al. [28]. BACs have been fitted to a training set consisting of 29 oxygenates and an additional 32 saturated and unsaturated hydrocarbons (see Table S5 in Appendix A). By using the values reported in Table 2-2, the MAD and the MD of this training set can be reduced to 1.28 kJ mol^{-1} and 0.05 kJ mol^{-1}, respectively. The statistics for the standard enthalpies of formation for the oxygenate compounds are provided in Table 2-1.

Table 2-1: Statistics for the deviation of the ab initio calculated thermochemical data of oxygenates from the corresponding experimental value.[a]

	CBS-QB3 + SO HO	CBS-QB3 + SO 1D-HR	CBS-QB3 + SO + BAC 1D-HR
		$\Delta_f H°_{CBS\text{-}QB3}$-$\Delta_f H°_{NIST}$ (kJ mol^{-1})	
MD	0.87	1.53	0.05
MAD	2.81	3.43	1.28
MAX	6.30	8.56	6.00
		$S°_{CBS\text{-}QB3}$ -$S°_{NIST}$ (J mol^{-1} K^{-1})	
MD	-8.65	-0.43	-0.43
MAD	8.94	0.85	0.85
MAX	29.8	4.33	4.33
		$C_p°_{CBS\text{-}QB3}$- $C_p°_{NIST}$ (J mol^{-1} K^{-1})	
MD	-1.2	-0.1	-0.1
MAD	2.9	1.0	1.0
MAX	14.6	2.9	2.9

[a] SO: spin – orbit correction; BAC: bond additive correction on $\Delta_f H°$; HO: harmonic oscillator approximation; 1D-HR: one dimensional hindered rotor correction; MD: mean deviation; MAD: mean absolute deviation; MAX: maximum deviation.

Table 2-2: Calculated Bond Additive Corrections (BACs) for the standard enthalpy of formation ($\Delta_f H°$).

Bond	C-C	C-H	C-O	C=O	O-H	C=C
BAC [kJ mol^{-1}]	-2.07	-0.19	1.58	3.11	-1.77	-3.45

To determine the ab initio GAVs, CBS-QB3 calculations were performed for a total set of 202 oxygenate molecules and 248 oxygenate radicals. The chemical compounds included in the training set for the GAVs were saturated and unsaturated, α- and β-branched, mono- and bifunctional oxygenate molecules, including alcohols, ethers, esters, aldehydes, ketones, acids and ketenes. The standard enthalpy of formation ($\Delta_f H°$) at 298 K, entropy ($S°$) at 298 K and heat capacity ($C_p°$) at 300 K, 400 K, 500 K, 600 K, 800 K, 1000 K and 1500 K were obtained for each compound. The whole database can be found in Table S6 of Appendix A for molecules and in Table S7 for radicals together with their corresponding number of optical isomers and their total symmetry number.

To calculate the GAVs for oxygenates, some hydrocarbon GAVs determined in previous work of Sabbe and co-workers [7, 8], which employed the same methodology, have been used. These GAVs used are summarized in Table S8 in Appendix A.

2.4.1 Oxygenate Molecules

From the database of 202 molecules (see Table S6 in Appendix A), 60 GAVs and 14 corrections for non-nearest neighbour interactions (NNIs) were estimated. From these groups, 28 new groups and a further 12 groups for which only Khan and Broadbelt have determined GAVs before were introduced [10]. Furthermore, the 14 NNIs have not been reported before. The species investigated were alcohols, ethers, esters, aldehydes, ketones, acids and ketenes, including bifunctional species.

Two estimation procedures can be followed: The NNI corrections can be estimated either simultaneously with or separately from the GAVs. In this work the GAVs and NNIs were estimated simultaneously. The GAVs were calculated within 97.5 % confidence intervals (CI).

To assess the reliability of the group additivity approximation, a statistical analysis was performed. Because nine GAVs and three NNI corrections are derived from a single molecular structure, the statistics on the regression are slightly biased because these parameters are formally calculated from the CBS-QB3 values and not determined by regression. To lift this bias, the parameters reflecting the quality of the regression were determined by neglecting both the GAVs or NNI corrections derived from a single molecule, and molecules from which a single GAV or NNI correction is determined. The reported significance of the regression (F), mean absolute deviation (MAD), root mean square deviation (RMS) and maximum deviation (MAX) correspond to the differences between the thermochemical data predicted by the group additivity method and the values calculated by using ab initio calculations.

GAVs for oxygenate molecules: The group additive model introduced is found to be accurate for the oxygenate compounds included in the training set with a MAD of 1.49 kJ mol^{-1} for standard enthalpies of formation, 2.11 J mol^{-1} K^{-1} for entropies, and less than 1.83 J mol^{-1} K^{-1} for heat capacities at the studied temperatures. The statistics for the regression estimates are presented in Table 2-3 and the details of the residual differences between the group additive predictions and ab initio calculated values for every molecule of the training set are provided in Table S9 in Appendix A.

Table 2-3: Statistics for the regression analysis of the GAVs and NNIs for the standard enthalpies of formation ($\Delta_f H°$) and entropies ($S°$) at 298 K, and the heat capacities ($C_p°$) at various temperatures for molecules.[a]

	$\Delta_f H°$ [kJ mol^{-1}]	$S°$ [J mol^{-1} K^{-1}]	$C_p°$ [J mol^{-1} K^{-1}] 300 K	400 K	500 K	600 K	800 K	1000 K	1500 K
F	64989	7354	1953	3713	6556	9480	13943	18887	38066
MAD	1.49	2.11	1.83	1.52	1.20	1.11	1.06	0.95	0.68
RMS	1.99	2.72	2.33	2.01	1.70	1.54	1.42	1.30	0.99
MAX	6.53	7.63	7.06	6.81	6.53	5.87	4.84	5.15	4.82

[a] F: Significance; MAD: mean absolute deviation; RMS: root mean square deviation; MAX: maximum deviation

Table 2-4 lists the GAVs obtained after regression for all of the unknown groups along with 97.5% CIs for the enthalpies and entropies at 298 K and heat capacities at 300 K. Because the

CIs for the heat capacities decrease with temperature, only confidence intervals at 300 K are provided because these provide an upper limit to the CIs at higher temperatures. The groups are presented in Table 2-4 with decreasing number of carbon atoms as ligands. First, groups for saturated oxygenates with oxygen or carbonyl atoms as ligands are presented, followed by groups for saturated ketenes, unsaturated oxygenates with oxygen or carbonyl atoms as ligands, and finally for unsaturated ketenes.

NNIs for oxygenate molecules: For all molecules included in the training set of oxygenate molecules, possible non-nearest neighbor interactions (NNIs) were identified and determined simultaneously with the GAVs by unweighed least-square analysis, minimizing the objective function (2-1). After a first regression, the NNIs for which all the calculated thermodynamic properties ($\Delta_f H°$, $S°$ and $C_p°$) are less than a threshold of 5 kJ mol^{-1} for $\Delta_f H°$ and 5 J mol^{-1}K^{-1} for $S°$ and $C_p°$ were omitted and a new regression was performed. This procedure was repeated until all the NNIs had at least one thermodynamic parameter greater than 5 kJ mol^{-1} for $\Delta_f H°$ and 5 J mol^{-1}K^{-1} for $S°$ and $C_p°$. From the initial 31 possible gauche interactions and 25 possible hydrogen bonds recognized, resulting in a total of 56 NNIs only 14 of them were finally retained (see Table 2-5).

The NNI corrections introduced in this work for oxygenate molecules can be divided into three main categories: Hydrogen-bonding interactions, which are mainly stabilizing interactions, gauche interactions and various other interactions due to the particular structure of the examined compound. The values for the non-nearest-neighbour-interactions (NNIs) along with the confidence intervals for the enthalpies and entropies at 298 K and the heat capacities at 300 K calculated in this work are listed in Table 2-5.

Hydrogen bonds: A hydrogen bond is an interaction between a covalently bound hydrogen atom and a region of high electron density on an electronegative atom such as an oxygen atom. The strongly stabilizing effects, mainly caused by electrostatic attraction between the positively charged hydrogen and the negatively charged heteroatom, require dedicated corrections in any group additivity scheme. The main criterion for introducing a hydrogen bond correction is for the distance between the hydrogen and electronegative atom to be less than 2.5 Å. After the regression only hydrogen bonds that appeared to have at least one significant value for one of the calculated thermodynamic parameters, that is, $\Delta_f H^\circ$ > 5 kJ mol^{-1} or $S°$, $C_p°$ > 5 J mol^{-1} K^{-1}, were retained. In this work, corrections for 10 hydrogen-bonding interactions were introduced and are presented in Figure 2-1.

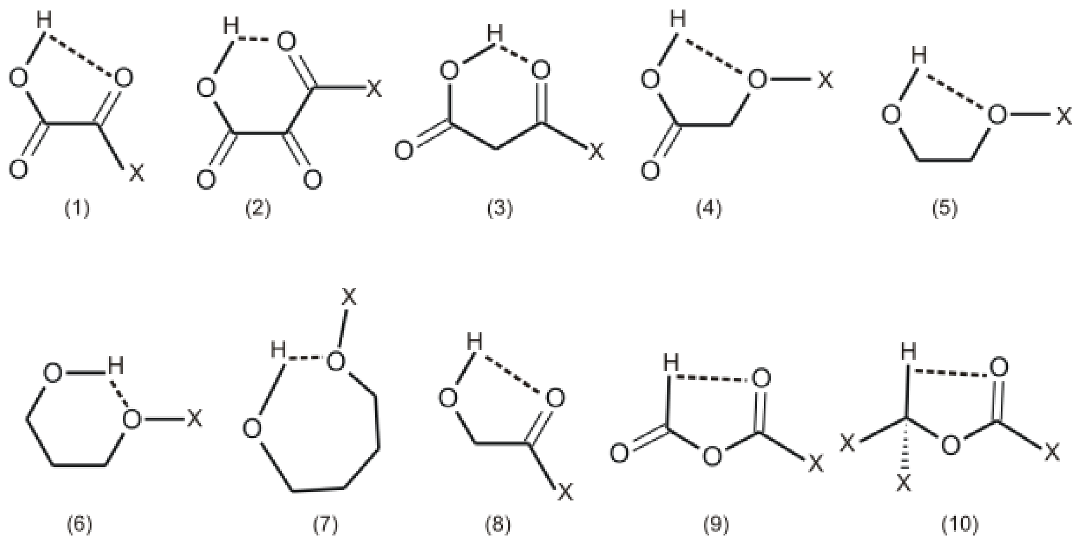

Figure 2-1: 3D structures of the hydrogen bonds introduced as NNIs (1) Hbr_H-O-CO-CO, (2) Hbr_ H-O-CO-CO-CO, (3) Hbr_ H-O-CO-C-CO, (4) Hbr_ H-O-CO-C-O, (5) Hbr_H-O-C-C-O, (6) Hbr_ H-O-C-C-C-O, (7) Hbr_ H-O-C-C-C-C-O, (8) Hbr_ H-O-C-CO, (9) Hbr_ H-CO-O-CO and (10) Hbr_ H-C-O-CO. X represents a generalized substituent.

As a result of their stabilizing effects hydrogen bonds are expected to have negative values for the standard enthalpy of formation. In this work some NNIs are, however, associated with a positive contribution to the enthalpy, for example, the hydrogen bond of the type H-O-CO-CO-CO (NNI12) has a value of +4.5 kJ mol^{-1} for the standard enthalpy. This can be explained by the fact that in the particular molecule in which this interaction is present another hydrogen bond of the type H-O-CO-CO (NNI1) is also present. The molecular structure of 2-oxopropanedionic acid is provided in Figure 2-2 as an example. Both of the interactions themselves, NNI1 (the lower hydrogen bond) and NNI2 (the upper hydrogen bond), are stabilizing, but the CO-$(CO)_2$ group experiences a certain amount of oxygen-oxygen repulsion, which cannot be included in either of the two NNIs. This oxygen-oxygen repulsion has a destabilizing influence on the molecular structure that causes one of the NNIs to have a positive value.

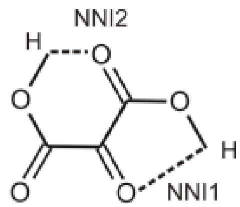

Figure 2-2: Molecular structure of 2-oxopropanedionic acid.

According to Benson's group additivity method, a GAV does not correspond to strain-free molecules but incorporates all the interactions that stem from atoms composing a particular GAV. Thus, the pure character of an NNI (e.g., the stabilizing character of a hydrogen bond) may be biased and differ from molecule to molecule in which this NNI is present.

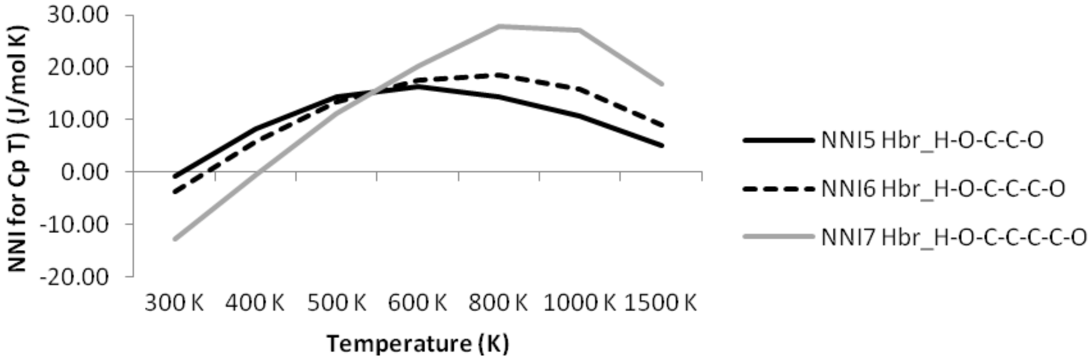

Figure 2-3: Temperature dependence of the heat capacities of the hydrogen bonds H-O-C-C-O (NNI5), H-O-C-C-C-O (NNI6) and H-O-C-C-C-C-O (NNI7) with increasing carbon-chain length.

Table 2-4: GAVs for the standard enthalpies of formation ($\Delta_f H°$) and entropies ($S°$) at 298 K, and the heat capacities ($C_p°$) at various temperatures for oxygenate molecules.[a]

group	$\Delta_f H°$ [kJ mol^{-1}]	$S°$ [J mol^{-1} K^{-1}]	$C_p°$ [J mol^{-1} K^{-1}]						
			300 K	400 K	500 K	600 K	800 K	1000 K	1500 K
saturated oxygenates other than ketenes									
C-(C)$_3$(O)	-20.34 ± 3.24	-144.38 ± 4.44	23.99 ± 3.81	31.20	34.89	36.47	36.78	36.05	34.4
C-(C)$_3$(CO)	4.57 ± 2.85	-140.94 ± 3.90	22.68 ± 3.34	27.48	30.12	31.51	32.36	32.39	32.42
C-(C)$_2$(O)$_2$	-69.23 ± 4.92	-163.77 ± 6.74	27.88 ± 5.77	43.75	51.85	54.00	50.77	45.94	38.31
C-(C)$_2$(CO)$_2$	14.95 ± 4.33	-146.69 ± 5.92	33.76 ± 5.08	33.42	32.60	31.91	31.01	30.55	30.35
C-(C)$_2$(CO)(O)	-10.87 ± 4.39	-148.70 ± 6.02	28.15 ± 5.16	35.17	38.11	38.72	37.49	35.88	33.45
C-(C)$_2$(O)(H)	-25.09 ± 2.83	-52.05 ± 3.88	21.99 ± 3.32	29.03	34.22	37.78	41.96	44.27	47.11
C-(C)$_2$(CO)(H)	-5.41 ± 2.85	-47.41 ± 3.90	23.68 ± 3.34	27.86	31.26	34.00	38.07	41.00	45.46
C-(C)(O)(H)$_2$	-34.33 ± 1.22	37.65 ± 1.67	25.01 ± 1.43	31.90	37.45	41.88	48.53	53.31	60.53
C-(C)(CO)(H)$_2$	-21.51 ± 1.30	40.32 ± 1.78	26.91 ± 1.53	30.80	34.98	38.91	45.56	50.73	58.93
C-(O)$_2$(H)$_2$	-67.53 ± 4.92	17.89 ± 6.74	27.35 ± 5.77	43.68	53.55	58.15	60.86	61.66	63.53
C-(CO)$_2$(H)$_2$	-10.01 ± 3.57	40.1 ± 4.88	27.77 ± 4.19	32.81	37.10	40.67	46.39	50.85	58.25
C-(O)(CO)(H)$_2$	-19.83 ± 3.70	31.54 ± 5.06	26.75 ± 4.34	34.37	40.77	45.37	51.2	54.96	60.79
C-(O)(H)$_3$	-42.90	127.12	25.31	32.07	38.44	44.06	53.36	60.63	72.47
C-(CO)(H)$_3$	-42.90	127.12	25.31	32.07	38.44	44.06	53.36	60.63	72.47
O-(C)$_2$	-98.62 ± 2.08	38.61 ± 2.85	14.70 ± 2.44	13.40	13.58	14.54	16.71	18.29	20.17
O-(C)(CO)	-102.16 ± 2.69	45.71 ± 3.68	11.49 ± 3.15	9.94	9.96	10.70	12.71	14.71	18.00
O-(CO)$_2$	-46.39 ± 5.54	80.80 ± 7.59	18.40 ± 6.51	11.55	6.97	3.72	-0.53	-2.57	-1.41
O-(C)(H)	-165.22 ± 2.16	125.32 ± 2.96	19.07 ± 2.54	19.80	20.85	22.07	24.57	26.95	31.66
O-(CO)(H) [c]	-165.22 ± 2.16	125.32 ± 2.96	19.07 ± 2.54	19.80	20.85	22.07	24.57	26.95	31.66
CO-(C)$_2$	-132.23 ± 1.77	61.78 ± 2.42	23.82 ± 2.08	27.70	31.22	34.19	38.37	40.85	43.26
CO-(C)(O)	-221.97 ± 2.43	43.52 ± 3.33	20.67 ± 2.85	28.39	34.60	39.48	46.23	50.09	52.68
CO-(C)(CO)	-122.03 ± 1.09	57.80 ± 1.50	26.77 ± 1.28	30.83	34.36	37.27	41.27	43.45	45.25
CO-(O)$_2$	-281.39 ± 5.11	22.66 ± 7.00	26.17 ± 6.00	39.30	48.25	53.88	58.97	59.63	56.09
CO-(CO)$_2$	-89.30 ± 2.05	64.51 ± 2.81	31.75 ± 2.41	33.35	34.10	34.51	35.19	36.06	38.14
CO-(O)(CO)	-196.18 ± 2.86	39.37 ± 3.92	27.18 ± 3.36	34.34	39.85	44.13	49.81	52.40	52.33
CO-(C)(H)	-123.42 ± 1.77	145.46 ± 2.42	26.24 ± 2.08	31.22	35.94	40.13	46.74	51.39	57.73
CO-(O)(H)	-211.83 ± 3.42	124.04 ± 4.68	25.88 ± 4.01	34.56	42.08	48.16	56.57	61.38	65.84
CO-(CO)(H)	-104.85 ± 1.45	140.49 ± 1.98	29.76 ± 1.70	34.63	39.25	43.32	49.57	53.77	59.32
saturated ketenes									
C-(C)$_3$(CCO) [b]	-4.55 ± 5.90	-144.08 ± 8.08	20.63 ± 6.93	27.65	31.98	34.41	36.16	36.25	35.2
C-(C)$_2$(CCO)(H) [b]	-11.05 ± 5.90	-47.59 ± 8.08	21.23 ± 6.93	27.55	32.36	35.85	40.37	43.16	46.94
C-(C)(CCO)(H)$_2$	-21.07 ± 2.95	40.95 ± 4.04	21.19 ± 3.46	28.00	33.91	38.75	46.07	51.36	59.45
C-(CCO)(H)$_3$	-42.90	127.12	25.31	32.07	38.44	44.06	53.36	60.63	72.47
CCO-(C)$_2$	0.54 ± 4.06	84.72 ± 5.55	42.55 ± 4.76	46.42	50.00	53.24	58.30	61.71	66.01
CCO-(C)(H)	-17.65 ± 3.41	169.15 ± 4.67	43.83 ± 4.00	50.10	55.50	60.05	67.09	72.13	79.55
unsaturated oxygenates other than ketenes									
C-(C)$_2$(C$_d$)(O)	-14.57 ± 3.24	-153.23 ± 4.44	29.24 ± 3.81	37.61	40.84	41.46	40.06	38.20	35.08
C-(C)$_2$(C$_d$)(CO)	9.78 ± 2.85	-146.74 ± 3.90	26.01 ± 3.34	30.13	32.44	33.51	33.75	33.26	32.55
C-(C)(C$_d$)(O)$_2$	-62.75 ± 4.92	-170.44 ± 6.74	27.95 ± 5.77	42.92	51.33	54.81	53.92	49.73	41.11
C-(C)(C$_d$)(CO)$_2$	19.86 ± 4.33	-150.69 ± 5.92	35.99 ± 5.08	39.53	39.94	39.09	36.71	34.80	32.51
C-(C)(C$_d$)(CO)(O)	-3.88 ± 3.66	-158.30 ± 5.02	33.75 ± 4.30	42.15	45.09	44.95	41.74	38.55	34.46
C-(C)(C$_d$)(O)(H)	-23.99 ± 3.19	-61.06 ± 4.36	29.84 ± 3.74	38.86	43.83	46.37	48.34	49.06	49.94
C-(C)(C$_d$)(CO)(H)	-2.17 ± 2.85	-50.47 ± 3.90	29.32 ± 3.34	32.99	35.49	37.28	39.75	41.6	44.96
C-(C$_d$)$_2$(O)$_2$	-55.74 ± 4.92	-179.76 ± 6.74	30.08 ± 5.77	45.85	54.70	58.39	57.78	53.65	44.31
C-(C$_d$)$_2$(CO)$_2$	25.20 ± 4.33	-168.67 ± 5.92	42.49 ± 5.08	50.96	52.27	50.54	45.33	41.10	35.70
C-(C$_d$)$_2$(CO)(O)	2.99 ± 3.49	-160.69 ± 4.77	36.85 ± 4.09	46.04	49.00	48.85	45.61	42.23	37.25
C-(C$_d$)$_2$(O)(H)	-17.40 ± 3.10	-64.14 ± 4.24	29.82 ± 3.64	38.47	43.27	45.70	47.5	48.09	48.78
C-(C$_d$)$_2$(CO)(H)	2.86 ± 2.85	-53.20 ± 3.90	29.26 ± 3.34	34.41	37.40	39.22	41.43	43.04	46.12
C-(C$_d$)(O)(H)$_2$	-26.64 ± 2.88	34.59 ± 3.95	28.42 ± 3.38	35.65	40.62	44.31	49.79	53.92	60.6
C-(C$_d$)(CO)(H)$_2$	-16.85 ± 2.85	40.18 ± 3.90	24.94 ± 3.34	31.41	36.47	40.49	46.72	51.49	59.29
C$_d$-(C)(O)	32.95 ± 4.34	-50.89 ± 5.94	12.79 ± 5.10	15.86	19.67	22.91	26.55	27.85	28.45
C$_d$-(C)(CO)	38.97 ± 4.82	-51.26 ± 6.60	15.33 ± 5.66	16.82	18.64	20.42	23.20	250	27.10

C_d-(O)$_2$	28.28 ± 6.30	-42.69 ± 8.63	11.34 ± 7.40	11.93	14.86	17.95	22.31	24.6	26.92
C_d-(O)(H)	36.37	33.51	18.08	21.17	24.43	27.41	32.22	35.73	40.97
C_d-(CO)(H)	36.37	33.51	18.08	21.17	24.43	27.41	32.22	35.73	40.97
C_d-(CCO)(H)	36.37	33.51	18.08	21.17	24.43	27.41	32.22	35.73	40.97
O-(C)(C_d)	-123.88 ± 2.96	18.91 ± 4.05	19.07 ± 3.47	23.32	25.26	25.92	25.50	24.52	22.72
O-(CO)(C_d)(b)	-100.6 ± 6.96	38.43 ± 9.53	20.02 ± 8.17	19.61	18.50	17.71	17.02	16.49	15.33
O-(C_d)(H)	-188.07 ± 3.56	106.30 ± 4.87	24.60 ± 4.18	30.30	32.52	33.15	33.29	33.55	34.97
CO-(C)(C_d)	-130.44 ± 4.17	47.38 ± 5.71	25.26 ± 4.90	30.66	34.68	37.69	41.62	43.93	46.69
CO-(O)(C_d)	-218.60 ± 6.36	33.44 ± 8.70	28.33 ± 7.46	37.84	44.54	49.34	55.45	58.73	60.61
CO-(C_d)(H)	-128.34 ± 5.90	129.26 ± 5.71	27.31 ± 4.90	34.00	39.42	43.77	50.16	54.55	60.77
unsaturated ketenes									
C-(C)$_2$(C_d)(CCO) (b)	2.86 ± 5.90	-144.60 ± 8.08	25.48 ± 6.93	31.89	35.19	36.68	37.19	36.66	34.96
C-(C)(C_d)(CCO)(H) (b)	-10.44 ± 5.90	-54.03 ± 8.08	24.45 ± 6.93	31.59	36.01	38.80	42.13	44.21	47.25
C-(C_d)$_2$(CCO)(H) (b)	-6.83 ± 5.90	-55.37 ± 8.08	27.62 ± 6.93	35.40	39.24	41.25	43.40	44.87	47.43
C-(C_d)(CCO)(H)$_2$ (b)	-22.24 ± 5.90	37.92 ± 8.08	25.85 ± 6.93	31.99	37.06	41.14	47.42	52.15	59.73
C_d-(C)(CCO) (b)	41.57 ± 6.82	-48.01 ± 9.33	22.68 ± 8.00	24.05	24.63	25.07	25.64	25.84	25.70
CCO-(C_d)(H) (b)	-35.99 ± 4.82	152.19 ± 6.60	43.67 ± 5.66	52.95	59.65	64.67	71.81	76.72	83.92

[a] 97.5 % confidence intervals for $\Delta_f H°$ and $S°$ at 298 K, and for $C_p°$ at 300 K are provided. The GAVs reported without confidence intervals were set equal to GAVs taken from previous work (see Table S1 of Appendix A).
[b] The GAV is derived from a single molecular structure.
[c] The GAV is set equal to GAV O-(C)(H) in order to avoid linear dependence of GAVs.

Table 2-5: Corrections for non-nearest-neighbor-interactions (NNIs) for the standard enthalpies of formation ($\Delta_f H°$) and entropies ($S°$) at 298 K, and heat capacities ($C_p°$) at various temperatures for oxygenate molecules.[a]

Inter. no.	Interaction	Occ.[b]	$\Delta_f H°$ [kJ mol^{-1}]	$S°$ [J mol^{-1} K^{-1}]	$C_p°$ [J mol^{-1} K^{-1}] 300 K	400 K	500 K	600 K	800 K	1000 K	1500 K
NNI1	Hbr_H-O-CO-CO	8	-6.60 ± 2.54	-10.30 ± 3.48	-1.85 ± 2.98	-0.09	0.72	0.76	0.27	0.46	2.90
NNI2	Hbr_H-O-CO-CO-CO (c)	1	4.50 ± 5.52	-31.85 ± 7.56	-6.30 ± 6.48	-1.41	2.46	5.13	7.47	7.84	8.05
NNI3	Hbr_H-O-CO-C-CO	3	-3.18 ± 3.67	-27.16 ± 5.02	-3.93 ± 4.30	-0.99	1.44	3.32	5.50	6.18	5.44
NNI4	Hbr_H-O-CO-C-O (c)	1	-1.06 ± 5.42	-14.92 ± 7.42	-1.41 ± 6.36	-1.19	-1.64	-1.73	-0.67	0.80	2.89
NNI5	Hbr_H-O-C-C-O	2	1.90 ± 4.96	-23.49 ± 6.80	-0.75 ± 5.82	8.30	14.25	16.25	14.31	10.72	4.95
NNI6	Hbr_H-O-C-C-C-O	2	-0.05 ± 4.96	-32.03 ± 6.80	-3.65 ± 5.82	5.72	13.28	17.49	18.57	15.79	8.98
NNI7	Hbr_H-O-C-C-C-C-O	2	-4.75 ± 4.96	-48.69 ± 6.80	-12.77 ± 5.82	-0.68	11.16	20.15	27.92	26.99	16.93
NNI8	Hbr_H-O-C-CO	10	-13.77 ± 2.42	-17.34 ± 3.32	1.97 ± 2.84	5.01	6.56	7.54	8.28	7.84	5.52
NNI9	Hbr_H-CO-O-CO	2	-5.88 ± 6.11	-26.91 ± 8.36	5.26 ± 7.17	9.86	12.00	12.75	12.91	12.62	10.77
NNI10	Hbr_H-C-O-CO	3	0.70 ± 4.08	11.18 ± 5.58	-4.98 ± 4.79	-4.72	-3.87	-2.75	-0.68	0.49	0.94
NNI11	gauche_C-C-O-CO	4	-3.50 ± 3.75	-10.29 ± 5.13	9.27 ± 4.40	8.99	8.06	7.09	5.52	4.62	3.7
NNI12	C-C-O-H	2	6.15 ± 3.92	0.70 ± 5.37	-4.44 ± 4.60	-3.69	-2.5	-1.54	-0.52	-0.22	-0.27
NNI13	cis_C-C=C-O (c)	1	5.12 ± 6.08	-5.10 ± 8.32	0.10 ± 7.13	-0.42	-1.85	-3.02	-3.72	-3.26	-1.76
NNI14	cis_C-C=C(O)-OH	2	12.59 ± 4.42	16.18 ± 6.05	-11.43 ± 5.19	-12.31	-11.36	-9.93	-7.16	-5.1	-2.43

[a] 97.5 % confidence intervals for $\Delta_f H°$ and $S°$ at 298 K, and for $C_p°$ at 300 K are provided.
[b] The number of occurrences of the NNI in the whole training set is indicated.
(c) NNI correction is derived from a single molecular structure.

The majority of hydrogen bonds have negative entropy and heat capacity values, at least at low temperatures. A negative entropy corresponds to a decrease in the internal flexibility of a molecule in which these interactions are present due to a stronger preference for the rotamer in which the hydrogen bond is present.

The results for the hydrogen bonds H-O-C-C-O (NNI5), H-O-C-C-C-O (NNI6) and H-O-C-C-C-C-O (NNI7) could be modeled on one NNI that is dependent only on the number of carbon atoms that participate in the hydrogen bond. Figure 2-3 shows the temperature dependence of the heat capacities of the above-mentioned hydrogen bonds, and suggests that the number of parameters of the group additive model could be reduced. However, in this work these three hydrogen bonds are considered as three different NNIs.

Gauche interactions: Gauche interactions usually have destabilizing effects, which result in positive contributions to the standard enthalpy of formation and restrict the internal flexibility in a molecule, resulting in a decrease in entropy and heat capacity. Gauche interactions in oxygenates need dedicated attention because the anomeric effect can cause an electronegative substituent to assume an axial rather than an equatorial conformation, which is the opposite of what one would expect from repulsive gauche interactions. In the current database of oxygenate compounds the anomeric effect can be detected in only three compounds but was found not to make a significant contribution and the only oxygenate-specific gauche interaction that is retained in this work is the interaction C-C-O-CO shown in Figure 2-4. In this gauche interaction the bond along the C and CO is a carbon-carbonyl interaction, which, according to the results, has a stabilizing effect on the molecules in which it is present.

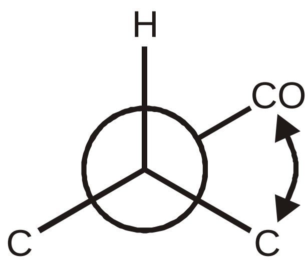

Figure 2-4: Gauche interaction C-C-O-CO (NNI11).

Other interactions: Three other types of interactions due to the orientation of functional groups within the molecule are present in this work. Two of them are *cis* interactions and correspond to unsaturated oxygenates and, more specifically to vinyl alcohols. The structures of these interactions, along with their corresponding Newman projections, are shown in Figure 2-5.

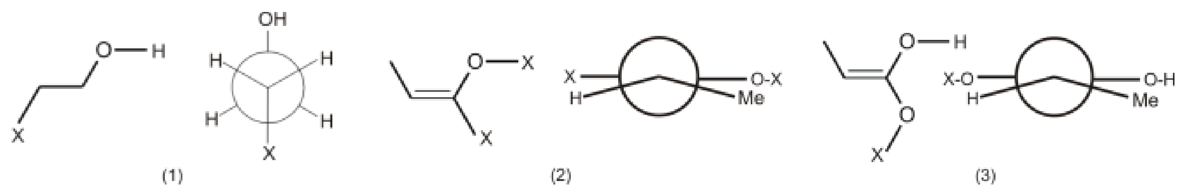

Figure 2-5: Interactions related to structures (1) C-C-O-H, (2) the *cis* interaction in *cis*-C-C=C-O, and (3) the *cis* interaction in *cis*-C-C=C(O)-OH along with their corresponding Newman projections. X represents a generalized substituent.

The first interaction involves small linear alcohols such as ethanol and 1-propanol in which the hydroxy group is at the end of the molecule and appears to have a destabilizing effect. The last two interactions are *cis*-destabilizing interactions that are present in vinyl alcohols. *cis*-C-C=C-O (NNI13) describes the interaction between a methyl and an oxygen-containing group in a *cis* relative disposition, whereas *cis*-C-C=C(O)-OH (NNI14) describes the interaction between a hydroxy group and a methyl group, also in a *cis* relative disposition, in which the C_d atom that has the hydroxy group attached also bears another oxygen ligand. The presence of the second oxygen ligand differentiates this *cis* interaction NNI14 from the *cis* interaction NNI13, assigning larger absolute values for all the thermodynamic properties for a particular NNI correction.

Comparison of reported GAVs with the corresponding values from the literature: The group additivity values along with the values of the NNI corrections obtained in this work were compared with the corresponding values presented in the compilation of thermochemical data provided by Poling et al. [5]. The results of this comparison, for all groups in common, are provided in Table S10 in Appendix A.

The majority of GAVs obtained in this work are similar to the values obtained from experimental sources by Poling et al. [5]. By excluding the GAVs that deviate significantly, the MAD between the corresponding GAVs is 4.4 kJ mol^{-1} for standard enthalpies of formation, 4.1 $Jmol^{-1}$ K^{-1} for the entropies and less than 3.5 J mol^{-1} K^{-1} for the heat capacities above 500 K, which is acceptable bearing in mind that different GAVs have been used for hydrocarbons, which influence all other values.

A direct comparison with the GAVs of Khan and Broadbelt obtained from ab initio calculations [10] is not straightforward because different assumptions were made to avoid the linear dependencies. The results of this comparison for all GAVs in common are provided in Table S11 in Appendix A, and the MAD, after excluding the GAVs that deviate significantly, is 4.7 kJ mol^{-1} for the standard enthalpies of formation, 7.8 J mol^{-1} K^{-1} for the entropies and less than 6 J mol^{-1} K^{-1} for the heat capacities. The GAVs that appear to have larger deviations, may be arise from the arbitrary fixing of values of certain groups to avoid linear dependencies in the model because fixing the contributions of certain groups affects the GAVs of other groups. For example, the GAVs for C-(O)$(H)_3$, C-(CO)$(H)_3$ and C-(CCO)$(H)_3$ were set equal to the GAV for C-(C)$(H)_3$, which was taken from the work of Sabbe and co-workers for hydrocarbons and hydrocarbon radicals [7, 8].

Comparison between the group additive predictions based on values provided by Poling et al. [5] and experimental values taken from the NIST web-book [14], and group additive predictions based on values from this work and the corresponding experimental values taken from the NIST web-book are provided in Table 2-6. Because in the work of Khan and Broadbelt [10] there are no GAVs for the structures for which experimental data are available, comparisons between GA prediction based on values provided by Khan and Broadbelt and ab initio values, and GA predictions based on values from this work and the corresponding ab initio values is provided in Table 2-7.

Table 2-6: Deviations between the group additive predictions based on the GAVs of Poling (GA) and experimental values (EXP)[14] and the GA predictions based on the GAVs from this work and experimental values for the standard enthalpies of formation ($\Delta_f H°$) and entropies ($S°$) at 298 K and heat capacities ($C_p°$) at 400 and 500 K for oxygenate molecules.

	Deviations (GA−EXP) using GAVs of Poling				Deviations (GA−EXP) using GAVs from this work			
MOLECULES	$\Delta_f H°$ [kJ mol^{-1}]	$S°$ [J mol^{-1} K^{-1}]	$C_p°$ [J mol^{-1} K^{-1}] 400 K	$C_p°$ [J mol^{-1} K^{-1}] 500 K	$\Delta_f H°$ [kJ mol^{-1}]	$S°$ [J mol^{-1} K^{-1}]	$C_p°$ [J mol^{-1} K^{-1}] 400 K	$C_p°$ [J mol^{-1} K^{-1}] 500 K
Methylpropyl ether	1.6	19.6			-0.3	0.6		
1,2-dimethoxy-ethane	-5.0				-8.9			
1,5-Pentanediol	2.6				0.7			
2-methyl-1-Butanol	-3.7				-4.6			
3-Hexanone	-2.3	-13.4	1.3	0.2	-0.7	-1.5	-0.5	-2.7
Methylisobutylketone	1.6		1.1		1.9		-0.3	
4,4-dimethyl-2-Pentanone	-1.2				-0.9			
Butanal	0.0	8.7			-1.3	-1.2		
Heptanal	-4.5	11.9			-5.8	2.0		
Pentanoic acid, methyl ester	-79.0				-0.4			
Carbonic acid, diethyl ester	-153.4				2.2			
Ethanol, 2-methoxy-, acetate	-80.5				-4.6			
4-Pentenoic acid, ethylester	-72.3				5.8			
Butanoic acid	-74.4	0.1			3.8	4.6		
1-methoxy-butane		21.4				2.5		
1-Hexadecanol		-3.7				-2.8		
Pentanal		13.5				3.7		
n-Propyl acetate			4.8				2.1	

Table 2-7: Deviations between the group additive prediction based on the GAVs of Khan and Broadbelt and ab initio values, and GA prediction based on the GAVs from this work and ab initio values for the standard enthalpies of formation ($\Delta_f H°$) and entropies ($S°$) at 298 K and heat capacities ($C_p°$) at different temperatures for oxygenate molecules.

	Deviation between the GA predictions and ab initio values					
	GAVs from Broadbelt					
MOLECULES	$\Delta_f H°$ [kJ mol^{-1}]	$S°$ [J mol^{-1} K^{-1}]	$C_p°$ [J mol^{-1} K^{-1}] 300 K	600 K	1000 K	1500 K
2-methoxy-2-methylpropanoic acid	-9.6	3.5	8	10.8	6.3	1.3
2-hydroxy-2-methylbutanal	7.3	15.1	0.1	-3.5	-4.3	-2.3
prop-1-en-2-yl-22-dimethylpropanoate	5.8	-3.5	6.5	8.5	3.4	0.9
2-methylpentan-3-one	-2.6	2.8	-0.3	2.4	2.9	2.7
	GAVs from this work					
MOLECULES	$\Delta_f H°$ [kJ mol^{-1}]	$S°$ [J mol^{-1} K^{-1}]	$C_p°$ [J mol^{-1} K^{-1}] 300 K	600 K	1000 K	300 K
2-methoxy-2-methylpropanoic acid	-2.3	-3.3	3.9	0.4	-1.1	-1.8
2-hydroxy-2-methylbutanal	1.8	5.8	-0.6	-4.6	-4.6	-2.9
prop-1-en-2-yl-22-dimethylpropanoate	1.4	1.2	0.1	2.2	1	-1.2
2-methylpentan-3-one	-1.1	4.9	-1.5	-1.5	-0.5	0

Based on the results from the comparison in Table 2-6, it can be concluded that the GA model developed in this work can provide an accurate prediction of thermodynamic values, and in most cases better than the prediction based on the GAVs derived from Poling et al. [5]. Large deviations of approximately −80 kJ mol^{-1} in $\Delta_f H°$ at 298 K are observed for all esters and acids and are due to the large deviations in GAVs for O-(C)(CO) and O-(CO)(H) between the work of Poling et al. [5] and our work.

Based on the results from the comparison in Table 2-7, it can be concluded that the GA model developed in this work can provide an accurate prediction of thermodynamic values and in all selected cases better than the predictions based on the GAVs from Khan and Broadbelt [10]. Because the model developed by Khan and Broadbelt extends to multisubstituted oxygenate compounds and the reported GAVs for oxygenate molecules are limited in all the above molecules, when a group value was not available from the work of Khan and Broadbelt, the corresponding value from this work was used.

2.4.2 Oxygenate Radicals

The thermochemistry of oxygenate radicals included in this work can be described by using 97 groups in addition to the nonradical groups mentioned in the previous section. For 40 out of these 97 groups, values have been recently reported by Khan and Broadbelt [10]. These 97 groups can be divided into 28 radical-centered groups and 69 radical-adjacent groups. Radical adjacent groups can be defined as groups in which the radical is one of the ligands of the central atom according to Benson's GA method, thus this ligand can be a carbon or an oxygen atom, a carbonyl or a ketene group. The estimation of these 97 GAVs and 12 NNI corrections, and the assessment of the accuracy of the group additivity method was achieved by using a training set consisting of 248 radicals of oxygenates (see Table S7 in Appendix A).

The radicals included in the particular training set were selected by taking into account the fact that the prediction of the thermochemical data of resonance-stabilized radicals by Benson's group additivity method is problematic. The enthalpy of formation can be determined unambiguously by the group additivity method only for molecules in which the ligands of the radical-centered group include information about all unsaturated bonds that are involved in electron delocalization. This is, for example, the case for radicals of dialdehydes as illustrated in Figure 2-6.

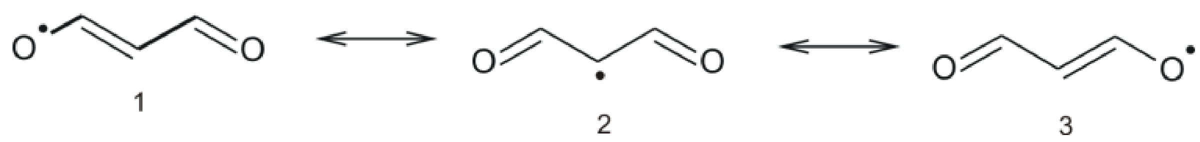

Figure 2-6: Resonance stabilization in radicals of dialdehydes.

The standard enthalpy of formation of the canonical structure 2 containing the O=C-C$^{\bullet}$-C=O sequence can be determined accurately because the radical-centered group C$^{\bullet}$-(CO)$_2$(X), in which X can be a hydrogen atom or a carbon chain, provides information about all possible delocalization. There is no such a group present in the other canonical structures. To prevent a misestimation of the C$_d$-(O$^{\bullet}$)(H) GAV present in the canonical structures 1 and 3, only canonical structures in which the radical-centered group includes information about all unsaturated bonds involved in electron delocalization are retained in this database.

The NNI corrections introduced were estimated simultaneously with GAVs used to describe the radicals. The GAVs are calculated within 97.5 % Confidence Intervals (CIs). Because there are 26 GAVs and 2 NNI corrections derived from a single radical structure, the statistics on the regression are slightly biased because these parameters are formally calculated from the CBS-QB3 values and not determined by regression. To lift this bias, the parameters reporting the quality of the regression were determined by neglecting the GAVs or NNI corrections derived from a single radical and radicals from which a single GAV or NNI correction is determined, similarly to the approach for molecules. The reported significance of the regression (*F*), MAD, RMS and MAX correspond to the differences between the thermochemical data predicted by the group additivity method and the values calculated using ab initio calculations.

GAVs for oxygenate radicals: The group additive model introduced for radicals has a MAD of less than 1.6 kJ mol^{-1} for the standard enthalpies of formation at 298 K, 2.0 J mol^{-1} K^{-1} for the entropies at 298 K and less than 1.5 J mol^{-1} K^{-1} for heat capacities at the studied temperatures. The statistics for the regression estimates along with the confidence intervals for enthalpies and entropies at 298 K and heat capacities at 300 K are presented in Table 2-8. The details of the residual differences between the group additive predictions and the ab initio calculated values for every molecule in the training set are provided in Table S12 in Appendix A. Table 2-9 lists the GAVs obtained after regression for all of the unknown groups along with 97.5% confidence intervals (CIs) for enthalpies and entropies at 298 K and heat capacities at 300 K.

Table 2-8: Statistics for the regression of the GAVs and NNIs in oxygenate radicals for the standard enthalpies of formation ($\Delta_f H°$) and entropies ($S°$) at 298 K and heat capacities ($C_p°$) at various temperatures.[a]

	$\Delta_f H°$	$S°$	$C_p°$ [J mol^{-1} K^{-1}]						
	[kJ mol^{-1}]	[J mol^{-1} K^{-1}]	300 K	400 K	500 K	600 K	800 K	1000 K	1500 K
F	3486	3163	907	1611	2349	3045	4257	5658	10440
MAD	1.51	1.98	1.44	1.27	1.14	1.04	0.93	0.84	0.64
RMS	1.99	2.68	1.80	1.62	1.50	1.42	1.31	1.19	0.92
MAX	6.18	9.73	6.12	4.93	5.11	5.22	5.14	4.88	3.34

[a] *F*:Significance; MAD: mean absolute deviation; RMS: root mean square deviation; MAX: maximum deviation

NNIs for oxygenate radicals: For all radicals included in the training set of oxygenate radicals, possible non-nearest neighbor interactions (NNIs) were identified and the GAVs and NNIs were determined simultaneously by unweighed least-squares analysis, minimizing the objective function (2-1). NNIs that have all their calculated thermodynamic properties ($\Delta_f H°$, $S°$ and $C_p°$) less than a threshold of 5 kJ mol^{-1} for $\Delta_f H°$ and 5 J mol^{-1}K^{-1} for $S°$ and $C_p°$ were omitted and a new regression followed until all NNIs had at least one thermodynamic parameter greater than 5 kJ mol^{-1} for $\Delta_f H°$ and 5 J mol^{-1}K^{-1} for $S°$ and $C_p°$. From the initial 32 possible radical gauche interactions and 26 possible radical hydrogen bonds identified, amounting to 58 NNIs in total, only 12 of them were finally retained and these are presented in Table 2-10 along with the confidence intervals for the enthalpies and entropies at 298 K and heat capacities at 300 K.

The NNIs introduced in this work for oxygen-containing radicals can be divided into three main categories: Hydrogen bonds, gauche interactions and other types of interactions present in particular radicals.

Hydrogen bonds: Eight different types of hydrogen bonds are introduced in this work (see Figure 2-7). The X ligands can be either hydrogen atoms or a carbon chain.

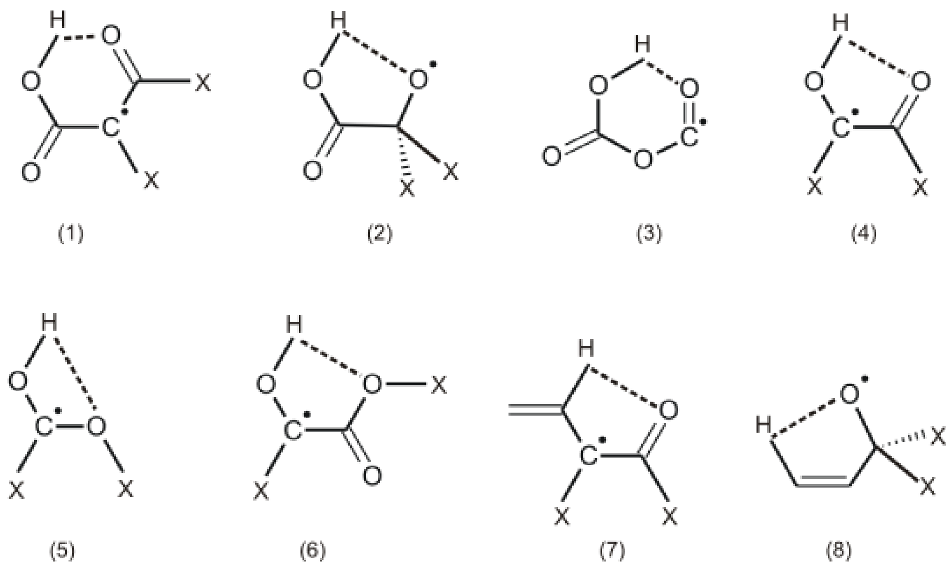

Figure 2-7: 3D structures of the hydrogen bonds introduced as NNIs (1) Hbr_H-O-CO-C$^{\bullet}$-CO, (2) Hbr_ H-O-CO-C-O$^{\bullet}$, (3) Hbr_ H-O-CO-O-CO$^{\bullet}$, (4) Hbr_ H-O-C$^{\bullet}$-CO, (5) Hbr_ H-O-C$^{\bullet}$-O, (6) Hbr_ H-O-C$^{\bullet}$-CO-O, (7) Hbr_ H-C$_d$-C$^{\bullet}$-CO and (8) Hbr_ H-C$_d$-C$_d$-C-O$^{\bullet}$. X represents a generalized substituent.

A hydrogen bond is a stabilizing interaction, but, similar to NNI corrections in oxygenate molecules, five out of the eight NNI corrections for hydrogen bonds have positive values for standard enthalpies of formation. From the database of radicals it can be concluded that NNIs for hydrogen bonds with positive corrections for the enthalpy of formation appear mainly in radicals with at least two functional groups. In all circumstances there was the tendency to create two hydrogen bonds in the same radical, one between the first functional group and a neighbouring hydrogen atom, and a second one between the second functional group and a neighbouring hydrogen atom. This will be clarified by the following example.

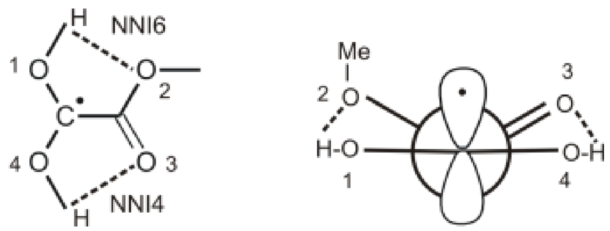

Figure 2-8: Structure of the methyloxycarbonyl(dihydroxy)methyl radical and its corresponding Newman projection.

The structure of the methyloxycarbonyl(dihydroxy)methyl radical is shown in Figure 2-8 along with its corresponding Newman projection. There are two hydrogen bonds present in this structure: H-O-C$^{\bullet}$-CO-O (NNI6) and H-O-C$^{\bullet}$-CO (NNI4). The hydrogen bond H-O-C$^{\bullet}$-CO (NNI4) has a negative correction on the standard enthalpy of formation, whereas the H-O-C$^{\bullet}$-CO-O hydrogen bond (NNI6) has a positive correction, that is, almost the same value as the former but with opposite sign. The same is also true for the other hydrogen bonds that have a positive correction for the standard enthalpy of formation. Both of the interactions are stabilizing, but the C$^{\bullet}$-(CO)(O)$_2$ group already implicitly involves a certain amount of hydrogen bonding: The hydrogen atoms attached to the oxygen atoms 1 and 4 can potentially form hydrogen bonds with the O atoms 4 and 1, respectively. Hence, the absence of these interactions has a positive enthalpy contribution, and the NNI6 H-O-C$^{\bullet}$-CO-O is positive to compensate for the lack of these two H bonds. However, two hydrogen bonds are created between the hydrogen atoms on the oxygen atoms 1 and 4 and the oxygen atoms 2 and 3, respectively. The NNI6 H-O-C$^{\bullet}$-CO-O is positive because it is only present in two radicals, whereas NNI14 is present in 21 radicals (see Table 2-10) and it therefore remains negative.

Similarly, the other hydrogen bonds that have positive values are usually present only in one, two or three radicals, but these are in most cases only present together with one of the other NNI corrections for hydrogen bonds.

Table 2-9: GAVs for the standard enthalpies of formation ($\Delta_f H°$) and entropies ($S°$) at 298 K, and heat capacities ($C_p°$) at various temperatures for oxygenate radicals.[a]

group	$\Delta_f H°$ [kJ mol^{-1}]	$S°$ [J mol^{-1} K^{-1}]	$C_p°$ [J mol^{-1} K^{-1}] 300 K	400 K	500 K	600 K	800 K	1000 K	1500 K
carbon-centered radicals									
C$^{\bullet}$-(C)$_2$(O)	155.16 ± 2.34	-39.23 ± 3.15	19.52 ± 2.12	21.73	23.91	25.6	27.45	27.99	27.5
C$^{\bullet}$-(C)$_2$(CO)	135.45 ± 2.79	-46.75 ± 3.76	14.56 ± 2.53	17.15	19.66	21.71	24.53	26.43	29.41
C$^{\bullet}$-(C)$_2$(CCO) (b)	132.75 ± 5.04	-44.13 ± 6.78	14.20 ± 4.56	17.53	20.49	22.93	26.24	28.14	30.01
C$^{\bullet}$-(C$_d$)$_2$(O) (b)	50.94 ± 5.04	-73.75 ± 6.78	21.49 ± 4.56	33.96	40.23	42.88	43.61	42.44	38.66
C$^{\bullet}$-(C$_d$)$_2$(CO)	78.16 ± 3.91	-81.87 ± 5.27	16.87 ± 3.54	24.89	29.53	32.09	34.37	35.51	38.04
C$^{\bullet}$-(C)(C$_d$)(O)	86.33 ± 3.56	-57.31 ± 4.79	25.39 ± 3.22	30.92	33.87	35.35	36.2	35.98	34.54
C$^{\bullet}$-(C)(C$_d$)(CO)	104.76 ± 2.79	-66.34 ± 3.76	15.79 ± 2.53	21.15	24.72	27.01	29.56	31.06	33.55
C$^{\bullet}$-(C)(C$_d$)(CCO) (b)	84.96 ± 5.04	-53.60 ± 6.78	17.65 ± 4.56	23.44	27.11	29.45	32.00	33.23	34.39
C$^{\bullet}$-(C$_d$)$_2$(CCO) (b)	62.27 ± 5.04	-82.90 ± 6.78	16.94 ± 4.56	26.08	31.17	34.02	36.63	37.68	38.61
C$^{\bullet}$-(C)(O)$_2$	120.38 ± 6.70	-50.23 ± 9.02	25.67 ± 6.07	30.78	33.92	35.16	34.78	33.35	30.35
C$^{\bullet}$-(C)(O)(CO)	104.46 ± 5.69	-52.70 ± 7.66	22.32 ± 5.15	25.83	28.30	29.66	30.63	30.96	31.64
C$^{\bullet}$-(C)(O)(H)	149.09 ± 3.05	40.56 ± 4.11	23.75 ± 2.76	29.14	33.07	35.69	38.76	40.53	42.76
C$^{\bullet}$-(C)(CO)(H)	134.59 ± 2.44	39.10 ± 3.28	22.17 ± 2.20	26.56	30.26	33.13	37.23	40.10	44.27
C$^{\bullet}$-(C)(CCO)(H)	128.25 ± 4.36	46.75 ± 5.87	20.95 ± 3.95	25.43	29.04	31.94	36.20	39.13	42.98
C$^{\bullet}$-(C$_d$)(O)$_2$	64.16 ± 6.70	-72.83 ± 9.02	30.75 ± 6.07	39.12	41.99	42.23	40.43	38.41	35.02
C$^{\bullet}$-(C$_d$)(O)(CO)	70.00 ± 5.69	-71.72 ± 7.66	26.65 ± 5.15	34.49	38.51	40.12	40.55	40.02	38.00
C$^{\bullet}$-(C$_d$)(O)(H)	89.65 ± 3.76	25.41 ± 5.06	22.35 ± 3.40	31.83	38.05	41.74	45.15	46.48	47.8
C$^{\bullet}$-(C$_d$)(CO)(H)	89.77 ± 3.10	22.04 ± 4.17	25.87 ± 2.81	32.67	37.04	39.85	43.39	45.86	49.62
C$^{\bullet}$-(C$_d$)(CCO)(H) (b)	77.76 ± 5.04	15.88 ± 6.78	20.38 ± 4.56	28.22	33.39	36.87	41.26	44.07	48.23
C$^{\bullet}$-(O)$_3$	83.12 ± 10.54	-51.50 ± 14.18	26.01 ± 9.54	31.07	33.94	34.98	34.75	33.59	30.85
C$^{\bullet}$-(O)$_2$(CO)	62.34 ± 7.71	-73.41 ± 10.37	24.21 ± 6.97	33.01	38.52	41.09	41.64	40.35	37.91
C$^{\bullet}$-(O)(CO)$_2$	102.56 ± 6.01	-73.51 ± 8.09	24.48 ± 5.44	29.10	32.19	33.75	34.54	34.48	35.58
C$^{\bullet}$-(O)$_2$(H)	125.07 ± 5.86	33.78 ± 7.88	28.53 ± 5.30	34.84	38.5	40.37	41.95	42.62	43.44
C$^{\bullet}$-(CO)$_2$(H)	137.10 ± 2.92	23.00 ± 3.93	26.42 ± 2.64	31.95	36.49	39.8	44.01	46.56	49.49
C$^{\bullet}$-(O)(CO)(H)	112.79 ± 3.94	29.33 ± 5.30	25.96 ± 3.56	32.08	36.61	39.55	42.75	44.33	46.24
C$^{\bullet}$-(O)(H)$_2$	147.15 ± 3.05	126.15 ± 4.11	27.47 ± 2.76	33.14	37.78	41.39	46.67	50.45	56.24
C$^{\bullet}$-(CO)(H)$_2$	136.53 ± 2.44	123.82 ± 3.28	26.91 ± 2.20	32.39	36.69	40.14	45.63	50.02	57.28
C$^{\bullet}$-(CCO)(H)$_2$	116.85 ± 4.36	122.13 ± 5.87	27.37 ± 3.95	33.6	38.13	41.57	46.78	50.8	57.44
unsaturated carbon-centered radicals									
C$_d^{\bullet}$-(O)	275.75 ± 5.04	53.38 ± 6.78	14.33 ± 4.56	12.36	12.60	13.76	16.25	18.02	20.31
C$_d^{\bullet}$ -(CO)	271.22 ± 5.04	43.59 ± 6.78	20.66 ± 4.56	20.93	21.20	21.48	22.02	22.40	22.83
carbon radicals adjacent to carbon-centered group									
C-(C)$_2$(C$^{\bullet}$)(O)	-18.85 ± 3.06	-149.06 ± 4.12	28.70 ± 2.77	35.09	38.15	39.30	39.10	37.96	35.30
C-(C)$_2$(C$^{\bullet}$)(CO)	5.14 ± 2.52	-144.98 ± 3.39	31.12 ± 2.28	34.25	35.35	35.47	34.66	33.74	32.81
C-(C)$_2$(C$^{\bullet}$)(CCO) (b)	-2.05 ± 5.04	-145.43 ± 6.78	27.51 ± 4.56	32.03	34.58	35.88	36.54	36.24	35.06
C-(C$^{\bullet}$)(C)(C$_d$)(O)	-12.34 ± 3.06	-153.98 ± 4.12	30.27 ± 2.77	37.69	40.74	41.45	40.34	38.61	35.47
C-(C$^{\bullet}$)(C)(C$_d$)(CO)	11.53 ± 2.52	-148.81 ± 3.39	31.34 ± 2.28	34.94	36.12	36.12	34.95	33.75	32.63
C-(C$^{\bullet}$)(C)(C$_d$)(CCO) (b)	2.16 ± 5.04	-148.26 ± 6.78	31.32 ± 4.56	36.01	37.61	37.94	37.33	36.43	34.78

C-(C)(C$^\bullet$)(O)2	-62.79 ± 2.91	-167.57 ± 3.91	32.81 ± 2.63	46.47	53.23	54.99	52.00	47.3	39.46
C-(C)(C$^\bullet$)(CO)2	13.05 ± 2.91	-149.76 ± 3.91	39.01 ± 2.63	40.17	39.54	38.40	36.17	34.52	32.67
C-(C)(C$^\bullet$)(CO)(O)	-11.04 ± 3.14	-156.02 ± 4.23	37.01 ± 2.84	44.26	46.68	46.30	43.00	39.81	35.56
C-(C)(C$^\bullet$)(O)(H)	-25.03 ± 2.91	-56.64 ± 3.91	31.46 ± 2.63	36.60	39.92	42.07	44.62	46.15	48.26
C-(C)(C$^\bullet$)(CO)(H)	-4.83 ± 2.52	-50.62 ± 3.39	29.81 ± 2.28	32.30	34.6	36.55	39.58	41.8	45.56
C-(C)(C$^\bullet$)(CCO)(H) [b]	-9.35 ± 5.04	-49.22 ± 6.78	25.79 ± 4.56	30.20	33.84	36.64	40.53	43.12	46.90
C-(C$^\bullet$)(C$_d$)(O)$_2$	-59.88 ± 2.91	-175.64 ± 3.91	31.43 ± 2.63	46.96	55.71	59.16	57.80	53.00	43.30
C-(C$^\bullet$)(C$_d$)(CO)$_2$	19.06 ± 2.91	-161.92 ± 3.91	44.76 ± 2.63	48.28	47.98	46.26	42.30	39.15	35.11
C-(C$^\bullet$)(C$_d$)(CO)(O)	-1.77 ± 2.27	-159.87 ± 3.05	39.35 ± 2.05	46.85	49.21	48.7	44.94	41.16	35.77
C-(C$^\bullet$)(O)(H)$_2$	-29.08 ± 1.78	38.21 ± 2.40	23.86 ± 1.61	31.47	37.48	42.05	48.57	53.14	60.10
C-(C$^\bullet$)(CO)(H)$_2$	-20.52 ± 2.52	34.29 ± 3.39	27.04 ± 2.28	31.42	35.82	39.7	46.02	50.88	58.96
C-(C$^\bullet$)(CCO)(H)$_2$	-23.12 ± 2.52	43.11 ± 3.39	22.39 ± 2.28	28.78	34.41	39.07	46.20	51.37	59.3
carbon radicals adjacent to unsaturated carbon-centered group									
C$_d$-(C$^\bullet$)(O)	41.89 ± 2.91	-45.61 ± 3.91	15.00 ± 2.63	16.75	18.92	20.93	23.64	25.10	27.04
C$_d$-(C$^\bullet$)(CO)	45.05 ± 2.52	-58.57 ± 3.39	17.47 ± 2.28	18.86	20.02	21.12	23.04	24.44	26.44
C$_d$-(C$^\bullet$)(CCO) [b]	48.57 ± 5.04	-46.90 ± 6.78	20.36 ± 4.56	21.64	22.71	23.76	25.48	26.62	28.05
carbon radicals adjacent to oxygen-centered group									
O-(C)(C$^\bullet$)	-99.36 ± 2.43	42.20 ± 3.27	14.87 ± 2.20	13.32	12.88	13.23	14.62	15.99	18.28
O-(C$^\bullet$)(C$_d$)	-119.21 ± 4.41	31.68 ± 5.94	13.74 ± 3.99	16.97	18.84	19.77	20.19	20.08	20.00
O-(C$^\bullet$)(CO)	-91.27 ± 3.20	47.93 ± 4.31	15.94 ± 2.90	14.61	14.28	14.41	14.88	15.30	16.28
O-(C$^\bullet$)(H) [c]	-165.22 ± 2.16	125.32 ± 2.96	19.07 ± 2.54	19.80	20.85	22.07	24.57	26.95	31.66
O-(C$_d^\bullet$)(H) [c]	-188.07 ± 3.56	106.30 ± 4.87	24.60 ± 4.18	30.30	32.52	33.15	33.29	33.55	34.97
carbon radicals adjacent to carbonyl-centered group									
CO-(C)(C$^\bullet$)	-122.60 ± 2.59	61.22 ± 3.48	22.86 ± 2.34	27.37	31.13	34.21	38.45	40.84	43.04
CO-(C$^\bullet$)(O)	-205.75 ± 1.62	40.93 ± 2.18	23.81 ± 1.47	31.34	37.29	42.01	48.47	51.79	52.59
CO-(C$^\bullet$)(CO)	-123.74 ± 2.77	49.23 ± 3.73	25.42 ± 2.51	31.40	36.06	39.55	43.81	45.83	47.15
CO-(C$^\bullet$)(H) [c]	-123.42 ± 1.77	145.46 ± 2.42	26.24 ± 2.08	31.22	35.94	40.13	46.74	51.39	57.73
CO-(C$_d^\bullet$)(H) [c]	-128.34 ± 5.90	129.26 ± 5.71	27.31 ± 4.90	34.00	39.42	43.77	50.16	54.55	60.77
carbon radicals adjacent to ketene-centered group									
CCO-(C)(C$^\bullet$)	-1.55 ± 5.04	86.07 ± 6.78	40.39 ± 4.56	44.31	48.23	51.78	57.24	60.89	65.70
CCO-(C$^\bullet$)(H) [c]	-17.65 ± 3.41	169.15 ± 4.67	43.83 ± 4.00	50.10	55.50	60.05	67.09	72.13	79.55
CCO-(C$_d^\bullet$)(H) [c]	-35.99 ± 4.82	152.19 ± 6.60	43.67 ± 5.66	52.95	59.65	64.67	71.81	76.72	83.92
unsaturated carbon radicals adjacent to oxygen- or carbonyl-centered group									
O-(C)(C$_d^\bullet$)	-123.91 ± 6.17	29.08 ± 8.30	15.59 ± 5.58	18.82	20.17	20.60	20.69	20.69	20.75
CO-(C$_d^\bullet$)(O)	-204.45 ± 6.17	32.70 ± 8.30	25.04 ± 5.58	34.88	42.15	47.35	53.29	55.42	54.78
carbonyl radicals adjacent to carbon-centered group									
C-(C)$_3$(CO$^\bullet$) [b]	36.40 ± 5.04	12.08 ± 6.78	46.18 ± 4.56	53.72	58.65	62.02	66.03	68.16	70.33
C-(C)$_2$(C$_d$)(CO$^\bullet$) [b]	40.21 ± 5.04	9.36 ± 6.78	50.75 ± 4.56	57.17	61.46	64.34	67.62	69.27	70.88
C-(C)$_2$(CO)(CO$^\bullet$)	48.67 ± 3.56	9.22 ± 4.79	56.21 ± 3.22	60.54	63.12	64.82	66.85	68.02	69.54
C-(C)$_2$(CO$^\bullet$)(O)	18.78 ± 3.14	4.55 ± 4.23	53.86 ± 2.84	62.50	67.63	70.49	72.73	73.15	72.64
C-(C)$_2$(CO$^\bullet$)(H) [b]	29.40 ± 5.04	104.72 ± 6.78	45.83 ± 4.56	53.26	59.28	64.17	71.31	76.14	82.83
C-(C)(C$_d$)(CO$^\bullet$)(CO)	51.98 ± 3.56	-4.05 ± 4.79	68.74 ± 3.22	73.32	73.50	72.75	71.45	70.83	70.61
C-(C)(C$_d$)(CO$^\bullet$)(O)	25.59 ± 3.14	-3.69 ± 4.23	59.23 ± 2.84	68.53	73.17	75.21	76.00	75.45	73.66
C-(C)(CO$^\bullet$)(H)$_2$	14.35 ± 3.56	192.69 ± 4.79	47.93 ± 3.22	55.32	62.41	68.61	78.36	85.45	96.03
C-(CO)(CO$^\bullet$)(H)$_2$	27.52 ± 2.25	186.05 ± 3.03	59.19 ± 2.04	65.45	70.35	74.45	81.21	86.59	95.78
C-(O)(CO$^\bullet$)(H)$_2$	12.63 ± 2.91	180.42 ± 3.91	54.18 ± 2.63	65.14	72.99	78.52	85.90	90.91	98.51
carbonyl radicals adjacent to unsaturated carbon-centered group									
C$_d$-(C)(CO$^\bullet$) [b]	74.28 ± 5.04	84.74 ± 6.78	41.36 ± 4.56	47.05	51.69	55.46	60.85	64.24	68.38
C$_d$-(CO$^\bullet$)(H) [b]	69.88 ± 5.04	169.93 ± 6.78	50.68 ± 4.56	57.68	62.76	66.67	72.47	76.61	82.88
carbonyl radicals adjacent to oxygen-centered group									
O-(C)(CO$^\bullet$)	-114.19 ± 3.56	181.11 ± 4.79	36.13 ± 3.22	40.41	44.74	48.53	54.03	57.31	60.47
O-(CO)(CO$^\bullet$)	-70.32 ± 2.91	184.73 ± 3.91	50.66 ± 2.63	53.45	54.69	54.88	54.10	53.39	53.71

carbonyl radicals adjacent to carbonyl-centered group								
CO-(C)(CO$^\bullet$)	-72.30 ± 3.56	201.4 ± 4.79	51.62 ± 3.22	58.62	64.25	68.73	75.07	79.08	84.08
CO-(CO)(CO$^\bullet$)	-81.92 ± 2.52	185.44 ± 3.39	56.26 ± 2.28	63.39	68.96	73.39	79.82	84.12	89.7
CO-(O)(CO$^\bullet$)	-139.11 ± 3.56	185.89 ± 4.79	55.89 ± 3.22	66.44	74.4	80.26	87.20	89.93	89.91
oxygen radicals adjacent to carbon-centered group									
C-(C)$_3$(O$^\bullet$) [(b)]	42.50 ± 5.04	-23.62 ± 6.78	36.87 ± 4.56	43.09	46.67	48.75	50.63	51.27	51.50
C-(C)$_2$(O)(O$^\bullet$)	-3.43 ± 3.56	-30.40 ± 4.79	35.18 ± 3.22	44.84	50.69	53.83	55.86	55.72	53.94
C-(C)$_2$(CO)(O$^\bullet$) [(b)]	51.22 ± 5.04	-24.39 ± 6.78	40.49 ± 4.56	46.07	49.23	50.89	51.97	51.97	51.52
C-(C)$_2$(O$^\bullet$)(H) [(b)]	39.30 ± 5.04	66.42 ± 6.78	35.76 ± 4.56	42.59	47.75	51.6	56.77	60.08	64.59
C-(C)$_2$(C$_d$)(O$^\bullet$) [(b)]	36.91 ± 8.28	-28.04 ± 11.14	36.77 ± 7.49	46.35	51.22	53.11	53.34	53.02	53.87
C-(C)(C$_d$)(O$^\bullet$)(O)	4.68 ± 3.56	-36.67 ± 4.79	39.82 ± 3.22	50.20	55.53	57.84	58.40	57.34	54.63
C-(C)(C$_d$)(CO)(O$^\bullet$)	55.34 ± 4.21	-37.23 ± 5.67	47.56 ± 3.81	55.00	57.99	58.76	57.84	56.29	53.68
C-(C)(O$^\bullet$)(H)$_2$	29.85 ± 3.56	161.05 ± 4.79	37.43 ± 3.22	44.74	50.99	56.14	63.97	69.61	78.05
C-(O)(O$^\bullet$)(H)$_2$	-6.30 ± 2.91	150.34 ± 3.91	33.50 ± 2.63	43.6	51.83	57.94	66.12	71.42	78.90
C-(O$^\bullet$)(CO)(H)$_2$	45.96 ± 2.76	149.09 ± 3.71	40.03 ± 2.50	47.94	54.47	59.59	66.94	71.83	78.90
oxygen radicals adjacent to unsaturated carbon-centered group									
C$_d$-(C)(O$^\bullet$) [(b)]	-18.32 ± 5.04	62.81 ± 6.78	28.18 ± 4.56	33.08	36.53	39.03	42.16	43.90	45.81
C$_d$-(O$^\bullet$)(H) [(b)]	-11.62 ± 5.04	143.17 ± 6.78	32.58 ± 4.56	37.98	42.39	45.94	51.18	54.78	59.95
oxygen radicals adjacent to carbonyl-centered group									
CO-(C)(O$^\bullet$)	-147.00 ± 3.56	172.38 ± 4.79	33.21 ± 3.22	39.93	45.25	49.29	54.54	57.57	61.03
CO-(O)(O$^\bullet$)	-203.06 ± 3.56	154.52 ± 4.79	37.04 ± 3.22	46.42	53.37	58.24	63.65	65.69	66.14
CO-(O$^\bullet$)(CO)	-108.14 ± 2.52	167.80 ± 3.39	40.82 ± 2.28	47.22	51.46	54.16	57.2	59.00	61.70
ketene radicals adjacent to carbon-centered group									
C-(C)$_3$(CCO$^\bullet$) [(b)]	185.60 ± 5.04	30.37 ± 6.78	64.94 ± 4.56	75.29	82.39	87.27	92.98	95.93	98.88
C-(C)$_2$(C$_d$)(CCO$^\bullet$) [(b)]	189.71 ± 5.04	24.66 ± 6.78	67.82 ± 4.56	77.34	83.69	88.02	93.11	95.82	98.70
C-(C)$_2$(CCO$^\bullet$)(H) [(b)]	177.10 ± 5.04	121.12 ± 6.78	63.65 ± 4.56	74.04	82.07	88.33	97.19	103.01	110.87
C-(C)(CCO$^\bullet$)(H)$_2$	163.50 ± 3.56	207.82 ± 4.79	63.44 ± 3.22	75.11	84.55	92.22	103.76	111.92	123.82
ketene radicals adjacent to unsaturated carbon-centered group									
C$_d$-(C)(CCO$^\bullet$) [(b)]	191.58 ± 5.04	109.81 ± 6.78	54.88 ± 4.56	63.29	69.70	74.72	81.78	86.22	91.75

[a] 97.5 % confidence intervals for $\Delta_f H°$ and $S°$ at 298 K, and for $C_p°$ at 300 K are provided.
[b] The GAV is derived from a single radical.
[c] The GAV is set equal to GAV of the corresponding nonradical group to avoid the linear dependence of the GAVs (see Table S1 in Appendix A).

Table 2-10: NNIs for the enthalpies of formation ($\Delta_f H°$) (kJ/mol) and entropies ($S°$) at 298 K and heat capacities ($C_p°$) at various temperatures for oxygenate radicals.[a]

Inter. no.	Interaction	Occ.[b]	$\Delta_f H°$ [kJ mol^{-1}]	$S°$ [J mol^{-1} K^{-1}]	$C_p°$ [J mol^{-1} K^{-1}] 300 K	400 K	500 K	600 K	800 K	1000 K	1500 K
NNI1	Hbr_H-O-CO-C$^\bullet$-CO	6	-7.93 ± 3.48	-9.18 ± 4.68	-5.24 ± 3.15	-3.92	-2.91	-2.26	-1.57	-0.83	2.07
NNI2	Hbr_H-O-CO-C-O$^\bullet$	2	6.45 ± 4.50	-10.80 ± 6.06	2.57 ± 4.08	2.89	2.19	1.31	0.07	-0.24	0.83
NNI3	Hbr_H-O-CO-O-CO$^\bullet$ [(c)]	1	22.33 ± 5.82	-5.59 ± 7.82	-3.86 ± 5.26	-7.74	-9.51	-9.37	-6.28	-2.58	2.62
NNI4	Hbr_H-O-C$^\bullet$-CO	21	-23.04 ± 4.77	-17.58 ± 6.42	-3.96 ± 4.32	-1.38	0.26	1.71	4.53	6.94	9.60
NNI5	Hbr_H-O-C$^\bullet$-O	10	-2.24 ± 4.87	-6.54 ± 6.55	-0.47 ± 4.41	1.11	1.99	2.40	2.38	1.90	0.69
NNI6	Hbr_H-O-C$^\bullet$-CO-O	2	22.53 ± 6.24	4.65 ± 8.40	3.13 ± 5.65	1.90	1.31	0.98	-0.63	-3.49	-8.86
NNI7	Hbr_H-C$_d$-C$^\bullet$-CO	2	7.22 ± 5.30	4.39 ± 7.13	2.18 ± 4.80	1.41	0.99	0.81	0.72	0.56	-0.61
NNI8	Hbr_H-C$_d$-C$_d$-C-O$^\bullet$ [(c)]	2	11.20 ± 6.57	2.77 ± 8.84	2.57 ± 5.94	-1.02	-2.44	-2.48	-1.36	-0.80	-1.89
NNI9	gauche-CO$^\bullet$-C-O-CO	3	3.13 ± 3.56	-12.80 ± 4.79	9.97 ± 3.22	9.80	8.35	6.85	4.67	3.49	2.12
NNI10	gauche-C$^\bullet$-C-O-CO	5	2.22 ± 2.88	-6.36 ± 3.88	5.68 ± 2.61	4.51	2.86	1.50	0.02	-0.35	0.08
NNI11	O-CO-C$^\bullet$-O-C	2	32.42 ± 5.64	11.54 ± 7.59	4.90 ± 5.11	3.27	1.65	0.43	-1.26	-3.02	-7.17
NNI12	CO-C$^\bullet$-CO-O-C	3	17.78 ± 4.25	12.73 ± 5.72	6.72 ± 3.85	6.45	6.52	6.55	6.10	4.58	-2.19

[a] 97.5 % confidence intervals for $\Delta_f H°$ and $S°$ at 298 K, and for $C_p°$ at 300 K are provided.
[b] The number of occurrences of the NNI in the whole training set is indicated.
(c) NNI correction is derived from a single radical structure.

Gauche interactions: The two gauche interactions that are present in the radicals of the training set are presented in Figure 2-9. Both interactions have only small corrections to the enthalpy of formation, but their corrections to the entropies are much higher. Both of them, NNI9 (CO•-C-O-CO) and NNI10 (C•-C-O-CO), have destabilizing effects resulting in positive enthalpies of formation and restrict the internal flexibility in the radicals, resulting in a decrease in entropy.

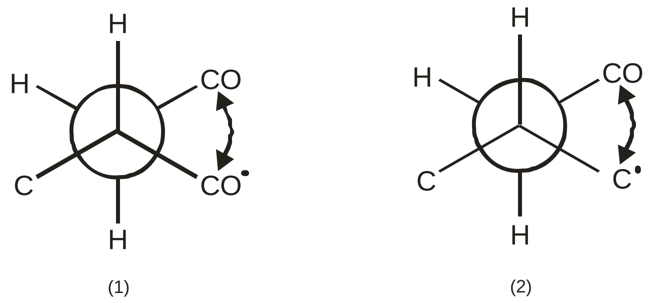

Figure 2-9: Gauche interactions (1) CO•-C-O-CO and (2) C•-C-O-CO.

Other interactions: In this work, two further corrections for NNIs in radicals that cannot be categorized as hydrogen bonds or gauche interactions have been considered. The structures incorporating these interactions, along with their corresponding Newman projections, are shown in Figure 2-10.

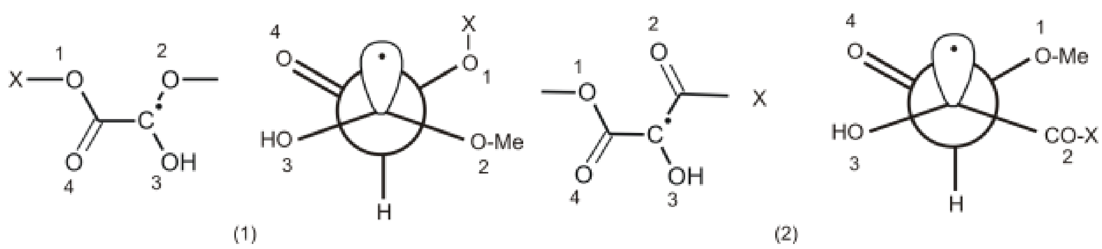

Figure 2-10: Interactions related with a particular geometry (1) O-CO-C•-O-C and (2) CO-C•-CO-O-C.

These two interactions have destabilizing effects on the radicals in which they are present. The destabilizing effect in the first interaction is caused by the presence of the additional leftmost oxygen atom (oxygen atom 1), which distorts the regular geometry of the ligands around the $C^{\bullet}$-$(O)_2(CO)$ group due to coulombic interactions between the electronegative oxygen atoms. The second interaction is very similar, but the upper left oxygen (oxygen atom 1) distorts the normal structure of the $C^{\bullet}$-$(O)(CO)_2$ group.

Comparison of reported GAVs with the corresponding values from the literature: The group additivity values obtained from this work along with the NNI corrections were compared with the corresponding values obtained from the GAVs provided by Khan and Broadbelt [10] based on ab initio calculations. The results of this comparison, for all oxygenate GAVs in common are provided in Table S13 in Appendix A and the MAD, after excluding the GAVs that deviate significantly, is 5.8 kJ mol^{-1} for the standard enthalpies of formation, 5.6 J mol^{-1} K^{-1} for the entropies and less than 3.1 J mol^{-1} K^{-1} for the heat capacities. The comparison was not straightforward because of the arbitrary fixing of values of certain groups to avoid linear dependencies in the model as fixing the contributions of certain groups affects the GAVs of other groups.

Because there are no experimental data available for radicals, comparisons between GA predictions based on the values provided by Khan and Broadbelt [10] and ab initio values, and the GA predictions based on values from this work and the corresponding ab initio values are provided in Table 2-11.

Based on the comparisons in Table 2-11, it can be concluded that the GA model developed in this work can provide an accurate prediction of thermodynamic values and in almost all selected cases better than the prediction based on the GAVs from Khan and Broadbelt [10]. Because the model developed by Khan and Broadbelt is extended to radicals in atmospheric chemistry and the reported GAVs for oxygenate radicals are limited in comparison with our determined groups, in all the above radicals when a group value was not available from the work of Khan and Broadbelt, the corresponding value from this work was used.

Table 2-11: Deviation between GA predictions based on GAVs from Khan and Broadbelt and ab initio values, and GA prediction based on GAVs from this work and the ab initio values for the standard enthalpies of formation ($\Delta_f H°$) and entropies ($S°$) at 298 K and the heat capacities ($C_p°$) at various temperatures for oxygenate radicals.[a]

	Deviation between GA predictions and ab initio values					
	GAVs from Broadbelt					
RADICALS	$\Delta_f H°$ [kJ mol^{-1}]	$S°$ [J mol^{-1} K^{-1}]	$C_p°$ [J mol^{-1} K^{-1}] 300 K	600 K	1000 K	1500 K
ethoxy-methyl	-5.4	0.4	2.8	1.3	-0.1	0.5
2-hydroxy-ethanoyl-methyl	10.3	1.4	6.6	7.4	3.5	-1.5
3-carboxybutan-2-yl	-0.3	-4	0.3	2.3	0.2	-0.5
2-methyl-3-oxopentan-2-yl	-4.7	-0.2	3	4	2.9	-2.2
2-hydroxypropyl	-7.1	1.7	4.5	4.2	3	2.9
3-ethoxy-2-methyl-3-oxopropyl	-2.7	-8.3	6.1	5.4	1.3	-1.3
	GAVs from this work					
RADICALS	$\Delta_f H°$ [kJ mol^{-1}]	$S°$ [J mol^{-1} K^{-1}]	$C_p°$ [J mol^{-1} K^{-1}] 300 K	600 K	1000 K	300 K
ethoxy-methyl	1.8	-4	4.9	2.3	1.1	0.8
2-hydroxy-ethanoyl-methyl	5.3	3.9	5.2	0.7	-1.2	-1.4
3-carboxybutan-2-yl	2.3	1.9	-2.2	-1	-0.9	0.6
2-methyl-3-oxopentan-2-yl	-1.1	5.4	0.3	-1	-1.7	-1.1
2-hydroxypropyl	-2	4.8	2.9	1.2	-0.1	-0.1
3-ethoxy-2-methyl-3-oxopropyl	0.1	-2.3	3.5	2	0.1	-0.5

2.4.3 Radical Adjacent Groups

To evaluate the need for assigning thermodynamic parameters to radical adjacent groups, another statistical analysis was performed in which the values for carbon radical-adjacent-groups were replaced by the corresponding values for the nonradical group counterparts. When the GAVs of radical adjacent groups could be considered equal to those of the corresponding nonradical groups, the number of parameters could be significantly reduced. The analysis was performed only for carbon-centered radical-adjacent groups because the radicalar oxygen, carbonyl and ketene “central atoms” only have a single valence and are consequently not considered as a group as such in the Benson method [1-3]. Therefore these have no central radical group ($O^\bullet$, $C^\bullet$=O, $C^\bullet$=C=O) and all radical character is accounted for by the radical-adjacent groups of these radicals, which was analogously performed by the $C_t^\bullet$ ligand by Sabbe and co-workers [7, 8]. In total, values for 30 radical-adjacent groups might be considered to be set equal to their corresponding values for nonradical groups. These groups are listed in Table 2-12.

Setting the GAVs for the radical-adjacent groups presented in Table 2-12 equal to the GAV of the corresponding nonradical group, the differences between the GA predicted and ab initio (AI) thermodynamic parameters for the 248 oxygenate radicals in the training set are presented in Table S14 in Appendix A.

Table 2-12: Carbon-radical-adjacent groups that may be considered to be set equal to their corresponding non-radical groups.[a]

Carbon-radical-adjacent group	Corresponding nonradical group
C-(C)$_2$(C$^\bullet$)(O)	C-(C)$_3$(O)
C-(C)$_2$(C$^\bullet$)(CO)	C-(C)$_3$(CO)
C-(C)$_2$(C$^\bullet$)(CCO)	C-(C)$_3$(CCO)
C-(C$^\bullet$)(C)(C$_d$)(O)	C-(C)$_2$(C$_d$)(O)
C-(C$^\bullet$)(C)(C$_d$)(CO)	C-(C)$_2$(C$_d$)(CO)
C-(C$^\bullet$)(C)(C$_d$)(CCO)	C-(C)$_2$(C$_d$)(CCO)
C-(C)(C$^\bullet$)(O)$_2$	C-(C)$_2$(O)$_2$
C-(C)(C$^\bullet$)(CO)$_2$	C-(C)$_2$(CO)$_2$
C-(C)(C$^\bullet$)(CO)(O)	C-(C)$_2$(CO)(O)
C-(C)(C$^\bullet$)(O)(H)	C-(C)$_2$(O)(H)
C-(C)(C$^\bullet$)(CO)(H)	C-(C)$_2$(CO)(H)
C-(C)(C$^\bullet$)(CCO)(H)	C-(C)$_2$(CCO)(H)
C-(C$^\bullet$)(C$_d$)(O)$_2$	C-(C)(C$_d$)(O)$_2$
C-(C$^\bullet$)(C$_d$)(CO)$_2$	C-(C)(C$_d$)(CO)$_2$
C-(C$^\bullet$)(C$_d$)(CO)(O)	C-(C)(C$_d$)(CO)(O)
C-(C$^\bullet$)(O)(H)$_2$	C-(C)(O)(H)$_2$
C-(C$^\bullet$)(CO)(H)$_2$	C-(C)(CO)(H)$_2$
C-(C$^\bullet$)(CCO)(H)$_2$	C-(C)(CCO)(H)$_2$
C$_d$-(C$^\bullet$)(O)	C$_d$-(C)(O)
C$_d$-(C$^\bullet$)(CO)	C$_d$-(C)(CO)
C$_d$-(C$^\bullet$)(CCO)	C$_d$-(C)(CCO)
O-(C)(C$^\bullet$)	O-(C)$_2$
O-(C$^\bullet$)(C$_d$)	O-(C)(C$_d$)
O-(C$^\bullet$)(CO)	O-(C)(CO)
CO-(C)(C$^\bullet$)	CO-(C)$_2$
CO-(C$^\bullet$)(O)	CO-(C)(O)
CO-(C$^\bullet$)(CO)	CO-(C)(CO)
CCO-(C)(C$^\bullet$)	CCO-(C)$_2$
O-(C)(C$_d^\bullet$)	O-(C)(C$_d$)
CO-(C$_d^\bullet$)(O)	CO-(C$_d$)(O)

[a] C$_d$ represents a double-bonded carbon atom.

The summary of the results of the statistical analysis in Table S15 shows that the MAD for the enthalpies of formation is 3.07 kJ mol^{-1}, for the entropies 2.64 J mol^{-1} K^{-1} and less than 2.4 J mol^{-1} K^{-1} for the heat capacities at every studied temperature. In comparison with the corresponding values obtained by the statistical analysis of the radicals presented in Table 2-8, the results seem to be reliable. However, a closer look at the detailed results in Table S14 in Appendix A reveals that the deviation between group additive predicted and ab initio values in many radicals is larger than the threshold of 5 kJ mol^{-1} for the enthalpies of formation at 298 K (in 51 out of the 248 radicals) and 5 J mol^{-1} K^{-1} for the entropies at 298 K (in 42 out of the 248 radicals) and the heat capacities, especially at low temperatures, for example, 300 K (in 34 out of the 248 radicals). This is due to the fact that, for the enthalpies of formation, 12 out of the 30 GAVs for carbon-radical-adjacent groups deviate by more than 5 kJ mol^{-1} from the corresponding nonradical group, whereas for the entropies 6 out of 30 deviate more than 5 J mol^{-1} K^{-1}. Therefore we should conclude that the group additive model for oxygenates, as developed in this work, cannot be used by setting the GAVs for carbon-radical-adjacent groups equal to the GAVs of corresponding nonradical groups. Hence, all 30 carbon-radical-adjacent groups from Table 2-12 need to be considered explicitly in our group additive model along with the other radical-adjacent groups (carbonyl, oxygen and ketene radical-adjacent groups) and all the radical-centered groups to improve its reliability in predicting thermodynamic values for oxygenate radicals.

2.4.4 Validation of the Group Additive Model

The group additivity model proposed in this work can be validated either by comparing the group additivity predictions with the ab initio values for a validation set containing both oxygenates molecules and radicals or by comparing these predictions directly with experimental data.

Ab initio validation: The validation set consists of 12 molecules and 11 radicals of oxygenates that are not included in the training set but which represent the different types of compounds included in the training set. The differences between the GA predictions and ab initio calculations for all species included in the validation set are given in Table 2-13 for molecules and radicals. The actual ab initio values for the enthalpies of formation, entropies, and heat capacities for molecules and radicals are collected in Tables S16 and S17 in Appendix A, respectively.

Table 2-13: Differences between the GA and ab initio values for the molecules and radicals of the validation set and averaged values for the standard enthalpies of formation ($\Delta_f H°$) and entropies ($S°$) at 298 K and heat capacities ($C_p°$) at various temperatures.[a]

	Deviation between the GA predictions and ab initio values (AI)								
	$\Delta_f H°$ [kJ mol^{-1}]	$S°$ [J mol^{-1} K^{-1}]	$C_p°$ [J mol^{-1} K^{-1}] 300 K	400 K	500 K	600 K	800 K	1000 K	1500 K
MOLECULES									
butanal	-2.93	-0.94	0.33	0.75	0.74	0.67	0.62	0.61	0.48
butanoic-acid	0.6	-6.46	4.38	2.41	1.02	0.13	-0.65	-0.73	-0.31
1-methoxy-2-methyl-propane	1.05	2.05	-1.03	-1.64	-2.14	-2.29	-2.02	-1.64	-0.87
4-methoxy-2-butanone	-2.29	-0.7	-3.04	-4.35	-3.76	-2.76	-1.21	-0.45	-0.24
propyl-methanoate	1.28	-1.12	4.21	2.25	0.79	-0.12	-0.85	-0.82	-0.22
2-methoxy-2-methylpropanoic-acid	-2.34	-3.31	3.89	3.5	1.79	0.39	-0.74	-1.06	-1.84
2-hydroxy-2-methylbutanal	1.82	5.8	-0.6	-1.53	-3.36	-4.63	-5.15	-4.6	-2.86
prop-1-en-2-yl-22-dimethylpropanoate	1.37	1.17	0.07	0.63	1.4	2.15	2.3	1.04	-1.23
ethenyl-ethylether	1.38	-0.74	-2.83	-1.89	-0.5	0.47	1.08	0.91	0.16
pent-1-en-3-ol	-0.32	-1.18	1.92	2.1	2.2	2.04	1.57	1.24	0.98
2-methylpentan-3-one	-1.05	4.85	-1.49	-2.09	-1.88	-1.51	-0.9	-0.49	-0.02
MAD	1.49	2.57	2.16	2.1	1.78	1.56	1.55	1.23	0.84
RMS	1.67	3.3	2.64	2.34	2.04	2.05	2	1.66	1.18
MAX	2.93	6.46	4.38	4.35	3.76	4.63	5.15	4.6	2.86
RADICALS									
ethoxy-methyl	1.77	-3.97	4.86	4.2	3.11	2.27	1.42	1.1	0.76
2-hydroxy-ethanoyl-methyl	5.25	3.86	5.18	3.67	1.88	0.66	-0.57	-1.16	-1.4
3-methoxy-propanoyl	-4.58	3.08	-4.92	-2.74	-1.76	-1.22	-0.69	-0.45	-0.24
3-carboxy-propyl	4.42	4.27	-0.99	-0.53	-0.62	-0.86	-1.22	-1.21	-0.78
3-carboxybutan-2-yl	2.3	1.85	-2.2	-1.02	-0.84	-1.03	-1.2	-0.86	0.55
2-methylpentan-2-yl-oxidanyl	-1	3.76	-0.69	-1	-0.79	-0.6	-0.35	-0.26	-0.15
2-methyl-3-oxopentan-2-yl	-1.06	5.36	0.31	-0.04	-0.55	-1.01	-1.56	-1.66	-1.06
3-methyl-1-oxopent-1-en-3-yl	-0.8	-3.77	-0.01	0.14	0.22	0.29	0.33	0.31	0.24
2-hydroxypropyl	-2	4.77	2.93	2.56	1.85	1.17	0.29	-0.05	-0.13
3-hydroxy-2-methylidenebutanoyl	-3.38	-0.98	4.43	5.6	5.37	4.62	3.05	2.09	1.52
3-ethoxy-2-methyl-3-oxopropyl	0.11	-2.25	3.54	3.05	2.5	1.97	0.94	0.14	-0.46
MAD	2.42	3.45	2.73	2.23	1.77	1.43	1.06	0.84	0.66
RMS	2.93	3.66	3.33	2.83	2.27	1.83	1.3	1.06	0.81
MAX	5.25	5.36	5.18	5.6	5.37	4.62	3.05	2.09	1.52

[a] MAD: mean absolute deviation; RMS: root mean square deviation; MAX: maximum deviation.

For the 12 molecules in the validation set, the GA method predicts values for standard enthalpies of formation within 3 kJ mol^{-1} with a MAD of 1.49. The MAD for the entropies is

2.57 J mol^{-1} K^{-1}, with very small differences for most molecules; only 2 out of the 12 molecules have a deviation of more than 5 J mol^{-1} K^{-1}. Finally, the MAD for the heat capacities is less than 2.2 J mol^{-1} K^{-1} for the whole temperature range.

For the 11 radicals in the validation set, the GA method predicts values for the standard enthalpy of formation with a MAD of 2.42 kJ mol^{-1} and only one out of 11 radicals deviates more than 5 kJ mol^{-1}. For the entropies, the majority of radicals have an absolute deviation of around 4 J mol^{-1} K^{-1} with a MAD of 3.45 J mol^{-1} K^{-1}, whereas the MAD for the heat capacities is less than 2.8 J mol^{-1} K^{-1} for all temperatures calculated.

Clearly, the GA model developed in this work predicts enthalpies of formation that are within about 5 kJ mol^{-1} of ab initio values, and entropies and heat capacities within around 5 J mol^{-1} K^{-1}.

Experimental validation: The experimental values for the standard enthalpies of formation, entropies, and heat capacities were taken from the NIST web-book [14]. In total, 53 gas-phase standard enthalpies of formation of molecules representative of the categories of compounds included in this work (six ethers, nine alcohols, nine ketones, three aldehydes, eighteen esters and eight acids), eight gas-phase entropies, and four gas-phase heat capacities were used for comparison with the results from the GA model.

The experimental value with the corresponding confidence intervals and the differences between GA predicted and experimental data for all species included in this set of molecules are presented in Tables (2-14)−(2-16) for the enthalpies of formation, entropies and heat capacities, respectively. The confidence intervals given in these tables relate to the average values obtained by an algorithm described in the NIST web-book [29].

Table 2-14: Comparison of the GA predicted values with the experimental data obtained from the NIST web-book[29] for the standard enthalpies of formation ($\Delta_f H°$) at 298 K. The experimental values are averages of the different cited references. The confidence intervals relate to this average and were calculated as a mean interval (see text).

molecule	NIST[a] $\Delta_f H°$ [kJ mol^{-1}]	$\Delta_f H°_{GAV}$-$\Delta_f H°_{NIST}$ [kJ mol^{-1}]
ETHERS		
Methylpropyl ether	-238.9 [30, 31]	-0.3
1-methoxy- butane	-258.1 [30]	-1.6
n-Butylether	-334 [32, 33]	-1.1
1-Methoxydecane	-381.1 [30]	-1.6
1,2-dimethoxy-ethane	-342.8 ± 25 [34, 35]	-8.9
1,2-diethoxy-ethane	-408.2 ± 1 [36, 37]	-12.1
ALCOHOLS		
1-Octanol	-356.4 ± 3.8 [38-41]	-2.9
1-Nonanol	-377 ± 2.4 [38, 40, 41]	-2.8
1-Decanol	-395 ± 2.9 [38, 40, 41]	-5.3
1-Dodecanol	-436.5 [38]	-4.8
1-Tetradecanol	-476.2 ±0.7 [38, 42]	-6.1
1-Hexadecanol	-516.8 ± 1.9 [38, 39, 43, 44]	-6.5
1,5-Pentanediol	-449 ± 3.5 [45-47]	0.7
2-methyl-1-Butanol	-302 [40]	-4.6
2-ethyl-1-Hexanol	-367.5 [48]	-0.6
KETONES		
2-Hexanone	-279.8 [39]	-0.7
3-Hexanone	-278.3 [39]	-3.3
4-Heptanone	-298.3 [49]	-3.8
2-Nonanone	-340.8 [50]	-1.2
5-Nonanone	-344.9 [39]	1.8
6-Undecanone	-387.4 [39]	3.3
Methylisobutylketone	-291.2 [49]	1.9
4,4-dimethyl-2-Pentanone	-320.5 [49]	-0.9
2,2,6,6-Tetramethyl-4-heptanone	-421.2 [51]	-3.7
ALDEHYDES		
Butanal	-207 ± 3.7 [48, 52-54]	-1.3
Heptanal	-264 [54]	-5.8
Octanal	-291.9 [55]	1.8
ESTERS		
Pentanoic acid, methyl ester	-472 ± 6.5 [56, 57]	-0.4
Hexanoic acid, methyl ester	-494 [56]	1.1
Heptanoic acid, methyl ester	-517 [56]	3.6
Pentanoic acid, ethyl ester	-507 ± 0.4 [52, 57, 58]	0.2
Hexanoic acid, ethyl ester	-528 [52]	0.7
Heptanoic acid, ethyl ester	-548 [52]	0.2
Octanoic acid, ethyl ester	-570 [52]	1.7
Nonanoic acid, ethyl ester	-590 [52]	1.2
Decanoic acid, ethyl ester	-612 [52]	2.7
Undecanoic acid, ethyl ester	-634 [52]	4.2
n-Butyl pentanoate	-560 [58]	11.2
Carbonic acid, diethyl ester	-642.4 ± 2.4 [37, 59]	2.2
Ethanol, 2-methoxy-, acetate	-572.6 [60]	-4.6
Propanoic acid ethoxymethyl ester	-617.4 [59]	-14.5
Butanoic acid, 3-methyl-, methyl ester	-511.7 [57]	-1.6
Pentanoic acid, 2-methylpropyl ester	-569 [58]	12.4
4-Pentenoic acid, ethylester	-385 [58]	5.8

4-Pentenoic, 2-methylpropylester	-437 [58]	8
ACIDS		
Butanoic acid	-475.9 [61]	3.8
Pentanoic acid	-491 ± 1.8 [56-58, 61]	-2.5
Hexanoic acid	-510 ± 2.2 [56, 61, 62]	-3.1
Heptanoic acid	-525.8 ± 1.5 [56, 61]	-7.8
Octanoic acid	-550.2 ± 1.1 [56, 61]	-3.9
Nonanoic acid	-566.1 ± 2 [56, 61]	-8.5
Hexadecanoic acid	-730 [61]	11.9
3-methyl-butanoic acid	-502.5 [57]	1.1
MAD		**3.8**

[a] First the mean and standard deviation were estimated and then the values greater than three standard deviations from the mean were excluded. If values have been excluded, the process was repeated with estimates based on the remaining values. The given error range corresponds to 1.96 times the final estimate of the standard deviation.

Table 2-15: Comparison of the GA predicted values with the experimental data in the NIST web-book [29] for molar entropies (S^o) at 298 K. The confidence intervals are given as a mean interval.

molecule	NIST $S°$ [J mol^{-1} K^{-1}]	$S°_{GAV}$ - $S°_{NIST}$ [J mol^{-1} K^{-1}]
Methyl propyl ether	352 [63]	0.6
1-methoxy-butane	390.1 [63]	2.5
1-Hexadecanol	853 ± 17 [44]	-2.8
3-Hexanone	409.6 [63]	-1.5
Butanal	344.8 ± 4.2 [64]	-1.2
Pentanal	379.9 ± 3.3 [65]	3.7
Heptanal	461.5 ± 4.2 [64]	2
Butanoic acid	353.3 [66]	4.6
MAD		**2.2**

Table 2-16: Comparison of the GA predicted values with experimental data in the NIST web-book [29] for heat capacities (C_p) at 400 and 500 K. The confidence intervals are given as a mean interval.

molecule	$C_p°$ [J mol^{-1} K^{-1}]			
	$C_p°_{400,NIST}$	$C_p°_{500,NIST}$	$C_p°_{400,GAV}$ - $C_p°_{400,NIST}$	$C_p°_{500,GAV}$ - $C_p°_{500,NIST}$
3-Hexanone	185.14 [67]	215.81 [67]	-0.5	-2.7
Methyl isobutyl ketone	182.26 ± 0.27 [68]		-0.3	
n-Propyl acetate	162.33 [69]		2.1	
MAD			**1.1**	**2.7**

The group additive prediction deviates by more than 5 kJ mol^{-1} for only 14 out of the 53 molecules, with five of these 14 molecules deviating by more than 10 kJ mol^{-1}. The MAD with the experimental standard enthalpies of formation is 3.8 kJ mol^{-1}. For the entropies, the set of eight molecules show very good agreement between experimental and GA values, with a MAD of 2.2 J mol^{-1} K^{-1} and no molecules that deviate by more than 5 J mol^{-1} K^{-1}. The heat capacities of only three molecules at 400 K and 500 K can be compared with reference data, with deviations of less than 3 J mol^{-1} K^{-1} in all cases. Thus, it can be concluded that there is good agreement between experimental and GA enthalpies of formation, whereas for the entropies and heat capacities, the agreement can be considered very good.

2.4.5 Hydrogen Bond Increments (HBIs) for Oxygenate Radicals

An alternative procedure for predicting the thermodynamic properties of oxygenate radicals is the hydrogen bond increment method first developed by Lay et al. [15]. The nomenclature used in this work is in accord with that used by Lay et al, and the HBIs are denoted by a symbolism in which J represents a radical site on the preceding carbon or oxygen atom, for example, CCJ(C)O indicates a radical that contains the structure $CH_2C^{\bullet}(CH_3)O$-. Based on the results for the GAVs provided in Tables 2-4 and 2-9, 77 thermodynamic values for HBIs can be calculated using the equations (2-4)−(2-6). In this work, 77 new HBI structures were introduced and their thermodynamic properties ($\Delta_f H°$, $S°$, $C_p°$) were determined (Table 2-17). To the best of our knowledge, the thermodynamic data for only 11 out of these 77 HBI structures have been calculated previously [16-19]. Table 2-17 first presents saturated carbon-centered radicals containing the hydroxyl/alkoxy functional group (alcohols, ethers, esters) from the simplest to the most complex structure followed by the saturated oxygen-centered radicals. Then, the corresponding unsaturated radicals follow (first carbon-centered, followed by oxygen-centered). Next, saturated carbon- and oxygen-centered radicals bearing a carbonyl moiety (aldehydes, ketones, acids, esters) are presented from the simplest to the most complex structure, followed by the saturated carbonyl-centered radical. Then, the corresponding unsaturated radicals follow (first carbon-centered, followed by carbonyl-centered). And finally, saturated carbon-centered radicals bearing the ketenyl moiety (ketenes) are presented from the simplest to the most complex structure followed by the saturated ketenyl-centered radicals (first carbon-centered followed by ketenyl-centered).

Table 2-17: Hydrogen Bond Increments (HBIs) for the calculation of standard enthalpies of formation ($\Delta_f H°$) and entropies ($S°$) at 298 K and heat capacities ($C_p°$) at various temperatures.

HBI	Nomenclature	$\Delta_f H°$ [kJ mol^{-1}]	$S°$ [J mol^{-1} K^{-1}]	$C_p°$ [J mol^{-1} K^{-1}] 300 K	400 K	500 K	600 K	800 K	1000 K	1500 K
saturated carbon-centered radicals bearing a hydroxy/alkoxy moiety (alcohols, ethers, esters)										
1	CJH2O	195.3	1.2	4.9	3.7	1.6	-0.9	-5.9	-10.3	-17.5
2	CJCO	212.0	6.1	0.8	-1.5	-4.1	-6.7	-11.1	-14.3	-19.2
3	CCJO	184.0	3.9	1.2	0.4	-1.5	-3.9	-8.6	-12.5	-18.7
4	OCJO	190.4	15.1	1.0	-8.2	-14.4	-17.5	-19.4	-20.1	-21.5
5	CCJCO	198.9	13.8	-6.9	-8.3	-10.0	-11.6	-14.5	-16.8	-20.3
6	CCJ(O)C	178.7	14.3	-4.4	-7.4	-9.8	-11.5	-13.9	-15.9	-19.2
7	CCJ(C)O	180.4	14.4	-2.0	-7.1	-10.7	-13.4	-16.6	-18.5	-21.2
8	CCJ(C)CO	151.4	-0.8	-7.8	-9.3	-10.3	-11.0	-12.4	-13.7	-16.1
9	CJC(C)OC	211.9	7.0	5.5	1.8	-2.0	-5.5	-11.0	-14.7	-19.8
10	CJC(C)2O	213.1	5.1	4.1	1.1	-2.1	-5.1	-9.7	-13.1	-18.5
11	CJC(O)2C	217.3	8.1	2.4	-1.5	-5.0	-7.4	-10.8	-13.6	-18.2
saturated oxygen-centered radicals										
12	CCOJ	224.9	3.8	-8.1	-12.2	-14.4	-15.1	-14.7	-14.5	-15.6
13	OCOJ	226.4	0.8	-10.9	-17.5	-19.8	-19.3	-16.2	-14.3	-14.3
14	CC(C)OJ	229.6	-6.8	-5.3	-6.3	-7.3	-8.3	-9.8	-11.2	-14.2
15	CC(C)2OJ	228.1	-4.6	-6.2	-7.9	-9.0	-9.9	-10.7	-11.7	-14.6
16	CC(C)(O)OJ	231.0	8.0	-11.8	-18.8	-22.1	-22.3	-19.5	-17.2	-16.0
unsaturated carbon-centered radicals bearing a hydroxyl/alkoxy moiety (alcohols, ethers, esters)										
17	C=CJO	239.4	26.7	-6.1	-11.8	-15.2	-17.2	-19.2	-20.3	-22.0
18	C=CCJO	115.9	-7.4	-6.0	-3.9	-3.0	-3.2	-5.7	-8.6	-13.8
19	C=COCJ	191.4	13.7	-4.9	-7.2	-8.9	-10.6	-13.6	-15.9	-19.7
20	C=CCJCO	117.4	-19.9	3.0	3.2	2.4	1.0	-1.8	-4.5	-9.8
21	C=C(O)CJ	158.8	-3.9	-1.7	-2.3	-4.6	-7.1	-11.0	-13.5	-16.6
22	C=CCJ(O)C	110.3	4.5	-5.7	-8.4	-10.0	-11.0	-12.1	-13.1	-15.5
23	C=CC(C)(O)CJ	213.9	9.0	0.5	-2.7	-5.5	-7.9	-11.8	-14.6	-19.0
24	C=CC(O)2CJ	213.8	6.7	1.0	-0.2	-2.0	-4.0	-8.1	-11.6	-17.2
25	C=CCJC(O)C=C	68.3	-9.6	-8.3	-4.5	-3.0	-2.8	-3.9	-5.6	-10.2
unsaturated oxygen-centered radicals										
26	C=COJ	140.1	3.3	-10.1	-13.5	-14.6	-14.6	-14.3	-14.5	-16.0
27	C=C(C)OJ	136.8	7.4	-9.2	-13.1	-15.6	-17.0	-17.7	-17.6	-17.6
28	C=CC(C)2OJ	227.9	2.7	-8.9	-12.1	-12.9	-12.9	-12.6	-12.9	-14.8
29	C=CC(C)(O)OJ	232.7	8.5	-7.2	-12.5	-16.7	-19.1	-20.1	-19.4	-18.2
saturated carbon-centered radicals bearing a carbonyl moiety (aldehydes, ketones, acids, esters)										
30	CJC=O	184.4	-7.8	1.5	1.1	-0.4	-2.3	-6.1	-9.2	-14.4
31	CJCC=O	212.0	6.1	0.8	-1.5	-4.1	-6.7	-11.1	-14.3	-19.2
32	CCJC=O	161.1	-5.7	-4.9	-3.4	-3.4	-4.2	-6.7	-9.2	-13.9
33	OCJC=O	138.6	0.2	-1.3	-3.3	-5.6	-7.4	-9.8	-11.2	-14.0
34	CCJCC=O	198.9	13.8	-6.9	-8.3	-10.0	-11.6	-14.5	-16.8	-20.3
35	C=OCJC=O	164.7	-13.0	1.9	1.5	0.9	0.0	-2.5	-5.1	-10.2
36	CJC(C)C=O	211.5	8.7	3.6	0.2	-3.0	-5.8	-10.5	-14.1	-19.3
37	CJC(C=O)2C	209.0	8.8	2.8	2.5	0.6	-1.9	-6.9	-10.9	-17.1
38	CJC(C)(C=O)O	212.9	3.7	6.6	5.1	2.3	-0.9	-6.8	-11.3	-17.8
39	CJC(C)2C=O	211.5	7.9	5.9	2.5	-1.1	-4.4	-9.7	-13.6	-19.0
saturated oxygen-centered radicals bearing a carbonyl moiety (aldehydes, ketones, acids, esters)										
40	C=OCOJ	243.0	2.6	-6.6	-9.3	-11.5	-13.2	-15.0	-16.0	-17.5
41	OC=OOJ	242.9	6.0	-8.5	-13.1	-16.3	-18.3	-20.4	-21.2	-21.4
42	C=OC=OOJ	261.5	16.0	-3.1	-6.8	-10.1	-13.0	-17.5	-20.9	-25.9
43	CC(C)(C=O)OJ	241.1	16.3	-8.6	-13.9	-16.3	-17.5	-18.4	-18.8	-19.1

saturated carbonyl-centered radicals										
44	CCCJ=O	160.0	8.3	-1.7	-3.9	-7.0	-9.9	-14.5	-17.5	-21.4
45	COCJ=O	197.2	-4.3	2.2	-0.2	-3.5	-6.5	-10.9	-13.6	-17.0
46	C=OCCJ=O	161.4	0.8	5.2	1.4	-2.8	-6.4	-12.0	-15.8	-20.4
47	OC=OCJ=O	158.2	4.6	-3.0	-4.7	-7.0	-9.5	-14.0	-17.2	-21.1
48	C=OC=OCJ=O	112.2	-19.6	-5.2	-4.6	-4.4	-4.5	-4.9	-5.7	-7.8
49	CC(C)CJ=O	158.2	6.7	-4.1	-5.8	-7.9	-9.9	-13.5	-16.2	-20.3
50	CC(C)2CJ=O	155.3	7.5	-2.7	-5.0	-7.4	-9.6	-13.1	-15.6	-19.9
51	CC(C)(O)CJ=O	156.9	6.8	0.9	-2.6	-5.6	-8.1	-12.0	-14.9	-19.6
52	CC(C)(C=O)CJ=O	157.2	10.4	-3.7	-4.0	-5.4	-7.2	-10.9	-13.9	-18.6
53	C=CJC=O	244.3	9.6	0.4	-2.2	-4.8	-7.2	-11.6	-15.5	-22.0
unsaturated carbon-centered radicals bearing a carbonyl moiety (aldehydes, ketones, acids, esters)										
54	C=C(C=O)CJ	156.0	-16.5	-1.8	-1.2	-2.4	-4.4	-8.2	-11.3	-15.9
55	C=CCJ(C)C=O	117.4	-17.3	-12.2	-10.5	-9.4	-9.0	-9.1	-9.7	-11.5
56	C=CCJ(C=O)C=C	89.4	-27.9	-10.0	-7.5	-6.1	-5.5	-5.6	-6.4	-8.5
57	C=CC(O)(C=O)CJ	214.3	6.9	4.0	0.9	-2.4	-5.2	-9.7	-13.0	-18.1
58	C=CC(C)(C=O)CJ	212.6	9.8	2.8	0.6	-2.7	-5.8	-10.8	-14.4	-19.3
59	C=CC(C=O)2CJ	211.8	5.5	4.7	2.4	-0.6	-3.5	-8.4	-12.1	-17.6
unsaturated oxygen-centered radicals bearing a carbonyl moiety (aldehydes, ketones, acids, esters)										
60	C=CC(C)(C=O)OJ	244.1	10.4	-5.5	-11.3	-14.6	-16.2	-17.2	-17.4	-18.4
unsaturated carbonyl-centered radicals										
61	C=CCJ=O	161.9	7.2	5.3	2.5	-1.1	-4.5	-9.9	-13.7	-18.9
62	C=C(C)CJ=O	163.7	6.7	-1.3	-3.8	-6.4	-8.8	-12.5	-15.3	-19.5
63	C=CC(C)2CJ=O	153.9	10.6	-1.5	-4.2	-7.0	-9.3	-12.8	-15.4	-19.4
64	C=CC(C)(O)CJ=O	157.3	8.7	-1.0	-4.5	-7.4	-9.7	-12.7	-15.1	-19.5
65	C=CC(C)(C=O)CJ=O	155.6	1.2	6.5	2.6	-2.4	-6.5	-12.0	-15.3	-19.7
saturated carbon-centered radicals bearing a ketenyl moiety (ketenes)										
66	CJC=C=O	155.5	-1.3	0.2	-0.7	-2.6	-4.5	-8.1	-11.0	-15.6
67	CJCC=C=O	202.3	16.4	-3.3	-5.8	-8.1	-10.1	-13.4	-15.9	-19.9
68	CJC(C)C=C=O	212.1	9.7	3.2	-0.5	-4.1	-7.2	-11.8	-15.0	-19.5
69	CCJ(C)C=C=O	143.8	3.5	-7.1	-10.0	-11.8	-12.9	-14.1	-15.1	-16.9
70	CCJC(C)=C=O	147.4	8.3	-1.3	-4.0	-6.2	-7.9	-10.8	-12.9	-16.9
saturated ketenyl-centered radicals										
71	CCCJ=C=O	202.2	-2.3	-1.6	-3.0	-4.9	-6.5	-9.4	-11.6	-15.1
72	CC(C)CJ=C=O	206.0	1.7	-0.8	-3.6	-6.0	-7.8	-10.6	-12.6	-15.8
unsaturated carbon-centered radicals bearing a ketenyl moiety (ketenes)										
73	C=CCJC=C=O	100.0	-22.0	-5.5	-3.8	-3.7	-4.3	-6.1	-8.1	-11.5
74	C=C(CJ)C=C=O	156.9	-8.1	-6.2	-5.6	-5.7	-6.4	-8.2	-10.0	-12.8
75	C=CCJ(C)C=C=O	95.4	0.5	-6.8	-8.2	-8.9	-9.3	-10.1	-11.0	-12.9
76	C=CCJ(C=C=O)C=C	69.1	-27.5	-10.7	-9.3	-8.1	-7.2	-6.8	-7.2	-8.8
unsaturated ketenyl-centered radicals										
77	C=C(C)CJ=C=O	186.0	5.6	-11.5	-13.7	-14.6	-15.0	-15.7	-16.3	-17.8

By using the HBIs presented in Table 2-17 in combination with the GAVs from Tables 2-4 and 2-9, the thermodynamic parameters ($\Delta_f H°$, $S°$, $C_p°$) of the oxygenate radicals in the training set are reproduced with a MAD of 3.0 kJ mol^{-1} for $\Delta_f H°$ at 298 K, 3.01 J mol^{-1} K^{-1} for $S°$ at 298 K and less than 1.95 J mol^{-1} K^{-1} for $C_p°$ in the temperature range 300−1500 K. The corresponding values for Benson's group additive method for radicals are 1.35 kJ mol^{-1} for

$\Delta_f H°$ at 298 K, 1.77 J mol^{-1} K^{-1} for $S°$ at 298 K and less than 1.29 mol^{-1} K^{-1} for $C_p°$ in the temperature range 300−1500 K.

Table 2-18: Comparison of the thermodynamic parameters of HBIs from this work for standard enthalpies of formation ($\Delta_f H°$) and entropies ($S°$) at 298 K and heat capacities ($C_p°$) at various temperatures with the corresponding literature values.

#	HBI		$\Delta_f H°$ [kJ mol^{-1}]	$S°$ [J mol^{-1} K^{-1}]	$C_p°$ [J mol^{-1} K^{-1}] 300 K	400 K	500 K	600 K	800 K	1000 K	1500 K
1	CCOJ	this work	224.9	3.8	-8.1	-12.2	-14.4	-15.1	-14.7	-14.5	-15.6
		Sun et al [17]	219.6	-5.9	-3.3	-4.6	-6.2	-7.5	-9.5	-10.9	-13.9
		difference	5.2	9.7	-4.7	-7.5	-8.2	-7.5	-5.3	-3.6	-1.7
2	CCJO	this work	184.0	3.9	1.2	0.4	-1.5	-3.9	-8.6	-12.5	-18.7
		Sun et al [17]	202.4	7.4	-2.6	-5.8	-8.6	-10.7	-13.4	-15.1	-17.9
		difference	-18.5	-3.5	3.9	6.2	7.1	6.9	4.8	2.6	-0.8
3	CJCO	this work	212.0	6.1	0.8	-1.5	-4.1	-6.7	-11.1	-14.3	-19.2
		Sun et al. [17]	211.1	0.4	3.1	0.3	-3.0	-5.9	-10.4	-13.7	-18.5
		difference	0.8	5.8	-2.4	-1.8	-1.1	-0.8	-0.7	-0.7	-0.7
4	CCOJ	this work	224.9	3.8	-8.1	-12.2	-14.4	-15.1	-14.7	-14.5	-15.6
		Sun et al [16]	215.9	-3.8	-2.2	-3.6	-5.2	-6.7	-8.8	-10.6	-13.9
		difference	9.0	7.6	-5.9	-8.6	-9.2	-8.4	-5.9	-4.0	-1.7
5	C(C)OJ	this work	229.6	-6.8	-5.3	-6.3	-7.3	-8.3	-9.8	-11.2	-14.2
		Sun et al [16]	223.4	-8.0	-4.4	-5.7	-7.2	-8.4	-10.1	-11.3	-13.9
		difference	6.2	1.1	-0.9	-0.6	-0.1	0.1	0.3	0.1	-0.3
6	CJO	this work	195.3	1.2	4.9	3.7	1.6	-0.9	-5.9	-10.3	-17.5
		Sun et al [16]	184.7	-9.0	1.8	1.4	-0.4	-2.8	-7.4	-11.2	-17.2
		difference	10.5	10.2	3.0	2.3	2.0	1.9	1.5	0.9	-0.3
7	CCJO	this work	184.0	3.9	1.2	0.4	-1.5	-3.9	-8.6	-12.5	-18.7
		Sun et al [16]	179.1	9.0	-2.1	-3.9	-5.9	-7.8	-11.2	-13.9	-18.3
		difference	4.8	-5.1	3.3	4.3	4.4	4.0	2.6	1.4	-0.4
8	CJCO	this work	212.0	6.1	0.8	-1.5	-4.1	-6.7	-11.1	-14.3	-19.2
		Sun et al [16]	211.1	0.4	3.1	0.3	-3.0	-5.9	-10.4	-13.7	-18.5
		difference	0.8	5.8	-2.4	-1.8	-1.1	-0.8	-0.7	-0.7	-0.7
9	C=CJC=O	this work	244.3	9.6	0.4	-2.2	-4.8	-7.2	-11.6	-15.5	-22.0
		Sebbar et al. [18]	253.9	7.4	-10.8	-14.9	-17.8	-19.8	-22.2	-23.4	-25.2
		difference	-9.6	2.2	11.2	12.7	13.0	12.6	10.5	7.9	3.1
10	C=CCJ=O	this work	161.9	7.2	5.3	2.5	-1.1	-4.5	-9.9	-13.7	-18.9
		Sebbar et al [18]	162.8	10.8	-13.4	-16.9	-19.5	-21.4	-23.7	-24.9	-26.3
		difference	-0.9	-3.6	18.7	19.4	18.4	16.9	13.8	11.2	7.5
11	COCJ=O	this work	197.2	-4.3	2.2	-0.2	-3.5	-6.5	-10.9	-13.6	-17.0
		Sebbar et al. [18]	179.9	-3.9	-7.2	-8.1	-7.7	-7.2	-7.5	-9.3	-14.4
		difference	17.4	-0.4	9.4	7.9	4.2	0.7	-3.4	-4.4	-2.6
12	CJC=O	this work	184.4	-7.8	1.5	1.1	-0.4	-2.3	-6.1	-9.2	-14.4
		Hudzik et al [19]	182.2	-9.9	0.0	-1.8	-4.3	-6.6	-11.5	-15.0	-18.2
		difference	2.3	2.1	1.5	2.9	3.9	4.3	5.4	5.8	3.7
13	CCJC=O	this work	161.1	-5.7	-4.9	-3.4	-3.4	-4.2	-6.7	-9.2	-13.9
		Hudzik et al [19]	162.5	-13.1	-7.0	-9.5	-10.9	-11.9	-15.2	-17.3	-19.0
		difference	-1.4	7.4	2.1	6.1	7.5	7.7	8.5	8.2	5.1
14	CJC(C)C=O	this work	211.5	8.7	3.6	0.2	-3.0	-5.8	-10.5	-14.1	-19.3
		Hudzik et al [19]	205.5	19.6	5.1	2.4	-1.4	-5.3	-11.7	-15.8	-20.9
		difference	6.0	-11.0	-1.5	-2.2	-1.6	-0.5	1.1	1.8	1.6
MAD			**6.7**	**5.4**	**5.1**	**6.0**	**5.8**	**5.2**	**4.6**	**3.8**	**2.1**

The thermodynamic properties for the HBIs in this work were compared with the corresponding HBIs available in the literature. The results of this comparison are provided in Table 2-18 and reveal that there are significant differences between values obtained in this work and those found in the literature. This could be attributed to differences in the approaches used for calculating the thermodynamic properties; isodesmic reactions were used to determine the values reported in the literature [16-19] whereas in this work Benson's group additive method was used. Moreover, the fact that an HBI structure is not strictly defined can pose significant interpretation problems, for example, the thermodynamic values for HBI CJC(C)(C=O)O are an average of the data derive from the radicals $CH_2^{\bullet}$-C(COH)(CH_3)-OH, $CH_2^{\bullet}$-C(COH)(CH_3)-OCH_3 and $CH_2^{\bullet}$-C(COH)(CH_3)-$OCOCH_3$. The characteristic moiety at the β position with respect to the radical center in the previously mentioned radicals (-OH, -CH_3, and -$OCOCH_3$, respectively) influence the HBIs. Therefore it can be concluded that in cases like the example given, the possibility of including additional hydrogen bond increments to more accurately predict thermodynamic values should be examined.

The calculated HBIs in this work for the thermodynamic parameters ($\Delta_f H°$, $S°$, $C_p°$) provide an alternative but less accurate method than Benson's group additive method for calculating the thermodynamic parameters of oxygenate radicals. Differences between the HBIs reported in this work and the corresponding literature values [16-19] can be attributed to uncertainties in the different approaches used to determine the HBIs and moreover to the need, in a few circumstances, to introduce additional HBI structures that can better describe some particular radical structures.

2.5 Conclusions

A database of enthalpies of formation, entropies and heat capacities for 450 saturated and unsaturated, α- and β-branched, mono- and bifunctional oxygenate compounds and their corresponding radicals has been constructed. The calculations were performed by using ideal gas statistical thermodynamics based on CBS-QB3 calculations including corrections for hindered rotation for all internal rotors.

A set of GAVs for the standard enthalpies of formation ($\Delta_f H°$) at 298 K, entropies at 298 K ($S°$), and heat capacities ($C_p°$) over a wide range of temperatures (300-1500 K) was determined for 60 molecules and 97 radicals. The group additive model was further developed by adopting 14 NNI corrections for molecules and 12 NNI corrections for radicals. The types of interactions recognized were hydrogen bonds, gauche interactions, and interactions arising from the structure of the particular compound. It can be concluded that the hydrogen bonds are on the periphery of the group additivity method: They are very difficult to model, yet make a significant contribution to the thermochemistry of a compound.

It was investigated as to whether the carbon-radical-adjacent groups could be set equal to the corresponding nonradical groups. However, the results of the regression statistics revealed that this is not feasible because some radicals show deviations of more than 10 kJ mol^{-1} for the enthalpies of formation and more than 10 J mol^{-1} K^{-1} for the entropies and heat capacities at lower temperatures.

The group additive values obtained were validated by using a set of 12 molecules and 11 radicals and also by a set of experimental values. A comparison of group additive predicted values with ab initio calculated values shows that the enthalpies were predicted to within 5 kJ mol^{-1} for the great majority of the compounds included in the validation set. In addition, the entropies and heat capacities were predicted to within 5 J mol^{-1} K^{-1} for almost every compound in the validation set. The agreement between the experimental values and the group additive predicted values is within 5 kJ mol^{-1} for the enthalpies of 39 out of the 53 molecules examined, whereas for the entropies and heat capacities, all the group additive predictions agree with the experimental values to within 5 J mol^{-1} K^{-1}.

Hence, the GAVs reported in this work can be reliably used to predict the thermochemical data for large oxygenate compounds, combining rapid prediction with a wide application range. In particular, this work significantly extends the application range for the enthalpy of formation, entropy and heat capacities of oxygenate radicals.

An alternative procedure to Benson's group additive method for calculating the thermodynamic parameters of oxygenate radicals is the hydrogen bond increment method. This method provides a less accurate prediction of the thermodynamic parameters of oxygenate radicals compared with Benson's group additive method, the MADs on the HBI predictions for the radicals in the training set being 3.0 kJ mol^{-1} for $\Delta_f H°$ at 298 K, 3.0 J mol^{-1} K^{-1} for $S°$ at 298 K and less than 1.95 J mol^{-1} K^{-1} for $C_p°$ in the temperature range 300−1500 K. Thus, the HBIs reported in this work can be used to predict the thermochemical data for large oxygenate radicals.

2.6 References

1. Benson, S.W., *Thermochemical Kinetics*. 1968, New York: John Wiley & Sons Ltd.
2. Benson, S.W. and J.H. Buss, *Additivity Rules for the Estimation of Molecular Properties. Thermodynamic Properties.* J Chem Phys, 1958. **29**(9): p. 546-561.
3. Benson, S.W., F.R. Cruickshank, D.M. Golden, G.R. Haugen, H.E. O'Neal, A.S. Rodgers, R. Shaw, and R. Walsh, *Additivity Rules for the Estimation of Thermochemical Properties.* Chem Rev, 1969. **69**: p. 279-324.
4. Cohen, N., *Revised group additivity values for enthalpies of formation (at 298 K) of carbon-hydrogen and carbon-hydrogen-oxygen compounds.* J Phys Chem Ref Data, 1996. **25**(6): p. 1411-1481.
5. Poling, B.E., J.M. Prausnitz, and J.P. O'Connel, *The properties of gases and liquids*. 2001, New York: McGraw-Hill.
6. Luo, Y.R., *Handbook of bond dissociation energies in organic compounds*. 2003, Boca Raton: CRC Press.
7. Sabbe, M.K., F. De Vleeschouwer, M.F. Reyniers, M. Waroquier, and G.B. Marin, *First Principles Based Group Additive Values for the Gas Phase Standard Entropy and Heat Capacity of Hydrocarbons and Hydrocarbon Radicals.* J Phys Chem A, 2008. **112**(47): p. 12235-12251.
8. Sabbe, M.K., M. Saeys, M.F. Reyniers, G.B. Marin, V. Van Speybroeck, and M. Waroquier, *Group additive values for the gas phase standard enthalpy of formation of hydrocarbons and hydrocarbon radicals.* J Phys Chem A, 2005. **109**(33): p. 7466-7480.
9. Sumathi, R. and W.H. Green, *Thermodynamic properties of ketenes: Group additivity values from quantum chemical calculations.* J Phys Chem A, 2002. **106**(34): p. 7937-7949.
10. Khan, S.S., X.R. Yu, J.R. Wade, R.D. Malmgren, and L.J. Broadbelt, *Thermochemistry of Radicals and Molecules Relevant to Atmospheric Chemistry: Determination of Group Additivity Values using G3//B3LYP Theory*. J Phys Chem A, 2009. **113**(17): p. 5176-5194.
11. Bhattacharya, A. and S. Shivalkar, *Re-tooling Benson's group additivity method for estimation of the enthalpy of formation of free radicals: C/H and C/H/O groups.* J Chem Eng Data, 2006. **51**(4): p. 1169-1181.
12. Holmes, J.L. and C. Aubry, *Group Additivity Values for Estimating the Enthalpy of Formation of Organic Compounds: An Update and Reappraisal. 1. C, H, and O.* J Phys Chem A, 2011. **115**(38): p. 10576-10586.
13. Holmes, J.L. and C. Aubry, *Group Additivity Values for Estimating the Enthalpy of Formation of Organic Compounds: An Update and Reappraisal. 2. C, H, N, O, S, and Halogens.* J Phys Chem A, 2012. **116**(26): p. 7196-7209.
14. *NIST Standard Reference Database Number 69, http://webbook.nist.gov/chemistry/*. 2009: NIST.

15. Lay, T.H., J.W. Bozzelli, A.M. Dean, and E.R. Ritter, *Hydrogen-Atom Bond Increments for Calculation of Thermodynamic Properties of Hydrocarbon Radical Species.* J Phys Chem-Us, 1995. **99**(39): p. 14514-14527.

16. Sun, H.Y. and J.W. Bozzelli, *Structures, rotational barriers, thermochemical properties, and additivity groups for 2-propanol, 2-chloro-2-propanol and the corresponding alkoxy and hydroxyalkyl radicals.* J Phys Chem A, 2002. **106**(15): p. 3947-3956.

17. Sun, H.Y. and J.W. Bozzelli, *Structures, intramolecular rotation barriers, and thermochemical properties: Ethanol, alpha-monoethanols, dichloroethanols, and corresponding radicals derived from H atom loss.* J Phys Chem A, 2001. **105**(41): p. 9543-9552.

18. Sebbar, N., H. Bockhorn, and J.W. Bozzelli, *Thermochemical properties, rotation barriers, and group additivity for unsaturated oxygenated hydrocarbons and radicals resulting from reaction of vinyl and phenyl radical systems with O-2.* J Phys Chem A, 2005. **109**(10): p. 2233-2253.

19. Hudzik, J.M. and J.W. Bozzelli, *Thermochemistry and Bond Dissociation Energies of Ketones.* J Phys Chem A, 2012. **116**(23): p. 5707-5722.

20. Frisch, M.J., G.W. Trucks, H.B. Schlegel, G.E. Scuseria, M.A. Robb, J.R. Cheeseman, J.A. Montgomery, T. Vreven, K.N. Kudin, et al., *Gaussian 03, revision B.03*, 2004, Gaussian, Inc.: Wallingford CT.

21. Vandeputte, A.G., M.K. Sabbe, M.F. Reyniers, and G.B. Marin, *Modeling the Gas-Phase Thermochemistry of Organosulfur Compounds.* Chem-Eur J, 2011. **17**(27): p. 7656-7673.

22. Van Speybroeck, V., P. Vansteenkiste, D. Van Neck, and M. Waroquier, *Why Does the Uncoupled Hindered Rotor Model Work Well for the Thermodynamics of n-Alkanes?* Chem Phys Lett, 2005. **402**(4-6): p. 479-484.

23. Vansteenkiste, P., D. Van Neck, V. Van Speybroeck, and M. Waroquier, *An extended hindered-rotor model with incorporation of Coriolis and vibrational-rotational coupling for calculating partition functions and derived quantities.* J Chem Phys, 2006. **124**(4): p. 044314.

24. Vansteenkiste, P., V. Van Speybroeck, G.B. Marin, and M. Waroquier, *Ab Initio Calculation of Entropy and Heat Capacity of Gas-Phase n-Alkanes Using Internal Rotations.* J Phys Chem A, 2003. **107**(17): p. 3139-3145.

25. Montgomery, J.A., A.M.J. Frisch, J.W. Ochterski, G.A. Petersson, K. Raghavachari, and V.G. Zakrzewski, *Comment on "Assessment of complete basis set methods for calculation of enthalpies of formation" [J. Chem. Phys. 188, 692 (1998)].* J Chem Phys, 1998. **109**(15): p. 6505-6506.

26. Reid, R.C., J.M. Prausnitz, and B.E. Poling, *The properties of gases & liquids*. 1987, New York: McGraw-Hill.

27. Cohen, N. and S.W. Benson, *Estimation of Heats of Formation of Organic-Compounds by Additivity Methods.* Chem Rev, 1993. **93**(7): p. 2419-2438.

28. Petersson, G.A., D.K. Malick, W.G. Wilson, J.W. Ochterski, J.A. Montgomery, and M.J. Frisch, *Calibration and comparison of the Gaussian-2, complete basis set, and density functional methods for computational thermochemistry*. J Chem Phys, 1998. **109**(24): p. 10570-10579.

29. *A Guide to the NIST Chemistry WebBook*, http://webbook.nist.gov/chemistry/site-cal.html. 2009: NIST.

30. Fenwick, J.O., D. Harrop, and A.J. Head, *Thermodynamic Properties of Organic Oxygen Compounds .41. Enthalpies of Formation of 8 Ethers.* J Chem Thermodyn, 1975. **7**(10): p. 943-954.

31. Pilcher, G., D.J. Coleman, and A.S. Pell, *Measurements of Heats of Combustion by Flame Calorimetry .2. Dimethyl Ether Methyl Ethyl Ether Methyl N-Propyl Ether Methyl Isopropyl Ether.* T Faraday Soc, 1964. **60**(4953): p. 499.

32. Colomina, M., A.S. Pell, H.A. Skinner, and D.J. Coleman, *Heats of Combustion of 4 Dialkylethers.* T Faraday Soc, 1965. **61**(516P): p. 2641.

33. Murrin, J.W.G., S., *Determination of the C-O bond energy from the heats of combustion of four aliphatic ethers.* NAVORD Report No. 5491, U.S. Naval Powder Factory Res. & Dev. Dept., 1957: p. 1-14.

34. Steele, W.V., R.D. Chirico, S.E. Knipmeyer, A. Nguyen, and N.K. Smith, *Thermodynamic properties and ideal-gas enthalpies of formation for butyl vinyl ether, 1,2-dimethoxyethane, methyl glycolate, bicyclo[2.2.1]hept-2-ene, 5-vinylbicyclo[2,2.1]hept-2-ene, trans-azobenzene, butyl acrylate, di-tert-butyl ether, and hexane-1,6-diol.* J Chem Eng Data, 1996. **41**(6): p. 1285-1302.

35. Wiberg, K.B., K.M. Morgan, and H. Maltz, *Thermochemistry of Carbonyl Reactions .6. A Study of Hydration Equilibria.* J Am Chem Soc, 1994. **116**(24): p. 11067-11077.

36. Gutner, N.M., N.D. Lebedeva, S.L. Dobychin, and N.N. Kiseleva, *Thermochemical Study of Aliphatic Ethers.* J Appl Chem-Ussr+, 1980. **53**(9): p. 1523-1525.

37. Mansson, M., *Non-bonded oxygen-oxygen interactions in straight-chain compounds.* J. Chem. Thermodyn., 1969: p. 141-151.

38. Mosselman, C. and H. Dekker, *Enthalpies of Formation of N-Alkan-1-Ols.* J Chem Soc Farad T 1, 1975. **71**(3): p. 417-424.

39. Gundry, H.A.H., D.; Head, A.J.; Lewis, G.B., *Thermodynamic properties of organic oxygen compounds. 21. Enthalpies of combustion of benzoic acid, pentan-1-ol, octan-1-ol, and hexadecan-1-ol.* J. Chem. Thermodyn., 1969. **321-332**.

40. Chao, J. and F.D. Rossini, *Heats of Combustion Formation and Isomerization of 19 Alkanols.* J Chem Eng Data, 1965. **10**(4): p. 374.

41. Green, J.H.S., *Thermodynamic properties of the normal alcohols C1-C12.* J. Appl. Chem., 1961. **11**(397-404).

42. Steele, W.V.C., R.D.; Nguyen, A.; Hossenlopp, I.A.; Smith, N.K., *DIPPR PROJECT 871: Determination of ideal-gas enthalpies of formation for key compounds: The 1989 project results.* J. Chem. Thermodyn., 1991. **101-134**.

43. Parks, G.S.M., J.R.; Peterson, P.V., Jr., *Heats of combustion and formation of some organic compounds containing oxygen.* J. Chem. Phys., 1950. **18**: p. 152.

44. R.C., W., *Physical and thermodynamic properties of aliphatic alcohols.* J. Phys. Chem. Ref. Data, 1973. **1**(Suppl.1): p. 1-420.

45. Knauth, P. and R. Sabbah, *Energetics of Intramolecular and Intermolecular Bonds in Omega-Alkanediols .3. Thermochemical Study of 1,6-Hexanediol, 1,7-Heptanediol, 1,8-*

Octanediol, 1,9-Nonanediol, and 1,10-Decanediol at 298.15k. Can J Chem, 1990. **68**(5): p. 731-734.

46. Gardner, P.J. and K.S. Hussain, *Standard Enthalpies of Formation of Some Aliphatic Diols.* J Chem Thermodyn, 1972. **4**(6): p. 819.
47. Miller, P., *The free energy of furfural and some of its derivatives.* Iowa State Coll. J. Sci., 1936. **10**: p. 91-93.
48. Tjebbes, J., *Heats of Combustion of Butanal and Some Related Compounds.* Acta Chem Scand, 1960. **14**(1): p. 180-188.
49. Dubois, J.E. and H. Herzog, *Heats of Formation of Aliphatic Ketones - Structure Correlation Based on Environment Treatment.* Journal of the Chemical Society-Chemical Communications, 1972(16): p. 932.
50. Sellers, P., *Enthalpies of Combustion and Formation of 2-Nonanone and 2-Dodecanone.* J Chem Thermodyn, 1977. **9**(2): p. 139-142.
51. C., S.P., *Enthalpy of formation of 2,2,6,6-tetramethyl-4-heptanone.* Acta Chem. Scand., 1971. **25**: p. 2099-2102.
52. Wiberg, K.B., L.S. Crocker, and K.M. Morgan, *Thermochemical Studies of Carbonyl-Compounds .5. Enthalpies of Reduction of Carbonyl Groups.* J Am Chem Soc, 1991. **113**(9): p. 3447-3450.
53. Buckley, E.C., J.D., *Chemical equilibria. Part 2.-Dehydrogenation of propanol and butanol.* Trans. Faraday Soc., 1967. **63**: p. 895-901.
54. Nicholson, G.R., *The Heats of Combustion of Butanal and Heptanal.* J Chem Soc, 1960(May): p. 2377-2379.
55. Geiseler, V.G.R., M., *Bildungsenthalpien stellungsisomerer n-Alkanderivate. 1. Mitteilung: Bildungsenthalpien des Octanals und der drei isomeren Octanone.* Ber. Bunsen-Ges. Phys. Chem., 1965. **69**: p. 485-488.
56. Adriaans.N, H. Dekker, and J. Coops, *Heats of Combustion of Normal Staturated Fatty Acids and Their Methyl Esters.* Recl Trav Chim Pay-B, 1965. **84**(3): p. 393-407.
57. Hancock, C.K.W., G.M.; Gilby, R.F., *Heats of combustion of five-carbon fatty acids and their methyl and ethyl esters.* J. Phys. Chem. Ref. Data, 1954(58): p. 127-129.
58. Schjanberg, E., *Die verbrennungswarmen und die refraktionsdaten einiger pentensaureeste.* Z. Phys. Chem., 1937(178): p. 274-281.
59. Mansson, M., *Enthalpies of combustion and formation of ethyl propionate and diethyl carbonate.* J. Chem. Thermodyn., 1972(4): p. 865-871.
60. Guthrie, J.P., *Cyclization of glycol monoesters to give hemiorthoesters: a test of the thermochemical method for determining free energies of tetrahedral intermediates.* Can. J. Chem., 1977. **55**: p. 3562-3574.
61. Lebedeva, N.D., *Heats of Combustion of Some Monocarboxylic Acids.* Zh Fiz Khim+, 1964. **38**(11): p. 2648-2651.
62. Fenwick, J.O., D. Harrop, and A.J. Head, *Thermodynamic Properties of Organic Oxygen Compounds .46. Enthalpies of Formation of Ethyl-Acetate and 1-Hexanoic Acid.* J Chem Thermodyn, 1978. **10**(7): p. 687-690.

63. Andon, R.J.L. and J.F. Martin, *Thermodynamic Properties of Organic Oxygen Compounds .40. Heat-Capacity and Entropy of 6 Ethers.* J Chem Thermodyn, 1975. **7**(6): p. 593-606.

64. Chermin, H.A.G., *Thermo data for petrochemicals. Part 27: Gaseous normal aldehydes. The important thermo properties are presented for all the gaseous normal aldehydes from formaldehyde through decaldehyde.* Pet. Refin., 1961. **40**: p. 181-184.

65. Connett, J.E., *Chemical Equilibria .3. Dehydrogenation of Pentan-1-Ol, Pentan-2-Ol, and 3-Methylbutan-2-Ol.* J Chem Soc A, 1970(8): p. 1284-1286.

66. Stull D.R., J., ed. *The Chemical Thermodynamics of Organic Compounds*. Wiley, New York. 1969.

67. Hales, J.L., E.B. Lees, and D.J. Ruxton, *Thermodynamic Properties of Organic Oxygen Compounds .18. Vapour Heat Capacities and Heats of Vaporization of Ethyl Ketone Ethyl Propyl Ketone Methyl Isopropyl Ketone and Methyl Phenyl Ether.* T Faraday Soc, 1967. **63**(536P): p. 1876.

68. Geiseler, G., K. Quitzsch, H.P. Hofmann, and R. Pfestorf, *Heat-Capacity and Heat of Vaporization of Isomeric Butylmethylketones and Propylacetates.* Z Phys Chem-Leipzig, 1973. **252**(3-4): p. 170-176.

69. Connett, J.E., J.F. Counsell, and D.A. Lee, *Thermodynamic Properties of Organic Oxygen Compounds .44. Vapor Heat-Capacities and Enthalpies of Vaporization of Methyl Acetate, Ethyl-Acetate, and Propyl Acetate.* J Chem Thermodyn, 1976. **8**(12): p. 1199-1203.

Chapter 3

Kinetic Modeling of α-Hydrogen Abstractions from Unsaturated and Saturated Oxygenate Compounds by Carbon-Centered Radicals

This chapter includes the following paper:

Paraskevas, P. D.; Sabbe, M. K.; Reyniers, M. F.; Papayannakos, N.; G.B. Marin, Kinetic Modeling of α-Hydrogen Abstractions from Unsaturated and Saturated Oxygenate Compounds by Carbon-Centered Radicals. *Chem Phys Chem* **2014**, *15*, 1849-1866.

3.1 Abstract

Hydrogen abstractions are important elementary reactions in a variety of reacting media at high temperatures in which oxygenates and hydrocarbon radicals are present. Accurate kinetic data are obtained from CBS-QB3 ab initio (AI) calculations by using conventional transition-state theory within the high-pressure limit, including corrections for hindered rotation and tunneling. From the obtained results, a group additive (GA) model is developed that allows the Arrhenius parameters and rate coefficients for abstraction of the α-hydrogen from a wide range of oxygenate compounds to be predicted at temperatures ranging from 300 to 1500 K. From a training set of 60 hydrogen abstractions from oxygenates by carbon-centered radicals, 15 GA values (ΔGAV^os) are obtained for both the forward and reverse reactions. Among them, four ΔGAV^os refer to primary contributions, and the remaining 11 ΔGAV^os refer to secondary ones. The accuracy of the model is further improved by introducing seven corrections for cross-resonance stabilization of the transition state from an additional set of 43 reactions. The determined ΔGAV^os are validated upon a test set of AI data for 17 reactions. The mean absolute deviation of the pre-exponential factors (log*A*) and activation energies (E_a) for the forward reaction at 300 K are 0.238 log(m^3 mol^{-1} s^{-1}) and 1.5 kJ mol^{-1}, respectively, whereas the mean factor of deviation $\langle\rho\rangle$ between the GA-predicted and the AI-calculated rate coefficients is 1.6. In comparison with a compilation of 33 experimental rate coefficients, the $\langle\rho\rangle$ between the GA-predicted values and these experimental values is only 2.2. Hence, the constructed GA model can be reliably used in the prediction of kinetics of α-hydrogen abstraction reactions between a broad range of oxygenates and oxygenate radicals.

3.2 Introduction

The conversion of biomass into fuels, commodities, and specialty chemicals is expected to play an important role worldwide in the coming years due to the increased concern for environmental protection and for security of supply. New technologies and new products will emerge from the need to process biomass. The high oxygen content in biomass results in the production of various oxygenates that are either to be separated from the main stream and used in specific applications or to be further processed and converted into final products. Fundamental kinetic modeling can facilitate the optimization of current technologies and the design of new processes. To simulate the conversion process or the final use of the biomass-derived products, as fuels, knowledge of the kinetic parameters for the most important reaction families is indispensable. Given that hydrogen-abstraction reactions involving oxygenate compounds are conceptually simple and yet play a prominent role in atmospheric and free-radical chemistry of many processes such as pyrolysis, steam cracking and polymerization, kinetic data for this reaction family are important for reaction network generation.

The required thermodynamic and kinetic data for process simulations are scarce, and their experimental determination is not straightforward because of the high reactivity and instability of the oxygenate radicals involved. Moreover, despite the increasing development of computational resources and methods, it is neither possible nor desirable to calculate all required kinetic parameters, in particular for the larger species in the network, from first principles. Because the need for accurate thermodynamic and kinetic data is indispensable a variety of methods has been developed.

These methods could be classified into methods that use kinetic correlations, such as Evans-Polanyi correlations [1, 2], the intersecting parabolas (IP) method [3] and the Blowers and

Masel model [4], and into highly detailed methods based on the structure of the transition state, which are related to Benson's group-additivity method [5, 6]. The former methods correlate the activation energy to the reaction enthalpy, and their main drawbacks are that they can be used only for the prediction of activation energies and that they do not allow the prediction of pre-exponential factors.

Benson's techniques of thermochemical kinetics provided the first framework to estimate rate coefficients on the basis of group-additive (GA) considerations. It was successfully used to determine accurate thermodynamic and kinetic data for reactions involving unsaturated oxygenates [7], peroxy radicals [8] and carbonyl-containing compounds such as aldehydes and ketones [9]. The contribution of Benson's group-additivity method in studying atmospheric [10] and free-radical chemistry of several processes such as pyrolysis [11] and oxidation and combustion [12, 13] is also distinguished. The techniques used are very powerful, and most of them are easily applied by hand on a specific reaction, depending on the available data. However, because implementing them into automatic reaction mechanism building programs is not straightforward, more systematic variants have been developed on the same idea.

The most detailed methods are based on the structure of the transition state such as the structural contribution method of Willems and Froment [14, 15], in which frequency factors and activation energies are calculated by adding contributions to the Arrhenius parameters of a reference reaction, and this accounts for structural differences between the latter and the considered reaction. Sumathi et al. [16-18] introduced a methodology to calculate transition-state theory rate coefficients by calculating the thermochemistry of the reactants and transition state with AI-derived group additivity by using supergroups that encompassed the reactive moiety of the transition-state structure. The major advantage of the supergroup approach is that they can account for contributions originating from interactions from nonadjacent groups.

However, the main limitation of this method is that it covers only hydrogen abstractions by $H^•$ and $^•CH_3$, and the number combinatorially increases if more abstracting radicals are considered. Carstensen and Dean [19] developed rate estimation rules where the pre-exponential factor and the exponent, *n*, in the temperature dependence of the rate expression of a reaction family was determined from a reference reaction or by averaging rate constants of a test set of reactions.

The reaction class transition-state theory developed by Truong [20] is able to predict rate coefficients for hydrogen-abstraction reactions in which the hydrogen is abstracted from alkanes [21], alkenes [22], and alcohols [23, 24]. According to this approach, the rate coefficient of a target reaction can be calculated by the rate coefficient of a reference reaction by multiplying it with four correction factors accounting for symmetry, tunneling, partition function, and potential energy effects. The reaction classes are very narrowly defined and cover hydrogen abstractions from alkanes by $H^•$, $O^•$, $HO^•$, $^•CHO$ and $^•CH_3$; from alkenes by $H^•$ and $HO^•$; and from alcohols by H. Zhang and Truong [25] proposed the extended reaction class transition-state theory, an approach that uses an Evans-Polanyi relationship to estimate reaction barriers and determines pre-exponential factors relative to a well-characterized reference reaction by performing cost-effective molecular mechanics or density functional theory (DFT) calculations.

In this work, the GA method developed by Saeys et al. [26] was adopted. This method determines activation energies of hydrogen-abstraction reactions between hydrocarbons, further extended by Sabbe et al. [27] to include pre-exponential factors also. In this method, the group additivity of enthalpy and entropy for reactants and transition state is reformulated in terms of the difference between transition state and reactants, which leads to direct group additivity for the pre-exponential factor ($\log A$) and activation energy (E_a). Furthermore, relating these GA values for $\log A$ and E_a to a reference reaction for each reaction family reduces the temperature dependence of these GA values to almost nonexistence. In practice, the Arrhenius parameters for a target reaction within a reaction family are obtained by combining the corresponding Arrhenius parameter of the reference reaction with a perturbation term that accounts for the structural differences between the transition-state structure of the target and reference reaction. The adequacy of this group-additivity scheme has been shown to be excellent for the prediction of kinetic parameters for hydrogen abstraction and addition reactions between hydrocarbons [26-28], for 1,2-hydrogen shifts and cyclization reactions of silicon-containing compounds [29-31], and for α-hydrogen abstractions from thiols, sulfides, and thiocarbonyl compounds [32]. Furthermore, this GA scheme has been shown to provide very good results for the simulation of an industrial ethane steam-cracking furnace [33] and for the thermal decomposition of methyl decanoate in a bench-scale pyrolysis setup [34].

The ab initio (AI) computational method used to obtain the GA values was the high-level CBS-QB3 compound method of Montgomery et al. [35]. The accuracy of this method has already been proven for hydrocarbon gas-phase chemistry [36-40], for organosulfur compounds in their gaseous phase [32, 41, 42], and for oxygenates gas-phase chemistry [43]. The results of this work are consistent with previous work for hydrocarbon, organosulfur, and oxygenate radical chemistry and can be implemented in automated reaction network generating programs such as RMG [44] (Reaction Mechanism Generator) and Genesys [45].

The aim of this study was to determine an accurate and consistent set of GA values (ΔGAV^os) for the prediction of Arrhenius parameters of α-hydrogen abstraction reactions between oxygenates by carbon-centered radicals, including a systematic evaluation of the effects of resonance stabilization on the kinetics of the investigated reactions. The temperature range covered was 300-1500 K, which encompasses most chemical applications except for combustion.

First, the activation energies and pre-exponential factors are calculated with the CBS-QB3 composite method by using corrections for one-dimensional hindered rotation (1D-HR) around the transition state and zero-curvature tunneling according to the Eckart scheme [26, 39]. Next, the necessity for including secondary and tertiary contributions was assessed followed by determining the GA values, assuring the constructed model was robust and accurate. Finally, the accuracy of the GA model is assessed by comparison of GA-predicted data with 1) CBS-QB3 obtained data for a validation set of 17 reactions and 2) experimental kinetic data obtained from the literature [46].

3.3 Computational Methods

3.3.1 Rate Coefficients

Rate coefficients were calculated on the basis of the procedure described by Vandeputte et al. [39] by using conventional transition state theory (TST) in the high-pressure limit [eq. (3-1)] [47]:

$$k(T) = \kappa_{\mathrm{Eckart}}(T)\frac{k_{\mathrm{B}}T}{h}\frac{q_{\ddagger}}{q_{\mathrm{A}}q_{\mathrm{B}}}e^{-\frac{\Delta E(0\,\mathrm{K})}{RT}} \qquad (3\text{-}1)$$

in which q is the total partition function per unit volume, k_{B} is the Boltzmann constant, h is the Planck constant, ΔE(0 K) is the electronic zero-point-corrected reaction barrier determined by the CBS-QB3 method of Montgomery et al. [35], and $\kappa_{\mathrm{Eckart}}(T)$ is the Eckart tunneling coefficient. All electronic structure calculations were performed with the Gaussian03 program [48]. Partition functions q were calculated at the B3LYP/6-311G(2d,d,p) level by using a default scale factor of 0.99. The partition function at the transition state was corrected for inharmonic behavior of the rotation around the forming/breaking bond by using the one-dimensional hindered rotor correction (1D-HR) based on the B3LYP/6-31 G(d) energy profile for the internal rotation [49]. Only in cases for which the barrier of rotation was less than 1 kJ mol^{-1}, which typically results in a scattered and discontinuous internal rotation energy profile, was the free rotor approximation applied.

Arrhenius parameters (E_a and log$A$) were obtained from linear least-square regression to AI rate coefficients on the Arrhenius equation [eq. (3-2)]:

$$\ln k = \ln A - \frac{E_a}{RT} \quad (3\text{-}2)$$

in the temperature range T= – 100 K to T= + 100 K with k sampled at intervals of 50 K, with T the temperature of interest. Rate coefficients for all reactions included in this study at temperatures ranging from 300-1500 K are presented in Tables S1-S3 of Appendix B.

3.3.2 Group Additivity Method

The group additivity model used in this work was based on the group-additivity method developed by Benson [6], and this method was appropriate for determining Arrhenius parameters for all reactions within a particular reaction family. The equation used to obtain rate coefficients within the GA method is [eq. (3-3)]:

$$k = \kappa_{Eckart} n_e k_{GA} = \kappa n_e \tilde{A} e^{-\frac{E_a}{RT}} \quad (3\text{-}3)$$

in which κ stands for the tunneling coefficient, n_e is the reaction path degeneracy or number of single events, $\tilde{A}$ is the single-event pre-exponential factor, and E_a is the activation energy. By applying Benson's group-additivity method for transition states, the Arrhenius parameters of a target reaction were calculated by adding perturbations to the Arrhenius parameters of a reference reaction [27]. These added perturbations relate to the structural differences between the transition state of the target reaction and that of the reference reaction.

According to Benson's group-additivity method, a group is defined as a polyvalent atom together with all of its ligands. Groups are hence characterized as X-$(A)_i(B)_j(C)_k(D)_l$ in which X represents the central atom surrounded by *i* A atoms, *j* B atoms, *k* C atoms and *l* D atoms. In this work, distinction was made between different carbon- and oxygen-related groups. The oxygen-related groups studied in this work involve O-centered groups and >C=O (carbonyl) groups, denoted as CO. Different types of carbon-related groups present in this work were distinguished and notated distinctly: sp^3C stands for a single-bonded carbon atom and sp^2C_d stands for a double-bonded carbon atom.

A schematic representation of the transition state of the hydrogen-abstraction reactions studied in this work is presented in Figure 3-1. To extend Benson's group-additivity scheme to transition states of hydrogen-abstraction reactions, two additional central atoms were introduced that were representative of the two atoms between which the hydrogen atom was exchanged [26]. During the reaction, the hydrogen atom migrates from the group on C_2 to the group on C_1. Thus, the carbon atom abstracting the hydrogen atom is labeled with the subscript 1, whereas the atom from which the hydrogen atom is abstracted is labeled by the subscript 2. As a reference reaction, the hydrogen abstraction by methyl from methane was adopted.

The major contributions to the Arrhenius parameters are from the two central groups between which the hydrogen atom is abstracted, and these are referred to as primary contributions. Contributions arising from the X and Y groups in Figure 3-1, that is, the groups adjacent to one of the two groups exchanging a hydrogen atom, are referred to as secondary contributions. Tertiary contributions are interactions that either arise from the K- and L-centered groups (Figure 3-1) with the primary groups or from repulsive/attractive interactions between secondary groups located on opposite sides of the transition state, which are denoted as non-nearest-neighbor interactions (NNIs).

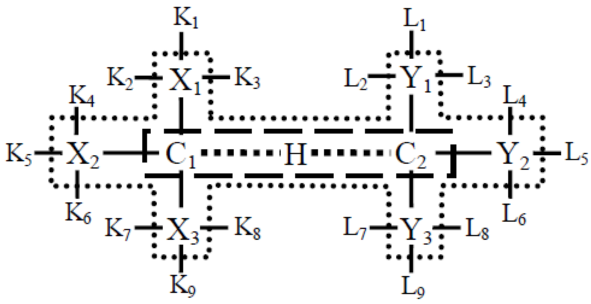

Figure 3-1: Schematic representation of the transition state for the abstraction of a hydrogen atom bonded to a carbon atom (C_2) by a carbon-centered radical ($C_1^{\bullet}$). The dashed line indicates the central atoms of the primary contributions. The dotted line indicates the central atoms of the primary and secondary contributions [32].

On the basis of the additivity of enthalpy, the activation energy of a target reaction can be written as a truncated sum of contributions to the activation energy of a reference reaction $E_{a,\mathrm{ref}}$ [eq. (3-4)] [26, 27]:

$$E_a(T) = E_{\alpha,\mathrm{ref}}\,(T) + \sum_{i=1}^{2} \Delta\mathrm{GAV}^{\mathrm{o}}_{\mathrm{E}_a}(C_i) + \sum_{i=1}^{3} \Delta\mathrm{GAV}^{\mathrm{o}}_{\mathrm{E}_\alpha}(X_i) + \sum_{i=1}^{3} \Delta\mathrm{GAV}^{\mathrm{o}}_{\mathrm{E}_\alpha}(Y_i) + \sum_{i} NNI_i^{o} + \Delta\mathrm{E}^{\mathrm{o}}_{\mathrm{E}_{\mathrm{a,res}}} \tag{3-4}$$

in which the first term refers to the activation energy of the reference reaction, whereas the other terms account for the structural differences between the transition state of the target and the reference reaction. Specifically, the second term refers to primary contributions, the third and fourth term refer to secondary contributions, and the fifth term refers to non-nearest-neighbor contributions. The last term, $\Delta E^{o}_{\alpha,res}$, represents the additional cross-resonance stabilization and hyperconjugative effects due to the simultaneous presence of groups centered on the atoms between which the hydrogen is abstracted and cannot be included in the $\Delta\mathrm{GAV}^{\mathrm{o}}$s.

As a reference reaction, the hydrogen abstraction from methane by methyl was chosen, analogous to the work of Sabbe et al. [27] and Vandeputte et al. [32]. The main advantage of introducing a reference reaction is that the temperature dependence of the activation energy, E_a, is incorporated in $E_{a,res}$ leaving the ΔGAV^{o}s almost temperature independent.

In earlier work [26] non-nearest-neighbor interactions only had a significant influence on the Arrhenius parameters in reactions with severe steric hindrance. In this work, tertiary contributions were neglected without significant influence on the accuracy of the model, because reactions with strong sterical hindrance between the reactants are uncommon in hydrogen-abstraction reactions. Sabbe et al. [27] previously showed that in hydrogen abstractions between hydrocarbons, secondary contributions appeared to be of minor importance and could be neglected, but in the case of organosulfur compounds, as shown by Vandeputte et al. [32], not all secondary contributions are negligible. Given that organosulfur compounds have many similarities with oxygenate compounds, secondary contributions could not a priory be omitted. The necessity of including secondary contributions in α-hydrogen abstractions between oxygenates was evaluated in this work.

Moreover, as the transition state for hydrogen-abstraction reactions originates from the competition between two radicals to bind with the same hydrogen atom, the location of the transition state and its energy depend on the strength of the forming and the breaking bond. Hence, resonance-stabilizing groups adjacent to the central atoms of the transition state greatly affect the kinetics of the particular reaction. In addition, the resonance stabilization of a neighbor group on a radical is accounted for by the primary contribution and hence, $\Delta E^{o}_{a,res}$ accounts for resonance and hyperconjugative effects due to the simultaneous presence of ligands other than H to the central C_1 and C_2 atoms between which the H atom is abstracted.

To illustrate the applicability of a group additive model for hydrogen-abstraction reactions involving oxygenate compounds, abstractions by methyl from the different secondary carbon atoms in 1-butanol were studied. This allowed the effect of a hydroxyl group on hydrogen-abstraction reactions in the *α*, *β*, and *γ* positions of this group to be investigated. The transition-state geometries and the CBS-QB3 barriers are presented in Figure 3-2. For hydrogen abstraction from a carbon atom in the *α*, *β* and *γ* positions of the oxygen atom, electronic barriers of 41.8, 49.2, and 49.5 kJ mol^{-1}, respectively, were retrieved. These data illustrate that an adjacent oxygen atom lowers the activation energy for hydrogen abstraction by approximately 8 kJ mol^{-1}. This decrease in activation energy is limited to the neighboring C atom. The barriers obtained for hydrogen abstraction from the carbon atoms in the *α* and *β* positions of the oxygen atom are in good agreement with the obtained for hydrogen abstraction from propane, that is, 49.0 kJ mol^{-1}. Adjacent oxygen atoms stabilize the forming radical and transition state by the *α* effect, that is, the sharing of its lone electron pair of electrons with a neighboring electron-deficient centre. This results in a stronger C−O bond and a decrease in the C−O bond length. This is also illustrated in Figure 3-2. In the transition states for hydrogen abstraction from carbon atoms in the *β* and *γ* positions of the oxygen atom, the C−O bond length amounts is 143 pm (which is equal to the C−O bond length in 1-butanol), compared to a value of 140 pm in the case of hydrogen abstraction from the carbon atom in the *α* position of the O atom.

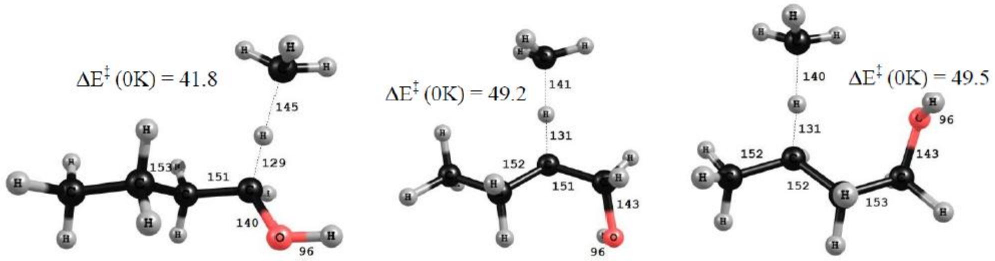

Figure 3-2: B3LYP/6-311G(2d,d,p) transition-state geometries for hydrogen abstractions from butan-1-ol by methyl. Transition states for abstraction from the carbon atom in *α*, *β*, and *γ* position of the hydroxyl group are shown. CBS-QB3 energy barriers Δ*E*‡ (0 K) are indicated in kJ mol^{-1}. Carbon, black, oxygen, red; hydrogen, light gray.

The necessity for including secondary contributions along with the primary ones to describe the transition state of α-hydrogen abstractions from oxygenates by carbon-centered radicals is shown by the abstraction from the carbon atom directly linked to the oxygen atom in methyl acetate (CH_3OCOCH_3) by a methyl radical [$^{\bullet}CH_3$, reaction (R-III)] as an example. The spin density plots presented in Figures 3-3 and 3-4 could be used as a qualitive tool to show that there are indeed fundamental differences on the basis of which the possibility of including secondary contributions and resonance corrections was considered. The actual effect of the possible secondary contributions and resonance corrections will be assessed in the Results section.

$$^{\bullet}CH_3 + CH_4 \leftrightarrow CH_4 + {}^{\bullet}CH_3 \qquad \text{(R-I)}$$

$$^{\bullet}CH_3 + CH_3OH \leftrightarrow CH_4 + {}^{\bullet}CH_2OH \qquad \text{(R-II)}$$

$$^{\bullet}CH_3 + CH_3OCOCH_3 \leftrightarrow CH_4 + {}^{\bullet}CH_2OCOCH_3 \qquad \text{(R-III)}$$

$$^{\bullet}CH_2OH + CH_3OH \leftrightarrow CH_3OH + {}^{\bullet}CH_2OH \qquad \text{(R-IV)}$$

The only primary ΔGAV^o required to model this reaction is the $\Delta GAV^o[C_2\text{-}(O)(H)_2]$, which accounts for the influence of an oxygen ligand on the C_2 group, and it can be derived as the difference between the Arrhenius parameters (E_a and $\log\tilde{A}$) of the hydrogen abstraction from the carbon atom in methanol (CH_3OH) by methyl ($^{\bullet}CH_3$), the reverse reaction of reaction (R-II) and the reference reaction (R-I).

Spin density contour plots and Mulliken atomic spin densities for the transition state of reaction (R-III) are presented in Figure 3-3 along with the corresponding data obtained for reference reaction (R-I) and training reaction (R-II) from which the $\Delta GAV^o[C_2\text{-}(O)(H)_2]$ was derived. From the transition state of the reference reaction presented in Figure 3-3**,** it is clear that the spin is mainly located on the two carbon atoms between which the hydrogen atom is exchanged. In the transition state of training reaction (R-II) in Figure 3-3**,** it can be concluded that the spin delocalization is limited to the oxygen atom next to the carbon radical center, and thus, it was included in the corresponding ΔGAV^{o}. In the transition state of reaction (R-III), the presence of a carbonyl ligand adjacent to the oxygen atom causes an additional spin delocalization, and the atomic spin density is further distributed to the carbonyl group next to the oxygen atom. Hence, the spin density cannot be captured into ΔGAV^{o}[C_2-(O)$(H)_2$] and the introduction of ΔGAV^{o}[O-($^{\bullet}C_2$)(CO)] accounting for the particular secondary contribution was of major importance. Therefore, the inclusion of secondary contributions along with the primary ones was necessary to increase the accuracy of the model.

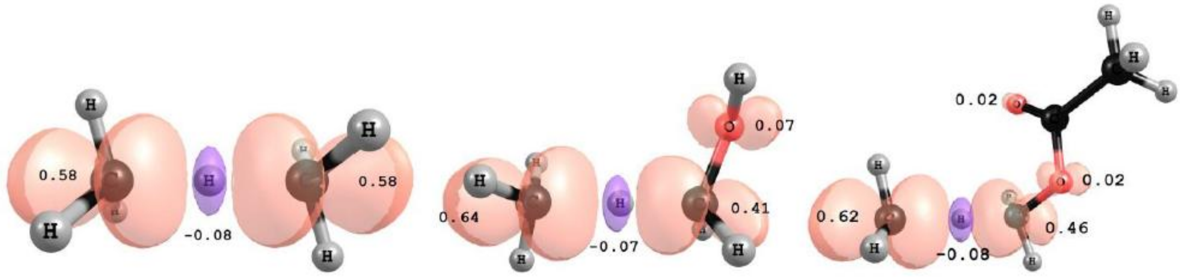

Figure 3-3: Spin density plots and Mulliken atomic spin densities for the transition state of hydrogen abstraction by methyl from methane [reaction (R-I)], by methyl from methanol [reaction (R-II)], and by methyl from methyl acetate [reaction (R-III); B3LYP/6-311G(2d,d,p), contour value=0.005]. Carbon, black, oxygen, red; hydrogen, light gray.

The necessity to include resonance corrections in the modeling of α-hydrogen abstractions from oxygenates by carbon-centered radicals is illustrated by the hydrogen abstraction from the carbon atom in methanol (CH_3OH) by the methanol radical [$^{\bullet}CH_2OH$, reaction (R-IV)].

The two ΔGAV^{o}s that were required to model this reaction are ΔGAV^{o}[C_1-(O)$(H)_2$] and ΔGAV^{o}[C_2-(O)$(H)_2$]. These two ΔGAV^{o}s account for the influence of an oxygen ligand on the C_1 and C_2 groups, respectively. The first one was determined as the difference between the Arrhenius parameters (E_a and log$\tilde{A}$) of the hydrogen abstraction by hydroxymethyl from methane [reaction (R-II)] and the corresponding Arrhenius parameters of reference reaction (R-I), which is the hydrogen abstraction by methyl from methane. Similarly, the $\Delta GAV^o[C_2-(O)(H)_2]$ was derived from the reverse of reaction (R-II) and reference reaction (R-I).

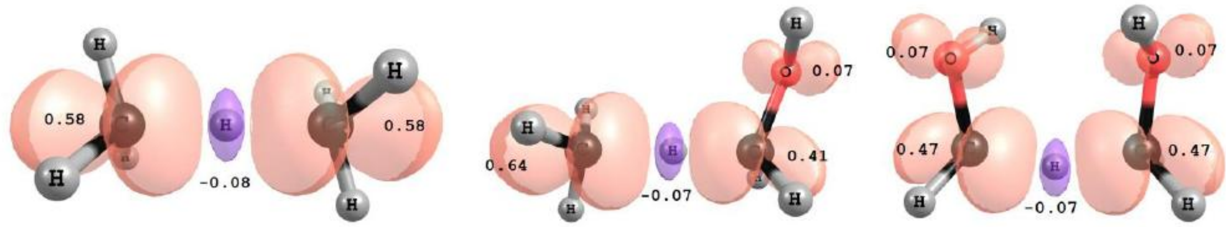

Figure 3-4. Spin-density plots and Mulliken atomic spin densities for the transition state of hydrogen abstraction by methyl from methane [reaction (R-I)], by methyl from methanol [reaction (R-II)], and hydrogen abstraction by hydroxymethyl from methanol [reaction (R-IV); (B3LYP/6-311G(2d,d,p), contour value=0.005). Carbon, black, oxygen, red; hydrogen, light gray.

Spin density contour plots and Mulliken atomic spin densities for the transition state of the reaction (R-IV) are presented in Figure 3-4, together with the corresponding data obtained for reference reaction (R-I) and training reaction (R-II) from which the ΔGAV^os were derived. From the transition state of the reference reaction presented in Figure 3-4**,** it can be concluded that the spin is mainly located on the two carbon atoms between which the hydrogen atom is exchanged. On the basis of the transition state of training reaction (R-II), the Mulliken atomic spin density on the carbon atom was found to be 0.41, whereas that on the neighboring oxygen atom was 0.07. This spin delocalization was captured by the particular ΔGAV^o, as it is limited to the oxygen atom adjacent to the carbon radical center. In the transition state of reaction (R-IV) presented in Figure 3-4**,** the simultaneous presence of oxygen ligands on both primary groups alters the spin distribution on both primary groups and is involved in the delocalization of the unpaired electron in the transition state. Hence, the spin density is distributed over the two carbon atoms exchanging the hydrogen atom and their adjacent oxygen atoms. This effect cannot be captured within the GA values, and therefore, corrections accounting for resonance and/or hyperconjugative effects in the transition state were introduced.

In analogy with eq (3-4), the single-event pre-exponential factor log$\tilde{A}$ of a given reaction can be modeled through the following relationship [eq. (3-5)]:

$$\log\tilde{A}(T) = \log\tilde{A}_{ref}(T) + \sum_{i=1}^{2}\Delta\mathrm{GAV}^{o}_{\log\tilde{A}}(C_i) + \sum_{i=1}^{3}\Delta\mathrm{GAV}^{o}_{\log\tilde{A}}(X_i) + \sum_{i=1}^{3}\Delta\mathrm{GAV}^{o}_{\log\tilde{A}}(Y_i) + \sum_{i} NNI_i^{o} + \Delta\log\tilde{A}^{o}_{res} \qquad (3\text{-}5)$$

In which the first term, log$\tilde{A}_{ref}(T)$, refers to the single-event pre-exponential factor of the reference reaction, whereas the other terms account for structural differences between the transition state of the target and the reference reaction. Specifically, the second term refers to primary contributions, the third and fourth terms refer to secondary contributions, and the fifth term refers to non-nearest-neighbor contributions. The last term, $\Delta log\tilde{A}^{o}_{res}$, is a correction term that accounts for the effect of transition-state resonance on log$\tilde{A}$.

The single-event pre-exponential factor $\tilde{A}$ was obtained by dividing the pre-exponential factor A with the number of single events, n_e, according to eq (3-6):

$$\log\tilde{A} = \log A - \log n_e \qquad (3\text{-}6)$$

in which the number of single events, n_e, is analogous to the reaction path degeneracy and is given by the following equation, as it is proposed by Pollak and Pechukas [50] and Coulson [51] [eq. (3-7)]:

$$n_e = \frac{n_{\mathrm{opt},\ddagger}}{n_{\mathrm{opt,A}}\,n_{\mathrm{opt,B}}}\frac{\sigma_{\mathrm{A}}\sigma_{\mathrm{B}}}{\sigma_{\ddagger}} \qquad (3\text{-}7)$$

In eq (3-7), σ represents the global symmetry number of the reactants A and B (σ_A and σ_B) and the transition state ($\sigma_{\ddagger}$) and n_{opt} the number of optical isomers (chiral species); a correction factor of 2 accounts for the mixing of optically active species. For symmetric reactions, n_e should be divided by a value of 2 to exclude the influence of the twofold symmetry axis that is present in the transition state and absent along the reaction path. The total symmetry number of a molecule is the product of the external and internal symmetry numbers according to the eq (3-8):

$$\sigma = \sigma_{ext} \prod \sigma_{\text{int},i} \qquad (3\text{-}8)$$

in which σ_{ext} and $\sigma_{\text{int},i}$ denote the external and internal symmetry numbers.

In this study primary and secondary contributions were calculated simultaneously by using unweighed least-square analysis, which minimized the following objective function [eq. (3-9)]:

$$SSQ = \sum^{n} (y_i - \hat{y}_i) \qquad (3\text{-}9)$$

in which y_i is the AI-calculated kinetic parameter (activation energy, E_a, or pre-exponential factor, A) and $\hat{y}_i$ is the group-additivity calculated value.

Next, the GA values assigned to the primary and secondary contributions for the reactions included in the training set were used to calculate resonance corrections. The remaining deviations between GA predictions and AI values for this training set of reactions were used to calculate the resonance corrections by a separate unweighed least-square analysis.

To avoid linear dependencies in the regression described above, the ΔGAV^os for single-event pre-exponential factors ($\log\tilde{A}$) and activation energies (E_a) for three secondary contributions were set to zero. These secondary contributions are the following: O-(C_i)(H), CO-(C_i)(H), C-(C_i)$(H)_3$, which correspond to the secondary contributions with the most hydrogen ligands, an approach consistent with the work of Sabbe et al. [27] and Vandeputte et al. [32]. Additionally, ΔGAV^os for six primary contributions [C_i-(C)$(H)_2$, C_i-$(C)_2$(H), C_i-$(C)_3$, C_i-$(C_d)(H)_2$, C_i-(C_d)(C)(H) and C_i-$(C_d)(C)_2$] were taken from the work of Sabbe et al. [27]. These ΔGAV^os for single-event pre-exponential factors ($\log\tilde{A}$) and activation energies (E_a) are provided in Table S4 of Appendix B.

The reported significance F of the regression, mean absolute deviation (MAD), root mean square deviation (RMS), and maximum deviation (MAX) correspond to the differences between the Arrhenius parameters predicted by the additivity method and the corresponding values obtained by CBS-QB3 AI method. The reported significance F of the regression is calculated as [eq. (3-10)]:

$$F = \frac{\sum_{i=1}^{n} \hat{y}_i^2 \Big/ p}{\sum_{i=1}^{n} (\hat{y}_i - y_i)^2 \Big/ (n-p)} \tag{3-10}$$

In which y is the CBS-QB3 AI Arrhenius parameter (activation energy or single-events pre-exponential factor), $\hat{y}$ the corresponding Arrhenius parameter predicted by our AI group-additivity method, n is the number of molecules in the regression, and p the number of parameters, that is, the number of estimated ΔGAV^os or resonance corrections.

The accuracy of the GA method implemented in this study was assessed by comparison of GA-predicted rate coefficients with AI-calculated and experimentally obtained rate coefficients. As a measure for the deviation between these values, a factor ρ was defined according to eq (3-11) completely in line with previous work [27, 28, 32, 38].

$$\begin{cases} \rho = \dfrac{k_{\mathrm{AI}}}{k_{\mathrm{GA}}} & k_{\mathrm{AI}} > k_{\mathrm{GA}} \\ \rho = \dfrac{k_{\mathrm{GA}}}{k_{\mathrm{AI}}} & k_{\mathrm{GA}} > k_{\mathrm{AI}} \end{cases} \tag{3-11}$$

The factor ρ is a value higher than 1 and gives a proper indication of the relative deviation between both rate coefficients. Moreover, it permits a significant arithmetic mean factor of deviation of rate coefficients for a set of reactions, $\langle\rho\rangle$, to be calculated.

3.3.3 Tunneling

Tunneling corrections on the calculated Arrhenius parameters of hydrogen-abstraction reactions have been shown by Vandeputte et al. [39] to be of major importance, particularly at low temperatures. They are strongly temperature dependent and can differ significantly for different reactions within a reaction family. Therefore, the modeling of tunneling would require knowledge of the energy along the reaction path and the imaginary frequency in the transition state, whereas the inclusion of tunneling into the ΔGAV°s would lead to strongly temperature-dependent ΔGAV°s. Given that the knowledge of the energy along a reaction path is practically unfeasible in the framework of group-additivity model and to avoid reporting ΔGAV°s that are only valid in a limited temperature interval, tunneling contributions were excluded from the calculated Arrhenius parameters and modeled separately.

Vandeputte et al. [39] evaluated the performance of three different zero-curvature tunneling methods for hydrogen-abstraction reactions between hydrocarbons: 1) Wigner [52], 2) Skodje and Truhlar (S&T) [53] and 3) Eckart [54]. On the basis of this study [39], at high temperatures all tunneling corrections were in fairly good agreement. However, at temperatures below 500 K the tunneling corrections proposed by Wigner significantly underestimated the tunneling contributions. In comparison to accurate tunneling coefficients calculated by using the centrifugal dominant small-curvature semi-classical (CD-SCS) tunneling method, the S&T tunneling correction slightly overestimated tunneling contributions for temperatures below 400 K, in contrast to the Eckart values. At lower temperatures, the agreement of CBS-QB3-calculated rate coefficients with the experimentally observed ones was also slightly better for the Eckart than the S&T method, though this result may also be dependent on the applied AI method. Therefore, the Eckart tunneling method was applied in this work.

In this work, the Eckart tunneling method was used to determine the tunneling contributions, as this method was shown in previous work [32] to yield adequate results for hydrogen-abstraction reactions. Calculation of the Eckart tunneling coefficients requires information concerning the reaction enthalpy, barrier height, and imaginary frequency for crossing this barrier. Given that 1) tunneling can only occur through the net electronic barrier and 2) within the same reaction family imaginary frequencies and barrier heights are strongly related, the activation energy of the exothermic reaction was considered as one of the main factors determining the tunneling contribution. Sabbe et al. [27] proposed a fourth-order polynomial equation with temperature-dependent coefficients that allowed the tunneling coefficients to be calculated on the basis of the GA-calculated activation energy of the exothermic reaction [eq. (3-12)]:

$$\kappa(T) = 1 + \left(\frac{162}{T}\right)^3 E_{\mathrm{a,exo}} + 2.71 \cdot 10^{-6} \exp\left(-\frac{T-300}{26}\right) E_{\mathrm{a,exo}}^4 \qquad (3\text{-}12)$$

in which $E_{\mathrm{a,exo}}$ is the activation energy for the exothermic reaction in kJ mol^{-1} and T is the temperature in K. In this work, the applicability of eq (3-12) for α-hydrogen abstractions from oxygenates by carbon-centered radicals was assessed. Eckart tunneling coefficients for all reactions considered in this work at temperatures ranging from 300 to 1500 K are provided in Table S5 of Appendix B.

3.4 Results and Discussion

3.4.1 Rate Coefficients and Arrhenius Parameters

The rate coefficients, tunneling coefficients, Arrhenius parameters, and standard reaction enthalpies and entropies over a wide temperature range (300, 600 and 1000 K) are provided in Tables S6−S8 of Appendix B, for a training set of 60 hydrogen-abstraction reactions by methyl radicals, from which the GA values for the primary and secondary contributions ware determined. The 43 reactions from which the influence of resonance stabilization in the transition state was evaluated are tabulated in Tables S9−S11 of Appendix B along with their thermodynamic and kinetic data at the same temperatures.

The reliability of the AI-calculated data was established by comparing the results of the CBS-QB3 AI calculations for three selected hydrogen-abstraction reactions with those obtained by using W1BD [55] calculations. Due to the heavy computational demands of this method, the comparison was limited to small reactions, and hence, only hydrogen abstraction from methane, methanol and ethanol by a methyl radical were included. For these reactions, the CBS-QB3 electronic reaction energies, $\Delta_r E(0\ \mathrm{K})$, were within 1 kJ mol^{-1} of the W1BD results. For electronic reactions barriers, the W1BD barriers were slightly larger than the CBS-QB3 barriers by 2 to 4 kJ mol^{-1}, but this was still within the kcal chemical accuracy range claimed by the CBS-QB3 method.

Additionally, the accuracy of the high-level CBS-QB3 compound method of Montgomery et al. [35] was already shown for the thermochemistry of gas-phase oxygenates in the recent work of Paraskevas et al. [43]. For standard enthalpies of formation, the mean absolute deviation (MAD) between 61 ab initio calculated and experimental values was 1.28 kJ mol^{-1}

only, from which a similar range of accuracy for the reaction enthalpies of the studied reactions in the current work was expected.

Experimental data concerning hydrogen-abstraction reactions between oxygenates and oxygenate radicals are very scarce, and it was possible to retrieve only a limited number of experimental rate coefficients. On the basis of the data available on the NIST Chemical Kinetics Database [46] for hydrogen abstractions by carbon centered-radicals from oxygenates, we collected the reactions in common with the reactions included in the training set of reactions (see Table S6 of Appendix B) to compare the reaction rate coefficients. The experimental rate coefficients reported in this paragraph were also used in the experimental validation set. On the basis of the results of this comparison, it was clear that the experimental rate coefficients were in good agreement with the AI-obtained data. Batt et al. [56] proposed a rate coefficient expression for the 373-473 K temperature range for hydrogen abstraction by methyl from dimethyl ether. The rate coefficient from this work at 400 K was 1.3 m^3 mol^{-1} s^{-1}, which agrees within a factor of 1.4 to the corresponding AI value (9.2 10^{-1} m^3 mol^{-1} s^{-1}) from the Table S1 of Appendix B (reaction 1/6). Arthur and Newitt [57] studied hydrogen abstraction by methyl from methyl acetate and reported rate coefficients in the temperature range from 389 to 497 K. The rate coefficient they reported at 400 K for the creation of the $^{\bullet}CH_2OCOCH_3$ radical was 2.0 10^{-1} m^3 mol^{-1} s^{-1}, which is almost a factor of 2 higher than the AI-calculated value (9.8 10^{-2} m^3 mol^{-1} s^{-1}, reaction 1/11 in Table S1 of Appendix B). To create the $^{\bullet}CH_2COOCH_3$ radical, they reported 3.7 10^{-1} m^3 mol^{-1} s^{-1}, which is almost 2.6 times higher that the corresponding AI (1.4 10^{-1} m^3 mol^{-1} s^{-1}, reaction 1/46, Table S1 of Appendix B). Rate coefficients within the 370-580 K temperature range were reported by Kinsman and Roscoe [58] for hydrogen abstraction by methyl from acetone. The reported rate coefficient was 7.9 10^{-1} m^3 mol^{-1} s^{-1}, which is within a factor of 3.6 higher than the corresponding AI rate coefficient (2.2 10^{-1} m^3 mol^{-1} s^{-1}; reaction 1/31, Table S1 of Appendix B). On the basis of the comparison between the experimentally retrieved data for the absolute values measured directly and the AI-calculated rate coefficients for the same reactions, it was concluded that the AI data determined in the framework of this work could be safely used to determine the GA values.

The training set of 60 reactions for the calculation of the ΔGAV^os involved hydrogen abstraction from alcohols, ethers, esters, ketones, aldehydes, acids, hydroxyperoxides, alkyl peroxides, diketones, unsaturated ketones, and unsaturated ethers, by a methyl radical covered a wide range of hydrogen abstractions from oxygenate compounds by methyl. In all studied reactions, the formed radical center had an oxygen atom or a CO group in the α position of the radical site. The effect of both primary and secondary contributions on the Arrhenius parameters was studied on the basis of the reactions presented in Table S6 of Appendix B, and the ΔGAV^os for the primary and secondary contributions were determined simultaneously by unweighed least-square analysis.

The training set of 43 reactions for the calculation of resonance and hyperconjugative corrections is presented in Table S9 of Appendix B and involves hydrogen abstractions by radicals such as ethyl, allyl, but-1-en-3-yl, hydroxymethyl, 1-hydroxyethyl, propan-2-yl, 3-methylbut-1-en-3-yl, 2-oxoethyl, and 1-oxopropan-2-yl from oxygenate compounds. Due to the simultaneous presence of ligands other than H on the central C_1 and C_2 atoms between which the H atom was exchanged, the kinetic parameters of the studied reactions were strongly affected by resonance and hyperconjugative interactions.

The data presented in Table S6 of Appendix B illustrate that hydrogen abstraction by a methyl radical from a carbon-centered oxygenate radical was generally exothermic and that the reaction enthalpy varied from −21 kJ mol^{-1} for esters (reaction 1/11) to −67 kJ mol^{-1} for diketones (reaction 1/52). This implies that C−H bonds in the *α* position of an oxygen-centered ligand are typically weaker than C−H bonds in methane, and consequently, the formed radicals are more stable than the methyl radical. On the basis of the data presented in Table S9 of Appendix B, it can be concluded that hydrogen abstraction by the ethyl radical, hydroxymethyl or 2-oxomethyl from oxygenate compounds is generally exothermic, whereas hydrogen abstraction by allyl radical, but-1-en-3-yl or 3-me-1-butenerad from oxygenates is generally endothermic.

The reaction entropy range from −44.6 J mol^{-1} K^{-1} (reaction 1/51) to 22.5 J mol^{-1} K^{-1} (reaction 2/42) and provided a general idea of the internal flexibility of the system around the forming and the breaking bonds. At 300 K, the reaction rate for the forward reaction varied from 6 10^{-12} m^3 mol^{-1} s^{-1} for hydrogen abstraction by but-1-en-3-yl from methanol (reaction 2/19) and 3 m^3 mol^{-1} s^{-1} for hydrogen abstraction by methyl from diketones (reaction 1/54). The highest barrier, 95.8 kJ mol^{-1}, was obtained for the reaction forming the $^{\bullet}CH_2OH$ radical in which the hydrogen was abstracted by $CH_2{=}CHCH_2CH_3$ (reaction 2/28), whereas the lowest activation energy, 28.8 kJ mol^{-1}, was caused by the stability of the $CH_3COCOCH^{\bullet}CH_3$ radical (reaction 2/33).

For hydrogen abstraction reactions by a carbon-centered radical from an oxygenate compound the pre-exponential factors fluctuated between 10^2 and 10^6 m^3 mol^{-1} s^{-1}. By comparing the pre-exponential factors between reactions included in Table S6 and those in Table S9 of Appendix B, it is clear that the pre-exponential factors for reactions stabilized by resonance and/or hyperconjugative effects were somewhat lower than the corresponding parameters for non-resonance stabilized reactions.

The results for tunneling coefficients for the hydrogen abstractions by methyl from oxygenates at 300 K ranged significantly between 4.8 and 37.3. This is completely in line with the previous work of Truong et al. [59] and Vandeputte et al. [39], which showed that, especially at lower temperatures, tunneling corrections have a profound effect on the calculated rate coefficients and thereby influence the Arrhenius parameters. Additionally, the same conclusion was reached on the basis of the results for reactions presented in Table S9 of Appendix B where the tunneling coefficients fluctuated from 5.7 to 70.2.

3.4.2 Resonance and Hyperconjugative Interactions

The simultaneous presence of ligands other than H centered on C_1 and C_2 atoms causes cross-resonance and/or cross-hyperconjugation effects in the transition state that cannot be incorporated in the calculated ΔGAV^{o}s, and hence, the usage of additional terms accounting for these effects should be evaluated. The influence of these cross-stabilization effects in hydrogen-abstraction reactions between oxygenate compounds was evaluated on the basis of the results presented in Table S9 of Appendix B and was completely in line with previous work [27, 32]. Generally, resonance effects are stabilizing interactions that result in lowering the activation energy for a given reaction and reducing the pre-exponential factors, as the relative motion of the two reactants in the transition state is hampered.

The training set of 43 reactions provided in Table S9 of Appendix B for the calculation of resonance and hyperconjugative corrections involve hydrogen abstractions by radicals such as ethyl, allyl, but-1-en-3-yl, hydroxymethyl, 1-hydroxyethyl, propan-2-yl, 3-methylbut-1-en-3-yl, 2-oxoethyl, and 1-oxopropan-2-yl from oxygenate compounds. These reactions facilitate the study to the resonance stabilization caused by 1) cross-stability interactions of a carbon-centered ligand on the C_1 atom with hyperconjugating C-H bonds, α-oxygen atoms, α-carbonyl ligands or π-conjugating systems on the C_2 atom, 2) cross-interactions of an oxygen ligand on the C_1 atom with hyperconjugating C-H bonds, α-oxygen atoms or α-carbonyl ligands on the C_2 atom; and 3) cross interactions of a carbonyl group on the C_1 atom with hyperconjugating C−H bonds and α-carbonyl ligands on the C_2 atom.

Along with two corrections determined in a previous work [27] for the stabilization in the transition state due to the simultaneous presence of hyperconjugating and π-conjugating groups on the C_1 and C_2 atoms, in this work seven more correction terms were introduced. The corrections for which values were taken from the work of Sabbe et al. [27] are 1) the interaction of a β C-H bond in the C_1 atom with a β C-H bond in the C_2 atom ($\sigma_{\beta C\text{-}H}$–$\sigma_{\beta C\text{-}H}$) and 2) the interaction of a π-conjugating system on the C_1 atom and a β C-H bond on the C_2 atom ($\pi_{C=C}$–$\sigma_{\beta C\text{-}H}$).

The 7 resonance and hyperconjugative correction terms introduced in this work can be summarized into cross-interactions between 1) an α-oxygen atom and a β C-H bond ($p_{\alpha O}$–$\sigma_{\beta C\text{-}H}$), 2) an α-oxygen atom and a π-conjugating system (both allylic and propargylic or an unsaturated oxygenate, $p_{\alpha O}$–$\pi_{C=C}$), 3) an α-oxygen atom and another α-oxygen atom ($p_{\alpha O}$–$p_{\alpha O}$), 4) an α-oxygen atom and a carbonyl group ($p_{\alpha O}$–$\pi_{C=O}$), 5) a carbonyl group and a π C−H bond ($\pi_{C=O}$–$\sigma_{\beta C\text{-}H}$), 6) a carbonyl group and a C=C group ($\pi_{C=O}$–$\pi_{C=C}$) and 7) a carbonyl group and another carbonyl group ($\pi_{C=O}$–$\pi_{C=O}$). Spin-density plots illustrating the electron delocalization in the transition state for the resonance corrections introduced in this work are presented in Appendix B.

Clearly, stabilizing interactions that act beyond the local groups are present in the transition state of reactions that have multiple ligands other than hydrogen atoms on the C_1 and C_2 atoms between which the hydrogen atom is abstracted. The number of the necessary corrections can be obtained by counting the number of all cross-interactions between the groups centered on the C_1 and C_2 atoms. In the cases of multisubstituted reactants, the application of equations (3-13) and (3-14) proposed by Vandeputte et al. [32] is very important to avoid any omission or overlooking of necessary resonance corrections.

$$n(X-X) = n_{X,C1} n_{X,C2} \qquad (3\text{-}13)$$

$$n(X-Y) = n_{X,C1} n_{Y,C2} + n_{Y,C1} n_{X,C2} \qquad (3\text{-}14)$$

with X, Y = $p_{\alpha O}$, $\sigma_{\beta C-H}$, $\pi_{C=C}$ or $\pi_{C=O}$. $n(X-X)$ in eq (3-13) is the number of resonance corrections needed to describe the cross-interactions caused by the simultaneous presence of the same X ligand on both the C_1 and C_2 atoms. $n(X-Y)$ in eq (3-14) represents the number of cross-interactions between two different ligands, X and Y, on the C_1 and C_2 atoms. $n_{x,C1}$ and $n_{x,C2}$ terms represent the number of X ligands on C_1 and C_2, respectively, whereas $n_{Y,C1}$ and $n_{Y,C2}$ are the number of Y ligands on C_1 and C_2, respectively.

The application of equations (3-13) and (3-14) is shown by using the example of the hydrogen-abstraction reaction by but-1-en-3-yl from ethanol (reaction 2/20, Table S9 of Appendix B) presented in Figure 3-5.

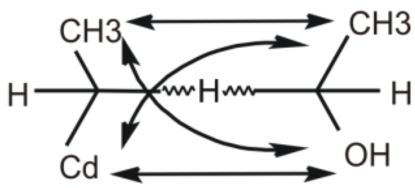

Figure 3-5: Resonance interactions in the transition state of the reaction between but-1-en-3-yl (CH_2=$CHCH^{\bullet}CH_3$) and ethanol (CH_3CH_2OH) (reaction 2/20).

Four types of cross-interactions can be recognized in the transition state presented in Figure 3-5: 1) The interaction between β C-H bond in the C_1 and C_2 atoms of the transition state ($\sigma_{\beta C-H}-\sigma_{\beta C-H}$). 2) The interaction between the β C-H bond in the C_1 atom and an α-oxygen atom ligand in the C_2 atom. 3) The interaction between a π-conjugating system on the C_1 atom and a β C-H bond on the C_2 atom ($\pi_{C=C}-\sigma_{\beta C-H}$). 4) The interaction between a π-conjugating system and an α-oxygen atom ($\pi_{C=C}-p_{\alpha O}$).

The total number of interactions present in the transition state in Figure 3-5 can be verified by using equations (3-13) and (3-14). Equation (3-13) accounts for the number of $\sigma_{\beta C\text{-}H}$–$\sigma_{\beta C\text{-}H}$ corrections ($n_{\sigma\beta C-H,C1} = n_{\sigma\beta C-H,C2} = 1$) and gives the result 1, whereas eq (3-14) provides the number 3, which corresponds to the $\pi_{C=C}$–$\sigma_{\beta C\text{-}H}$, $\pi_{C=C}$–$p_{\alpha O}$ and $\sigma_{\beta C\text{-}H}$–$p_{\alpha O}$ interactions.

3.4.3 Group Additivity Model

The group additivity values (ΔGAV^os) required to describe the kinetics of hydrogen-abstraction reactions between carbon-centered oxygenate radicals, were derived from the Arrhenius parameters of Table S6 of Appendix B. As a reference reaction, the hydrogen abstraction from methane by methyl was chosen to ensure that the ΔGAV°s presented in this work could be combined with those reported in previous work for α-hydrogen abstraction reactions between hydrocarbons [27] and those reported for α-hydrogen-abstraction reactions in thiols, sulfides, and thiocarbonyl compounds [32]. Arrhenius parameters for the reference reaction over a wide range of temperatures 300-1500 K can be found in Table S12 of Appendix B.

The 60 reactions presented in Table S6 of Appendix B are divided into 12 categories of 5 reactions each, and within the same category, all reactions contain the same primary contributions but different secondary contributions. For example, the first category contains alcohols, the second contains ethers, the third contains esters, and so on. If the ΔGAV^os for primary contributions were adequate to describe kinetic parameters for these reactions, then the difference in the activation energies ($E_{a,react}$–$E_{a,ref}$) and single-event pre-exponential factors ($\log\tilde{A}_{react}$–$\log\tilde{A}_{ref}$) would have almost the same values for the reactions having the same primary contribution. From the results of this comparison, it is clear that there are significant deviations between values calculated for reactions with the same primary contributions. Hence, the inclusion of secondary contributions along with the primary ones seems to be of major importance to increase the accuracy of the model. The differences in single-events pre-exponential factors ($\log\tilde{A}_{react}-\log\tilde{A}_{ref}$) and activation energies ($E_{a,react}-E_{a,ref}$) for the forward and reverse reaction for every reaction presented in Table S6 of Appendix B can be found in Tables S13−S15 at 300 K, 600 K, and 1000 K, respectively. Applied symmetry numbers and corresponding reaction path degeneracy for all reactions of Tables S6, S9, 3-5 and 3-6 are presented in Table S16 of Appendix B.

In Table 3-1 ΔGAV^os at 300, 600 and 1000 K for primary and secondary contributions for α-hydrogen abstractions from oxygenates by carbon centered radicals are presented. On the basis of these values, it can be concluded that for the temperature range from 300 K to 1000 K the ΔGAV^os are almost temperature independent (see Figure 3-6). The maximum variation in going from 300 to 1000 K in $\Delta GAV^o_{Ea}(C_1)$ was 3.2 kJ mol^{-1}, whereas in $\Delta GAV^o_{Ea}(C_2)$ it was only 0.6 kJ mol^{-1}. For pre-exponential factors, the maximum variation in $\Delta GAV^o_{log\tilde{A}}(C_1)$ was 0.339 J mol^{-1} s^{-1}, whereas in $\Delta GAV^o_{log\tilde{A}}(C_2)$ it was only 0.083 J mol^{-1} s^{-1}. The largest temperature dependence pertains to ΔGAV^os that correspond to primary contributions, whereas those corresponding to secondary contributions are almost temperature independent. The temperature dependence of the ΔGAV^os for activation energies and pre-exponential factors reported in Table 3-1 is further illustrated in Figure 3-6.

On the basis of the graphs presented in Figure 3-6, it can be concluded that only ΔGAV^os for the C_1 group and for primary contributions appear to have a limited temperature dependence, whereas ΔGAV^os for the secondary contributions are almost temperature independent.

The limited temperature dependence of the $\Delta GAV°$s allows their use over a broad temperature range, in particular at higher temperatures, without losing prediction accuracy. Deviations in $\log\tilde{A}$ and E_a due to the limited temperature dependence of the $\Delta GAV°$s compensate to a large extend for each other resulting in accurate reaction rates.

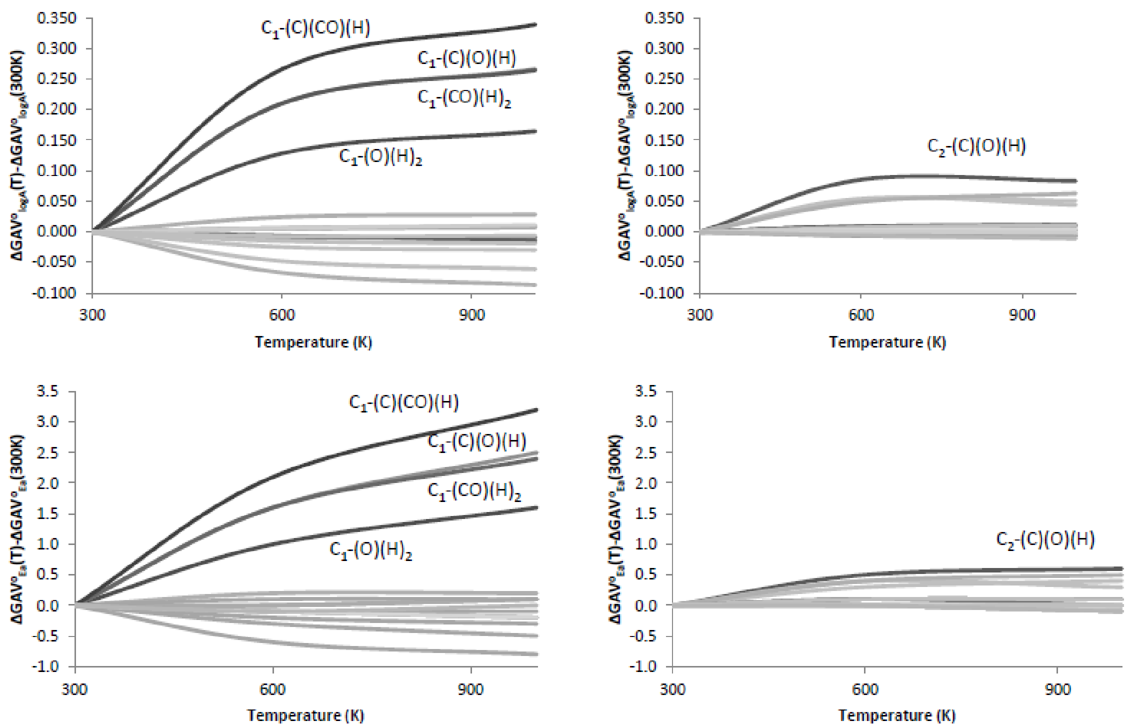

Figure 3-6: Temperature dependence of the 15 ΔGAV°s presented in Table 3-1. C_1 group on the left, C_2 group on the right, for log*A* on the top line and E_a on the bottom line. $\Delta GAV^o_{\log\tilde{A}}$ in log(m^3 mol^{-1} s^{-1}) and ΔGAV^o_{Ea} in kJ mol^{-1}. The grey lines are only included to illustrate the very low temperature dependence of the majority of the groups, while the black lines are the exceptions for which more extreme temperature variations occur.

Table 3-1: ΔGAV°s at 300 K, 600 K and 1000 K for α-hydrogen abstractions from oxygenates by carbon-centered radicals.

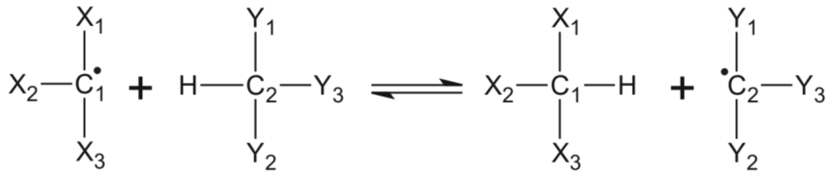

	Forward / ΔGAV° (C_1)						Reverse / ΔGAV° (C_2)					
	300 K		600 K		1000 K		300 K		600 K		1000 K	
Group	log$\tilde{A}$[a]	E_a[b]	log$\tilde{A}$[a]	E_a[b]	log$\tilde{A}$[a]	E_a[b]	log$\tilde{A}$[a]	E_a[b]	log$\tilde{A}$[a]	E_a[b]	log$\tilde{A}$[a]	E_a[b]
Reference Reaction												
$^{\bullet}CH_3 + CH_4$	8.268	69.7	8.865	74.8	9.510	84.4	8.268	69.7	8.865	74.8	9.510	84.4
Primary Contributions												
C_i-(O)(H)$_2$	-0.297	17.2	-0.169	18.2	-0.133	18.8	-0.512	-18.2	-0.46	-17.9	-0.461	-17.8
C_i-(C)(O)(H)	-0.119	17.1	0.091	18.7	0.147	19.6	0.02	-25.6	0.105	-25.1	0.103	-25.0
C_i-(CO)(H)$_2$	-0.097	19.4	0.113	21.0	0.167	21.8	-0.693	-22.8	-0.686	-22.8	-0.699	-22.9
C_i-(C)(CO)(H)	-0.222	32.0	0.044	34.1	0.117	35.2	-0.127	-31.1	-0.073	-30.7	-0.083	-30.8
Secondary Contributions												
O-(C)(C_i)	-0.223	-1.9	-0.232	-2.0	-0.233	-2.0	-0.062	-0.7	-0.053	-0.6	-0.053	-0.7
O-(C_i)(CO)	-0.272	-9.9	-0.339	-10.5	-0.359	-10.7	-0.222	3.7	-0.222	3.7	-0.219	3.7
O-(C_i)(O)	-0.071	-5.7	-0.077	-5.8	-0.086	-5.9	-0.047	1.3	-0.038	1.4	-0.035	1.4
O-(C_i)(C_d)	0.268	-2.1	0.292	-1.9	0.296	-1.9	0.48	6.8	0.529	7.2	0.543	7.3
CO-(C)(C_i)	-0.631	-6.0	-0.656	-6.2	-0.661	-6.3	-0.33	-1.5	-0.329	-1.4	-0.328	-1.4
CO-(C_i)(O)	-0.118	-14.0	-0.166	-14.3	-0.179	-14.5	-0.227	2.0	-0.22	2.1	-0.216	2.1
CO-(C_i)(CO)	0.003	-4.1	0.009	-4.1	0.012	-4.0	-0.389	-7.3	-0.396	-7.3	-0.397	-7.4
CO-(C_i)(C_d)	-0.074	-5.0	-0.089	-5.1	-0.093	-5.2	-0.049	-4.2	-0.046	-4.2	-0.045	-4.2
C-(C)(C_i)(H)$_2$	-0.186	-2.9	-0.181	-2.9	-0.179	-2.8	-0.115	-1.8	-0.118	-1.8	-0.118	-1.8
C-(C)$_2$(C_i)(H)	-0.399	-4.1	-0.393	-4.0	-0.388	-4.0	-0.114	-1.7	-0.113	-1.7	-0.115	-1.8
C-(C)$_3$(C_i)	-0.295	-5.2	-0.302	-5.3	-0.301	-5.2	-0.286	-1.6	-0.292	-1.6	-0.297	-1.7

[a] Units = [log($m^3\ mol^{-1}\ s^{-1}$)]. [b] Units = [$kJ\ mol^{-1}$].

3.4.4 Resonance Corrections

As mentioned in previous section, resonance and hyperconjugative effects are stabilizing interactions in the transition state due to the simultaneous presence of ligands other than the hydrogen atom on the C_1 and C_2 atoms that cannot be included in the GA values. To evaluate the necessity of including resonance and hyperconjugative corrections, the ΔGAV^os determined in the previous step (Table 3-1) were used to predict Arrhenius parameters for the reactions of Table S9 of Appendix B. The deviations in the GA-predicted values from the corresponding AI values for the activation energies and the pre-exponential factors for every reaction included in Table S9 of Appendix B and over a wide temperature range (300 K, 600 K and 1000 K) are provided in Table S17 of Appendix B. On the basis of the statistics of the differences between GA-predicted and AI-calculated values illustrated in Table 3-2 for three different temperatures (300, 600 and 1000 K), it can be concluded that the remaining deviations are significant and the introduction of additional correction parameters is necessary to improve the accuracy of the model.

Table 3-2: Average deviations for the comparison between GA-predicted and AI-calculated values for the reactions of Table S9 of Appendix B by using ΔGAV^os from the Table 3-1[a].

	300 K				600 K				1000 K			
	forward		reverse		forward		reverse		forward		reverse	
	$\log\tilde{A}$[b]	E_a[c]	$\log\tilde{A}$[b]	E_a[c]	$\log\tilde{A}$[b]	E_a[c]	$\log\tilde{A}$[b]	E_a[c]	$\log\tilde{A}$[b]	E_a[c]	$\log\tilde{A}$[b]	E_a[c]
MAD	0.591	7.7	0.583	7.6	0.520	7.0	0.505	6.9	0.496	6.5	0.475	6.5
RMS	0.805	9.8	0.791	9.7	0.680	9.0	0.665	9.0	0.629	8.6	0.608	8.5
MAX	1.986	19.3	2.015	19.4	1.675	18.2	1.723	18.1	1.454	18.5	1.516	18.3

[a] MAD: mean absolute deviation, RMS: root mean square deviation, MAX: maximum deviation). Single-event pre-exponential factors $\log\tilde{A}$ [log(m^3 mol^{-1} s^{-1})] and activation energies E_a (kJ mol^{-1}).
[b] Units = [log(m^3 mol^{-1} s^{-1})].
[c] Units = [kJ mol^{-1}].

From the training set of reactions presented in Table S9 of Appendix B, all possible ΔGAV^os for the primary and secondary contributions were recognized and their values are illustrated in Table 3-1. All possible resonance and hyperconjugative interactions in the transition state were recognized and corrections were introduced for every single interaction.

For the 43 reactions included in Table S9 of Appendix B all possible ΔGAV^{o}s for the primary and secondary contributions describing every single transition state were recognized and their values illustrated in Table 3-1 used. In a next step, the AI-calculated value for every reaction was subtracted from the corresponding GA-predicted value (e.g. $E_{a,GA} - E_{a,AI}$) and the remainder of the subtraction was attributed to the resonance or hyperconjugative effects in the particular transition state. Finally, all corrections needed for a particular transition state were identified by a procedure similar to that described by the equations (3-13) and (3-14). The values of the existent resonance corrections were determined by unweighed least-square analysis, which minimized the objective function [eq. (3-9)]. The results of this regression are presented in Table 3-3. The values for the $\sigma_{\beta C\text{-}H}$–$\sigma_{\beta C\text{-}H}$ and $\pi_{C=C}$–$\sigma_{\beta C\text{-}H}$ corrections were taken from previous work [27].

Table 3-3: Correction factors to account for additional stabilization in the transition state at 300, 600 and 1000 K. Italic values were taken from the work of Sabbe et al. [27].

Entry	Correction	Corresponding structure	300 K log$\tilde{A}$[a]	300 K E_a[b]	600 K log$\tilde{A}$[a]	600 K E_a[b]	1000 K log$\tilde{A}$[a]	1000 K E_a[b]	Average log$\tilde{A}$[a]	Average E_a[b]
1	$\sigma_{\beta C\text{-}H}$–$\sigma_{\beta C\text{-}H}$	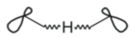	-0.049	-0.3	-0.05	-0.3	-0.051	-0.3	-0.05	-0.3
2	$\pi_{C=C}$–$\sigma_{\beta C\text{-}H}$	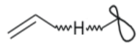	-0.061	-3.4	-0.052	-3.3	-0.053	-3.4	-0.055	-3.4
3	$p_{\alpha O}$–$\sigma_{\beta C\text{-}H}$	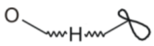	-0.053	-0.4	-0.04	-0.3	-0.04	-0.3	-0.044	-0.3
4	p_{aO}–$\pi_{C=C}$	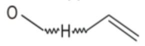	-0.605	-9.0	-0.475	-8.0	-0.454	-7.7	-0.511	-8.2
5	p_{aO}– p_{aO}	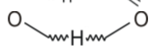	-1.128	-6.5	-0.834	-4.0	-0.717	-2.5	-0.893	-4.3
6	p_{aO}–$\pi_{C=O}$	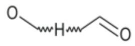	-1.672	-17.6	-1.415	-15.4	-1.258	-13.2	-1.448	-15.4
7	$\pi_{C=O}$–$\sigma_{\beta C\text{-}H}$	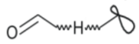	-0.089	-4.8	-0.090	-4.9	-0.093	-4.9	-0.091	-4.9
8	$\pi_{C=O}$–$\pi_{C=C}$	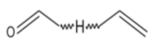	-0.252	-9.4	-0.283	-9.7	-0.297	-9.9	-0.277	-9.7
9	$\pi_{C=O}$–$\pi_{C=O}$		-0.359	-1.5	-0.345	-1.3	-0.348	-1.6	-0.351	-1.5

[a] Units = [log(m^3 mol^{-1} s^{-1})]. [b] Units = [kJ mol^{-1}].

The correction factors applied for the resonance and hyperconjugative effects were generally temperature independent in 300-1000 K range. Only for $p_{\alpha O}$–$p_{\alpha O}$ and $\pi_{C=O}$–$\pi_{C=C}$ [correction factors 5 and 8 from Table 3-3] did there seem to be a temperature dependence for both pre-exponential factors and activation energies. The temperature dependence of the resonance corrections reported in Table 3-3 is further illustrated in Figure 3-7.

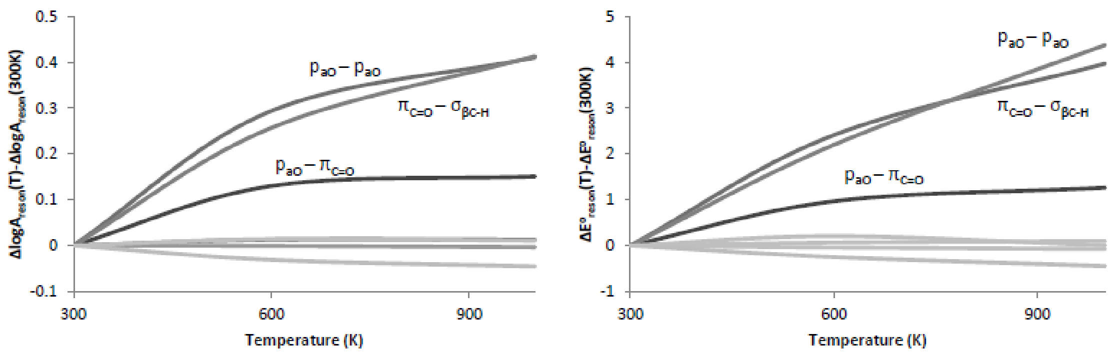

Figure 3-7: Temperature dependence of the seven correction factors for ΔE^{o}_{res} and $\Delta\log A_{res}$ presented in Table 3-3. $\Delta GAV^{o}_{\log\tilde{A}}$ in log(m^3 mol^{-1} s^{-1}) and ΔGAV^{o}_{Ea} in kJ mol^{-1}. Only the most temperature dependent resonance corrections are labeled, whereas the temperature dependence of the other groups is only provided as an indication of the small temperature dependence.

The strongest stabilizing effect was obtained for the cross-interaction of a carbonyl group and a β C−H bond ($\pi_{C=O}$−$\sigma_{\beta C-H}$). Due to this interaction, the activation energy could be lowered to about 18 kJ mol^{-1} at 300 K, whereas the contribution of $\pi_{C=O}$−$\sigma_{\beta C-H}$ to the single-event pre-exponential factor is up to −1.672 log(m^3 mol^{-1} s^{-1}) at 300 K. In contrast, the smallest correction factors were those describing the cross-interaction of an α-oxygen atom and a hyperconjugating β C-H bond ($p_{\alpha O}$−$\sigma_{\beta C-H}$) with a contribution to the activation energy up to −0.4 kJ mol^{-1} at 300 K and to $\log\tilde{A}$ up to −0.053 log(m^3 mol^{-1} s^{-1}) at the same temperature.

In Table S18 of Appendix B the deviations in the comparison between the GA-predicted (with resonance corrections taken from Table 3-3) and AI-calculated pre-exponential factors and activation energies are illustrated at several temperatures (300, 600 and 1000 K). On the basis of the statistics of the differences between the GA-predicted and AI-calculated values provided in Table 3-4 for three different temperatures (300, 600 and 1000 K), it can be concluded that the deviations are much smaller than those of the corresponding values presented in Table 3-2 and, in any case, are within chemical accuracy. Particularly, after introducing resonance corrections, the MAD between the GA-predicted and AI-calculated values dropped for activation energies for the forward reaction from 7.7 kJ mol^{-1} to 1.0 kJ mol^{-1} at 300 K and for pre-exponential factors from 0.591 to 0.192 log(m^3 mol^{-1} s^{-1}) at the same temperature. Thus, the inclusion of resonance corrections is of major importance for an accurate prediction of Arrhenius parameters in hydrogen-abstraction reactions between oxygenates.

Table 3-4: Average deviations between GA-predicted and AI-calculated values for $\Delta\log\tilde{A}$ and ΔE_a in the prediction of the Arrhenius parameters of the reactions of Table S9 of Appendix B after using resonance corrections from Table 3-3[a].

	300 K				**600 K**				**1000 K**			
	forward		**reverse**		**forward**		**reverse**		**forward**		**reverse**	
	log$\tilde{A}$[b]	**E_a[c]**	**log$\tilde{A}$[b]**	**E_a[c]**	**log$\tilde{A}$[b]**	**E_a[c]**	**log$\tilde{A}$[b]**	**E_a[c]**	**log$\tilde{A}$[b]**	**E_a[c]**	**log$\tilde{A}$[b]**	**E_a[c]**
MAD	0.192	1.1	0.209	1.0	0.187	1.0	0.198	1.0	0.184	1.0	0.191	1.0
RMS	0.278	1.3	0.270	1.3	0.267	1.2	0.248	1.3	0.271	1.3	0.238	1.4
MAX	0.988	3.2	0.766	3.5	0.994	2.4	0.621	3.5	0.991	3.2	0.592	3.8

[a] MAD: mean absolute deviation, RMS: root mean square deviation, MAX: maximum deviation). Single-event pre-exponential factors log$\tilde{A}$ [log(m^3 mol^{-1} s^{-1})] and activation energies E_a (kJ mol^{-1}).
[b] Units = [log(m^3 mol^{-1} s^{-1})].
[c] Units = [kJ mol^{-1}].

To illustrate the applicability of the proposed resonance correction method, Arrhenius parameters were calculated for the hydrogen-abstraction reaction from butan-2-one by allyl radical (reaction 2/37, Table S9 of Appendix B) at 300 K:

$$CH_2{=}CHCH_2^{\bullet} + CH_3COCH_2CH_3 \leftrightarrow CH_2{=}CHCH_3 + CH_3COCH^{\bullet}CH_3$$

The transition state of this reaction is presented in Figure 3-8. From this figure, two stabilizing cross-interactions of the transition state can be recognized: the interaction of an allylic fragment (a π-conjugating system) on the C_1 atom with a β C-H bond on the C_2 atom ($\pi_{C=C}$–$\sigma_{\beta C\text{-}H}$) and the interaction of the ethenyl ligand (a π-conjugating system) on the C_1 with a carbonyl ligand on the C_2 atom ($\pi_{C=O}$–$\pi_{C=C}$).

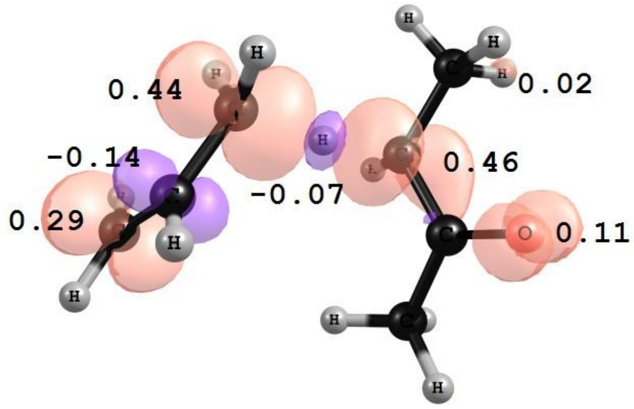

Figure 3-8. Spin-density plot and Mulliken atomic spin densities illustrating the resonance stabilization in the transition state for the hydrogen-abstraction reaction by the allyl radical from butan-2-one [reaction 2/23 from Table S9 of Appendix B; B3LYP/6-311G(2d,d,p), contour value=0.005]. Carbon, black; oxygen, red; hydrogen, light gray.

By using the group additivity model developed in this work, the Arrhenius parameters, activation energy, and pre-exponential factor for the reaction 2/37 were calculated:

$$E_a(300\text{K}) = E_{a,\text{ref}}(300\text{K}) + \Delta\text{GAV}_{E_a}{}^{\circ}(\text{C}_1\text{-(C}_d\text{)(H)}_2) + \Delta\text{GAV}_{E_a}{}^{\circ}(\text{C}_2\text{-(C)(CO)(H)}) + \Delta\text{GAV}_{E_a}{}^{\circ}(\text{C}_d\text{-(C}_1\text{)(H)}) + \Delta\text{GAV}_{E_a}{}^{\circ}(\text{CO-(C}_2\text{)(C)}) + \Delta\text{GAV}_{E_a}{}^{\circ}(\text{C-(C}_2\text{)(H)}_3) + \pi_{C=C}-\sigma_{\beta C\text{-}H} + \pi_{C=O}-\pi_{C=C} = 69.7 + 49.2 - 31.1 + 0 - 1.5 + 0 - 3.4 - 9.4 = 73.5 \text{ kJ mol}^{-1}$$

$$\log A(300\text{K}) = \log\tilde{A}_{\text{ref}}(300\text{K}) + \Delta\text{GAV}_{\log\tilde{A}}{}^{\circ}(\text{C}_1\text{-(C}_d\text{)(H)}_2) + \Delta\text{GAV}_{\log\tilde{A}}{}^{\circ}(\text{C}_2\text{-(C)(CO)(H)}) + \Delta\text{GAV}_{\log\tilde{A}}{}^{\circ}(\text{C}_d\text{-(C}_1\text{)(H)}) + \Delta\text{GAV}_{\log\tilde{A}}{}^{\circ}(\text{CO-(C}_2\text{)(C)}) + \Delta\text{GAV}_{\log\tilde{A}}{}^{\circ}(\text{C-(C}_2\text{)(H}_3\text{)}) + \pi_{C=C}-\sigma_{\beta C\text{-}H} + \pi_{C=O}-\pi_{C=C} + \log(n_e) = 5.268 + 0.097 - 0.127 + 0 - 0.330 + 0 - 0.061 - 0.252 + \log(2) = 4.595 + 0.301 = 4.896$$

in which n_e is the number of single events for the forward reaction[1]. The predicted GA model

----

[1] n_e for this reaction amounts to 4, but is for this comparison taken as 2 since the number of optical isomers are excluded from n_e because log*A* is derived from ab initio data directly and, hence, does not contain any contribution of optical isomers.

values are in very good agreement with the corresponding AI-calculated values 73.9 kJ mol^{-1} and 4.690 $\log(m^3\ mol^{-1}\ s^{-1})$, with deviations [(GA-predicted)−(AI-calculated)] equal to 0.4 kJ mol^{-1} and 0.206 for the activation energies and pre-exponential values, respectively.

3.4.5 Tunneling Model

As mentioned previously, the reported GA values do not include tunneling contributions to avoid strong temperature dependence on the ΔGAV^os. Therefore, a correlation, the fourth-order polynomial with temperature-dependent coefficients developed by Sabbe et al. [27], was used in this work to determine the Eckart tunneling coefficients for hydrogen-abstraction reactions between oxygenates included in Tables S6 and S9 of Appendix B. Eckart tunneling coefficients, determined by eq (3-12), were reproduced on average within a mean factor of deviation, $<\rho>$, of 1.29, 1.09 and 1.02 at 300, 600 and 1000 K, respectively [the ρ factor was determined by using eq (3-11)]. Equation (3-11) provides an indication for the relative deviation between the AI-calculated tunneling coefficients and the predicted values by the fourth-order polynomial. This relative deviation decreased with an increase in the temperature (T), as the tunneling coefficient also decreased with an increase in T.

Figure 3-9 presents the tunneling coefficients for the reactions of the training set included in Tables S6 and S9 of Appendix B versus the AI activation energy of the exothermic reaction, $E_{a,exo}$, at 300 K.

The maximum deviation at 300 K amounted to a factor of 1.8 and was obtained for reaction 51 of Table S6 of Appendix B, the hydrogen abstraction by methyl radical from 2,3-butadione. Additionally, more than 90% of the tunneling coefficients at 300 K were reproduced on average within a factor of 1.6.

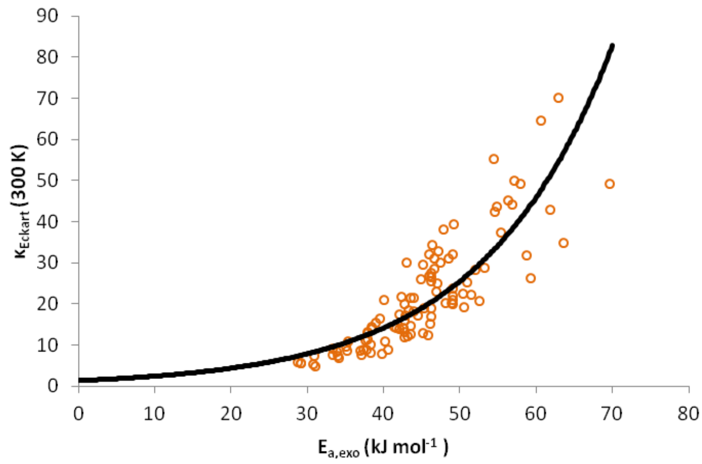

Figure 3-9. Tunneling coefficients as function of the AI activation energy of the exothermic reaction, for the reactions of Tables S6 and S9 of Appendix B (o) and fit from eq (3-12).

3.5 Validation

The validation of the group-additivity model proposed in this work could be achieved either 1) by comparing the GA predictions with the AI values for a validation set containing reactions that have not been used previously for the determination of group additive values or resonance corrections, 2) by comparing these predictions with the predictions of other models such as the Blowers and Masel model [4] and the intersecting parabolas model [3], and (iii) by comparing the GA predictions directly with experimentally obtained data.

3.5.1 Ab Initio Validation

The ab initio validation set consisted of 17 reactions that were representative of the variety of the oxygenate compounds and the resonance corrections that the developed group-additivity model covers. The rate coefficients, Arrhenius parameters, tunneling coefficients, and standard reaction enthalpies and entropies for the AI validation set of 17 α-hydrogen-abstraction reactions between oxygenates by carbon-centered radicals at 300, 600 and 1000 K are provided in Tables S19-S21 of Appendix B, respectively.

Table 3-5 illustrates the performance of the group-additivity model at 300 K, because at lower temperatures the differences between the GA-predicted and the AI-calculated values are expected to be larger due to the strong sensitivity of the activation energies and the tunneling coefficients at that temperature. The MAD for the difference between the GA-predicted and the AI-calculated values for the forward reaction for the pre-exponential factors was 0.238 $\log(m^3\ mol^{-1}\ s^{-1})$, whereas it was 1.5 kJ mol^{-1} for the activation energies. The corresponding deviations for the reverse reactions were 0.247 $\log(m^3\ mol^{-1}\ s^{-1})$ and 1.8 kJ mol^{-1} for the pre-exponential factors and the activation energies respectively. The largest deviation for $\log\tilde{A}$ amounted to an underestimation of 0.652 $\log(m^3\ mol^{-1}\ s^{-1})$ for the AI pre-exponential factor. The largest deviation for the activation energies corresponded to an underestimation of 4.5 kJ mol^{-1} for the AI activation energy. The largest deviations in the pre-exponential factors and activation energies for both the forward and the reverse reactions were observed for the same reaction, the hydrogen abstraction by 2-oxoethyl from ethyl methyl ether (reaction 3/15).

Regarding the rate coefficients, the $<\rho>$ factor [see eq. (3-11)] for the differences between the GA predictions and the AI calculations was 1.6 for the forward reaction and 1.8 for the reverse reaction. The largest deviation was observed for the hydrogen-abstraction reaction by hydroxymethyl from acetone (reaction 3/10) and was within a factor of 2.7 still limited. For the reverse reactions, the largest deviation in the rate coefficients amounted to a ratio of 3.3 for the same reaction (reaction 3/10).

Thermodynamic consistency was preserved for the reactions in which both the reactants and the products were included in the group-additivity training set, that is, the reactions from which the ΔGAV^os were derived. Therefore, the deviation for the forward and reverse

Table 3-5. Comparison between GA and AI kinetic parameters at 300 K for the AI validation set of 17 reactions[a].

	Reactions	κ/κ_{AI}	forward $\Delta\log A$[b]	forward ΔE_a[c]	forward k_{GA}/k_{AI}	reverse $\Delta\log A$[b]	reverse ΔE_a[c]	reverse k_{GA}/k_{AI}
3/1	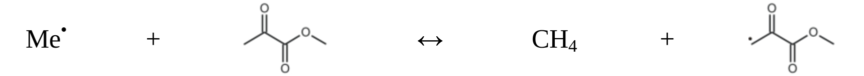	1.6	-0.191	0.3	1.7	0.053	1.7	1.6
3/2	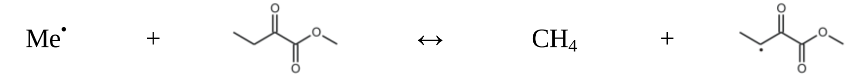	1.7	0.345	0.3	2.0	0.330	-0.4	2.6
3/3		1.2	0.034	1.1	1.4	-0.052	0.7	1.4
3/4	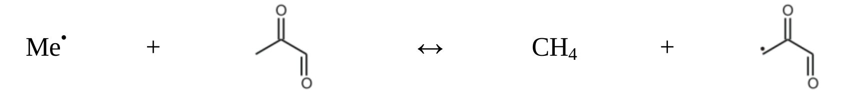	1.7	-0.166	1.0	2.1	0.020	2.7	2.6
3/5		0.6	-0.483	-2.9	1.1	-0.453	-3.7	1.6
3/6	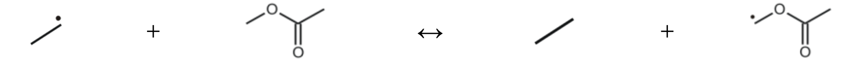	0.9	-0.066	1.4	1.9	0.285	1.6	1.1
3/7		0.6	-0.477	-3.5	1.5	-0.405	-3.0	1.4
3/8		0.6	-0.026	0.2	1.1	-0.292	-0.1	1.8
3/9		0.7	0.065	0.9	1.1	0.065	0.9	1.1
3/10	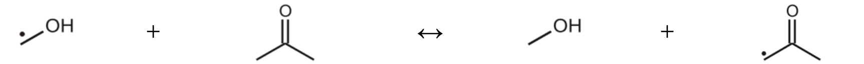	1.5	-0.249	1.2	2.7	-0.417	0.7	3.3
3/11		0.8	-0.182	-2.7	2.1	-0.163	-3.3	2.8
3/12		0.7	-0.124	-0.1	1.2	0.105	1.4	1.3
3/13		1.6	0.467	2.5	1.1	0.458	2.5	1.1
3/14	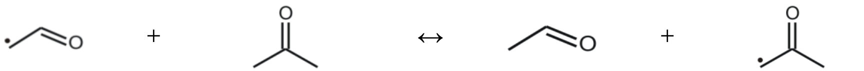	1.6	0.160	2.2	1.6	-0.098	1.7	2.3
3/15		2.0	-0.652	-4.5	1.5	-0.681	-3.8	1.1
3/16		1.0	-0.108	0.6	1.5	-0.138	0.9	1.9
3/17	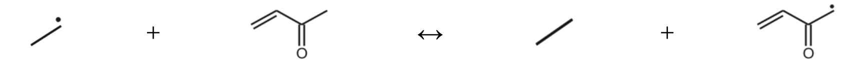	1.3	-0.259	0.7	2.3	-0.191	0.6	1.9
	MAD		0.238	1.5		0.247	1.8	
	RMS		0.298	2.0		0.307	2.1	
	MAX		0.652	4.5	2.7	0.681	3.8	3.3
	<ρ>	1.5			1.6			1.8

[a] $\Delta\log A = \log A_{GA} - \log A_{AI}$; $\Delta E_a = E_{a,GA} - E_{a,AI}$; MAD: mean absolute deviation; RMS: root mean square deviation; MAX: maximum deviation; <ρ> = factor of deviation between two values taken from eq (3-11). [a] Units = [log(m^3 mol^{-1} s^{-1})]. [b] Units = [kJ mol^{-1}].

reaction was expected to be identical. For other radicals not included in the training set, thermodynamic consistency could not be maintained by the group additivity method. Therefore, to maintain thermodynamic consistency in a reaction mechanism it is recommended to estimate the Arrhenius parameters for the exothermic reaction by using the GA scheme, whereas those for the endothermic reaction should be obtained by using the thermodynamic equilibrium coefficient and the corresponding Arrhenius parameter for the exothermic reaction.

Table 3-5 also provides information about the performance of the model-predicted tunneling coefficients by using eq (3-11) and the Eckart's tunneling coefficients. The average deviation between the predicted and Eckart's tunneling coefficient was 1.5 at 300 K, whereas the maximum deviation corresponded to a factor of 2 for the reaction between 2-oxoethyl and ethyl methyl ether (reaction 3/15). At 600 and 1000 K the mean factor of deviation $<\rho>$ of rate coefficients for the forward reaction was 2.2 and 1.8, respectively (see Tables S22 and S23 of Appendix B). Hence, it can be concluded that the group-additivity model developed in this work can provide an accurate prediction for the rate coefficients and the Arrhenius parameters of hydrogen-abstraction reactions included in the AI validation set.

3.5.2 Comparison with other Models

The accuracy of the GA model is compared to the model developed by Blowers and Masel [4] [eq. (3-15)] and the IP model developed by Denisov [3]. The Blowers and Masel model is based on the eq (3-15) for calculating activation energies on the basis of the standard enthalpy of formation of the particular reaction.

$$E_{\mathrm{a}} = \left(\frac{w_{\mathrm{b}} + w_{\mathrm{f}} + \Delta_{\mathrm{r}} H}{2} \right) \frac{\left(V_{\mathrm{p}} - \left(w_{\mathrm{b}} + w_{\mathrm{f}} \right) + \Delta_{\mathrm{r}} H \right)^2}{V_{\mathrm{p}}^2 - \left(w_{\mathrm{b}} + w_{\mathrm{f}} \right)^2 + \Delta_{\mathrm{r}} H^2} \qquad (3\text{-}15)$$

in which w_b corresponds to the bond-dissociation energy of the breaking bond, w_f stands for the bond-dissociation energy of the forming bond and V_p is a parameter related to the intrinsic barrier E_a^o.

The parameters of eq (3-15) were fitted by minimizing the MAD between the predictions of the Blowers and Masel model in the activation energies and the corresponding AI-calculated values for the training set of reactions included in Table S6 of Appendix B. The parameters derived by this fit of parameters were for w_b+w_f=692.4 kJ/mol and for V_P=986.4 kJ/mol. These parameters were used to determine the activation energies for the 17 reactions included in the AI validation set presented in Table 3-5. The MAD for the deviation of the AI-calculated values from the corresponding values predicted by eq (3-15) was 6.6 kJ mol^{-1}, and it is larger than the MAD between the GA-predicted and the AI-calculated values, which amounted to only 1.5 kJ mol^{-1}. Additionally, for 8 out of the 17 reactions included in the particular validation set, the activation energies predicted by the Blowers and Masel model deviated by more than 5 kJ mol^{-1} compared to the corresponding AI values.

The IP model is based on the correlation of the activation energy and the reaction enthalpy, as expressed in eq (3-16):

$$b = a\left(E_a - \Delta_r H^o\right)^{1/2} - E_a^{1/2} \qquad (3\text{-}16)$$

in which α and b are two fitting parameters that relate to the force constants of the broken and formed carbon-hydrogen bond and the hydrogen atom displacement during abstraction.

Completely in line with the previously explained comparison, the parameters of the IP model were fitted by minimizing the MAD between the predictions of the IP model in the activation energies and the corresponding AI-calculated values for the reactions included in the training set of reactions in Table S6 of Appendix B.The minimum MAD between these values was yielded for α = 0.6 and b = 12.1. These values for the parameters were used in eq (3-16) to determine the activation energies for the AI validation set of reactions. The MAD between the IP model predicted and the AI-calculated values was 13.7 kJ mol^{-1}, which is higher than the corresponding MAD between the GA-predicted and the AI-calculated values for the same set of reactions. Moreover, the majority of the activation energies predicted by the IP model deviated more than 5 kJ mol^{-1} compared to the corresponding AI values.

The 17 reactions of the AI validation set presented in Table 3-5 were the reactions used to compare the reliability among the three models. In Figure 3-10, the parity plot for the activation energies at 300 K calculated from CBS-QB3 rate coefficients and those obtained 1) by using the GA method presented in this work, 2) by the Blowers and Masel model with w_f + w_b = 692.4 kJ mol^{-1} and V_p = 986.4 kJ mol^{-1}, and 3) by the intersecting parabolas model with a = 0.6 and b = 12.1 is presented.

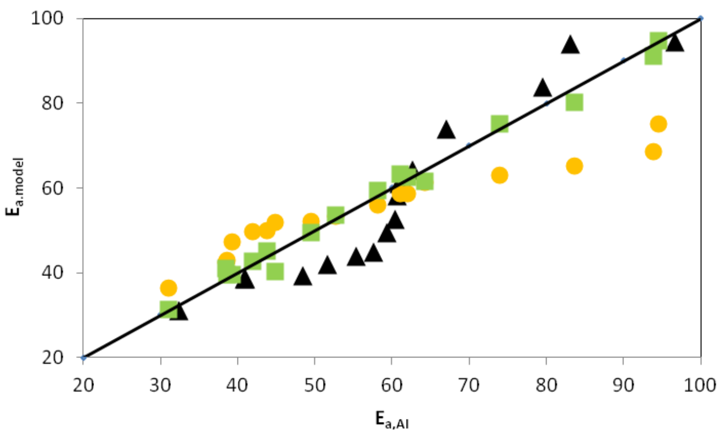

Figure 3-10. Parity plot of the activation energies at 300 K showing the improved performance of the GA model developed in this work (□), in comparison with the Blowers and Masel model with w_f + w_b = 692.4 kJ mol^{-1} and V_p = 986.4 kJ mol^{-1} (Δ) and the intersecting parabolas model with a = 0.6 and b = 12.1 (o). Activation energies, E_a, in kJ mol^{-1}).

3.5.3 Experimental Validation

Experimental values for reaction rates were taken from the NIST Chemical Kinetics Database [46]. Given that reactions between oxygenates and oxygenate radicals were very difficult to retrieve from the Chemical Kinetics Database [46], a limited number of experimental data concerning hydrogen-abstraction reactions between oxygenates was used. Thus, a compilation of 33 experimentally derived rate coefficients for 8 different reactions was used to compare with the results of the GA model and is presented in Table 3-6. In this compilation, the rate coefficients were subdivided into categories on the basis of the data categories provided by the NIST Chemical Kinetics Database [46]. Following this classification, in the current experimental validation set of reaction rates, 7 rate coefficients were absolute values that were measured directly, 1 was from a limited review, and 25 were experimental values derived from fitting to a complex mechanism. All the experimental data referred to hydrogen abstractions by methyl radicals from oxygenate compounds, which implies that only ΔGAV^os and not resonance correction factors were validated by this compilation of experimental data.

The rate coefficients were compared at the temperature within the experimental temperature range, preferably at 300, 600, and 1000 K for which the ΔGAV^os were determined. For experimental temperature ranges not containing the preferred temperatures (300, 600 and 1000 K), the rate coefficients were evaluated at the center of the reported temperature range rounded to the nearest hundred. Arrhenius parameters for the reference reaction over a wide range of temperatures can be found in Table S12 of Appendix B. The ΔGAV^os used were those corresponding to the numerical interpolation between the already determined ΔGAV^os.

Table 3-6. Experimental validation set of 33 experimental reaction rates.[a]

			Reaction					T[b]	k_{exp}[c]	k_{calc}/k_{exp}	ρ
Absolute value measured directly											
1a	$Me^{\bullet}$	+	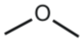	↔	CH_4	+	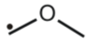	400	$1.3\ 10^{0}$ [56]	0.56	1.8
1b								900	$7.0\ 10^{3}$ [60]	0.37	2.7
2a	$Me^{\bullet}$	+	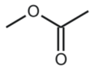	↔	CH_4	+	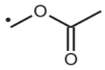	400	$2.0\ 10^{-1}$ [57]	0.37	2.7
3a	$Me^{\bullet}$	+	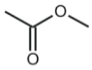	↔	CH_4	+	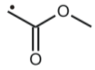	400	$3.7\ 10^{-1}$ [57]	0.75	1.3
4a	$Me^{\bullet}$	+	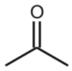	↔	CH_4	+	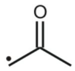	500	$1.1\ 10^{1}$ [58]	0.55	1.8
4b								400	$2.0\ 10^{0}$ [61]	0.29	3.5
4c								400	$4.1\ 10^{0}$ [62]	0.14	7.1
Experimental value and limited review											
1c	$Me^{\bullet}$	+	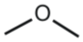	↔	CH_4	+	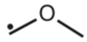	600	$2.6\ 10^{2}$ [63]	0.27	3.7
Experimental value derived from fitting to a complex mechanism											
1d	$Me^{\bullet}$	+	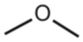	↔	CH_4	+	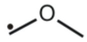	1000	$1.5\ 10^{4}$ [64]	0.37	2.7
1e								500	$1.8\ 10^{1}$ [65, 66]	0.58	1.7
1f								500	$8.6\ 10^{0}$ [67]	1.21	1.2
2b	$Me^{\bullet}$	+	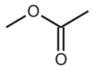	↔	CH_4	+	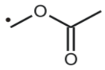	500	$9.9\ 10^{-1}$ [68]	1.34	1.3
3b	$Me^{\bullet}$	+	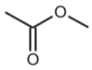	↔	CH_4	+	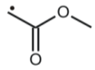	500	$9.8\ 10^{0}$ [68]	0.36	2.8
4d	$Me^{\bullet}$	+	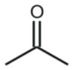	↔	CH_4	+	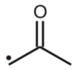	1000	$4.4\ 10^{3}$ [69]	0.76	1.3
4e								900	$5.9\ 10^{3}$ [70]	0.27	3.7
4f								500	$2.3\ 10^{1}$ [71]	0.53	1.9
4g								400	$1.8\ 10^{0}$ [72]	0.64	1.6
4h								500	$2.0\ 10^{1}$ [73]	0.62	1.6
4i								500	$2.4\ 10^{1}$ [74]	0.51	2.0
4j								400	$1.8\ 10^{0}$ [75]	0.65	1.5
4k								500	$1.9\ 10^{1}$ [68]	0.63	1.6
4l								500	$2.1\ 10^{1}$ [76]	0.57	1.7
4m								500	$2.5\ 10^{1}$ [77]	0.49	2.0
4n								500	$1.8\ 10^{1}$ [66, 78]	0.69	1.4
4o								400	$1.4\ 10^{0}$ [79, 80]	0.82	1.2
4p								500	$1.9\ 10^{1}$ [81]	0.63	1.6
4q								500	$1.6\ 10^{1}$ [78]	0.77	1.3
4r								500	$2.6\ 10^{1}$ [79]	0.47	2.1
5	$Me^{\bullet}$	+	CH4	↔	CH_4	+	$Me^{\bullet}$	600	$3.1\ 10^{0}$ [79]	0.71	1.4
6	$Me^{\bullet}$	+	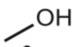	↔	CH_4	+	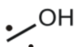	400	$5.0\ 10^{-1}$ [81]	0.69	1.5
7a	$Me^{\bullet}$	+	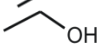	↔	CH_4	+	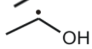	400	$2.0\ 10^{0}$ [66]	3.13	3.1
7b								400	$1.6\ 10^{0}$ [82]	3.91	3.9
8	$Me^{\bullet}$	+	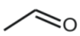	↔	CH_4	+	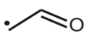	800	$7.5\ 10^{0}$ [83]	0.70	1.4
										$\langle\rho\rangle$	**2.2**

[a] ρ the factor of deviation between two values taken from eq (3-10); $k_{calc} = \kappa\tilde{A}_{GA}\exp(-E_{a,GA}/RT)$.
[b] Units = [K]
[c] Units = [$m^3\ mol^{-1}\ s^{-1}$]

For example, given that the ΔGAV^o of the activation energy of the C_1-(O)(H)$_2$ at 500 K was needed, it was calculated as $[(\Delta GAV^o_{C1\text{-}(O)(H)2}(600\ K) - \Delta GAV^o_{C1\text{-}(O)(H)2}(300\ K)) / 3] \times 2 + \Delta GAV^o_{C1\text{-}(O)(H)2}(300\ K)$, which is equal to $[(18.2-17.2)/3] \times 2 + 17.2 = 0.7 + 17.2 = 17.9$ kJ mol^{-1}. This linear interpolation can slightly improve the accuracy of the prediction, but due to the low T dependence of the ΔGAV^os it was omitted. Thus, there was almost no difference (only 0.3 kJ mol^{-1}) between using this interpolation and taking directly the $\Delta GAV^o_{C1\text{-}(O)(H)2}(600\ K)$.

The mean factor of deviation $<\rho>$ was 2.2; consequently, there was an excellent agreement of the GA prediction with the experimental reaction rate coefficients. In seven out of the eight different reactions, the reaction rates were predicted within a factor of 2 and only in one case (reaction 7) did the $<\rho>$ factor amount to 3.5. The largest deviation observed for the absolute value measured directly by Pritchard et al. [62] for the hydrogen abstraction by methyl from propane-2-one at 400 K (reaction 4c) amounted to a factor of 7.1. Given that for the same reaction there were additional two values measured directly and 15 values derived from fitting to a complex mechanism, for which the mean $<\rho>$ factor amounted to 1.9, it could be concluded that this quite large deviation from the experimental rate coefficient for reaction 4c was not due to limitations in the group-additivity method.

To conclude, the methodology presented in this work allows rate coefficients for hydrogen-abstraction reactions between oxygenates by carbon-centered radicals to be obtained within a mean factor of deviation, $<\rho>$, of 2.2 between the GA predictions and the experimental rate coefficients.

3.6 Conclusion

In this work, a group-additivity model was developed that allowed estimation of the Arrhenius parameters and rate coefficients for α-hydrogen abstractions from oxygenates by carbon-centered radicals in the temperature range from 300 to 1500 K. The GA values (ΔGAV^os) determined cover a wide range of oxygenate compounds such as alcohols, ethers, esters, acids, ketones, diketones, aldehydes, hydroxyperoxides, alkyl peroxides and unsaturated ethers and ketones. This model is a consistent extension of previously constructed models for hydrogen abstractions from hydrocarbons and from thiols, sulfides, and thiocarbonyl compounds towards hydrogen-abstraction reactions between oxygenates.

All kinetic and thermodynamic data were obtained from the accurate CBS-QB3 method, incorporating Eckart tunneling coefficients and corrections for 1D hindered rotation about the forming/breaking bond in the transition state. From an extensive training set, 15 ΔGAV^os were determined, of which 4 were for primary and 11 for secondary contributions. These secondary contributions, which are related to substituents on the substituents of the radical center, were shown to play a significant role, and their inclusion significantly improved the accuracy of the model. The temperature dependence of the ΔGAV^os is very small, in particular the ΔGAV^os for the secondary contributions were as good as temperature independent. This allowed the use of a set ΔGAV^o over a broad temperature range without loss of accuracy.

Resonance and hyperconjugation stabilization of the transition state played a significant role on the energy and the internal flexibility of the transition state. These stabilizing interactions, which pertain to the transition state only, lowered the activation energy and hampered the relative motion of the two reactants in the transition state. Therefore, seven additional correction terms were introduced, which, along with the corresponding correction terms from previous work for hydrogen abstractions from hydrocarbons, could describe this effect, and this resulted in a significant increase in the accuracy of the model. For the prediction of tunneling coefficients, the fourth order polynomial that correlates the tunneling coefficients with the GA activation energy, developed earlier for hydrogen abstractions between hydrocarbons, was shown to perform equally well for hydrogen abstractions between oxygenates.

Using the developed GA scheme, the rate coefficients for 17 reactions of the AI validation set were reproduced on average within a factor of 2 at 300 K, and for a compilation of 33 experimentally determined rate coefficients the mean factor of deviation between the GA prediction, and these experimental values amounts to only 2.2. Furthermore, it was shown that the GA model outperformed the Blowers and Masel and the intersecting parabolas model in the prediction of the activation energies. Hence, the developed model can be reliably applied for the prediction of Arrhenius parameters and reaction rates for a wide variety of gas-phase hydrogen-abstraction reactions between oxygenates by carbon-centered radicals at temperatures ranging from 300 to 1500 K, combining fast prediction with wide applicability.

A future challenge consists in the extension of the current kinetic model concerning hydrogen abstractions involving oxygenates by carbon-centered radicals towards the corresponding abstractions by hydrogen radicals and oxygen-centered radicals.

3.7 References

1. Evans, M.G. and M. Polanyi, *Further Considerations on the Thermodynamics of Chemical Equilibria and Reaction Rates.* Proc. Roy. Soc. A, 1936. **154**: p. 1333-1360.
2. Evans, M.G. and M. Polanyi, *Inertia and Driving Force of Chemical Reactions.* Trans. Faraday Soc., 1938. **1938**(34): p. 11-29.
3. Denisov, E.T., *New Empirical Models of Free Radical Abstraction Reactions.* Usp Khim+, 1997. **66**(10): p. 953-971.
4. Blowers, P. and R. Masel, *Engineering Approximations for Activation Energies in Hydrogen Transfer Reactions.* Aiche J, 2000. **46**(10): p. 2041-2052.
5. Benson, S.W. and J.H. Buss, *Additivity Rules for the Estimation of Molecular Properties. Thermodynamic Properties.* J Chem Phys, 1958. **29**(9): p. 546-561.
6. Benson, S.W., *Thermochemical Kinetics*. 1968, New York: John Wiley & Sons Ltd.
7. Benson, S.W., *Oxygen Initiated Combustion: Thermochemistry and Kinetics of Unsaturated Hydrocarbons.* Int J Chem Kinet, 1996. **28**(9): p. 665-672.
8. Benson, S.W., *Some Observations on the Thermochemistry and Kinetics of Peroxy Radicals.* J Phys Chem-Us, 1996. **100**(32): p. 13544-13547.
9. Benson, S.W., *Some Observations on the Kinetics and Thermochemistry of the Reactions of HO2 Radicals with Aldehydes and Ketones.* Int J Chem Kinet, 2001. **33**(9): p. 509-512.
10. Benson, S.W., *Probing the Chemical Kinetics of Air Pollution.* Environ Sci Technol, 2002. **36**(1): p. 28-32.
11. Shum, L.G.S. and S.W. Benson, *The Pyrolysis of Dimethyl Sulfide, Kinetics and Mechanism.* Int J Chem Kinet, 1985. **17**(7): p. 749-761.
12. Benson, S.W., *Some Key Reactions in Oxidation and Combustion - Thermochemistry and Kinetics.* Abstr Pap Am Chem S, 1982. **183**(Mar): p. 35-41.
13. Benson, S.W., *The Kinetics and Thermochemistry of Chemical Oxidation with Application to Combustion and Flames.* Prog Energ Combust, 1981. **7**(2): p. 125-134.
14. Willems, P.A. and G.F. Froment, *Kinetic Modeling of the Thermal-Cracking of Hydrocarbons .1. Calculation of Frequency Factors.* Ind Eng Chem Res, 1988. **27**(11): p. 1959-1966.
15. Willems, P.A. and G.F. Froment, *Kinetic Modeling of the Thermal-Cracking of Hydrocarbons .2. Calculation of Activation-Energies.* Ind Eng Chem Res, 1988. **27**(11): p. 1966-1971.
16. Sumathi, R., H.H. Carstensen, and W.H. Green, *Reaction Rate Prediction via Group Additivity Part 1: H Abstraction from Alkanes by H and CH3.* J Phys Chem A, 2001. **105**(28): p. 6910-6925.
17. Sumathi, R., H.H. Carstensen, and W.H. Green, *Reaction Rate Prediction via Group Additivity, Part 2: H-Abstraction from Alkenes, Alkynes, Alcohols, Aldehydes and Acids by H Atoms.* J Phys Chem A, 2001. **105**(39): p. 8969-8984.

18. Sumathi, R. and W.H. Green, *Oxygenate, Oxyalkyl and Alkoxycarbonyl Thermochemistry and Rates for Hydrogen Abstraction from Oxygenates.* Phys Chem Chem Phys, 2003. **5**(16): p. 3402-3417.

19. Carstensen, H.H. and A.M. Dean, *Rate Constant Rules for the Automated Generation of Gas-Phase Reaction Mechanisms.* J Phys Chem A, 2009. **113**(2): p. 367-380.

20. Truong, T.N., *Reaction Class Transition State Theory: Hydrogen Abstraction Reactions by Hydrogen Atoms as Test Cases.* J Chem Phys, 2000. **113**(12): p. 4957-4964.

21. Kungwan, N. and T.N. Truong, *Kinetics of the Hydrogen Abstraction CH3 + Alkane -> CH4 Plus Alkyl Reaction Class: An Application of the Reaction Class Transition State Theory.* J Phys Chem A, 2005. **109**(34): p. 7742-7750.

22. Huynh, L.K., S. Panasewicz, A. Ratkiewicz, and T.N. Truong, *Ab Initio Study on the Kinetics of Hydrogen Abstraction for the H+Alkene -> H2+Alkenyl Reaction Class.* J Phys Chem A, 2007. **111**(11): p. 2156-2165.

23. Ratkiewicz, A. and T.N. Truong, *Kinetics of the Hydrogen Abstraction R-OH+H -> R-O-center + H2 Reaction Class.* Int J Chem Kinet, 2010. **42**(7): p. 414-429.

24. Ratkiewicz, A., J. Bieniewska, and T.N. Truong, *Kinetics of the Hydrogen Abstraction R-OH+H -> R-center-OH+H2 Reaction Class: An Application of the Reaction Class Transition State Theory.* Int J Chem Kinet, 2011. **43**(2): p. 78-98.

25. Zhang, S.W. and T.N. Truong, *Kinetics of hydrogen abstraction reaction class H+H-C(sp(3)): First-principles predictions using the reaction class transition state theory.* J Phys Chem A, 2003. **107**(8): p. 1138-1147.

26. Saeys, M., M.F. Reyniers, V. Van Speybroeck, M. Waroquier, and G.B. Marin, *Ab Initio Group Contribution Method for Activation Energies of Hydrogen Abstraction Reactions.* Chem Phys Chem, 2006. **7**(1): p. 188-199.

27. Sabbe, M.K., A.G. Vandeputte, M.F. Reyniers, M. Waroquier, and G.B. Marin, *Modeling the Influence of Resonance Stabilization on the Kinetics of Hydrogen Abstractions.* Phys Chem Chem Phys, 2010. **12**(6): p. 1278-1298.

28. Sabbe, M.K., M.F. Reyniers, M. Waroquier, and G.B. Marin, *Hydrogen radical addition to unsaturated hydrocarbons and reverse beta-scission reactions: modeling of activation energies and pre-exponential factors.* Chemphyschem, 2009. **11**(1): p. 195-210.

29. Adamczyk, A.J., M.F. Reyniers, G.B. Marin, and L.J. Broadbelt, *Kinetics of Substituted Silylene Addition and Elimination in Silicon Nanocluster Growth Captured by Group Additivity.* Chem Phys Chem, 2010. **11**(9): p. 1978-1994.

30. Adamczyk, A.J., M.F. Reyniers, G.B. Marin, and L.J. Broadbelt, *Kinetic Correlations for H2 Addition and Elimination Reaction Mechanisms During Silicon Hydride Pyrolysis.* Phys Chem Chem Phys, 2010. **12**(39): p. 12676-12696.

31. Adamczyk, A.J., M.F. Reyniers, G.B. Marin, and L.J. Broadbelt, *Hydrogenated Amorphous Silicon Nanostructures: Novel Structure-Reactivity Relationships for Cyclization and Ring Opening in the Gas Phase.* Theor Chem Acc, 2011. **128**(1): p. 91-113.

32. Vandeputte, A.G., M.K. Sabbe, M.F. Reyniers, and G.B. Marin, *Kinetics of Alpha Hydrogen Abstractions from Thiols, Sulfides and Thiocarbonyl Compounds.* Phys Chem Chem Phys, 2012. **14**(37): p. 12773-12793.

33. Sabbe, M.K., K.M. Van Geem, M.F. Reyniers, and G.B. Marin, *First Principle-Based Simulation of Ethane Steam Cracking.* Aiche J, 2011. **57**(2): p. 482-496.
34. Pyl, S.P., K.M. Van Geem, P. Puimege, M.K. Sabbe, M.F. Reyniers, and G.B. Marin, *A comprehensive study of methyl decanoate pyrolysis.* Energy, 2012. **43**(1): p. 146-160.
35. Montgomery, J.A., M.J. Frisch, J.W. Ochterski, and G.A. Petersson, *A Complete Basis Set Model Chemistry. VI. Use of Density Functional Geometries and Frequencies.* J Chem Phys, 1999. **110**(6): p. 2822-2827.
36. Sabbe, M.K., M. Saeys, M.F. Reyniers, G.B. Marin, V. Van Speybroeck, and M. Waroquier, *Group additive values for the gas phase standard enthalpy of formation of hydrocarbons and hydrocarbon radicals.* J Phys Chem A, 2005. **109**(33): p. 7466-7480.
37. Sabbe, M.K., F. De Vleeschouwer, M.F. Reyniers, M. Waroquier, and G.B. Marin, *First Principles Based Group Additive Values for the Gas Phase Standard Entropy and Heat Capacity of Hydrocarbons and Hydrocarbon Radicals.* J Phys Chem A, 2008. **112**(47): p. 12235-12251.
38. Sabbe, M.K., A.G. Vandeputte, M.F. Reyniers, V. Van Speybroeck, M. Waroquier, and G.B. Marin, *Ab Initio Thermochemistry and Kinetics for Carbon-Centered Radical Addition and Beta Scission Reactions.* J Phys Chem A, 2007. **111**(34): p. 8416-8428.
39. Vandeputte, A.G., M.K. Sabbe, M.F. Reyniers, V. Van Speybroeck, M. Waroquier, and G.B. Marin, *Theoretical Study of the Thermodynamics and Kinetics of Hydrogen Abstractions from Hydrocarbons.* J Phys Chem A, 2007. **111**(46): p. 11771-11786.
40. Saeys, M., M.F. Reyniers, G.B. Marin, V. Van Speybroeck, and M. Waroquier, *Ab Initio Calculations for Hydrocarbons: Enthalpy of Formation, Transition State Geometry, and Activation Energy for Radical Reactions.* J Phys Chem A, 2003. **107**(43): p. 9147-9159.
41. Vandeputte, A.G., M.F. Reyniers, and G.B. Marin, *A theoretical study of the thermodynamics and kinetics of small organosulfur compounds.* Theor Chem Acc, 2009(123): p. 391-412.
42. Vandeputte, A.G., M.K. Sabbe, M.F. Reyniers, and G.B. Marin, *Modeling the Gas-Phase Thermochemistry of Organosulfur Compounds.* Chem-Eur J, 2011. **17**(27): p. 7656-7673.
43. Paraskevas, P.D., M.K. Sabbe, M.F. Reyniers, N. Papayannakos, and G.B. Marin, *Group Additive Values for the Gas Phase Standard Enthalpy of Formation, Entropy and Heat Capacity of Oxygenates.* Chem-Eur J, 2013. **19**: p. 16431-16452.
44. William H. Green, Joshua W. Allen, Beat A. Buesser, Robert W. Ashcraft, Gregory J. Beran, Caleb A. Class, Connie Gao, C. Franklin Goldsmith, Michael R. Harper, et al., *RMG - Reaction Mechanism Generator v4.0.1*, 2013.
45. Vandewiele, N.M., K.M. Van Geem, M.F. Reyniers, and G.B. Marin, *Genesys: Kinetic Model Construction Using Chemo-Informatics.* Chem Eng J, 2012. **207**: p. 526-538.
46. *Chemical Kinetics Database, NIST Standard Reference Database 17, Version 7.0 (Web Version), Release 1.6.7, Data Version 2013*, 2013.
47. Laidler, K.J., *Chemical Kinetics*. 1987, New York: Harper & Row.
48. Frisch, M.J., G.W. Trucks, H.B. Schlegel, G.E. Scuseria, M.A. Robb, J.R. Cheeseman, J.A. Montgomery, T. Vreven, K.N. Kudin, et al., *Gaussian 03, revision B.03*, 2004, Gaussian, Inc.: Wallingford CT.

49. Van Speybroeck, V., P. Vansteenkiste, D. Van Neck, and M. Waroquier, *Why Does the Uncoupled Hindered Rotor Model Work Well for the Thermodynamics of n-Alkanes?* Chem Phys Lett, 2005. **402**(4-6): p. 479-484.

50. Pollak, E.L.I. and P. Pechukas, *Symmetry Numbers, Not Statistical Factors, Should be Used in Absolute Rate Theory and in Bronsted Relations.* J Am Chem Soc, 1978. **100**(10): p. 2984-2991.

51. Coulson, D.R., *Statistical Factors in Reaction-Rate Theories.* J Am Chem Soc, 1978. **100**(10): p. 2992-2996.

52. Wigner, E., *Calculation of the Rate of Elementary Association Reactions.* J Chem Phys, 1937. **5**: p. 720-725.

53. Skodje, R.T., D.G. Truhlar, and B.C. Garrett, *A General Small-Curvature Approximation for Transition-State-Theory Transmission Coefficients.* J Phys Chem-Us, 1981. **85**(21): p. 3019-3023.

54. Eckart, C., *The Penetration of a Potential Barrier by Electrons.* Phys Rev, 1930. **35**: p. 1303-1309.

55. Barnes, E.C., G.A. Petersson, J.A. Montgomery, M.J. Frisch, and J.M.L. Martin, *Unrestricted Coupled Cluster and Brueckner Doubles Variations of W1 Theory*. J Chem Theory Comput, 2009. **5**(10): p. 2687-2693.

56. Batt L., Alvarado-Salinas G., Reid I.A.B., Robinson C., and S. D.B., *The Pyrolysis of Dimethyl Ether and Formaldehyde.* Symp. Int. Combust. Proc., 1982. **19**.

57. Arthur, N.L. and P.J. Newitt, *Reactions of Methyl Radicals .3. Hydrogen Abstraction from Methyl Acetate and Methyl [H-2(3)] Acetate.* Aust J Chem, 1979. **32**(8): p. 1697-1708.

58. Kinsman, A.C. and J.M. Roscoe, *A Kinetic-Analysis of the Photolysis of Mixtures of Acetone and Propylene.* Int J Chem Kinet, 1994. **26**(1): p. 191-200.

59. Truong, T.N., W.T. Duncan, and M. Tirtowidjojo, *A Reaction Class Approach for Modeling Gas Phase Reaction Rates.* Phys Chem Chem Phys, 1999. **1**(6): p. 1061-1065.

60. Pacey, P.D., *Initial-Stages of Pyrolysis of Dimethyl Ether.* Can J Chem, 1975. **53**(18): p. 2742-2747.

61. March, R.E. and J.C. Polanyi, *Photolysis by Pulsed Illumination.* Proc R Soc Lon Ser-A, 1963. **273**(1352): p. 360.

62. Pritchard, G.O., H.O. Pritchard, and A.F. Trotman-Dickenson, *The reactions of methyl radicals with acetone, diethyl ketone, and di-tert.-butyl peroxide.* J. Chem. Soc., 1954.

63. Zhao, Z., M. Chaos, A. Kazakov, and F.L. Dryer, *Thermal decomposition reaction and a comprehensive kinetic model of dimethyl ether.* Int J Chem Kinet, 2008. **40**(1): p. 1-18.

64. Hidaka, Y., K. Sato, and M. Yamane, *High-Temperature Pyrolysis of Dimethyl Ether in Shock Waves.* Combust Flame, 2000. **123**(1-2): p. 1-22.

65. Arthur, N.L., P. Gray, and A.A. Herod, *Methyl and Trifluoromethyl Radical Attack on Ethers.* Can J Chemistry, 1969. **47**(8): p. 1347-&.

66. Gray, P. and A.A. Herod, *Methyl Radical Reactions with Ethanol and Deuterated Ethanols.* T Faraday Soc, 1968. **64**(546P): p. 1568-&.

67. Loucks, L.F. and K.J. Laidler, *Mercury-Photosensitized Decomposition of Dimethyl Ether .I. Mechanism.* Can J Chemistry, 1967. **45**(22): p. 2763-&.

68. Ferguson, K.C. and J.T. Pearson, *Methyl and Trifluoromethyl Radical Reactions with Methyl Acetate and Deuterated Methyl Acetates.* T Faraday Soc, 1970. **66**(568): p. 910-&.

69. Sato, K. and Y. Hidaka, *Shock-Tube and Modeling Study of Acetone Pyrolysis and Oxidation.* Combust Flame, 2000. **122**(3): p. 291-311.

70. Mousavipour, S.H. and P.D. Pacey, *Initiation and abstraction reactions in the pyrolysis of acetone.* J Phys Chem-Us, 1996. **100**(9): p. 3573-3579.

71. Arican, H. and N.L. Arthur, *Reactions of Methyl Radicals .4. Hydrogen Abstraction from Tetramethylsilane by Methyl Radicals Produced by the Photolysis of Both Acetone and Azomethane.* Aust J Chem, 1983. **36**(11): p. 2185-2194.

72. Duke, M.G. and K.A. Holbrook, *Reactions of Methyl Radicals with Oxetan, 2-Methyloxetan and 2,4-Dimethyloxetan.* J Chem Soc Farad T 1, 1980. **76**: p. 1232-1239.

73. Arthur, N.L. and P.J. Newitt, *Reactions of Methyl Radicals .2. Hydrogen Abstraction from Methyl Trifluoroacetate.* Aust J Chem, 1979. **32**(5): p. 1025-1030.

74. Arthur, N.L. and M.S. Lee, *Reactions of Methyl Radicals .1. Hydrogen Abstraction from Dimethyl Sulfide.* Aust J Chem, 1976. **29**(7): p. 1483-1492.

75. Donovan, T.R., W. Dorko, and A.G. Harrison, *Hydrogen Abstraction from Methyl Formate by Methyl Radicals.* Can J Chemistry, 1971. **49**(6): p. 828-&.

76. Gray, P. and L.J. Leyshon, *Hydrogen Abstraction from Amides - Isotope Effects Reactivity of Different Sites and Secondary Effects in Reaction of Methyl Radicals with Formamide and Acetamide.* T Faraday Soc, 1969. **65**(555P): p. 780-&.

77. Shaw, H. and S. Toby, *Photochemistry of Gaseous Acetone.* J Phys Chem-Us, 1968. **72**(7): p. 2337-&.

78. Thynne, J.C.J. and P. Gray, *Methyl-Radical-Sensitized Decomposition of Gaseous Dimethyl Carbonate.* T Faraday Soc, 1962. **58**(Dec): p. 2403-&.

79. Dainton, F.S. and D.E. Mcelcheran, *The Reaction Ch3 + Cd4-]Ch3d + Cd3.* T Faraday Soc, 1955. **51**(5): p. 657-664.

80. Greig, G. and J.C.J. Thynne, *Hydrogen and Deuterium Atom Abstraction from Trideuteromethyl Mercaptan by Methyl Radicals . Reactivity of Methylthio Radicals.* T Faraday Soc, 1966. **62**(518P): p. 379-&.

81. Shannon, T.W. and A.G. Harrison, *Reaction of Methyl Radicals with Methyl Alcohol.* Can J Chem, 1963. **41**(10): p. 2455-&.

82. Bansal, K.M. and G.R. Freeman, *Gamma Radiolysis of Ethanol Vapor.* J Am Chem Soc, 1968. **90**(26): p. 7183-7189.

83. Laidler, K.J. and M.T.H. Liu, *Mechanism of Acetaldehyde Pyrolysis.* Proc R Soc Lon Ser-A, 1967. **297**(1450): p. 365-&.

Chapter 4

Kinetic Modeling of α-Hydrogen Abstractions from Unsaturated and Saturated Oxygenate Compounds by Hydrogen Atoms

This chapter includes the following paper:

Paraskevas, P. D.; Sabbe, M. K.; Reyniers, M. F.; Papayannakos, N.; G.B. Marin, Kinetic Modeling of α-Hydrogen Abstractions from Unsaturated and Saturated Oxygenate Compounds by Hydrogen Atom. *J Phys Chem A*, **2014**, *118*, 9296-9309.

4.1 Abstract

Hydrogen abstraction reactions play a significant role in thermal biomass conversion processes, as well as regular gasification, pyrolysis or combustion. In this work a group additivity model is constructed that allows prediction of reaction rates and Arrhenius parameters of hydrogen abstractions by hydrogen atoms from alcohols, ethers, esters, peroxides, ketones, aldehydes, acids and diketones in a broad temperature range (300-2000 K). A training set of 60 reactions was developed with rate coefficients and Arrhenius parameters calculated by the CBS-QB3 method in the high-pressure limit with tunneling corrections using Eckart tunneling coefficients. From this set of reactions, 15 group additive values were derived for the forward and the reverse reaction, 4 referring to primary and 11 to secondary contributions. The accuracy of the model is validated upon an ab initio and an experimental validation set of 19 and 23 reactions, respectively, showing that reaction rates can be predicted with a mean factor of deviation of 2 for the ab initio and 3 for the experimental values. Hence, this work illustrates that the developed group additive model can be reliably applied for the accurate prediction of kinetics of α-hydrogen abstractions by hydrogen atoms from a broad range of oxygenates.

4.2 Introduction

Biomass is an important source for renewable energy, and thermally converted biomass can be used as a substitute for fossil fuels. Moreover, energy from biomass conversion has a considerable contribution toward alleviating the impacts on humanity of the greenhouse effects and problems related to climate change. The three main thermal biomass conversion processes are combustion, gasification and pyrolysis, with hydrogen-abstraction reactions playing a dominant role in all three processes. Despite the indisputable importance of oxygenate compounds in biomass, many thermodynamic and kinetic data required for reactor simulations are still lacking or are only inaccurately known. In particular, the complex radical chemistry makes it difficult to extract reliable rate coefficients from experimental data only, since the short-lived radical intermediates lead to large reaction networks and they are not present in the final products.

Because of the rapid increase in computational resources and the accuracy of newly developed levels of theory, computational chemistry offers a reliable complementary tool to experiment, allowing studying the reaction pathways in detail. Even though the computational performance is still increasing, ab initio methods are computationally too demanding to provide the kinetic data for all the reactions in a reaction network; in particular, larger reactants can lead to thousands of reactions. Therefore, methods have been developed that require only a limited set of parameters to predict the kinetics for the thousands of reactions of large radical reaction networks.

The most popular method is the Evans-Polanyi relation [1, 2], which correlates the activation energy with the reaction enthalpy for an homologous set of reactions. Further refinement to the previous method involves the intersecting parabolas (IP) method [3] and the Blowers and

Masel model [4]. The disadvantage of all these methods is that they only provide activation energies.

The thermochemical kinetics framework introduced by Benson [5, 6], based on group additivity, was successfully used in determining thermodynamic and kinetic data for reactions involving unsaturated oxygenates [7], peroxy radicals [8], and carbonyl-containing compounds such as aldehydes and ketones [9]. Benson's group additivity method also made a large contribution to the field of atmospheric [10] and free-radical chemistry, including processes such as pyrolysis [11], oxidation, or combustion [12]. The thermochemical kinetic techniques are versatile, and most are easy to apply by hand on a specific reaction. However, since implementing these techniques in programs for automatic reaction mechanism construction is not straightforward, more systematic variants have been developed on the same idea.

An early systematic structure-based method is the structural contribution method developed by Willems and Froment [13, 14], in which activation energies and frequency factors are calculated by adding contributions that account for structural differences between the target and the reference reaction to the Arrhenius parameters of a reference reaction. Alternatively, Truong [15] used reaction class transition state theory to calculate rate coefficients for hydrogen-abstraction reactions where the hydrogen is abstracted from alkanes [16] by methyl and from alkenes [17] and alcohols [18, 19] by hydrogen atoms. In this approach, the rate coefficient of a target reaction is calculated by multiplying the rate coefficient of a reference reaction with a set of four correction factors that account for effects of electronic barrier, partition function, symmetry, and tunneling. A more Benson-inspired method is that of Sumathi et al. [20-22], who proposed a method to obtain Arrhenius parameters for hydrogen abstractions using supergroups that comprise the whole reactive moiety in the transition state. The main limitation of this method is that it currently only deals with abstractions by $H^\bullet$ and

$^{\bullet}CH_3$, and more importantly, that the number of parameters needed increases combinatorially when more abstracting radicals are considered.

Saeys et al. [23] proposed a group additive method for determining activation energies for hydrogen abstractions between hydrocarbons, which was further extended by Sabbe et al. [24] to include also pre-exponential factors. Within this method, group additive values for Arrhenius parameters are determined in terms of the difference in enthalpy and entropy between transition state and reactants. Since the resulting "kinetic" group additive values are temperature dependent, they are furthermore expressed relative to a reference reaction. For every reaction family, the most simple representative reaction is chosen as a reference reaction. The activation energies and pre-exponential factors of a target reaction are obtained by adding perturbations to the corresponding parameters of the reference reaction, with the perturbation terms referring to the structural differences between the transition states of the studied and the reference reaction, expressed in group additive terms. This method has shown to yield excellent results in predicting rate coefficients for 1,2-hydrogen shifts and cyclization reactions for silicon-containing compounds [25-27], for α-hydrogen abstractions from thiols, sulfides, thiocarbonyl and other sulfur compounds [28, 29] and for α-hydrogen abstractions from oxygenate compounds by carbon-centered radicals [30].

The group additivity based methods discussed above are very promising tools in the sense that they grasp most effects that govern the reaction kinetics, while at the same time, these methods can be easily implemented into existing programs for automated mechanism generation like RMG [31] and Genesys [32].

The aim of this study is to provide an extension to the previously developed models for hydrogen abstractions from hydrocarbons [23, 24], sulfur compounds [28, 29] and oxygenates by carbon-centered radicals [30] toward hydrogen-abstraction reactions involving oxygenates by hydrogen atoms. Particularly, an accurate and consistent set of group additive values (ΔGAV^os) is determined for the prediction of Arrhenius parameters of α-hydrogen abstraction reactions from oxygenates by hydrogen atoms in the temperature range 300-2000 K, which includes most chemical applications. Accurate kinetic data for abstraction by the H radical from oxygenates are very scarce, despite their importance in many free-radical processes. The set of ΔGAV^os will be constructed based on the accurate CBS-QB3 method [33] with rate coefficients obtained in the high pressure limit, and incorporating Eckart tunneling coefficients, similar to earlier work [23, 34]. Finally, the developed group additive model will be evaluated by comparing group additive predictions with both ab initio calculated and experimentally obtained kinetic parameters.

4.3 Computational Methods

4.3.1 Rate Coefficients

Rate coefficients for bimolecular reactions are calculated in the high-pressure limit using the conventional transition state theory (TST) [35] as expressed by eq (4-1):

$$k(T) = \kappa_{\mathrm{Eckart}}(T)\frac{k_{\mathrm{B}}T}{h}\frac{q_{\ddagger}}{q_{\mathrm{A}}q_{\mathrm{B}}}e^{-\frac{\Delta E(0\ \mathrm{K})}{RT}} \qquad (4\text{-}1)$$

In eq (4-1), q is the total partition function per unit volume, k_{B} is the Boltzmann constant, h is the Planck constant, ΔE(0 K) is the electronic reaction barrier determined using the CBS-QB3 method of Montgomery et al. [33], including zero-point corrections, and $\kappa_{\mathrm{Eckart}}(T)$ is the one-dimensional (1D) Eckart [36] tunneling coefficient. Although Eckart tunneling coefficients are zero-curvature, the neglect of curve-crossing is partially compensated for by the narrow barrier, and it is known that they give fairly reliable results at a negligible computational cost

[37]. Because of the metathesis nature of the hydrogen-abstraction reaction, its rate coefficients can be considered to be in the high-pressure limit, and falloff effects should not be accounted for.

All electronic structure calculations are performed with the Gaussian-03 program [38]. Partition functions *q* are obtained at the B3LYP/6-311G(2d,d,p) level using the standard CBS-QB3 scale factor of 0.99, in the rigid rotor and harmonic oscillator approximation and assuming that translational, rotational, rovibrational, and electronic contributions are uncoupled and can be separated. The symmetry numbers for external and internal rotations are included in the partition functions. For the reactants, products, and transition state, the lowest-energy conformer at the B3LYP/6-311G(d,p) level was determined by screening possible conformers, and then, CBS-QB3 was used to obtain electronic energies. Higher-energy conformers were not further included in the evaluation.

It is generally assumed that internal rotational modes that only exist either in the reactants or in the transition state, and in particular the internal rotation around the forming/breaking bond, significantly contribute to the rate coefficient. The contribution of most of the other internal rotations can be considered similar in reactants and the transition state, and these are expected to have a minor effect on the rate coefficient. For the considered reaction family of hydrogen abstractions by the H radical, the abstracting radical is a single atom and there is no internal rotation around the forming/breaking bond. According to the work of Ratkiewicz et al. [19], the contributions of the other internal rotations for reactions of the type R-OH + $H^\bullet \rightarrow R^\bullet$-OH + H_2 were found to be of minor importance. For the hydrogen abstractions considered in this work, this assumption is validated by comparing the rate coefficients for five H-abstraction reactions calculated with the applied harmonic oscillator (HO) approximation with those obtained considering all internal rotations (see Appendix C for a detailed discussion). The difference in rate coefficients calculated using HO and one-dimensional hindered rotor (1-D

HR) approximation is limited even at higher temperature and on average remains within the chemical accuracy that the CBS-QB3 method claims (4 kJ mol^{-1} on the energy, which results in a difference of a factor 2-5 on the rate coefficients in the 300-1000 K range). Therefore, no corrections for internal rotations have been applied in this work.

Although more accurate computational methods might be available, CBS-QB3 was used in this work since it has been shown [37] to yield the most accurate yet cost-effective thermochemical and kinetic data for hydrogen abstractions between hydrocarbons, in a comparison of rate coefficients calculated at the CBS-QB3, G3B3, BMK/6-311G(2d,p,p), and MPW1PW91/6-311G(2d,d,p) level with experiment. Additionally, the CBS-QB3 method has already shown its accuracy for gas-phase oxygenate thermochemistry [39] and for the kinetics of hydrogen abstraction reactions between carbon-centered radicals and oxygenates [30].

For the applied CBS-QB3 method, the reliability can be illustrated for two selected hydrogen abstractions, comparing its results to high-level calculations accounting for variational effects and multidimensional tunneling. The reaction energy ($\Delta_r H^o$) obtained using CBS-QB3 for the reaction $H^\bullet + CH_3OH \rightarrow H_2 + {}^\bullet CH_2OH$ amounts to −35.6 kJ mol^{-1} which is very close to the value of −35.1 kJ mol^{-1} obtained with coupled-cluster theory, CCSD(T)/cc-pVTZ in the study of Carvalho et al. [40]. The CBS-QB3 rate coefficient for the reaction $H^\bullet + CH_3CH_2OH \rightarrow H_2 + CH_3C^\bullet H_2OH$ amounts to 1.8×10^3 m^3 mol^{-1} s^{-1} at 300 K and deviates a factor of 1.6 from the value (1.1×10^3 m^3 mol^{-1} s^{-1} at 300 K) obtained using G2M method incorporating small-curvature tunneling reported in the work of Park et al. [41].

Arrhenius parameters (E_a and log$A$) have been estimated from ab initio rate coefficients using linear least squares regression on the Arrhenius equation, in the temperature range $T \pm 100$ K with k sampled at 50 K intervals.

4.3.2 Group Additivity Method

The group additive model that is applied in this work has its roots in Benson's group additivity method [6], and it allows estimating of the Arrhenius parameters for all reactions within a reaction family based on a limited number of parameters. A detailed description of this Benson's group additive method can be found in earlier work concerning H abstractions from oxygenate compounds by carbon centered radicals [30].

A schematic representation of a transition-state representative for the H abstractions studied in this work is shown in Figure 4-1. In order to enable the application of Benson's group additivity scheme to the transition states studied in this work, the groups centered on atoms H_1 and C_2 between which migration of the hydrogen atom occurs, need to be introduced. Since the hydrogen abstraction from methane by a hydrogen atom is the simplest reaction of the particular reaction family, it is selected as reference reaction. The choice of the simplest reaction of a particular reaction family has the drawback that long-range interactions such as the neighboring-groups effects are not incorporated on this reaction. This is not the case in this work, since for hydrogen abstractions by hydrogen atoms, the reacting compounds are not only very far apart, also the H atom is a very small reaction partner, and consequently, long-range interactions between reactants are not present. The main advantage of introducing a reference reaction is that it yields the ΔGAV^os almost temperature independent by incorporating the temperature dependence of the Arrhenius parameters into the Arrhenius parameters of the reference reaction.

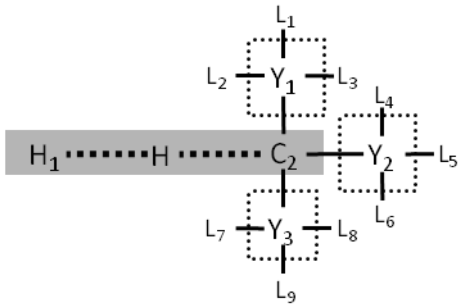

Figure 4-1: Scheme representing the transition state of the abstraction of a hydrogen atom that is bonded to carbon atom C_2 by a hydrogen atom ($H_1^{\bullet}$). The grey zone encompasses the central atoms of the primary contributions. The dotted line indicates the central atoms of the secondary contributions.

A detailed explanation of the types of contributions involved in such a transition state as the one presented in Figure 4-1 can be found in earlier work of H abstractions by carbon-centered radicals from oxygenate compounds [30]. The activation energy and single-event pre-exponential factors can be determined as the difference between the corresponding parameters of the transition state and the reactants. Hence, Arrhenius parameters can be expressed as a sum of contributions added to the corresponding Arrhenius parameters of the reference reaction (eq 4-2).

$$E_{\mathrm{a}}(T) = E_{\mathrm{a,ref}}(T) + \Delta\mathrm{GAV}^{\mathrm{o}}_{\mathrm{Ea}}(C_2) + \sum_{i=1}^{3}\Delta\mathrm{GAV}^{\mathrm{o}}_{\mathrm{Ea}}(Y_i) \tag{4-2}$$

$$\log A(T) = \log \tilde{A}_{ref}(T) + \Delta\mathrm{GAV}^{\mathrm{o}}_{\log\tilde{\mathrm{A}}}(C_2) + \sum_{i=1}^{3}\Delta\mathrm{GAV}^{\mathrm{o}}_{\log\tilde{\mathrm{A}}}(Y_i) + \log n_e$$

In eq (4-2) $E_{\mathrm{a,ref}}(T)$ and $\log\tilde{A}_{ref}(T)$ refer to the corresponding Arrhenius parameters of the reference reaction, $\Delta\mathrm{GAV}^{\mathrm{o}}(C_2)$ and $\Delta\mathrm{GAV}^{\mathrm{o}}(Y_i)$ are the group additive values for the primary and secondary contributions, respectively, and n_e is the number of single events for the particular reaction. The single-event pre-exponential factor $\tilde{A}$ is the pre-exponential factor A divided by the number of single events, n_e, according to eq (4-3):

$$\log \tilde{A} = \log A - \log n_e \tag{4-3}$$

In this work, since the first reactant is a hydrogen atom in all cases, secondary contributions arise only from the groups adjacent to the carbon atom from which the hydrogen is abstracted. The requirement to include secondary contributions for α-hydrogen abstractions by H atoms from oxygenates will be evaluated in this work. Tertiary contributions, which capture non-nearest-neighbor interactions, are less important in this reaction family, since their main contribution, sterical hindrance between the reactants, is absent due to the small nature of the abstracting hydrogen atom [24, 28, 29]. The primary and secondary contributions are determined simultaneously using least-square regression. A detailed description of this applied methodology can be found in earlier work concerning hydrogen abstractions from oxygenate compounds by carbon-centered radicals [30].

As a result of the definition of a group, each group contains information about the neighboring groups, which ultimately leads to linearly dependent subsets in the whole set of groups for this reaction family. Because of the linear dependence between some of the ΔGAV^os for Arrhenius parameters (E_a and $\log\tilde{A}$), three of ΔGAV°s referring to secondary contributions were set equal to zero in the estimation procedure. These ΔGAV^os pertain to the secondary groups O-(C_i)(H), CO-(C_i)(H), and C-(C_i)$(H)_3$: the secondary contributions with the largest number of hydrogen ligands within every linearly dependent subset. This procedure is consistent with previous work [24, 28, 29].

To evaluate the reliability of the group additivity model, a statistical analysis is performed. The reported mean absolute deviation (MAD), root-mean-square deviation (RMS), and maximum deviation (MAX) are calculated based on the differences between the Arrhenius parameters (activation energies, E_a, and single-event pre-exponential factors, $\log\tilde{A}$) predicted by the group additivity method and those obtained from CBS-QB3.

Analogously with previous studies [24, 28-30, 34, 42], the accuracy of the group additive method developed in this study is assessed by comparing group additively predicted rate coefficients with (a) ab initio calculated rate coefficients and (b) experimentally determined rate coefficients from literature. To provide an adequate measure to quantify the deviation between group additive and reference values, an absolute factor of deviation ρ is defined according to eq (4-4).

$$\begin{cases} \rho = \dfrac{k_{\mathrm{AI}}}{k_{\mathrm{GA}}} & k_{\mathrm{AI}} > k_{\mathrm{GA}} \\ \rho = \dfrac{k_{\mathrm{GA}}}{k_{\mathrm{AI}}} & k_{\mathrm{GA}} > k_{\mathrm{AI}} \end{cases} \tag{4-4}$$

The factor ρ is always larger than 1, providing the relative deviation between the rate coefficients. The advantage is that this factor ρ can be averaged out for a set of reactions, leading to a mean factor of deviation of rate coefficients for a set of reactions, $<\rho>$.

4.3.3 Tunneling Corrections

For hydrogen-transfer reactions, in which a very light particle – the H atom − is transferred between two other molecules, the contribution of tunneling to the rate coefficient can be significant [43]. Particularly at lower temperatures, it has a profound effect on the kinetic parameters of hydrogen abstractions [23, 28, 37, 44]. Tunneling contributions are strongly dependent on temperature, and they can differ significantly from reaction to reaction, also within a reaction family. Including tunneling in the ΔGAV°s would cause the ΔGAV°s to depend very strongly on temperature. On the other hand, calculating the tunneling contributions accurately requires at least the energy profile along the reaction path and knowledge of the imaginary frequency in the transition state. Since these properties are not accessible during the application of the group additivity model, and because including tunneling in the ΔGAV°s would cause them to be only valid in a limited temperature interval, tunneling contributions were not included in the calculated Arrhenius parameters but modeled separately.

Tunneling contributions are determined using the 1D Eckart tunneling potential [36]. The Eckart model, as a zero-curvature tunneling method, assumes that the reaction and the tunneling path coincide. The tunneling factor is calculated by fitting an Eckart potential through the zero-point-corrected energies of the reactants, the saddle point, and the products, using the curvature at the transition state. Since these are not available during the application of the group additive method, Sabbe et al. [24] proposed a fourth-order polynomial in the exothermic activation energy, with temperature-dependent coefficients, for H-abstraction reactions by carbon-centered radicals. Equation (4-5) allows calculating tunneling coefficients based on the group additive calculated activation energy of the exothermic reaction $E_{\text{a,exo}}$ (in kJ mol^{-1}):

$$\kappa(\mathrm{T}) = 1 + \left(\frac{162}{T}\right)^3 E_{\alpha,\mathrm{exo}} + 2.71\times10^{-6} \exp\left(-\frac{T-300}{26}\right) E_{\alpha,\mathrm{exo}}^4 \qquad (4\text{-}5)$$

where T is the temperature (K). The applicability of eq (4-5) for α-hydrogen abstractions from oxygenates by hydrogen atoms will be evaluated. In the case that this equation cannot accurately reproduce tunneling coefficients for the studied reaction families, the possibility of refitting the parameters of this equation will be thoroughly examined.

4.4 Results and Discussion

4.4.1 Rate Coefficients and Arrhenius Parameters

A training set of 60 hydrogen-abstraction reactions by a hydrogen atom is constructed, based on which the group additive values for both the primary and the secondary contributions can be determined. The reactions included in this training set presented in Table 4-1. For these reactions, rate coefficients, tunneling coefficients, activation energies, pre-exponential factors and standard reaction enthalpies and entropies at 300 K are provided in Table S1 (Appendix C). The corresponding parameters for this training set at 600, 1000, 1500 and 2000 K are given in Tables S2-S5 (Appendix C), respectively. Rate coefficients and Eckart tunneling coefficients for all reactions in this study (300-2000 K) are reported in Tables S6 and S7 (Appendix C), respectively.

Table 4-1: Training set of Hydrogen-Abstraction Reactions from Oxygenates by Hydrogen Atoms.

Reference Reaction

$H^{\bullet}$ + CH_4 ↔ H_2 + $Me^{\bullet}$

Training Set of Reactions

1/1	$H^{\bullet}$	+	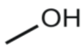	↔	H_2	+	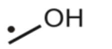	1/31	$H^{\bullet}$	+	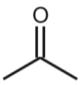	↔	H_2	+	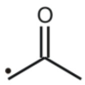
1/2	$H^{\bullet}$	+	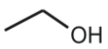	↔	H_2	+	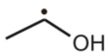	1/32	$H^{\bullet}$	+	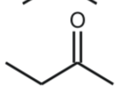	↔	H_2	+	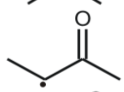
1/3	$H^{\bullet}$	+	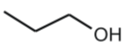	↔	H_2	+	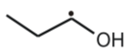	1/33	$H^{\bullet}$	+	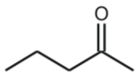	↔	H_2	+	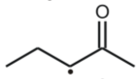
1/4	$H^{\bullet}$	+	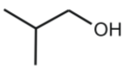	↔	H_2	+	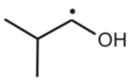	1/34	$H^{\bullet}$	+	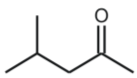	↔	H_2	+	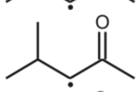
1/5	$H^{\bullet}$	+	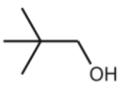	↔	H_2	+	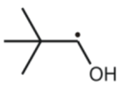	1/35	$H^{\bullet}$	+	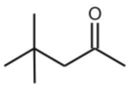	↔	H_2	+	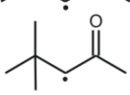
1/6	$H^{\bullet}$	+	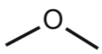	↔	H_2	+	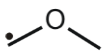	1/36	$H^{\bullet}$	+	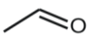	↔	H_2	+	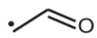
1/7	$H^{\bullet}$	+	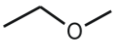	↔	H_2	+	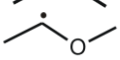	1/37	$H^{\bullet}$	+	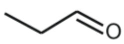	↔	H_2	+	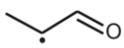
1/8	$H^{\bullet}$	+		↔	H_2	+		1/38	$H^{\bullet}$	+		↔	H_2	+	
1/9	$H^{\bullet}$	+	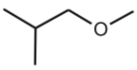	↔	H_2	+	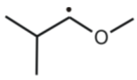	1/39	$H^{\bullet}$	+	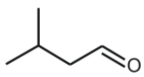	↔	H_2	+	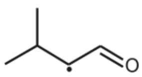

No.		Reactant		Product
		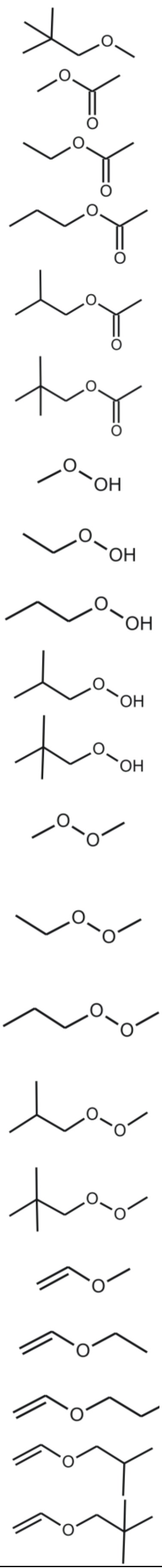		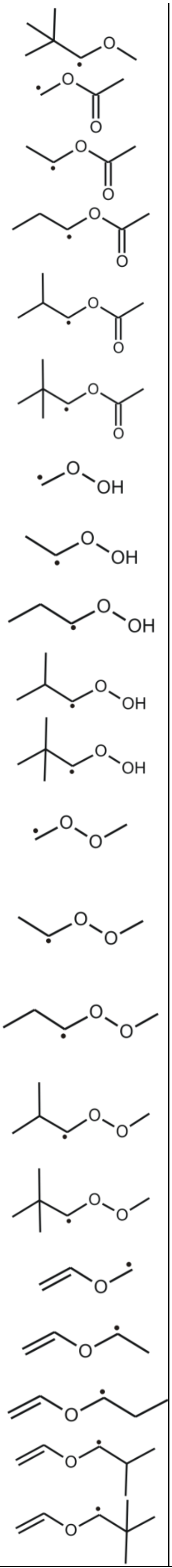
1/10	$H^{\bullet}$ +		↔ H_2 +	
1/11	$H^{\bullet}$ +		↔ H_2 +	
1/12	$H^{\bullet}$ +		↔ H_2 +	
1/13	$H^{\bullet}$ +		↔ H_2 +	
1/14	$H^{\bullet}$ +		↔ H_2 +	
1/15	$H^{\bullet}$ +		↔ H_2 +	
1/16	$H^{\bullet}$ +		↔ H_2 +	
1/17	$H^{\bullet}$ +		↔ H_2 +	
1/18	$H^{\bullet}$ +		↔ H_2 +	
1/19	$H^{\bullet}$ +		↔ H_2 +	
1/20	$H^{\bullet}$ +		↔ H_2 +	
1/21	$H^{\bullet}$ +		↔ H_2 +	
1/22	$H^{\bullet}$ +		↔ H_2 +	
1/23	$H^{\bullet}$ +		↔ H_2 +	
1/24	$H^{\bullet}$ +		↔ H_2 +	
1/25	$H^{\bullet}$ +		↔ H_2 +	
1/26	$H^{\bullet}$ +		↔ H_2 +	
1/27	$H^{\bullet}$ +		↔ H_2 +	
1/28	$H^{\bullet}$ +		↔ H_2 +	
1/29	$H^{\bullet}$ +		↔ H_2 +	
1/30	$H^{\bullet}$ +		↔ H_2 +	

No.		Reactant		Product
		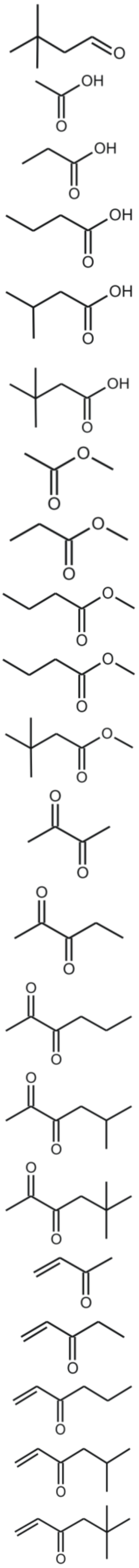		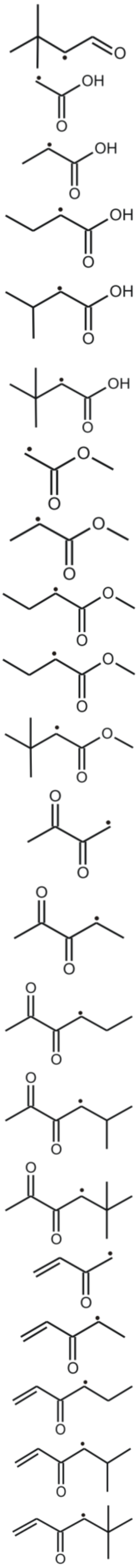
1/40	$H^{\bullet}$ +		↔ H_2 +	
1/41	$H^{\bullet}$ +		↔ H_2 +	
1/42	$H^{\bullet}$ +		↔ H_2 +	
1/43	$H^{\bullet}$ +		↔ H_2 +	
1/44	$H^{\bullet}$ +		↔ H_2 +	
1/45	$H^{\bullet}$ +		↔ H_2 +	
1/46	$H^{\bullet}$ +		↔ H_2 +	
1/47	$H^{\bullet}$ +		↔ H_2 +	
1/48	$H^{\bullet}$ +		↔ H_2 +	
1/49	$H^{\bullet}$ +		↔ H_2 +	
1/50	$H^{\bullet}$ +		↔ H_2 +	
1/51	$H^{\bullet}$ +		↔ H_2 +	
1/52	$H^{\bullet}$ +		↔ H_2 +	
1/53	$H^{\bullet}$ +		↔ H_2 +	
1/54	$H^{\bullet}$ +		↔ H_2 +	
1/55	$H^{\bullet}$ +		↔ H_2 +	
1/56	$H^{\bullet}$ +		↔ H_2 +	
1/57	$H^{\bullet}$ +		↔ H_2 +	
1/58	$H^{\bullet}$ +		↔ H_2 +	
1/59	$H^{\bullet}$ +		↔ H_2 +	
1/60	$H^{\bullet}$ +		↔ H_2 +	

It is very important to investigate the accuracy of the ab initio calculated parameters by comparing them with the available experimental data. Perusal of the literature shows that experimental data concerning hydrogen abstractions from oxygenates by hydrogen atoms are scarce, and only a limited amount of experimental rate coefficients can be found in the NIST Chemical Kinetics Database [45]. The experimental rate coefficients reported in this paragraph are also used later in the set of reactions to validate the group additive method. From the different categories in which the NIST Chemical Kinetics Database subdivides experimental rate coefficients, only the “absolute values measured directly” were selected for comparison with the ab initio values calculated in this work.

Li and Williams [46] reported absolute rate coefficients for the hydrogen abstraction from methanol by a hydrogen atom (reaction 1/1, Table 4-1) for temperatures ranging from 300 to 2700 K. Their reported value of 7.7×10^{2} m^3 mol^{-1} s^{-1} at 400 K agrees within 10% with the corresponding ab initio value of 7.2×10^{2} m^3 mol^{-1} s^{-1}. For the hydrogen abstraction from dimethyl ether (reaction 1/6, Table 4-1) Lee et al. [47] proposed absolute rate coefficients for temperatures 273-426 K. The reaction rate at 300 K, 3.8×10^{2} m^3 mol^{-1} s^{-1} is also within 10% of the ab initio calculated value of $4.0\text{x}10^{2}$ m^3 mol^{-1} s^{-1}. Tranter and Walker [48] measured directly the reaction rates for the hydrogen abstraction from (i) acetone (CH_3COCH_3) (reaction 1/31, Table 4-1) and (ii) butan-2-one ($CH_3CH_2COCH_3$) (reaction 1/32, Table 4-1) at 753 K. The reported values of 2.3×10^{5} m^3 mol^{-1} s^{-1} for reaction (i) and 7.2×10^{5} m^3 mol^{-1} s^{-1} for reaction (ii) are by a factor of 5.7 and 4.8 higher than the ab initio calculated values 4×10^{4} m^3 mol^{-1} s^{-1} and 1.5×10^{5} m^3 mol^{-1} s^{-1}, respectively. Though for the latter reactions the agreement is not so good as for the other two, the agreement between the ab initio calculated rate coefficients and the experimentally obtained data for absolute values measured directly remains below a factor of 6, which can be considered sufficient to guarantee the use of the calculated kinetic parameters for the determination of group additive values.

A wide range of hydrogen-abstraction reactions is covered by the 60 reactions of the training set, including hydrogen abstractions by a hydrogen atom from alcohols, ethers, esters, ketones, diketones, aldehydes, acids, hydroxyl and alkyl peroxides, and unsaturated ketones and ethers. The training set of reactions can be divided into 12 subsets including 5 reactions each (see Table S1, Appendix C). In all of the studied reactions, the first reactant is a hydrogen atom, and the created radical center is in α position to an oxygen atom or a carbonyl (CO) group. The effect of the secondary contributions on the Arrhenius parameters is also studied in the framework of the same training set. This can be achieved by calculating parameters for a nonsubstituted, monosubstituted, disubstituted, and trisubstituted oxygenate compound for every type of the studied reaction families. ΔGAV^os for both primary and secondary contributions are calculated simultaneously by unweighed least-squares regression.

On the basis of the data retrieved from Table S1 (Appendix C) it can be concluded that all hydrogen abstractions of the training set at 300 K are exothermic with reaction enthalpies varying from −67 kJ mol^{-1} for the H abstraction from 2,3-pentadione (reaction 1/52, Table 4-1) to −22 kJ mol^{-1} for the H abstraction from methyl acetate (reaction 1/11, Table 4-1). This relates to the H−H bond typically being stronger than the broken C−H bonds. Generally, α-hydrogen abstractions from diketones, aldehydes, and unsaturated ketones are the most exothermic, while α-hydrogen abstractions from esters and unsaturated ethers are the least exothermic reactions.

Reaction entropies are positive for all reactions studied fluctuating from 7 J mol^{-1} K^{-1} for hydrogen abstractions from esters (reaction 1/46, Table 4-1) to 37 J mol^{-1} K^{-1} for abstractions from ketones (reaction 1/34, Table 4-1). The introduction of the external rotation of H_2 along with the translation energy leads to positive values in reaction entropies for all reactions included in the training set. Pre-exponential factors vary for the forward reaction from ≈3x10^{6} m^{3} mol^{-1} s^{-1} for the hydrogen abstraction from alkyl peroxides (reaction 1/25, Table 4-1) to almost one order of magnitude higher (≈ $4x10^7$ m^3 mol^{-1} s^{-1}) for the abstraction from saturated ethers (reaction 1/27, Table 4-1).

Regarding the activation energies, their values cover a range from 23 kJ mol^{-1} for the H abstraction from saturated ketones (reaction 1/60, Table 4-1) to 44 kJ mol^{-1} for the abstraction from esters (reaction 1/11, Table 4-1). The highest barrier in reaction 1/11 is caused by the instability of the formed acetyloxy methyl radical ($^{\bullet}CH_2OCOCH_3$). The lowest barrier is obtained for reaction 1/60 in which the radical CH_2=CHCOC$^{\bullet}$H$(CH_3)_3$ is formed, which is stabilized by the hyperconjugation of the two methyl groups adjacent to the formed carbon radical center. In general, the lowest barriers are observed for hydrogen abstractions from ethers, diketones, alcohols and saturated ketones, while the highest barriers are observed for esters, saturated ethers, and acids.

At 300 K, the rate coefficients for the forward reaction range between 1.2 m^3 mol^{-1} s^{-1} and $3.1x10^3$ m^3 mol^{-1} s^{-1}. The H abstraction from methyl acetate has the lowest rate coefficient (reaction 1/11, Table 4-1), while the highest one corresponds to the hydrogen abstraction from CH_2=CHCOC$^{\bullet}$HCH$(CH_3)_2$ (5-methyl-3-methylidene-hex-1-ene) (reaction 1/59, Table 4-1). Unsaturated ketones, ethers and diketones are the most reactive in α-hydrogen abstractions while esters and acids are the least reactive.

Tunneling has a significant effect on reaction rates particularly at low temperatures, with tunneling coefficients ranging from 2.8 for abstractions from diketones (reactions 1/52 and 1/54, Table 4-1) to 6.5 for abstractions from unsaturated ketones (reaction 1/56, Table 4-1). However, the effect of tunneling is not so profound as for hydrogen abstractions by carbon-centered radical, in which the higher activation barriers and imaginary frequencies lead to tunneling coefficients up to 37.3.

4.4.2 Group Additivity Model

Group Additivity Values: The data included in Table S1 (Appendix C) can be used to calculate ΔGAV^os at 300 K for H-abstraction reactions by hydrogen atoms from carbon atoms in the α position of an oxygen or a carbonyl group. The hydrogen abstraction from methane by a hydrogen atom is selected as a reference reaction. As explained above, this is the most simple reaction of the reaction family, in which a transition state of the H--H--C type is formed. Arrhenius parameters for the reference reaction over a wide temperature range (300-2000 K) can be found in Table S8 (Appendix C).

The training set of the 60 reactions presented in Table S1 (Appendix C) can be divided into 12 subsets each one containing 5 reactions. Within each of the 12 subsets, all 5 reactions contain the same secondary contributions of the oxygenate side but different secondary contributions of the carbon side of the formed radical center. For example, the first subset contains alcohols, the second ethers, the third esters, and so forth. If the restriction to primary contributions was sufficient to describe the kinetic parameters for this set of reactions, then the activation energies and single-event pre-exponential factors should have very similar values for all reactions with the same primary contribution. However, there are clearly large differences in these values for reactions that share the same primary contribution. The Arrhenius parameters (E_a and log$A$) for reactions sharing the same primary groups differ up to ~10 kJ mol^{-1} and ~0.550 log(m^3 mol^{-1} s^{-1}) for activation energies and single-event pre-exponential factors, respectively. Hence, secondary contributions need to be included to remain within chemical accuracy. The applied symmetry numbers and corresponding number of single events for all reactions of Table S1 are presented in Table S9 (Appendix C).

Table 4-2: ΔGAV°s at 300 K, 600 K and 1000 K for α-Hydrogen Abstractions from Oxygenates by Hydrogen Atoms. [a]

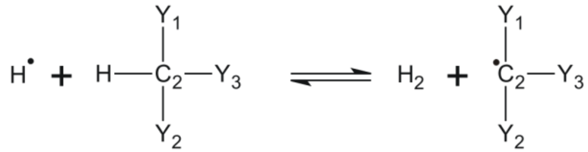

	Forward						Reverse					
	300 K		600 K		1000 K		300 K		600 K		1000 K	
	log$\tilde{A}$	E_a	log$\tilde{A}$	E_a	log$\tilde{A}$	E_a	log$\tilde{A}$	E_a	log$\tilde{A}$	E_a	log$\tilde{A}$	E_a
Reference Reaction												
$H^{\bullet} + CH_4$	7.605	55.9	8.058	59.7	8.504	66.4	6.364	55.9	6.440	56.8	6.859	63.2
	ΔGAV° (C_1)						ΔGAV° (C_2)					
	300 K		600 K		1000 K		300 K		600 K		1000 K	
Group	log$\tilde{A}$	E_a	log$\tilde{A}$	E_a	log$\tilde{A}$	E_a	log$\tilde{A}$	E_a	log$\tilde{A}$	E_a	log$\tilde{A}$	E_a
Primary Contributions												
C_i-(O)(H)$_2$	-1.076	-21.7	-1.089	-21.8	-1.098	-22.0	-0.862	13.8	-0.797	14.2	-0.770	14.7
C_i-(C)(O)(H)	-0.556	-30.3	-0.551	-30.2	-0.560	-30.4	-0.696	12.5	-0.563	13.6	-0.516	14.2
C_i-(CO)(H)$_2$	-1.061	-17.6	-1.083	-17.8	-1.091	-17.9	-0.465	24.6	-0.284	26.0	-0.224	26.9
C_i-(C)(CO)(H)	-0.557	-27.3	-0.561	-27.3	-0.574	-27.6	-0.651	35.9	-0.443	37.5	-0.373	38.5
Secondary Contributions												
O-(C)(C_i)	0.087	-1.0	0.107	-0.9	0.106	-0.9	-0.074	-2.2	-0.072	-2.3	-0.073	-2.3
O-(C_i)(CO)	-0.019	9.7	0.007	9.9	0.014	10.0	-0.069	-3.8	-0.110	-4.1	-0.125	-4.3
O-(C_i)(O)	-0.128	3.4	-0.113	3.6	-0.108	3.6	-0.151	-3.6	-0.152	-3.6	-0.158	-3.7
O-(C_i)(C_d)	0.552	8.7	0.618	9.2	0.638	9.5	0.340	-0.1	0.381	0.2	0.392	0.3
CO-(C)(C_i)	-0.140	-1.3	-0.138	-1.3	-0.136	-1.3	-0.441	-5.9	-0.465	-6.1	-0.470	-6.1
CO-(C_i)(O)	-0.077	3.1	-0.063	3.3	-0.057	3.3	0.032	-12.9	-0.009	-13.2	-0.021	-13.3
CO-(C_i)(CO)	-0.303	-3.6	-0.305	-3.7	-0.311	-3.7	0.089	-0.5	0.100	-0.4	0.096	-0.4
CO-(C_i)(C_d)	-0.023	-3.8	-0.012	-3.8	-0.009	-3.7	-0.047	-4.6	-0.055	-4.7	-0.057	-4.7
C-(C)(C_i)(H)$_2$	-0.085	-1.2	-0.088	-1.2	-0.088	-1.2	-0.156	-2.3	-0.152	-2.3	-0.149	-2.2
C-(C)$_2$(C_i)(H)	-0.014	-0.8	-0.017	-0.8	-0.019	-0.8	-0.299	-3.2	-0.297	-3.1	-0.292	-3.1
C-(C)$_3$(C_i)	-0.156	-1.4	-0.160	-1.4	-0.163	-1.5	-0.165	-5.0	-0.171	-5.1	-0.168	-5.0

[a] $\tilde{A}$ in $m^3\ mol^{-1}\ s^{-1}$ and E_a in $kJ\ mol^{-1}$. Y_1 and Y_2 ligands correspond to either a hydrogen or an alkyl group, while Y_3 ligand corresponds to either an oxygen or a carbonyl containing group ($Y_3 \equiv$ O−Z or CO−Z. Z could be H, O, CO, or an alkyl group). In C_i, i=1 refers to the forward and i=2 to the reverse reaction, C_d refers to a double-bonded carbon atom.

ΔGAV^os for pre-exponential factors and activation energies at 300, 600 and 1000 K for hydrogen-abstraction reactions by hydrogen are available in Table 4-2. ΔGAV^os for the corresponding Arrhenius parameters at higher temperatures (1500 and 2000 K) can be retrieved from Table S10 (Appendix C). The low-temperature-dependence of the ΔGAV^os for both pre-exponential factors and activation energies reported in Table 4-2 is illustrated in Figure S1 (Appendix C). It is clear that ΔGAV^os for both the forward and the reverse reaction are almost temperature independent. The average change in ΔGAV^o_{Ea} from 300 to 2000 K amounts to 0.3 and 0.9 kJ mol^{-1} for the forward and the reverse reactions, respectively, while the average $\Delta GAV^o_{\log\tilde{A}}$ deviation for the same temperature range amounts to 0.022 and 0.078 for the forward and the reverse reactions, respectively. Also, the largest variations in ΔGAV^os for E_a and $\log\tilde{A}$ in this wide temperature range are limited to 1.2 kJ mol^{-1} and 0.100 log(m^3 mol^{-1} s^{-1}) respectively, while for the reverse reaction, the corresponding values are up to 3.4 kJ mol^{-1} and 0.310 log(m^3 mol^{-1} s^{-1}), respectively.

The most pronounced temperature dependencies for both pre-exponential factors and activation energies are observed for ΔGAV^os concerning primary contributions and mainly for ΔGAV^os C_i-(C)(CO)(H) and C_i-(CO)$(H)_2$. It can be concluded that the very small temperature dependence allows using of the $\Delta GAV°$s over a wide range of temperatures, in particular, at higher temperatures, without losing accuracy. Moreover, the small deviations in $\log\tilde{A}$ and E_a due to the limited temperature dependence of the $\Delta GAV°$s compensate each other for the largest extent, resulting in a temperature dependence of the rate coefficients that is even lower than that of the Arrhenius parameters.

ΔGAV^os for the primary contributions to pre-exponential factors and activation energies are larger than for the secondary contributions. Comparing the secondary contributions among themselves, the following conclusions can be inferred: secondary contributions with an oxygen atom linked to the carbon radical center have higher values than the corresponding contributions with a carbonyl group linked to the carbon radical center, while the lowest values obtained for secondary contributions with a carbon atom linked to the carbon radical center. The ΔGAV^os for C-(C)(C_i)$(H)_2$, C-$(C)_2$(C_i)(H), C-$(C)_3$(C_i) appear to have almost the same values for the forward reaction, and it seems that they could be modeled in one single ΔGAV^o. In this work, they are treated as being three different ΔGAV^os, since their values for the reverse reaction have significant variations between each other.

The application of the proposed model is illustrated by two examples, starting with reaction 1/60 of Table 4-1:

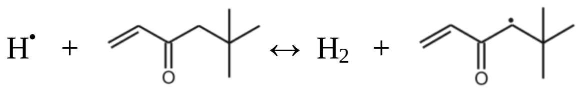

In the following calculations the subscript “1” in the carbon radical center refers to the corresponding ΔGAV^o for the forward reaction. The activation energy and the single-event pre-exponential factor for the forward reaction 1/60 at 300 K can be calculated from the proposed group values in Table 4-2 as follows:

$$E_a(300\text{ K}) = E_{a,ref}(300\text{ K}) + \Delta GAV_{E_a}^\circ({}^\bullet C_1\text{-(C)(CO)(H)}) + \Delta GAV_{E_a}^\circ(\text{CO-}({}^\bullet C_1)(C_d)) +$$

$$+ \Delta GAV_{E_a}^\circ(\text{C-}(C)_3({}^\bullet C_1)) = 55.9 - 27.3 - 3.8 - 1.4 = 23.4\text{ kJ mol}^{-1}$$

$$\log A(300\text{ K}) = \log\tilde{A}_{ref}(300\text{ K}) + \Delta GAV_{\log\tilde{A}}^\circ({}^\bullet C_1\text{-(C)(CO)(H)}) + \Delta GAV_{\log\tilde{A}}^\circ(\text{CO-}({}^\bullet C_1)(C_d)) +$$

$$+ \Delta GAV_{\log\tilde{A}}^\circ(\text{C-}(C)_3({}^\bullet C_1)) + \log(n_e)^{[1]} = 7.605 - 0.557 - 0.023 - 0.156 + \log(1) = 6.869$$

In the calculation of log$A$, n_e is the number of single events for the forward reaction[1]; n_e for

----

[1]n_e for this reaction amounts to 2, but is for this comparison taken as 1 since the number of optical isomers are excluded from n_e because log$A$ is derived from ab initio data directly and, hence, does not contain any contribution of optical isomers.

the reaction of the example is equal to 1. The values predicted by the group additive model agree well to the corresponding ab initio calculated values, respectively, 23.2 kJ mol^{-1} and 6.943, with differences of the group additively predicted versus the ab initio value of 0.2 kJ mol^{-1} and −0.074 for the activation energies and pre-exponential factors, respectively.

The second example refers to the reverse reaction 1/8 of Table 4-1:

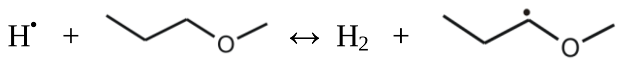

The subscript “2” in the carbon radical center refers to the corresponding ΔGAV^{o} for the reverse reaction. The Arrhenius parameters for the reverse of reaction 1/8 at 300 K can be calculated by the proposed group additive model as follows:

$$E_a(300\text{ K}) = E_{a,ref}(300\text{ K}) + \Delta GAV_{E_a}°(^{\bullet}C_2\text{-}(C)(O)(H)) + \Delta GAV_{E_a}°(C\text{-}(^{\bullet}C_2)(C)(H)_2) +$$

$$+ \Delta GAV_{E_a}°(O\text{-}(^{\bullet}C_2)(C)) = 55.9 + 12.5 - 2.3 - 2.2 = 63.9\text{ kJ mol}^{-1}$$

$$\log A(300\text{ K}) = \log\tilde{A}_{ref}(300\text{ K}) + \Delta GAV_{\log\tilde{A}}°(^{\bullet}C_2\text{-}(C)(O)(H)) + \Delta GAV_{\log\tilde{A}}°(C\text{-}(^{\bullet}C_2)(C)(H)_2) +$$

$$+ \Delta GAV_{\log\tilde{A}}°(O\text{-}(^{\bullet}C_2)(C)) + \log(n_e)^1 = 6.364 - 0.696 - 0.156 - 0.074 + \log(1)$$

$$= 5.438$$

The GA predicted values are in excellent agreement with the corresponding ab initio calculated values 63.8 kJ mol^{-1} and 6.348, with the differences between the group additively predicted and the ab initio values amounting to only 0.1 kJ mol^{-1} and 0.050 for the activation energies and pre-exponential factors, respectively[1].

----

[1] n_e for this reaction amounts to 2, but is for this comparison taken as 1 since the number of optical isomers are excluded from n_e because log$A$ is derived from ab initio data directly and, hence, does not contain any contribution of optical isomers.

Tunneling Model: As mentioned above, the group additive values exclude contributions from tunneling. Equation (4-5), proposed by Sabbe et al. [24] for hydrogen-abstraction reactions of the C--H--C type, involving hydrocarbons, was shown to yield accurate results also for hydrogen abstractions of the C--H--C type involving organosulfur [28] and oxygenate compounds [30]. This equation correlates tunneling with the Arrhenius activation energy, which can be obtained from group additivity. Tunneling coefficients are proportional to the net barriers, that is, the smallest value among the forward and the reverse activation energies, which corresponds to the activation barrier for the exothermic direction of the reaction.

The model of eq (4-5) however overestimated the Eckart tunneling coefficients with a factor of 2.2 on average at 300 K (see Figure 4-2) with the deviations increasing with the barrier height of the exothermic reaction. This overestimation is mainly due to the significant differences in imaginary frequencies between the hydrogen abstractions with transition states of the H--H--C type and those of the C--H--C type. Particularly, imaginary frequencies for the abstraction by hydrogen atoms (H--H--C type) amount to 1000-1200 cm^{-1} for the reactions in this work, while the corresponding imaginary frequencies for the same reactions but with methyl instead of hydrogen as abstracting radical are ~400 cm^{-1} higher. Therefore, the three parameters of the fourth-order polynomial were refitted to the Eckart's tunneling coefficients for all reactions of the training set, for temperatures ranging from 300 to 2000 K. This leads to eq (4-6):

$$\kappa(\mathrm{T}) = 1 + \left(\frac{97}{T}\right)^3 E_{\alpha,\mathrm{exo}} + 1.73\times10^{-6}\exp\left(-\frac{T-300}{26}\right)E_{\alpha,\mathrm{exo}}^4 \tag{4-6}$$

By using eq (4-6) tunneling coefficients are reproduced with an average factor of deviation of 1.3 at 300 K, and only for one out of the 60 reactions of the training set the tunneling coefficient differ by more than a factor 2 from the Eckart tunneling coefficient. In the two graphs presented in Figure 4-2, the improvement compared to the tunneling coefficients obtained with eq (4-6) is obvious. The agreement improves with increasing temperatures, and the mean factor of deviation is only 1.2 and 1.1 on average at 600 and 1000 K respectively, while for higher temperatures tunneling contributions can be neglected.

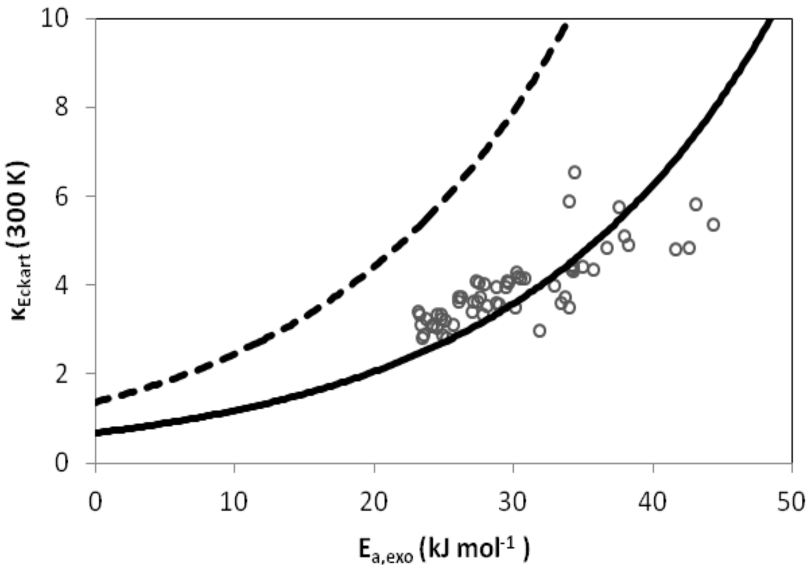

Figure 4-2: Comparison of the performance of the improved reparametrized tunneling model (eq 4-6) (full line) and the original tunneling model (eq 4-5) (dashed line). Eckart tunneling coefficients (circles) are expressed as a function of the ab initio activation energy of the exothermic reaction for the reactions in Table 4-1 (o) at 300 K.

4.4.3 Model Performance

The performance of the group additivity model developed in this work is evaluated by comparing the group additivity predictions with (i) the ab initio kinetic parameters for a validation set of reactions that were not present in the training set of reactions from which the group additive values have been determined, (ii) experimentally obtained data directly, and (iii) the predictions of other models such as the Blowers and Masel model [4], the IP model [3], and the model developed by Ratkiewicz et al. [19] using the reaction class transition state theory.

Ab initio Validation: The ΔGAV^{o}s determined from the kinetic data provided in Table S1 (Appendix C) are validated using an ab initio validation set including 19 reactions. For these reactions, the calculated Arrhenius parameters and rate and tunneling coefficients at 300, 600, 1000, 1500 and 2000 K can be found in Tables S11-S15 (Appendix C). In Table 4-3, the performance of the group additivity model is illustrated at 300 K based on the deviations between group additively predicted and ab initio calculated parameters. The comparison at 300 K is the strictest, since the lower the temperatures the lower the differences that can be expected between the GA and AI calculated rate coefficients, due to the strong sensitivity of rate coefficients on the activation energies and the tunneling coefficients at low temperatures. The deviations between group additive predictions and ab initio values for the reactions included in the ab initio validation set at 600, 1000, 1500 and 2000 K are provided in Tables S16-S19 (Appendix C). Additionally, symmetry numbers and the applied number of single events for the reactions used in the ab initio validation set are presented in Table S9 (Appendix C).

The MAD between group additivity predictions and ab initio calculated values for the pre-exponential factors and activation energies for the forward reactions at 300 K amount to 0.127 and 1.4 kJ mol^{-1}, respectively, while for the reverse reactions the corresponding values are 0.126 and 1.8 kJ mol^{-1}, respectively. The largest deviation for the pre-exponential factors at 300 K is observed for the H-abstraction from pentan-3-one (reaction 2/8, Table 4-3) and amounts to 0.554. Regarding the activation energies the largest deviation is observed for the abstraction from 3-methoxybut-1-ene (reaction 2/11, Table 4-3), amounting to 4.2 kJ mol^{-1}.

The average deviation between the predicted and the calculated rate coefficients (including tunneling effects) amounts to a factor of 1.9 for the forward and 2.5 for the reverse reaction. This indicates that the GA model developed in this work reproduces the calculated rate coefficients accurately. The agreement between group additive predicted and ab initio calculated rate coefficients improves with increasing temperatures, since the mean factor of deviation amounting to 1.4 for the forward reaction at both 600 and 1000 K. Only for one forward reaction, the hydrogen abstraction from 3-methoxybut-1-ene (reaction 2/11, Table 4-3), the group additive prediction deviates more than a factor of 2 from the corresponding AI value (6.6). The same reaction also shows the lowest agreement for the reverse reaction. Table 4-3 also provides the ratio of the estimated tunneling coefficient by using eq (4-6) and the ab initio calculated Eckart tunneling coefficient. On the basis of these results, the tunneling coefficients are reproduced accurately within a factor of 1.2 at 300 K, in agreement with the observed factor of deviation of 1.3 on the training set.

In principle, a fully complete group additive model that based on the thermochemistry of the transition state and the reactants, without any approximation, omission, or simplification and that captures all non-nearest neighbor interactions, leads to built-in thermodynamical consistency, that is, the differences between the forward and reverse activation energies and entropies are the reaction enthalpy and reaction entropy, respectively [24]. However, the neglect of tertiary contributions for reactants, the transition state, and products can disturb this thermodynamic consistency, particularly for reactions in which a strong difference in steric and/or resonance effects between the reactant and product sides is present. Hence, to avoid erroneous prediction of the reaction equilibrium, especially for reactions of that type, it is advisable to introduce thermodynamic consistency, taking the reverse rate coefficient as the ratio of the forward rate coefficient and the equilibrium coefficient. The latter can be determined using group additivity to predict the thermochemistry of reactants and products, using the consistent GAVs presented in previous work [39].

In previous work [24, 28-30], it was shown that the accuracy of truncated group additive predictions can be different for both the forward and the reverse reaction rates, and hence, $\Delta GAV°$s for both directions have been determined in this work. On the basis of the results

Table 4-3: Comparison between Group Additive (GA) and ab Initio (AI) kinetic parameters at 300 K for the ab Initio Validation Set of 19 Reactions. [a]

Reactions									forward				reverse	
								κ/κ_{AI}	$\Delta\log A$	ΔE_a	k_{GA}/k_{AI}	$\Delta\log A$	ΔE_a	k_{GA}/k_{AI}
2/1	$H^\bullet$	+	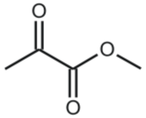	↔	H_2	+	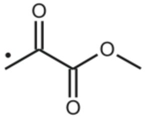	0.8	-0.008	0.3	0.9	-0.065	1.7	0.4
2/2	$H^\bullet$	+	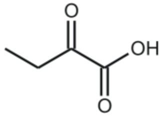	↔	H_2	+	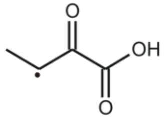	0.9	-0.167	-1.4	1.3	-0.042	-3.8	4.3
2/3	$H^\bullet$	+	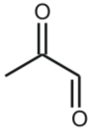	↔	H_2	+	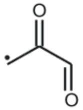	0.7	0.059	1.0	0.8	-0.056	2.7	0.3
2/4	$H^\bullet$	+	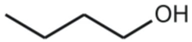	↔	H_2	+	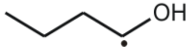	1.0	-0.059	0.1	0.9	0.009	1.4	0.6
2/5	$H^\bullet$	+	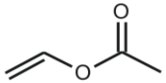	↔	H_2	+	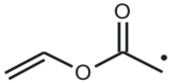	1.0	0.176	0.2	1.4	-0.072	-1.7	1.7
2/6	$H^\bullet$	+	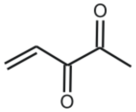	↔	H_2	+	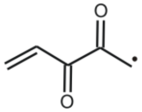	1.1	0.103	0.8	0.9	-0.139	-0.9	1.0
2/7	$H^\bullet$	+	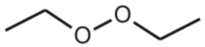	↔	H_2	+	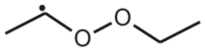	0.9	0.241	1.9	0.8	0.140	1.9	0.7
2/8	$H^\bullet$	+	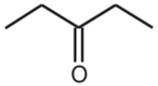	↔	H_2	+	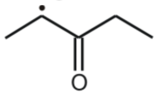	0.9	0.554	1.0	2.5	-0.271	1.2	0.3
2/9	$H^\bullet$	+	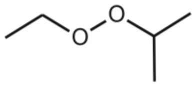	↔	H_2	+	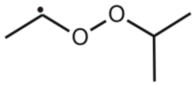	0.9	-0.036	1.7	0.5	0.169	1.4	0.8
2/10	$H^\bullet$	+	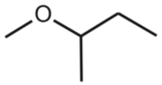	↔	H_2	+	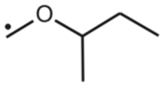	0.9	0.160	2.5	0.5	-0.275	-1.6	1.0
2/11	$H^\bullet$	+	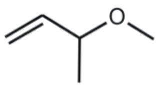	↔	H_2	+	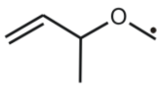	0.9	0.078	-4.2	6.6	-0.231	3.7	0.1

2/12	$H^{\bullet}$	+	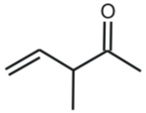	↔	H_2	+	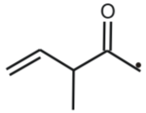	0.7	-0.037	4.1	0.2	-0.153	3.8	0.2
2/13	$H^{\bullet}$	+	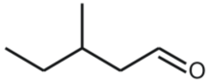	↔	H_2	+	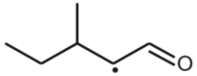	0.8	0.012	-0.3	1.2	0.071	-1.1	1.8
2/14	$H^{\bullet}$	+	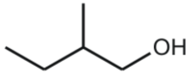	↔	H_2	+	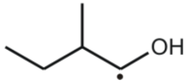	0.9	-0.018	1.1	0.6	-0.130	0.6	0.6
2/15	$H^{\bullet}$	+		↔	H_2	+	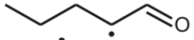	0.8	0.136	2.4	0.5	-0.026	1.4	0.5
2/16	H•	+	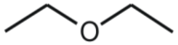	↔	H_2	+	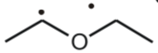	0.9	0.045	1.3	0.7	0.115	1.9	0.6
2/17	$H^{\bullet}$	+	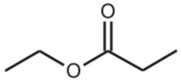	↔	H_2	+	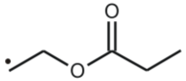	0.9	0.191	1.0	1.0	0.191	1.1	1.0
2/18	$H^{\bullet}$	+	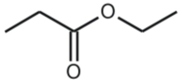	↔	H_2	+	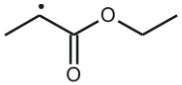	0.8	0.220	1.7	0.9	0.064	1.4	0.7
2/19	$H^{\bullet}$	+	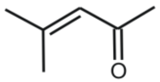	↔	H_2	+	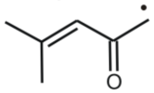	0.7	0.111	0.1	1.3	-0.178	1.6	0.3
							MAD		0.127	1.4		0.126	1.8	
							RMS		0.177	1.9		0.148	2.1	
							MAX		0.554	4.2	6.6	0.275	3.8	7.5
							<ρ>	1.2			1.9			2.5

[a] $\Delta\log A = \log A_{GA} - \log A_{AI}$ in m^3 mol^{-1} s^{-1}, $\Delta E_a = E_{a,GA} - E_{a,AI}$ in kJ mol^{-1}. MAD: mean absolute deviation; RMS: root-mean-square deviation; MAX: maximum deviation; <ρ>: factor of deviation between two values taken from eq (4-4). Tunneling effects are not included in the reported $\Delta\log A$, but only included in the reported k_{GA} and k_{AI}.

presented in Table 4-3, the best accuracy is obtained by calculating the forward rate coefficient using the ΔGAV°s presented in this work, and the reverse rate coefficient from thermodynamic consistency.

Experimental Validation: The group additive model developed in this work is also validated by comparing group additive predictions with experimental reaction rates taken from the NIST Chemical Kinetics Database [45]. In Table 4-4, group additively predicted rate coefficients are compared with a selection of 21 experimental rate coefficients for 7 different reactions. These experimental rate coefficients are classified by the NIST Chemical Kinetics Database into categories depending on the way they have been determined, including "reaction rates measured directly", "experimental values obtained by a limited review", or "experimental values from fitting to a complex mechanism or from detailed balance/reverse rate". The uncertainty in the experimental rate coefficients is large, and the temperature and pressure ranges in which they are valid are in the majority of cases limited. Even for absolute values measured directly there are significant uncertainties due to the experimental method or the setup used to measure the reaction rates. This illustrates the need for developing a reliable and accurate model for this reaction family.

The rate coefficients are compared at a temperature included in the temperature range of the experiment, preferably at 300, 600, and 1000 K. For experimental temperature ranges not including these preferred temperatures, the rate coefficients were evaluated at the mean value of the reported temperature range, rounded to the nearest hundred, while for experimental rate coefficients at a fixed temperature, rate coefficients were evaluated at the nearest decade. The Arrhenius parameters of the reference reaction are given for a broad range of temperatures in Table S8 (Appendix C). Since ΔGAV^os are almost temperature independent, ΔGAV^os reported in Table 4-2 can be used over a broad temperature range. For example, if rate coefficients at 400 K are to be determined, ΔGAV^os at 300 K can be used without any loss of accuracy.

The mean factor of deviation $<\rho>$ between the group additively predicted and the experimentally obtained rate coefficients amounts to 3.1, indicating a very good agreement between compared values. If the rather unreliable "experimental values derived from fitting to a complex mechanism" are omitted, $<\rho>$ even drops to a factor 2.6. In the 7 reactions of this set, the reaction rates are predicted within an average factor of ~3 except for the reaction 1 where the rate coefficient is predicted within a factor of ~5. This is mainly due to the largest deviation between the GA predicted and the experimental reaction rate that amounts to 12 and is observed for a value derived from fitting to a complex mechanism by the work of Vandooren and Van Tiggelen [49]. For the particular reaction rate the uncertainty in the experimental value provided by the author amounts to a factor of 2.

Table 4-4: Experimental Validation Set of 21 Experimental Reaction Rates.[a]

	Reaction							T	k_{exp}	k_{calc}/k_{exp}	ρ
Absolute value measured directly											
1a	$H^\bullet$	+	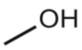	↔	H_2	+	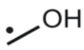	600	$1.3x10^5$ [46]	0.24	4.1
1b								600	$9.9x10^4$ [50]	0.33	3.0
2a	$H^\bullet$	+	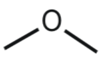	↔	H_2	+	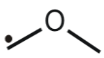	400	$2.0x10^4$ [47]	0.19	5.2
2b								600	$2.5x10^5$ [51]	0.40	2.5
2c								300	$7.8x10^2$ [52]	0.45	2.2
3a	$H^\bullet$	+	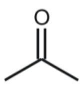	↔	H_2	+	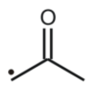	750	$2.3x10^5$ [48]	0.60	1.7
3b								1000	$1.9x10^6$ [53]	0.44	2.3
3c								900	$9.6x10^4$ [54]	4.64	4.6
4a	$H^\bullet$	+	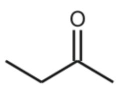	↔	H_2	+	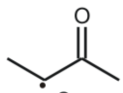	750	$7.2x10^5$ [48]	0.96	1.0
5a	$H^\bullet$	+	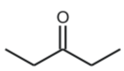	↔	H_2	+	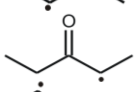	750	$1.2x10^6$ [48]	1.16	1.2
6a	$H^\bullet$	+	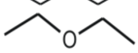	↔	H_2	+	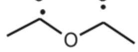	600	$4.9x10^5$ [51]	1.23	1.2
Experimental value and limited review											
2d	$H^\bullet$	+	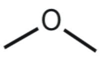	↔	H_2	+	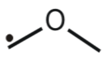	600	$3.0x10^5$ [55]	0.33	3.0
Experimental value derived from fitting to a complex mechanism											
1c	$H^\bullet$	+	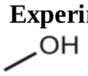	↔	H_2	+	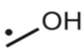	1000	$2.4x10^5$ [56]	3.15	3.2

1d								1000	9.2×10^{6} [49]	0.08	12.0
2e	$H^{\bullet}$	+	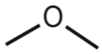	↔	H_2	+	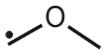	1000	5.0×10^{6} [55]	0.44	2.3
2f								1000	2.5×10^{6} [57]	0.87	1.2
2g								1000	1.1×10^{7} [58]	0.20	5.0
2h								1000	1.0×10^{7} [59]	0.22	4.6
7a	$H^{\bullet}$	+	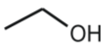	↔	H_2	+	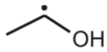	600	9.5×10^{4} [60]	2.06	2.1
7b								400	1.3×10^{4} [61]	1.17	1.2
Experimental value derived from detailed balance/reverse rate											
1e	$H^{\bullet}$	+	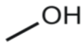	↔	H_2	+	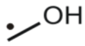	1000	9.4×10^{7} [62]	1.23	1.2
										<ρ>	**3.1**

[a] T in K, k_{exp} in $m^3\ mol^{-1}\ s^{-1}$, ρ the factor of deviation between two values taken from eq (4-4), $k_{calc} = \kappa\tilde{A}_{GA}\ exp(-E_{a,GA}/RT)$).

Excluding this large deviation as outlier, the methodology presented in this work shows to predict rate coefficients for α-hydrogen-abstraction reactions from oxygenates by hydrogen atoms with a mean factor of deviation with experimental rate coefficients, <ρ>, of better than 3. Clearly, the accuracy of the group additive method in comparison with experimental values is determined not only by the accuracy of the group additive method itself but also by the accuracy of the CBS-QB3 method from which the ΔGAV° values have been derived. Hence, the overall conclusion is that the accuracy of the group additive method is of a similar order as the accuracy of the CBS-QB3 method.

Comparison with other Models: The predictions of the group additive model developed in this work are compared with the corresponding predictions of three other models, that is, the model of Blowers and Masel [4], the IP model, developed by Denisov [3], and Ratkiewicz's model [19] based on the reaction class transition state theory. In Figure 4-3, CBS-QB3 activation energies at 300 K of the ab initio validation set are compared in a parity plot to those obtained using (a) the group additive method presented in this work, (b) the Blowers and Masel model and (c) the IP model.

The Blowers and Masel model calculates activation energies from the standard reaction enthalpy, $\Delta_r H$ of the particular reaction based on eq (4-7):

$$E_a = \left(\frac{w_b + w_f + \Delta_r H}{2} \right) \frac{\left(V_p - (w_b + w_f) + \Delta_r H\right)^2}{V_p^2 - (w_b + w_f)^2 + \Delta_r H^2} \tag{4-7}$$

in which w_b and w_f formally correspond to the bond dissociation energy of the breaking bond and the forming bond, respectively, and V_p is related to the intrinsic barrier E_α^{o}. The sum w_b + w_f is estimated as a single parameter.

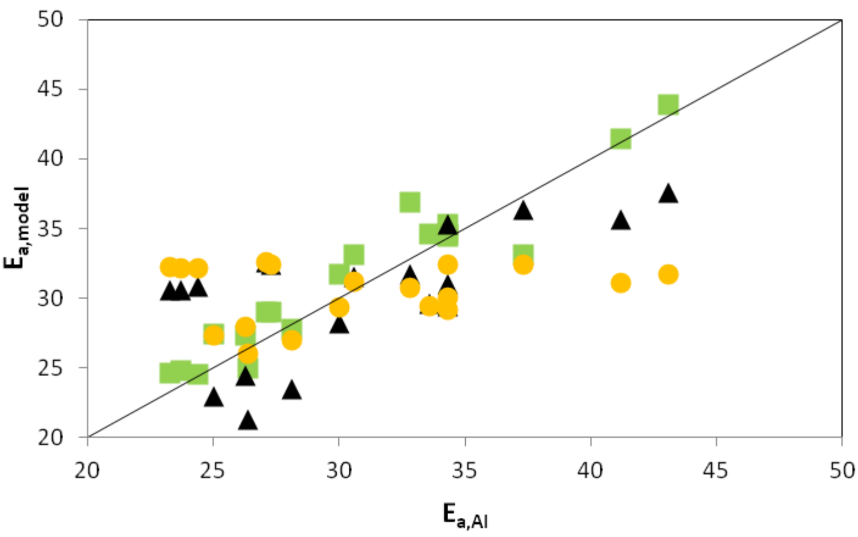

Figure 4-3: Parity plot of predicted activation energies at 300 K vs ab initio calculated activation energies showing the improved performance of the group additive model developed in this work (□), in comparison with the Blowers and Masel model with w_f + w_b = 291.4 kJ mol^{-1} and V_p = 582.8 kJ mol^{-1} (Δ) and the IP model with a = 0.3 and b = 8.3 (o) (Activation energies, E_a, in kJ mol^{-1}, for the 19 reactions of the ab initio validation set of Table S11, Appendix C).

All parameters present in eq (4-7) were estimated by minimizing the residual sum of squares (RSSQ) of the deviation between the Blowers and Masel model predictions for activation energies and the corresponding ab initio calculated values, for the same training set of reactions as used for the determination of ΔGAV°s (Table S1, Appendix C). The estimated parameters for this model are w_b+w_f=291.4 kJ mol^{-1} and V_P=582.8 kJ mol^{-1}. Next, the obtained parameters were used for the determination of the activation energies of the 19 reactions of the ab initio validation set (Table S11, Appendix C). The MAD for the deviation of predicted by eq (4-7) from the corresponding ab initio calculated values amounts to 3.9 kJ mol^{-1}, while the MAD between the group additively predicted and the ab initio calculated values amounts to only 1.4 kJ mol^{-1}. Additionally, for 8 out of the 19 reactions included in the validation set the Blowers and Masel model predicts activation energies that deviate more than 5 kJ mol^{-1} from their ab initio counterparts.

The MAD between the group additively predicted and the ab initio calculated values is compared with the corresponding value for the comparison between predictions of the IP model and the ab initio calculated values of the validation set presented in Table S11 (Appendix C). The IP model correlates the activation energy to the reaction enthalpy as follows:

$$b = a\left(E_{\mathrm{a}} - \Delta_{\mathrm{r}} H^{\mathrm{o}}\right)^{1/2} - E_{\mathrm{a}}^{1/2} \qquad (4\text{-}8)$$

where a and b are parameters that relate to the force constants of the broken and formed carbon–hydrogen bond and the magnitude of the displacement of the migrating hydrogen atom. Similar to the Blowers and Masel model, the IP model parameters were determined by minimizing the RSSQ of the deviation between the activation energies predicted by the IP model and the corresponding ab initio calculated values, for all reactions in the training set (Table S1, Appendix C). The resulting values of the parameters are a = 0.3 and b = 8.3, which are consecutively used in eq (4-8) to determine the activation energies for the ab initio validation set. The MAD between the IP model and the ab initio calculated values amounts to 4.5 kJ mol^{-1}, which is also larger than the corresponding value for the group additive predictions for the same set of reactions (1.4 kJ mol^{-1}). Moreover, 7 out of the 19 activation energies predicted by the IP model deviate more than 5 kJ mol^{-1} from the ab initio values.

An overview of the comparative performance of the three models on the ab initio validation set at 300 K, that is, the group additive model developed in this work, the Blowers and Masel model and the IP model is presented in Table 4-5. It is clear that the group additive model has an MAD about three times lower than the two other models, although the parameters of all models have been fitted to the same training set and applied to the same validation set.

Table 4-5: Average Deviations between Predicted by Three Different Models (Group Additive Model Developed in This Work, Blowers and Masel [4] and the Intersecting Parabolas [3] Model) and ab Initio Activation Energies, E_a, for the Exothermic Reaction at 300 K for the Reactions Included in Table S11 (Appendix C)[a]

	Group Additivity	Blowers and Masel	Intersecting Parabolas
MAD	1.4	3.9	4.5
RMS	1.8	4.4	5.6
MAX	4.2	7.3	11.4

[a] E_a in kJ mol^{-1}

The method developed by Ratkiewicz et al. [19], reaction class transition state theory (RC-TST), is based on four correction factors that account for effects of electronic activation energy, partition function, symmetry, and tunneling on the rate coefficient of a reference reaction. Unfortunately, for abstractions by H atoms, this method is currently only parameterized for alcohols. Experimental reaction rates from the NIST Chemical Kinetics Database [45] are scarce, and for hydrogen abstractions by hydrogen from alcohols, only a single reaction is found, that is, the hydrogen abstraction from ethanol. Hence, next to the comparison with experimental values, Ratkiewicz' method is also compared to the alcohol-related reactions from the ab initio validation set. Alcohols are involved only for two reactions included in the ab initio validation set, that is, the H-abstraction from 1-butanol and from 2-methylbutan-1-ol (reactions 2/4 and 2/14 from Table 4-3, respectively). Both of them along with the one experimental reaction rate available belong to the hydrogen abstractions from primary α-carbon sites. After applying the appropriate equation for reference reaction rate constants (eq 4-9) and the corresponding correction factors, as they are summarized for α-hydrogen abstractions from the alcohol class by Ratkiewicz et al. [19] (see Table IV) the results summarized in Table 4-6.

$$k_\alpha(T) = 2.97\times10^{-19}\times T^{2.53}\times\exp\left(\frac{-1721}{T}\right)\times10^{-6}\quad (\mathrm{m^3\ s^{-1}\ molecule^{-1}}) \qquad (4\text{-}9)$$

Table 4-6: Comparison of the Performance of the Group Additive Model Developed in this Work and the Reaction Class Transition State Theory (RC-TST) Method Developed by Ratkiewicz et al [19]. Predictions of the two Models Compared with the Available Experimental and ab Initio Calculated Reaction Rates.[a]

	Reaction	*T*	k_{exp}	k_{AI}	ρ GA	ρ Ref. [19]
1a	$H^{\bullet}$ + 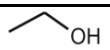 ↔ H_2 + 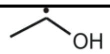	400	$1.3x10^4$ [61]		1.2	1.9
1b		600	$9.5x10^4$ [60]		2.1	1.3
2a	$H^{\bullet}$ + 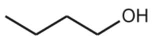 ↔ H_2 + 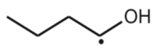	300		$1.4x10^3$	1.2	1.9
2b		1000		$1.4x10^6$	1.1	1.5
2c		2000		$1.5x10^7$	1.0	1.2
3a	$H^{\bullet}$ + 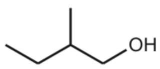 ↔ H_2 + 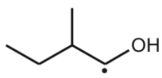	300		$2.2x10^3$	1.7	3.0
3b		1000		$1.7x10^6$	1.3	1.9
3c		2000		$1.8x10^7$	1.2	1.4
				<ρ>	1.3	1.8

[a] *T* in K, k_{exp} and k_{AI} in m^3 mol^{-1} s^{-1}, ρ the factor of deviation between the model predicted value and the corresponding experimental or ab initio rate coefficient.

The mean factor of deviation between the model predicted and ab initio rate coefficients in Table 4-6 amounts in average to 1.3 for the group additive method and 1.8 for the RC-TST method of Ratkiewicz et al. [19]. While the group additive model performs slightly better, the difference is not sufficient to conclude that this model outperforms the RC-TST method; furthermore, the comparison is for two out of three reactions made to rate coefficients calculated using the CBS-QB3 approach, the same from which the ΔGAV° values have been determined. From the two experimental data points of the first reaction in Table 4-6, one is predicted better by the GA model and the other better by the RC-TST model. If a large experimental set would exist, most probably both methods would give similar results.

To conclude, the group additive model constructed in this work outperforms the model of Blowers and Masel and the IP model for activation energies. Furthermore, these models assume a fixed pre-exponential factor for the whole reaction family, while the GA model also allows to model pre-exponential factors.

Additionally, the rate coefficients calculated by the model developed by Ratkiewicz et al. [19] for the reactions involving alcohols differ only slightly from the reference rate coefficients than the group additive predictions. However, the group additive model developed in this work is also applicable to a range of oxygenates other than alcohols, and it allows to distinguish between mono-, di-, and trisubstituted carbon atoms adjacent to the carbon-centered radical, two aspects that are not covered by the model developed by Ratkiewicz et al. [19].

4.5 Conclusions

In this work, a group additive scheme is developed to model the Arrhenius parameters (activation energies and pre-exponential factors) and the rate and tunneling coefficients for hydrogen-abstraction reactions by hydrogen atoms from oxygenate compounds in the temperature range of 300-2000 K. This model is valid for a wide range of oxygenates in which the oxygen or the carbonyl group is in α position related to the carbon atom from which the hydrogen is abstracted, including alcohols, ethers, esters, acids, ketones, diketones, aldehydes, hydro- and alkyl peroxides, and unsaturated ethers and ketones.

This work is an extension of the recent work on hydrogen abstractions by carbon-centered radicals from oxygenates where the oxygen or the carbonyl group is also in α position to the carbon atom from which the hydrogen is abstracted.

The kinetic and thermodynamic data are obtained using the accurate CBS-QB3 method with kinetics in the high-pressure limit, incorporating Eckart tunneling coefficients. From a set of 60 hydrogen abstraction reactions by hydrogen atoms from oxygenate compounds, four primary and eleven secondary contributions are determined. The inclusion of secondary contributions is shown to be necessary for improving the accuracy of the model. Since the temperature dependence of the Arrhenius parameters is incorporated in the corresponding values for the well-chosen reference reaction, the ΔGAV^{o}s are almost temperature independent. Tunneling coefficients can be accurately predicted by a fourth-order polynomial that correlates the tunneling coefficient to the temperature and the activation energy of the exothermic direction of the reaction.

This group additive model is validated upon an ab initio validation set and an experimental validation set. Furthermore, the results of this model are compared with the results obtained by three models: the Blowers and Masel, the IP and Ratkiewicz's RC-TST model. The rate coefficients of the ab initio validation set can be reproduced on average with a mean factor of 2 at 300 K and even better in higher temperatures. The mean absolute deviations at 300 K between group additively predicted and ab initio calculated Arrhenius parameters (activation energies and pre-exponential factors) amount to 1.4 kJ mol^{-1} and 0.127, resp. Additionally, the 23 experimental rate coefficients are well predicted by the model, with a mean factor of deviation of 3 between the GA predicted and the experimental rate coefficients.

Therefore, the model developed in this work can be used for a reliable prediction of Arrhenius parameters and rate coefficients for a wide range of hydrogen abstraction reactions between gas-phase oxygenates and hydrogen atoms at temperatures ranging between 300 and 2000 K, combining fast prediction with a wide applicability. This model fits seamlessly with previously constructed models, which broadens the application range in a consistent way.

4.6 References

1. Evans, M.G. and M. Polanyi, *Further Considerations on the Thermodynamics of Chemical Equilibria and Reaction Rates.* Proc. Roy. Soc. A, 1936. **154**: p. 1333-1360.
2. Evans, M.G. and M. Polanyi, *Inertia and Driving Force of Chemical Reactions.* Trans. Faraday Soc., 1938. **1938**(34): p. 11-29.
3. Denisov, E.T., *New Empirical Models of Free Radical Abstraction Reactions.* Usp Khim+, 1997. **66**(10): p. 953-971.
4. Blowers, P. and R. Masel, *Engineering Approximations for Activation Energies in Hydrogen Transfer Reactions.* Aiche J, 2000. **46**(10): p. 2041-2052.
5. Benson, S.W. and J.H. Buss, *Additivity Rules for the Estimation of Molecular Properties. Thermodynamic Properties.* J Chem Phys, 1958. **29**(9): p. 546-561.
6. Benson, S.W., *Thermochemical Kinetics*. 1968, New York: John Wiley & Sons Ltd.
7. Benson, S.W., *Oxygen Initiated Combustion: Thermochemistry and Kinetics of Unsaturated Hydrocarbons.* Int J Chem Kinet, 1996. **28**(9): p. 665-672.
8. Benson, S.W., *Some Observations on the Thermochemistry and Kinetics of Peroxy Radicals.* J Phys Chem-Us, 1996. **100**(32): p. 13544-13547.
9. Benson, S.W., *Some Observations on the Kinetics and Thermochemistry of the Reactions of HO2 Radicals with Aldehydes and Ketones.* Int J Chem Kinet, 2001. **33**(9): p. 509-512.
10. Benson, S.W., *Probing the Chemical Kinetics of Air Pollution.* Environ Sci Technol, 2002. **36**(1): p. 28-32.
11. Shum, L.G.S. and S.W. Benson, *The Pyrolysis of Dimethyl Sulfide, Kinetics and Mechanism.* Int J Chem Kinet, 1985. **17**(7): p. 749-761.
12. Benson, S.W., *Some Key Reactions in Oxidation and Combustion - Thermochemistry and Kinetics.* Abstr Pap Am Chem S, 1982. **183**(Mar): p. 35-41.
13. Willems, P.A. and G.F. Froment, *Kinetic Modeling of the Thermal-Cracking of Hydrocarbons .1. Calculation of Frequency Factors.* Ind Eng Chem Res, 1988. **27**(11): p. 1959-1966.
14. Willems, P.A. and G.F. Froment, *Kinetic Modeling of the Thermal-Cracking of Hydrocarbons .2. Calculation of Activation-Energies.* Ind Eng Chem Res, 1988. **27**(11): p. 1966-1971.
15. Truong, T.N., *Reaction Class Transition State Theory: Hydrogen Abstraction Reactions by Hydrogen Atoms as Test Cases.* J Chem Phys, 2000. **113**(12): p. 4957-4964.
16. Kungwan, N. and T.N. Truong, *Kinetics of the Hydrogen Abstraction CH3 + Alkane -> CH4 Plus Alkyl Reaction Class: An Application of the Reaction Class Transition State Theory*. J Phys Chem A, 2005. **109**(34): p. 7742-7750.
17. Huynh, L.K., S. Panasewicz, A. Ratkiewicz, and T.N. Truong, *Ab Initio Study on the Kinetics of Hydrogen Abstraction for the H+Alkene -> H2+Alkenyl Reaction Class.* J Phys Chem A, 2007. **111**(11): p. 2156-2165.

18. Ratkiewicz, A. and T.N. Truong, *Kinetics of the Hydrogen Abstraction R-OH+H -> R-O-center + H2 Reaction Class.* Int J Chem Kinet, 2010. **42**(7): p. 414-429.

19. Ratkiewicz, A., J. Bieniewska, and T.N. Truong, *Kinetics of the Hydrogen Abstraction R-OH+H -> R-center-OH+H2 Reaction Class: An Application of the Reaction Class Transition State Theory.* Int J Chem Kinet, 2011. **43**(2): p. 78-98.

20. Sumathi, R. and W.H. Green, *Oxygenate, Oxyalkyl and Alkoxycarbonyl Thermochemistry and Rates for Hydrogen Abstraction from Oxygenates.* Phys Chem Chem Phys, 2003. **5**(16): p. 3402-3417.

21. Sumathi, R., H.H. Carstensen, and W.H. Green, *Reaction Rate Prediction via Group Additivity Part 1: H Abstraction from Alkanes by H and CH3.* J Phys Chem A, 2001. **105**(28): p. 6910-6925.

22. Sumathi, R., H.H. Carstensen, and W.H. Green, *Reaction Rate Prediction via Group Additivity, Part 2: H-Abstraction from Alkenes, Alkynes, Alcohols, Aldehydes and Acids by H Atoms.* J Phys Chem A, 2001. **105**(39): p. 8969-8984.

23. Saeys, M., M.F. Reyniers, V. Van Speybroeck, M. Waroquier, and G.B. Marin, *Ab Initio Group Contribution Method for Activation Energies of Hydrogen Abstraction Reactions.* Chem Phys Chem, 2006. **7**(1): p. 188-199.

24. Sabbe, M.K., A.G. Vandeputte, M.F. Reyniers, M. Waroquier, and G.B. Marin, *Modeling the Influence of Resonance Stabilization on the Kinetics of Hydrogen Abstractions.* Phys Chem Chem Phys, 2010. **12**(6): p. 1278-1298.

25. Adamczyk, A.J., M.F. Reyniers, G.B. Marin, and L.J. Broadbelt, *Kinetics of Substituted Silylene Addition and Elimination in Silicon Nanocluster Growth Captured by Group Additivity.* Chem Phys Chem, 2010. **11**(9): p. 1978-1994.

26. Adamczyk, A.J., M.F. Reyniers, G.B. Marin, and L.J. Broadbelt, *Kinetic Correlations for H2 Addition and Elimination Reaction Mechanisms During Silicon Hydride Pyrolysis.* Phys Chem Chem Phys, 2010. **12**(39): p. 12676-12696.

27. Adamczyk, A.J., M.F. Reyniers, G.B. Marin, and L.J. Broadbelt, *Hydrogenated Amorphous Silicon Nanostructures: Novel Structure-Reactivity Relationships for Cyclization and Ring Opening in the Gas Phase.* Theor Chem Acc, 2011. **128**(1): p. 91-113.

28. Vandeputte, A.G., M.K. Sabbe, M.F. Reyniers, and G.B. Marin, *Kinetics of Alpha Hydrogen Abstractions from Thiols, Sulfides and Thiocarbonyl Compounds.* Phys Chem Chem Phys, 2012. **14**(37): p. 12773-12793.

29. Vandeputte, A.G., M.F. Reyniers, and G.B. Marin, *Kinetic Modeling of Hydrogen Abstractions Involving Sulfur Radicals.* Chem Phys Chem, 2013. **14**(16): p. 3751-3771.

30. Paraskevas, P.D., M.K. Sabbe, M.F. Reyniers, N. Papayannakos, and G.B. Marin, *Kinetic Modeling of α-Hydrogen Abstractions from Unsaturated and Saturated Oxygenate Compounds by Carbon-Centered Radicals.* Chem Phys Chem, 2014. **15**(9): p. 1849-1866.

31. William H. Green, Joshua W. Allen, Beat A. Buesser, Robert W. Ashcraft, Gregory J. Beran, Caleb A. Class, Connie Gao, C. Franklin Goldsmith, Michael R. Harper, et al., *RMG - Reaction Mechanism Generator v4.0.1*, 2013.

32. Vandewiele, N.M., K.M. Van Geem, M.F. Reyniers, and G.B. Marin, *Genesys: Kinetic Model Construction Using Chemo-Informatics.* Chem Eng J, 2012. **207**: p. 526-538.

33. Montgomery, J.A., M.J. Frisch, J.W. Ochterski, and G.A. Petersson, *A Complete Basis Set Model Chemistry. VI. Use of Density Functional Geometries and Frequencies.* J Chem Phys, 1999. **110**(6): p. 2822-2827.

34. Sabbe, M.K., A.G. Vandeputte, M.F. Reyniers, V. Van Speybroeck, M. Waroquier, and G.B. Marin, *Ab Initio Thermochemistry and Kinetics for Carbon-Centered Radical Addition and Beta Scission Reactions.* J Phys Chem A, 2007. **111**(34): p. 8416-8428.

35. Laidler, K.J., *Chemical Kinetics*. 1987, New York: Harper & Row.

36. Eckart, C., *The Penetration of a Potential Barrier by Electrons.* Phys Rev, 1930. **35**: p. 1303-1309.

37. Vandeputte, A.G., M.K. Sabbe, M.F. Reyniers, V. Van Speybroeck, M. Waroquier, and G.B. Marin, *Theoretical Study of the Thermodynamics and Kinetics of Hydrogen Abstractions from Hydrocarbons.* J Phys Chem A, 2007. **111**(46): p. 11771-11786.

38. Frisch, M.J., G.W. Trucks, H.B. Schlegel, G.E. Scuseria, M.A. Robb, J.R. Cheeseman, J.A. Montgomery, T. Vreven, K.N. Kudin, et al., *Gaussian 03, revision B.03*, 2004, Gaussian, Inc.: Wallingford CT.

39. Paraskevas, P.D., M.K. Sabbe, M.F. Reyniers, N. Papayannakos, and G.B. Marin, *Group Additive Values for the Gas Phase Standard Enthalpy of Formation, Entropy and Heat Capacity of Oxygenates.* Chem-Eur J, 2013. **19**: p. 16431-16452.

40. Carvalho, E.F.V., A.N. Barauna, F.B.C. Machado, and O. Roberto, *Theoretical Calculations of Energetics, Structures and Rate Constants for the H+CH3OH Hydrogen Abstraction Reactions.* Chem Phys Lett, 2008. **463**(1-3): p. 33-37.

41. Park, J., Z.F. Xu, and M.C. Lin, *Thermal Decomposition of Ethanol. II. A Computational Study of the Kinetics and Mechanism for the H+C2H5OH Reaction.* J Chem Phys, 2003. **118**(22): p. 9990-9996.

42. Sabbe, M.K., M.F. Reyniers, M. Waroquier, and G.B. Marin, *Hydrogen Radical Addition to Unsaturated Hydrocarbons and Reverse Beta-Scission Reactions: Modeling of Activation Energies and Pre-Exponential Factors.* Chem Phys Chem, 2009. **11**(1): p. 195-210.

43. Wigner, E., *Calculation of the Rate of Elementary Association Reactions.* J Chem Phys, 1937. **5**: p. 720-725.

44. Truong, T.N., W.T. Duncan, and M. Tirtowidjojo, *A Reaction Class Approach for Modeling Gas Phase Reaction Rates.* Phys Chem Chem Phys, 1999. **1**(6): p. 1061-1065.

45. *Chemical Kinetics Database, NIST Standard Reference Database 17, Version 7.0 (Web Version), Release 1.6.7, Data Version 2013*, 2013.

46. Li, S.C. and F.A. Williams, *Experimental and Numerical Studies of Two-Stage Methanol Flames.* Twenty-Sixth Symposium (International) on Combustion, 1996. **1-2**: p. 1017-1024.

47. Lee, J.H., R.C. Machen, D.F. Nava, and L.J. Stief, *Rate Parameters for the Reaction of Atomic-Hydrogen with Dimethyl Ether and Dimethyl Sulfide.* J Chem Phys, 1981. **74**(5): p. 2839-2844.

48. Tranter, R.S. and R.W. Walker, *Rate Constants for H and OH Attack on Propanone, Butanone and Pentan-3-one at 753 K and the Oxidation Chemistry of the Radicals Formed.* Phys Chem Chem Phys, 2001. **3**(7): p. 1262-1270.

49. Vandooren, J.P. and P.J. Van Tiggelen, *Experimental Investigation of Methanol Oxidation in Flames: Mechanism and Rate Constants of Elementary Steps.* Symp. Int. Combust. Proc., 1981. **18**: p. 473-483.

50. Hoyermann, K., R. Sievert, and H.G. Wagner, *Mechanism of the Reaction of H-Atoms with Methanol.* Ber Bunsen Phys Chem, 1981. **85**(2): p. 149-153.

51. Faubel, C., K. Hoyermann, E. Strofer, and H.G. Wagner, *Gas-Phase Reaction of Hydrogen-Atoms with Dimethylether, Diethylether and Butylmethylether.* Ber Bunsen Phys Chem, 1979. **83**(5): p. 532-538.

52. Slemr, F. and P. Warneck, *Kinetics of Reaction of Atomic-Hydrogen with Methyl Hydroperoxide.* Int J Chem Kinet, 1977. **9**(2): p. 267-282.

53. Sato, K. and Y. Hidaka, *Shock-Tube and Modeling Study of Acetone Pyrolysis and Oxidation.* Combust Flame, 2000. **122**(3): p. 291-311.

54. Azatyan, V., Z. Gyulbeky, L. Romanovi, and A. Nalbandy, *Reactions of Hydrogen and Oxygen with Acetone.* Arm Khim Zh, 1972. **25**(9): p. 727-731.

55. Takahashi, K., O. Yamamoto, T. Inomata, and M. Kogoma, *Shock-Tube Studies on the Reactions of Dimethyl Ether with Oxygen and Hydrogen Atoms.* Int J Chem Kinet, 2007. **39**(2): p. 97-108.

56. Cribb, P.H., J.E. Dove, and S. Yamazaki, *A Kinetic-Study of the Pyrolysis of Methanol Using Shock-Tube and Computer-Simulation Techniques.* Combust Flame, 1992. **88**(2): p. 169-185.

57. Hidaka, Y., K. Sato, and M. Yamane, *High-Temperature Pyrolysis of Dimethyl Ether in Shock Waves.* Combust Flame, 2000. **123**(1-2): p. 1-22.

58. Aronowitz, D. and D. Naegeli, *High-Temperature Pyrolysis of Dimethyl Ether.* Int J Chem Kinet, 1977. **9**(3): p. 471-479.

59. Fernandes, R.X., C. Fittschen, and H. Hippler, *Kinetic Investigations of the Unimolecular Decomposition of Dimethylether Behind Shock Waves.* React Kinet Catal L, 2009. **96**(2): p. 279-289.

60. Aders, W.K. and H.G. Wagner, *Studies on Reaction of Hydrogen-Atoms with Ethanol and Tert-Butanol.* Ber Bunsen Phys Chem, 1973. **77**(9): p. 712-718.

61. Bansal, K.M. and G.R. Freeman, *Gamma Radiolysis of Ethanol Vapor.* J Am Chem Soc, 1968. **90**(26): p. 7183-7189.

62. Westbrook, C.K. and F.L. Dryer, *Comprehensive Mechanism for Methanol Oxidation.* Combust Sci Technol, 1979. **20**(3-4): p. 125-140.

Chapter 5

Group Additive Kinetics for Hydrogen Transfer Between Oxygenates

This chapter includes the following paper:

Paraskevas, P.D.; M.K. Sabbe,; M.F. Reyniers; N. Papayannakos; G.B. Marin, Group Additive Kinetics for Hydrogen Transfer Between Oxygenates, *J Phys Chem A*, **2015**, *119*, 6961-6980.

5.1 Abstract

Hydrogen abstraction reactions involving oxygenates in gaseous phase play an important role in many biomass-related conversion processes. In this work, group additivity is used to provide Arrhenius parameters in a temperature range of 300-2500 K for hydrogen abstractions between oxygenate compounds such as alcohols, ethers, esters, acids, ketones, diketones, aldehydes, hydroxyperoxides, alkyl peroxides and unsaturated ethers and ketones. The group additive values for Arrhenius parameters of hydrogen transfer reactions of the type O--H--C and O--H--O are derived from CBS-QB3 calculations in the high-pressure limit. From a total set of 118 reactions, 43 group additivity values are determined. Inclusion of an additional 37 corrections accounting for cross-resonance effects in the transition state further improves the accuracy of the model. For a set of 25 ab initio calculated and 60 experimental rate coefficients, group additive modeling reproduces rate coefficients within a mean factor of deviation of ~3. Hence, the developed group additive models can be reliably used for an accurate and fast prediction of the kinetics of hydrogen abstractions involving oxygenates.

5.2 Introduction

In the last decades there has been an increasing concern for sustainable development and a worldwide protection of the environment. The key point of the sustainable development is the use of renewable resources. Most of the compounds originating from biological sources contain oxygen in various functional groups. The upgrading of these molecules can be achieved by employing processes like pyrolysis, steam-cracking, polymerization, and oxidation, most of which involve oxygenate molecules and radicals in gaseous phase, but their chemistry at reaction conditions remains largely unexplored. Accurate and robust modelling of such processes requires fundamental reaction networks, and because hydrogen abstraction reactions form a substantial part of most radical reaction networks, data for such reactions are necessary. To acquire all these data through experiment is subject to financial and instrumental limitations because experimental equipment can often only cover a narrow range of conditions and the number of experiments that can be performed in a certain period is limited.

More recently, computational tools such as the density functional theory (DFT) B3LYP [1], BMK [2] and Minnesota functionals [3], the composite methods of Gaussian [4-6], and the complete basis set [7] (CBS) and Weizmann [8, 9] methods, make it feasible to determine kinetic and thermodynamic parameters for several complex radical reactions. However, even those tools have their own constraints, especially for larger species where ab initio calculations still remain computationally too expensive. To overcome this restriction, methods have been developed that can predict thermodynamics and kinetics for larger species based on a limited set of parameters.

Kinetic parameters are often obtained by correlations like the Evans−Polanyi [10, 11] relationship, where activation energies for reactions within the same reaction family are correlated with their reaction enthalpy. Variations of this model and more extended ones are the Intersecting Parabolas (IP) method [12] and the Blowers and Masel model [13], providing more detailed but simple correlations. The disadvantage is that these methods only provide activation energies; pre-exponential factors have to be obtained from other sources, or they are considered fixed for the whole reaction family.

More accurate Arrhenius parameters (activation energies and pre-exponential factors) are obtained by means of group additivity. Additivity rules are still widely applied, mainly for thermochemistry [14] and kinetics [15], but it is particularly group additivity as developed within the framework of thermochemical kinetics by Benson and co-workers [16-18] that has gained most popularity. This method has been successfully applied in a variety of processes such as pyrolysis [19], oxidation or combustion [20] and also in the study of free-radical atmospheric chemistry [21]. Since implementing these thermochemical kinetics techniques in automatic reaction mechanism building programs is not straightforward, more systematic variants have been developed based on the same idea [22-24].

Group additive models (GA) for Arrhenius parameters are of major importance for reaction network generation programs such as RMG [25] (Reaction Mechanism Generator) and Genesys [26] in which group recognition algorithms that identify all required contributions are implemented. These automated reaction network generators are indispensable in studying large, complex radical reaction mechanisms.

In this work, a GA model is developed that allows us to determine rate coefficients and Arrhenius parameters for hydrogen abstraction reactions from oxygenate compounds by oxygen-centered radicals. This GA model is completely in agreement with previous models for hydrogen abstractions from oxygenate compounds by carbon-centered [27] and by hydrogen radicals [28], and these models can be used seamlessly in combination with earlier developed models for abstraction from hydrocarbons [29, 30] and from sulfur compounds [31, 32].

Rate coefficients have been obtained from CBS-QB3 calculations with corrections for tunneling and the internal rotation around the forming/breaking bond in the transition state. From these calculated rate coefficients, the group additive values for the calculation of Arrhenius parameters with the group additive model are derived using least-squares regression, along with corrections accounting for possible resonance and/or hyperconjugative effects in the transition state. The results in this paper are structured according to the two reaction families considered, i.e., hydrogen abstractions by oxygen-centered radicals from (a) a carbon atom and (b) an oxygen atom. The first one covers transition states of the O--H--C type, while the second one refers to transition states of the O--H--O type. Finally, the accuracy of the constructed group additive models is validated by comparing group additive predictions with a set of ab initio calculated data and a set of experimental data taken from literature.

5.3 Computational Methods

5.3.1 Rate Coefficients

Rate coefficients are calculated using conventional transition-state theory (TST) in the high-pressure limit [33] as it is expressed by eq (5-1):

$$k(T) = \kappa_{\mathrm{Eckart}}(T)\frac{k_{\mathrm{B}}T}{h}\frac{q_{\ddagger}}{q_{\mathrm{A}}q_{\mathrm{B}}}e^{-\frac{\Delta E(0\,\mathrm{K})}{RT}} \tag{5-1}$$

with q the total partition function per unit volume; k_B and h the Boltzmann and the Planck constants, respective; $\Delta E(0\text{ K})$ the electronic zero-point corrected reaction barrier determined using the CBS-QB3 method of Montgomery et al. [7]; and $\kappa_{Eckart}(T)$ the one-dimensional (1D) Eckart [34] tunneling coefficient. All electronic structure calculations have been performed with the Gaussian 09 [35] program.

Partition functions, q, are calculated at the B3LYP/6-311G(2d,d,p) level using a default scale factor of 0.99, while the one-dimensional hindered rotor (1D-HR) potential [36-38] was calculated at the B3LYP/6-31G(d) level of theory as a function of the torsional angle in steps of 10^{o}. Based on the results of previous work [39, 40], the internal rotation around the forming/breaking bond in the transition state is treated explicitly because its contribution cannot cancel out between transition state and reactants: it exists only in the transition state and can therefore significantly contribute to the rate coefficient. The contribution of most of the other internal rotations can be considered similar in reactants and transition state, and they are expected to have a minor effect on the rate coefficient. Hence, the other rotational modes are considered as harmonic oscillators in the calculation of the rate coefficients.

Electronic energies are obtained using the CBS-QB3 composite method. In a benchmark study, the CBS-QB3 method has, among the G3B3 composite method and the MPW1PW91/ 6-311G(2d,d,p) and BMK/6-311G(2d,p,p) density functional theory (DFT) methods, been shown [41] to yield the best agreement with experimental thermochemical and kinetic data for hydrogen abstractions between hydrocarbons. There are methods available that can yield even more accurate thermochemistry, such as the Weizmann methods [2, 9, 42], Gaussian-4 theory (G4) method [43], high-accuracy extrapolated ab initio thermochemistry (HEAT) [44], or CCSD(T) calculations with up to 6ζ basis sets and complete basis set extrapolations [45]. However, these methods are limited to smaller compounds and hence, cannot be used in the framework of this study. Also, consistency of the group additive model in this work with previous work is an argument for the CBS-QB3 method, with the previous work already showing CBS-QB3's accuracy for the thermochemistry of the gas phase oxygenates [40] and for the kinetics of hydrogen abstractions from oxygenates by carbon-centered [27] and by hydrogen [28] atoms.

The reliability of the applied CBS-QB3 method can, in the absence of abundant experimental data, be illustrated by comparing its results for a few reactions to other ab initio calculations for the same reactions, among which some are of a high level. Particularly, Jodkowski et al. [46] performed ab initio calculations at the MP2/6-311G** level of theory for the hydrogen abstraction by a methoxy radical from hydrogen, methane, and water at temperatures ranging from 300 to 2000 K. Rate coefficients obtained by the CBS-QB3 method for the reaction $CH_3O^{\bullet} + H_2 \leftrightarrow CH_3OH + H^{\bullet}$ for the whole temperature range (300-2500 K) deviate by a mean factor of 4.0, whereas for the reaction $CH_3O^{\bullet} + CH_4 \leftrightarrow CH_3OH + {}^{\bullet}CH_3$ the mean factor of deviation is 2.4 and even lower for the reaction $CH_3O^{\bullet} + H_2O \leftrightarrow CH_3OH + {}^{\bullet}OH$ in which the mean deviation factor is 1.9. Truong and Ratkiewicz [47] used the BH&HLYP/cc-pVDZ level of theory to determine rate coefficients for the hydrogen abstraction by hydrogen atom from methanol producing a methoxy radical and hydrogen. The resulting rate coefficients in the temperature range 300-2500 K differ with a mean factor of deviation of only 1.5 with the CBS-QB3 rate coefficients. In addition to that, Jorgensen et al. [48] show that for the gas phase hydrogen abstraction from methyl acetate by hydroxyl the rate coefficients obtained by the CBS-QB3 method at 298 K are in very good agreement with the results of MC-QCISD//MP2/6-311G(d.p), CCSC(T)/VTZ//BH&HLYP/aVTZ, and G3, with the differences being only a factor of 1, 1.3 and 3.2 respectively.

The determination of the transition state can be very difficult for some hydrogen abstractions from oxygenates by hydroxyl, because the B3LYP functional is the built-in geometry optimizer of CBS-QB3. B3LYP's tendency to predict transition states that are too early and barriers that are too low [49] causes some transition-state searches for this reaction family to fail. To overcome this, it was also shown [32] that the BMK functional provides reliable geometries for CBS-QB3 saddle points for hydrogen abstractions by sulfur radicals in cases where the standard B3LYP geometry optimization procedure of the CBS-QB3 method fails to determine transition-state geometries. The geometry optimization strength of the BMK method was shown also by a benchmark study performed by Zheng et al. [50] in which the G3//BMK method was found to produce results that were more accurate than those of G3//MP2 and G3//B3LYP in reproducing bond dissociation energies.

Hence, for the transition states in this work, a three-step optimization procedure was chosen. First, the standard B3LYP/6-311G(d,p) geometry optimization procedure of the CBS-QB3 method is used. For the exceptional case where a transition state could not be located, the transition-state search proceeds to the second step in which the BMK/6-311G(2d,d,p) method is used to determine the transition-state geometry. The resulting geometry is then used in a third step, a new B3LYP/6-311G(d,p) optimization in which the length of the two forming/breaking bonds in the transition state are constrained to the BMK value, after which the CBS-QB3 single-point energy calculations are performed.

To validate this approach, it has been applied to four reactions for which the B3LYP method has no problem finding the transition state. The resulting activation energies differ by only 0.8 kJ mol^{-1} in average and 1.3 kJ mol^{-1} at most from the default CBS-QB3 calculation based on a B3LYP geometry, and 0.105 and 0.213 log(m^3 mol^{-1} s^{-1}) for pre-exponential factors at 300 K (see Appendix D Table S1 for the details). From these values it can be concluded that the BMK method predicts transition-state geometries that can be combined with those predicted by B3LYP. The BMK method has been used in this work only to locate the transition state of a hydrogen abstraction when the B3LYP method fails, which was the case for 20 of the 118 hydrogen abstractions included in the training set of reactions.

Arrhenius parameters (E_a and log$A$) were obtained from linear least-squares regression of the ab initio rate coefficients to the Arrhenius equation in the temperature range T – 100 K to T + 100 K with k sampled at intervals of 50 K and with T the temperature of interest.

The accuracy of the group additive method implemented in this study is assessed by comparison of group additively predicted rate coefficients with ab initio calculated and experimentally obtained rate coefficients. As a measure for the deviation between these values, a factor of deviation, ρ, is defined according to eq (5-2), completely in line with previous work [27, 28, 30-32].

$$\begin{cases} \rho = \dfrac{k_{\mathrm{AI}}}{k_{\mathrm{GA}}} & k_{\mathrm{AI}} > k_{\mathrm{GA}} \\ \rho = \dfrac{k_{\mathrm{GA}}}{k_{\mathrm{AI}}} & k_{\mathrm{GA}} > k_{\mathrm{AI}} \end{cases} \qquad (5\text{-}2)$$

For this factor ρ>1 always holds, which permits us to calculate an arithmetic mean factor of deviation of rate coefficients for a set of reactions, $<\rho>$.

5.3.2 Group Additivity Method

The group additivity model developed in this work is based on Benson's group additivity method [17]. Arrhenius parameters for all reactions within a particular reaction family can be determined based on a limited number of parameters. Details of the use of this method for the calculation of Arrhenius parameters can be found in earlier work [27, 28]. Within this GA method the rate coefficient is expressed by eq (5-3):

$$k = \kappa_{Eckart} n_{\mathrm{e}} k_{\mathrm{GA}} = \kappa n_{\mathrm{e}} \widetilde{A} e^{-\frac{E_{\mathrm{a}}}{RT}} \qquad (5\text{-}3)$$

with κ the tunneling coefficient, n_e the reaction path degeneracy, $\tilde{A}$ the single-event pre-exponential factor, and E_a the activation energy. The single-event pre-exponential factor, $\tilde{A}$, is obtained by dividing the pre-exponential factor, A, with the reaction path degeneracy [51, 52].. A detailed description of how this GA model can be applied for hydrogen abstractions of that type is provided in section 1 of Appendix D.

Two reaction families are studied in this work: the abstraction by an oxygen-centered radical of a hydrogen atom bound (a) to a carbon atom and (b) to an oxygen atom of an oxygenate compound. Consequently, these two reaction families are characterized by transition states of the O--H--C and O--H--O type, respectively. A schematic representation of these types of transition states is presented in Figure 5-1. The subscripts 1 and 2 indicate the direction of the reaction. With O_1 the attacking radical, the hydrogen atom migrates from the group on C_2 or O_2 to the group on O_1 during the reaction. This means that the radical atom abstracting the hydrogen atom is labeled with the subscript 1, while the atom from which the hydrogen is abstracted is labeled with the subscript 2. According to the GA method, Arrhenius parameters for a given reaction can then be expressed as perturbations, which are usually referred to as contributions, to the corresponding kinetic parameters of a well chosen reference reaction [27, 28].

These contributions to Arrhenius parameters are denoted ΔGAV^os [53], which are derived from thermodynamic group additivity as follows: if a GAV describes the group additive value to the standard enthalpy of formation of a species, then ΔGAV is the difference in this GAV between reactant and transition state, now describing the contribution to the activation energy. ΔGAV^o is the difference between the ΔGAV of a target reaction and that of the reference reaction. These ΔGAV^os can be categorized into primary, secondary and tertiary contributions. Primary contributions are the major ones and arise from the central groups between which the hydrogen atom is transferred, while secondary contributions originate from the groups adjacent to the two groups exchanging the hydrogen atom. Finally, tertiary contributions, also referred to as non-nearest-neighbor interactions (NNIs), are those arising from interactions between (a) groups adjacent to the secondary groups with primary groups or (b) secondary groups located on opposite sides of the transition state. A detailed description of these three types of contributions and how they arise in the transition state can be found in earlier work of hydrogen abstractions by carbon-centered radicals from oxygenate compounds [27].

Based on the additivity of standard enthalpy of formation and standard entropy between the transition state and the reactants, the activation energy and pre-exponential factor, respectively, of a given reaction, can be expressed as a truncated sum of contributions to the corresponding Arrhenius parameters of a reference reaction as presented in eq (5-4):

$$E_{\mathrm{a}}(T) = E_{\mathrm{a,ref}}(T) + \sum_{i=1}^{2} \Delta\mathrm{GAV}^{\mathrm{o}}_{\mathrm{E_a}}(C_i) + \sum_{i=1}^{3} \Delta\mathrm{GAV}^{\mathrm{o}}_{\mathrm{E_a}}(X_i) + \sum_{i=1}^{3} \Delta\mathrm{GAV}^{\mathrm{o}}_{\mathrm{E_a}}(Y_i) + \sum_{i} NNI_i^o + \Delta\mathrm{E}^{\mathrm{o}}_{\mathrm{E_{a,res}}}$$

$$\log \tilde{A}(T) = \log \tilde{A}_{ref}(T) + \sum_{i=1}^{2} \Delta\mathrm{GAV}^{\mathrm{o}}_{\log\tilde{\mathrm{A}}}(C_i) + \sum_{i=1}^{3} \Delta\mathrm{GAV}^{\mathrm{o}}_{\log\tilde{\mathrm{A}}}(X_i) + \sum_{i=1}^{3} \Delta\mathrm{GAV}^{\mathrm{o}}_{\log\tilde{\mathrm{A}}}(Y_i) + \sum_{i} NNI_i^o + \Delta \log \tilde{A}^o_{res} \tag{5-4}$$

In equation (5-4) the first term refers to the Arrhenius parameter (E_a or $\log\tilde{A}$ respectively) of the reference reaction, the second term corresponds to the primary contributions; the third and fourth terms correspond to the secondary contributions, whereas the fifth term refers to the tertiary contributions. The last term represents the additional cross-resonance stabilization and hyperconjugative effects due to the simultaneous presence of stabilizing groups centered on the atoms between which the hydrogen is transferred, which cannot be included in the $\Delta\mathrm{GAV}^{\mathrm{o}}$s.

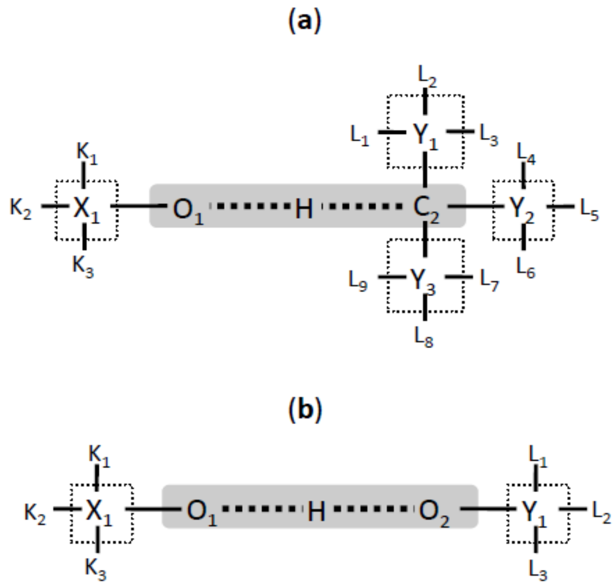

Figure 5-1: Schematic representation of the transition state for abstraction of a hydrogen atom bound (a) to a carbon atom and (b) to an oxygen atom by an oxygen-centered radical. The grey zone indicates the central atoms of the primary contributions. The dotted line encompasses the central atoms of the secondary contributions.

As a reference reaction, usually the simplest reaction that captures the characteristics of the studied reaction family is chosen. In this work, the hydrogen abstraction by a methoxy radical ($CH_3O^{\bullet}$) from methane is selected as the reference reaction for the O--H--C reaction family, and the hydrogen abstraction by a methoxy radical from methanol is chosen as the reference reaction for the O--H--O reaction family. The main advantage of introducing a reference reaction is that the temperature dependence of the Arrhenius parameters, E_a and $\log\tilde{A}$, is incorporated into $E_{a,ref}$ and $\log\tilde{A}_{ref}$, respectively, leaving the ΔGAV^os almost temperature independent.

Saeys et al. [29] have shown that for hydrogen abstractions between hydrocarbons, non-nearest-neighbor interactions have a significant influence only on the Arrhenius parameters for reactions with severe steric hindrance. In this work, tertiary contributions can be neglected without significant influence on the accuracy of the model because there are no reactions with strong steric hindrance in the studied reactions: hydrogen abstractions usually form transition states in which the reactants are widely separated from each other. In previous work concerning hydrogen abstraction reactions between oxygenates [27, 28], the inclusion of secondary contributions was shown to be of major importance for the accuracy of the model. Thus, it can be expected that the secondary contributions are also necessary in this work for developing an accurate and reliable model.

To avoid linear dependencies in the estimation of ΔGAV^os by regression to the Arrhenius parameters of the training set, ΔGAV^os for six secondary groups, O-(C_i)(H), O-(O_i)(H), CO-(C_i)(H), C_d-(C_i)(H), C_d-(O_i)(H) and C-(C_i)$(H)_3$, of the O--H--C reaction family and for three secondary groups, O-(O_i)(H), CO-(O_i)(H) and C_d-(O_i)(H), of the O--H--O reaction family were set equal to zero. These groups correspond to the secondary contributions with the most hydrogen ligands, an approach consistent with the work of Sabbe et al. [30] and Vandeputte et al. [31].

Because the transition state for hydrogen abstraction reactions originates from the competition between two radicals to bind with the same hydrogen atom, the location of the transition state and its energy depends on the strength of the forming and the breaking bond. Hence, resonance-stabilizing groups that are bound to the central atoms of the transition state (O_i or C_i) not only modify the bond strength of the migrating hydrogen but also greatly affect the abstraction kinetics. Because the resonance and hyperconjugative effects due to the simultaneous presence of ligands other than H on the central atoms between which the H atom is abstracted (O_1 and C_2/O_2) cannot be grasped by primary or other groups, a separate correction is often required. The importance of including resonance correction terms for increasing the accuracy of the developed group additive model is illustrated in section 2 of Appendix D.

To model hydrogen abstraction reactions of the O--H--C and the O--H--O type, two sets of 20 and 17 resonance corrections, respectively, are introduced. Each correction accounts for a single type of cross-interaction, and the total number of resonance corrections needed to describe the resonance and/or hyperconjugative effects in the transition state can be determined by counting all the cross-interactions between ligands on the two primary groups, as shown in the work of Vandeputte et al. [32] and explained in detail in section 1 of Appendix D.

5.3.3 Tunneling Corrections

Tunneling corrections on the ab initio rate coefficients are calculated using the Eckart tunneling model [34], which is based on the Eckart potential derived from the imaginary frequency in the transition state and the reaction barrier heights for both the forward and the reverse reaction. The significant contribution of the tunneling corrections on the calculated Arrhenius parameters of hydrogen abstractions, especially at lower temperatures, has been shown in previous studies [22, 41, 54].

The main advantage of not including tunneling corrections in the ΔGAV^os is that determined group additive values remain almost temperature independent. The temperature dependence is incorporated both in the corresponding Arrhenius parameters of the reference reaction and the tunneling coefficient, which can be modeled explicitly using correlations such as those developed in previous works [30, 47, 55].

Within a reaction family the imaginary frequencies have rather similar values, while the activation energy of the exothermic direction of the reaction is a good measure for the net electronic barrier through which tunneling can occur. Therefore, the activation energy for the exothermic direction of the reaction can be considered as one of the main factors, controlling the tunneling contribution within a reaction family. Sabbe et al. [30] proposed the fourth-order polynomial of the eq (5-5), with temperature-dependent coefficients for calculating tunneling coefficients for hydrogen abstractions with transition states of the C--H--C type, based on the group additively calculated activation energy of the exothermic direction for the particular reaction. Similar fourth-order polynomial equations were found to provide tunneling coefficients for hydrogen abstractions of the S--H--C and S--H--S type [32] and also the H--H--C type [28]. The parameters *A*, *B* and *C* in eq (5-5) for the above-mentioned tunneling equations are summarized in Table 5-1.

$$\kappa(\mathrm{T}) = 1 + \left(\frac{A}{T}\right)^3 E_{\mathrm{a,exo}} + B\exp\left(-\frac{T-300}{C}\right) E_{\mathrm{a,exo}}^4 \qquad (5\text{-}5)$$

In eq (5-5) *A*, *B* and *C* are calculated parameters.

In this work the applicability of eq (5-5) will be assessed for hydrogen abstractions involving oxygenates by oxygen-centered radicals. If required, refitting the parameters of this equation for the studied reaction families will be considered.

Table 5-1: Parameters for the Fourth-Order Polynomial of eq (5-5) to Calculate Tunneling Coefficients for the Reaction Families Studied Previously.

reaction family	*A*	*B*	*C*
C--H--C [30]	162	$2.71\ 10^{-06}$	26
S--H--C [32] S--H--S [32]	146	$1.30\ 10^{-06}$	19
H--H--C [28]	97	$1.73\ 10^{-06}$	26

5.4 Results and Discussion

5.4.1 O--H--C Hydrogen Abstractions

Group Additivity Values and Resonance Corrections: A set of 43 hydrogen abstraction reactions by oxygen-centered radicals with transition states of the O--H--C type was constructed to provide a training set from which group additive values for Arrhenius parameters for this reaction family can be determined. This set is presented in Table 5-2 and involves hydrogen abstractions by the methoxy radical ($CH_3O^{\bullet}$) from saturated and unsaturated hydrocarbons and from saturated oxygenate compounds like alcohols; ethers; esters; alkyl peroxides; aldehydes; ketones; acids; diketones; and unsaturated alcohols, ethers and ketones. Rate and tunneling coefficients, standard reaction enthalpies and entropies, along with Arrhenius parameters (activation energies and pre-exponential factors) for the reactions included in this training set in the temperature range of 300-2500 K are provided in Tables S2-S7 of Appendix D.

An additional 39 O--H--C hydrogen abstraction reactions are studied to quantify the influence of resonance and/or hyperconjugative effects. The training set of reactions for determining resonance corrections involves hydrogen abstractions by hydroxyl ($^{\bullet}OH$), vinyloxy ($CH_2{=}CHO^{\bullet}$), hydroperoxy ($HOO^{\bullet}$), and formyl ($HCOO^{\bullet}$) radicals from a wide range of hydrocarbons and oxygenates and is presented in Table 5-3. The corresponding kinetic parameters for this training set in the temperature range 300-2500 K can be retrieved from Tables S8-S13 of Appendix D. Rate coefficients for all reactions with transition states of the O--H--C type for temperatures 300-2500 K are provided in Tables S14 and S15 of Appendix D. Eckart tunneling coefficients for the same reactions for temperatures 300-1500 K (at higher temperatures tunneling coefficients are ~1 for all reactions) and applied symmetry numbers are provided in Tables S16 and S17 of Appendix D.

The majority of the hydrogen abstraction reactions by a methoxy radical ($CH_3O^•$) (see Tables 5-2 and 5-3) are exothermic at 300 K because in most cases the formed radicals are more stable than the methoxy radical, and consequently the formed O−H bond is typically stronger than the broken C−H bond. In contrast, hydrogen abstraction reactions by the vinyloxy (CH_2=$CHO^•$) or hydroperoxy ($HOO^•$) radical appeared to be endothermic at 300 K in the majority of cases.

Single-event pre-exponential factors at 300 K fluctuate between 10^4 and 10^7 m^3 mol^{-1} s^{-1} and are highly related to the rotation of the formed –OH bond in the transition state (TS), which is treated as a hindered rotor. The characteristic frequency of this rotation is low; hence, the contributions to the pre-exponential factor for the forward reaction is not negligible.

Among the 82 reactions in Tables 5-1 and 5-2, there are 4 barrierless reactions for which the activation energy is negative at 300 K, while another 16 reactions have ab initio activation energies lower than 10 kJ mol^{-1} at the same temperature. For these barrierless reactions the negative activation energies are used in the regression for the determination of the ΔGAV^os, an approach similar to the one followed in previous work [32]. The reason is that this same ΔGAV^o will not necessarily yield a negative activation energy in combination with another reactant. The activation energies are highly related to the corresponding reaction enthalpies, and a formally negative activation energy is usually due to a very unstable reactant radical, which results in a very negative reaction enthalpy for the corresponding hydrogen abstraction. In combination with a reactant that turns into an unstable product radical, the activation energy can be positive. If not, the reaction should be considered barrierless, and at least the activation energy should be set to zero if no more appropriate method is used.

Table 5-2: Training Set of Hydrogen Abstraction Reactions from Oxygenates by Oxygen-Centered Radicals with Transition States of the O--H--C Type for the Determination of Primary and Secondary ΔGAV°s.

Reference Reaction

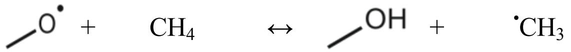

Training Set of Reactions

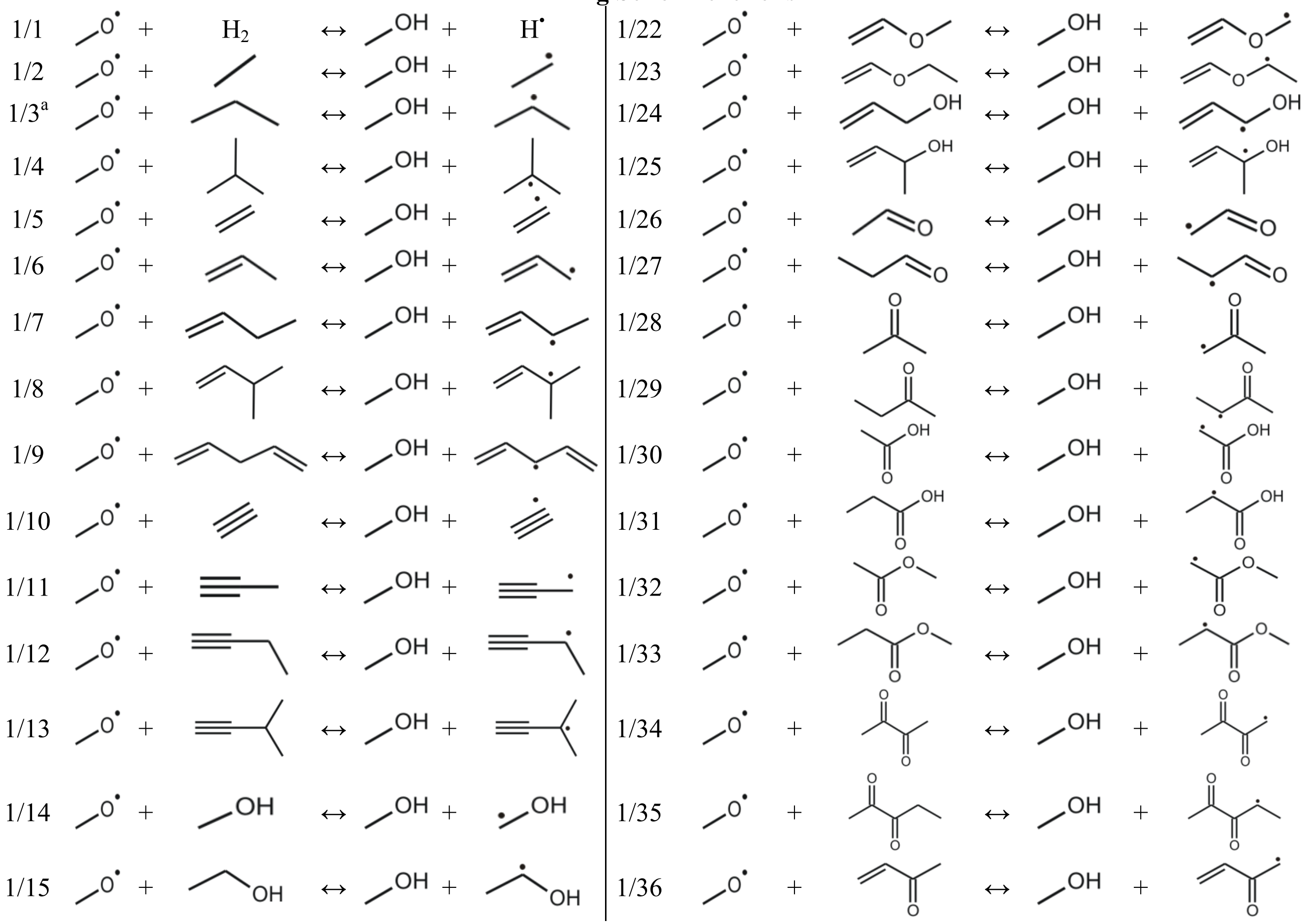

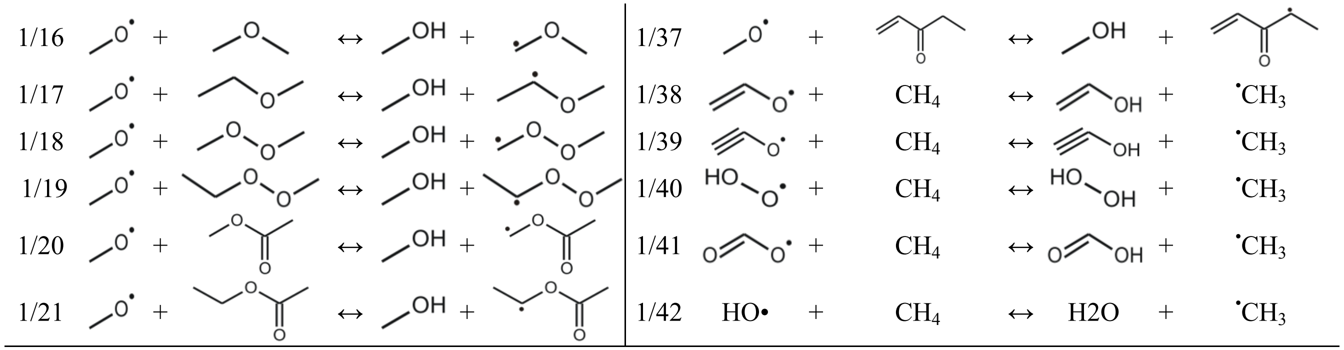

[a] Geometry optimization performed using the BMK/6-311G(2d,d,p) and the electronic energy obtained using CBS-QB3 method based on the BMK optimized geometry.

Table 5-3: Training Set of Hydrogen Abstraction Reactions from Oxygenates by Oxygen-Centered Radicals with Transition States of the O--H--C Type for the Determination of Resonance Corrections.

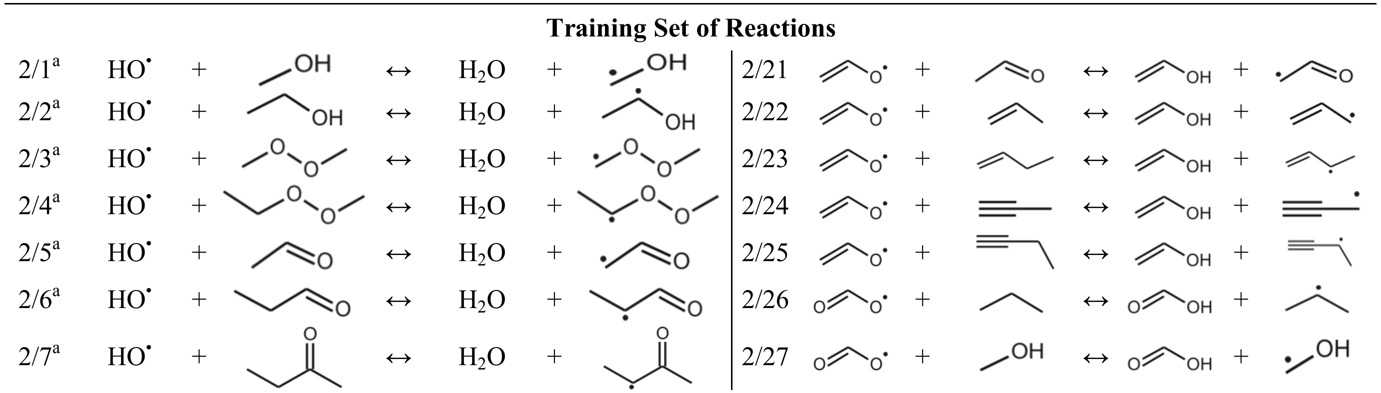

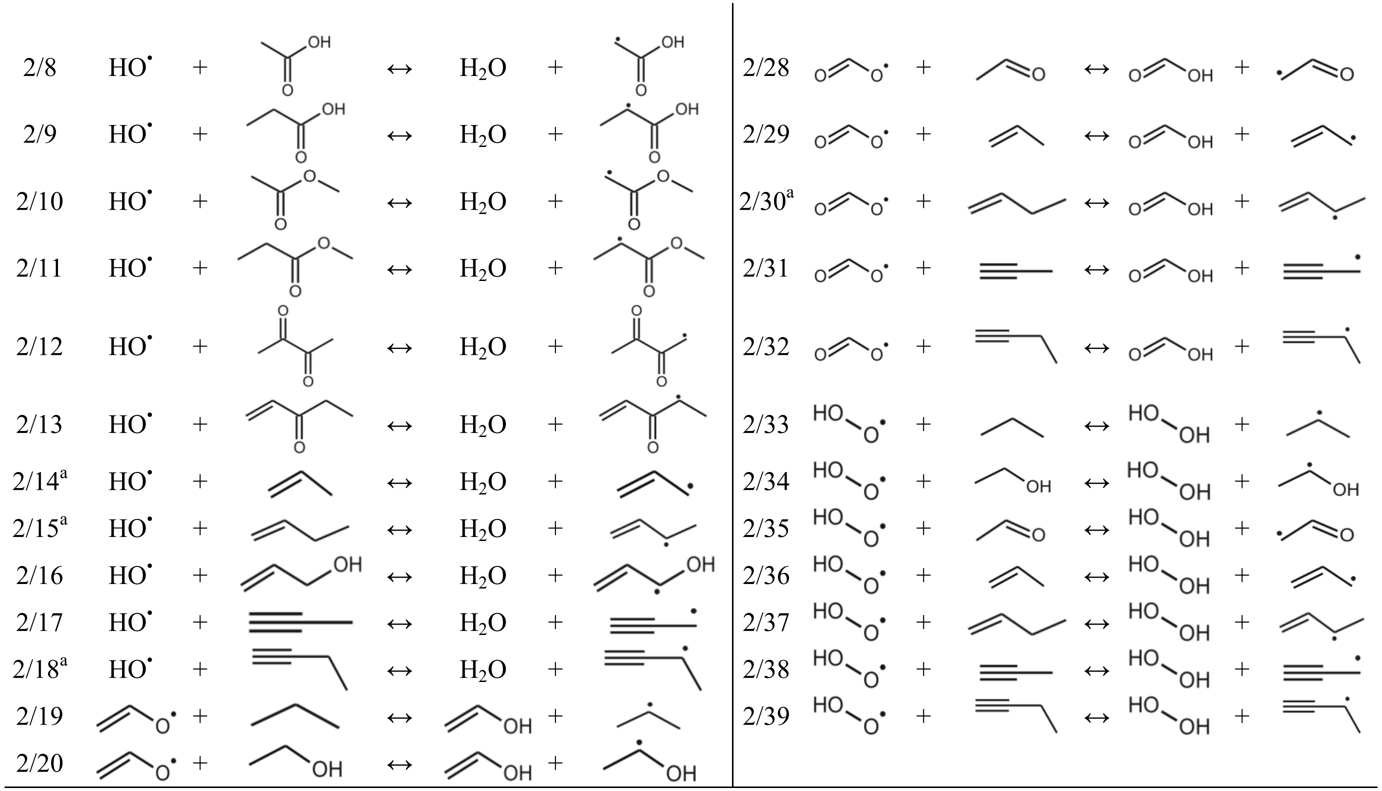

[a] Geometry optimization performed using the BMK/6-311G(2d,d,p) and the electronic energy obtained using CBS-QB3 method based on the BMK optimized geometry.

As a reference reaction, the hydrogen abstraction by a methoxy radical from methane was chosen, which, although one of the smallest reactions, still captures the main characteristics of the particular reaction family. Arrhenius parameters for the reference reaction in a broad temperature range (300-2500 K) can be found in Table S18 of Appendix D. The rate coefficients of this reaction are also regressed to a modified Arrhenius equation over the temperature range 300-2500 K. This was achieved by a linear regression of the natural logarithm of the rate coefficient (ln$k$) versus T^{-1} (T, temperature in K), which resulted in eq (5-6):

$$k = AT^{n}e^{-\frac{E_{\mathrm{a}}}{RT}} = 1.7\ 10^{-7}\ T^{4.1}\exp\left(-\frac{23}{RT}\right) \qquad (5\text{-}6)$$

In eq (5-6), A and k are expressed in m^3 mol^{-1} s^{-1} for the bimolecular hydrogen abstraction reactions, whereas E_a is in kJ mol^{-1}. The apparent strong temperature dependence expressed by the fourth power in the temperature is caused by tunneling contributions for T<600 K; excluding tunneling from the parameter estimation results in a temperature exponent of 2.9, which is between 2 and 3 as can be expected for bimolecular reactions. The rate coefficients provided by eq (5-6) at 300-2500 K are compared with rate coefficients available in the literature [56], resulting in mean deviations of about 2.3 when compared with MP2 and MP4 ab initio data, from the work of Jodkowsi et al. [46] at 300-2000 K. A similar deviation, of about 2.5, is obtained when data from this work are compared with experimental data [57] at 700, 800 and 900 K. The results and discussion of this comparison can be found in section 3 of Appendix D. Parameters for the modified Arrhenius equation for all reactions included in Tables 5-2 and 5-3 can be found in Table S19 of Appendix D.

As shown in previous work [27, 28], secondary contributions play an important role in hydrogen abstractions between oxygenates, and their inclusion is necessary to obtain high accuracy with the group additive model. In this work, the group additive values for secondary contributions are determined simultaneously with the primary contributions by unweighed least square analysis. A set of 32 ΔGAV^os for single-event pre-exponential factors and activation energies, among which 24 for primary and 8 for secondary contributions, was determined. These values for temperatures of 300 K and 1000 K are provided in Table 5-4, while for intermediate and higher temperatures the corresponding data are provided in Table S20 of Appendix D.

Because the hydrogen abstraction by a methoxy radical from methane was chosen as the reference reaction, resonance effects due to alkyl ligands on the oxygen atom are already accounted for in the ΔGAV^os. Thus, the reactions included in Table 5-3 facilitate the study of the resonance stabilization caused by the simultaneous presence in the transition state of a hydrogen, a vinyl, a carbonyl or an oxygen ligand on the oxygen side of the transition state along with a hyperconjugating C-H bond, an α-oxygen atom, or π-conjugating ligands (C=C or C=O) on the carbon side.

An overview of the 20 resonance and hyperconjugative correction terms introduced in this work along with their values for the single-event pre-exponential factors and the activation energies at 300 K and 1000 K are presented in Table 5-5. At intermediate and higher temperatures the corresponding corrections for the Arrhenius parameters are provided in Table S21 of Appendix D. The largest correction at 300 K for the pre-exponential factors is obtained for the interaction between an α-oxygen atom on the oxygen side with a carbonyl π-conjugating system on the carbon side of the transition state that amounts to a negative contribution of −0.746 log(m^3 mol^{-1} s^{-1}) (#18). For activation energies at 300 K, the largest contribution corresponds to the interaction between a double bond π-conjugating system on the oxygen side with another double bond π-conjugating system on the carbon side of the transition state, amounting to a value of −20 kJ mol^{-1} (#9).

Table 5-4: ΔGAV°s at 300 and 1000 K for α-Hydrogen Abstractions from Saturated and Unsaturated Oxygenate Compounds by Oxygen-Centered Radicals with Transition States of the O--H--C type[a] .

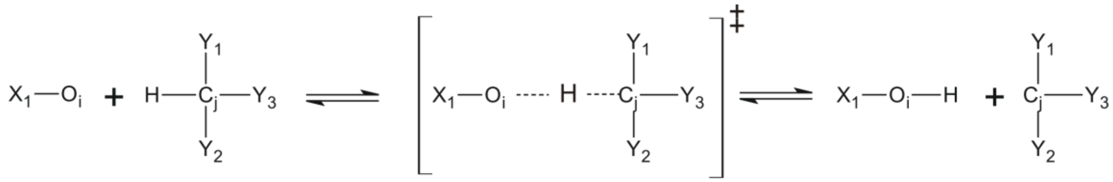

	forward (i=1, j=2)				reverse (i=2, j=1)			
	300 K		**1000 K**		**300 K**		**1000 K**	
	log$\tilde{A}$	**E_a**	**log$\tilde{A}$**	**E_a**	**log$\tilde{A}$**	**E_a**	**log$\tilde{A}$**	**E_a**
reference reaction								
$CH_3O^{\bullet} + CH_4$	5.367	45.7	6.859	62.6	5.193	45.2	6.335	58.9
	$\Delta GAV^{o}_{forward}$				**$\Delta GAV^{o}_{reverse}$**			
	300 K		**1000 K**		**300 K**		**1000 K**	
group	**log$\tilde{A}$**	**E_a**	**log$\tilde{A}$**	**E_a**	**log$\tilde{A}$**	**E_a**	**log$\tilde{A}$**	**E_a**
Oxygen-Centered Groups								
primary contributions								
O_i-(H)	1.016	-28.9	0.751	-31.5	-0.094	29.3	-0.293	27.5
O_i-(C_d)	-0.146	78.3	-0.027	79.7	0.063	-7.0	0.118	-6.5
O_i-(C_t)	1.135	101.3	1.850	109.3	0.197	-32.2	0.232	-31.8
O_i-(O)	0.138	50.3	0.381	52.9	-0.077	-22.8	-0.112	-23.2
O_i-(CO)	-0.178	-11.0	-0.086	-10.0	0.005	19.6	0.078	20.2
Carbon-Centered Groups								
primary contributions								
H_i	1.860	6.9	1.528	2.7	0.619	6.8	-0.116	-0.4
C_i-(C)$(H)_2$	-1.465	-0.2	-1.935	-5.6	-0.581	-15.8	-1.073	-21.4
C_i-$(C)_2$(H)	-0.773	2.8	-0.643	3.9	0.082	-24.4	0.136	-24.0
C_i-$(C)_3$	-1.807	-1.9	-2.104	-5.6	-0.796	-36.4	-1.288	-42.0
C_i-(C_d)$(H)_2$	0.118	50.5	0.323	52.2	-0.559	-25.6	-0.544	-25.5

C_i-(C)(C_d)(H)	-0.084	56.1	0.152	58.2	-0.083	-33.0	-0.015	-32.6
C_i-(C_d)$_2$(H)	0.027	87.0	0.196	88.3	-0.435	-36.2	-0.509	-37.2
C_i-(C)$_2$(C_d)	-0.874	58.7	-0.680	60.3	-0.257	-37.0	-0.263	-37.3
C_i-(C_t)(H)$_2$	-0.216	37.7	-0.018	39.5	-0.665	-20.7	-0.565	-19.8
C_i-(C_t)(C)(H)	-0.644	41.9	-0.372	44.4	-0.084	-29.1	0.063	-27.9
C_i-(C_t)(C)$_2$	-0.840	44.3	-0.513	47.3	-0.132	-36.3	0.024	-35.0
$C_{i,d}$-(H)	0.007	-22.2	0.267	-19.8	0.026	-0.4	0.112	0.3
$C_{i,t}$-(H)	1.223	-38.4	1.150	-40.2	1.587	77.3	1.119	71.4
C_i-(O)(H)$_2$	-0.510	12.2	-0.339	13.7	-0.775	-23.5	-0.724	-23.3
C_i-(C)(O)(H)	-0.568	10.2	-0.296	12.5	-0.273	-32.6	-0.189	-32.1
C_i-(C_d)(O)(H)	-0.881	72.2	-0.615	74.4	-0.953	-36.0	-0.846	-35.4
C_i-(C_d)(C)(O)	-0.939	77.6	-0.809	78.6	-0.376	-36.0	-0.445	-37.0
C_i-(CO)(H)$_2$	-0.112	28.9	0.214	31.8	-0.729	-13.4	-0.674	-12.9
C_i-(C)(CO)(H)	-0.273	39.6	0.093	43.0	-0.140	-23.9	-0.071	-23.5
secondary contributions								
O-(C_i)(C)	-0.286	-3.0	-0.225	-2.5	-0.127	-1.8	-0.043	-1.0
O-(C_i)(C_d)	0.826	-1.4	0.837	-1.4	0.862	7.9	0.908	8.4
O-(C_i)(O)	-0.773	-4.2	-0.843	-4.9	-1.046	2.7	-1.066	2.7
O-(C_i)(CO)	-0.378	-5.8	-0.462	-6.6	-0.319	8.1	-0.291	8.4
CO-(C_i)(C)	-0.703	-8.1	-0.690	-8.0	-0.503	-3.8	-0.462	-3.4
CO-(C_i)(C_d)	0.344	-6.4	0.324	-6.6	0.165	-5.6	0.173	-5.5
CO-(C_i)(O)	-0.070	-13.3	-0.129	-13.8	-0.408	2.5	-0.391	2.7
CO-(C_i)(CO)	-0.336	-1.4	-0.245	-0.6	-0.748	-3.8	-0.669	-3.2

[a] $\tilde{A}$ in m^3 mol^{-1} s^{-1} and E_a in kJ mol^{-1}. Y_1 and Y_2 ligands correspond to either a hydrogen or an alkyl group, whereas Y_3 ligand corresponds to either an oxygen- or a carbonyl-containing group ($Y_3 \equiv$ O−Z or CO−Z; Z could be H, O, CO or an alkyl group). X_1 ligand corresponds to a hydrogen, an alkyl group, an oxygen, or a carbonyl-containing group. C_d and C_t refer to a double and a triple bonded carbon atom, respectively.

Table 5-5: Correction Factors Accounting for Cross-Resonance Stabilization in Transition States of the O--H--C Type at 300 and 1000 K for Hydrogen Abstractions from Oxygenates by Oxygen-Centered Radicals[a].

			300 K		1000 K	
#	Correction	Corresponding structure	log$\tilde{A}$	E_a	log$\tilde{A}$	E_a
1	${}_{H}O{-}C_{\sigma\beta C\text{-}H}$	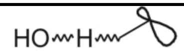	-0.014	3.8	-0.091	3.0
2	${}_{H}O{-}C_{paO}$		0.115	7.5	0.072	7.1
3	${}_{H}O{-}C_{\pi C=O}$	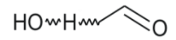	-0.165	6.7	-0.178	6.5
4	${}_{H}O{-}C_{\pi C=C}$	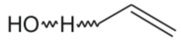	0.209	10.9	0.207	10.8
5	${}_{H}O{-}C_{\pi C\equiv C}$	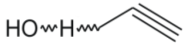	0.166	12.3	-0.026	10.3
6	${}_{\pi C=C}O{-}C_{\sigma\beta C\text{-}H}$	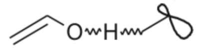	0.020	-4.2	0.013	-4.3
7	${}_{\pi C=C}O{-}C_{paO}$	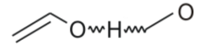	-0.663	-14.7	-0.430	-12.6
8	${}_{\pi C=C}O{-}C_{\pi C=O}$	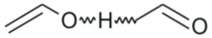	-0.217	-11.1	-0.146	-10.6
9	${}_{\pi C=C}O{-}C_{\pi C=C}$		-0.141	-20.3	-0.090	-19.9
10	${}_{\pi C=C}O{-}C_{\pi C\equiv C}$		-0.075	-16.2	-0.053	-16.2
11	${}_{\pi C=O}O{-}C_{\sigma\beta C\text{-}H}$	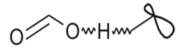	-0.047	1.9	-0.093	1.4
12	${}_{\pi C=O}O{-}C_{paO}$	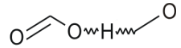	-0.022	7.0	-0.194	5.1
13	${}_{\pi C=O}O{-}C_{\pi C=O}$		-0.715	-9.5	-0.544	-7.8
14	${}_{\pi C=O}O{-}C_{\pi C=C}$		0.477	7.3	0.340	5.8
15	${}_{\pi C=O}O{-}C_{\pi C\equiv C}$	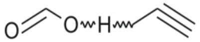	0.376	7.5	0.274	6.4
16	${}_{p\alpha O}O{-}C_{\sigma\beta C\text{-}H}$	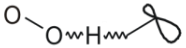	-0.055	-3.8	-0.074	-3.9
17	${}_{p\alpha O}O{-}C_{paO}$	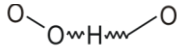	-0.574	-7.2	-0.494	-6.6
18	${}_{p\alpha O}O{-}C_{\pi C=O}$		-0.746	-9.4	-0.478	-7.0
19	${}_{p\alpha O}O{-}C_{\pi C=C}$	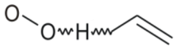	-0.434	-14.2	-0.305	-13.1
20	${}_{p\alpha O}O{-}C_{\pi C\equiv C}$		-0.276	-10.1	-0.271	-10.2

[a] log$\tilde{A}$ in log(m^3 mol^{-1} s^{-1}) and E_a in kJ mol^{-1}.

The vast majority of ΔGAV^{o}s presented in Table 5-4 are temperature independent over a temperature range from 300 to 2500 K, varying less than 5 kJ mol^{-1} or 0.3 log(m^{3} mol^{-1} s^{-1}) in this wide temperature range (see section 5, Figure S39 of Appendix D). Only for 5 of the 32 groups the temperature dependence is larger, but it remains even for these groups below 1 kJ mol^{-1} or 0.050 log(m^{3} mol^{-1} s^{-1}) per 100 K in activation energies and pre-exponential factors respectively, for both the forward and the reverse reaction. The groups that exhibit a larger temperature dependence pertain to groups such as the O_1-(C_t), C_1-($C)_3$, and the H_1 group, which are associated with reactions with differences in internal mobility of the reactants and/or transition state compared to those in the reference reaction. The related change in temperature dependence of the respective partition functions can result in an increased temperature dependence of the ΔGAV^{o}s. The reactions related to the O_1-(C_t) and the H_1 group (reactions 1/39 and 1/1, respectively) could even be considered to belong to another reaction family, which is part of the explanation for the different temperature dependence of their Arrhenius parameters than that of the reference reaction.

For corrections for resonance and/or hyperconjugative effects the temperature dependence is even smaller than for ΔGAV^{o}s, limited to 3 kJ mol^{-1} for the E_a corrections end ~0.3 for the log$\tilde{A}$ corrections, in the same 300-2500 K temperature interval. The full overview of the temperature dependence of the resonance corrections for activation energies and pre-exponential factors for both the forward and reverse reactions is provided in Figure S40 of Appendix D.

Table 5-6 provides a comparison of the statistics for the deviation between GA predictions and ab initio (AI) calculations for the reactions included in Table 5-3, not including (top) and including (bottom) corrections for resonance and/or hyperconjugative effects at 300 K and 1000 K. The inclusion of resonance corrections reduces the mean absolute deviation (MAD) between GA predicted and AI calculated values from 0.3 log(m^{3} mol^{-1} s^{-1}) to ~0.15 log(m^{3}

mol^{-1} s^{-1}) for the pre-exponential factors and from 11 kJ mol^{-1} to less than 1 kJ mol^{-1} for the activation energies for the forward reactions at 300 K. At higher temperatures, i.e. at 1000 K, the MAD between GA predicted and AI calculated values for pre-exponential factors and activation energies is even lower.

At higher temperatures, the accuracy of the model is expected to be higher because the comparison at lower temperatures is the most rigorous one due to the stronger sensitivity of the rate coefficient on errors in the activation energy. Additional accuracy was achieved at all temperatures because deviations between GA predictions and AI calculations for log$\tilde{A}$ and E_a compensate to a large extent for each other.

Table 5-6: Average Deviation for the Comparison between GA predicted and ab initio (AI) Calculated Values for the Reactions Included in Table 5-3 Using (a) ΔGAV^{o}s from Table 5-4 and (b) ΔGAV^{o}s from Table 5-4 along with Corrections for Resonance and/or Hyperconjugative Effects from Table 5-5 at 300 and 1000 K^a.

	300 K				1000 K			
	forward		reverse		forward		reverse	
	no corrections for resonance and/or hyperconjugating effects included							
	log$\tilde{A}$	E_a	log$\tilde{A}$	E_a	log$\tilde{A}$	E_a	log$\tilde{A}$	E_a
MAD	0.287	11.2	0.306	11.3	0.277	10	0.635	11.1
RMS	0.380	12.1	0.403	12.2	0.343	11.1	0.762	12.4
MAX	0.781	23.1	1.076	23.2	0.898	22.9	1.987	22.4
	corrections for resonance and/or hyperconjugating effects included							
	log$\tilde{A}$	E_a	log$\tilde{A}$	E_a	log$\tilde{A}$	E_a	log$\tilde{A}$	E_a
MAD	0.144	0.9	0.200	0.9	0.149	0.6	0.169	0.6
RMS	0.199	1.3	0.272	1.3	0.208	0.9	0.241	0.8
MAX	0.478	3.5	0.755	3.7	0.558	2.8	0.610	2.2

^{a} MAD: mean absolute deviation; RMS: root mean square deviation; MAX: maximum deviation. Single-event pre-exponential factors log$\tilde{A}$ [log(m^3 mol^{-1} s^{-1})] and activation energies E_a (kJ mol^{-1}).

Summarizing, the inclusion of resonance corrections was shown to significantly improve the performance of the GA model. An example of the calculation of the Arrhenius parameters from ΔGAV^{o}s and resonance corrections is given in section 1 of Appendix D.

Tunneling: To avoid strong temperature dependence of the ΔGAV^{o}s, the reported ΔGAV^o group additive values do not include tunneling contributions. The fourth-order polynomial introduced by Sabbe et al. [30] (see Table 5-1) was shown to accurately reproduce the Eckart tunneling coefficients for hydrogen abstraction reactions of the C--H--C type involving hydrocarbon [30], organosulfur [31] and oxygenate [28] compounds.

Using the equations developed for hydrogen abstractions of the C--H--C, the S--H--C, and the H--H--C type from Table 5-1 to predict tunneling coefficients for the hydrogen abstractions involving oxygenates with transition state of the O--H--C type at 300 K (see Tables 5-2 and 5-3), Eckart tunneling coefficients are reproduced with a mean factor of deviation, $<\rho>$, amounting to 1.7, 2.0 and 2.4, respectively. Among the total of 82 reactions used for this comparison, there are four hydrogen abstractions for which the forward reaction is barrierless at 300 K. These reactions were excluded from the set of reactions used to evaluate the performance of the particular equation. At higher temperatures the agreement is excellent using all the three of the above-mentioned equations with mean absolute deviations less than 1.2 at every temperature studied.

Hence, it was opted to refit the three parameters of the fourth-order polynomial to Eckart's tunneling coefficients for the reactions included in Tables 5-2 and 5-3 except for the barrierless reactions, in the temperature range 300-1000 K (at higher temperatures, tunneling effects are negligible). After refit of the parameters mentioned in Table 5-1, eq (5-7) is obtained:

$$\kappa(\mathrm{T}) = 1 + \left(\frac{126}{T}\right)^3 E_{\mathrm{a,exo}} + 8.30 \cdot 10^{-6} \exp\left(-\frac{T-300}{26}\right) E_{\mathrm{a,exo}}^4 \qquad (5\text{-}7)$$

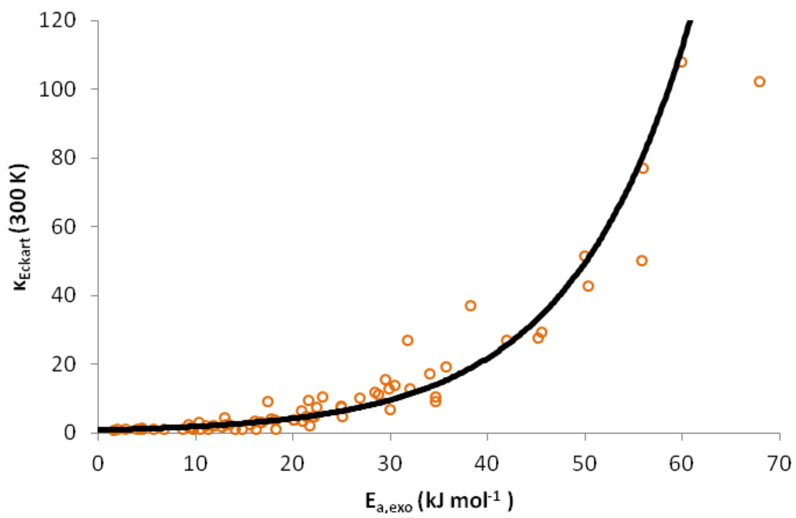

Figure 5-2: Eckart tunneling coefficients at 300 K for the reactions included in Tables 5-2 and 5-3 (circles) and fit from eq (5-5) of tunneling coefficients as a function of the ab initio activation energy of the exothermic reaction, $E_{a,exo}$ (solid line).

Using eq (5-7) tunneling coefficients are reproduced with an average factor of deviation of 1.4 at 300 K, with only two tunneling coefficients deviating more than a factor of 2.5 and maximum deviation of ~3. Tunneling coefficients for the reactions included in Tables 5-2 and 5-3 versus the ab initio activation energy of the exothermic reaction, $E_{a,exo}$, are presented in Figure 5-2. The solid line indicates the values calculated for tunneling coefficients using eq (5-7).

5.4.2 O--H--O Hydrogen Abstractions

Group Additivity Values and Resonance Corrections: Because the group additive model for hydrogen abstractions with transition state of the O--H--O type is fully consistent with the model developed for hydrogen abstractions with TS of the O--H--C type, only a brief description is provided here. As reference reaction the symmetric hydrogen abstraction reaction by methoxy radical ($CH_3O^\bullet$) from methanol (CH_3OH) was chosen. The simplest hydrogen abstraction reaction with the O--H--O type of transition state is the reaction between hydroxyl and water. Because it was observed that hydrogen abstractions by hydroxyl radical typically have reaction barriers and imaginary frequencies much lower than the corresponding abstractions by methoxy radicals, the reaction between methoxy radical and methanol was preferred as the reference reaction.

The training set for hydrogen abstractions of the O--H--O type includes reactions in which an oxygen-centered radical abstracts a hydrogen attached to an oxygen atom. There are 13 hydrogen abstractions by methoxy radical ($CH_3O^{\bullet}$) from saturated alcohols, acids, peroxides, and unsaturated alcohols included in this training set, which are provided in Table 5-7. Rate and tunneling coefficients, Arrhenius parameters, and standard reaction enthalpies and entropies at several temperatures (300-2500 K) for the reactions included in this training set are provided in Tables S22-S27 of Appendix D.

The influence of resonance and/or hyperconjugative effects in the transition state of the O--H--O type was studied using the training set of 22 hydrogen abstraction reactions that is presented in Table 5-8. Kinetic parameters for this training set of reactions in a wide range of temperatures (300-2500 K) can be retrieved from Tables S28-S33 of Appendix D. Rate coefficients for all reactions considered in this reaction family at temperatures 300-2500 K are provided in Tables S34 and S35 of Appendix D, while Eckart tunneling coefficients for the same reactions for 300-1500 K (at higher temperatures, tunneling coefficients are ~1 for all reactions) and applied symmetry numbers are provided in Tables S36 and S37 of Appendix D. Arrhenius parameters for the reference reaction at temperatures ranging from 300 to 2500 K can be retrieved from Table S38 of Appendix D.

Table 5-7: Training Set of Hydrogen Abstraction Reactions from Oxygenates by Oxygen-Centered Radicals with Transition States of the O--H--O Type for the Determination of Primary and Secondary ΔGAV°s.

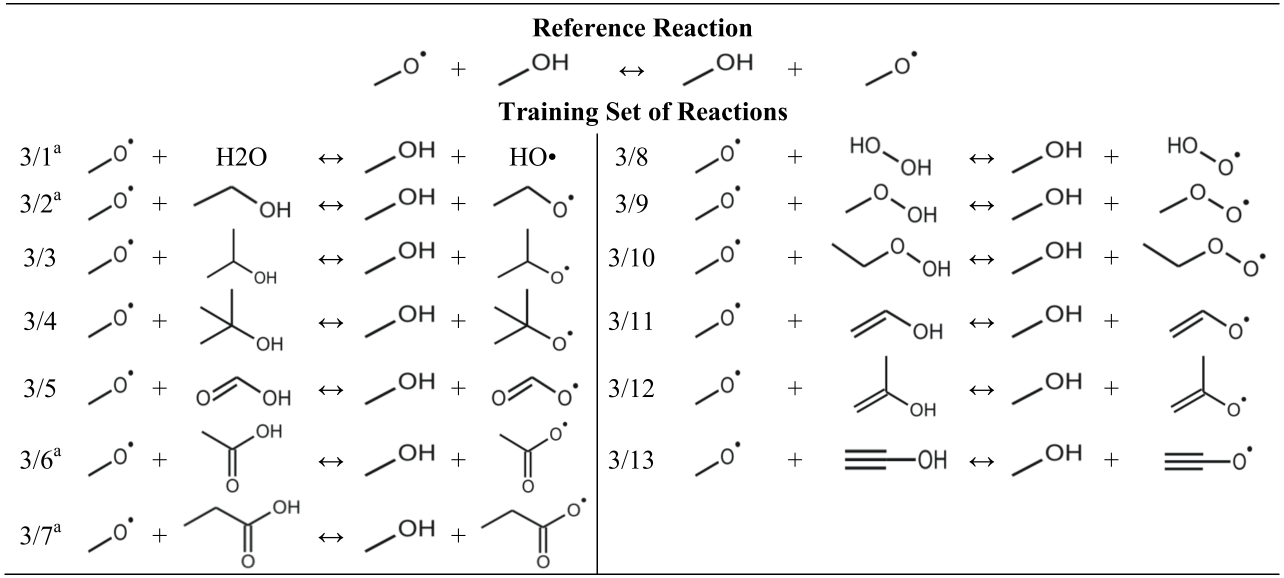

[a] Geometry optimization performed using the BMK/6-311G(2d,d,p) and the electronic energy obtained using CBS-QB3 method based on the BMK optimized geometry.

Table 5-8: Training Set of Hydrogen Abstraction Reactions from Oxygenates by Oxygen-Centered Radicals with Transition States of the O--H--O Type for the Determination of Resonance Corrections.

Training Set of Reactions

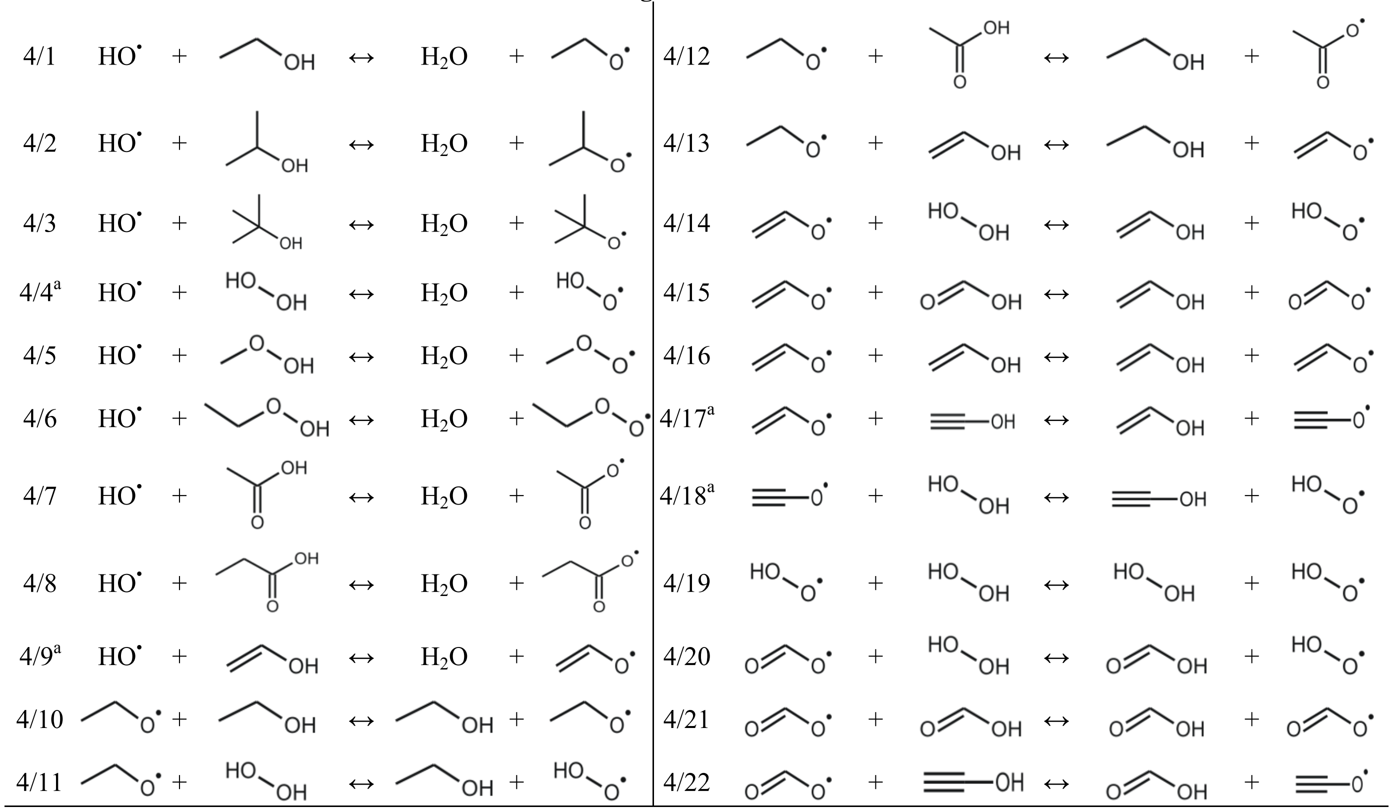

[a] Geometry optimization performed using the BMK/6-311G(2d,d,p) and the electronic energy obtained using CBS-QB3 method based on the BMK optimized geometry.

The rate coefficients for this reference reaction are regressed to a modified Arrhenius equation over the temperature range studied (300-2500 K). This was done by a linear regression of the natural logarithm of the rate coefficient (ln$k$) versus T^{-1} (T, temperature in K), that resulted in the eq (5-8):

$$k = AT^{n}e^{-\frac{E_a}{RT}} = 4.0\ 10^{-7}\ T^{3.78}\exp\left(-\frac{18}{RT}\right) \qquad (5\text{-}8)$$

in which A and k are expressed in $m^3\ mol^{-1}\ s^{-1}$ for the bimolecular hydrogen abstraction reactions, whereas E_a is in kJ mol^{-1}. Parameters for the modified Arrhenius equation for all reactions included in Tables 5-7 and 5-8 can be found in Table S39 of Appendix D.

Among the reactions included in Tables 5-7 and 5-8, there are two barrierless reactions, in both of which the hydrogen is abstracted from ethynol. In these reactions, the transition state has lower energy than the reactants; this is mainly due to the reactant ethynol, which is extremely unstable. The majority of the lowest values in rate coefficients, Arrhenius parameters, and tunneling coefficients are observed for hydrogen abstractions in which ethynol is involved. Generally, very low barriers are observed in reactions in which the hydrogen is abstracted by hydroxyl, resulting also in very high rate coefficients. Hydrogen abstractions by hydroxyl are the most exothermic reactions included in this training set, while there are a few endothermic reactions, including mostly abstractions by methoxy radical.

Using the ab initio calculated values included in Tables S22-S27 of Appendix D at 300-2500 K, 11 ΔGAV^{o}s are determined by unweighed least-squares regression, accounting for 5 primary and 6 secondary contributions. These GA values for activation energies and single-

Table 5-9: ΔGAV°s at 300 and 1000 K for Hydrogen Abstractions from Saturated and Unsaturated Oxygenate Compounds by Oxygen-Centered Radicals with Transition States of the O--H--O Type[a].

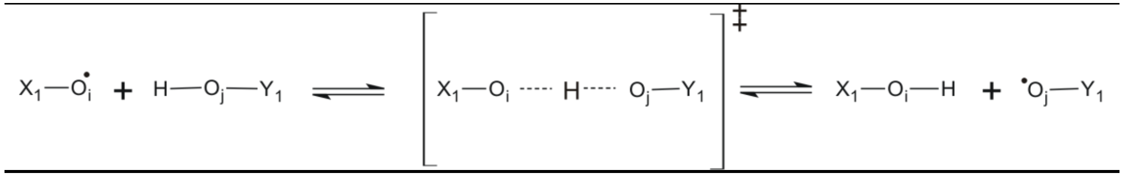

	forward (i=1, j=2)				reverse (i=2, j=1)			
	300 K		1000 K		300 K		1000 K	
	log$\tilde{A}$	E_a	log$\tilde{A}$	E_a	log$\tilde{A}$	E_a	log$\tilde{A}$	E_a
reference reaction								
$CH_3O^\bullet + CH_3OH$	4.940	37.5	6.426	54.2	4.940	37.5	6.426	54.2
	ΔGAV°$_{forward}$				**ΔGAV°$_{reverse}$**			
	300 K		1000 K		300 K		1000 K	
group	log$\tilde{A}$	E_a	log$\tilde{A}$	E_a	log$\tilde{A}$	E_a	log$\tilde{A}$	E_a
primary contributions								
O_i-(H)	0.513	-22.6	0.307	-24.6	-0.598	35.5	-0.737	34.4
O_i-(C_d)	0.335	76.1	0.335	76.1	0.544	-9.3	0.48	-10.2
O_i-(C_t)	0.761	81.5	1.443	88.9	-0.36	-51.8	-0.362	-52.0
O_i-(O)	-0.347	57.7	-0.039	60.8	-0.562	-15.4	-0.532	-15.3
O_i-(CO)	-0.945	-30.4	-0.797	-28.3	-0.762	0.1	-0.632	1.9
secondary contributions								
C-(O_i)(C)$(H)_2$	0.234	-0.6	0.732	5.1	0.195	-3.5	0.256	-2.8
C-(O_i)$(C)_2$(H)	-0.269	-10.1	-0.05	-7.6	-0.087	-4.4	0.062	-2.7
C-(O_i)$(C)_3$	-0.462	-13.2	-0.238	-10.6	-0.242	-5.9	-0.115	-4.4
C_d-(O_i)(C)	-0.949	-3.0	-1.085	-4.3	-0.315	-4.3	-0.388	-4.9
O-(O_i)(C)	-0.318	0.9	-0.406	0.1	-0.2	-6.2	-0.292	-6.9
CO-(O_i)(C)	0.955	34.3	0.992	34.3	1.228	23.0	1.234	22.7

[a] ΔGAV°$_{\log\tilde{A}}$ in log(m^3 mol^{-1} s^{-1}) and ΔGAV°$_{Ea}$ in kJ mol^{-1}. $\tilde{A}$ in m^3 mol^{-1} s^{-1} and E_a in kJ mol^{-1}. Y_1 and X_1 ligands correspond to a hydrogen or an oxygen, a carbonyl, or a carbon (single-, double-, or triple-bonded) containing group. C_d and C_t refer to a double- and a triple-bonded carbon atom, respectively.

Table 5-10: Correction Factors Accounting for Additional Stabilization in Transition States of the O--H--O Type at 300 and 1000 K for Hydrogen Abstractions from Oxygenates by Oxygen-Centered Radicals[a].

#	Correction	Corresponding structure	300 K		1000 K	
			$\log\tilde{A}$	E_a	$\log\tilde{A}$	E_a
1	${}_{\mathrm{H}}\mathrm{O{-}O}_{\sigma\beta\mathrm{C\text{-}H}}$		0.367	0.8	0.358	0.4
2	${}_{\mathrm{H}}\mathrm{O{-}O}_{\mathrm{paO}}$	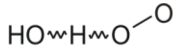	0.863	18.5	0.897	18.5
3	${}_{\mathrm{H}}\mathrm{O{-}O}_{\pi\mathrm{C{=}O}}$	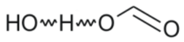	-0.037	5.8	-0.061	5.3
4	${}_{\mathrm{H}}\mathrm{O{-}O}_{\pi\mathrm{C{=}C}}$	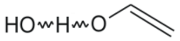	0.243	13.4	0.352	14.4
5	${}_{\sigma\beta\mathrm{C\text{-}H}}\mathrm{O{-}O}_{\sigma\beta\mathrm{C\text{-}H}}$		-0.763	0.4	-0.731	0.7
6	${}_{\sigma\beta\mathrm{C\text{-}H}}\mathrm{O{-}O}_{\mathrm{paO}}$	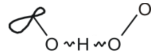	-0.336	3.8	-0.348	3.7
7	${}_{\sigma\beta\mathrm{C\text{-}H}}\mathrm{O{-}O}_{\pi\mathrm{C{=}O}}$	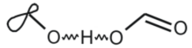	-0.170	0.9	-0.124	1.3
8	${}_{\sigma\beta\mathrm{C\text{-}H}}\mathrm{O{-}O}_{\pi\mathrm{C{=}C}}$	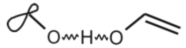	-0.029	1.1	-0.051	0.8
9	${}_{\pi\mathrm{C{=}C}}\mathrm{O{-}O}_{\mathrm{paO}}$	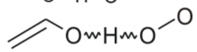	-0.134	-17.6	0.004	-15.8
10	${}_{\pi\mathrm{C{=}C}}\mathrm{O{-}O}_{\pi\mathrm{C{=}O}}$	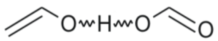	-1.507	-51.9	-1.703	-54.1
11	${}_{\pi\mathrm{C{=}C}}\mathrm{O{-}O}_{\pi\mathrm{C{=}C}}$	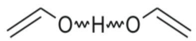	-1.121	-51.9	-1.156	-52.0
12	${}_{\pi\mathrm{C{=}C}}\mathrm{O{-}O}_{\pi\mathrm{C{\equiv}C}}$	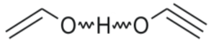	0.407	-48.8	0.319	-49.5
13	${}_{\pi\mathrm{C{\equiv}C}}\mathrm{O{-}O}_{\mathrm{paO}}$	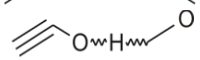	0.637	-13.3	0.685	-12.7
14	${}_{\mathrm{paO}}\mathrm{O{-}O}_{\mathrm{paO}}$	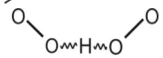	0.514	-18.5	0.300	-20.5
15	${}_{\pi\mathrm{C{=}O}}\mathrm{O{-}O}_{\mathrm{paO}}$	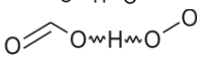	1.870	35.0	1.536	30.9
16	${}_{\pi\mathrm{C{=}O}}\mathrm{O{-}O}_{\pi\mathrm{C{=}O}}$	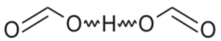	1.564	57.6	1.394	54.6
17	${}_{\pi\mathrm{C{=}O}}\mathrm{O{-}O}_{\pi\mathrm{C{\equiv}C}}$	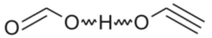	0.428	20.0	0.604	22.9

[a] $\log\tilde{A}$ in $\log(\mathrm{m^3\ mol^{-1}\ s^{-1}})$ and E_a in $\mathrm{kJ\ mol^{-1}}$.

event pre-exponential factors at 300 and 1000 K are provided in Table 5-9, while the corresponding values at intermediate and higher temperatures can be found in Table S40 of Appendix D.

An additional set of 17 corrections introduced to account for all possible stabilizing interactions resulting from resonance and/or hyperconjugative cross-effects in the transition state. These corrections are determined after the calculation of the ΔGAV^os in a subsequent least-squares regression for the reactions included in the corresponding training set.

Because the hydrogen abstraction by methoxy radical from methanol was chosen as reference reaction, the training set of reactions used for the determination of the ΔGAV^os already includes resonance effects by the simultaneous presence in the transition state of a hyperconjugating C−H bond at the oxygen atoms between which the hydrogen is transferred. Hence, the absence of this cross-resonance effect in the hydrogen abstraction reactions by hydroxyl results in underestimating both the pre-exponential factors and activation energies. This means that corrections accounting for the presence of a hydrogen atom instead of the methyl group as a ligand of the oxygen radical from which the hydrogen atom is abstracted should be introduced. Moreover, the presence of ligands other than hydrogen and carbon to the oxygen atoms between which the hydrogen is transferred results in resonance and/or hyperconjugative effects that need to be determined. The values for these 17 cross-resonance corrections for single-event pre-exponential factors and activation energies at 300 and 1000 K are presented in Table 5-10. The corresponding values at intermediate and higher temperatures can be found in Table S41 of Appendix D.

ΔGAV^os and corrections for cross-resonance effects in transition states of the O--H--O type can be considered to be temperature independent, with the temperature dependence for the vast majority limited to 6 kJ mol^{-1}/0.4 $\log(m^3\ mol^{-1}\ s^{-1})$ in the studied temperature range (300-

2500 K). Only 3 ΔGAV°s deviate more, and even for these the change per 100 K is limited to less than 0.05 log(m^3 mol^{-1} s^{-1}) and 1.0 kJ mol^{-1} for pre-exponential factors and activation energies, respectively. The overview of the limited temperature dependence for all the ΔGAV°s and resonance corrections reported in Tables 5-9 and 5-10 is given in section S5 in Figures S41 and S42 of Appendix D.

The inclusion of corrections for resonance and/or hyperconjugative effects significantly improves the accuracy of the model. The application of the proposed model with corrections for cross-effects for hydrogen abstractions with transition states of the O--H--O type is in agreement with the proposed model for transition states of the O--H--C type. A comparison of the statistics for the deviation between GA predictions and AI calculations for the hydrogen abstractions of the O--H--O type included in Table 5-8, not including (top) and including (bottom) corrections for resonance and/or hyperconjugative effects at 300 and 1000 K is provided in Table 5-11.

Table 5-11: Average Deviation for the Comparison between GA Predicted and AI Calculated Values for the Reactions Included in Table 5-8 using (a) ΔGAV°s from Table 5-9 and (b) ΔGAV°s from Table 5-9 along with corrections for resonance and/or hyperconjugative effects from Table 5-10 at 300 and 1000 K[a].

	300 K				1000 K			
	forward		reverse		forward		reverse	
	no corrections for resonance and/or hyperconjugating effects included							
	log$\tilde{A}$	$\boldsymbol{E_a}$	**log$\tilde{A}$**	$\boldsymbol{E_a}$	**log$\tilde{A}$**	$\boldsymbol{E_a}$	**log$\tilde{A}$**	$\boldsymbol{E_a}$
MAD	0.745	18.9	0.713	18.6	0.668	19.3	0.635	18.9
RMS	0.914	26.8	0.881	26.8	0.834	26.5	0.799	26.4
MAX	1.871	57.6	1.870	57.6	1.703	54.6	1.703	54.6
	Corrections for resonance and/or hyperconjugating effects included							
	log$\tilde{A}$	$\boldsymbol{E_a}$	**log$\tilde{A}$**	$\boldsymbol{E_a}$	**log$\tilde{A}$**	$\boldsymbol{E_a}$	**log$\tilde{A}$**	$\boldsymbol{E_a}$
MAD	0.046	0.3	0.046	0.3	0.026	0.3	0.026	0.3
RMS	0.094	0.5	0.094	0.5	0.059	0.5	0.059	0.5
MAX	0.268	1.3	0.268	1.3	0.182	1.2	0.182	1.2

[a] MAD: mean absolute deviation; RMS: root mean square deviation; MAX: maximum deviation. Single-event pre-exponential factors log$\tilde{A}$ [log(m^3 mol^{-1} s^{-1})] and activation energies E_a (kJ mol^{-1}).

Tunneling: The training set of hydrogen abstractions for determining ΔGAV^os and resonance corrections for reactions with transition states of the O--H--O type contains two barrierless reactions and a few reactions with very low barriers and consequently very low imaginary frequencies in the transition state. For the other reactions included in this training set imaginary frequencies are comparable with those determined for hydrogen abstractions involving sulfur compounds with transition states of the S--H--S type [32]. Hence, the equation parameters included in Table 5-1 for obtaining tunneling coefficients for hydrogen abstractions of the S--H--S type perform better for the reactions of the O--H--O type compared to the other equations of Table 5-1.

Eckart tunneling coefficients for the reactions included in Tables 5-7 and 5-8 at 300 K can be reproduced using this equation with a mean factor of deviation, $<\rho>$, of ~1.9, while the majority of tunneling coefficients at the same temperature deviate less than a factor of 3. At 600 K, tunneling coefficients are predicted within 20% of the corresponding Eckart values and even better at higher temperatures.

Because refit of the parameters of the polynomial presented in Table 5-1 does not improve the description of tunneling coefficients compared to the equation that expresses tunneling for hydrogen abstractions of the S--H--S type, with the mean factor of deviation between tunneling coefficients and the model decreasing from 1.93 to 1.92 only, the S--H--S type equation was retained for the reactions belonging to this O--H--O reaction family.

5.5 Model Performance

The group additive models developed in this work for reaction families with transition states of the O--H--C and O--H--O type are validated by comparing (i) the group additive predictions with the corresponding ab initio calculated values for a validation set containing hydrogen abstraction reactions that have not been used previously for the determination of the group additive values, ΔGAV^{o}; (ii) the GA predictions directly with experimentally obtained data; and (iii) the GA predictions with the predictions of other models such as the Blowers and Masel model [13] and the intersecting parabolas (IP) model [12].

5.5.1 Ab Initio Validation

The presented ΔGAV^{o}s and corrections for resonance and/or hyperconjugative effects in the transition state of the O--H--C and O--H--O type determined in this work are validated upon a test set of ab initio calculated data for 25 reactions covering a representative number of ΔGAV^{o}s and corrections for resonance effects. Rate and tunneling coefficients, Arrhenius parameters and standard reaction enthalpies and entropies for the 25 hydrogen abstraction reactions included in the ab initio validation set at temperatures ranging from 300 to 2500 K are provided in Tables S42-S47 of Appendix D. Using data calculated by the same ab initio method has the advantage that one really tests the group additivity method, and not the comparison of CBS-QB3-derived data with other literature data.

Table 5-12: Comparison between Group Additive (GA) and Ab Initio (AI) Kinetic Parameters at 300 K for the Ab Initio Validation Set of 25 Reactions (16 and 9 Reactions with Transition States of the O--H--C and O--H--O Type, Respectively)[c].

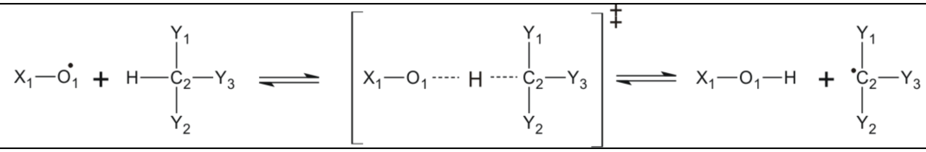

Reactions								κ/κ_{AI} [b]	forward				reverse		
									$\Delta\log A$	ΔE_a	k_{GA}/k_{AI}	$\log(k_{AI}/k_{GA})$	$\Delta\log A$	ΔE_a	k_{GA}/k_{AI}
5/1	$HO^{\bullet}$	+	H_2	↔	H_2O	+	$H^{\bullet}$	1.7	-0.196	-3.3	2.5	0.40	-0.196	-3.1	2.3
5/2	$HO^{\bullet}$	+		↔	H_2O	+		0.7	0.139	0.6	0.8	-0.10	0.139	0.7	0.7
5/3[a]	$HO^{\bullet}$	+		↔	H_2O	+		0.9	-0.274	1.3	0.3	-0.52	-0.273	1.4	0.3
5/4[a]	$HO^{\bullet}$	+	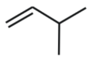	↔	H_2O	+	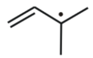	0.8	0.110	1.1	0.9	-0.05	0.109	1.2	0.8
5/5[a]	$HO^{\bullet}$	+		↔	H_2O	+		0.8	0.447	4.6	0.5	-0.30	0.447	4.7	0.4
5/6[a]	$HO^{\bullet}$	+	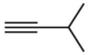	↔	H_2O	+	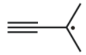	0.8	0.049	2.9	0.4	-0.40	0.049	3.0	0.4
5/7	$HO^{\bullet}$	+	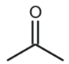	↔	H_2O	+	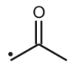	1.5	-0.262	-4.4	3.4	0.53	-0.295	-4.8	3.6
5/8	$HO^{\bullet}$	+	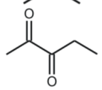	↔	H_2O	+	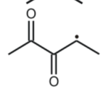	0.8	0.422	2.3	1.1	0.04	0.389	1.4	1.5
5/9	$HO^{\bullet}$	+	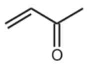	↔	H_2O	+	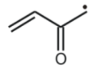	1.5	-0.337	-5.3	4.0	0.60	-0.343	-5.2	3.8
5/10[a]	$HO^{\bullet}$	+	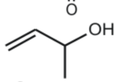	↔	H_2O	+	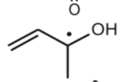	0.9	0.277	4.9	0.3	-0.52	-0.024	5.0	0.1
5/11	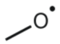	+	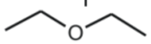	↔	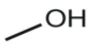	+	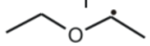	1.1	-0.055	0.2	1.3	0.11	-0.138	0.7	0.9
5/12	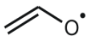	+	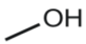	↔	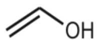	+	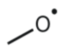	0.6	0.051	1.7	0.6	-0.22	0.114	1.8	0.7
5/13	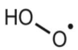	+	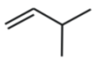	↔	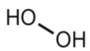	+	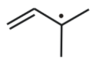	1.4	-0.200	-2.5	1.4	0.15	-0.201	-2.4	1.3
5/14	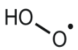	+	H_2	↔	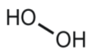	+	$H^{\bullet}$	1.0	-0.002	4.9	0.3	-0.52	-0.002	5.0	0.3
5/15	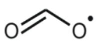	+	H_2	↔	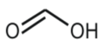	+	$H^{\bullet}$	0.5	-0.114	1.3	1.2	0.08	-0.113	1.5	1.1
5/16	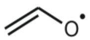	+	H_2	↔	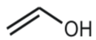	+	$H^{\bullet}$	2.6	0.071	3.1	0.4	-0.40	0.071	3.3	0.3
							MAD		0.188	2.8			0.181	2.8	
							RMS		0.230	3.2			0.223	3.3	

							MAX		0.447	5.3			0.447	5.2	
							<ρ>/< log(k_{AI}/k_{GA})>	1.4			2.2	-0.07			2.7

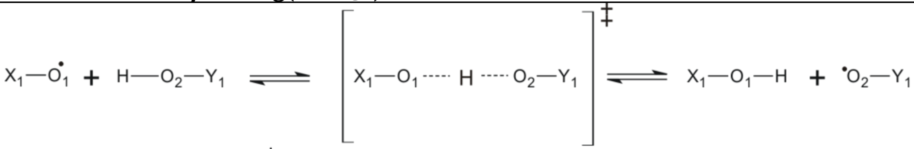

5/17[a]	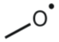	+	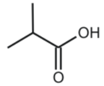	↔	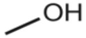	+	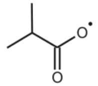	1.0	0.393	2.1	1.2	0.08	0.194	0.6	1.4
5/18	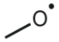	+	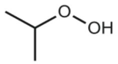	↔	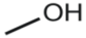	+	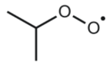	1.3	-0.016	0.8	1.0	0.00	0.049	-1.8	3.2
5/19	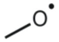	+	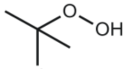	↔	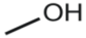	+	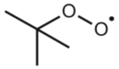	1.2	-0.125	6.0	0.1	-1.00	-0.001	0.6	1.0
5/20	$HO^{\bullet}$	+	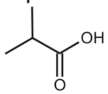	↔	H_2O	+	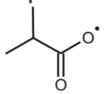	5.8	0.353	-1.1	3.8	0.58	0.153	-2.6	4.4
5/21	$HO^{\bullet}$	+	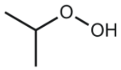	↔	H_2O	+	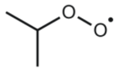	0.7	0.107	-0.7	1.3	0.11	0.170	-3.2	4.1
5/22[a]	$HO^{\bullet}$	+	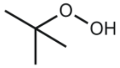	↔	H_2O	+	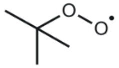	1.6	-0.288	2.8	0.3	-0.52	-0.164	-2.6	3.3
5/23	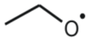	+	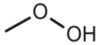	↔	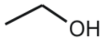	+	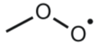	1.2	-0.082	-1.2	1.5	0.18	-0.137	-0.8	1.1
5/24[a]	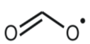	+	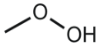	↔	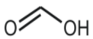	+	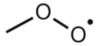	3.7	-0.338	-1.9	0.6	-0.22	-0.392	-1.4	0.4
5/25		+	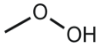	↔	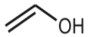	+	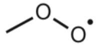	0.4	-0.251	-0.7	0.8	-0.10	-0.305	-0.3	0.6
							MAD		0.217	1.9			0.174	1.5	
							RMS		0.252	2.5			0.207	1.8	
							MAX		0.393	6.0			0.392	3.2	
							<ρ>/< log(k_{AI}/k_{GA})>	2.2			2.9	-0.10			2.5

[a] Geometry optimization performed using the BMK/6-311G(2d,d,p) and the electronic energy obtained using CBS-QB3 method based on the BMK optimized geometry

[b] κ/κ_{AI} is the ratio between the tunneling coefficient calculated using the fourth-order polynomial and the Eckart ab initio calculated tunneling coefficient. The polynomial pertains to eq (5-7) (upper panel) and eq (5-5) with parameters from Table 5-1 (A=146, B=1.30 10^{-6}, C=19) (lower panel).

[c] $\Delta\log A = \log A_{GA} - \log A_{AI}$ in $m^3\ mol^{-1}\ s^{-1}$; $\Delta E_a = E_{a,GA} - E_{a,AI}$ in kJ mol^{-1}. MAD: mean absolute deviation; RMS: root mean square deviation; MAX: maximum deviation; <ρ>, factor of deviation between two values taken from eq (5-2)).

In Table 5-12, the performance of the two group additive models developed in this work at 300 K is illustrated by providing the deviation between group additively predicted and ab initio calculated pre-exponential factors and activation energies along with deviations in tunneling and rate coefficients. The comparison at 300 K is the most rigorous because the sensitivity to errors in activation energies and tunneling coefficients at low temperatures is higher than at higher temperatures. The corresponding data at higher temperatures (600-2500 K) are presented in Tables S48-S52 of Appendix D.

For the comparison with ab initio kinetic parameters in Table 5-12, both the forward and reverse kinetic parameters have been determined based on ΔGAV^o group additive values. As was shown in previous work [27, 28, 30-32], the accuracy of the predictions of the truncated group additive model can be different for the forward and the reverse rate coefficients. Hence, ΔGAV^os for both directions of the particular reaction families have been determined and GA predicted Arrhenius parameters and rate coefficients have been compared to the corresponding ab initio values for the forward and reverse directions of the reactions studied.

In Table 5-12, it can be observed that for reactions of the O--H--C type the deviations on the forward and reverse rate coefficients are often the same, or at least very similar. For reactions of the O--H--O type, however, the deviations on the rate parameters for the forward and reverse rate can even differ in sign, which means that in this case the resulting equilibrium does not match the thermodynamic equilibrium. Therefore, based on the results of Table 5-12, it is suggested that in practice the best accuracy can be guaranteed by calculating the kinetic parameters for one direction using GA values determined in this work and calculating the rate coefficient for the reverse direction from thermodynamic consistency, based on $k_{rev} = k_{for}/K_{eq}$. In this equation, the forward and reverse direction can be chosen arbitrarily for this reaction family because the reference reaction is symmetric. In Table 5-12 and the discussion below, however, the Arrhenius parameters and the rate coefficients are directly calculated from the group additive model.

Equation (5-7) succeeds in accurately reproducing tunneling coefficients for reactions with O--H--C transition states included in the ab initio validation set, because the $\langle\rho\rangle$ factor defined by eq (5-2) amount to only 1.4. For reactions with transition states of the O--H--O type, the equation proposed for S--H--S transition states as provided in Table 5-1 performs well with tunneling coefficients reproduced with a mean factor of deviation of ~2.2.

The mean absolute deviation (MAD) between group additivity prediction and ab initio calculated pre-exponential factors amounts to ~0.2 log(m^3 mol^{-1} s^{-1}) for both reaction families. The largest deviation in pre-exponential factors amounts to 0.447 and corresponds to the hydrogen abstraction by hydroxyl from 1,4-pentadiene (reaction 5/5).

The MAD between GA prediction and AI determined activation energies amounts to 2.8 kJ mol^{-1} for both the forward and the reverse reaction with TS of the O--H--C type, while for reactions with TS of the O--H--O type it is slightly better (1.9 and 1.5 kJ mol^{-1} for the forward/reverse reaction). Only in two cases is the deviation between GA prediction and AI calculation greater than 5 kJ mol^{-1}. For the hydrogen abstraction reaction by hydroxyl from but-3-ene-2-one (CH_2=$CHCOCH_3$) (reaction 5/9), the activation energy is underestimated by ~5.3 kJ mol^{-1} for both the forward and the reverse reaction, while for the hydrogen abstraction by methoxy radical from *tert*-butyl hydroperoxide ($CH_3C(CH_3)_2OOH$) (reaction 5/19) there is an overestimation by 6 kJ mol^{-1} of the activation energy for the forward reaction.

Rate coefficients at 300 K can be reproduced with a mean factor of deviation of 2.2 for the forward and 2.7 for the reverse reactions with TS of the O--H--C type. For reactions with TS of the O--H--O type, the values are 2.9 and 2.5 for the two directions of the reaction, respectively. However, deviations can amount up to a factor of ~11 at 300 K for the forward reaction 5/19. Even for this reaction, agreement between the ab initio calculated and the group additively predicted rate coefficients for the forward reaction is much better at higher temperatures with a deviation of ~4 at 600 K, ~2.5 at 1000 K; the agreement is even better at temperatures up to 2500 K. The values of −0.07 and −0.10 for the mean value of the logarithmic deviations, $<\log(k_{AI}/k_{GA})>$, (see Table 5-12) for both studied reaction families correspond to a mean underestimation of 15 and 20 % respectively, which is very small, almost negligible average underestimation of the AI rate coefficients by the GA model.

Generally, larger deviations are observed for hydrogen abstractions that involve primary groups with multiple ligands, in which non-nearest-neighbor-interactions between ligands on both primary groups can cause rate coefficients calculated by the GA method to deviate from the ab initio calculated rate coefficients. This is the case for example in reactions 5/6 and 5/10 with O--H--C TS, where the triply substituted radical products, $HC{\equiv}C\text{-}{}^{\bullet}C(CH_3)_2$ and $CH_2{=}CH\text{-}{}^{\bullet}C(CH_3)OH$ respectively, cause deviations from the GA calculated values.

5.5.2 Experimental Validation

Group additively predicted rate coefficients are compared with a compilation of 60 experimental rate coefficients obtained from NIST Chemical Kinetics Database [58] and the IUPAC Kinetics Database [59, 60]. These experimental rate coefficients correspond to 26 hydrogen abstraction reactions with transition states of the O--H--C and the O--H--O type, and the results of this comparison are presented in Table 5-13. The experimental data available are divided into three main categories according to the classification of experimental methodology followed by the NIST Chemical Kinetics Database [58]. Following this classification, in the experimental validation set used in this work, 46 rate coefficients are absolute values measured directly, 14 rate coefficients are derived from fitting to a complex mechanism, and one stems from detailed balance/reverse rate. All data retrieved from the IUPAC Kinetics Database [59, 60] are absolute data based on laboratory measurements.

The majority of the available experimental data in Table 5-13 refer to reactions with transition state of the O--H--C type (21 of the 26 reactions), and in most of the cases the hydrogen is abstracted by hydroxyl (22 of the 26 reactions). For hydrogen abstractions of the O--H--O type there is only very limited experimental data available, of which most is at pressures below the pressure range of interest (e.g. at pressure < 10^{-4} bar), leading to only five reactions of the O--H--O type that could be included (reactions 18, 19, 20, 21 and 26 of Table 5-13).

Table 5-13: Experimental Validation Set of 60 Experimental Rate Coefficients[a].

	Reaction							T	$k$exp	k_{GA}/k_{exp}	ρ
				Absolute value measured directly							
1a	$HO^{\bullet}$	+	H_2	↔	H_2O	+	$H^{\bullet}$	300	$4.2\ 10^{3}$ [61]	1.37	1.4
1b								300	$4.3\ 10^{3}$ [62]	1.33	1.3
1c								300	$3.5\ 10^{3}$ [63]	1.65	1.6
1d								300	$4.2\ 10^{3}$ [59]	1.36	1.4
2a	$HO^{\bullet}$	+	CH_4	↔	H_2O	+	$^{\bullet}CH_3$	300	$4.0\ 10^{3}$ [64]	6.86	6.9
2b								300	$5.5\ 10^{3}$ [65]	4.92	4.9
2c								300	$4.0\ 10^{3}$ [66]	6.79	6.8
2d								1000	$1.0\ 10^{6}$ [67]	0.24	4.2
2e								300	$4.0\ 10^{3}$ [60]	6.82	6.8
3a	$HO^{\bullet}$	+		↔	H_2O	+		300	$1.7\ 10^{5}$ [68]	3.87	3.9
3b								300	$1.6\ 10^{5}$ [69]	4.09	4.1
3c								300	$1.5\ 10^{5}$ [70]	4.32	4.3
3d								300	$1.5\ 10^{5}$ [71]	4.31	4.3
3e								1000	$5.1\ 10^{6}$ [72]	0.37	2.7
3f								300	$1.5\ 10^{5}$ [60]	4.27	4.3
4	$HO^{\bullet}$	+		↔	H_2O	+		300	$6.6\ 10^{5}$ [60]	1.44	1.4
5	$HO^{\bullet}$	+	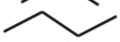	↔	H_2O	+	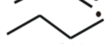	300	$5.1\ 10^{6}$ [60]	0.67	1.5
6a	$HO^{\bullet}$	+	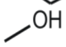	↔	H_2O	+	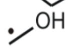	300	$6.4\ 10^{5}$ [73]	1.81	1.8
6b								1000	$2.2\ 10^{6}$ [74]	1.51	1.5
6c								300	$5.5\ 10^{5}$ [60]	2.35	2.4
7	$HO^{\bullet}$	+	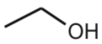	↔	H_2O	+	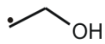	300	$5.1\ 10^{6}$ [60]	9.93	9.9
8	$HO^{\bullet}$	+	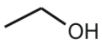	↔	H_2O	+	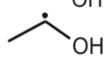	300	$2.0\ 10^{6}$ [60]	2.86	2.9
9	$HO^{\bullet}$	+	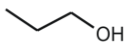	↔	H_2O	+	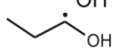	300	$3.4\ 10^{6}$ [60]	1.71	1.7
10a	$HO^{\bullet}$	+	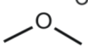	↔	H_2O	+	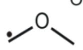	300	$1.7\ 10^{6}$ [75]	1.73	1.7
10b								300	$1.4\ 10^{6}$ [76]	2.11	2.1
10c								300	$1.5\ 10^{6}$ [77]	2.01	2.0
10d								300	$2.1\ 10^{6}$ [78]	1.40	1.4
10f								600	$4.2\ 10^{6}$ [64]	0.66	1.5
10g								600	$3.9\ 10^{6}$ [79]	0.71	1.4
10h								300	$1.7\ 10^{6}$ [60]	1.75	1.8
11	$HO^{\bullet}$	+	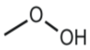	↔	H_2O	+	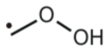	300	$1.2\ 10^{6}$ [80]	0.09	11.3
12	$HO^{\bullet}$	+	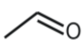	↔	H_2O	+	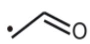	300	$4.5\ 10^{5}$ [60]	0.19	5.4

13	$HO^\bullet$	+	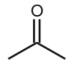	↔	H_2O	+	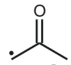	300	$1.1\ 10^5$ [60]	0.83	1.2
14	$HO^\bullet$	+	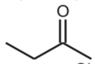	↔	H_2O	+	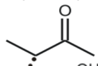	300	$6.7\ 10^5$ [60]	1.21	1.2
15a	$HO^\bullet$	+	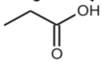	↔	H_2O	+	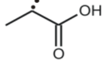	300	$7.2\ 10^5$ [81]	0.24	4.1
15b								300	$9.6\ 10^5$ [82]	0.14	7.3
15c								300	$7.2\ 10^5$ [60]	0.23	4.1
16	$HO^\bullet$	+	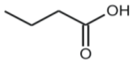	↔	H_2O	+	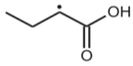	300	$1.1\ 10^6$ [60]	0.32	3.2
17a	$HO^\bullet$	+	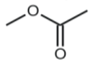	↔	H_2O	+	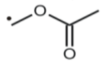	300	$2.1\ 10^5$ [83]	0.32	3.1
17b								300	$2.1\ 10^5$ [84]	0.32	3.2
17c								300	$1.1\ 10^5$ [85]	0.61	1.7
18	$HO^\bullet$	+	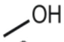	↔	H_2O	+	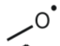	300	$7.8\ 10^4$ [60]	0.23	4.4
19	$HO^\bullet$	+	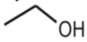	↔	H_2O	+	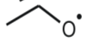	300	$9.6\ 10^4$ [60]	0.27	3.6
20	$HO^\bullet$	+	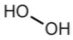	↔	H_2O	+	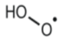	300	$1.0\ 10^6$ [59]	0.12	8.7
21	$HO^\bullet$	+	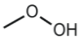	↔	H_2O	+	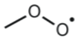	300	$1.2\ 10^6$ [59]	1.17	1.2
			Experimental value derived from fitting to a complex mechanism								
1e	$HO^\bullet$	+	H_2	↔	H_2O	+	$H^\bullet$	1000	$1.3\ 10^6$ [86]	3.79	3.8
3g	$HO^\bullet$	+		↔	H_2O	+		1000	$5.2\ 10^6$ [86]	0.36	2.8
6d	$HO^\bullet$	+	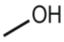	↔	H_2O	+	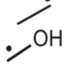	1000	$5.0\ 10^6$ [87]	0.66	1.5
6e								1000	$1.5\ 10^6$ [88]	2.22	2.2
10i	$HO^\bullet$	+	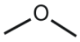	↔	H_2O	+	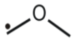	300	$1.7\ 10^6$ [89]	1.72	1.7
10j								300	$1.4\ 10^6$ [90]	2.15	2.1
10k								1000	$8.8\ 10^6$ [91]	0.77	1.3
17d	$HO^\bullet$	+	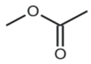	↔	H_2O	+	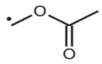	300	$2.3\ 10^5$ [92]	0.29	3.5
22	$HO^\bullet$	+	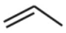	↔	H_2O	+	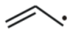	700	$7.6\ 10^6$ [93]	062	1.6
23	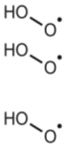	+	CH4	↔	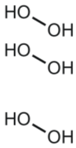	+	$^\bullet CH_3$	1000	47 [94]	1.45	1.5
24a		+		↔		+		700	6.9 [95]	0.81	1.2
24b								800	30 [96]	1.04	1.0
25		+		↔		+		800	48 [96]	4.92	4.9
26	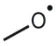	+	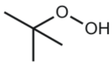	↔	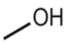	+	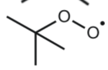	400	$4.2\ 10^3$ [97]	0.26	3.9
			Experimental value derived from detailed balance/reverse rate								
6f	$HO^\bullet$	+	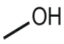	↔	H_2O	+	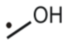	1000	$1.4\ 10^6$ [98]	2.29	2.3
										<ρ>	**3.2**

[a] T in K; k_{exp} in $m^3\ mol^{-1}\ s^{-1}$; ρ the factor of deviation between two values taken from eq (5-2), $k_{calc} = \kappa\tilde{A}_{GA}\ exp(-E_{a,GA}/RT)$.

The available rate coefficients are compared at temperatures within the experimental temperature range, preferably at temperatures for which ΔGAV°s have been determined. For experimental temperature ranges not including the preferred temperatures, the rate coefficients have been calculated at the closest temperature for which ΔGAV°s are available. Because the majority of ΔGAV°s is almost temperature independent, and ΔGAV°s have been determined at several intermediate temperatures, GA values to the closest temperature for which ΔGAV^os are available can be used without any loss of accuracy. Arrhenius parameters for the reference reaction for the two reaction families at 300-2500 K can be found in Tables S18 and S38 of Appendix D.

The mean factor of deviation between the GA prediction and the experimental value, $<\rho>$, amounts to only 3.2 for the reactions included in the experimental validation set, implying a very good agreement of the GA prediction with the experimental rate coefficients. In 21 out of the 25 available reactions the rate coefficients are predicted within a factor lower than ~5, and for 13 out of the latter 21 reactions, this deviation factor is lower than ~3.

The largest deviation amounts to a factor of ~11 for the hydrogen abstraction by hydroxyl from methyl hydroperoxide (reaction 11), whereas there are two other reactions with deviations of a factor of ~9. These reactions are the hydrogen abstraction by hydroxyl from ethanol (reaction 7) and from hydrogen peroxide (reaction 20). For reaction 11, the deviation can be partially attributed to the low temperature and pressure of the experiment (249 K and 0.27-0.53 bar), with tunneling coefficients more difficult to predict at the lowest temperature. Regarding reaction 7, the formed radical center is in β-position to the hydroxyl group, which can cause an additional stabilization of the transition state and the product radical. Such interactions can in principle be accounted for by secondary contributions, but for the C--H--O reaction family, secondary interactions for carbon-centered groups have been neglected in line with earlier work on hydrogen abstractions between hydrocarbons [30]. The large deviation for reaction 7 indicates that neglecting carbon-centered secondary contributions for the C--H--O reaction family may not be justified for all reactions. For the structurally similar reactions 8 and 9, the agreement with experiment is with a factor of 2.9 and 1.7 much better, respectively, because of the oxygen-centered secondary contributions of the O-(C_i)(H) group, which are accounted for by the model. Finally, reaction 20 has to be considered particular in the sense that two very small oxygenate compounds react, whereas the group additive method is actually intended for reactions between larger molecules. Therefore, the correction for the resonance effect between the hydrogen atom of hydroxyl and an oxygen in α position to the oxygen radical center was determined from reactions in which larger compounds are involved.

Hence, it can be concluded that the two GA models for hydrogen abstractions with TS of the O--H--C and O--H--O type presented in this work allow obtaining rate coefficients for hydrogen abstraction reactions between oxygenates by oxygen centered radicals within a mean factor of deviation, $\langle\rho\rangle$, of ~3 between GA predictions and experimental rate coefficients.

5.5.3 Comparison with other models

The activation energies predicted by the GA model developed in this work are compared with the corresponding values predicted by two other models available: (a) the Blowers and Masel [13] model and (b) the intersecting parabolas (IP) model developed by Denisov [12]. The results of this comparison are presented as parity plots of activation energies for the 16 hydrogen abstraction reactions of the O--H--C type (see Figure 5-3) and the 9 reactions of the O--H--O type included in the ab initio validation set (see Figure 5-4).

According to Blowers and Masel model, eq (5-9) can be used for the calculation of the activation energy on the basis of the standard enthalpy of formation of the particular reaction.

$$E_{\mathrm{a}} = \left(\frac{w_{\mathrm{b}} + w_{\mathrm{f}} + \Delta_{\mathrm{r}} H}{2} \right) \frac{\left(V_{\mathrm{p}} - \left(w_{\mathrm{b}} + w_{\mathrm{f}} \right) + \Delta_{\mathrm{r}} H \right)^2}{V_{\mathrm{p}}^2 - \left(w_{\mathrm{b}} + w_{\mathrm{f}} \right)^2 + \Delta_{\mathrm{r}} H^2} \tag{5-9}$$

In eq (5-6), w_b and w_f correspond to the bond dissociation energy of the breaking and the forming bond, respectively, and V_p is a parameter related to the intrinsic barrier E_a^o. The sum $w_b + w_f$ is estimated as a single parameter.

The parameters of the eq (5-9) were estimated by minimizing the residual sum of squares (RSSQ) of the deviation between the predictions of the Blowers and Masel model in activation energies and the corresponding ab initio calculated values at 300 K for the training set of reactions included in Tables 5-2 and 5-3 for H-abstractions of the O--H--C type and Tables 5-7 and 5-8 for H-abstractions of the O--H--O type of transition states. The fitted parameters are w_b+w_f = 788.3 kJ mol^{-1} and V_P = 995.0 kJ mol^{-1} for the O--H--C reaction family and w_b+w_f = 888.3 kJ mol^{-1} and V_P = 1092.0 kJ mol^{-1} for the O--H--O reaction family. Using these values, the activation energies for the forward hydrogen abstraction reactions included in the ab initio validation set at 300 K are predicted with a mean absolute deviation of 8.4 and 9.2 kJ mol^{-1} for the two reaction families, respectively, which is significantly higher than the corresponding MAD between the GA predictions and the AI calculated values that amounts to only 2.6 and 1.5 kJ mol^{-1}, respectively.

The IP model derives from a correlation between the activation energy and the reaction enthalpy within a particular reaction family and is expressed as in eq (5-10):

$$b = a\left(E_\mathrm{a} \text{-} \Delta_\mathrm{r} H^\mathrm{o}\right)^{1/2} - E_\mathrm{a}^{1/2} \qquad (5\text{-}10)$$

where α and b are parameters that relate to the force constants of the broken and formed carbon−hydrogen or oxygen−hydrogen bond and the hydrogen atom displacement during abstraction.

In line with the procedure described previously for the Blowers and Masel model, the parameters of the IP model were fitted by minimizing the RSSQ of the predictions by the IP model in activation energies and the corresponding ab initio calculated values at 300 K for the reactions included in the training set of reactions in Tables 5-2 and 5-3 and in Tables 5-7 and 5-8 for the O--H--C and O--H--O type H-abstractions, respectively.

The minimum MAD between these values is obtained for α = 1.0 and b = 13.9 for the O--H--C reaction family and α = 0.5 and b = 9.6 for the O--H--O reaction family. Using these values for the prediction of the activation energies for the forward reactions included in the ab initio validation set, activation energies are reproduced with a MAD of 13.1 and 21.6 kJ mol^{-1} for the two reaction families, respectively, which is clearly less accurate than the prediction made by the GA model developed in this work.

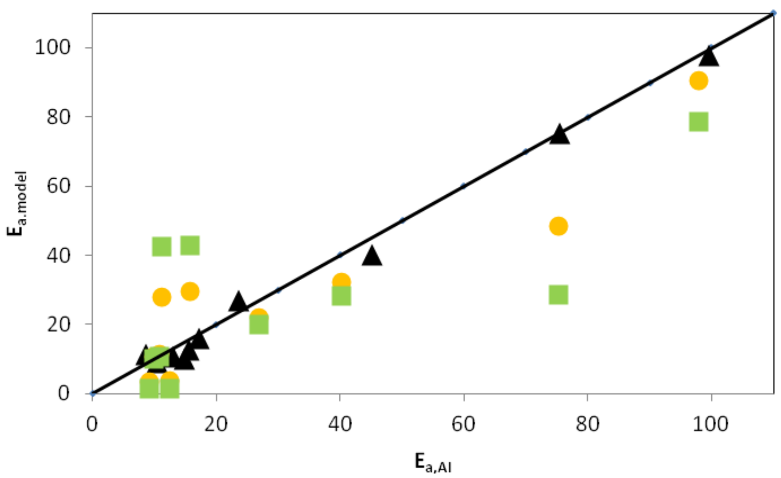

Figure 5-3: Parity plot of predicted activation energies at 300 K for hydrogen abstractions with transition state of the O--H--C type versus ab initio calculated activation energies showing the improved performance of the GA model developed in this work (Δ), in comparison with the Blowers and Masel model with $w_f + w_b$ = 788.3 kJ mol^{-1} and V_p = 995.0 kJ mol^{-1} (o), and the intersecting parabolas model with a = 1.0 and b = 13.9 (□). Activation energies, E_a in kJ mol^{-1}, at 300 K for the 25 reactions of the ab initio validation set provided in Table S42 of Appendix D.

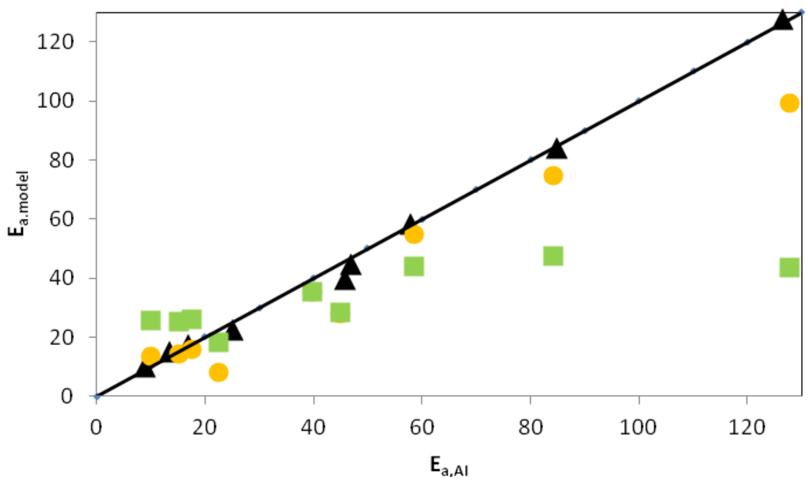

Figure 5-4: Parity plot of predicted activation energies at 300 K for hydrogen abstractions with transition state of the O--H--O type versus ab initio calculated activation energies showing the improved performance of the GA model developed in this work (Δ), in comparison with the Blowers and Masel model with $w_f + w_b$ = 888.3 kJ mol^{-1} and V_p = 1092.0 kJ mol^{-1} (o), and the intersecting parabolas model with a = 0.5 and b = 9.6 (□). Activation energies, E_a, in kJ mol^{-1}, at 300 K for the 25 reactions of the ab initio validation set presented in Table S42 of Appendix D.

Based on the performance of the three models in predicting activation energies for the two reaction families studied − (a) the GA model developed in this work, (b) the Blowers and Masel model and, (c) the IP model developed by Denisov − it can be safely concluded that the GA model outperforms the two others. Moreover, the GA model allows the prediction of the pre-exponential factors of a given reaction within the studied reaction families, while the other two models assume a fixed pre-exponential factor for the whole reaction family.

5.6 Conclusions

This work provides an extension to the previously developed group additivity schemes for hydrogen abstractions from oxygenates by carbon centered and by hydrogen radicals toward hydrogen abstractions between oxygenates by oxygen centered radicals. In particular, hydrogen abstraction reactions of the O--H--C and the O--H--O type are studied, and the compounds involved cover a variety of oxygenate compounds such as alcohols, ethers, esters, acids, ketones, diketones, aldehydes, hydroxyperoxides, alkyl peroxides and unsaturated ethers and ketones. The developed models allow the prediction of Arrhenius parameters and rate and tunneling coefficients in a broad temperature range (300-2500 K).

Group additive values for Arrhenius parameters for the two reaction families are derived from an extensive training set of ab initio calculated data for more than 100 hydrogen abstraction reactions. For all the ab initio calculations the CBS-QB3 method was employed, incorporating Eckart tunneling coefficients and corrections for 1-D hindered rotation around the forming/ breaking bond in the transition state. For reactions with transition states of the O--H--C type, a set of 32 ΔGAV^os (24 accounting for primary and 8 for secondary contributions) and 20 corrections for resonance and/or hyperconjugative interactions was derived. In line with the previously developed models for hydrogen abstractions between oxygenates, secondary contributions were shown to play an important role in determining Arrhenius parameters for reactions of the O--H--C type. Similarly, 11 ΔGAV^os (5 for primary and 6 for secondary contributions) and 17 corrections for cross-effects around the transition state were determined for reactions with transition state of the O--H--O type.

These two group additive models were validated upon an ab initio validation set containing 25 hydrogen abstraction reactions not previously used for the determination of the ΔGAV^os. Mean absolute deviations in Arrhenius parameters amounted to 2.8 kJ mol^{-1} for activation energies and 0.188 log(m^3 mol^{-1} s^{-1}) for pre-exponential factors for the forward reaction of the O--H--C type at 300 K, while rate coefficients for the same reactions could be reproduced on average within a factor of ~2.5 for both the forward and the reverse reaction. For reactions of the O--H--O type the corresponding values for the forward reaction at 300 K are 1.9 kJ mol^{-1} for activation energies, 0.217 log(m^3 mol^{-1} s^{-1}) for pre-exponential factors and ~2.9 for rate coefficients.

Comparable results were obtained from the experimental validation set where 60 experimental rate coefficients of 26 different reactions could be group additively predicted with a mean factor of deviation of ~3.2. Additionally, it was shown that this GA model outperforms the Blowers and Masel model and the intersecting parabolas (IP) model in the prediction of activation energies.

Consequently, the models developed in this work extrapolate successfully the previously established models toward the accurate prediction of Arrhenius parameters and rate coefficients for a wide variety of gas-phase hydrogen abstraction reactions between oxygenates by oxygen-centered radicals at temperatures ranging from 300 to 2500 K.

5.7 References

1. Becke, A.D., *A New Mixing of Hartree-Fock and Local Density-Functional Theories.* J Chem Phys, 1993. **98**(2): p. 1372-1377.
2. Boese, A.D. and J.M.L. Martin, *Development of density functionals for thermochemical kinetics.* J Chem Phys, 2004. **121**(8): p. 3405-3416.
3. Zhao, Y. and D.G. Truhlar, *A new local density functional for main-group thermochemistry, transition metal bonding, thermochemical kinetics, and noncovalent interactions.* J Chem Phys, 2006. **125**(19).
4. Curtiss, L.A., K. Raghavachari, P.C. Redfern, V. Rassolov, and J.A. Pople, *Gaussian-3 (G3) theory for molecules containing first and second-row atoms.* J Chem Phys, 1998. **109**(18): p. 7764-7776.
5. Baboul, A.G., L.A. Curtiss, P.C. Redfern, and K. Raghavachari, *Gaussian-3 theory using density functional geometries and zero-point energies.* J Chem Phys, 1999. **110**(16): p. 7650-7657.
6. Henry, D.J., M.B. Sullivan, and L. Radom, *G3-RAD and G3X-RAD: Modified Gaussian-3 (G3) and Gaussian-3X (G3X) procedures for radical thermochemistry*. J Chem Phys, 2003. **118**(11): p. 4849-4860.
7. Montgomery, J.A., M.J. Frisch, J.W. Ochterski, and G.A. Petersson, *A Complete Basis Set Model Chemistry. VI. Use of Density Functional Geometries and Frequencies.* J Chem Phys, 1999. **110**(6): p. 2822-2827.
8. Boese, A.D., M. Oren, O. Atasoylu, J.M.L. Martin, M. Kallay, and J. Gauss, *W3 theory: Robust computational thermochemistry in the kJ/mol accuracy range.* J Chem Phys, 2004. **120**(9): p. 4129-4141.
9. Karton, A., E. Rabinovich, J.M.L. Martin, and B. Ruscic, *W4 theory for computational thermochemistry: In pursuit of confident sub-kJ/mol predictions.* J Chem Phys, 2006. **125**(14).
10. Evans, M.G. and M. Polanyi, *Further Considerations on the Thermodynamics of Chemical Equilibria and Reaction Rates.* Proc. Roy. Soc. A, 1936. **154**: p. 1333-1360.
11. Evans, M.G. and M. Polanyi, *Inertia and Driving Force of Chemical Reactions.* Trans. Faraday Soc., 1938. **1938**(34): p. 11-29.
12. Denisov, E.T., *New Empirical Models of Free Radical Abstraction Reactions.* Usp Khim+, 1997. **66**(10): p. 953-971.
13. Blowers, P. and R. Masel, *Engineering Approximations for Activation Energies in Hydrogen Transfer Reactions.* Aiche J, 2000. **46**(10): p. 2041-2052.
14. Lucarini, M., G.F. Peduli, and M. Guerra, *A Critical Evaluation of the Factors Determining the Effect of Intramolecular Hydrogen Bonding on the O-H Bond Dissociation Enthalpy of Catechol and of Flavonoid Antioxidants.* Chem-Eur J, 2004. **10**(4): p. 933-939.
15. Bentley, T.W., *Additivity Rules Using Similarity Models for Chemical Reactivity: Calculation and Interpretation of Electrofugality and Nucleofugality.* Chem-Eur J, 2006. **12**(25): p. 6514-6520.

16. Benson, S.W. and J.H. Buss, *Additivity Rules for the Estimation of Molecular Properties. Thermodynamic Properties.* J Chem Phys, 1958. **29**(9): p. 546-561.
17. Benson, S.W., *Thermochemical Kinetics*. 1968, New York: John Wiley & Sons Ltd.
18. Benson, S.W., F.R. Cruickshank, D.M. Golden, G.R. Haugen, H.E. O'Neal, A.S. Rodgers, R. Shaw, and R. Walsh, *Additivity Rules for the Estimation of Thermochemical Properties.* Chem Rev, 1969. **69**: p. 279-324.
19. Shum, L.G.S. and S.W. Benson, *The Pyrolysis of Dimethyl Sulfide, Kinetics and Mechanism.* Int J Chem Kinet, 1985. **17**(7): p. 749-761.
20. Benson, S.W., *Some Key Reactions in Oxidation and Combustion - Thermochemistry and Kinetics.* Abstr Pap Am Chem S, 1982. **183**(Mar): p. 35-41.
21. Benson, S.W., *Probing the Chemical Kinetics of Air Pollution.* Environ Sci Technol, 2002. **36**(1): p. 28-32.
22. Sumathi, R., H.H. Carstensen, and W.H. Green, *Reaction Rate Prediction via Group Additivity Part 1: H Abstraction from Alkanes by H and CH3.* J Phys Chem A, 2001. **105**(28): p. 6910-6925.
23. Sumathi, R., H.H. Carstensen, and W.H. Green, *Reaction Rate Prediction via Group Additivity, Part 2: H-Abstraction from Alkenes, Alkynes, Alcohols, Aldehydes and Acids by H Atoms.* J Phys Chem A, 2001. **105**(39): p. 8969-8984.
24. Sumathi, R. and W.H. Green, *Oxygenate, Oxyalkyl and Alkoxycarbonyl Thermochemistry and Rates for Hydrogen Abstraction from Oxygenates.* Phys Chem Chem Phys, 2003. **5**(16): p. 3402-3417.
25. William H. Green, Joshua W. Allen, Beat A. Buesser, Robert W. Ashcraft, Gregory J. Beran, Caleb A. Class, Connie Gao, C. Franklin Goldsmith, Michael R. Harper, et al., *RMG - Reaction Mechanism Generator v4.0.1*, 2013.
26. Vandewiele, N.M., K.M. Van Geem, M.F. Reyniers, and G.B. Marin, *Genesys: Kinetic Model Construction Using Chemo-Informatics.* Chem Eng J, 2012. **207**: p. 526-538.
27. Paraskevas, P.D., M.K. Sabbe, M.F. Reyniers, N. Papayannakos, and G.B. Marin, *Kinetic Modeling of α-Hydrogen Abstractions from Unsaturated and Saturated Oxygenate Compounds by Carbon-Centered Radicals.* Chem Phys Chem, 2014. **15**(9): p. 1849-1866.
28. Paraskevas, P.D., M.K. Sabbe, M.F. Reyniers, N. Papayannakos, and G.B. Marin, *Kinetic Modeling of α-Hydrogen Abstractions from Unsaturated and Saturated Oxygenate Compounds by Hydrogen Atoms.* J Phys Chem A, 2014. **118**(40): p. 9296-9309.
29. Saeys, M., M.F. Reyniers, V. Van Speybroeck, M. Waroquier, and G.B. Marin, *Ab Initio Group Contribution Method for Activation Energies of Hydrogen Abstraction Reactions.* Chem Phys Chem, 2006. **7**(1): p. 188-199.
30. Sabbe, M.K., A.G. Vandeputte, M.F. Reyniers, M. Waroquier, and G.B. Marin, *Modeling the Influence of Resonance Stabilization on the Kinetics of Hydrogen Abstractions.* Phys Chem Chem Phys, 2010. **12**(6): p. 1278-1298.
31. Vandeputte, A.G., M.K. Sabbe, M.F. Reyniers, and G.B. Marin, *Kinetics of Alpha Hydrogen Abstractions from Thiols, Sulfides and Thiocarbonyl Compounds.* Phys Chem Chem Phys, 2012. **14**(37): p. 12773-12793.

32. Vandeputte, A.G., M.F. Reyniers, and G.B. Marin, *Kinetic Modeling of Hydrogen Abstractions Involving Sulfur Radicals.* Chem Phys Chem, 2013. **14**(16): p. 3751-3771.

33. Laidler, K.J., *Chemical Kinetics*. 1987, New York: Harper & Row.

34. Eckart, C., *The Penetration of a Potential Barrier by Electrons.* Phys Rev, 1930. **35**: p. 1303-1309.

35. Frisch, M.J., G.W. Trucks, H.B. Schlegel, G.E. Scuseria, M.A. Robb, J.R. Cheeseman, G. Scalmani, V. Barone, B. Mennucci, et al., *Gaussian 09, Revision D.01*, 2009, Gaussian, Inc.: Wallingford CT.

36. Vansteenkiste, P., V. Van Speybroeck, G.B. Marin, and M. Waroquier, *Ab Initio Calculation of Entropy and Heat Capacity of Gas-Phase n-Alkanes Using Internal Rotations.* J Phys Chem A, 2003. **107**(17): p. 3139-3145.

37. Van Speybroeck, V., P. Vansteenkiste, D. Van Neck, and M. Waroquier, *Why Does the Uncoupled Hindered Rotor Model Work Well for the Thermodynamics of n-Alkanes?* Chem Phys Lett, 2005. **402**(4-6): p. 479-484.

38. Vansteenkiste, P., V. Van Speybroeck, G. Verniest, N. De Kimpe, and M. Waroquier, *Applicability of the hindered rotor scheme to the puckering mode in four-membered rings.* J Phys Chem A, 2006. **110**(10): p. 3838-3844.

39. Sabbe, M.K., F. De Vleeschouwer, M.F. Reyniers, M. Waroquier, and G.B. Marin, *First Principles Based Group Additive Values for the Gas Phase Standard Entropy and Heat Capacity of Hydrocarbons and Hydrocarbon Radicals.* J Phys Chem A, 2008. **112**(47): p. 12235-12251.

40. Paraskevas, P.D., M.K. Sabbe, M.F. Reyniers, N. Papayannakos, and G.B. Marin, *Group Additive Values for the Gas Phase Standard Enthalpy of Formation, Entropy and Heat Capacity of Oxygenates.* Chem-Eur J, 2013. **19**: p. 16431-16452.

41. Vandeputte, A.G., M.K. Sabbe, M.F. Reyniers, V. Van Speybroeck, M. Waroquier, and G.B. Marin, *Theoretical Study of the Thermodynamics and Kinetics of Hydrogen Abstractions from Hydrocarbons.* J Phys Chem A, 2007. **111**(46): p. 11771-11786.

42. Martin, J.M.L. and G. de Oliveira, *Towards standard methods for benchmark quality ab initio thermochemistry - W1 and W2 theory*. J Chem Phys, 1999. **111**(5): p. 1843-1856.

43. Curtiss, L.A., P.C. Redfern, and K. Raghavachari, *Gaussian-4 theory*. J Chem Phys, 2007. **126**(8).

44. Tajti, A., P.G. Szalay, A.G. Csaszar, M. Kallay, J. Gauss, E.F. Valeev, B.A. Flowers, J. Vazquez, and J.F. Stanton, *HEAT: High accuracy extrapolated ab initio thermochemistry*. J Chem Phys, 2004. **121**(23): p. 11599-11613.

45. Feller, D., K.A. Peterson, and J.G. Hill, *On the effectiveness of CCSD(T) complete basis set extrapolations for atomization energies.* J Chem Phys, 2011. **135**(4).

46. Jodkowski, J.T., M.T. Rayez, J.C. Rayez, T. Berces, and S. Dobe, *Theoretical study of the kinetics of the hydrogen abstraction from methanol. 3. Reaction of methanol with hydrogen atom, methyl, and hydroxyl radicals.* J Phys Chem A, 1999. **103**(19): p. 3750-3765.

47. Ratkiewicz, A. and T.N. Truong, *Kinetics of the Hydrogen Abstraction R-OH+H -> R-O-center + H2 Reaction Class.* Int J Chem Kinet, 2010. **42**(7): p. 414-429.

48. Jorgensen, S., V.F. Andersen, E.J.K. Nilsson, O.J. Nielsen, and M.S. Johnson, *Theoretical study of the gas phase reaction of methyl acetate with the hydroxyl radical: Structures, mechanisms, rates and temperature dependencies.* Chem Phys Lett, 2010. **490**(4-6): p. 116-122.

49. Vandeputte, A.G., M.F. Reyniers, and G.B. Marin, *A theoretical study of the thermodynamics and kinetics of small organosulfur compounds.* Theor Chem Acc, 2009(123): p. 391-412.

50. Zheng, J.J., Y. Zhao, and D.G. Truhlar, *Representative benchmark suites for barrier heights of diverse reaction types and assessment of electronic structure methods for thermochemical kinetics.* J Chem Theory Comput, 2007. **3**(2): p. 569-582.

51. Pollak, E.L.I. and P. Pechukas, *Symmetry Numbers, Not Statistical Factors, Should be Used in Absolute Rate Theory and in Bronsted Relations.* J Am Chem Soc, 1978. **100**(10): p. 2984-2991.

52. Coulson, D.R., *Statistical Factors in Reaction-Rate Theories.* J Am Chem Soc, 1978. **100**(10): p. 2992-2996.

53. Saeys, M., M.F. Reyniers, G.B. Marin, V. Van Speybroeck, and M. Waroquier, *Ab Initio Group Contribution Method for Activation Energies for Radical Additions.* Aiche J, 2004. **50**(2): p. 426-444.

54. Truong, T.N., W.T. Duncan, and M. Tirtowidjojo, *A Reaction Class Approach for Modeling Gas Phase Reaction Rates.* Phys Chem Chem Phys, 1999. **1**(6): p. 1061-1065.

55. Ratkiewicz, A., J. Bieniewska, and T.N. Truong, *Kinetics of the Hydrogen Abstraction R-OH+H -> R-center-OH+H2 Reaction Class: An Application of the Reaction Class Transition State Theory.* Int J Chem Kinet, 2011. **43**(2): p. 78-98.

56. *Chemical Kinetics Database,NIST Standard Reference Database 17, Version 7.0 (Web Version), Release 1.3*. 2005; Available from: http://kinetics.nist.gov/.

57. Wantuck, P.J., R.C. Oldenborg, S.L. Baughcum, and K.R. Winn, *Direct Measurements of Methoxy Removal Rate Constants for Collisions with CH4, Ar, N2, Xe, and CF4 in the Temperature Range 673-973 K.* Symp. Int. Combust. Proc., 1988. **22**: p. 973 - 981.

58. *Chemical Kinetics Database, NIST Standard Reference Database 17, Version 7.0 (Web Version), Release 1.6.7, Data Version 2013*, 2013.

59. Atkinson, R., D.L. Baulch, R.A. Cox, J.N. Crowley, R.F. Hampson, R.G. Hynes, M.E. Jenkin, M.J. Rossi, and J. Troe, *Evaluated Kinetic and Photochemical Data for Atmospheric Chemistry: Volume I - Gas Phase Reactions of Ox, HOx, NOx, and SOx, Species.* Atmos Chem Phys, 2004. **4**(4): p. 1461-1738.

60. Atkinson, R., D.L. Baulch, R.A. Cox, J.N. Crowley, R.F. Hampson, R.G. Hynes, M.E. Jenkin, M.J. Rossi, and J. Troe, *Evaluated Kinetic and Photochemical Data for Atmospheric Chemistry: Volume II - Gas Phase Reactions of Organic Species.* Atmos Chem Phys, 2006. **6**(6): p. 3625-4055.

61. Orkin, V.L., S.N. Kozlov, G.A. Poskrebyshev, and M.J. Kurylo, *Rate Constant for the Reaction of OH with H-2 Between 200 and 480 K.* J Phys Chem A, 2006. **110**(21): p. 6978-6985.

62. Talukdar, R.K., T. Gierczak, L. Goldfarb, Y. Rudich, B.S.M. Rao, and A.R. Ravishankara, *Kinetics of Hydroxyl Radical Reactions with Isotopically Labeled Hydrogen.* J Phys Chem-Us, 1996. **100**(8): p. 3037-3043.

63. Schmidt, V., G.Y. Zhu, K.H. Becker, and E.H. Fink, *Study of Oh Reactions at High-Pressures by Excimer Laser Photolysis - Dye-Laser Fluorescence*. Ber Bunsen Phys Chem, 1985. **89**(3): p. 321-322.

64. Bonard, A., V. Daele, J.L. Delfau, and C. Vovelle, *Kinetics of OH Radical Reactions with Methane in the Temperature Range 295-660 K and with Dimethyl Ether and Methyl-tert-butyl Ether in the Temperature Range 295-618 K.* J Phys Chem A, 2002. **106**(17): p. 4384-4389.

65. Calpini, B., F. Jeanneret, M. Bourqui, A. Clappier, R. Vajtai, and H. van den Bergh, *Direct measurement of the total reaction rate of OH in the atmosphere.* Analysis, 1999. **27**(4): p. 328-336.

66. Gierczak, T., R.K. Talukdar, S.C. Herndon, G.L. Vaghjiani, and A.R. Ravishankara, *Rate coefficients for the reactions of hydroxyl radicals with methane and deuterated methanes.* J Phys Chem A, 1997. **101**(17): p. 3125-3134.

67. Bryukov, M.G., V.D. Knyazev, S.M. Lomnicki, C.A. McFerrin, and B. Dellinger, *Temperature-dependent kinetics of the gas-phase reactions of OH with Cl-2, CH4, and C3H8.* J Phys Chem A, 2004. **108**(47): p. 10464-10472.

68. Heathfield, A.E., C. Anastasi, P. Pagsberg, and A. McCulloch, *Atmospheric lifetimes of selected fluorinated ether compounds.* Atmos Environ, 1998. **32**(4): p. 711-717.

69. Donahue, N.M., J.G. Anderson, and K.L. Demerjian, *New rate constants for ten OH alkane reactions from 300 to 400 K: An assessment of accuracy*. J Phys Chem A, 1998. **102**(18): p. 3121-3126.

70. Clarke, J.S., J.H. Kroll, N.M. Donahue, and J.G. Anderson, *Testing frontier orbital control: Kinetics of OH with ethane, propane, and cyclopropane from 180 to 360K.* J Phys Chem A, 1998. **102**(48): p. 9847-9857.

71. Crowley, J.N., J.P. Campuzano, and G.K. Moortgat, *Temperature dependent rate constants for the gas-phase reaction between OH and CH3OCl.* J Phys Chem-Us, 1996. **100**(9): p. 3601-3606.

72. Koffend, J.B. and N. Cohen, *Shock tube study of OH reactions with linear hydrocarbons near 1100 K.* Int J Chem Kinet, 1996. **28**(2): p. 79-87.

73. Overend, R. and G. Paraskevopoulos, *Rates of Oh Radical Reactions .4. Reactions with Methanol, Ethanol, 1-Propanol, and 2-Propanol at 296-K.* J Phys Chem-Us, 1978. **82**(12): p. 1329-1333.

74. Li, S.C. and F.A. Williams, *Experimental and Numerical Studies of Two-Stage Methanol Flames.* Twenty-Sixth Symposium (International) on Combustion, 1996. **1-2**: p. 1017-1024.

75. Mellouki, A., S. Teton, and G. Lebras, *Kinetics of Oh Radical Reactions with a Series of Ethers.* Int J Chem Kinet, 1995. **27**(8): p. 791-805.

76. Nelson, L., O. Rattigan, R. Neavyn, H. Sidebottom, J. Treacy, and O.J. Nielsen, *Absolute and Relative Rate Constants for the Reactions of Hydroxyl Radicals and Chlorine Atoms with a Series of Aliphatic-Alcohols and Ethers at 298-K.* Int J Chem Kinet, 1990. **22**(11): p. 1111-1126.

77. Wallington, T.J., R.Z. Liu, P. Dagaut, and M.J. Kurylo, *The Gas-Phase Reactions of Hydroxyl Radicals with a Series of Aliphatic Ethers over the Temperature-Range 240-440-K.* Int J Chem Kinet, 1988. **20**(1): p. 41-49.

78. Perry, R.A., R. Atkinson, and J.N. Pitts, *Rate Constants for Reaction of Oh Radicals with Ch2=Chf, Ch2=Chcl, and Ch2=Chbr over Temperature-Range 299 Degrees-K-426 Degreesk.* J Chem Phys, 1977. **67**(2): p. 458-462.

79. Arif, M., B. Dellinger, and P.H. Taylor, *Rate coefficients of hydroxyl radical reaction with dimethyl ether and methyl tert-butyl ether over an extended temperature range.* J Phys Chem A, 1997. **101**(13): p. 2436-2441.

80. Vaghjiani, G.L. and A.R. Ravishankara, *Kinetics and Mechanism of Oh Reaction with Ch3ooh.* J Phys Chem-Us, 1989. **93**(5): p. 1948-1959.

81. Dagaut, P., T.J. Wallington, R.Z. Liu, and M.J. Kurylo, *The Gas-Phase Reactions of Hydroxyl Radicals with a Series of Carboxylic-Acids over the Temperature-Range 240-440-K.* Int J Chem Kinet, 1988. **20**(4): p. 331-338.

82. Zetzsch, C.S., F., *Rate constants for reactions of OH with carbonic acids.* Phys. Chem. Behav. Atmos. Pollut. Proc. Eur. Symp., 1982. **2**: p. 129-137.

83. El Boudali, A., S. Le Calve, G. Le Bras, and A. Mellouki, *Kinetic studies of OH reactions with a series of acetates.* J Phys Chem-Us, 1996. **100**(30): p. 12364-12368.

84. Wallington, T.J., P. Dagaut, R.H. Liu, and M.J. Kurylo, *The Gas-Phase Reactions of Hydroxyl Radicals with a Series of Esters over the Temperature-Range 240-440-K.* Int J Chem Kinet, 1988. **20**(2): p. 177-186.

85. Campbell, I.M. and P.E. Parkinson, *Rate Constants for Reactions of Hydroxyl Radicals with Ester Vapors at 292-K.* Chem Phys Lett, 1978. **53**(2): p. 385-387.

86. Krasnoperov, L.N. and J.V. Michael, *Shock tube studies using a novel multipass absorption cell: Rate constant results for OH+H-2 and OH+C2H6.* J Phys Chem A, 2004. **108**(26): p. 5643-5648.

87. Vandooren, J.V.T., P.J., *Experimental Investigation of Methanol Oxidation in Flames: Mechanism and Rate Constants of Elementary Steps.* Symp. Int. Combust. Proc., 1981. **18**.

88. Bowman, C.T., *Shock-Tube Investigation of High-Temperature Oxidation of Methanol.* Combust Flame, 1975. **25**(3): p. 343-354.

89. DeMore, W.B. and K.D. Bayes, *Rate constants for the reactions of hydroxyl radical with several alkanes, cycloalkanes, and dimethyl ether.* J Phys Chem A, 1999. **103**(15): p. 2649-2654.

90. Wallington, T.J., J.M. Andino, L.M. Skewes, W.O. Siegl, and S.M. Japar, *Kinetics of the Reaction of Oh Radicals with a Series of Ethers under Simulated Atmospheric Conditions at 295-K.* Int J Chem Kinet, 1989. **21**(11): p. 993-1001.

91. Cook, R.D., D.F. Davidson, and R.K. Hanson, *High-Temperature Shock Tube Measurements of Dimethyl Ether Decomposition and the Reaction of Dimethyl Ether with OH.* J Phys Chem A, 2009. **113**(37): p. 9974-9980.

92. Smith, D.F., C.D. Mciver, and T.E. Kleindienst, *Kinetics and Mechanism of the Atmospheric Oxidation of Tertiary Amyl Methyl-Ether.* Int J Chem Kinet, 1995. **27**(5): p. 453-472.

93. Baldwin, R.R., M.W.M. Hisham, and R.W. Walker, *Elementary reactions involved in the oxidation of propene: Arrhenius parameters for the reaction HO2 + C3H6 = C3H6O + OH.* Symp. Int. Combust. Proc., 1984. **20**: p. 743-750.

94. Baldwin, R.R., P.N. Jones, and R.W. Walker, *Determination of the Rate-Constant for Ho2+Ch4-]H2o2+Ch3 at 443-Degrees-C.* J Chem Soc Farad T 2, 1988. **84**: p. 199-207.

95. Baldwin, R.R., C.E. Dean, M.R. Honeyman, and R.W. Walker, *Arrhenius Parameters for the Reaction Ho2+C2h6-]C2h5+H2o2 over the Temperature-Range 400-500-Degrees-C.* J Chem Soc Farad T 1, 1986. **82**: p. 89-102.

96. Baldwin, R.R., A.R. Fuller, D. Longthorn, and R.W. Walker, *The Oxidation of Formaldehyde as a Source of HO2 Radicals*, in *Combust. Inst. European Symp.*, F.J. Weinberg, Editor 1973, Academic Press: London.

97. Kirsch, L.J. and D.A. Parkes, *Recombination of Tertiary Butyl Peroxy-Radicals .1. Product Yields between 298-K and 373-K.* J Chem Soc Farad T 1, 1981. **77**: p. 293-307.

98. Held, T.J. and F.L. Dryer, *A comprehensive mechanism for methanol oxidation.* Int J Chem Kinet, 1998. **30**(11): p. 805-830.

Chapter 6

Group Additive Kinetic Modeling for Carbon-centered Radical Addition to Oxygenates and *β*-Scission of Oxygenates

6.1 Abstract

A consistent set of group additive values is determined for the Arrhenius parameters of carbon-centered radical addition to oxygenates and the reverse *β*-scission of oxygenate compounds, covering a wide temperature range (300-2500 K). These values are derived based on a training set of 66 reactions for which the Arrhenius parameters are calculated using the CBS-QB3 method in the high-pressure limit, including corrections for hindered internal rotation. Using linear least-square regression a set of 32 group additive values is derived for activation energies and pre-exponential factors. Among them, 18 refer to values accounting for primary contributions, and 14 to secondary contributions, which are shown to be essential to obtain a highly accurate model. In the absence of experimental data in literature, the accuracy of the model is established by comparing model predictions with an ab initio validation set containing 24 reactions. The mean factor of deviation between the group additively calculated rate coefficients and the ab initio values is 3, for both the radical additions and the *β*-scissions. Therefore, the developed group additive model, constituting an extension of the existing group additive model for carbon-centered radical additions and *β*-scissions of hydrocarbons, can be safely applied for an accurate prediction of kinetics of the corresponding reactions involving oxygenate compounds.

6.2 Introduction

Radical addition and their reverse β-scission reactions play a significant role in various processes based on radical chemistry. Processes such as pyrolysis, steam-cracking, oxidation or combustion are among the most important industrial production processes in which the reaction family of carbon-centered radical addition/β-scission is of major importance.

Recently, the growing concern for environmental issues has led to the investigation of the use of alternative feedstock based on biomass. This kind of feedstock implies a high oxygen content in the reactant compounds and often also in the products. Accurate description of the kinetics that govern these processes is not only important for reliable process simulations, but it is crucial for a detailed understanding and optimization of the pertinent processes. However, the lack of experimental data for such reactions due to the reactive nature of oxygenate radicals makes it imperative to obtain kinetic data from other sources.

The last few decades a variety of methods have been developed for the prediction of kinetic parameters for radical reactions. The rapidly developed computational chemistry provides a powerful tool for determining the necessary thermodynamic and kinetic data, yet there are significant limitations in its use since ab initio methods are computationally too demanding for larger compounds. An alternative approach for predicting thermodynamics and kinetics for the thousands of reactions present in larger reaction networks, based on a limited amount of parameters, is therefore desirable.

Evans-Polanyi [1, 2] correlations and its variations [3, 4] are among the most common methods that correlate the activation energy of a given reaction to the reaction enthalpy within a particular reaction family. The main drawback of these methods is that they consider a constant pre-exponential factor for all reactions within the same reaction family.

The most popular method that makes use of group additivity for predicting thermochemical kinetics is Benson's group contribution method [5, 6]. Within the framework of this predictive method, thermodynamic and kinetic parameters were shown to be accurately predicted for a variety of compounds, such as unsaturated oxygenates [7], peroxy radicals [8] and aldehydes and ketones [9].

Based on the idea of group additivity Willems and Froment [10, 11] developed a method according to which structural differences between the target and the reference reaction can be added as contributions to the Arrhenius parameters of the reference reaction. Another approach, the reaction class transition state theory developed by Truong [12] was shown to be adequate for predicting rate coefficients for hydrogen abstraction reactions for several reaction families such as alkanes [13], alkenes [14] and alcohols [15, 16]. The concept of introducing supergroups for hydrogen abstraction reactions that encompass the reactive moiety of the transition state structure is attributed to Sumathi et al. [17-19]. According to this method rate coefficients can be obtained by calculating thermochemistry for the reactants and the transition state based on supergroups that account for contributions from the reaction center as a whole, an entity which contains several polyvalent atoms.

In this work the group additive method proposed by Saeys et al. [20] was chosen; within this method, group additive values for Arrhenius parameters can be determined in terms of activation enthalpy and entropy, such as the difference between the reactants and the transition state. Particularly, activation energies and pre-exponential factors for a considered reaction are obtained by adding perturbations to a well chosen reference reaction. These perturbations correspond to the structural differences between the reactants and the transition state. The main advantage of this method is that the group additive values remain almost temperature independent since temperature dependence is expressed by the Arrhenius parameters of the reference reaction. This method was shown to provide accurate results for determining kinetic parameters, not only for radical additions [21, 22], but also for hydrogen abstractions covering a wide range of compounds involved such as hydrocarbons [23, 24], sulfur [25, 26] and oxygenate compounds [27-29].

Group additive values for kinetic parameters such as activation energies and pre-exponential factors are of major importance since they grasp the main effects that govern the reaction kinetics and are compatible with reaction mechanism generation programs such as PRIM [30], RMG [31] and Genesys [32]. These programs can be used for the development of detailed chemical kinetic networks combining a reliable yet computationally inexpensive prediction for complex reaction mechanisms in radical chemistry.

This study intends to be fully consistent with the already developed group additive model for carbon-centered radical addition and β-scission reactions between hydrocarbons [21], and provides an extension towards carbon-centered radical additions to oxygenates and β-scissions of oxygenates. Since it was shown that the inclusion of secondary contributions is necessary for an accurate prediction of rate coefficients for hydrogen abstractions involving oxygenates [27-29] the necessity of including secondary contributions for the oxygenate reaction family studied in this work is investigated.

The aim of this work is to determine an accurate set of group additive values (ΔGAV^os) for the calculation of activation energies and pre-exponential factors for carbon-centered radical addition to oxygenates and the reverse β-scission of oxygenates at temperatures ranging from 300 K to 2500 K. Initially, accurate kinetic data are obtained at various temperatures (300-2500 K) with the CBS-QB3 composite ab initio method [33] along with corrections for the one-dimensional hindered rotation [34] (1D-HR) around the transitional bond for the oxygenate reaction family studied. Based on these data, group additive values are determined at the same temperature range (300-2500 K) using linear least-square regression. The accuracy of the ΔGAV^{o}s determined in this work is assessed by comparing the group additive predictions with a set of ab initio calculated values.

6.3 Computational Methods

6.3.1 Rate Coefficients

In conventional transition state theory (CTST) the rate coefficient in the high pressure limit for bimolecular reactions such as radical additions is expressed by the eq (6-1):

$$k(T) = \frac{k_B T}{h} \frac{q_{\ddagger}}{q_A q_B} e^{-\frac{\Delta E(0\ \mathrm{K})}{RT}} \qquad (6\text{-}1)$$

with q the total partition function per unit volume, k_B and h the Boltzmann and the Planck constants respectively and ΔE(0 K) the electronic zero-point corrected reaction barrier determined using the CBS-QB3 method of Montgomery et al. [33]. All electronic structure calculations in this study have been performed with the Gaussian-09 [35] program.

For the monomolecular β-scission reactions the rate coefficients are expressed by the eq (6-2):

$$k(T) = \frac{k_B T}{h} \frac{q_{\ddagger}}{q_P} e^{-\frac{\Delta E(0\ \mathrm{K})}{RT}} \qquad (6\text{-}2)$$

Tunneling is neglected for the reaction family studied in this work, since the maximal tunneling coefficient for the reactions included in the training set of reactions is only 1.5 at 300 K. At higher temperatures, for instance 1000 K, where most of the chemical processes like steam-cracking or pyrolysis occur, tunneling coefficients are less than 1.1. It has been shown previously [36] that for radical additions the neglect of tunneling contributions does not reduce the accuracy of the CBS-QB3 calculated rate coefficients in comparison to experimentally observed rate coefficients. Hence, the value for *κ(T)* in eq (6-1) and (6-2) is set to 1.

Partition functions per unit volume, *q*, are calculated by the rigid-rotor and harmonic oscillator approximation at the B3LYP/6-311G(2d,d,p) level using a default scale factor of 0.99. Completely in line with previous work in carbon radical additions [21], the internal rotation around the forming/breaking bond in the transition state is always treated explicitly as one-dimensional hindered rotor (1D-HR) [34, 37, 38], since its contribution cannot cancel out between transition state and reactants: it only exists in the transition state, and can therefore significantly contribute to the rate coefficient. The contribution of most of the other internal rotations can be considered similar in reactants and transition state and therefore these are expected to have a minor effect on the rate coefficient. The correction in partition functions for the internal rotation about the formed bond in the addition product can be significant in some cases, up to a factor of three for the studied reactions. Since this mode is treated as a hindered internal rotor in the transition state, the same approach is applied to this rotational mode in the radical addition product to avoid inconsistencies.

The localization of the transition state of carbon-centered radical addition reactions is difficult using the default CBS-QB3 optimization step, the B3LYP method. This is due to B3LYP tendency to overestimate the length of the weak C−C bond in the transition state of radical addition reactions [39, 40]. Saeys et al. [20, 41] proposed a methodology according to which the location of the B3LYP/6-311G(d,p) transition state, which is the geometry optimization step within the CBS-QB3 method, is improved using a bond length scaling correlation derived from an IRCMax(CBS-QB3; B3LYP/6-311G(d,p)) [42] analysis. The length of the forming C−C bond in the transition state of radical additions was determined by the B3LYP/6-311G(d,p) method for the 66 reactions included in the training set. This forming bond length varies from 206.6 to 261.7 pm. This range of C−C bond lengths for the radical addition transition states in this work is much larger than the range of the bond lengths used by Saeys et al. [41] in the construction of the bond length scaling correlation, which covers C−C bond lengths between 214.3 and 246.5 pm. Therefore, the scaling correlation proposed by Saeys et al. [41] is inadequate to correlate the C−C bond lengths for the reactions studied in this work and a new scaling correlation based on data from the reactions studied here is required.

Hence, from the training set of 66 reactions, nine reactions were selected covering the whole range of B3LYP/6-311G(d,p) C−C bond lengths and for this set of nine reactions IRCMax calculations were performed in order to accurately locate the transition state on the CBS-QB3 potential energy surface. The derived correlation between the length of the forming C−C bond in the radical addition transition state at the IRCMax and the B3LYP level is provided in eq (6-3):

$$\begin{aligned} &C{-}C_{IRCMax} = 0.6783\ C{-}C_{B3LYP} + 69.89\ \text{pm} && \text{if } C{-}C_{B3LYP} > 217.25\ \text{pm} \\ &C{-}C_{IRCMax} = C{-}C_{B3LYP}\ \text{pm} && \text{if } C{-}C_{B3LYP} < 217.25\ \text{pm} \end{aligned} \tag{6-3}$$

A detailed description of how this correlations derived can be found in Section S1 of Appendix E. Hence, the transition state optimization in this work is performed in two steps. First, the $C{-}C_{B3LYP}$ length of the forming bond is determined at the B3LYP/6-311G(d,p) level of theory, the default CBS-QB3 optimization method. In a following step, the transition state is reoptimized at the same B3LYP level, but now constraining the length of the forming C−C bond at the improved $C{-}C_{IRCMax}$ length, which is determined using the eq (6-3). On the resulting geometry the CBS-QB3 energy is calculated, which should be close to the energy of the actual transition state on the CBS-QB3 potential energy surface.

Arrhenius parameters (E_a and log$A$) were obtained from linear least square regression to the ab initio rate coefficients, k, on the Arrhenius equation in the temperature range T – 100 K to

T + 100 K with k sampled at intervals of 50 K and with T the temperature of interest. The accuracy of the group additivity method used in this study is assessed by comparison of group additively predicted with ab initio calculated rate coefficients. As a measure for the deviation between these values, a factor ρ, larger than 1, is defined according to eq (6-4), which provides a proper indication for the relative deviation between the two rate coefficients:

$$\begin{cases} \rho = \dfrac{k_{\mathrm{AI}}}{k_{\mathrm{GA}}} & k_{\mathrm{AI}} > k_{\mathrm{GA}} \\ \rho = \dfrac{k_{\mathrm{GA}}}{k_{\mathrm{AI}}} & k_{\mathrm{GA}} > k_{\mathrm{AI}} \end{cases} \tag{6-4}$$

6.3.2 Group Additivity Method

Benson's group additivity method [6] as modified by Saeys et. al. [20] is adopted in this work for determining activation energies and pre-exponential factors for carbon radical additions and β-scissions among oxygenates. The additivity of enthalpy of formation and entropy in the transition state as developed by Benson [5, 43] allows the calculation of activation energies and pre-exponential factors, respectively. A detailed description of the derivation of this method is provided in earlier work concerning carbon-centered radical additions and β-scissions between hydrocarbons [20, 21].

Within the group additive method for Arrhenius parameters, the rate coefficients can be expressed by the eq (6-5):

$$k = n_{\mathrm{e}} k_{\mathrm{GA}} = n_{\mathrm{e}} \tilde{A} e^{-\frac{E_{\mathrm{a}}}{RT}} \tag{6-5}$$

in which n_{e} stands for the reaction path degeneracy [44, 45], $\tilde{A}$ is the single-event pre-exponential factor and E_{a} is the activation energy. Since for the studied radical additions tunneling coefficients are, even at 300 K, lower than 1.5, and lower at higher temperatures, the tunneling coefficient in this work is set to 1. The single-event pre-exponential factor, $\tilde{A}$, is obtained by dividing the pre-exponential factor, A, by the reaction path degeneracy [21]..

A schematic representation of the transition state of the carbon radical additions and *β*-scissions studied in this work is provided in Figure 6-1, according to which the transition-state-specific groups are those that involve carbon atoms C_1, C_2 and C_3. Possible oxygenate-specific groups can be present on X_i, Y_i and Z_i. During the addition of the C_3 radical these three atoms undergo the following changes: C_1 changes from double bonded carbon atom (C_d) into carbon radical ($C^{\bullet}$), C_2 changes from C_d into C and C_3 changes from $C^{\bullet}$ into C.

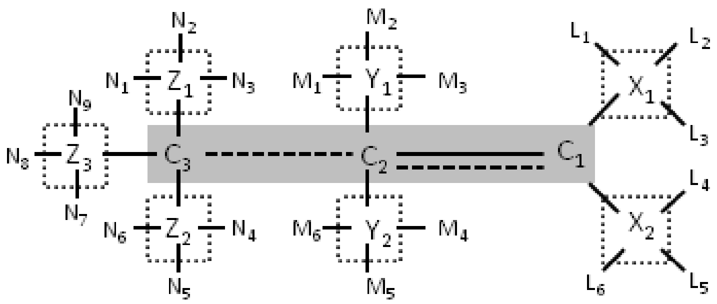

Figure 6-1: Transition state of a carbon radical addition/*β*-scission reaction, the dashed lines indicate partially formed bonds. The grey zone indicates the central atoms of the primary contributions. The dotted line encompasses the central atoms of the secondary contributions.

The contributions to the Arrhenius parameters can be categorized into primary, secondary and tertiary contributions. The former refer to ligands related to the central atoms involved in the studied reaction (C_1, C_2 and C_3), while secondary contributions relate to groups further away from the reaction center that have these atoms, C_i (i=1,2,3), as a ligand (X_i, Y_i and Z_i, see Figure 6-1). Tertiary contributions originate from non-nearest neighbor interactions. A detailed overview of these three different types of contributions can be found in earlier studies [20, 21] related to carbon-centered radical additions involving hydrocarbons.

As shown in previous works [27-29] for hydrogen abstractions involving oxygenate compounds, secondary contributions are, along with the primary contributions, of major importance for an accurate group additive model for oxygenate radical kinetics, while tertiary contributions can be safely neglected without any significant influence in the accuracy of the model. Hence, it is expected that secondary contributions are also necessary for an accurate and reliable group additive model for the kinetics of the radical additions studied in this work. The expression of the group additive model for the calculation of the Arrhenius parameters, truncated after the secondary contributions is provided in eq (6-6):

$$
\begin{aligned}
E_{\mathrm{a}}(T) &= E_{\mathrm{a,ref}}(T) + \sum_{i=1}^{3} \Delta\mathrm{GAV}^{\mathrm{o}}_{\mathrm{E_a}}(C_i) + \sum_{i=1}^{2} \Delta\mathrm{GAV}^{\mathrm{o}}_{\mathrm{E_a}}(X_i) + \sum_{i=1}^{2} \Delta\mathrm{GAV}^{\mathrm{o}}_{\mathrm{E_a}}(Y_i) + \sum_{i=1}^{3} \Delta\mathrm{GAV}^{\mathrm{o}}_{\mathrm{E_a}}(Z_i) \\
\log \tilde{A}(T) &= \log \tilde{A}_{ref}(T) + \sum_{i=1}^{3} \Delta\mathrm{GAV}^{\mathrm{o}}_{\log\tilde{\mathrm{A}}}(C_i) + \sum_{i=1}^{2} \Delta\mathrm{GAV}^{\mathrm{o}}_{\log\tilde{\mathrm{A}}}(X_i) + \sum_{i=1}^{2} \Delta\mathrm{GAV}^{\mathrm{o}}_{\log\tilde{\mathrm{A}}}(Y_i) + \sum_{i-1}^{3} \Delta\mathrm{GAV}^{\mathrm{o}}_{\log\tilde{\mathrm{A}}}(Z_i)
\end{aligned}
\tag{6-6}
$$

In eq (6-6), the 1st term refers to the Arrhenius parameter (E_a and $\log\tilde{A}$ respectively) of the reference reaction, the 2nd term to primary contributions and the other three terms to secondary contributions. Starting from a well-chosen reference reaction, representative of the reaction family studied, the determined group additive values for the Arrhenius parameters are added perturbations related to the structural differences between the transition state of the studied reaction and the reference reaction.

As a reference reaction the addition of methyl radical to ethene was chosen, with the *β*-scission of 1-propyl radical into methyl and ethene as its reverse reaction. Besides being the simplest reaction of the studied reaction family, it also allows this study to be fully consistent with the model developed in previous work [21], using the same reference reaction. The main advantage of introducing a reference reaction is that the temperature dependence of the Arrhenius parameters is mainly incorporated in the corresponding parameters of the reference reaction leaving the group additive contributions almost temperature independent.

An important characteristic of group additivity models is that every group includes information about its neighboring groups. This can lead to linear dependent subsets in the whole set of groups for a given reaction family, therefore a few groups corresponding to secondary contributions should be set equal to zero. These groups are: O-(C_1)(H), CO-

$(C_1)(H)$, $O\text{-}(C_2)(H)$, $CO\text{-}(C_2)(H)$, $O\text{-}(C_3)(H)$, $CO\text{-}(C_3)(H)$, $C\text{-}(C_{3,d})(H)_3$, $O\text{-}(C_{3,d})(H)$, which correspond to groups describing secondary contributions with the highest number of hydrogen ligands, an approach that is fully consistent with the work of Sabbe et al. [24].

6.4 Results and Discussion

6.4.1 Rate Coefficients and Arrhenius Parameters

The training set of reactions considered in this work for the study of carbon-centered radical additions to oxygenates and β-scissions of oxygenates contains 66 reactions (see Table 6-1), which have been grouped into three categories: (a) additions of a methyl radical to the unsubstituted carbon atom of various unsaturated oxygenates, (b) methyl radical additions to the substituted carbon atom of various unsaturated oxygenates and (c) additions of various oxygenate radicals to ethene. These three categories of reactions can be used for the evaluation of the effect of substituents on (a) the formed radical, (b) the attacked carbon atom and (c) the attacking radical, respectively. In these reactions several types of oxygenate compounds are included, such as alcohols, ethers, esters, ketones, aldehydes and acids, which are the main compounds involved in pyrolysis reaction networks of oxygenate compounds.

For the reactions included in the training set described above, ab initio calculated rate coefficients, Arrhenius parameters (activation energies and pre-exponential factors), standard reaction enthalpies and entropies at temperatures 300-2500 K are provided in Tables S2-S7 of Appendix E. Since tunneling coefficients are close to 1, even at the lowest temperatures for the reactions of the particular reaction family, Eckart tunneling coefficients are provided only at 300 K. This only in order to justify their neglect, and in the remainder of this work, tunneling coefficients are neglected and considered to be equal to unity.

Table 6-1: Training set of carbon-centered radical additions to oxygenates and β-scissions of oxygenates.

Reference Reaction

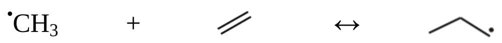

Training Set of Reactions

(a) Influence of the Structure of the Formed Radical

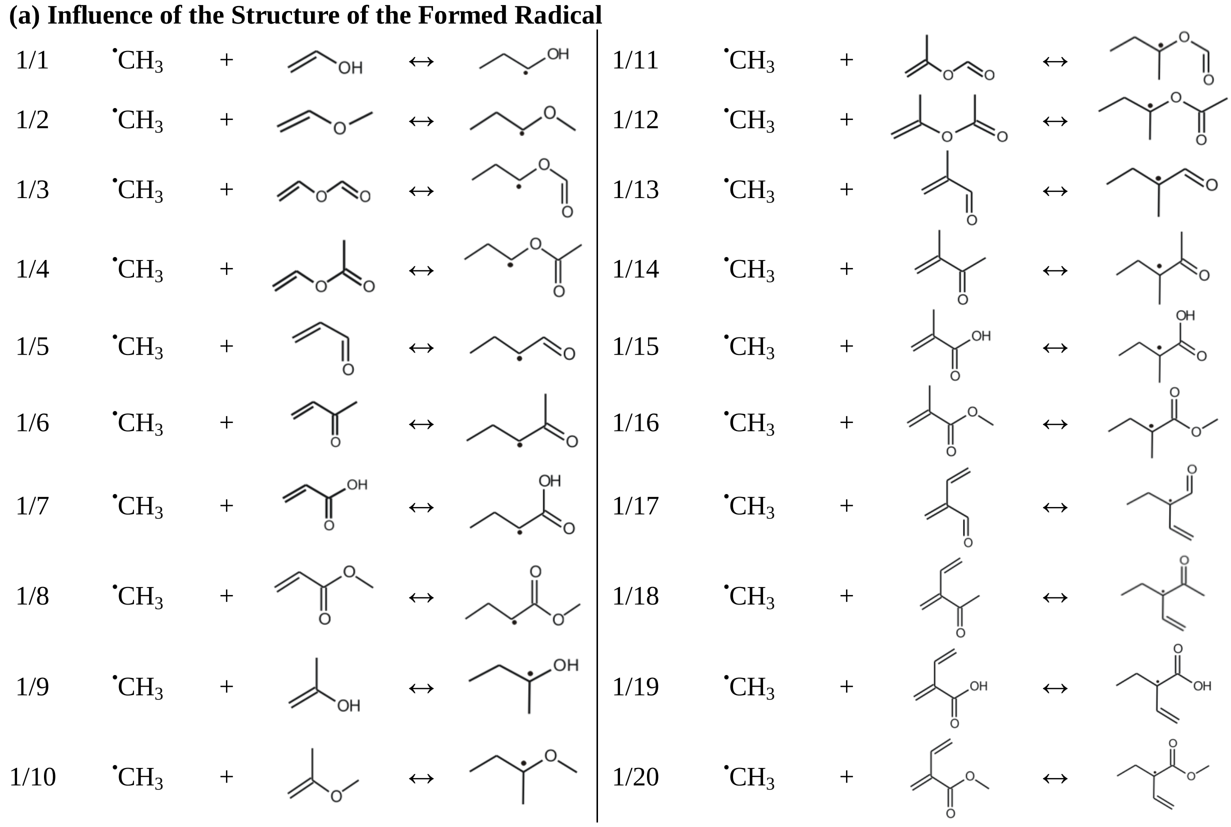

(b) Influence of the Structure of the Attacked Carbon Atom

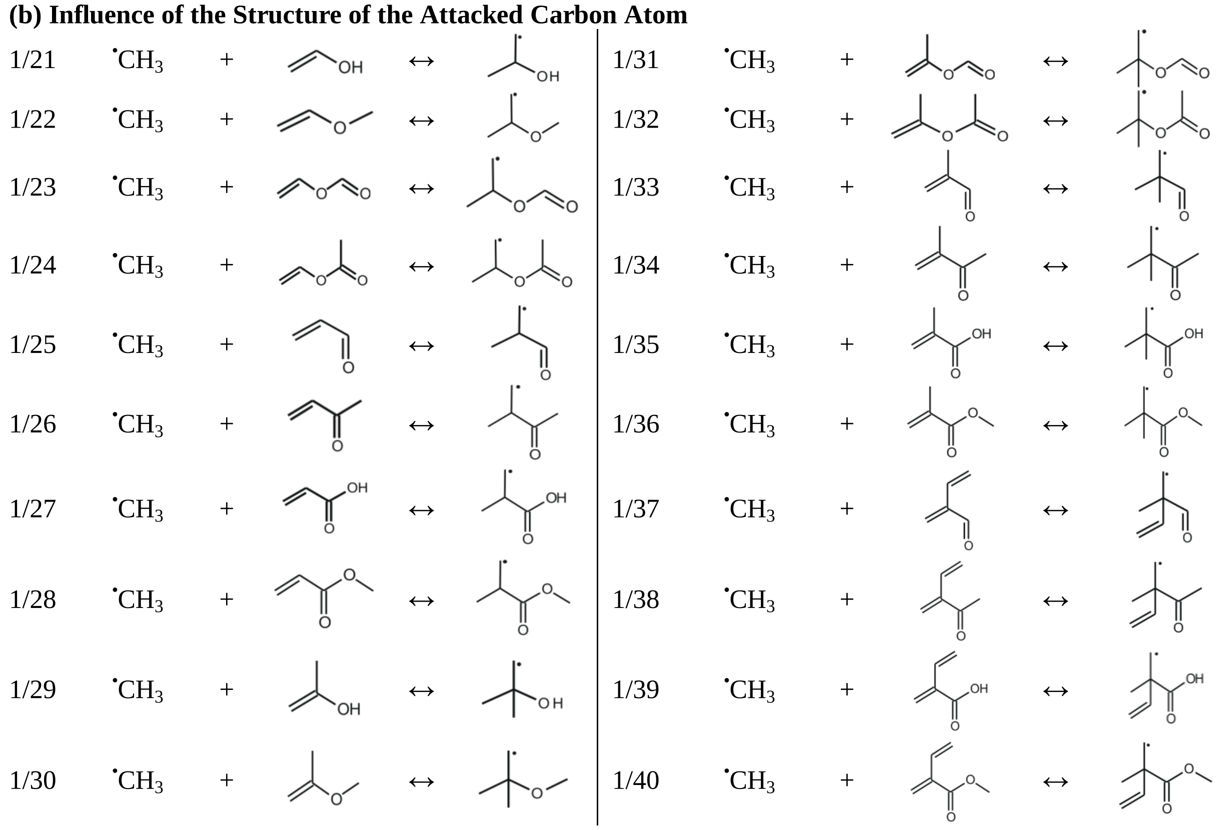

(c) Influence of the Structure of the Attacking Radical

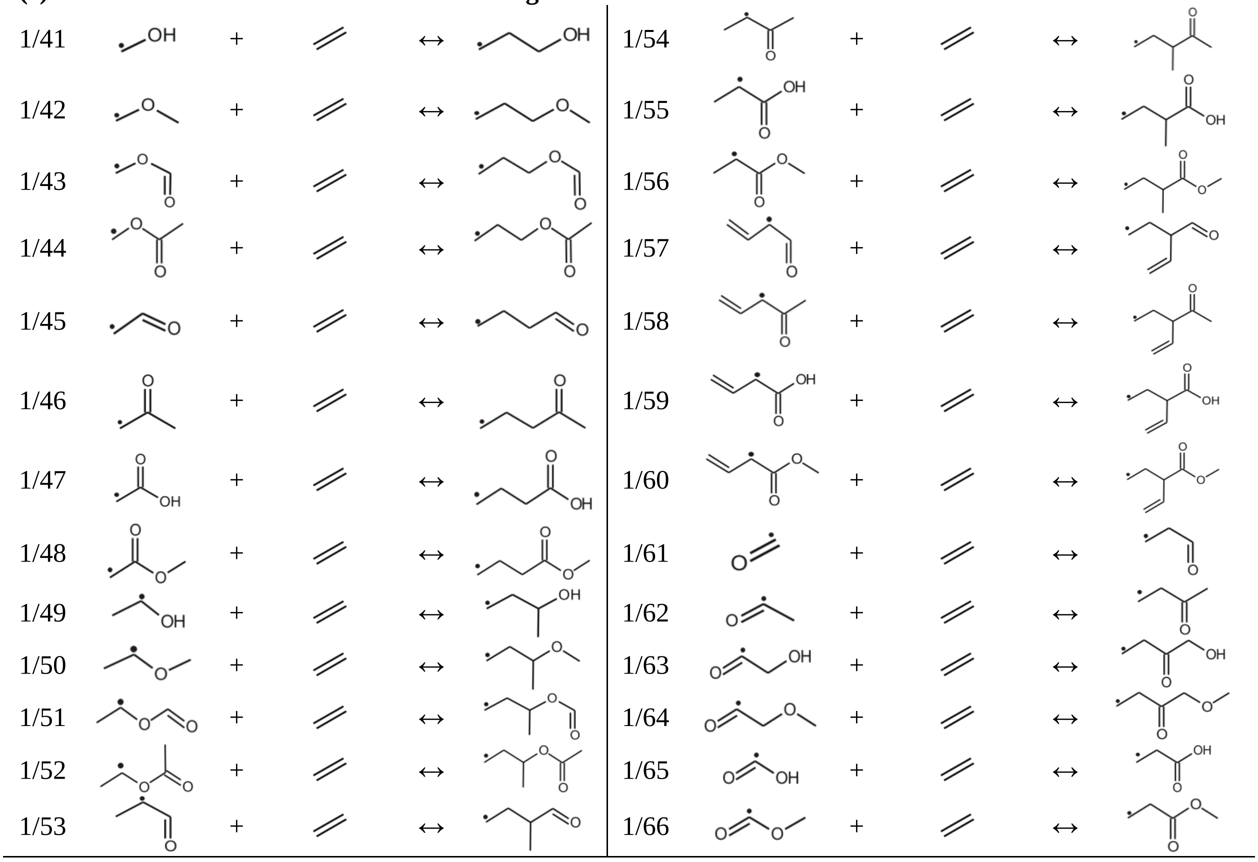

All radical reactions included in the training set are exothermic with standard reaction enthalpies varying from −175 to −2.5 kJ mol^{-1} at 300 K, see Table S2 of Appendix E. Strongly exothermic values correspond to reactions of the first category, while the reactions of the third category are weakly exothermic, which can be attributed to the fact that many of the reactant radicals in this category of reactions are resonance stabilized. Moreover, in all cases, the reactions of the second category have higher reaction enthalpy values than the corresponding reactions of the first category in which the same compounds react, mostly due to the increased steric interaction in the product radical resulting from the addition to the substituted end of the double bond. Standard reaction entropies are negative for all reactions included in the training set, and all of the same magnitude at 300 K. The reaction entropies, which fluctuate between −130 and −90 J mol^{-1} K^{-1}, mainly reflect the loss of the translational entropy in going from two reactants to a single product radical.

Activation energies vary between 6 and 59 kJ mol^{-1}. The highest barriers occur for the reactions of the second category, for which almost all activation barriers are above 30 kJ mol^{-1}. This can mainly be attributed to significant steric hindrance in the transition state for the reactions of this category, in which the substitution at the attacked carbon atom is varied. Lowest barriers correspond to reactions of the first category, for which most barriers are below 20 kJ mol^{-1} at 300 K. This can be explained by the strong exothermicity of these reactions, which is related to the varying substituents on the formed radical center. The activation energies for the reverse β-scission reactions at 300 K are much higher and lie between 55 and 182 kJ mol^{-1} at 300 K, with lowest values observed for the third category of reactions for which the β-scissions are only weakly endothermic. For the reactions of the second category all reaction barriers are higher than 100 kJ mol^{-1} while for the reactions of the first category all reaction barriers are even higher than 120 kJ mol^{-1}.

Pre-exponential factors fluctuate between 10^3 and 10^6 m^3 mol^{-1} s^{-1} for all radical addition reactions included in this training set at 300 K. Pre-exponential factors correlate well with the degree of substitution of the reactants. Generally, increasing substitution of the attacking radical or the attacked carbon atom leads to lower pre-exponential factors due to reduced internal mobility in the transition state. Therefore, pre-exponential factors for the reactions of the first category are almost an order of magnitude higher than the corresponding values for the reactions of the second category at 300 K. For β-scissions of oxygenates, pre-exponential factors are much higher than the corresponding values for the carbon radical addition reactions and amount to values of 10^9–10^{11} m^3 mol^{-1} s^{-1} at 300 K.

At the same temperature rate coefficients for the carbon radical additions to oxygenates have values between 5 10^{-6} and 1.5 10^4 m^3 mol^{-1} s^{-1}. The reactions of the first category tend to the higher values for the rate coefficients and the reactions of the second category to the lower values, with intermediate rate coefficients for the reactions of the third category. For the β-

scission reactions of oxygenates rate coefficients are much lower leading to values between 3.4 10^{-21} and 3 m^3 mol^{-1} s^{-1} at 300 K, indicating that at lower temperatures the carbon radical addition to oxygenates is the favorable reaction compared to its reverse reaction, the β-scission of oxygenates. At higher temperatures, approximately above 1000 K, β-scission of oxygenates become the favorable direction of the reaction.

For the first and second category of reactions included in the training set, the attacking radical is a methyl radical and the associated rotation around the formed bond in the product radical is a methyl rotor. The internal rotation energy profile for a methyl rotor not only has the same threefold symmetric shape for all reactions, but also the barrier height for this rotation is approximately the same (about 12 kJ mol^{-1}) for all reactions. For this type of internal rotation, the correction to the partition function is very limited, especially at lower temperatures below 1000 K. The inclusion of corrections for the internal rotation around the formed bond in the addition product can have significant influence in the rate coefficients for both the addition to oxygenates and the β-scission of oxygenates, especially for the reactions of the third category. Particularly, at 300 K the rate coefficients for the radical addition reactions of the third category are more than two times higher than the rate coefficients at the same temperature where the internal rotation around the formed bond in the addition product is treated as an harmonic oscillator. An overview of the averaged values for the rate coefficients, k_{HR} / k_{HO}, for the additions and β-scissions for the three categories of reactions included in the training set at 300 and 1000 K is presented in Table S8 of Appendix E.

6.4.2 Group Additivity Values

ΔGAV^os necessary for describing the kinetics of carbon-centered radical additions to oxygenates and their reverse β-scissions of oxygenates are derived by means of least-square regression based on the ab initio calculated Arrhenius parameters included in Tables S2-S7 of

Appendix E at temperatures ranging from 300 K to 2500 K. The ΔGAV^os for activation energies and pre-exponential factors for the reaction family studied at 300, 600 and 1000 K can be found in Table 6-2, whilst at higher temperatures (1500-2500 K) the corresponding parameters are provided in Table S9 of Appendix E. Rate coefficients for all carbon-centered radical additions and their reverse β-scissions included in the training set for temperatures between 300 and 2500 K can be retrieved from Table S10 of Appendix E. For the same reactions, applied symmetry numbers and number of single events are provided in Table S11 of Appendix E.

As a reference reaction the addition of methyl radical to ethene was chosen, with reverse reaction the β-scission of 1-propyl radical into methyl and ethene. Arrhenius parameters for the reference reaction at temperatures 300-2500 K are derived from Table S12 of Appendix E. Along with ΔGAV^os for primary contributions, also values for secondary contributions are determined. The inclusion of secondary contributions improves the mean absolute deviation (MAD) between group additive predictions and ab initio calculations for the Arrhenius parameters considerably. For instance, for activation energies at 300 K, the MAD reduces from 2.1 to 1.0 kJ mol^{-1} for additions and from 3.5 to 1.5 kJ mol^{-1} for β-scissions. Similar reductions hold for log$\tilde{A}$, while the full comparison between the corresponding parameters with or without inclusion of secondary contributions at temperatures up to 1000 K can be found in Table S13 of Appendix E.

Group additive values ΔGAV^o for pre-exponential factors for the radical addition reactions have positive values for primary contributions to C_1 (see Figure 6-1) in the temperature range 300-2500 K, whereas the corresponding values for primary contributions to C_2 and C_3 have mainly negative values in the same temperature range. Positive ΔGAV^o values for pre-exponential factors imply that the internal flexibility of the molecule is increased leading to an increase in the activation entropy of the reacting system compared to the reference reaction.

Table 6-2: ΔGAV°s at 300 K, 600 K and 1000 K for carbon-centered radical additions to oxygenates and their reverse *β*-scissions of oxygenates. ($\tilde{A}$ in m^3 mol^{-1} s^{-1} and E_a in kJ mol^{-1}). Y_1, Y_2 and X_1, X_2 ligands correspond to O, CO, C, C_d or H whereas Z_1, Z_2 and Z_3 ligands can be O, O_d, CO, C, C_d or H. C_d and O_d refer to a double-bonded carbon or oxygen atom, respectively.

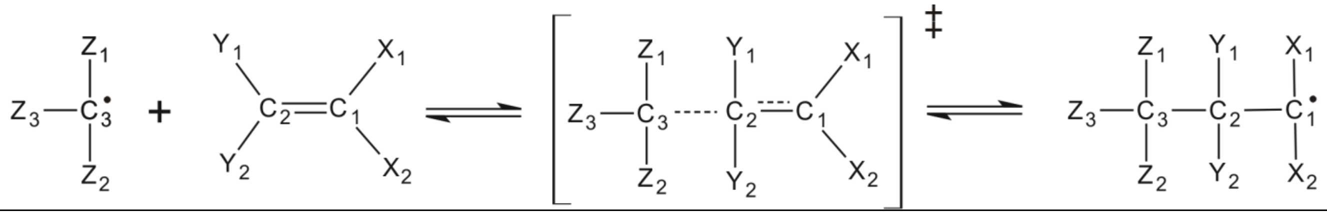

	addition						β-scission					
	300 K		600 K		1000 K		300 K		600 K		1000 K	
	log$\tilde{A}$	E_a	log$\tilde{A}$	E_a	log$\tilde{A}$	E_a	log$\tilde{A}$	E_a	log$\tilde{A}$	E_a	log$\tilde{A}$	E_a
Reference Reaction												
$^{\bullet}CH_3 + CH_2{=}CH_2$	4.882	30.5	5.439	35.2	5.968	43.1	10.184	125.1	10.458	127.3	10.547	128.5
	ΔGAV°$_{addition}$						ΔGAV°$_{β\text{-scission}}$					
	300 K		600 K		1000 K		300 K		600 K		1000 K	
Group	log$\tilde{A}$	E_a	log$\tilde{A}$	E_a	log$\tilde{A}$	E_a	log$\tilde{A}$	E_a	log$\tilde{A}$	E_a	log$\tilde{A}$	E_a
Primary Contributions												
C_1-(O)(H)	0.214	3.4	0.247	3.6	0.246	3.6	0.661	2.9	0.784	3.9	0.825	4.5
C_1-(CO)(H)	0.004	-17.7	0.002	-17.7	-0.003	-17.7	0.429	18.0	0.521	18.7	0.527	18.9
C_1-(C)(O)	0.025	-0.5	0.022	-0.6	0.007	-0.7	0.586	-0.5	0.742	0.7	0.799	1.6
C_1-(C)(CO)	0.123	-15.9	0.125	-16.0	0.118	-16.0	0.539	22.4	0.692	23.6	0.741	24.3
C_1-(C_d)(CO)	0.082	-25.5	0.137	-25.1	0.147	-24.9	1.130	57.0	1.320	58.4	1.364	59.1
C_2-(O)(H)	-0.141	11.1	-0.061	11.7	-0.043	12.0	0.058	-3.7	-0.006	-4.2	-0.059	-4.9
C_2-(CO)(H)	-0.248	-5.5	-0.224	-5.4	-0.218	-5.3	0.183	-11.6	0.129	-12.0	0.123	-12.0
C_2-(C)(O)	-0.498	17.8	-0.401	18.5	-0.381	18.8	0.157	-1.8	0.036	-2.9	-0.051	-4.1
C_2-(C)(CO)	-0.597	0.7	-0.530	1.1	-0.516	1.3	0.307	-14.1	0.227	-14.8	0.192	-15.2
C_2-(C_d)(CO)	-0.299	-1.3	-0.196	-0.6	-0.171	-0.2	0.449	-22.0	0.343	-22.9	0.290	-23.6
C_3-(O)$(H)_2$	-0.553	-2.5	-0.328	-0.8	-0.277	0.0	0.240	-14.2	0.243	-14.3	0.192	-15.0

C_3-(CO)(H)$_2$	-0.327	0.1	-0.141	1.4	-0.105	2.0	-0.038	-29.6	-0.237	-31.2	-0.315	-32.2
C_3-(C)(O)(H)	-0.847	-8.7	-0.492	-6.0	-0.412	-4.9	0.516	-21.7	0.477	-22.1	0.385	-23.4
C_3-(C)(CO)(H)	-0.968	3.6	-0.708	5.6	-0.651	6.4	0.104	-42.9	-0.104	-44.6	-0.205	-46.0
C_3-(C_d)(CO)(H)	-0.701	26.9	-0.350	29.5	-0.265	30.8	-0.450	-67.4	-0.609	-68.8	-0.694	-69.9
C_3-(O_d)(H)	-0.297	-2.6	-0.020	-0.5	0.084	1.1	0.042	-26.5	0.056	-26.4	0.083	-25.9
C_3-(O_d)(C)	-0.393	-6.6	-0.085	-4.2	0.016	-2.7	0.403	-31.1	0.357	-31.5	0.339	-31.7
C_3-(O_d)(O)	-0.004	-16.2	0.225	-14.5	0.287	-13.6	0.683	6.3	0.505	4.9	0.448	4.1
Secondary Contributions												
O-(C_1)(C)	0.245	-0.2	0.259	-0.1	0.263	-0.1	0.085	6.9	0.096	7.1	0.102	7.1
O-(C_1)(CO)	-0.150	-5.7	-0.172	-5.8	-0.173	-5.9	-0.302	1.0	-0.336	0.8	-0.338	0.8
CO-(C_1)(C)	-0.109	1.3	-0.108	1.3	-0.109	1.3	-0.274	-1.6	-0.257	-1.4	-0.241	-1.2
CO-(C_1)(O)	-0.147	2.6	-0.130	2.8	-0.127	2.8	-0.109	-6.8	-0.119	-6.8	-0.135	-7.1
O-(C_2)(C)	0.141	0.8	0.131	0.7	0.131	0.8	0.304	-0.4	0.320	-0.2	0.344	0.2
O-(C_2)(CO)	-0.333	-8.1	-0.338	-8.1	-0.338	-8.2	0.027	13.5	0.084	14.0	0.121	14.5
CO-(C_2)(C)	-0.127	-0.8	-0.140	-0.9	-0.146	-0.9	-0.011	2.7	-0.018	2.7	-0.020	2.6
CO-(C_2)(O)	-0.159	-0.7	-0.141	-0.6	-0.138	-0.5	-0.133	1.9	-0.142	1.8	-0.160	1.6
O-(C_3)(C)	0.067	1.1	-0.082	-0.1	-0.110	-0.5	-0.323	-3.4	-0.495	-4.7	-0.514	-5.0
O-(C_3)(CO)	-0.258	-2.8	-0.446	-4.3	-0.490	-4.9	-0.195	9.9	-0.322	9.0	-0.329	8.9
CO-(C_3)(C)	-0.451	-5.1	-0.432	-4.9	-0.427	-4.8	0.119	-1.9	0.102	-2.0	0.094	-2.2
CO-(C_3)(O)	-0.095	-8.1	-0.123	-8.4	-0.131	-8.4	-0.236	5.9	-0.211	6.1	-0.200	6.3
C-($C_{3,d}$)(O)(H)$_2$	0.033	1.1	0.032	1.1	0.025	0.9	-0.007	9.8	-0.007	9.8	-0.023	9.6
O-($C_{3,d}$)(C)	-0.043	0.8	-0.037	0.9	-0.038	0.9	0.110	-1.9	0.124	-1.9	0.128	-1.8

For ΔGAV^os on the C_1 carbon atom, the typically present resonance or hyperconjugative stabilization in the reactant radical is partially lifted in the transition state. The associated increase in flexibility increases the activation entropy with respect to the reference reaction. For the C_2 and C_3 groups, ligands on the carbon atoms between which a new C−C bond is formed lead to a decrease in the internal flexibility of the reactant molecules and consequently to a decrease in pre-exponential factor of the particular reaction compared to the reference reaction. Generally, ΔGAV^os for primary contributions to the Arrhenius parameters of the radical addition and the β-scission reactions are much higher in absolute terms than the corresponding values of the secondary contributions. Hence in following paragraphs the discussion will mainly focus on the primary contributions.

For carbon radical additions to oxygenates, the largest contribution in absolute values, for pre-exponential factors at 300 K, corresponds to ΔGAV^o C_3-(C)(CO)(H) and amounts to −0.968 log(m^3 mol^{-1} s^{-1}), while for β-scissions at the same temperature the largest contribution corresponds to ΔGAV^o C_1-(C_d)(CO) and is equal to +1.130 log(m^3 mol^{-1} s^{-1}). Generally, ΔGAV^os for pre-exponential factors of the β-scissions of oxygenates referring to contributions to C_1 (see Figure 6-1) have the highest values going up to +1.130 log(m^3 mol^{-1} s^{-1}), whereas lowest values derived for contributions to C_3 resulting in negative values down to −0.450 log(m^3 mol^{-1} s^{-1}).

At 300 K, the most positive contribution for activation energies for the carbon radical additions corresponds to the ΔGAV^o C_3-(C_d)(CO)(H) and amounts to +26.9 kJ mol^{-1} while the largest negative ΔGAV^o is that of the C_1-(C_d)(CO) group, equaling −25.5 kJ mol^{-1}. The ΔGAV^os for activation energies are mainly determined by the amount of resonance stabilization of the reactant (for the C_3 groups centered on the reactant radical) or product radical (for the C_1 groups centered on the formed radical), and for the C_2 groups also steric repulsion in the transition state needs to be considered.

The highest positive and negative ΔGAV^os for β-scission activation energies at 300 K correspond to the ΔGAV^os C_1-(C_d)(CO) and C_3-(C_d)(CO)(H) with values +57 kJ mol^{-1} and −67.4 kJ mol^{-1}, respectively. The strongly negative contribution of the group C_3-(C_d)(CO)(H) is due to the stability of the resonance-stabilized radical formed by the β-scission. All groups centered on C_2 and C_3 (see Figure 6-1), except for ΔGAV^o C_3-(O_d)(O), have negative contributions to the activation energy of the reference reaction for β-scissions of oxygenates. Contrary to that, all ΔGAV^os for groups centered on C_1 (see Figure 6-1) corresponding to primary contributions for activation energies for β-scissions are positive, with as only exception the ΔGAV^o C_1-(C)(O). Positive values in the activation energies for groups centered on C_1 are caused by an additional stabilization of the radical undergoing β-scission compared to that radical in the reference reaction.

In the group additivity method, the major part of the temperature dependence on the Arrhenius parameters of the reactions in the training set is accounted for by the corresponding parameters of the reference reaction, leaving the ΔGAV^os almost temperature independent. This is illustrated in Figure S2 of Appendix E, which provides the temperature dependence of the ΔGAV^os derived from Table 6-2 and Table S9 of Appendix E. Based on Figure S2, it can be claimed that ΔGAV^os for primary and secondary contributions are temperature independent, since for log$\tilde{A}$ the mean absolute deviation in going from 300 K to 2500 K is less than 0.140 log(m^3 mol^{-1} s^{-1}) for both addition and β-scission reactions and the maximum deviation amounts to ~0.48 log(m^3 mol^{-1} s^{-1}) only. For activation energies, E_a, the same conclusion holds, with the mean absolute deviation in the temperature range 300-2500 K less than 1.6 kJ mol^{-1} for additions and their reverse β-scissions and with a maximum deviation of 5 kJ mol^{-1}, which is still limited accounting for the wide temperature range of 2200 K.

The applicability of the group additive model developed in this work can be shown by the following examples for reactions included in Table 6-1. The Arrhenius parameters, single-event pre-exponential factor and activation energy for the carbon radical addition 1/15 from Table 6-1 at 1000 K can be calculated using ΔGAV^os from Table 6-2 as follows:

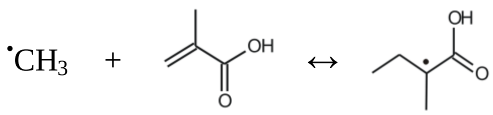

$\log A(1000\ K) = \log\tilde{A}_{ref}(1000\ K) + \Delta GAV_{\log\tilde{A}}^{o}\ (C_1\text{-(C)(CO)}) + \Delta GAV_{\log\tilde{A}}^{o}\ (CO\text{-}(C_1)\text{(O)}) + \log(n_e) = 5.968 + 0.118 - 0.127 + \log(4) = 6.561$

$E_a(1000\ K) = E_{a,ref}(1000\ K) + \Delta GAV_{Ea}^{o}\ (C_1\text{-(C)(CO)}) + \Delta GAV_{Ea}^{o}(CO\text{-}(C_1)\text{(O)}) = 43.1 - 16.0 + 2.8 = 29.9$ kJ mol^{-1}

In the calculation of the pre-exponential factors n_e is the number of single events, which in this reaction equals to 4. The values predicted by the GA model are in perfect agreement with the corresponding ab initio values that amount to 6.601 and 29.0 kJ mol^{-1}, respectively and differences between the GA and the AI values are equal to −0.040 and +0.9 kJ mol^{-1} respectively. Using eq (6-5), the rate coefficient for this carbon radical addition is calculated to be 9.98 10^4 m^3 mol^{-1} s^{-1}, being only 20% lower than the corresponding ab initio calculated value (1.23 10^5 m^3 mol^{-1} s^{-1}).

The second example refers to the calculation of the Arrhenius parameters for the β-scission reaction 1/44 from Table 6-1 at 1000 K using ΔGAV^os from Table 6-2:

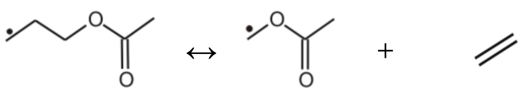

$\log A(1000\ K) = \log\tilde{A}_{ref}(1000\ K) + \Delta GAV_{\log\tilde{A}}^{o}\ (C_3\text{-(O)(H)}_2) + \Delta GAV_{\log\tilde{A}}^{o}\ (O\text{-}(C_3)\text{(CO)}) + \log(n_e) = 10.547 + 0.192 - 0.329 + \log(2) = 10.711$

$E_a(1000\text{ K}) = E_{a,ref}(1000\text{ K}) + \Delta GAV_{Ea}^{o}(C_3\text{-(O)(H)}_2) + \Delta GAV_{Ea}^{o}(\text{O-(C}_3\text{)(CO)}) = 128.5 - 15.0 + 8.9 = 122.4\text{ kJ mol}^{-1}$

The GA predicted values agree well with the corresponding ab initio calculated values that are 10.734 and 122.1 kJ mol^{-1} respectively, leading to differences between GA predicted and AI calculated values of −0.023 and +0.3 kJ mol^{-1}, respectively. The rate coefficient for the β-scission reaction is 2.08 10^4 m^3 mol^{-1} s^{-1} based on eq (6-5), that is 1.6 times higher than the corresponding AI determined value (1.27 10^4 m^3 mol^{-1} s^{-1}).

6.5 Validation

The GA model developed in this work is validated by comparing GA predictions with (a) a set of ab initio calculated values not previously used in the training set for determining ΔGAV^os and (b) predictions of other available models such as the Blowers and Masel [4] (BM) model and the Intersecting Parabolas (IP) model developed by Denisov [3]. Unfortunately, no experimental data for this reaction family could be found, despite a wide literature search, including the NIST Chemical Kinetics Database [46] and the IUPAC Kinetics Database [47, 48], neither for radical additions to oxygenates nor for β-scissions of oxygenates.

6.5.1 Ab initio validation

For the ab initio validation a set containing 24 carbon radical additions to oxygenates and β-scission reactions of oxygenates was developed with reactions not included in the training set for the determination of the ΔGAV^os. This set of reactions is representative of all types of ΔGAV^os provided in Table 6-2, allowing validation of primary groups centered on C_1, C_2 and C_3 along with the validation of secondary contributions. Ab initio Arrhenius parameters and rate coefficients for the 24 reactions of the ab initio validation set are compared with the corresponding group additively predicted values at 300 K, 600 K and 1000 K. Rate coefficients, Arrhenius parameters and standard reaction enthalpies and entropies for the 24 reactions included in the ab initio validation set at temperatures ranging from 300 to 1000 K are provided in Tables S14-S16 of Appendix E.

In Table 6-3 the performance of the group additive model is illustrated at 300 K by comparing the GA predictions with the AI determined values. The comparison at 300 K is the most stringent one due to the higher sensitivity of rate coefficients to errors in activation energies at lower than at higher temperatures. The comparison between GA predictions and AI calculated values for the reactions included in the validation set at higher temperatures (600 K and 1000 K) can be found in Tables S17-S18 of Appendix E, respectively. Moreover, symmetry numbers and reaction path degeneracy factors for the reactions included in the validation set are given in Table S19 of Appendix E.

In Table 6-3 the comparison between GA predictions and AI calculations is presented for both the forward and the reverse direction of the particular reaction. This is provided to allow comparing the corresponding deviations for the two directions of the same reaction, and the resulting effect on the equilibrium coefficient. Only for 11 of the 24 reaction the equilibrium coefficient k_{for}/k_{rev} is less than a deviation factor, $<\rho>$, of 2 from the ab initio equilibrium coefficient K_{AI}. This is better at higher temperatures, but will even then lead to thermodynamically inconsistent results. In order to avoid this, the best accuracy in the GA model can be achieved by calculating the kinetic parameters for one direction using GA values determined in this work, and calculating the rate coefficient for the reverse direction from thermodynamic consistency, based on $k_{rev} = k_{for} / K_{eq}$. Values for the equilibrium

Table 6-3: Comparison between group additive (GA) predicted and ab initio (AI) calculated kinetic parameters at 300 K for the ab initio validation set of 24 reactions. ($\Delta\log A$ = $\log A_{GA}-\log A_{AI}$ in log(m^3 mol^{-1} s^{-1}), ΔE_a = $E_{a,GA}-E_{a,AI}$ in kJ mol^{-1}). (MAD: mean absolute deviation, RMS: root mean square deviation, MAX: maximum deviation, <ρ>: factor of deviation between two values taken from eq (6-4)).

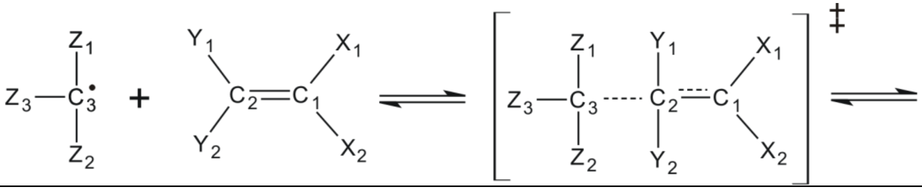

	Reactions	addition $\Delta\log A$	addition ΔE_a	addition k_{GA}/k_{AI}	β-scission $\Delta\log A$	β-scission ΔE_a	β-scission k_{GA}/k_{AI}	$\frac{K_{GA}^{eq}}{K_{AI}^{eq}}$
2/1	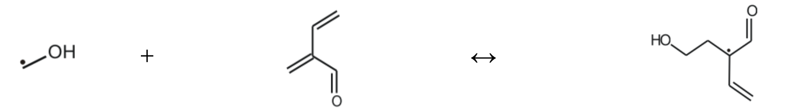	0.393	6.5	0.2	0.206	3.6	0.4	0.5
2/2	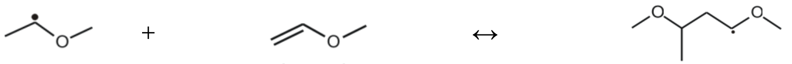	0.081	-2.1	2.4	0.162	1.3	0.7	3.3
2/3	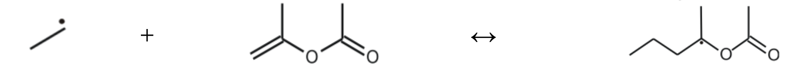	0.188	1.4	0.7	0.261	-0.2	1.6	0.5
2/4		0.146	4.6	0.2	0.170	5.6	0.1	1.5
2/5	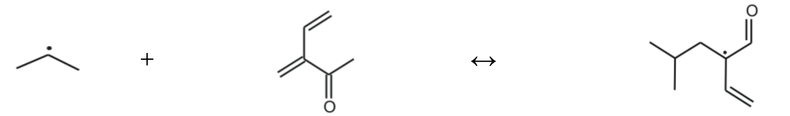	-0.177	4.0	0.1	-0.300	0.5	0.4	0.3
2/6	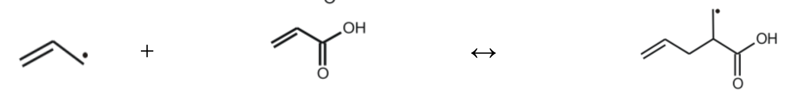	0.060	2.2	0.4	-0.211	3.5	0.1	3.2
2/7	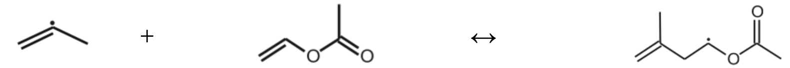	0.055	2.7	0.4	0.071	1.9	0.5	0.7
2/8		-0.326	-2.5	1.1	-0.184	-5.4	4.6	0.2
2/9		-0.083	4.5	0.1	-0.039	2.1	0.3	0.4
2/10		0.353	3.2	0.5	0.631	0.5	2.9	0.2

2/11	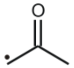	+		↔	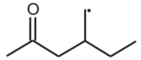	0.458	6.7	0.2	0.209	3.1	0.4	0.5
2/12	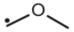	+	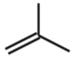	↔	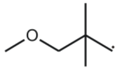	0.591	5.2	0.4	-0.585	-1.8	0.4	0.9
2/13	$^{\bullet}CH_3$	+	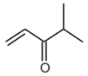	↔	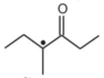	0.139	0.2	1.1	0.143	0.7	0.9	1.2
2/14	$^{\bullet}CH_3$	+	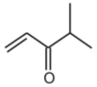	↔	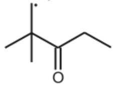	0.053	0.0	0.9	-0.023	1.7	0.4	2.5
2/15		+	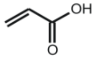	↔	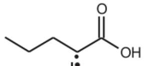	0.286	2.9	0.6	0.270	3.7	0.4	1.5
2/16		+	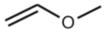	↔	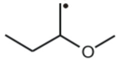	0.177	-0.5	1.4	-0.126	-4.2	3.0	0.5
2/17	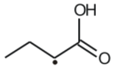	+		↔	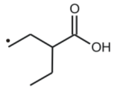	0.104	4.0	0.2	-0.065	-0.6	0.9	0.3
2/18	$^{\bullet}CH_3$	+	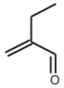	↔	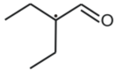	0.202	-1.3	2.4	0.093	0.8	0.8	3.1
2/19	$^{\bullet}CH_3$	+	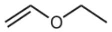	↔	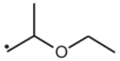	-0.310	-2.4	1.0	-0.567	-4.3	1.1	0.9
2/20	$^{\bullet}CH_3$	+	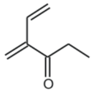	↔	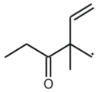	-0.117	1.0	0.4	-0.161	-2.6	1.6	0.3
2/21	$^{\bullet}CH_3$	+	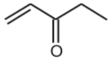	↔	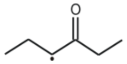	-0.001	-0.7	1.2	0.073	-1.8	2.2	0.6
2/22	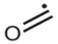	+	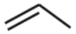	↔	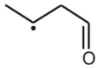	-0.078	2.5	0.3	0.638	1.0	2.5	0.1
2/23	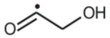	+	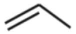	↔	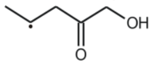	-0.224	2.3	0.3	-0.371	-6.3	4.6	0.1
2/24	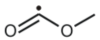	+	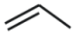	↔	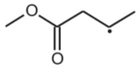	-0.035	2.7	0.3	0.761	1.3	3.1	0.1
					MAD	0.193	2.8		0.263	2.4		
					RMS	0.248	3.3		0.302	2.8		
					MAX	0.591	6.7		0.761	6.3		
					$\langle\rho\rangle$			3.0			2.8	

coefficient, K_{eq}, can be obtained either by ab initio calculations or from other sources, such as the consistent CBS-QB3 derived group additive method for thermochemistry [49]. It is advisable to calculate the rate coefficient for the carbon-centered radical addition to oxygenates, that is the bimolecular direction of the reaction, and obtain the rate coefficient for the β-scission reaction from thermodynamic consistency.

Based on the results of the comparison presented in Table 6-3 the mean factor of deviation between GA and AI rate coefficients amounts to a factor of 3.0 for carbon radical additions to oxygenates. It is slightly better for β-scissions of oxygenates, for which the mean factor of deviation is 2.8. At higher temperatures this deviation factor is much lower, resulting in deviations less than 1.8 for both additions and β-scissions at 600 K and even lower at higher temperatures. The resulting deviations, lower than a factor of 3.0 for both additions and β-scissions at 300 K, are still within the chemical accuracy claimed by the CBS-QB3 method. Particularly, the 4 kJ mol^{-1} (1 kcal mol^{-1}) accuracy claimed on the energy results in a difference of a factor of 5 to 2 on the rate coefficients for temperatures of 300 to 1000 K, respectively. Also, the very similar performance for the addition and β-scission direction of the reaction means that both directions can be considered 'forward' in the scheme to maintain thermodynamic consistency given in previous paragraph.

The mean absolute deviation (MAD) between the GA predicted and AI calculated activation energies is limited to 2.8 kJ mol^{-1} and 2.4 kJ mol^{-1} for the carbon radical addition and β-scission reactions, respectively. However, there are three addition and three β-scissions reactions with deviations larger than 5 kJ mol^{-1}. The largest deviation is observed for the β-scission of $CH_3{}^{\bullet}CHCH_2COCH_2OH$ into $O{=}{}^{\bullet}CCH_2OH$ and $CH_2{=}CHCH_3$ (reaction 2/23) and amounts to an underestimation of the CBS-QB3 activation energy of 6.3 kJ mol^{-1}.

For the single-event pre-exponential factors the MAD between GA predictions and AI calculations for the reactions included in the validation set amounts to 0.193 and 0.263 log(m^3 mol^{-1} s^{-1}) for the carbon radical additions and β-scission reactions, respectively. The majority of deviations are still very limited, but there are a few reactions, especially β-scissions, for which deviations are larger than 0.500 log(m^3 mol^{-1} s^{-1}). The largest deviation corresponds to the β-scission of $CH_3OCOCH_2{}^{\bullet}CHCH_3$ into $O={}^{\bullet}COCH_3$ and $CH_2=CHCH_3$ (reaction 2/24), for which the GA model results in a 0.761 log(m^3 mol^{-1} s^{-1}) overestimation of the corresponding single-event pre-exponential factor due to a low-frequency mode in the product radical. At higher temperatures, the GA predictions are much closer to the corresponding AI determined values. In general, the larger deviations are observed for reactions involving multisubstituted attacking radicals or multisubstituted attacked carbon atoms resulting in multisubstituted formed radicals. But even though the validation set deliberately included some reaction for which strong interactions were expected, the rate coefficients are for three out of four reactions predicted within a factor of 3, even at the most demanding temperature of 300 K at which the rate coefficients are most sensitive to deviations on the activation energy.

6.5.2 Comparison with other models

The predictions for the activation energies based on the GA model developed in this work are compared with the corresponding values predicted by two other available models: (a) the Blowers and Masel model [4] and (b) the intersecting parabolas model developed by Denisov [3]. Both models assume a fixed pre-exponential factor for all reactions in the same reaction family and correlate the activation energy of a particular reaction with the corresponding reaction enthalpy. Activation energies can be calculated using eq (6-7) for the BM and (6-8) for the IP model:

$$E_{\mathrm{a}} = \left(\frac{w_{\mathrm{b}} + w_{\mathrm{f}} + \Delta_{\mathrm{r}} H}{2}\right)\frac{\left(V_{\mathrm{p}} - \left(w_{\mathrm{b}} + w_{\mathrm{f}}\right) + \Delta_{\mathrm{r}} H\right)^2}{V_{\mathrm{p}}^2 - \left(w_{\mathrm{b}} + w_{\mathrm{f}}\right)^2 + \Delta_{\mathrm{r}} H^2} \qquad (6\text{-}7)$$

In eq (6-7) w_b and w_f correspond to the bond dissociation energy of the breaking and forming bond, respectively and their sum, $w_b + w_f$, is estimated as a single parameter, while V_p is another estimated parameter, which can be linked to the intrinsic barrier $E_{\mathrm{a}}^{\mathrm{o}}$ of the reaction family.

$$b = a\left(E_{\mathrm{a}} - \Delta_{\mathrm{r}} H^{\mathrm{o}}\right)^{1/2} - E_{\mathrm{a}}^{1/2} \qquad (6\text{-}8)$$

The parameters a and b in the IP model, eq (6-8), are related to the force constants of the broken and formed carbon-carbon bond during the addition reaction.

For the training set of reactions used for the determination of ΔGAV°s (Table S2 of Appendix E) the activation energies are calculated using the BM model and the IP model at 300 K. The parameters of these two models are determined by minimizing the residual sum of squares (RSSQ) for the deviation between the model predictions and the ab initio values. This optimization procedure resulted in $w_{\mathrm{b}}+w_{\mathrm{f}}$ = 692.5 kJ mol^{-1} and V_{P} = 956.7 kJ mol^{-1} for the BM model and in a = 0.6 and b = 11.7 for the IP model.

The resulting parameters for the two models were used to determine the activation energies for the 24 reactions of the ab initio validation set of Table 6-3. The MAD of the deviation between the ab initio calculated values at 300 K and the corresponding values predicted (a) by eq (6-7) of the BM model and (b) by eq (6-8) of the IP model amounts to 5.7 kJ mol^{-1} and 8 kJ mol^{-1}, respectively. Compared to the MAD between the GA predictions and the AI values for the same set of reactions at 300 K, which amounts to only 2.7 kJ mol^{-1}, these results attest the better performance of the GA model developed in this study as compared with the two other models considered. Moreover, with the GA model only 3 of the 24 activation energies for addition reactions deviate more than 5 kJ mol^{-1}, with a maximum deviation of 6.7 kJ mol^{-1}. For the two other models almost half of the activation energies deviate more than 5 kJ mol^{-1}, with maximum deviations of 16.6 and 22.0 kJ mol^{-1} for the MB and the IP model, respectively. The comparative performance of the three models in predicting activation energies for the reactions included in the validation set of reactions is provided in Table 6-4.

Table 6-4: Average deviations between predicted by (a) the group additive model developed in this work, (b) the Blowers and Masel [4] and (c) the Intersecting Parabolas [3] model and ab initio calculated activation energies, E_a, for carbon-centered radical additions to oxygenates at 300 K for the reactions included in Table 6-3. (E_a in kJ mol^{-1}).

	Group Additivity	Blowers and Masel	Intersecting Parabolas
MAD	2.7	5.7	8.0
RMS	3.3	7.3	10.0
MAX	6.7	16.6	22.0

Figure 6-2 provides a parity plot of the predicted activation energies for addition reactions versus the CBS-QB3 calculated activation energies for the ab initio validation set at 300 K (Table S14 of Appendix E), including (a) the GA method presented in this work, (b) the Blowers and Masel model and (c) the intersecting parabolas model. Based on the results of the comparison of the three models in predicting the activation energies for the reactions included in the validation set at 300 K, it is clear that the GA model developed in this work outperforms the two other models. An additional advantage of the GA model is that it also allows the determination of the pre-exponential factor of a given reaction, while the two other models assume a fixed pre-exponential factor within a given reaction family.

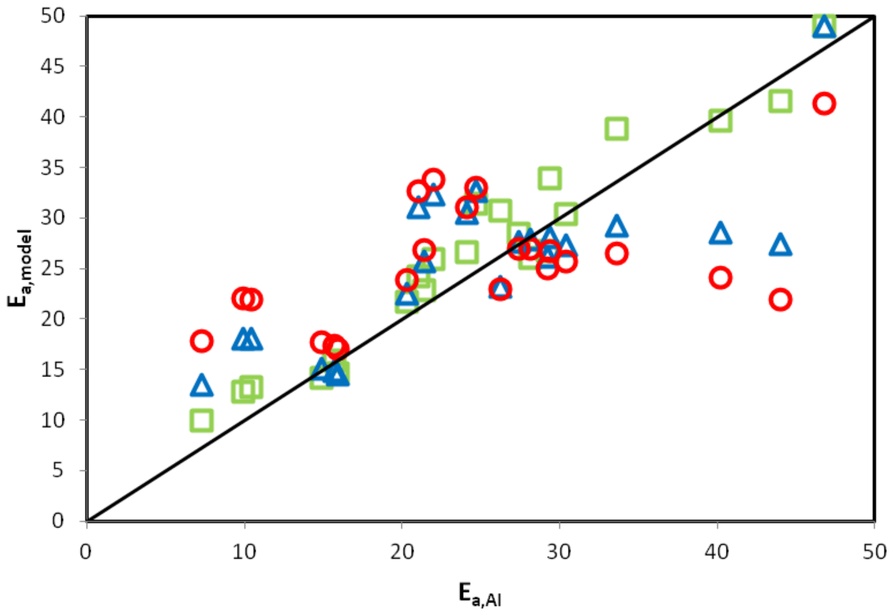

Figure 6-2: Parity plot of the predicted activation energies at 300 K for the carbon-centered radical addition reactions vs ab initio calculated activation energies showing the improved performance of the group additive model developed in this work (□), in comparison with the Blowers and Masel model with $w_f + w_b$ = 692.5 kJ mol^{-1} and V_p = 956.7 kJ mol^{-1} (Δ) and the intersecting parabolas model with a = 0.6 and b = 11.7 (○) (Activation energies, E_a, in kJ mol^{-1}, at 300 K for the 24 reactions of the ab initio validation set provided in Table S14 of Appendix E).

6.6 Conclusions

In this study a group additivity scheme is provided that allows the calculation of Arrhenius parameters and rate coefficients for carbon-centered radical additions to oxygenates and their reverse β-scissions of oxygenates, over a wide temperature range (300-2500 K). The derived model is an extension of the already existent group additive model for radical additions and β-scissions between hydrocarbons, and these two models can be used combinatorially.

All kinetic data used in this study derived from conventional transition-state theory applying CBS-QB3 ab initio calculations in the high pressure limit with corrections for internal hindered rotation around the forming/breaking bond in the transition state and the product radical. A linear correlation was used to improve the length of the forming bond in the transition state based on IRCMax calculations for the reactions studied.

From an extensive training set covering the majority of oxygenate-containing functional groups, 32 group additive values (ΔGAV^os) are obtained accounting for primary and secondary contributions to the Arrhenius parameters of the reference reaction. These ΔGAV^os were shown to be almost temperature independent in the studied temperature range (300-2500 K) and hence, temperature dependence in the Arrhenius parameters of the studied reactions is expressed by the corresponding parameters of the reference reaction.

Since to our knowledge no experimental data for carbon-centered radical additions to oxygenates and β-scissions of oxygenates is available, the validation of the developed model is attempted by comparison of the group additive (GA) predictions with ab initio (AI) calculated values for reactions not previously involved in the determination of the ΔGAV^os. The deviation between GA predicted and AI calculated rate coefficients for an AI validation set including 24 reactions amounts to a factor of ~3 at 300 K and ~1.5 at 1000 K, showing the good performance of the developed in this work GA model. The accuracy of the prediction at 300 K is slightly better than the results of the comparison between CBS-QB3 and experimental rate coefficients for hydrocarbons. Moreover, it was shown that the GA model developed in this work performs better in predicting activation energies for the AI validation set compared to the Blowers and Masel model and the Intersecting Parabolas model.

The lack of experimental data for the studied reaction family makes the results of this work even more important, since a powerful group additive tool is provided for the fast and accurate prediction of Arrhenius parameters and rate coefficients for carbon-centered radical additions to oxygenates and their reverse β-scissions of oxygenates.

6.7 References

1. Evans, M.G. and M. Polanyi, *Further Considerations on the Thermodynamics of Chemical Equilibria and Reaction Rates.* Proc. Roy. Soc. A, 1936. **154**: p. 1333-1360.
2. Evans, M.G. and M. Polanyi, *Inertia and Driving Force of Chemical Reactions.* Trans. Faraday Soc., 1938. **1938**(34): p. 11-29.
3. Denisov, E.T., *New Empirical Models of Free Radical Abstraction Reactions.* Usp Khim+, 1997. **66**(10): p. 953-971.
4. Blowers, P. and R. Masel, *Engineering Approximations for Activation Energies in Hydrogen Transfer Reactions.* Aiche J, 2000. **46**(10): p. 2041-2052.
5. Benson, S.W. and J.H. Buss, *Additivity Rules for the Estimation of Molecular Properties. Thermodynamic Properties.* J Chem Phys, 1958. **29**(9): p. 546-561.
6. Benson, S.W., *Thermochemical Kinetics*. 1968, New York: John Wiley & Sons Ltd.
7. Benson, S.W., *Oxygen Initiated Combustion: Thermochemistry and Kinetics of Unsaturated Hydrocarbons.* Int J Chem Kinet, 1996. **28**(9): p. 665-672.
8. Benson, S.W., *Some Observations on the Thermochemistry and Kinetics of Peroxy Radicals.* J Phys Chem-Us, 1996. **100**(32): p. 13544-13547.
9. Benson, S.W., *Some Observations on the Kinetics and Thermochemistry of the Reactions of HO2 Radicals with Aldehydes and Ketones.* Int J Chem Kinet, 2001. **33**(9): p. 509-512.
10. Willems, P.A. and G.F. Froment, *Kinetic Modeling of the Thermal-Cracking of Hydrocarbons .1. Calculation of Frequency Factors.* Ind Eng Chem Res, 1988. **27**(11): p. 1959-1966.
11. Willems, P.A. and G.F. Froment, *Kinetic Modeling of the Thermal-Cracking of Hydrocarbons .2. Calculation of Activation-Energies.* Ind Eng Chem Res, 1988. **27**(11): p. 1966-1971.
12. Truong, T.N., *Reaction Class Transition State Theory: Hydrogen Abstraction Reactions by Hydrogen Atoms as Test Cases.* J Chem Phys, 2000. **113**(12): p. 4957-4964.
13. Kungwan, N. and T.N. Truong, *Kinetics of the Hydrogen Abstraction CH3 + Alkane -> CH4 Plus Alkyl Reaction Class: An Application of the Reaction Class Transition State Theory*. J Phys Chem A, 2005. **109**(34): p. 7742-7750.
14. Huynh, L.K., S. Panasewicz, A. Ratkiewicz, and T.N. Truong, *Ab Initio Study on the Kinetics of Hydrogen Abstraction for the H+Alkene -> H2+Alkenyl Reaction Class.* J Phys Chem A, 2007. **111**(11): p. 2156-2165.
15. Ratkiewicz, A. and T.N. Truong, *Kinetics of the Hydrogen Abstraction R-OH+H -> R-O-center + H2 Reaction Class.* Int J Chem Kinet, 2010. **42**(7): p. 414-429.
16. Ratkiewicz, A., J. Bieniewska, and T.N. Truong, *Kinetics of the Hydrogen Abstraction R-OH+H -> R-center-OH+H2 Reaction Class: An Application of the Reaction Class Transition State Theory.* Int J Chem Kinet, 2011. **43**(2): p. 78-98.

17. Sumathi, R., H.H. Carstensen, and W.H. Green, *Reaction Rate Prediction via Group Additivity Part 1: H Abstraction from Alkanes by H and CH3.* J Phys Chem A, 2001. **105**(28): p. 6910-6925.

18. Sumathi, R., H.H. Carstensen, and W.H. Green, *Reaction Rate Prediction via Group Additivity, Part 2: H-Abstraction from Alkenes, Alkynes, Alcohols, Aldehydes and Acids by H Atoms.* J Phys Chem A, 2001. **105**(39): p. 8969-8984.

19. Sumathi, R. and W.H. Green, *Oxygenate, Oxyalkyl and Alkoxycarbonyl Thermochemistry and Rates for Hydrogen Abstraction from Oxygenates.* Phys Chem Chem Phys, 2003. **5**(16): p. 3402-3417.

20. Saeys, M., M.F. Reyniers, G.B. Marin, V. Van Speybroeck, and M. Waroquier, *Ab Initio Group Contribution Method for Activation Energies for Radical Additions.* Aiche J, 2004. **50**(2): p. 426-444.

21. Sabbe, M.K., M.F. Reyniers, V. Van Speybroeck, M. Waroquier, and G.B. Marin, *Carbon-centered Radical Addition and Beta-Scission Reactions: Modeling of Activation Energies and Pre-Exponential Factors.* Chem Phys Chem, 2008. **9**(1): p. 124-140.

22. Sabbe, M.K., M.F. Reyniers, M. Waroquier, and G.B. Marin, *Hydrogen Radical Additions to Unsaturated Hydrocarbons and the Reverse beta-Scission Reactions: Modeling of Activation Energies and Pre-Exponential Factors.* Chem Phys Chem, 2010. **11**(1): p. 195-210.

23. Saeys, M., M.F. Reyniers, V. Van Speybroeck, M. Waroquier, and G.B. Marin, *Ab Initio Group Contribution Method for Activation Energies of Hydrogen Abstraction Reactions.* Chem Phys Chem, 2006. **7**(1): p. 188-199.

24. Sabbe, M.K., A.G. Vandeputte, M.F. Reyniers, M. Waroquier, and G.B. Marin, *Modeling the Influence of Resonance Stabilization on the Kinetics of Hydrogen Abstractions.* Phys Chem Chem Phys, 2010. **12**(6): p. 1278-1298.

25. Vandeputte, A.G., M.K. Sabbe, M.F. Reyniers, and G.B. Marin, *Kinetics of Alpha Hydrogen Abstractions from Thiols, Sulfides and Thiocarbonyl Compounds.* Phys Chem Chem Phys, 2012. **14**(37): p. 12773-12793.

26. Vandeputte, A.G., M.F. Reyniers, and G.B. Marin, *Kinetic Modeling of Hydrogen Abstractions Involving Sulfur Radicals.* Chem Phys Chem, 2013. **14**(16): p. 3751-3771.

27. Paraskevas, P.D., M.K. Sabbe, M.F. Reyniers, N. Papayannakos, and G.B. Marin, *Kinetic Modeling of α-Hydrogen Abstractions from Unsaturated and Saturated Oxygenate Compounds by Carbon-Centered Radicals.* Chem Phys Chem, 2014. **15**(9): p. 1849-1866.

28. Paraskevas, P.D., M.K. Sabbe, M.F. Reyniers, N. Papayannakos, and G.B. Marin, *Kinetic Modeling of α-Hydrogen Abstractions from Unsaturated and Saturated Oxygenate Compounds by Hydrogen Atoms.* J Phys Chem A, 2014. **118**(40): p. 9296-9309.

29. Paraskevas, P.D., M.K. Sabbe, M.F. Reyniers, N. Papayannakos, and G.B. Marin, *Group Additive Kinetics for Hydrogen Transfer Between Oxygenates.* J Phys Chem A, 2015. **119**(27): p. 6961-6980.

30. Clymans, P.J. and G.F. Froment, *Computer-Generation of Reaction Paths and Rate-Equations in the Thermal-Cracking of Normal and Branched Paraffins.* Computers & Chemical Engineering, 1984. **8**(2): p. 137-142.

31. William H. Green, Joshua W. Allen, Beat A. Buesser, Robert W. Ashcraft, Gregory J. Beran, Caleb A. Class, Connie Gao, C. Franklin Goldsmith, Michael R. Harper, et al., *RMG - Reaction Mechanism Generator v4.0.1*, 2013.
32. Vandewiele, N.M., K.M. Van Geem, M.F. Reyniers, and G.B. Marin, *Genesys: Kinetic Model Construction Using Chemo-Informatics.* Chem Eng J, 2012. **207**: p. 526-538.
33. Montgomery, J.A., M.J. Frisch, J.W. Ochterski, and G.A. Petersson, *A Complete Basis Set Model Chemistry. VI. Use of Density Functional Geometries and Frequencies.* J Chem Phys, 1999. **110**(6): p. 2822-2827.
34. Vansteenkiste, P., V. Van Speybroeck, G.B. Marin, and M. Waroquier, *Ab Initio Calculation of Entropy and Heat Capacity of Gas-Phase n-Alkanes Using Internal Rotations.* J Phys Chem A, 2003. **107**(17): p. 3139-3145.
35. Frisch, M.J., G.W. Trucks, H.B. Schlegel, G.E. Scuseria, M.A. Robb, J.R. Cheeseman, G. Scalmani, V. Barone, B. Mennucci, et al., *Gaussian 09, Revision D.01*, 2009, Gaussian, Inc.: Wallingford CT.
36. Sabbe, M.K., A.G. Vandeputte, M.F. Reyniers, V. Van Speybroeck, M. Waroquier, and G.B. Marin, *Ab Initio Thermochemistry and Kinetics for Carbon-Centered Radical Addition and Beta Scission Reactions.* J Phys Chem A, 2007. **111**(34): p. 8416-8428.
37. Van Speybroeck, V., D. Van Neck, M. Waroquier, S. Wauters, M. Saeys, and G.B. Marin, *Ab Initio Study of Radical Addition Reactions: Addition of a Primary Ethylbenzene Radical to Ethene (I).* J Phys Chem A, 2000. **104**(46): p. 10939-10950.
38. Van Speybroeck, V., P. Vansteenkiste, D. Van Neck, and M. Waroquier, *Why Does the Uncoupled Hindered Rotor Model Work Well for the Thermodynamics of n-Alkanes?* Chem Phys Lett, 2005. **402**(4-6): p. 479-484.
39. Heuts, J.P.A., R.G. Gilbert, and L. Radom, *Determination of Arrhenius Parameters for Propagation in Free-Radical Polymerizations: An assessment of Ab Initio Procedures.* J Phys Chem-Us, 1996. **100**(49): p. 18997-19006.
40. Lynch, B.J., P.L. Fast, M. Harris, and D.G. Truhlar, *Adiabatic connection for kinetics.* J Phys Chem A, 2000. **104**(21): p. 4811-4815.
41. Saeys, M., M.F. Reyniers, G.B. Marin, V. Van Speybroeck, and M. Waroquier, *Ab Initio Calculations for Hydrocarbons: Enthalpy of Formation, Transition State Geometry, and Activation Energy for Radical Reactions.* J Phys Chem A, 2003. **107**(43): p. 9147-9159.
42. Malick, D.K., G.A. Petersson, and J.A. Montgomery, *Transition states for chemical reactions I. Geometry and classical barrier height.* J Chem Phys, 1998. **108**(14): p. 5704-5713.
43. Cohen, N. and S.W. Benson, *Estimation of Heats of Formation of Organic-Compounds by Additivity Methods.* Chem Rev, 1993. **93**(7): p. 2419-2438.
44. Pollak, E.L.I. and P. Pechukas, *Symmetry Numbers, Not Statistical Factors, Should be Used in Absolute Rate Theory and in Bronsted Relations.* J Am Chem Soc, 1978. **100**(10): p. 2984-2991.
45. Coulson, D.R., *Statistical Factors in Reaction-Rate Theories.* J Am Chem Soc, 1978. **100**(10): p. 2992-2996.
46. *Chemical Kinetics Database, NIST Standard Reference Database 17, Version 7.0 (Web Version), Release 1.6.7, Data Version 2013*, 2013.

47. Atkinson, R., D.L. Baulch, R.A. Cox, J.N. Crowley, R.F. Hampson, R.G. Hynes, M.E. Jenkin, M.J. Rossi, and J. Troe, *Evaluated Kinetic and Photochemical Data for Atmospheric Chemistry: Volume I - Gas Phase Reactions of Ox, HOx, NOx, and SOx, Species.* Atmos Chem Phys, 2004. **4**(4): p. 1461-1738.

48. Atkinson, R., D.L. Baulch, R.A. Cox, J.N. Crowley, R.F. Hampson, R.G. Hynes, M.E. Jenkin, M.J. Rossi, and J. Troe, *Evaluated Kinetic and Photochemical Data for Atmospheric Chemistry: Volume II - Gas Phase Reactions of Organic Species.* Atmos Chem Phys, 2006. **6**(6): p. 3625-4055.

49. Paraskevas, P.D., M.K. Sabbe, M.F. Reyniers, N. Papayannakos, and G.B. Marin, *Group Additive Values for the Gas Phase Standard Enthalpy of Formation, Entropy and Heat Capacity of Oxygenates.* Chem-Eur J, 2013. **19**: p. 16431-16452.

Chapter 7

First Principles Based Microkinetic Modeling of Methyl Butanoate Pyrolysis

7.1 Abstract

A consistent set of ab initio obtained thermodynamic and kinetic data is applied to simulate the thermal decomposition of methyl butanoate (MB). A reaction mechanism for the MB pyrolysis was developed using the Genesys reaction mechanism generation software. Reactor simulations were performed for the MB pyrolysis at a temperature range of 1013-1113 K and the results were validated with experimental data obtained in a bench-scale set-up. All thermodynamic data needed were determined by either ab initio calculations or group additivity based on ab initio data. Kinetic data for the simulations were obtained mainly from ab initio based group additivity, next to a set of experimental data to describe the kinetics of the thermal decomposition of small saturated and unsaturated oxygenated hydrocarbon species. The MB conversion is predicted within 3 % of the experimental conversion, whereas product yields are satisfactorily predicted within 1 wt% for the majority of products. However, important discrepancies are observed for CO, ethane and methyl propenoate, which can be attributed to the lack of a decomposition mechanism for methyl propenoate. The results of this study indicate the potential of integrating ab initio methods with engineering tools for accurate reactor simulations.

7.2 Introduction

The worldwide energy demand has increased in recent years and is expected to continue to grow in the foreseeable future. Fossil fuels and particularly petroleum-based compounds are widely used to cover the ever growing energy demand. However, the extensive use of fossil fuels is held responsible for the climate change, which will have a significant impact on humanity in the near future. The combination of this factor with the declining global oil production capacity has created the need for sustainable development. The need for sustainable development makes it progressively imperative to allocate fossil fuels more wisely, develop ways to diminish existing dependencies, and search for alternative sources.

Among the potential alternative fuels that are already on the market is biodiesel, which is made from renewable sources and is safely used directly in diesel engines, in pure form or blended with petroleum diesel, without major modifications to the engine system or the fuel distribution infrastructure. Biodiesel is typically derived from vegetable oils, animal fat or waste cooking oil [1], and it is composed of a mixture of saturated and unsaturated alkyl esters containing carbon chains of more than 12 carbon atoms [2]. The high oxygen content of biodiesel lowers the energy density of the fuel compared to the oil-derived diesel fuels and causes significant differences in the performance and combustion characteristics compared to fossil fuels, including a different emission of gases and particulate matter [3].

Kinetic modeling provides a useful way to investigate the chemical characteristics of this potential fuel and can greatly contribute to the design and optimization of processes in which biodiesel is involved. Due to its complexity and the varying size of the constituent molecules, direct modelling of biodiesel chemistry, such as the thermal decomposition of biodiesel, is unfeasible. An alternative is to use model molecules that match the characteristics of the biodiesel but avoid the complexity of the mixture. Among the latter is methyl butanoate

(MB), $CH_3CH_2CH_2C(=O)OCH_3$. MB is a relatively short methyl ester that still incorporates all essential chemical structure features of the typical biofuel, which can therefore be used as a convenient model compound for large biofuel methyl ester molecules.

Recently, Lai et al. [4] extensively reviewed the most recent experimental and ab initio studies aiming at the development of detailed kinetic models for the thermal decomposition of biodiesel. The first detailed chemical kinetic model for MB combustion was developed by Fisher et al. [5]. This model simulated the combustion of MB in closed vessels at low temperatures and sub-atmospheric conditions and indicated lower overall reactivities comparing to the limited experimental data available. A modification of this model was provided by Gail et al. [6] based on experimental data obtained in (a) a jet stirred reactor, (b) an opposed-flow diffusion flame and (c) a variable pressure flow reactor. The reaction mechanism for the MB combustion was further modified by Metcalfe et al. [7] performing a shock tube study for mixtures of MB, oxygen (O_2) and argon (Ar) in order to measure the ignition delay times behind the reflected shock wave. This work was further expanded by Dooley et al. [8] including experimental auto-ignition data from a rapid compression engine, based on which unimolecular decomposition reaction data were further refined.

El-Nahas et al. [9] added a six-centered unimolecular elimination reaction to the already existent reaction mechanism of MB, based on CBS-QB3 ab initio investigation of bond dissociation energies for unimolecular decomposition reactions of MB. Sub-mechanisms for the reaction of MB radicals using ab initio methods were proposed in the studies of Huynh et al. [10, 11]. The results from this work are in very good agreement with the recent experimental shock tube data for ignition delay obtained by Farooq et al. [12]. A more recent study of Ali and Violi [13] reported a detailed study of the unimolecular decomposition pathways of MB based on ab initio DFT calculations. Besides that, a significant amount of studies has been performed towards revealing reaction mechanisms for thermal decomposition of esters smaller than methyl butanoate [14-17] or for larger carbon-chain oxygenate compounds [18-21].

In previous work of our group, group additive models were developed for the prediction of the thermochemistry and kinetics for the radical gas-phase chemistry of hydrocarbons [22-25], sulfur-containing compounds [26-29] and oxygenates [30-33]. All these models are based on ab initio calculations, resulting in a consistent set of thermodynamic and kinetic data for the most important reaction families involved in radical chemistry including C/S/O/H containing compounds. The applied methodology is based on Benson’s group additive method [34, 35], using ab initio data obtained with the CBS-QB3 method of Montgomery et al. [36, 37]. In a further step, Sabbe et al. [38] used only these ab initio-based group additive models and ab initio obtained data, without any input from experiment or data fitting, to accurately simulate the steam-cracking of ethane in a pilot and an industrial cracker. This successful simulation provided a proof-of-principle that the available computational quantum chemical methods can be integrated with engineering models to provide a full ab initio modeling of gas phase reactions from molecular to industrial scale.

There are several reaction mechanism generator software packages available such as, KING [39], NetGen [40], RMG [41] and, at the Laboratory of Chemical Technology at Ghent University, PRIM [42] and Genesys [43]. The latter was opted to be used in this study because all reaction rules and chemical databases in Genesys are externalized from the network generation code, which gives full control to the user over the chemistry that needs to be included. This means that the available thermochemistry and kinetic models for hydrocarbons and oxygenates mentioned above can be easily implemented into Genesys.

In this work the simulation of a bench-scale reactor for MB thermal decomposition is performed using the CHEMKIN software package [44] in order to validate the use of the ab initio based group additively models in the microkinetic modelling of ester pyrolysis. Reaction path analysis is used to identify the dominant paths for the MB thermal decomposition at the studied conditions. The predictions of this model for the MB pyrolysis are compared with available experimental data obtained in a bench-scale pyrolysis set-up in the Laboratory for Chemical Technology (LCT) of Ghent University.

7.3 Reaction Network Generation

The Genesys [43] software package for reaction network generation was used in this work for the construction of a MB pyrolysis reaction network consisting solely of elementary reactions. The Genesys software includes many independent functional modules and databases. These modules contain algorithms that can execute a particular function within Genesys, for example calculating thermodynamic or kinetic data. As stated by Vandewiele et al. [43], the automated construction of kinetic models with Genesys consists of three sequential parts: (1) the input of the required information, (2) the processing step, in which the reaction network is generated, and (3) the post-processing step, in which the output file is produced in a format that can be read by microkinetic or reactor simulation programs.

For the construction of the input file for Genesys an extended literature review was performed in order to find all possible MB decomposition pathways [10, 11, 14-16, 21]. A detailed description of how the reaction families are defined in order to be used as an input file to Genesys can be found elsewhere [43]. All reaction types that were found to be important for the MB thermal decomposition according to the extended literature review were considered. The termination of the reaction network generation is achieved with a rule-based criterion [45]. A more detailed description of the termination criteria and constraints in generating chemical reaction networks can be found elsewhere [43].

One of the prerequisites for simulating chemical processes is to know the thermodynamics and kinetics for all compounds and reactions in the reaction network. For thermochemistry, Genesys first verifies whether thermodynamic parameters for the particular molecule/radical are included in one of the user-defined databases. These databases are ab initio based and contain thermochemistry data for hydrocarbon [22, 46] or oxygenate compounds [30] calculated with the CBS-QB3 composite method or with higher accuracy methods [47]. If not, prediction techniques, such as group additivity and the hydrogen bond increment method are applied to obtain thermochemical properties for molecules and radicals, respectively.

In this study, Benson's group additivity method [34, 35] is used for molecules, with the GAVs derived from our earlier work [22, 30, 46]. For the estimation of thermodynamic parameters of radical species the hydrogen bond increment (HBI) method developed by Lay et al. [48] is implemented. According to this method the thermochemistry of radical species is determined by adding a hydrogen atom bond increment to the corresponding thermodynamic parameter of the non-radicalar parent molecule. All the ab initio calculations for the determination of thermodynamic parameters for hydrocarbons and oxygenate compounds were performed using the CBS-QB3 compound method of Montgomery et al. [36, 37] including corrections for all internal rotations [49-51]. All thermodynamic parameters for the species involved are of ab initio origin, stemming from either ab initio calculations or from group additive methods based on ab initio data.

Rate coefficients for the elementary reactions included in the reaction mechanism were determined using the group additive values obtained in previous work [23-25, 31-33, 52]. Group additive values (ΔGAV^os) for the Arrhenius parameters of a particular reaction were determined on the basis of the group additivity method developed by Saeys et al. [53] for the determination of activation energies for radical addition reactions between hydrocarbons. This methodology was extended by Sabbe et al. [23] to include also pre-exponential factors using corrections for one-dimensional hindered rotation around the forming/breaking bond in the transition state (TS). According to this method, group additivity can be used in terms of differences between the transition state and the reactants to calculate accurate activation energies, E_a, and pre-exponential factors, log$A$, for a wide range of reaction types. These contributions were added to the corresponding Arrhenius parameters of the reference reaction for the studied reaction family. Rate coefficients can be calculated within the group additive scheme described above by using the eq (7-1):

$$k = \kappa n_e k_{GA} = \kappa n_e \tilde{A} e^{-\frac{E_a}{RT}} \quad (7\text{-}1)$$

In eq (7-1) κ stands for the tunneling coefficient, n_e is the reaction path degeneracy [54, 55] or the number of single events, $\tilde{A}$ is the single-event pre-exponential factor [23] and E_a is the activation energy. The Arrhenius parameters are obtained from group additivity, and the tunneling coefficients for hydrogen abstraction reactions are calculated using a user-defined correlation. In this work, a fourth order polynomial [25] was used, derived from Eckart [56] tunneling coefficients for a large set of reactions, as determined earlier [31-33]. A detailed description of the group additive method used can be found in previous work [31-33].

Although for hydrocarbons [23-25] secondary contributions were shown to be negligible and can be safely omitted, this is not the case for reactions involving oxygenate compounds. Hence, it was shown that for hydrogen abstractions involving oxygenates [31-33] and for carbon-centered radical additions to oxygenates (Chapter 6 of this PhD Dissertation), secondary contributions are of major importance and should be included. Moreover, it was shown that cross-resonance and hyperconjugative effects in the transition state contribute significantly in the Arrhenius parameters of hydrogen abstractions between hydrocarbons [25] and between oxygenates [31]. Consequently, the corresponding Genesys module for the determination of kinetic parameters for reactions of these types were modified correspondingly to include also secondary contributions and corrections for resonance/ hyperconjugative effects. In Genesys, the number of single events is calculated automatically. Reverse rate coefficients are determined using thermodynamic consistency as the ratio between the rate coefficient for the forward direction of the reaction and the thermodynamic equilibrium coefficient.

Seven group additive models were used for the reaction mechanism generation in this study: (1) carbon-centered radical additions to hydrocarbons and oxygenates, (2) hydrogen radical additions to hydrocarbons, (3) hydrogen abstractions by carbon-centered radicals and (4) by hydrogen atoms, from hydrocarbons and hydrocarbon side chains, and (5) hydrogen abstractions by carbon-centered radicals, (6) by hydrogen atoms and (7) by oxygen-centered radicals from oxygenates. In the developed kinetic model, the reported group additive values and the Arrhenius parameters at 1000 K were applied.

These reaction families cover the majority of hydrogen abstraction and radical addition reactions involved in the simulation of MB pyrolysis. However, for 34 hydrogen radical additions to oxygenates in the model generated by Genesys, group additive values have not been determined. For this reaction family of hydrogen radical additions to oxygenates, the kinetics are approximated by adding the ΔGAV^{o}s for carbon-centered radical additions to oxygenates (see Chapter 6 of this PhD dissertation) to the reference reaction for hydrogen addition to oxygenates, i.e., the hydrogen radical addition of a hydrogen atom to ethene. This assumption can be justified by the similarities in structure between the same unsaturated bond attacked by a carbon-centered radical and by a hydrogen radical.

Rate coefficients for bond scissions and their reverse radical recombinations cannot be determined by the CBS-QB3 approach used for the other reaction families. Radical recombination reactions are barrierless and hence, there is no clear transition state on the potential energy surface for these reactions. Since canonical transition state theory (CTST) [57] does not yield accurate results for reactions of this type, variational transition state theory (VTST) [58-60] should be used. According to this method the dividing surface is shifted along the reaction path to minimize possible recrossing effects and also maximizing the Gibbs free energy, which consequently minimizes the calculated rate coefficient. Furthermore, common single-reference ab initio methods such as CBS-QB3 cannot be used due to the multi reference character of bond scission transition states.

Therefore, this approach is computationally too expensive even for small compounds and, hence, its use is not affordable for the large number of radical recombination reactions involved in the reaction mechanism of this study. To overcome this limitation it was opted to use Arrhenius parameters for bond scission reactions and their reverse radical recombinations from the work of Huynh and Violi [11] and Ali and Violi [13] calculated using VTST. The reactions from these studies that have been used in this work are summarized in Table S1 of Appendix F. Rate coefficients for the bond scission reactions for which rate coefficients have not been determined by these authors were assumed in this work to be equal to the rates of structurally similar reactions included in the studies of Huynh and Violi [11] and Ali and Violi [13]. For example, it was assumed that the Arrhenius parameters of the C-O bond scission of MB into the $CH_3CH_2CH_2C^{\bullet}{=}O$ and $CH_3O^{\bullet}$ radicals are the same as the C-O bond scission of methyl propanoate ($CH_3CH_2COOCH_3$) into $CH_3CH_2C^{\bullet}{=}O$ and $CH_3O^{\bullet}$.

Also for hydrogen shift/isomerization reactions no group additive models are available due to the strong ring strain dependence for most of these reactions, which makes them difficult to model group additively. The ab initio studies of MB thermal decomposition of Huynh and Violi [11] and Ali and Violi [13] provide Arrhenius parameters for this type of reactions included in the reaction network developed. Energy barriers for these reactions are highly dependent on the type of the hydrogen migration; generally reactions that proceed through a transition state with a low ring strain energy, mainly six-membered transition states, have lower energy barriers than those proceeding through a more strained transition state, e.g., four-ring transition states.

The reaction network developed using Genesys for MB pyrolysis consists of 619 species and 722 reversible reactions. Among the 619 species, there are 384 radical and 235 molecular species, with maximum five carbon and three oxygen atoms in their molecular structure. These 722 reactions correspond mostly to radical additions/β-scissions (450 reactions), almost 26 % of them (187 reactions) are hydrogen abstractions, whereas there are also 75 radical recombinations/bond scissions along with 10 hydrogen shift reactions.

The Genesys software is designed to cope with every kind of reaction, depending on the chemical knowledge of the user. However, group additivity methods have been developed to calculate accurate thermodynamic and kinetic parameters for larger compounds starting from smaller structures. During MB pyrolysis a lot of smaller species are produced which are further decomposed into smaller ones. To describe all these decomposition reactions, numerous reaction families need to be included, each of them corresponding only to a limited number of reactions. Moreover, the accuracy of group additivity methods for smaller species is limited and it is highly recommended to obtain thermodynamic or kinetic data for smaller species directly from experimental resources or from high level ab initio calculations.

Hence, it was opted, in order to improve the accuracy of the developed reaction mechanism, to obtain data for the decomposition of smaller compounds containing up to two carbon atoms from the work of Metcalfe et al. [16]. This reaction mechanism developed for the oxidation of small hydrocarbon and oxygenated hydrocarbon species was merged with the reaction network generated by Genesys. For the limited cases of overlapping reactions derived from

Genesys that are also present in the mechanism developed by Metcalfe et al. [16], the latter data are used because they are expected to be the most accurate. Rate coefficients for the 762 reactions included in this seed mechanism have been assembled through critical evaluation of the literature and describe important reactions associated with methane, ethane, ethylene, formaldehyde, methanol, acetaldehyde and ethanol.

Moreover, the group additive models developed in the framework of this dissertation [31-33] (see also Chapter 6 of this PhD dissertation) focus mainly on saturated oxygenates and include only a limited number of ΔGAV^os for unsaturated oxygenates. Hence, the decomposition of small unsaturated esters such as methyl propenoate cannot be accurately described by the ΔGAV^os available. However, methyl propenoate is among the most important products during MB decomposition according to Huynh and Violi [11]. Bennadji et al. [14] proposed detailed mechanisms for the combustion of four small unsaturated methyl and ethyl esters based on experimental ignition delay times measured behind reflected shock waves for wide range of temperatures, pressures and concentrations. To further complete the reaction mechanism developed in this work for the MB pyrolysis, the nine hydrogen abstractions from methyl propenoate proposed by Bennadji et al. [14] are included to this mechanism. Arrhenius parameters for these nine hydrogen abstraction reactions can be found in Table S2 of Appendix F. An overview of the sources of the thermodynamic and kinetic data used in this work for the reaction mechanism for the MB pyrolysis is provided in Table 7-1.

In total, the reaction network constructed in this work for the MB pyrolysis contains 1493 reactions. Rate coefficients for bimolecular reactions are calculated in the high-pressure limit using the conventional transition state theory (TST) [61] as expressed at 50 K intervals.

Table 7-1: Source of the thermodynamic and kinetic data used for the reaction mechanism generated in this study for the MB pyrolysis.

		Thermodynamics	**Source**
1		Hydrocarbons	Sabbe et al. [22, 46] Goldsmith et al. [47]
2		Oxygenates	Paraskevas et al. [30] Goldsmith et al. [47]
		Kinetics	
1		***Hydrogen abstractions between hydrocarbons***	
	a	by carbon-centered radicals	Sabbe et al. [25]
	b	by hydrogen atoms (unpublished work)	Sabbe (unpublished work)
2		***Hydrogen Abstractions between oxygenates***	
	a	by carbon-centered radicals	Paraskevas et al. [31]
	b	by hydrogen atoms	Paraskevas et al. [32]
	c	by oxygen-centered radicals	Paraskevas et al. [33]
3		***Carbon-centered radical additions (reverse: β-scissions)***	
	a	to hydrocarbons	Sabbe et al. [23]
	b	to oxygenates	Chapter 6 of this PhD Dissertation
4		***Hydrogen radical additions (reverse: β-scissions)***	
	a	to hydrocarbons [24]	Sabbe et al. [24]
	b	to oxygenates	ΔGAV^os taken from Sabbe et al. [24] using the corresponding reference reaction for the particular reaction family
5		***Bond scissions (reverse: radical recombinations)***	Huynh and Violi [11] Ali and Violi [13]
6		***Hydrogen shifts (isomerization reactions)***	Huynh and Violi [11] Ali and Violi [13]
7		***Reactions for the decomposition of smaller compounds (up to two carbon atoms)***	Metcalfe et al. [16]
8		***Reactions for the decomposition of small unsaturated esters (up to four heavy atoms)***	Bennadji et al. [14]

7.4 Bench-Scale Pyrolysis Reactor and Reactor Model

The bench-scale pyrolysis set-up has been discussed in details previously [62, 63] and consists of three parts; the feed section, the furnace/reactor section and the analysis section. The reactor has a length of 1.475 m, an internal diameter of 6 mm and it is made of Incoloy 800HT (Ni, 30−35; Cr, 19−23; and Fe, > 39.5 wt%). The process gas temperature is measured by two thermocouples, one at the inlet and one at the outlet of the reactor, and by eight thermocouples placed at different intermediate positions. The reactor is placed vertically in a rectangular furnace and heated electrically. During MB pyrolysis the reactor is operated near isothermally, with a steep temperature increase at the inlet and a steep temperature drop at the outlet of the reactor. A downstream back pressure regulator is used for the pressure control of the reactor and the pressure drop over its length was found to be negligible. A schematic overview of the set-up is provided in Figure S1 of Appendix F.

Since in the bench-scale reactor used to validate the model, the radial temperature, the pressure and the concentration gradients are limited, as can be derived from the appropriate dimensionless number as the Peclét and Damhöhler number [62], one-dimensional reactor equations can be safely used. A plug flow reactor (PFR) is chosen in the CHEMKIN program for the simulation of the bench-scale reactor, using the process gas temperature and pressure profile from the corresponding bench-scale reactor experiment. Inlet mass flow rate and gas phase composition in CHEMKIN are taken from the bench-scale reactor experiments. For simulating the process in CHEMKIN [44] the temperature profile measured experimentally and a fixed pressure of 1.7 bar are used, see Tables S3-S4 of Appendix F. The initial feed to the reactor was set to 257 g/h MB and 40 g/h N_2, which corresponds to a 0.6 mol_{N2}/mol_{MB} dilution. The diluent nitrogen gas is used as an internal standard that reduces component partial pressures, and therefore condensation and coke formation.

7.5 Microkinetic Simulations

The extensive reaction network obtained in this study was used to simulate six bench-scale experiments all performed at the same feed flow rates and pressure but at different temperature settings varying from 1013 K to 1113 K in 20 K increments in order to cover a wide conversion range. For each studied condition, three repetition experiments were performed. A summary of the conversion and the measured product yields for the 18 experiments, along with details of process conditions concerning temperature profiles, mass flow rates and product composition, is provided in Tables S3 and S4 of Appendix F. It should be noted that in these Tables only products with yields higher than 0.1 wt% are presented.

A qualitative comparison of the produced compounds obtained from the reaction mechanism generated in this study and the experimental data shows that the majority of compounds which are present in the reactor effluent of MB pyrolysis are also present in the simulations. For the simulation, all data described in Table 7-1 have been implemented, including along with the ab initio data also experimental data from the work of Metcalfe et al. [16] and Bennadji et al. [14] . However, there are a few species missing from the simulation results, such as aromatics, cyclic compounds, and some other species with more than five carbon atoms. This is related to the restriction during the generation of the reaction mechanism by Genesys to limit molecules to contain maximally five carbon and three oxygen atoms, and therefore aromatics, cyclic compounds and other larger species are excluded from the mechanism. Although this assumption reduces the size of the developed mechanism, it only marginally affects the accuracy of the model: the overall production of compounds with more than five carbon and three oxygen atoms during MB pyrolysis experiments is less than 3.5 wt% even at the highest temperature of 1113 K (see Table S3-S4 of Appendix F).

Table 7-2 provides a comparison between simulated and experimentally observed conversion and product yields (wt %) for the bench-scale reactor experiment at 1013 K. The comparison is performed only for products with experimental yields larger than 1 wt%. For higher temperatures (1033-1113 K) the comparison between the simulated bench-scale reactor MB conversion and the product yields (wt %) can be found in Table S5 of Appendix F.

Table 7-2: Comparison between simulated and experimental product yields (wt %) at 1013 K (pressure: 0.17 MPa; flow rate of methyl butanoate: 257 g/h; dilution: 0.6 mol_{N2}/mol_{MB}).

	Exp	Simulated
CO_2	11.26	11.28
CH_4	10.53	9.56
CO	14.87	6.42
C_2H_6	1.45	0.28
C_2H_4	8.10	7.79
C_3H_6	6.38	7.48
CH_2O	3.17	2.90
Methyl Propenoate	5.09	12.04
Other	3.47	8.25
Methyl Butanoate	35.69	34.00
Total	100.00	100.00
Conversion of MB [%]	64.31	66.00

Based on the results provided in Table 7-2 it can be concluded that the simulated conversion of MB of 66% is in good agreement with the experimental MB conversion of 64.3%. The ab initio predicted versus the experimental MB conversion as function of the temperature in Figure 7-1 shows that the conversion can be accurately predicted, with deviations within 5% relative intervals for the studied experimental conditions.

The product yields for the major products of the MB pyrolysis in the bench-scale reactor at temperatures 1013-1113 K are predicted satisfactorily for most of them, as can be observed in Figure 7-2. Good agreement between the simulated and the experimental product yields is obtained for the majority of products, such as CO_2, CH_4, C_2H_4, and formaldehyde, which are predicted within 10% relative deviation from the corresponding experimental yields. The prediction for C_3H_6 is slightly worse since it deviates ~15% from the corresponding experimental yield.

However, major deviations pertain to three products: ethane, methyl propenoate, (CH_2=$CHCOOCH_3$), and carbon monoxide. Methyl propenoate is overpredicted by the reaction mechanism proposed in this work; the experimental product yield is 5 wt%, whereas the model predicts a yield of 12 wt%. Contrary to that, carbon monoxide is significantly underpredicted, since its experimental yield is about 15 wt%, whereas the model predicts only about 6.5 wt% CO yield at 1013 K. Finally, ethane is also underpredicted; the experimental product yield for ethane at 1013 K is 1.45 wt%, while the ab initio simulated process yields only 0.28 wt% ethane in the products of MB pyrolysis at 1013 K.

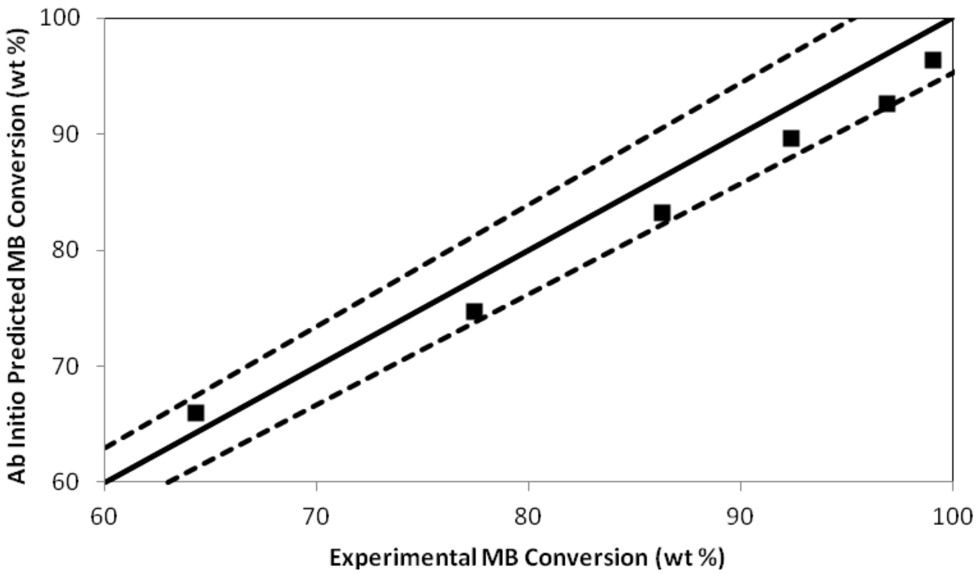

Figure 7-1: Simulated versus experimental methyl butanoate conversion (wt %) at temperatures ranging from 1013 to 1113 K. Dashed lines indicate 5% deviation from parity. (pressure: 0.17 MPa; flow rate of MB: 257 g/h; dilution: 0.6 mol_{N2}/mol_{MB}).

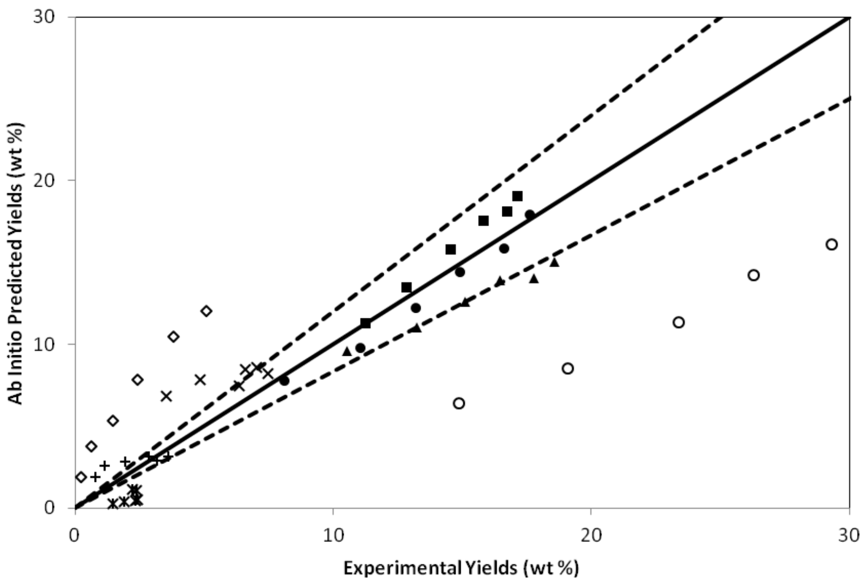

Figure 7-2: Simulated predicted versus experimental product yields (wt %) for CO_2 (■), CH_4 (▲), CO (○), C_2H_6 (*), C_2H_4 (•), C_3H_6 (x), CH_2O (+) and Methyl Propenoate (◊) at temperatures ranging from 1013 to 1113 K. Dashed lines indicate 20% relative intervals. Pressure: 0.17 MPa; flow rate of methyl butanoate: 257 g/h; dilution: 0.6 mol_{N2}/mol_{MB}.

Figures 7-3 and 7-4 show that the expected trends for the main products as a function of the MB conversion are satisfactorily reproduced by the model. In Figure 7-3, the yields for CO, CO_2, methane and ethylene increase with increasing MB conversion, which in its turn increases with temperature in the studied range 1013-1113 K, with the strongest increase for CO and ethylene. Figure 7-4 presents compounds for which the product yields decrease with increasing MB conversion. These products are ethane, propene, formaldehyde and methyl propenoate. The strongest decrease is clearly observed for methyl propenoate, for which the simulated product yield reduces from almost 12 wt% at 1013 K to less than 2 wt% at 1113 K. The experimental yield for this product is significantly lower, as it was discussed previously, decreasing from 5 wt% to almost 0.2 wt% with temperature. Although product yields for CO and methyl propenoate are significantly under- and overpredicted, respectively, the trends for these compounds presented in Figures 7-3 and 7-4 qualitatively coincide with the corresponding experimental trends.

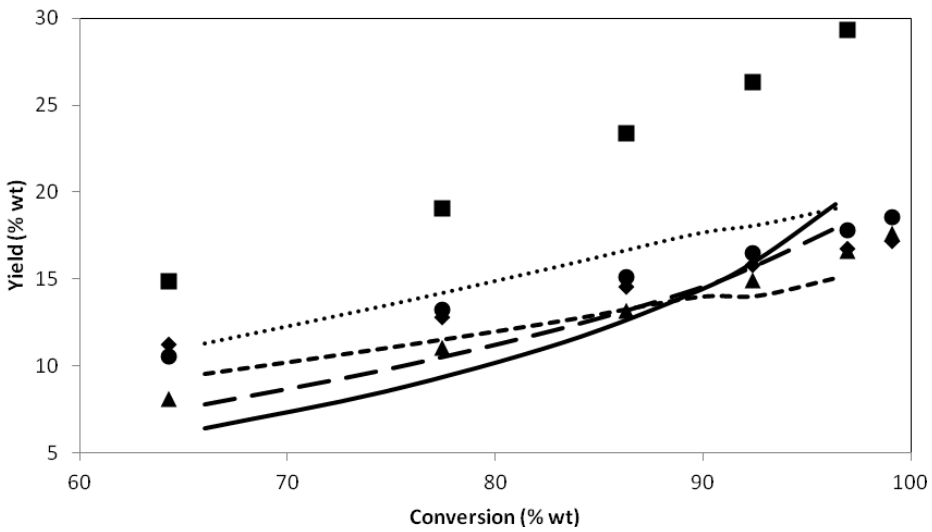

Figure 7-3: Simulated (lines) and experimentally obtained (dots) product yields versus the simulated and the experimental methyl butanoate conversion, respectively, for carbon dioxide (¨¨ ab initio, ♦ experimental), methane (--- ab initio, ● experimental), carbon monoxide (▬ ab initio, ■ experimental) and ethene (—— ab initio, ▲ experimental). (pressure: 0.17 MPa; flow rate of MB: 257 g/h; dilution: 0.6 mol_{N2}/mol_{MB}).

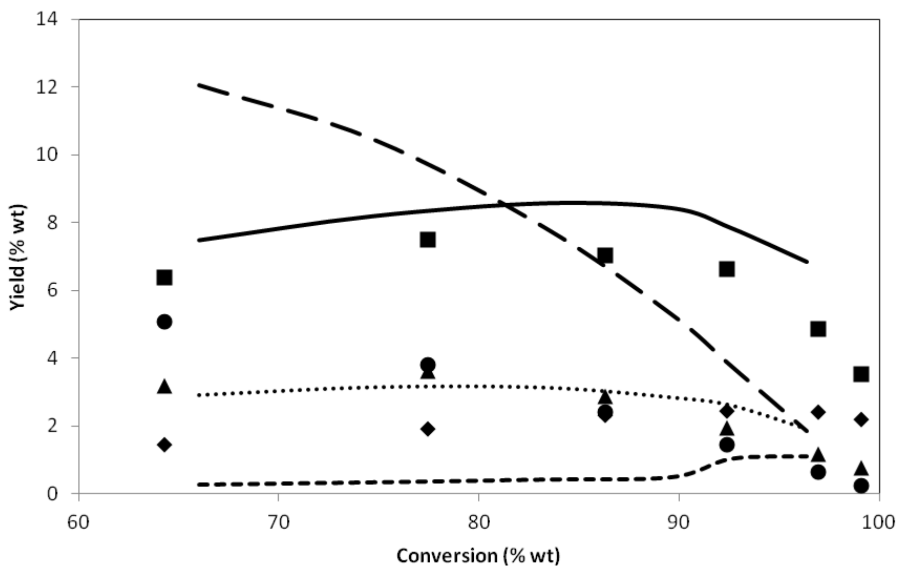

Figure 7-4: Simulated (lines) and experimentally obtained (dots) product yields versus the simulated and the experimental methyl butanoate conversion, respectively, for ethane (--- ab initio, ♦ experimental), propene (▬ ab initio, ■ experimental,), formaldehyde (¨¨ ab initio, ▲ experimental) and methyl propenoate (MP) (—— ab initio, ● experimental). (pressure: 0.17 MPa; flow rate of MB: 257 g/h; dilution: 0.6 mol_{N2}/mol_{MB}).

The inaccuracies on the predicted ethane, CO and methyl propenoate yields deserve further discussion. Perusal of the literature for data concerning the thermal decomposition of unsatured methyl esters, such as methyl propenoate, shows that there is a clear link between the decomposition of an unsaturated methyl ester and the production of carbon monoxide and small hydrocarbons. Particularly, Bennadji et al. [14] studied the oxidation of small unsaturated methyl esters, among which was methyl propenoate (methyl acrylate), using shock tube experiments, investigating the ignition delay times. Bennadji et al. [14] proposed a reaction mechanism for the oxidation of methyl propenoate at a temperature of 1440 K and pressure around 8 bar.

According to this mechanism methyl propenoate reacts by addition reactions, mainly additions of hydrogen atoms or hydroxyl, hydrogen abstraction reactions, and unimolecular bond scission reactions. The most important reaction pathways for methyl propenoate result in producing carbon monoxide, ethyl and vinyl radicals, in several successive elementary reactions. Direct implementation of the full mechanism proposed by Bennadji et al. [14] for the oxidation of unsaturated methyl esters is impossible, since due to the nature of combustion it refers to significantly higher temperatures than the experiments simulated in this work, and needs to be modified. Therefore, as it was discussed in previous chapter, nine hydrogen abstractions from methyl propenoate were included in the reaction mechanism obtained from this study. In the absence of these reactions from Bennadji et al. [14], the methyl propenoate yield at 1013 K would even be 18 wt% instead of the current 12 wt%, where the experimental product yield for methyl propenoate is 5 wt%. The yield for CO is 4 wt% without these reactions, instead of 6.4 wt% after including them. A possible explanation for the remaining deviation is the high temperature for which the model of Bennadji et al. [14] has been developed, 1280-1930 K, which probably excludes pathways that are important at the lower temperatures of this study (1013-1113 K).

To gain more insight into the reaction pathways for the MB thermal decomposition, the initial steps of the MB degradation are investigated. The reaction pathways for the primary decomposition of MB included in Table 7-3 can be categorized into two reaction families: reaction paths 1−5 involve unimolecular bond scission reactions, whereas reaction paths 6−10, involve hydrogen abstraction reactions. Among all these reaction channels, reaction pathways 2 and 8 have the largest rate coefficient at the studied temperature regime, whereas reaction pathway 10 has the smallest rate coefficient. Generally, reaction channels 1-5 have more than an order of magnitude higher pre-exponential factors compared to the corresponding parameter of reaction pathways 6-10, which can be attributed to the fact that homolytic bond scission reactions are entropically more favorable than the hydrogen transfer reactions. The reaction pathways for the primary decomposition of MB are in line with the results of a study based on ab initio data [13] about the unimolecular decomposition pathways of MB.

The products of the unimolecular decomposition of MB react further according to the reaction pathway scheme provided in Figure 7-5. This pathway scheme is based on the rate of production analysis for MB pyrolysis and shows only the main MB decomposition pathways. The analysis in Figure 7-5 is performed at the point of the maximum rate of MB consumption for the first experiment at 1013 K presented in Table S3 of Appendix F, corresponding to about 210 mm away from the reactor inlet.

Table 7-3: Arrhenius parameters for the modified Arrhenius equation, k(T) = AT^n exp($-E_a/RT$), used in the constructed reaction mechanism for the unimolecular decomposition pathways of MB. (A in cm^3 mol^{-1} s^{-1}, E_a in kJ mol^{-1}). Values for the Arrhenius parameters were taken from the ab initio study for the MB decomposition pathways by Ali and Violi [13].

	Reactions					A	n	E_a
1	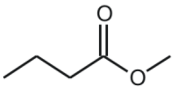	↔	$^{\bullet}CH_3$	+	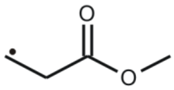	3.62 10^{14}	0	334.7
2	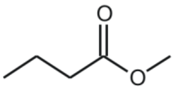	↔		+	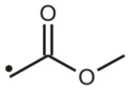	1.13 10^{15}	0	325.1
3	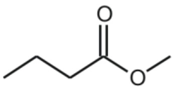	↔		+	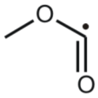	3.92 10^{15}	0	366.5
4	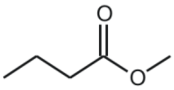	↔	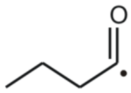	+	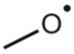	6.09 10^{14}	0	387.0
5	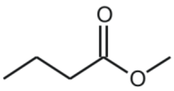	↔	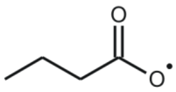	+	$^{\bullet}CH_3$	1.46 10^{15}	0	349.8
6	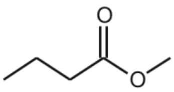	↔	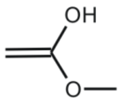	+		1.08 10^{13}	0	287.0
7	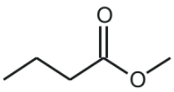	↔	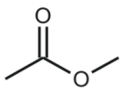	+		5.91 10^{13}	0	416.7
8	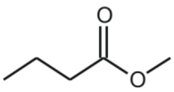	↔	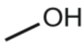	+	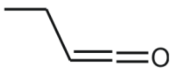	1.12 10^{14}	0	305.4
9	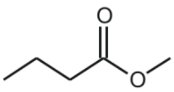	↔	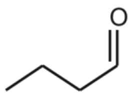	+	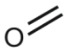	6.01 10^{13}	0	315.5
10	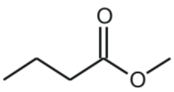	↔	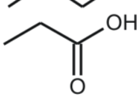	+		1.97 10^{13}	0	416.7

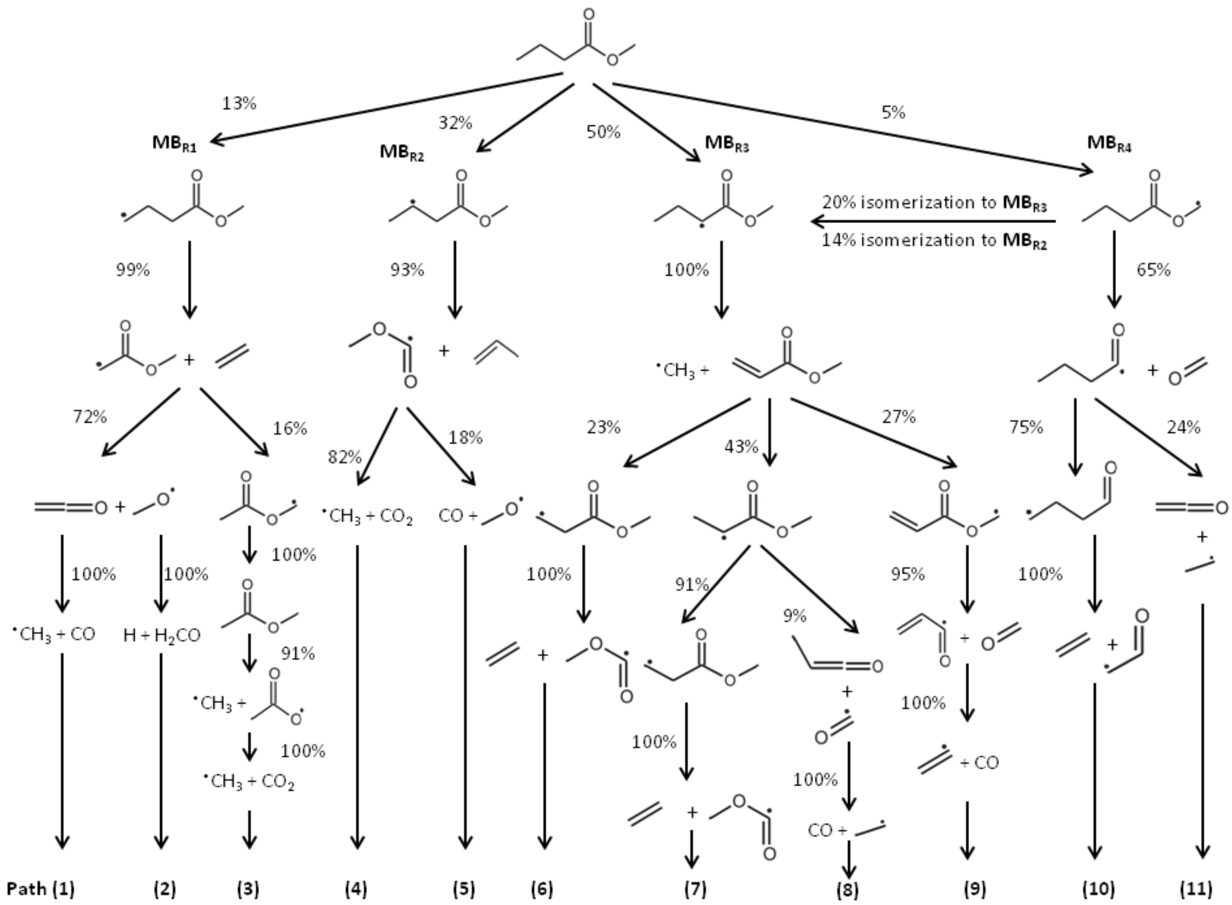

Figure 7-5: Reaction pathways for the MB thermal decomposition performed at the point of the maximum rate of consumption of MB for the experiment with a temperature set-point of 1013 K. The percentages indicates the fraction of the total decomposition rate of the reactant from which the reaction arrow originates.

The first step in MB thermal decomposition is the formation of four MB radicals, which are formed via hydrogen abstraction reactions, mostly by the abundant methyl radical. The four MB radicals produced are: (1) $^{\bullet}CH_2CH_2CH_2COOCH_3$, ($MB_{R1}$), (2) $CH_3{}^{\bullet}CHCH_2COOCH_3$, ($MB_{R2}$), (3) $CH_3CH_2{}^{\bullet}CHCOOCH_3$, ($MB_{R3}$), and (4) $CH_3CH_2CH_2COOCH_2{}^{\bullet}$, ($MB_{R4}$). These four initial radicals can either undergo isomerization reactions or break down to form smaller compounds through, mainly, β-scission reactions. Due to the larger bond dissociation energy of the C−H bond compared to the C−C bond, mainly C−C bonds are broken in the β-scission reactions. In the reaction mechanism presented in Figure 7-5 only reaction pathways that are chemically important according to the rate of production/consumption of the species involved are included.

Almost half of the MB is decomposed into $MB_{R3,}$ whereas yields for the other three MB radicals are 13% for $MB_{R1,}$ 32% for MB_{R2} and only 5% for $MB_{R4.}$ This is in line with Huynh's study [11] which states that the hydrogen atom linked to the carbon atom next to carbonyl in MB has the lowest bond energy and hence, it can be abstracted easier compared to the hydrogens linked to carbon atoms in MB. In the following, the decomposition pathways of intermediate radicals MB_{R1} to MB_{R4} are briefly discussed.

Almost all the produced $\mathbf{MB_{R1}}$ radical undergoes a β-scission reaction to produce ethylene and the methyl acetate radical $^{\bullet}CH_2COOCH_{3.}$ This radical can follow two possible reaction channels: 72% is decomposed through a C−C bond cleavage into ketene (CH_2=C=O) and a methoxy radical ($CH_3O^{\bullet}$) (paths 1&2) and 16% is isomerized into $CH_3COO^{\bullet}CH_2$, which is eventually decomposed in carbon dioxide and methyl (path 3). The formed ketene is decomposed into carbon monoxide and methyl by breaking a C−C bond (path 1), whereas the methoxy radical yields hydrogen and formaldehyde (path 2). Compared to previous work [11], this study reveals a new pathway for the consumption of the methyl acetate radical through isomerization and the final production of carbon dioxide (path 3).

Of the **$\mathbf{MB_{R2}}$ radical**, 93% is converted into methoxy-carbonyl ($CH_3OC^{\bullet}$=O) and propene (CH_2=$CHCH_3$) (paths 4&5). The former can follow two possible pathways, C−C or C−O bond cleavage, to produce CO_2 or CO (paths 4&5), respectively. According to several studies [10-12, 19, 21] these reactions are the main pathways for producing both carbon dioxide and carbon monoxide (see Figure 7-6). The same also holds for the reaction mechanism developed in this study.

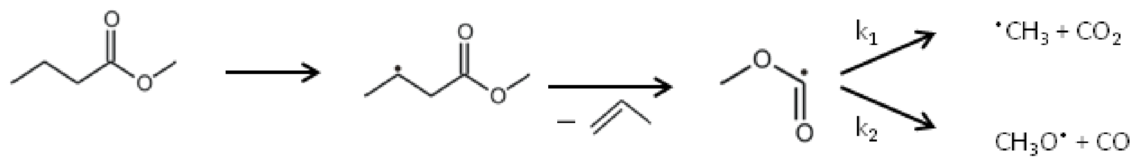

Figure 7-6: Main reaction pathway for CO_2/CO formation [10].

The rate coefficients for these two significant reactions are expressed in eq (7-2) and (7-3) as it was suggested by Glaude et al. [64]:

$$k_1 = 5.56\ 10^7 \exp\left(-\frac{61.5}{RT}\right) \qquad (7\text{-}2)$$

$$k_2 = 2.26\ 10^8 \exp\left(-\frac{95.0}{RT}\right) \qquad (7\text{-}3)$$

Pre-exponential factors in eq (7-2) and (7-3) are expressed in $m^3\ mol^{-1}\ s^{-1}$, whereas activation energies are in kJ mol^{-1}. The proposed rate coefficients for these reactions reveal that for the CO_2 formation the rate coefficient is about 14 times higher than the corresponding coefficient for the CO formation at 1000 K. Almost the entire CO_2 yield of the MB pyrolysis studied in this work stems from this reaction, and almost 58% of the CO yield.

The **MB_{R3}** radical is, as it was stated before, the most abundant radical formed from MB decomposition. The formed MB_{R3} leads, through a C−C β-scission reaction, to the formation of methyl and methyl propenoate (CH_2=$CHCOOCH_3$), an unsaturated methyl ester. According to the proposed reaction mechanism (see Figure 7-5) there are three main reaction pathways for decomposing methyl propenoate. Among these three pathways two involve hydrogen radical additions and one corresponds to hydrogen abstraction reaction. In the former, methyl propenoate (MP) decomposition pathway presented in Figure 7-5 (path 6), 23% of MP is converted into the $^{\bullet}CH_2CH_2COOCH_3$ (MP_{R1}) radical, which is, in a further C−C β-scission converted into ethylene and $CH_3OC^{\bullet}{=}O$. $CH_3OC^{\bullet}{=}O$ further decomposes, resulting in CO and CO_2 formation. The dominant path for the methyl propenoate decomposition is the second path: 43% of the formed MP is converted into $CH_3{}^{\bullet}CHCOOCH_3$ (MP_{R2}). This radical, MP_{R2}, is mainly isomerized (91%) yielding the radical MP_{R1} and then follows the MP_{R1} decomposition pathway into ethylene and $CH_3OC^{\bullet}{=}O$, finally leading to CO and CO_2 formation (path 7).

The methyl propenoate decomposition through the formation of MP_{R1} has been identified by Gail et al. [6] as one of the main pathways in MB oxidation in a jet stirred reactor, an opposed flow flame and a variable pressure flow reactor. The same route (path 7) is shown to be one of the most important pathways for the MB thermal decomposition (see Figure 7-7) based on the results of this study. However, there is a portion of 9% that decomposes into methyl ketene ($CH_3CH{=}C{=}O$) and the carbonyl ($H^{\bullet}C{=}O$) radical. Methyl ketene finally decomposes into ethyl and carbon monoxide (path 8).

The third reaction pathway is the one through which almost 27% of methyl propenoate decomposes to produce $CH_2{=}CHCOOCH_2{}^{\bullet}$, ($MP_{R3}$). MP_{R3} undergoes a C−O bond scission that leads to the formation of formaldehyde and 1-oxoprop-2-enyl ($CH_2{=}CH^{\bullet}C{=}O$). This latter is further decomposed into ethenyl and carbon monoxide (path 9). This reaction pathway differs from the corresponding reaction channel proposed by Huynh and Violi [11], in which MP_{R3} decomposes into $^{\bullet}CH_2CH{=}C{=}O$ and $H_2C{=}O$. The formed $^{\bullet}CH_2CH{=}C{=}O$ radical in a further step leads to the formation of vinyl radical ($^{\bullet}CH{=}CH_2$) and CO, the same final products as those described in this simulation. The lack of this reaction path can be attributed to the inability of our model to accurately describe the decomposition of small unsaturated esters and the formation of ketene products, as it was stated previously.

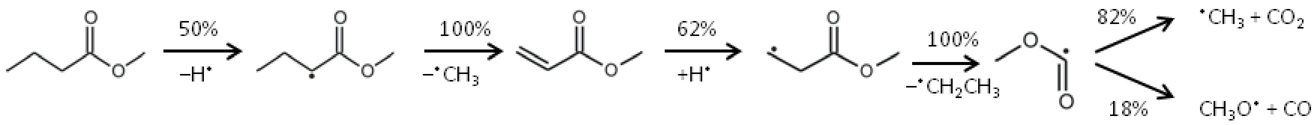

Figure 7-7: Main reaction pathway for the MB thermal decomposition. The percentages indicate the total decomposition rate of the particular compound for the simulation at the set-up temperature of 1013 K.

The proposed reaction mechanism for the decomposition of methyl propenoate, as described in Figure 7-5, has two reaction pathways missing compared to the reaction network proposed by Huynh and Violi [11]. According to this study, methyl propenoate is consumed following four reaction pathways that correspond to hydrogen abstraction or addition reactions, which result in four radicals: $^{\bullet}CH{=}CHCOOCH_3$, $CH_2{=}C^{\bullet}COOCH_3$, $CH_2{=}CHCOO^{\bullet}CH_2$ and $^{\bullet}CH2CH_2COOCH_3$. The lack of the ΔGAV^os necessary to describe decomposition reactions involving unsaturated oxygenates resulted in Genesys missing out the decomposition pathways to the two former radicals, $^{\bullet}CH{=}CHCOOCH_3$ and $CH_2{=}C^{\bullet}COOCH_3$, which were therefore introduced in the network using Arrhenius parameters from the work of Huynh and Violi [11]. However, the rate coefficients for these two reactions at 1000 K, as they are provided by Huynh and Violi [11], are very low compared to the other reactions decomposing methyl propenoate as they are presented in Figure 7-5.

MB_{R4} The fourth reaction channel for the decomposition of MB is the least important. This pathway, via the $CH_3CH_2CH_2COO^{\bullet}CH_2$ (MB_{R4}) radical, consumes only 5% of the MB. Almost one third of MB_{R4} isomerizes into two other MB radicals (20% into MB_{R2} and 14% into MB_{R3}). The remaining 65% of MB_{R4}, after a C−O *β*-scission MB_{R4} decomposes into formaldehyde and butanoyl ($CH_3CH_2CH_2C^{\bullet}{=}O$). The latter radical further decomposes into (a) the main path (75%) through isomerization to 4-oxobutyl ($^{\bullet}CH_2CH_2CH_2CH{=}O$) and (b) the secondary path (24%) through C−C β-scission resulting in the formation of ethyl and ketene. The radical 4-oxobutyl can be further decomposed into ethene and 2-oxoethyl ($^{\bullet}CH_2CH{=}O$).

Summarizing, despite the significant overprediction of methyl propenoate and the underprediction of carbon monoxide and ethane, the overall ab initio prediction for MB pyrolysis remains very good. The prediction of the MB conversion is excellent compared to experimental values, with differences below 5 % at the whole temperature range (1013-1113 K). Moreover, the ab initio prediction of the yields of the most significant products of the MB thermal decomposition such as carbon dioxide, methane, ethene, propene and formaldehyde is very good with differences up to 20 % only for the whole temperature range. An increase in temperature leads to the significant increase in MB conversion and in the yields of products such as CO, CO_2, methane and ethene. Contrary to that, yields of products such as ethane, formaldehyde and methyl propenoate decrease with increasing process temperature.

Based on these results it can be concluded that the developed reaction mechanism describes all the relevant chemistry during MB thermal decomposition and leads to qualitative and quantitative agreement to experimental results for all products except for CO, ethane and methyl propenoate. Moreover, it should be highlighted that none of the applied kinetic parameters has been fitted to experimental values. Hence, it can be stated that ab initio methods in combination with group additive methods can provide a useful tool in reactor simulation studies. The extension of the already obtained group additive models towards including more reaction types, such as bond scission and their reverse recombination reactions, isomerization or cyclization reactions will further contribute in increasing the accuracy of the predictions for the pyrolysis of bio-based feedstocks.

7.6 Conclusions

In this study the thermal decomposition of methyl butanoate (MB) was studied using Genesys, an automated reaction network generation program. All thermodynamic data required for the generation of the reaction mechanism were derived from either quantum chemical calculations on the CBS-QB3 level of theory or by means of group additivity based on CBS-QB3 data. Kinetic data were mainly obtained from ab initio calculations or group additivity methods based on ab initio calculations. For the chemistry of smaller compounds (less than two carbon and two oxygen atoms), experimentally derived kinetic data are used in order to improve the accuracy of the developed reaction mechanism.

The MB conversion and the product yields of the ab initio simulated process were compared with bench-scale set-up experimental data available from our group. Using the reaction mechanism developed in this work, the MB conversion is excellently predicted over the studied temperature regime of 1013-1113 K, whereas the majority of the main products was simulated within 10%, except for propene, which was simulated within 20%, and the three products ethane, CO and methyl propenoate, which have larger deviations compared to experimental yields. Most likely, the larger deviations are caused by lack of detailed mechanism for the methyl propenoate decomposition. Improvement of the methyl propenoate decomposition pathways would most likely decrease the overpredicted methyl propenoate yield and in the meantime would increase the underpredicted yields for CO and ethane.

According to the simulations, the main reaction pathway for decomposing MB is the one resulting in the formation of methyl propenoate, which in a further step leads to methoxy-carbonyl ($CH_3OC^{\bullet}=O$) formation, and in a final step to CO and CO_2 formation. The reaction pathway through methoxy-carbonyl is also the prevailing reaction channel for both CO and CO_2 formation.

This work has shown that thermal decomposition of oxygenate compounds can be studied in detail by combining first-principle data with complex algorithms for the construction of reaction network mechanisms. It was also shown that the use of ab initio thermodynamic data next to ab initio and experimental kinetic data is adequate for the development of reaction networks. Further extension of the already existing group additive models towards describing more reaction types, such bond scissions and isomerizations, and also hydrogen abstractions from unsaturated oxygenates, could lead to the development of reaction networks for methyl ester pyrolysis based solely on ab initio data.

The applicability of the developed reaction mechanism is not restricted to MB thermal decomposition. It can be implemented as a seed mechanism to describe other processes based on gas phase radical chemistry involving oxygenates, such as partial oxidation or combustion processes. As such, this is a significant step towards optimization of current technologies or designing new processes involving bio-based feedstock.

7.7 References

1. Ulber, R., D. Sell, and T. Hirth, eds. *Renewable Raw Materials: New Feedstocks for the Chemical Industry*. 2011, Wiley-VCH Verlag GmbH & Co: Weinheim, Germany.

2. Demirbas, A., *Biodiesel production from vegetable oils via catalytic and non-catalytic supercritical methanol transesterification methods.* Prog Energ Combust, 2005. **31**(5-6): p. 466-487.

3. Muralidharan, K., D. Vasudevan, and K.N. Sheeba, *Performance, emission and combustion characteristics of biodiesel fuelled variable compression ratio engine.* Energy, 2011. **36**(8): p. 5385-5393.

4. Lai, J.Y.W., K.C. Lin, and A. Violi, *Biodiesel combustion: Advances in chemical kinetic modeling.* Prog Energ Combust, 2011. **37**(1): p. 1-14.

5. Fisher, E.M., W.J. Pitz, H.J. Curran, and C.K. Westbrook, *Detailed chemical kinetic mechanisms for combustion of oxygenated fuels.* P Combust Inst, 2000. **28**: p. 1579-1586.

6. Gail, S., M.J. Thomson, S.M. Sarathy, S.A. Syed, P. Dagaut, P. Dievart, A.J. Marchese, and F.L. Dryer, *A wide-ranging kinetic modeling study of methyl butanoate combustion.* P Combust Inst, 2007. **31**: p. 305-311.

7. Metcalfe, W.K., S. Dooley, H.J. Curran, J.M. Simmie, A.M. El-Nahas, and M.V. Navarro, *Experimental and modeling study of C5H10O2 ethyl and methyl esters.* J Phys Chem A, 2007. **111**(19): p. 4001-4014.

8. Dooley, S., H.J. Curran, and J.M. Simmie, *Autoignition measurements and a validated kinetic model for the biodiesel surrogate, methyl butanoate.* Combust Flame, 2008. **153**(1-2): p. 2-32.

9. El-Nahas, A.M., M.V. Navarro, J.M. Simmie, J.W. Bozzelli, H.J. Curran, S. Dooley, and W. Metcalfe, *Enthalpies of formation, bond dissociation energies and reaction paths for the decomposition of model biofuels: Ethyl propanoate and methyl butanoate.* J Phys Chem A, 2007. **111**(19): p. 3727-3739.

10. Huynh, L.K., K.C. Lin, and A. Violi, *Kinetic Modeling of Methyl Butanoate in Shock Tube.* J Phys Chem A, 2008. **112**(51): p. 13470-13480.

11. Huynh, L.K. and A. Violi, *Thermal decomposition of methyl butanoate: Ab initio study of a biodiesel fuel surrogate.* J Org Chem, 2008. **73**(1): p. 94-101.

12. Farooq, A., W. Ren, K.Y. Lam, D.F. Davidson, R.K. Hanson, and C.K. Westbrook, *Shock tube studies of methyl butanoate pyrolysis with relevance to biodiesel.* Combust Flame, 2012. **159**(11): p. 3235-3241.

13. Ali, M.A. and A. Violi, *Reaction Pathways for the Thermal Decomposition of Methyl Butanoate.* J Org Chem, 2013. **78**(12): p. 5898-5908.

14. Bennadji, H., L. Coniglio, F. Billaud, R. Bounaceur, V. Warth, P.A. Glaude, and F. Battin-Leclerc, *Oxidation of Small Unsaturated Methyl and Ethyl Esters.* Int J Chem Kinet, 2011. **43**(4): p. 204-218.

15. Hakka, M.H., H. Bennadji, J. Biet, M. Yahyaoui, B. Sirjean, V. Warth, L. Coniglio, O. Herbinet, P.A. Glaude, et al., *Oxidation of Methyl and Ethyl Butanoates.* Int J Chem Kinet, 2010. **42**(4): p. 226-252.

16. Metcalfe, W.K., S.M. Burke, S.S. Ahmed, and H.J. Curran, *A Hierarchical and Comparative Kinetic Modeling Study of C-1 - C-2 Hydrocarbon and Oxygenated Fuels.* Int J Chem Kinet, 2013. **45**(10): p. 638-675.

17. Tao, H.R. and K.C. Lin, *Pathways, kinetics and thermochemistry of methyl-ester peroxy radical decomposition in the low-temperature oxidation of methyl butanoate: A computational study of a biodiesel fuel surrogate.* Combust Flame, 2014. **161**(9): p. 2270-2287.

18. Glaude, P.A., O. Herbinet, S. Bax, J. Biet, V. Warth, and F. Battin-Leclerc, *Modeling of the oxidation of methyl esters-Validation for methyl hexanoate, methyl heptanoate, and methyl decanoate in a jet-stirred reactor.* Combust Flame, 2010. **157**(11): p. 2035-2050.

19. Herbinet, O., P.A. Glaude, V. Warth, and F. Battin-Leclerc, *Experimental and modeling study of the thermal decomposition of methyl decanoate.* Combust Flame, 2011. **158**(7): p. 1288-1300.

20. Dievart, P., S.H. Won, S. Dooley, F.L. Dryer, and Y.G. Ju, *A kinetic model for methyl decanoate combustion.* Combust Flame, 2012. **159**(5): p. 1793-1805.

21. Pyl, S.P., K.M. Van Geem, P. Puimege, M.K. Sabbe, M.F. Reyniers, and G.B. Marin, *A comprehensive study of methyl decanoate pyrolysis.* Energy, 2012. **43**(1): p. 146-160.

22. Sabbe, M.K., F. De Vleeschouwer, M.F. Reyniers, M. Waroquier, and G.B. Marin, *First Principles Based Group Additive Values for the Gas Phase Standard Entropy and Heat Capacity of Hydrocarbons and Hydrocarbon Radicals.* J Phys Chem A, 2008. **112**(47): p. 12235-12251.

23. Sabbe, M.K., M.F. Reyniers, V. Van Speybroeck, M. Waroquier, and G.B. Marin, *Carbon-centered Radical Addition and Beta-Scission Reactions: Modeling of Activation Energies and Pre-Exponential Factors.* Chem Phys Chem, 2008. **9**(1): p. 124-140.

24. Sabbe, M.K., M.F. Reyniers, M. Waroquier, and G.B. Marin, *Hydrogen Radical Additions to Unsaturated Hydrocarbons and the Reverse beta-Scission Reactions: Modeling of Activation Energies and Pre-Exponential Factors.* Chem Phys Chem, 2010. **11**(1): p. 195-210.

25. Sabbe, M.K., A.G. Vandeputte, M.F. Reyniers, M. Waroquier, and G.B. Marin, *Modeling the Influence of Resonance Stabilization on the Kinetics of Hydrogen Abstractions.* Phys Chem Chem Phys, 2010. **12**(6): p. 1278-1298.

26. Vandeputte, A.G., M.K. Sabbe, M.F. Reyniers, and G.B. Marin, *Modeling the Gas-Phase Thermochemistry of Organosulfur Compounds.* Chem-Eur J, 2011. **17**(27): p. 7656-7673.

27. Vandeputte, A.G., M.K. Sabbe, M.F. Reyniers, and G.B. Marin, *Kinetics of Alpha Hydrogen Abstractions from Thiols, Sulfides and Thiocarbonyl Compounds.* Phys Chem Chem Phys, 2012. **14**(37): p. 12773-12793.

28. Vandeputte, A.G., M.F. Reyniers, and G.B. Marin, *Kinetics of Homolytic Substitutions by Hydrogen Atoms at Thiols and Sulfides.* Chem Phys Chem, 2013. **14**(8): p. 1703-1722.

29. Vandeputte, A.G., M.F. Reyniers, and G.B. Marin, *Kinetic Modeling of Hydrogen Abstractions Involving Sulfur Radicals.* Chem Phys Chem, 2013. **14**(16): p. 3751-3771.
30. Paraskevas, P.D., M.K. Sabbe, M.F. Reyniers, N. Papayannakos, and G.B. Marin, *Group Additive Values for the Gas Phase Standard Enthalpy of Formation, Entropy and Heat Capacity of Oxygenates.* Chem-Eur J, 2013. **19**: p. 16431-16452.
31. Paraskevas, P.D., M.K. Sabbe, M.F. Reyniers, N. Papayannakos, and G.B. Marin, *Kinetic Modeling of α-Hydrogen Abstractions from Unsaturated and Saturated Oxygenate Compounds by Carbon-Centered Radicals.* Chem Phys Chem, 2014. **15**(9): p. 1849-1866.
32. Paraskevas, P.D., M.K. Sabbe, M.F. Reyniers, N. Papayannakos, and G.B. Marin, *Kinetic Modeling of α-Hydrogen Abstractions from Unsaturated and Saturated Oxygenate Compounds by Hydrogen Atoms.* J Phys Chem A, 2014. **118**(40): p. 9296-9309.
33. Paraskevas, P.D., M.K. Sabbe, M.F. Reyniers, N. Papayannakos, and G.B. Marin, *Group Additive Kinetics for Hydrogen Transfer Between Oxygenates.* J Phys Chem A, 2015. **119**(27): p. 6961-6980.
34. Benson, S.W. and J.H. Buss, *Additivity Rules for the Estimation of Molecular Properties. Thermodynamic Properties.* J Chem Phys, 1958. **29**(9): p. 546-561.
35. Benson, S.W., *Thermochemical Kinetics*. 1968, New York: John Wiley & Sons Ltd.
36. Montgomery, J.A., M.J. Frisch, J.W. Ochterski, and G.A. Petersson, *A Complete Basis Set Model Chemistry. VI. Use of Density Functional Geometries and Frequencies.* J Chem Phys, 1999. **110**(6): p. 2822-2827.
37. Montgomery, J.A., M.J. Frisch, J.W. Ochterski, and G.A. Petersson, *A complete basis set model chemistry. VII. Use of the minimum population localization method.* J Chem Phys, 2000. **112**(15): p. 6532-6542.
38. Sabbe, M.K., K.M. Van Geem, M.F. Reyniers, and G.B. Marin, *First Principle-Based Simulation of Ethane Steam Cracking.* Aiche J, 2011. **57**(2): p. 482-496.
39. Dimaio, F.P. and P.G. Lignola, *King, a Kinetic Network Generator.* Chem Eng Sci, 1992. **47**(9-11): p. 2713-2718.
40. Susnow, R.G., A.M. Dean, W.H. Green, P. Peczak, and L.J. Broadbelt, *Rate-based construction of kinetic models for complex systems.* J Phys Chem A, 1997. **101**(20): p. 3731-3740.
41. William H. Green, Joshua W. Allen, Beat A. Buesser, Robert W. Ashcraft, Gregory J. Beran, Caleb A. Class, Connie Gao, C. Franklin Goldsmith, Michael R. Harper, et al., *RMG - Reaction Mechanism Generator v4.0.1*, 2013.
42. Clymans, P.J. and G.F. Froment, *Computer-Generation of Reaction Paths and Rate-Equations in the Thermal-Cracking of Normal and Branched Paraffins.* Computers & Chemical Engineering, 1984. **8**(2): p. 137-142.
43. Vandewiele, N.M., K.M. Van Geem, M.F. Reyniers, and G.B. Marin, *Genesys: Kinetic Model Construction Using Chemo-Informatics.* Chem Eng J, 2012. **207**: p. 526-538.
44. Design, R., *CHEMKIN-PRO 15131*, 2013, Reaction Design, Inc: San Diego.

45. Broadbelt, L.J., S.M. Stark, and M.T. Klein, *Termination of Computer-Generated Reaction-Mechanisms - Species Rank-Based Convergence Criterion.* Ind Eng Chem Res, 1995. **34**(8): p. 2566-2573.

46. Sabbe, M.K., M. Saeys, M.F. Reyniers, G.B. Marin, V. Van Speybroeck, and M. Waroquier, *Group additive values for the gas phase standard enthalpy of formation of hydrocarbons and hydrocarbon radicals.* J Phys Chem A, 2005. **109**(33): p. 7466-7480.

47. Goldsmith, C.F., G.R. Magoon, and W.H. Green, *Database of Small Molecule Thermochemistry for Combustion.* J Phys Chem A, 2012. **116**(36): p. 9033-9057.

48. Lay, T.H., J.W. Bozzelli, A.M. Dean, and E.R. Ritter, *Hydrogen-Atom Bond Increments for Calculation of Thermodynamic Properties of Hydrocarbon Radical Species.* J Phys Chem-Us, 1995. **99**(39): p. 14514-14527.

49. Vansteenkiste, P., V. Van Speybroeck, G.B. Marin, and M. Waroquier, *Ab Initio Calculation of Entropy and Heat Capacity of Gas-Phase n-Alkanes Using Internal Rotations.* J Phys Chem A, 2003. **107**(17): p. 3139-3145.

50. Van Speybroeck, V., P. Vansteenkiste, D. Van Neck, and M. Waroquier, *Why Does the Uncoupled Hindered Rotor Model Work Well for the Thermodynamics of n-Alkanes?* Chem Phys Lett, 2005. **402**(4-6): p. 479-484.

51. Vansteenkiste, P., D. Van Neck, V. Van Speybroeck, and M. Waroquier, *An extended hindered-rotor model with incorporation of Coriolis and vibrational-rotational coupling for calculating partition functions and derived quantities (vol 124, pg 044314, 2006).* J Chem Phys, 2006. **125**(4): p. Art. No. 049902.

52. Paraskevas, P.D., M.K. Sabbe, M.F. Reyniers, N. Papayannakos, and G.B. Marin, *Group Additive Kinetic Modeling for Carbon-centered Radical Addition to Oxygenates and β-Scission of Oxygenates*, 2015.

53. Saeys, M., M.F. Reyniers, G.B. Marin, V. Van Speybroeck, and M. Waroquier, *Ab Initio Group Contribution Method for Activation Energies for Radical Additions.* Aiche J, 2004. **50**(2): p. 426-444.

54. Pollak, E.L.I. and P. Pechukas, *Symmetry Numbers, Not Statistical Factors, Should be Used in Absolute Rate Theory and in Bronsted Relations.* J Am Chem Soc, 1978. **100**(10): p. 2984-2991.

55. Coulson, D.R., *Statistical Factors in Reaction-Rate Theories.* J Am Chem Soc, 1978. **100**(10): p. 2992-2996.

56. Eckart, C., *The Penetration of a Potential Barrier by Electrons.* Phys Rev, 1930. **35**: p. 1303-1309.

57. Eyring, H., *The Activated Complex in Chemical Reactions.* J Chem Phys, 1935. **3**: p. 107-115.

58. Truhlar, D.G. and B.C. Garrett, *Variational Transition-State Theory.* Accounts Chem Res, 1980. **13**(12): p. 440-448.

59. Truhlar, D.G. and B.C. Garrett, *Variational Transition-State Theory.* Annu Rev Phys Chem, 1984. **35**: p. 159-189.

60. Hu, W.P., Y.P. Liu, and D.G. Truhlar, *Variational Transition-State Theory and Semiclassical Tunneling Calculations with Interpolated Corrections - a New Approach to Interfacing Electronic-Structure Theory and Dynamics for Organic-Reactions.* J Chem Soc Faraday T, 1994. **90**(12): p. 1715-1725.

61. Laidler, K.J., *Chemical Kinetics*. 1987, New York: Harper & Row.
62. Harper, M.R., K.M. Van Geem, S.P. Pyl, G.B. Marin, and W.H. Green, *Comprehensive reaction mechanism for n-butanol pyrolysis and combustion.* Combust Flame, 2011. **158**(1): p. 16-41.
63. Pyl, S.P., C.M. Schietekat, K.M. Van Geem, M.F. Reyniers, J. Vercammen, J. Beens, and G.B. Marin, *Rapeseed oil methyl ester pyrolysis: On-line product analysis using comprehensive two-dimensional gas chromatography*. J Chromatogr A, 2011. **1218**(21): p. 3217-3223.
64. Glaude, A.P., J.W. Pitz, and J.M. Thomson, *Chemical Kinetic Modeling of Dimethyl Carbonate in an Opposed-Flow Diffusion Flame.* P Combust Inst, 2005. **30**(1): p. 1111-1118.

Chapter 8

Conclusions and Perspectives

Due to the rapid increase in computational resources and the accuracy of newly developed levels of theory, computational chemistry offers a reliable alternative to experiment for investigating the gas phase chemistry, allowing to study the reaction pathways of large kinetic networks in detail. In this work, ab initio calculations are employed to develop a database of accurate thermochemical data for oxygenate compounds and a database of accurate kinetic data for two main families of radical reactions involving oxygenates. The obtained ab initio data are successfully used to develop group additivity models based on Benson's group additivity method [1, 2], enabling a reliable prediction of thermodynamic parameters for oxygenate compounds and Arrhenius parameters for the complex radical chemistry that occurs during oxygenate conversion processes.

Ab initio calculated thermodynamic parameters have been determined using ideal gas statistical thermodynamics based on CBS-QB3 calculations, including corrections for hindered rotation for all internal rotors. Within the group additivity method used, next to the group additive values (GAVs), also corrections for non-nearest-neighbor interactions (NNIs) have been incorporated. This group additive model was shown to accurately reproduce thermodynamic parameters for oxygenate molecules and radicals, since model predictions are in agreement with experimentally obtained data. As an alternative to the group additive method for determining the thermochemistry of oxygenate radicals, hydrogen bond increments (HBIs) calculated according to the method developed by Lay et al. [3].

Kinetic parameters were determined based on CBS-QB3 ab initio calculations with corrections for one-dimensional hindered rotation around the forming/breaking bond. Two types of reactions have been studied that is, hydrogen abstractions and radical additions along with their reverse β-scissions. Rate coefficients were calculated using the conventional transition state theory in the high-pressure limit [4], with Eckart tunneling corrections [5] for hydrogen abstraction reactions only. Based on these data, group additive values (ΔGAV^os) for primary and secondary contributions were calculated. The present work has shown that all secondary contributions have a significant contribution and, hence, their inclusion in the developed kinetic models is indispensable to increase the accuracy of the prediction. Moreover, in order to consider effects caused by cross-resonance and/or hyperconjugation in the transition state also corrections for these cross-stabilization effects are included. Their inclusion can shed light on non-local effects that cannot be incorporated in the ΔGAV^os and, as was shown, their contribution to the Arrhenius parameters of the studied reactions is significant in many cases. Tunneling coefficients were modeled separately from ΔGAV^os using a fourth-order polynomial with temperature dependent coefficients [6].

The validation of the applied methodology in comparison with experimental rate coefficients, ab initio calculated data and predictions by other models has shown that it provides an accurate yet fast prediction for the studied reactions involving oxygenates. Moreover, the main advantage of using a group additive method is the application of the calculated group additive data to a much broader range than the actual set of ab initio calculated or experimentally obtained data.

The group additivity values for the thermochemistry of oxygenate compounds and the kinetic parameters of reactions involving oxygenates that were derived in this study were finally used to generate a reaction network for the thermal decomposition of methyl butanoate (MB), a widely used model biodiesel compound. The group contribution models developed in this study were implemented into Genesys [7], a kinetic model generation tool, for the estimation of thermodynamic properties of the molecules and the rate coefficients of elementary reactions involved in the developed reaction network. In Genesys [7] the chemical data libraries are separate from the code. This means that integration of new species with new functional groups or replacement of obsolete predictive models with more efficient and accurate solutions is feasible. In this work, new libraries have been added to allow the study of oxygenate compounds and, moreover, the Genesys code was modified to include secondary contributions along with corrections for resonance and/or hyperconjugative effects.

The parameters used in the generated reaction mechanism are based on ab-initio group additivity for the reactions between larger compounds, and the experiment-based seed mechanism of Metcalfe et al. [8] for the decomposition reactions of the smaller compounds and a set of nine hydrogen abstraction reactions from the study of Bennadji et al. [9] regarding the decomposition of small unsaturated methyl esters, without any optimization of rate coefficients. The results from the generated reaction network for the methyl butanoate pyrolysis are compared with the corresponding data from a series of experiments available in the Laboratory for Chemical Technology (LCT) of Ghent University. The predicted MB conversion and the predicted yields for the majority of the products agreed very well with the corresponding experimental values. However, the model cannot accurately predict product yields for three compounds; ethane, CO and methyl propenoate, mainly due to the lack of a mechanism for the thermal decomposition of small unsaturated esters, such as methyl propenoate.

Although the developed group additive models for thermochemistry and kinetics involving oxygenate compounds were shown to reproduce accurate parameters when compared to experimental data, further improvements are always possible. The extension of the already developed group additive models towards covering more reaction types and more reaction families would make it feasible to obtain more detailed and accurate models, without the necessity of including also experimental data.

First of all, based on the results of the comparison between predictions for the product yields of the MB pyrolysis and experimental data it can be concluded that a mechanism for the thermal decomposition of small unsaturated methyl esters, such as methyl propenoate, is missing. According to an experimental study [9] for the decomposition of such small unsaturated esters a significant amount of reactions occur involving smaller compounds. Extending the already developed group additive models towards including ΔGAV^os for these reaction families or adapting the relative seed mechanism [9] will most probably improve the already developed reaction network for the MB pyrolysis.

Additionally, radical recombination reactions and their reverse bond scissions were shown to be very important reaction families in the thermal decomposition of methyl butanoate. However, these types of reactions were not studied in detail in this work. Conventional Transition State Theory (CTST) [10] employed in this study fails to accurately locate the transition state for low-activated and barrierless reactions, such as radical recombination reactions. A computationally more demanding transition state optimization for this type of reactions, Variational Transition State Theory (VTST) [11-13], can provide much better results.

Moreover, the methyl butanoate thermal decomposition reaction network has shown that a significant amount of hydrogen radical addition reactions are involved. In the framework of this study only carbon-centered radical additions and their reverse β-scission reactions are investigated. Since hydrogen radical additions have a different behavior compared to carbon-radical additions, mainly due to the lack of steric hindrance in the transition state of the former reaction type, it is recommended that ΔGAV^os for this type of reactions should be determined.

Furthermore, for all reactions studied in this work, rate coefficients are determined in the high-pressure limit. This approach provides satisfactory results for many reactions involved in thermal decomposition processes of biomass feedstock. However, for very small compounds and especially for some radical recombination reactions or hydrogen radical additions, accounting for pressure dependence of the rate coefficients could improve the accuracy of the calculated rate coefficients [14].

Genesys reaction network generation software [7] uses the HBI method for the determination of ideal gas thermodynamic properties for radical species. However, Benson's group additive method was shown to yield more accurate thermodynamic parameters for hydrocarbon [15, 16] and oxygenate [17] radicals compared to the HBI method. Hence, it is expected that adapting the corresponding Genesys module for the calculation of thermodynamic parameters for radicals using GAVs when available instead of HBI method, would increase the accuracy of the determined thermodynamic parameters. This would most probably result in more accurate reaction networks generated by Genesys.

Approximately, 200 group additivity values and non-nearest-neighbor interactions for the thermochemistry of oxygenates, and 150 group additivity values and corrections for cross-resonance effects for hydrogen abstractions and carbon radical additions involving oxygenates are provided in this work. The majority of these values have never been reported before. However, these data cover only a part of the groups needed to describe complex reaction networks with species other than hydrocarbons, sulfur or oxygenate compounds. For example, some missing groups might be important when investigating multisubstituted species or additional groups will be also required to describe reaction networks containing complex sulfur, nitrogen or phosphorus containing compounds. Extension of the already existing models towards including feedstocks containing cyclic or aromatic components or developing group additive models to cover also hydrogen shifts or radical recombination reactions that remain unexplored in the ab initio level, would be of major importance.

The final conclusion of this work is that ab initio methods can be considered a useful tool for the thermodynamic and kinetic modeling of chemical processes based on the gas phase radical chemistry. The investigation of the thermal decomposition of methyl butanoate and the study of the several reaction pathways involved shows that computational chemistry tools provide better insight into several chemical processes. This can contribute significantly to the direction of optimizing current technologies and introduce new processes involving bio-based feedstock. The future challenge will be to apply the models and methodology developed in this work in the investigation of unexplored reaction conditions, different bio-based feedstock and novel conversion processes.

8.1 References

1. Benson, S.W. and J.H. Buss, *Additivity Rules for the Estimation of Molecular Properties. Thermodynamic Properties.* J Chem Phys, 1958. **29**(9): p. 546-561.
2. Benson, S.W., *Thermochemical Kinetics*. 1968, New York: John Wiley & Sons Ltd.
3. Lay, T.H., J.W. Bozzelli, A.M. Dean, and E.R. Ritter, *Hydrogen-Atom Bond Increments for Calculation of Thermodynamic Properties of Hydrocarbon Radical Species.* J Phys Chem-Us, 1995. **99**(39): p. 14514-14527.
4. Laidler, K.J., *Chemical Kinetics*. 1987, New York: Harper & Row.
5. Eckart, C., *The Penetration of a Potential Barrier by Electrons.* Phys Rev, 1930. **35**: p. 1303-1309.
6. Sabbe, M.K., A.G. Vandeputte, M.F. Reyniers, M. Waroquier, and G.B. Marin, *Modeling the Influence of Resonance Stabilization on the Kinetics of Hydrogen Abstractions.* Phys Chem Chem Phys, 2010. **12**(6): p. 1278-1298.
7. Vandewiele, N.M., K.M. Van Geem, M.F. Reyniers, and G.B. Marin, *Genesys: Kinetic Model Construction Using Chemo-Informatics.* Chem Eng J, 2012. **207**: p. 526-538.
8. Metcalfe, W.K., S.M. Burke, S.S. Ahmed, and H.J. Curran, *A Hierarchical and Comparative Kinetic Modeling Study of C-1 - C-2 Hydrocarbon and Oxygenated Fuels.* Int J Chem Kinet, 2013. **45**(10): p. 638-675.
9. Bennadji, H., L. Coniglio, F. Billaud, R. Bounaceur, V. Warth, P.A. Glaude, and F. Battin-Leclerc, *Oxidation of Small Unsaturated Methyl and Ethyl Esters.* Int J Chem Kinet, 2011. **43**(4): p. 204-218.
10. Eyring, H., *The Activated Complex in Chemical Reactions.* J Chem Phys, 1935. **3**: p. 107-115.
11. Truhlar, D.G. and B.C. Garrett, *Variational Transition-State Theory.* Accounts Chem Res, 1980. **13**(12): p. 440-448.
12. Truhlar, D.G. and B.C. Garrett, *Variational Transition-State Theory.* Annu Rev Phys Chem, 1984. **35**: p. 159-189.
13. Hu, W.P., Y.P. Liu, and D.G. Truhlar, *Variational Transition-State Theory and Semiclassical Tunneling Calculations with Interpolated Corrections - a New Approach to Interfacing Electronic-Structure Theory and Dynamics for Organic-Reactions.* J Chem Soc Faraday T, 1994. **90**(12): p. 1715-1725.
14. Wong, B.M., D.M. Matheu, and W.H. Green, *Temperature and molecular size dependence of the high-pressure limit.* J Phys Chem A, 2003. **107**(32): p. 6206-6211.
15. Sabbe, M.K., M. Saeys, M.F. Reyniers, G.B. Marin, V. Van Speybroeck, and M. Waroquier, *Group additive values for the gas phase standard enthalpy of formation of hydrocarbons and hydrocarbon radicals.* J Phys Chem A, 2005. **109**(33): p. 7466-7480.
16. Sabbe, M.K., F. De Vleeschouwer, M.F. Reyniers, M. Waroquier, and G.B. Marin, *First Principles Based Group Additive Values for the Gas Phase Standard Entropy and Heat Capacity of Hydrocarbons and Hydrocarbon Radicals.* J Phys Chem A, 2008. **112**(47): p. 12235-12251.

17. Paraskevas, P.D., M.K. Sabbe, M.F. Reyniers, N. Papayannakos, and G.B. Marin, *Group Additive Values for the Gas Phase Standard Enthalpy of Formation, Entropy and Heat Capacity of Oxygenates.* Chem-Eur J, 2013. **19**: p. 16431-16452.

Appendix

- Appendix A for Chapter 2 is available online:

http://onlinelibrary.wiley.com/doi/10.1002/chem.201301381/suppinfo

- Appendix B for Chapter 3 is available online:

http://onlinelibrary.wiley.com/doi/10.1002/cphc.201400039/suppinfo

- Appendix C for Chapter 4 is available online:

http://pubs.acs.org/doi/suppl/10.1021/jp503570e

- Appendix D for Chapter 5 is available online:

http://pubs.acs.org/doi/suppl/10.1021/acs.jpca.5b01668

Appendix E

Appendix E for Chapter 6.

1.1 C−C Bond Length Correlation Between B3LYP/CBS-QB3 and IRCMax(CBS-QB3;B3LYP) Method

The determination of transition states for radical additions is generally difficult, mainly due to the increase of the dynamical electron correlation in proceeding from the reactants to the transition state (TS) and the spin contamination of the unrestricted Hartree-Fock wave function at the TS (M. Saeys, M. F. Reyniers, G. B. Marin, V. Van Speybroeck, M. Waroquier *J Phys Chem A*. 2003, 107, 9147-9159).

For the carbon-radical addition reactions to oxygenates studied in this work the transition state is located following the approach proposed by Saeys et al.[1]. Following this methodology the location of the B3LYP/6-311G(d,p) transition state, which is the geometry optimization step within the CBS-QB3 method, is improved using a bond length scaling correlation derived from an IRCMax(CBS-QB3; B3LYP/6-311G(d,p)) analysis. Using this approach, Saeys et al. derived equation (E1) for carbon-centered radical additions between hydrocarbons:

$$C{-}C_{IRCMax} = 0.7381\ C{-}C_{B3LYP} + 58.03\ \text{pm} \qquad \text{if } C{-}C_{B3LYP} > 225\ \text{pm}$$

(E1)

$$C{-}C_{IRCMax} = C{-}C_{B3LYP} - 0.957\ \text{pm} \qquad \text{if } C{-}C_{B3LYP} < 225\ \text{pm}$$

The accuracy of this correlation was evaluated for the reactions of carbon-radical additions to oxygenates studied in this work. To this end, a subset of nine reactions was selected from the training set of 66 reactions studied. The length of the forming C−C bond in the transition state of these nine radical additions ranges from 206.6 to 261.7 pm.

For every reaction included in this subset single-point CBS-QB3 energies were calculated at different points along the B3LYP/6-311G(d,p) intrinsic reaction coordinate (IRC) path. Steps were taken until three consecutive points were found of which the middle one is higher in CBS-QB3 (0 K) energy than the other two. In a next step, a parabola was determined through those three points to locate the transition state, which is called the IRCMax(CBS-QB3; B3LYP/6-311G(d,p)) transition state.

The length of the forming C-C bond in the radical addition transition state derived from the B3LYP/6-311G(d,p) and IRCMax(CBS-QB3; B3LYP/6-311G(d,p)) methods can be found in Table S1. It can be concluded that the overestimation of the B3LYP method is systematic compared to the IRCMax C−C distance. Moreover, equation S1 overestimates most of the data points compared to the IRCMax C−C distance. Hence, the agreement between B3LYP and IRCMax C−C bond lengths can be improved by introducing the linear correlation provided in equation (E2):

$$C{-}C_{IRCMax} = 0.6783\ C{-}C_{B3LYP} + 69.89\ \text{pm} \qquad \text{if } C{-}C_{B3LYP} > 217.25\ \text{pm}$$

(E2)

$$C{-}C_{IRCMax} = C{-}C_{B3LYP}\ \text{pm} \qquad \text{if } C{-}C_{B3LYP} < 217.25\ \text{pm}$$

In Figure E1 the IRCMax C−C distance is plotted versus the corresponding B3LYP value. The improved performance of equation (E2) compared to equation (E1) in correlating B3LYP with IRCMax C−C bond lengths for carbon-radical additions to oxygenates is highlighted in Table S1.

Table S1: Length of the forming C-C bond in the radical addition transition state from the computational methods of B3LYP/6-311G(d,p) and IRCMax(CBS-QB3; B3LYP/6-311G(d,p)) and also the correlation S2. The numbers in the 1st column correspond to the numbering of Table 6-1. Bond distance in pm.

			Reaction			Forming C-C bond in the radical addition transition state		
						B3LYP/6-311G(d,p)	**IRCMax**	**Correlation S2**
1/2	$^{\bullet}CH_3$	+	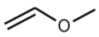	↔		236.6	230.5	230.4
1/6	$^{\bullet}CH_3$	+	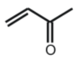	↔	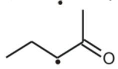	247.1	237.8	237.5
1/17	$^{\bullet}CH_3$	+	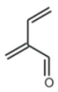	↔	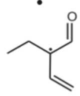	261.7	246.8	247.4
1/21	$^{\bullet}CH_3$	+	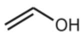	↔	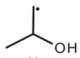	225.9	222.9	223.1
1/26	$^{\bullet}CH_3$	+	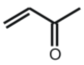	↔	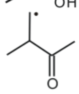	232.7	229.0	227.7
1/41	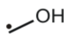	+		↔	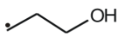	227.9	224.9	224.5
1/46	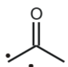	+		↔	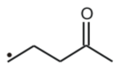	222.3	219.4	220.7
1/53	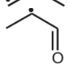	+		↔	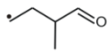	216.8	216.3	216.8
1/57	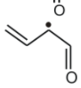	+		↔	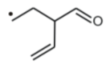	206.6	207.2	206.6

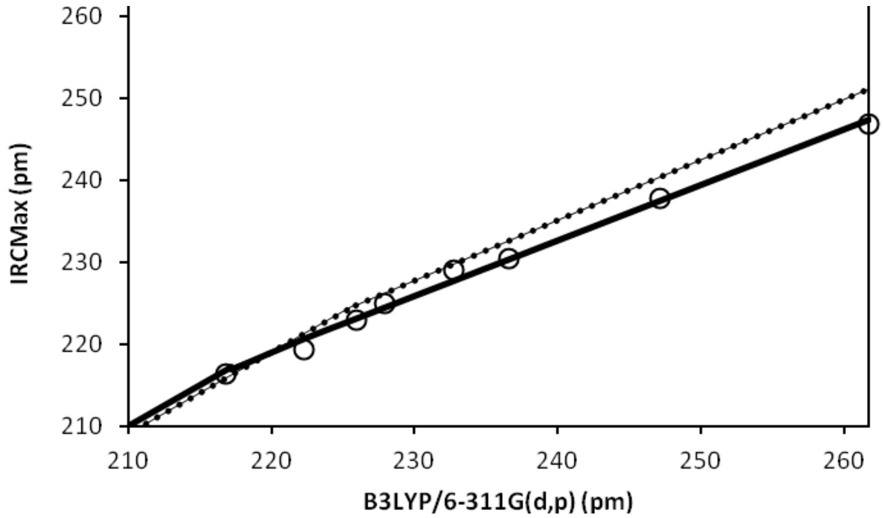

Figure S1: Bond lengths in pm of the forming C-C bond in the radical addition transition state of the carbon-centered radical addition to oxygenates, IRCMax(CBS-QB3; B3LYP/6-311G(d,p)) values versus B3LYP/6-311G(d,p) values using equation S2 (full line) and equation S1 (dotted line).

1.2 Temperature Dependence of ΔGAV°s

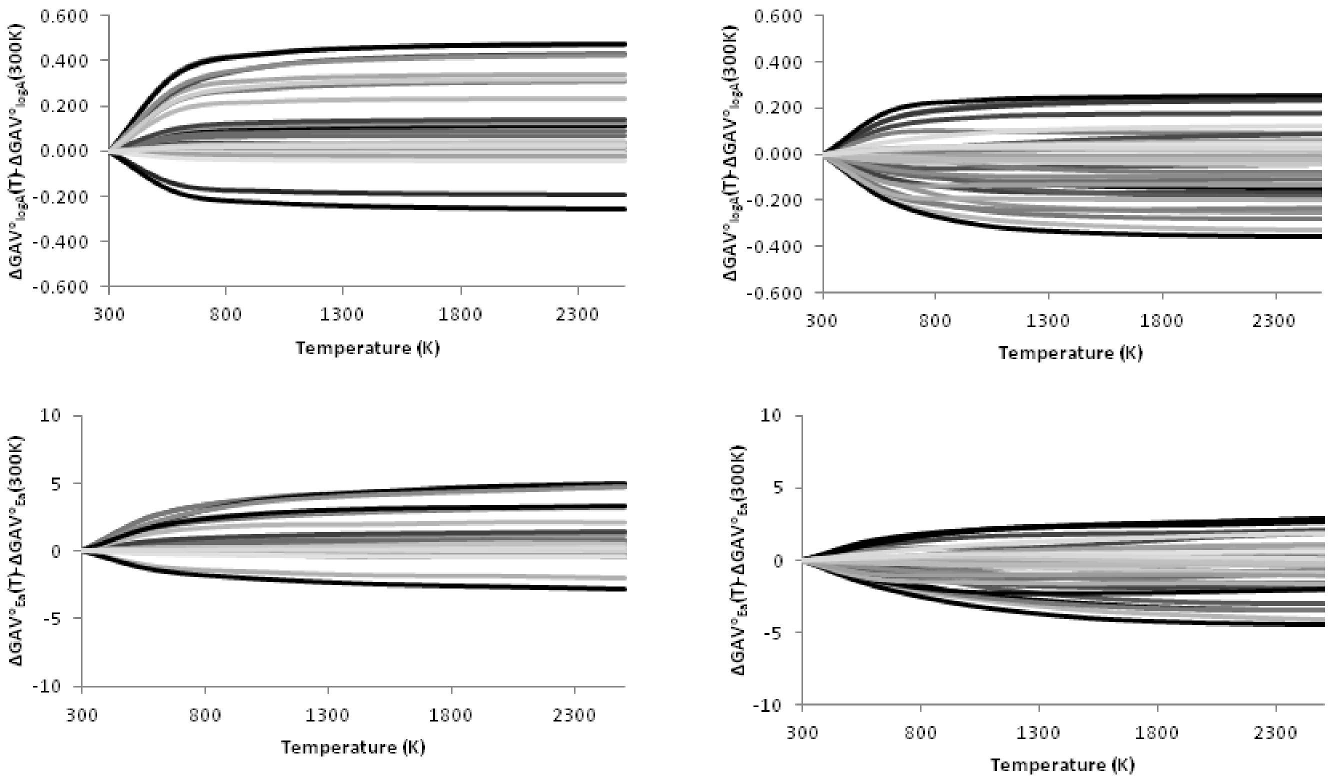

Figure S2: Temperature dependence of the ΔGAV°s presented in Table 6-3. ΔGAV°s for carbon radical additions on the left, ΔGAV°s for the corresponding β-scissions on the right, for $\log\tilde{A}$ on the top line and E_a on the bottom line. $\Delta GAV^{o}_{\log\tilde{A}}$ in $\log(m^3\ mol^{-1}\ s^{-1})$ and ΔGAV^{o}_{Ea} in kJ mol^{-1}. The grey lines are only included to illustrate the very low temperature dependence of the majority of the groups, while the black lines indicate the ΔGAV°s with the strongest temperature dependence, which is still very limited for the whole temperature range.

1.3 Tables

Table S2: Tunneling coefficients κ, standard reaction enthalpies $\Delta_r H^o$ (kJ mol^{-1}), standard reaction entropies $\Delta_r S^o$ (J mol^{-1} K^{-1}), pre-exponential factors log$A$ [log(m^3 mol^{-1} s^{-1})], activation energies E_a (kJ mol^{-1}) and rate coefficients k (m^3 mol^{-1} s^{-1}), at 300 K for the training set of 66 carbon radical additions/β-scissions, from which the primary and secondary contributions are determined. [$k = \kappa A\ exp(-E_a/RT)$]. Arrhenius parameters do not include tunneling contributions.

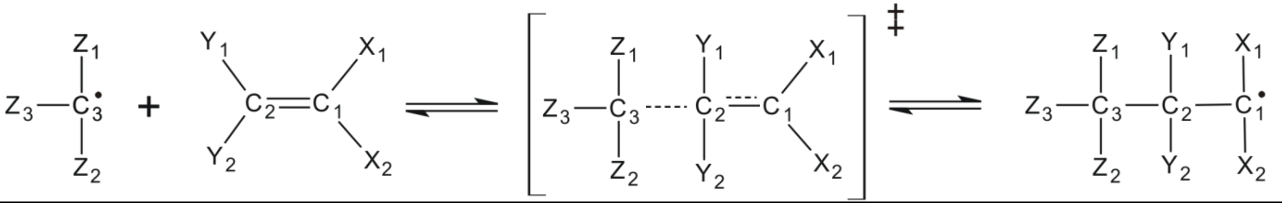

Reactions						κ	addition $\Delta_r H^o$	addition $\Delta_r S^o$	addition log A	addition E_a	addition k_{for}	β-scission log A	β-scission E_a	β-scission k_{rev}
ref	$^{\bullet}CH_3$	+		↔		1.2	-94.6	-90.0	5.785	30.5	3.5E+00	10.485	125.1	6.0E-12
1/1	$^{\bullet}CH_3$	+	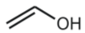	↔	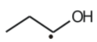	1.3	-95.4	-105.0	5.328	33.9	3.2E-01	10.811	129.3	2.4E-12
1/2	$^{\bullet}CH_3$	+	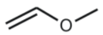	↔		1.3	-96.2	-97.7	5.924	36.3	4.9E-01	11.030	132.5	1.1E-12
1/3	$^{\bullet}CH_3$	+	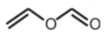	↔	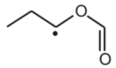	1.3	-103.4	-103.4	5.059	26.6	3.3E+00	10.460	130.0	8.2E-13
1/4	$^{\bullet}CH_3$	+	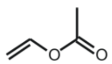	↔	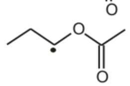	1.3	-102.0	-102.2	5.222	27.1	3.9E+00	10.559	129.1	1.4E-12
1/5	$^{\bullet}CH_3$	+	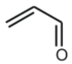	↔		1.2	-134.9	-108.9	4.995	8.9	3.1E+03	10.686	143.8	5.1E-15
1/6	$^{\bullet}CH_3$	+	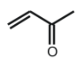	↔	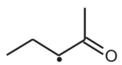	1.2	-128.8	-95.8	5.209	14.7	5.0E+02	10.213	143.5	1.9E-15
1/7	$^{\bullet}CH_3$	+	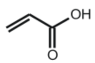	↔	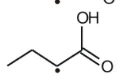	1.2	-118.2	-103.9	5.129	16.8	1.8E+02	10.554	135.0	1.3E-13

1/8	$^{\bullet}CH_3$	+	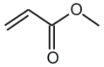	↔	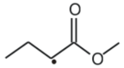	1.2	-117.6	-105.2	5.010	17.5	1.1E+02	10.506	135.1	1.1E-13
1/9	$^{\bullet}CH_3$	+	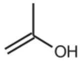	↔	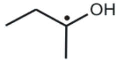	1.3	-93.3	-105.8	5.277	30.0	1.4E+00	10.804	123.3	2.7E-11
1/10	$^{\bullet}CH_3$	+	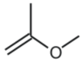	↔	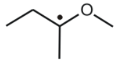	1.2	-87.6	-101.8	5.438	46.3	2.9E-03	10.754	133.9	3.3E-13
1/11	$^{\bullet}CH_3$	+	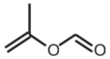	↔	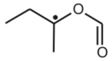	1.3	-101.1	-104.5	5.149	26.7	3.9E+00	10.608	127.8	2.8E-12
1/12	$^{\bullet}CH_3$	+	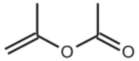	↔	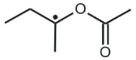	1.3	-97.7	-99.8	5.178	24.7	9.3E+00	10.393	122.4	1.5E-11
1/13	$^{\bullet}CH_3$	+	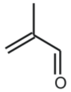	↔	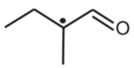	1.2	-130.8	-104.5	5.326	16.1	3.9E+02	10.786	146.9	1.8E-15
1/14	$^{\bullet}CH_3$	+	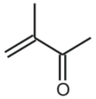	↔	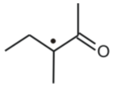	1.2	-129.4	-102.2	5.172	15.8	3.1E+02	10.508	145.2	1.9E-15
1/15	$^{\bullet}CH_3$	+	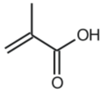	↔	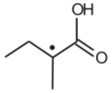	1.2	-124.7	-96.5	5.201	16.4	2.5E+02	10.241	141.1	5.3E-15
1/16	$^{\bullet}CH_3$	+	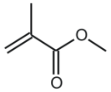	↔	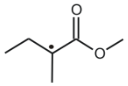	1.2	-124.9	-110.0	5.121	16.6	2.0E+02	10.866	141.5	1.9E-14
1/17	$^{\bullet}CH_3$	+	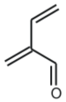	↔	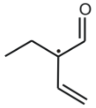	1.1	-174.6	-109.9	5.436	7.4	1.5E+04	11.178	182.0	3.4E-21
1/18	$^{\bullet}CH_3$	+	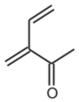	↔	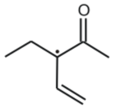	1.1	-173.3	-116.0	5.050	5.9	1.1E+04	11.107	179.2	8.7E-21
1/19	$^{\bullet}CH_3$	+	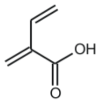	↔	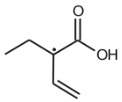	1.1	-169.9	-116.0	5.185	6.6	1.2E+04	11.242	176.5	3.4E-20
1/20	$^{\bullet}CH_3$	+	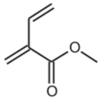	↔	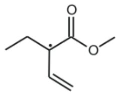	1.1	-168.9	-119.7	4.985	6.7	7.0E+03	11.239	175.6	5.0E-20
1/21	$^{\bullet}CH_3$	+	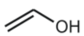	↔	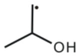	1.4	-80.8	-103.8	5.010	42.9	4.6E-03	10.430	123.7	1.0E-11
1/22	$^{\bullet}CH_3$	+	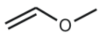	↔	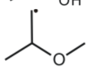	1.4	-81.4	-104.7	5.313	44.6	4.6E-03	10.782	126.0	9.3E-12

1/23	$^{\bullet}CH_3$	+	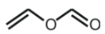	↔	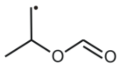	1.4	-100.4	-104.9	4.681	31.6	2.0E-01	10.161	132.0	2.0E-13
1/24	$^{\bullet}CH_3$	+	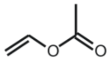	↔	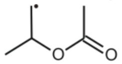	1.4	-98.8	-101.7	4.640	31.8	1.7E-01	9.951	130.6	2.2E-13
1/25	$^{\bullet}CH_3$	+	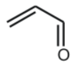	↔	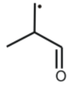	1.2	-92.8	-106.5	4.814	23.0	7.7E+00	10.376	115.8	2.0E-10
1/26	$^{\bullet}CH_3$	+	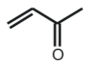	↔	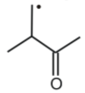	1.2	-91.3	-106.2	4.833	24.1	5.1E+00	10.379	115.4	2.4E-10
1/27	$^{\bullet}CH_3$	+	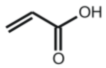	↔	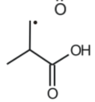	1.3	-89.4	-103.2	4.798	25.2	3.1E+00	10.190	114.6	2.1E-10
1/28	$^{\bullet}CH_3$	+	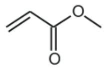	↔	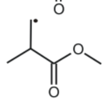	1.3	-89.6	-103.4	4.847	25.3	3.4E+00	10.247	114.9	2.2E-10
1/29	$^{\bullet}CH_3$	+	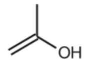	↔	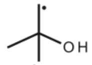	1.4	-74.0	-104.1	4.717	47.0	4.7E-04	10.153	121.0	1.7E-11
1/30	$^{\bullet}CH_3$	+	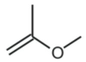	↔	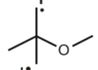	1.4	-71.1	-109.4	4.695	46.9	4.7E-04	10.409	118.0	1.0E-10
1/31	$^{\bullet}CH_3$	+	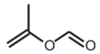	↔	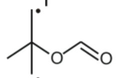	1.5	-99.1	-119.2	4.389	41.9	1.7E-03	10.615	141.0	1.7E-14
1/32	$^{\bullet}CH_3$	+	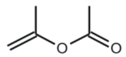	↔	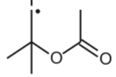	1.5	-97.7	-117.4	4.411	42.1	1.7E-03	10.546	139.8	2.3E-14
1/33	$^{\bullet}CH_3$	+	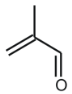	↔	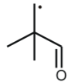	1.3	-78.0	-114.2	4.585	31.9	1.3E-01	10.548	109.9	3.2E-09
1/34	$^{\bullet}CH_3$	+	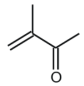	↔	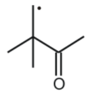	1.3	-81.7	-115.5	4.379	30.8	1.3E-01	10.412	112.5	8.4E-10
1/35	$^{\bullet}CH_3$	+	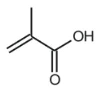	↔	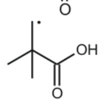	1.3	-83.7	-112.7	4.460	30.0	2.2E-01	10.347	113.7	4.6E-10
1/36	$^{\bullet}CH_3$	+	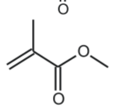	↔	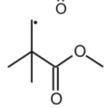	1.3	-84.7	-113.1	4.474	29.7	2.5E-01	10.381	114.4	3.7E-10

1/37	$^{\bullet}CH_3$	+	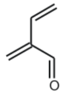	↔	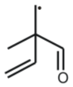	1.3	-71.6	-106.5	5.005	30.4	6.2E-01	10.567	102.0	8.0E-08
1/38	$^{\bullet}CH_3$	+	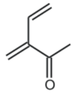	↔	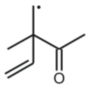	1.3	-79.9	-112.1	4.810	28.0	1.1E+00	10.668	107.9	9.5E-09
1/39	$^{\bullet}CH_3$	+	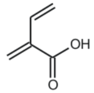	↔	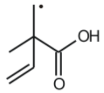	1.3	-76.7	-111.2	4.700	28.2	7.5E-01	10.507	104.9	2.2E-08
1/40	$^{\bullet}CH_3$	+	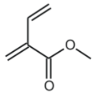	↔	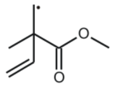	1.3	-76.4	-113.8	4.573	27.9	6.3E-01	10.515	104.3	2.9E-08
1/41	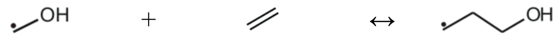					1.2	-83.5	-106.9	5.016	28.2	1.5E+00	10.600	111.7	1.7E-09
1/42						1.2	-77.4	-95.5	4.955	28.8	1.0E+00	9.944	106.2	3.3E-09
1/43						1.2	-96.4	-106.4	4.633	25.2	2.1E+00	10.192	121.6	1.3E-11
1/44						1.2	-95.2	-106.8	4.669	25.3	2.1E+00	10.246	120.5	2.2E-11
1/45	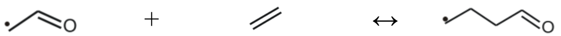					1.3	-63.7	-97.7	5.121	29.4	1.2E+00	10.224	93.1	1.3E-06
1/46	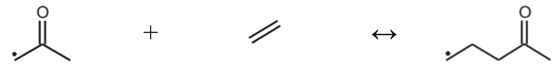					1.3	-68.4	-102.1	4.949	26.6	2.5E+00	10.283	95.0	7.0E-07
1/47						1.2	-79.8	-93.4	5.125	22.2	2.2E+01	10.005	102.0	2.2E-08
1/48	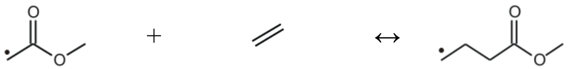					1.3	-79.2	-94.3	5.093	22.7	1.6E+01	10.018	101.9	2.3E-08
1/49						1.2	-81.0	-114.3	4.552	21.6	6.9E+00	10.524	102.6	5.1E-08
1/50						1.2	-78.1	-110.8	4.746	23.2	5.8E+00	10.535	101.3	9.3E-08
1/51						1.2	-94.4	-117.4	4.466	19.1	1.6E+01	10.597	113.5	8.2E-10
1/52						1.2	-93.9	-116.7	4.337	18.7	1.4E+01	10.432	112.6	8.0E-10
1/53						1.3	-47.2	-105.7	4.618	34.2	5.7E-02	10.140	81.4	1.2E-04
1/54	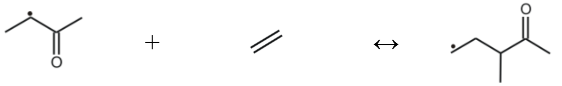					1.3	-49.4	-126.3	3.735	30.3	3.5E-02	10.330	79.7	3.7E-04

1/55	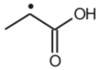	+		↔	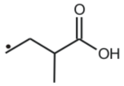	1.3	-63.0	-108.9	4.530	25.2	1.6E+00	10.219	88.2	9.3E-06
1/56	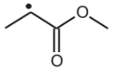	+		↔	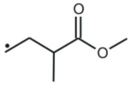	1.3	-64.2	-106.6	4.540	25.3	1.6E+00	10.111	89.5	4.3E-06
1/57	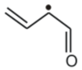	+		↔	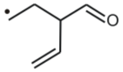	1.4	-2.5	-97.4	4.718	58.4	4.7E-06	9.804	60.9	2.2E-01
1/58	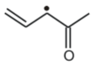	+		↔	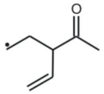	1.4	-5.1	-105.2	4.419	49.9	7.1E-05	9.912	55.0	3.0E+00
1/59	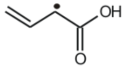	+		↔	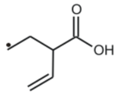	1.4	-11.9	-92.0	4.686	50.1	1.2E-04	9.494	62.0	6.9E-02
1/60	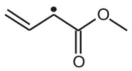	+		↔	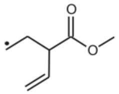	1.4	-13.0	-90.0	4.669	49.7	1.4E-04	9.371	62.7	4.0E-02
1/61	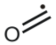	+		↔	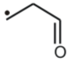	1.2	-70.7	-96.5	5.187	27.9	2.5E+00	10.226	98.6	1.3E-07
1/62	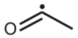	+		↔	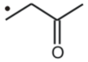	1.1	-70.1	-105.2	5.131	23.9	9.1E+00	10.628	94.0	1.9E-06
1/63	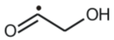	+		↔	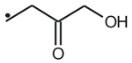	1.1	-84.3	-109.8	5.213	23.8	2.4E+01	10.947	108.1	2.9E-08
1/64	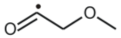	+		↔	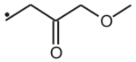	1.2	-73.4	-99.2	5.035	26.1	3.4E+00	10.215	99.5	8.9E-08
1/65	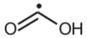	+		↔	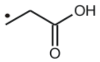	1.1	-117.1	-103.1	5.478	14.3	1.3E+03	10.865	131.4	1.4E-12
1/66	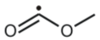	+		↔	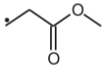	1.1	-114.4	-106.0	5.417	15.1	7.9E+02	10.956	129.5	3.6E-12

Table S3: Standard reaction enthalpies $\Delta_r H^o$ (kJ mol^{-1}), standard reaction entropies $\Delta_r S^o$ (J mol^{-1} K^{-1}), pre-exponential factors log$A$ [log(m^3 mol^{-1} s^{-1})], activation energies E_a (kJ mol^{-1}) and rate coefficients k (m^3 mol^{-1} s^{-1}), at 600 K for the training set of 66 carbon radical additions/β-scissions, from which the primary and secondary contributions are determined. [$k = \kappa A\ exp(-E_a/RT)$]. Arrhenius parameters do not include tunneling contributions.

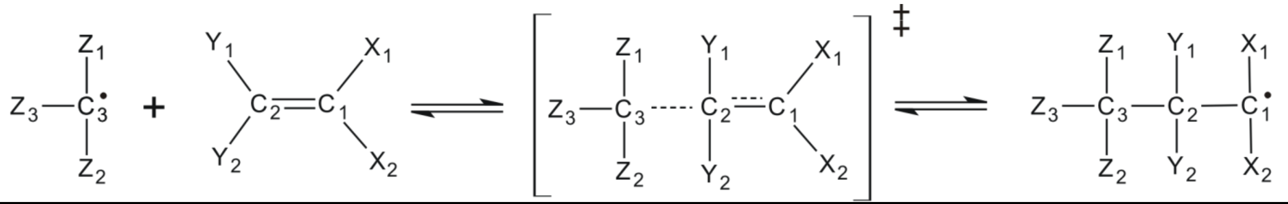

Reactions						addition					β-scission		
						$\Delta_r H^o$	$\Delta_r S^o$	log A	E_a	k_{for}	log A	E_a	k_{rev}
ref	$^\bullet CH_3$	+		↔		-92.1	-84.6	6.342	35.2	2.0E+03	10.759	127.3	5.0E-01
1/1	$^\bullet CH_3$	+	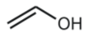	↔		-93.7	-101.4	5.930	38.9	3.6E+02	11.227	132.6	5.1E-01
1/2	$^\bullet CH_3$	+	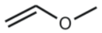	↔		-94.5	-93.9	6.540	41.4	9.0E+02	11.445	135.9	4.4E-01
1/3	$^\bullet CH_3$	+	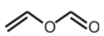	↔	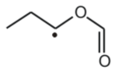	-101.5	-99.3	5.613	31.2	8.2E+02	10.799	132.7	1.9E-01
1/4	$^\bullet CH_3$	+	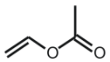	↔	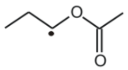	-100.3	-98.5	5.779	31.8	1.1E+03	10.922	132.1	2.8E-01
1/5	$^\bullet CH_3$	+	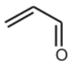	↔		-133.1	-105.2	5.546	13.5	2.4E+04	11.040	146.6	2.0E-02
1/6	$^\bullet CH_3$	+	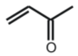	↔	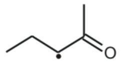	-127.4	-93.0	5.783	19.5	1.2E+04	10.641	146.9	7.3E-03
1/7	$^\bullet CH_3$	+	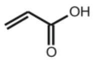	↔	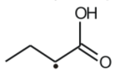	-115.8	-98.7	5.701	21.6	6.8E+03	10.856	137.4	8.2E-02
1/8	$^\bullet CH_3$	+	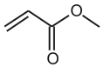	↔	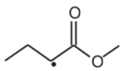	-115.9	-101.7	5.571	22.2	4.5E+03	10.884	138.1	7.6E-02
1/9	$^\bullet CH_3$	+	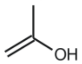	↔	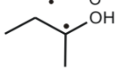	-92.0	-103.3	5.819	34.5	6.8E+02	11.215	126.5	1.7E+00
1/10	$^\bullet CH_3$	+	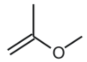	↔	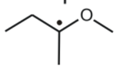	-105.5	-104.6	5.727	31.8	9.5E+02	11.189	137.3	1.8E-01
1/11	$^\bullet CH_3$	+	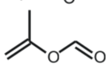	↔	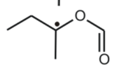	-99.8	-101.9	5.703	31.3	1.0E+03	11.024	131.1	4.3E-01

1/12	$^{\bullet}CH_3$	+	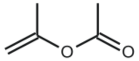	↔	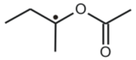	-96.4	-97.2	5.716	29.2	1.6E+03	10.796	125.6	7.7E-01
1/13	$^{\bullet}CH_3$	+	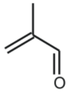	↔	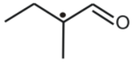	-129.6	-102.1	5.889	20.8	1.2E+04	11.223	150.4	1.4E-02
1/14	$^{\bullet}CH_3$	+	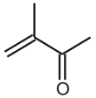	↔	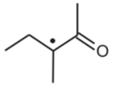	-128.2	-99.5	5.732	20.4	9.2E+03	10.930	148.6	1.0E-02
1/15	$^{\bullet}CH_3$	+	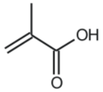	↔	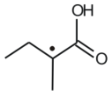	-123.2	-93.4	5.776	21.2	8.8E+03	10.656	144.4	1.3E-02
1/16	$^{\bullet}CH_3$	+	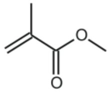	↔	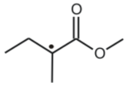	-123.5	-107.2	5.695	21.4	7.0E+03	11.295	144.9	5.0E-02
1/17	$^{\bullet}CH_3$	+	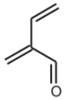	↔	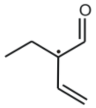	-173.1	-107.1	6.049	12.5	9.2E+04	11.644	185.6	3.1E-05
1/18	$^{\bullet}CH_3$	+	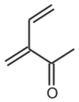	↔	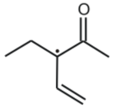	-171.9	-113.3	5.645	10.9	5.0E+04	11.564	182.8	4.5E-05
1/19	$^{\bullet}CH_3$	+	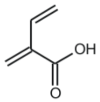	↔	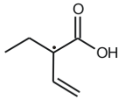	-168.4	-112.9	5.823	11.9	6.2E+04	11.722	180.3	1.1E-04
1/20	$^{\bullet}CH_3$	+	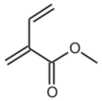	↔	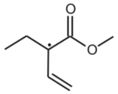	-167.1	-116.1	5.622	12.0	3.8E+04	11.685	179.1	1.3E-04
1/21	$^{\bullet}CH_3$	+	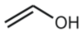	↔	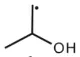	-77.3	-95.8	5.651	48.2	3.0E+01	10.653	125.5	5.8E-01
1/22	$^{\bullet}CH_3$	+	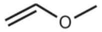	↔	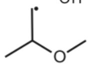	-78.0	-97.1	5.952	49.9	4.3E+01	11.025	127.9	8.3E-01
1/23	$^{\bullet}CH_3$	+	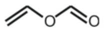	↔	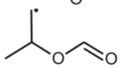	-97.2	-97.8	5.305	36.8	1.3E+02	10.412	134.0	6.1E-02

1/24	$^{\bullet}CH_3$	+	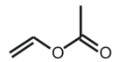	↔	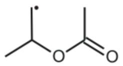	-95.7	-94.6	5.263	37.0	1.2E+02	10.207	132.7	4.9E-02
1/25	$^{\bullet}CH_3$	+	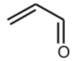	↔	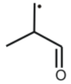	-89.7	-99.6	5.388	27.8	9.7E+02	10.592	117.5	2.4E+00
1/26	$^{\bullet}CH_3$	+	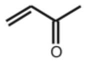	↔	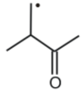	-88.2	-99.2	5.410	28.9	8.1E+02	10.593	117.1	2.6E+00
1/27	$^{\bullet}CH_3$	+	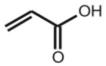	↔	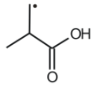	-86.0	-95.6	5.395	30.2	6.1E+02	10.390	116.2	2.0E+00
1/28	$^{\bullet}CH_3$	+	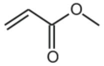	↔	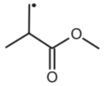	-86.4	-96.2	5.449	30.3	6.8E+02	10.472	116.7	2.2E+00
1/29	$^{\bullet}CH_3$	+	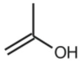	↔	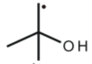	-69.6	-94.3	5.367	52.4	6.9E+00	10.293	122.0	5.1E-01
1/30	$^{\bullet}CH_3$	+	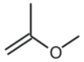	↔	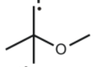	-67.1	-100.2	5.328	52.1	6.7E+00	10.561	119.2	1.7E+00
1/31	$^{\bullet}CH_3$	+	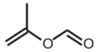	↔	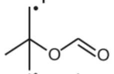	-95.4	-110.8	5.046	47.3	9.1E+00	10.833	142.7	2.8E-02
1/32	$^{\bullet}CH_3$	+	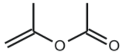	↔	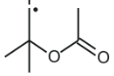	-94.0	-109.2	5.072	47.6	9.2E+00	10.777	141.6	3.1E-02
1/33	$^{\bullet}CH_3$	+	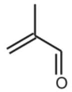	↔	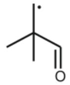	-74.3	-105.9	5.210	37.1	1.0E+02	10.741	111.4	1.2E+01
1/34	$^{\bullet}CH_3$	+	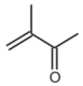	↔	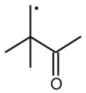	-77.9	-106.9	4.995	35.9	7.7E+01	10.580	113.8	5.0E+00
1/35	$^{\bullet}CH_3$	+	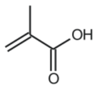	↔	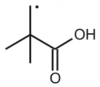	-79.8	-104.2	5.097	35.3	1.1E+02	10.539	115.1	3.5E+00
1/36	$^{\bullet}CH_3$	+	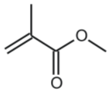	↔	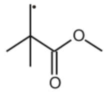	-80.9	-104.5	5.116	35.0	1.2E+02	10.576	115.9	3.3E+00
1/37	$^{\bullet}CH_3$	+	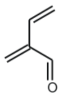	↔	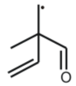	-67.4	-97.0	5.672	35.9	3.7E+02	10.740	103.3	5.9E+01
1/38	$^{\bullet}CH_3$	+	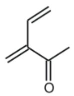	↔	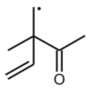	-76.1	-103.4	5.445	33.2	3.7E+02	10.846	109.3	2.3E+01

1/39	$^{\bullet}CH_3$	+	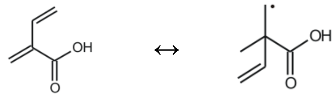	-72.5	-101.7	5.378	33.8	2.9E+02	10.692	106.3	2.9E+01
1/40	$^{\bullet}CH_3$	+	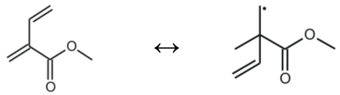	-71.5	-102.7	5.257	33.6	2.3E+02	10.623	105.1	3.2E+01
1/41	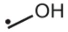	+	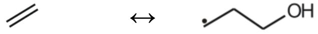	-79.0	-96.9	5.779	34.5	6.2E+02	10.843	113.5	9.6E+00
1/42	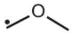	+	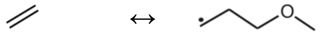	-73.0	-85.2	5.627	34.3	4.5E+02	10.080	107.3	5.7E+00
1/43	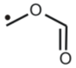	+	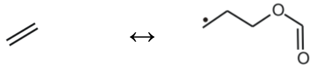	-92.8	-98.2	5.212	30.0	4.1E+02	10.341	122.8	4.7E-01
1/44	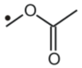	+	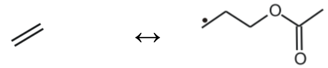	-91.4	-98.4	5.262	30.3	4.4E+02	10.402	121.7	6.7E-01
1/45	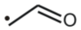	+	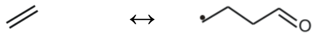	-58.0	-84.5	5.880	35.6	6.3E+02	10.296	93.6	1.5E+02
1/46	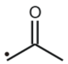	+	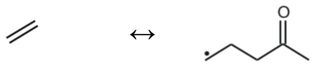	-62.5	-88.3	5.700	32.7	7.4E+02	10.311	95.2	1.1E+02
1/47	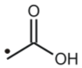	+	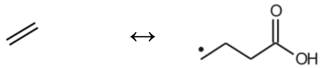	-75.1	-82.5	5.832	28.0	2.6E+03	10.141	103.1	1.5E+01
1/48	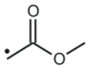	+	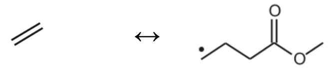	-74.1	-82.4	5.810	28.6	2.2E+03	10.116	102.7	1.6E+01
1/49	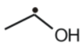	+	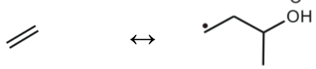	-75.6	-101.7	5.483	29.1	9.1E+02	10.793	104.7	5.0E+01
1/50	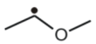	+	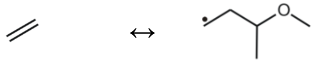	-72.3	-97.5	5.471	29.2	8.8E+02	10.565	101.5	5.6E+01
1/51	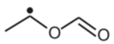	+	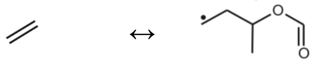	-89.2	-105.5	5.189	25.1	1.1E+03	10.699	114.3	5.9E+00
1/52	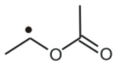	+	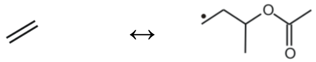	-88.6	-104.6	5.077	24.8	8.6E+02	10.542	113.4	4.9E+00
1/53	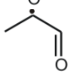	+	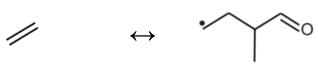	-41.0	-91.3	5.439	40.9	8.0E+01	10.206	81.9	1.3E+03
1/54	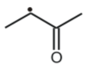	+	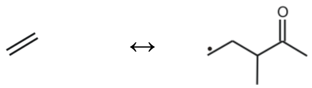	-42.8	-110.9	4.545	36.9	2.2E+01	10.336	79.7	2.7E+03

1/55	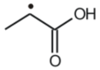	+		↔	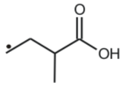	-57.3	-95.9	5.322	31.7	3.8E+02	10.333	89.0	4.1E+02
1/56	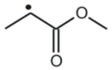	+		↔	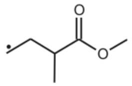	-58.4	-93.3	5.347	31.9	3.9E+02	10.221	90.3	2.4E+02
1/57	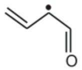	+		↔	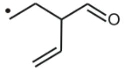	3.8	-82.7	5.604	65.6	8.4E-01	9.922	61.8	3.8E+04
1/58	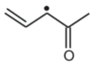	+		↔	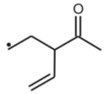	1.4	-90.0	5.383	57.7	2.5E+00	10.083	56.3	1.7E+05
1/59	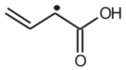	+		↔	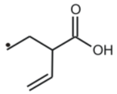	-5.8	-77.6	5.555	57.1	4.1E+00	9.610	62.9	1.5E+04
1/60	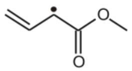	+		↔	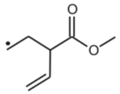	-6.6	-75.0	5.543	56.8	4.2E+00	9.462	63.4	9.6E+03
1/61	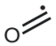	+		↔	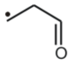	-66.2	-86.0	6.021	34.7	1.0E+03	10.514	100.9	5.6E+01
1/62	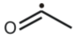	+		↔	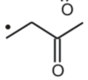	-64.8	-93.0	5.977	31.0	1.9E+03	10.836	95.8	3.2E+02
1/63	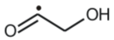	+		↔	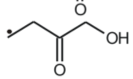	-79.6	-99.3	6.041	30.5	3.4E+03	11.228	110.1	6.1E+01
1/64	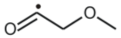	+		↔	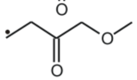	-67.4	-85.2	5.952	33.6	1.1E+03	10.404	101.0	4.2E+01
1/65	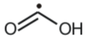	+		↔	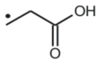	-111.5	-89.9	6.265	20.7	3.3E+04	10.963	132.2	3.3E-01
1/66	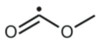	+		↔	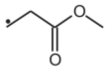	-108.7	-93.0	6.221	21.6	2.4E+04	11.079	130.3	6.0E-01

Table S4: Standard reaction enthalpies $\Delta_r H^o$ (kJ mol^{-1}), standard reaction entropies $\Delta_r S^o$ (J mol^{-1} K^{-1}), pre-exponential factors log*A* [log(m^3 mol^{-1} s^{-1})], activation energies E_a (kJ mol^{-1}) and rate coefficients *k* (m^3 mol^{-1} s^{-1}), at 1000 K for the training set of 66 carbon radical additions/*β*-scissions, from which the primary and secondary contributions are determined. [$k = \kappa A\ exp(-E_a/RT)$]. Arrhenius parameters do not include tunneling contributions.

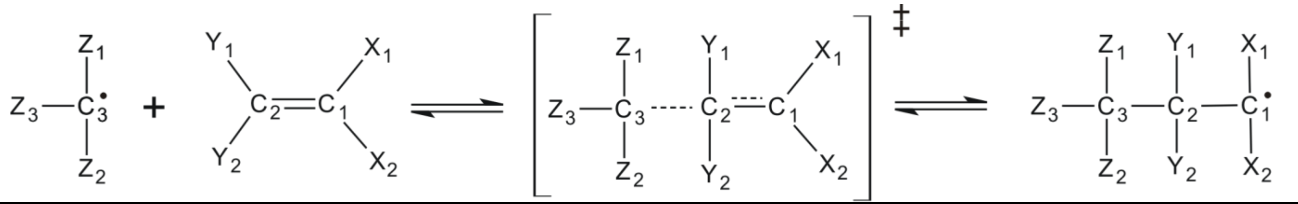

Reactions						addition					*β*-scission		
						$\Delta_r H^o$	$\Delta_r S^o$	log *A*	E_a	k_{for}	log *A*	E_a	k_{rev}
ref	$^\bullet CH_3$	+		↔		-85.4	-76.1	6.871	43.1	4.2E+04	10.848	128.5	1.4E+04
1/1	$^\bullet CH_3$	+	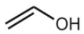	↔		-87.6	-93.8	6.462	46.9	1.0E+04	11.362	134.5	2.2E+04
1/2	$^\bullet CH_3$	+	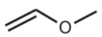	↔		-88.4	-86.3	7.075	49.4	3.2E+04	11.581	137.8	2.5E+04
1/3	$^\bullet CH_3$	+	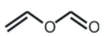	↔	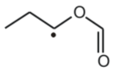	-95.2	-91.5	6.136	39.1	1.3E+04	10.914	134.3	8.1E+03
1/4	$^\bullet CH_3$	+	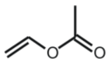	↔	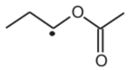	-94.4	-91.0	6.301	39.6	1.7E+04	11.056	134.0	1.2E+04
1/5	$^\bullet CH_3$	+	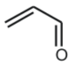	↔		-126.3	-96.8	6.068	21.4	9.0E+04	11.123	147.7	2.6E+03
1/6	$^\bullet CH_3$	+	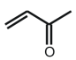	↔	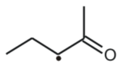	-121.6	-85.6	6.310	27.4	7.6E+04	10.784	149.0	1.0E+03
1/7	$^\bullet CH_3$	+	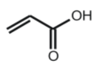	↔	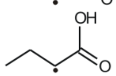	-108.8	-89.9	6.228	29.5	4.9E+04	10.922	138.3	5.1E+03
1/8	$^\bullet CH_3$	+	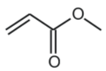	↔	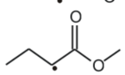	-109.1	-93.1	6.095	30.0	3.4E+04	10.957	139.1	5.0E+03

1/9	$^{\bullet}CH_3$	+	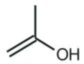	↔	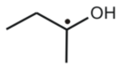	-86.4	-96.2	6.329	42.2	1.4E+04	11.356	128.6	4.5E+04
1/10	$^{\bullet}CH_3$	+	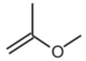	↔	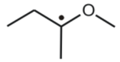	-100.0	-97.6	6.241	39.5	1.5E+04	11.340	139.5	1.2E+04
1/11	$^{\bullet}CH_3$	+	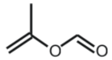	↔	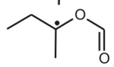	-94.2	-94.8	6.220	39.0	1.5E+04	11.171	133.2	1.7E+04
1/12	$^{\bullet}CH_3$	+	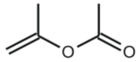	↔	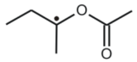	-90.8	-90.2	6.231	36.9	2.0E+04	10.944	127.7	1.9E+04
1/13	$^{\bullet}CH_3$	+	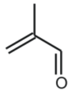	↔	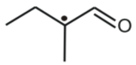	-124.0	-95.0	6.412	28.6	8.4E+04	11.373	152.6	2.6E+03
1/14	$^{\bullet}CH_3$	+	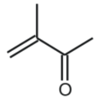	↔	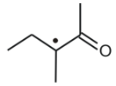	-122.1	-92.0	6.254	28.3	6.1E+04	11.061	150.4	1.6E+03
1/15	$^{\bullet}CH_3$	+	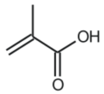	↔	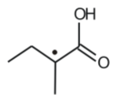	-117.2	-85.7	6.300	29.0	6.1E+04	10.779	146.2	1.4E+03
1/16	$^{\bullet}CH_3$	+	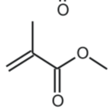	↔	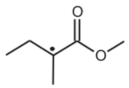	-117.6	-99.7	6.220	29.2	5.0E+04	11.426	146.8	5.9E+03
1/17	$^{\bullet}CH_3$	+	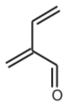	↔	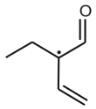	-166.9	-99.3	6.589	20.6	3.3E+05	11.777	187.5	9.7E+01
1/18	$^{\bullet}CH_3$	+	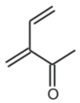	↔	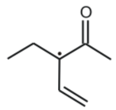	-165.9	-105.8	6.177	18.9	1.6E+05	11.704	184.8	1.1E+02
1/19	$^{\bullet}CH_3$	+	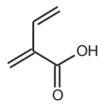	↔	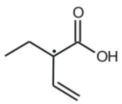	-162.5	-105.4	6.367	20.0	2.1E+05	11.874	182.5	2.2E+02
1/20	$^{\bullet}CH_3$	+	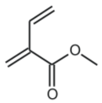	↔	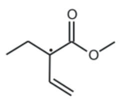	-160.3	-107.4	6.166	20.1	1.3E+05	11.777	180.4	2.3E+02
1/21	$^{\bullet}CH_3$	+	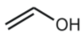	↔	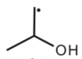	-69.7	-86.1	6.200	56.4	1.8E+03	10.697	126.1	1.3E+04
1/22	$^{\bullet}CH_3$	+	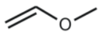	↔	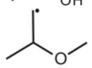	-70.7	-87.8	6.502	58.2	3.0E+03	11.090	128.9	2.4E+04
1/23	$^{\bullet}CH_3$	+	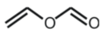	↔	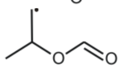	-89.8	-88.5	5.851	45.0	3.2E+03	10.472	134.8	2.8E+03

1/24	$^{\bullet}CH_3$	+	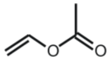	↔	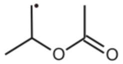	-88.6	-85.6	5.808	45.1	2.9E+03	10.278	133.7	2.0E+03
1/25	$^{\bullet}CH_3$	+	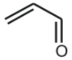	↔	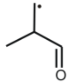	-82.9	-91.0	5.920	35.7	1.1E+04	10.672	118.6	3.0E+04
1/26	$^{\bullet}CH_3$	+	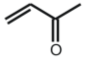	↔	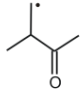	-81.4	-90.6	5.942	36.9	1.0E+04	10.676	118.3	3.2E+04
1/27	$^{\bullet}CH_3$	+	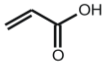	↔	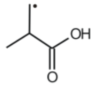	-78.7	-86.3	5.932	38.2	8.8E+03	10.442	116.9	2.2E+04
1/28	$^{\bullet}CH_3$	+	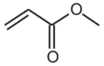	↔	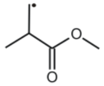	-79.4	-87.4	5.987	38.4	9.8E+03	10.550	117.8	2.5E+04
1/29	$^{\bullet}CH_3$	+	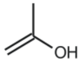	↔	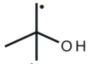	-61.3	-83.7	5.915	60.6	5.8E+02	10.287	121.9	8.6E+03
1/30	$^{\bullet}CH_3$	+	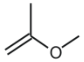	↔	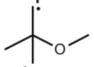	-59.2	-90.1	5.874	60.3	5.5E+02	10.582	119.5	2.3E+04
1/31	$^{\bullet}CH_3$	+	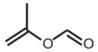	↔	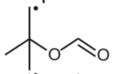	-87.8	-101.1	5.596	55.5	5.1E+02	10.876	143.3	2.6E+03
1/32	$^{\bullet}CH_3$	+	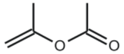	↔	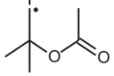	-86.5	-99.6	5.624	55.8	5.2E+02	10.826	142.3	2.6E+03
1/33	$^{\bullet}CH_3$	+	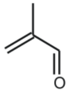	↔	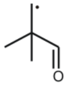	-67.1	-96.6	5.753	45.2	2.5E+03	10.798	112.3	8.8E+04
1/34	$^{\bullet}CH_3$	+	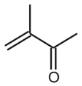	↔	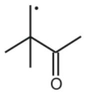	-70.4	-97.4	5.534	44.0	1.8E+03	10.620	114.4	4.5E+04
1/35	$^{\bullet}CH_3$	+	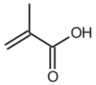	↔	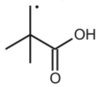	-72.3	-94.5	5.642	43.4	2.4E+03	10.579	115.7	3.5E+04
1/36	$^{\bullet}CH_3$	+	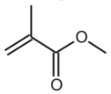	↔	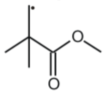	-73.3	-94.9	5.663	43.2	2.6E+03	10.619	116.5	3.5E+04

1/37	$^{\bullet}CH_3$ + 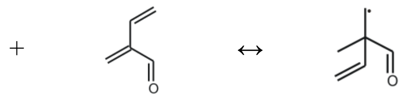	-59.6	-87.0	6.229	44.2	8.4E+03	10.776	103.8	2.3E+05
1/38	$^{\bullet}CH_3$ + 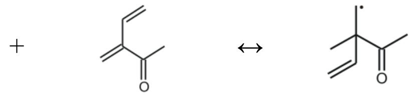	-68.5	-93.8	5.989	41.4	6.9E+03	10.889	109.9	1.4E+05
1/39	$^{\bullet}CH_3$ + 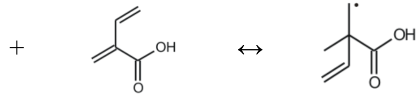	-64.7	-91.7	5.937	42.1	5.5E+03	10.729	106.8	1.4E+05
1/40	$^{\bullet}CH_3$ + 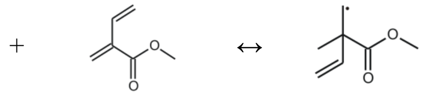	-63.1	-91.9	5.816	41.9	4.3E+03	10.615	105.0	1.4E+05
1/41	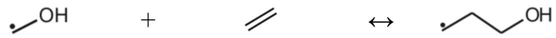	-70.7	-86.3	6.357	43.1	1.3E+04	10.867	113.8	8.5E+04
1/42	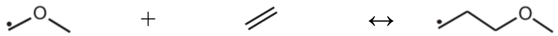	-65.0	-75.1	6.187	42.7	9.2E+03	10.109	107.7	3.1E+04
1/43		-85.2	-88.7	5.743	38.0	5.8E+03	10.374	123.2	8.8E+03
1/44	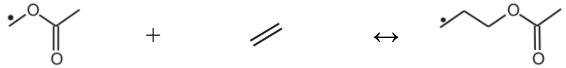	-83.8	-88.8	5.796	38.3	6.4E+03	10.433	122.1	1.2E+04
1/45	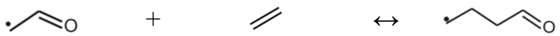	-49.6	-73.7	6.448	44.1	1.4E+04	10.299	93.7	2.6E+05
1/46	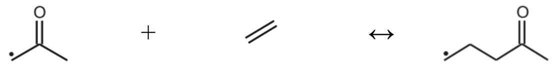	-54.0	-77.3	6.267	41.2	1.3E+04	10.307	95.2	2.2E+05
1/47	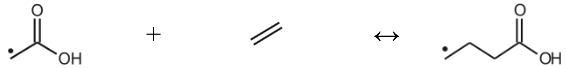	-67.3	-72.6	6.388	36.3	3.2E+04	10.180	103.6	6.0E+04
1/48		-66.0	-72.1	6.369	37.0	2.8E+04	10.135	103.0	5.8E+04
1/49		-66.6	-90.1	6.094	38.2	1.3E+04	10.803	104.8	2.2E+05
1/50		-63.3	-85.9	6.045	37.7	1.2E+04	10.533	101.0	1.8E+05
1/51		-80.6	-94.5	5.754	33.5	1.0E+04	10.688	114.1	5.5E+04
1/52		-79.9	-93.5	5.647	33.3	8.2E+03	10.531	113.2	4.2E+04
1/53	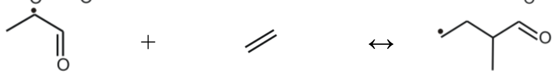	-32.1	-79.8	6.025	49.6	2.8E+03	10.194	81.7	8.7E+05
1/54	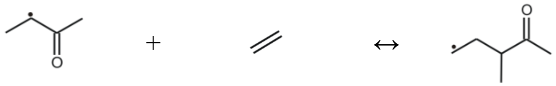	-33.6	-99.1	5.132	45.7	5.7E+02	10.311	79.3	1.5E+06

1/55	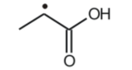	+		↔	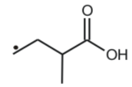	-48.8	-84.9	5.900	40.3	6.3E+03	10.336	89.1	5.0E+05
1/56	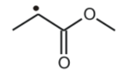	+		↔	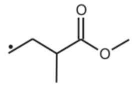	-49.7	-82.1	5.930	40.6	6.6E+03	10.221	90.3	3.3E+05
1/57	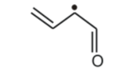	+		↔	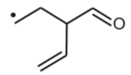	12.7	-71.2	6.217	74.7	2.1E+02	9.934	62.0	5.1E+06
1/58	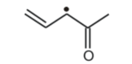	+		↔	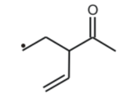	10.6	-78.1	6.009	67.0	3.3E+02	10.091	56.4	1.4E+07
1/59	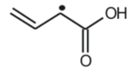	+		↔	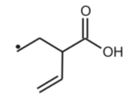	3.1	-66.2	6.158	66.1	5.2E+02	9.617	63.0	2.2E+06
1/60	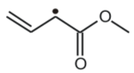	+		↔	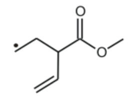	2.5	-63.5	6.148	65.9	5.2E+02	9.465	63.4	1.5E+06
1/61		+		↔	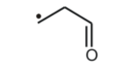	-58.4	-76.1	6.654	44.2	2.2E+04	10.630	102.6	1.9E+05
1/62		+		↔	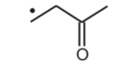	-56.4	-82.3	6.596	40.4	3.1E+04	10.896	96.8	7.1E+05
1/63	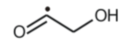	+		↔	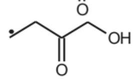	-71.6	-89.0	6.653	39.5	4.6E+04	11.304	111.1	3.8E+05
1/64	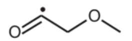	+		↔	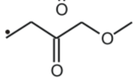	-58.5	-73.8	6.593	43.1	2.2E+04	10.446	101.6	1.4E+05
1/65	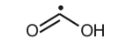	+		↔	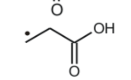	-103.1	-79.2	6.856	29.5	2.2E+05	10.995	132.6	1.3E+04
1/66	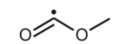	+		↔	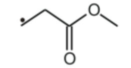	-100.4	-82.4	6.816	30.4	1.8E+05	11.120	130.8	2.0E+04

Table S5: Standard reaction enthalpies $\Delta_r H^o$ (kJ mol^{-1}), standard reaction entropies $\Delta_r S^o$ (J mol^{-1} K^{-1}), pre-exponential factors log*A* [log(m^3 mol^{-1} s^{-1})], activation energies E_a (kJ mol^{-1}) and rate coefficients *k* (m^3 mol^{-1} s^{-1}), at 1500 K for the training set of 66 carbon radical additions/*β*-scissions, from which the primary and secondary contributions are determined. [$k = \kappa A\ exp(-E_a/RT)$]. Arrhenius parameters do not include tunneling contributions.

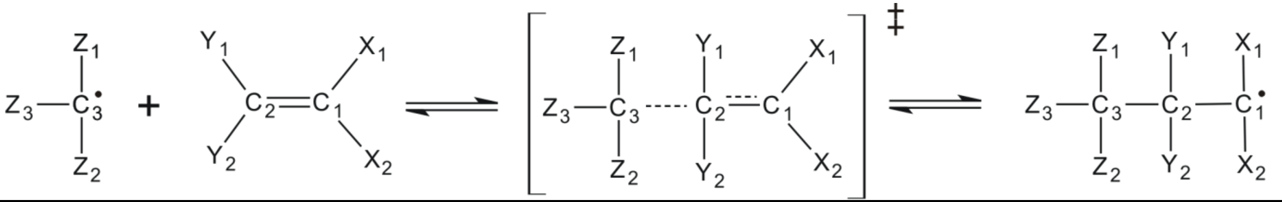

Reactions						addition					β-scission		
						$\Delta_r H^o$	$\Delta_r S^o$	log *A*	E_a	k_{for}	log *A*	E_a	k_{rev}
ref	$^{\bullet}CH_3$	+		↔		-75.3	-68.0	7.309	53.5	2.8E+05	10.860	128.8	2.4E+06
1/1	$^{\bullet}CH_3$	+	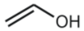	↔		-77.9	-85.9	6.900	57.2	8.1E+04	11.387	135.1	4.9E+06
1/2	$^{\bullet}CH_3$	+	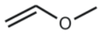	↔		-78.6	-78.3	7.517	59.8	2.7E+05	11.608	138.4	6.2E+06
1/3	$^{\bullet}CH_3$	+	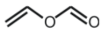	↔	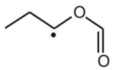	-85.5	-83.5	6.572	49.3	7.2E+04	10.934	134.8	1.8E+06
1/4	$^{\bullet}CH_3$	+	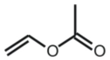	↔	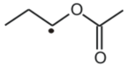	-84.7	-83.2	6.737	49.9	1.0E+05	11.085	134.6	2.5E+06
1/5	$^{\bullet}CH_3$	+	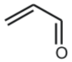	↔		-116.2	-88.5	6.504	31.6	2.5E+05	11.125	147.8	9.6E+05
1/6	$^{\bullet}CH_3$	+	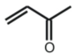	↔	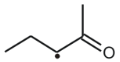	-112.0	-77.9	6.746	37.7	2.7E+05	10.816	149.7	4.0E+05
1/7	$^{\bullet}CH_3$	+	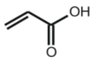	↔	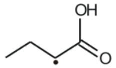	-98.3	-81.4	6.664	39.8	1.9E+05	10.914	138.1	1.3E+06
1/8	$^{\bullet}CH_3$	+	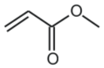	↔	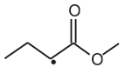	-98.5	-84.5	6.531	40.3	1.3E+05	10.946	138.8	1.3E+06
1/9	$^{\bullet}CH_3$	+	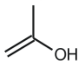	↔	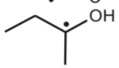	-76.8	-88.5	6.762	52.4	8.7E+04	11.386	129.2	7.8E+06
1/10	$^{\bullet}CH_3$	+	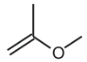	↔	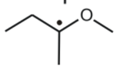	-90.5	-89.9	6.676	49.7	8.8E+04	11.373	140.2	3.1E+06
1/11	$^{\bullet}CH_3$	+	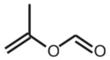	↔	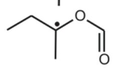	-84.7	-87.1	6.655	49.3	8.7E+04	11.204	134.0	3.5E+06

1/12	$^{\bullet}CH_3$	+	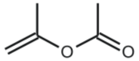	↔	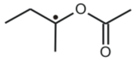	-81.3	-82.5	6.666	47.2	1.1E+05	10.978	128.5	3.2E+06
1/13	$^{\bullet}CH_3$	+	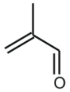	↔	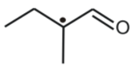	-114.5	-87.3	6.848	38.9	3.1E+05	11.409	153.4	1.2E+06
1/14	$^{\bullet}CH_3$	+	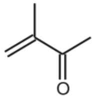	↔	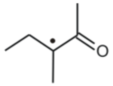	-112.5	-84.2	6.690	38.5	2.2E+05	11.086	151.0	6.8E+05
1/15	$^{\bullet}CH_3$	+	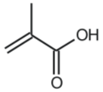	↔	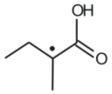	-107.4	-77.8	6.736	39.3	2.3E+05	10.800	146.7	5.0E+05
1/16	$^{\bullet}CH_3$	+	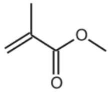	↔	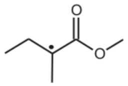	-107.8	-91.8	6.657	39.5	1.9E+05	11.452	147.3	2.1E+06
1/17	$^{\bullet}CH_3$	+	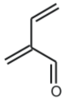	↔	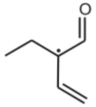	-157.1	-91.4	7.029	31.0	8.9E+05	11.802	188.1	1.8E+05
1/18	$^{\bullet}CH_3$	+	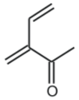	↔	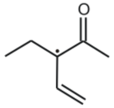	-156.3	-98.0	6.614	29.2	4.0E+05	11.733	185.5	1.9E+05
1/19	$^{\bullet}CH_3$	+	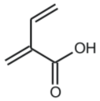	↔	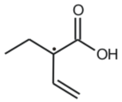	-152.9	-97.6	6.809	30.4	5.6E+05	11.909	183.3	3.4E+05
1/20	$^{\bullet}CH_3$	+	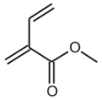	↔	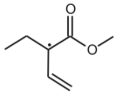	-149.7	-98.8	6.607	30.5	3.5E+05	11.770	180.2	3.1E+05
1/21	$^{\bullet}CH_3$	+	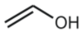	↔	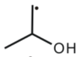	-59.1	-77.5	6.646	66.9	2.1E+04	10.692	126.0	2.0E+06
1/22	$^{\bullet}CH_3$	+	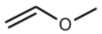	↔	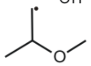	-60.3	-79.4	6.951	68.7	3.6E+04	11.096	129.0	4.1E+06
1/23	$^{\bullet}CH_3$	+	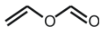	↔	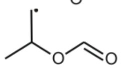	-79.3	-80.0	6.296	55.5	2.3E+04	10.474	134.8	6.1E+05

1/24	$^{\bullet}CH_3$	+	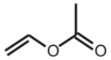	↔	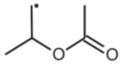	-78.3	-77.2	6.252	55.6	2.1E+04	10.287	133.9	4.3E+05
1/25	$^{\bullet}CH_3$	+	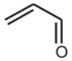	↔	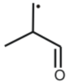	-72.9	-82.9	6.359	46.1	5.7E+04	10.690	119.0	3.5E+06
1/26	$^{\bullet}CH_3$	+	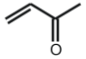	↔	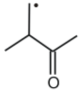	-71.6	-82.6	6.380	47.2	5.5E+04	10.696	118.8	3.7E+06
1/27	$^{\bullet}CH_3$	+	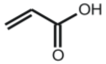	↔	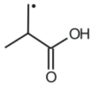	-68.4	-77.9	6.373	48.6	4.8E+04	10.444	117.0	2.4E+06
1/28	$^{\bullet}CH_3$	+	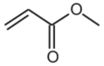	↔	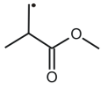	-69.5	-79.2	6.428	48.7	5.4E+04	10.566	118.2	2.9E+06
1/29	$^{\bullet}CH_3$	+	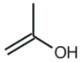	↔	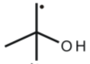	-50.3	-74.7	6.360	71.1	7.8E+03	10.264	121.4	1.1E+06
1/30	$^{\bullet}CH_3$	+	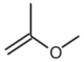	↔	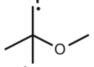	-48.5	-81.5	6.319	70.8	7.3E+03	10.575	119.3	2.7E+06
1/31	$^{\bullet}CH_3$	+	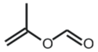	↔	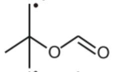	-77.3	-92.6	6.041	66.0	5.6E+03	10.878	143.3	7.9E+05
1/32	$^{\bullet}CH_3$	+	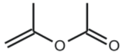	↔	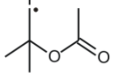	-76.1	-91.1	6.070	66.3	5.8E+03	10.831	142.4	7.6E+05
1/33	$^{\bullet}CH_3$	+	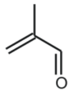	↔	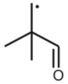	-56.9	-88.3	6.195	55.6	1.8E+04	10.810	112.5	7.9E+06
1/34	$^{\bullet}CH_3$	+	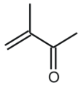	↔	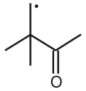	-60.1	-89.0	5.974	54.4	1.2E+04	10.624	114.5	4.4E+06
1/35	$^{\bullet}CH_3$	+	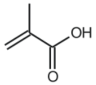	↔	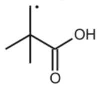	-62.0	-86.1	6.085	53.8	1.6E+04	10.581	115.8	3.6E+06
1/36	$^{\bullet}CH_3$	+	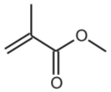	↔	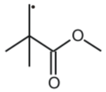	-63.0	-86.5	6.106	53.6	1.7E+04	10.623	116.6	3.7E+06
1/37	$^{\bullet}CH_3$	+	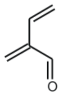	↔	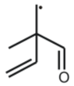	-49.1	-78.5	6.676	54.8	5.9E+04	10.778	103.9	1.5E+07
1/38	$^{\bullet}CH_3$	+	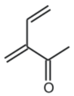	↔	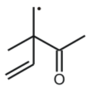	-58.2	-85.4	6.431	51.8	4.3E+04	10.893	110.0	1.2E+07

1/39	$^{\bullet}CH_3$	+	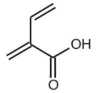	↔	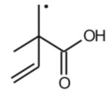	-54.1	-83.2	6.384	52.7	3.6E+04	10.729	106.8	1.0E+07
1/40	$^{\bullet}CH_3$	+	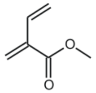	↔	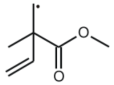	-51.9	-82.8	6.263	52.5	2.8E+04	10.589	104.4	9.1E+06
1/41	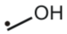	+		↔	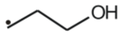	-59.6	-77.3	6.814	53.9	8.7E+04	10.853	113.5	8.0E+06
1/42	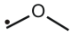	+		↔		-54.2	-66.3	6.637	53.3	6.1E+04	10.102	107.5	2.3E+06
1/43	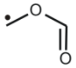	+		↔	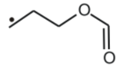	-74.6	-80.1	6.183	48.4	3.2E+04	10.366	123.0	1.2E+06
1/44	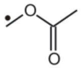	+		↔	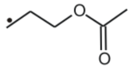	-73.4	-80.2	6.236	48.6	3.5E+04	10.425	122.0	1.5E+06
1/45	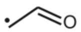	+		↔		-38.5	-64.7	6.896	54.6	9.9E+04	10.277	93.1	1.1E+07
1/46	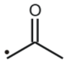	+		↔	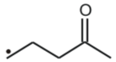	-42.9	-68.3	6.715	51.7	8.2E+04	10.285	94.6	9.9E+06
1/47	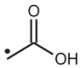	+		↔	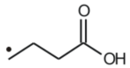	-56.7	-63.9	6.831	46.7	1.6E+05	10.171	103.4	3.8E+06
1/48	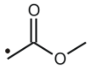	+		↔	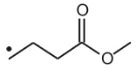	-55.2	-63.3	6.814	47.4	1.5E+05	10.121	102.6	3.6E+06
1/49	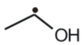	+		↔	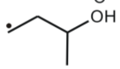	-55.2	-80.9	6.558	49.1	7.1E+04	10.785	104.3	1.4E+07
1/50	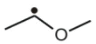	+		↔	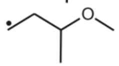	-51.9	-76.7	6.495	48.3	6.5E+04	10.500	100.2	1.0E+07
1/51	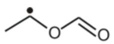	+		↔	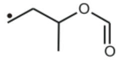	-69.5	-85.5	6.201	44.0	4.7E+04	10.665	113.5	5.2E+06
1/52	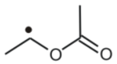	+		↔	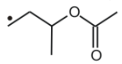	-69.0	-84.5	6.095	43.8	3.7E+04	10.511	112.8	3.9E+06
1/53	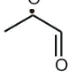	+		↔	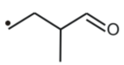	-20.8	-70.7	6.478	60.3	2.4E+04	10.171	81.1	2.2E+07
1/54	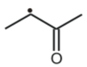	+		↔	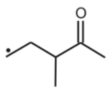	-22.3	-90.0	5.585	56.4	4.2E+03	10.287	78.7	3.5E+07

1/55	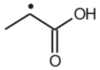	+		↔	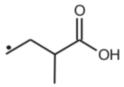	-37.8	-76.0	6.350	50.9	3.8E+04	10.320	88.7	1.7E+07
1/56	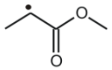	+		↔	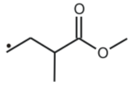	-38.7	-73.2	6.381	51.2	4.0E+04	10.204	89.9	1.2E+07
1/57	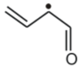	+		↔	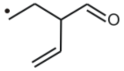	23.9	-62.0	6.681	85.6	5.1E+03	9.921	61.7	6.0E+07
1/58	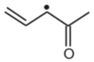	+		↔	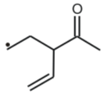	22.0	-68.9	6.477	78.0	5.8E+03	10.076	56.0	1.4E+08
1/59	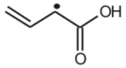	+		↔	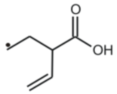	14.3	-57.2	6.619	77.0	8.8E+03	9.606	62.7	2.7E+07
1/60	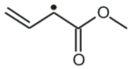	+		↔	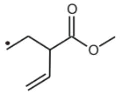	13.5	-54.4	6.610	76.7	8.8E+03	9.454	63.2	1.8E+07
1/61	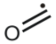	+		↔	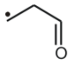	-48.1	-67.7	7.127	55.3	1.6E+05	10.666	103.4	1.2E+07
1/62	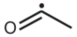	+		↔	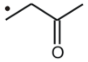	-45.7	-73.6	7.064	51.5	1.9E+05	10.907	97.2	3.4E+07
1/63	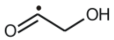	+		↔	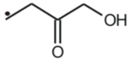	-60.9	-80.3	7.120	50.4	2.6E+05	11.315	111.3	3.1E+07
1/64	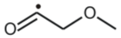	+		↔	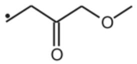	-47.2	-64.6	7.073	54.4	1.5E+05	10.445	101.6	8.1E+06
1/65	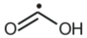	+		↔	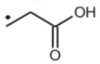	-92.5	-70.6	7.312	40.3	8.6E+05	11.001	132.8	2.5E+06
1/66	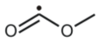	+		↔	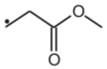	-89.7	-73.7	7.275	41.2	7.1E+05	11.124	130.9	3.8E+06

Table S6: Standard reaction enthalpies $\Delta_r H^o$ (kJ mol^{-1}), standard reaction entropies $\Delta_r S^o$ (J mol^{-1} K^{-1}), pre-exponential factors log$A$ [log(m^3 mol^{-1} s^{-1})], activation energies E_a (kJ mol^{-1}) and rate coefficients k (m^3 mol^{-1} s^{-1}), at 2000 K for the training set of 66 carbon radical additions/β-scissions, from which the primary and secondary contributions are determined. [$k = \kappa A\ exp(-E_a/RT)$]. Arrhenius parameters do not include tunneling contributions.

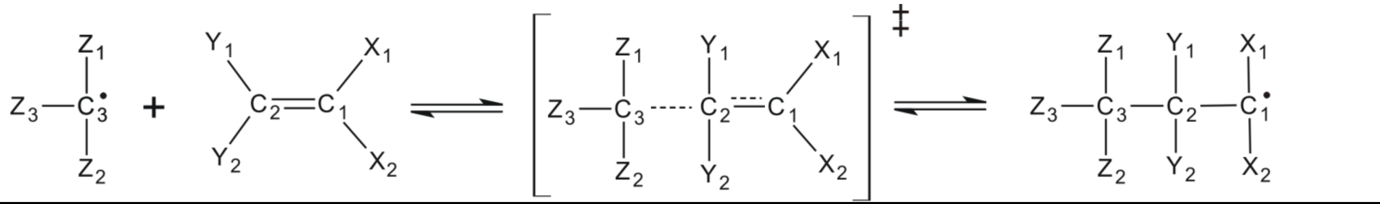

Reactions						addition					β-scission		
						$\Delta_r H^o$	$\Delta_r S^o$	log A	E_a	k_{for}	log A	E_a	k_{rev}
ref	$^{\bullet}CH_3$	+		↔		-64.8	-61.9	7.622	63.9	9.0E+05	10.857	128.7	3.1E+07
1/1	$^{\bullet}CH_3$	+	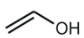	↔		-67.5	-79.9	7.212	67.6	2.8E+05	11.388	135.1	7.3E+07
1/2	$^{\bullet}CH_3$	+	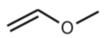	↔		-68.1	-72.3	7.832	70.3	9.9E+05	11.609	138.4	9.9E+07
1/3	$^{\bullet}CH_3$	+	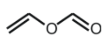	↔	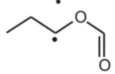	-75.1	-77.5	6.884	59.7	2.1E+05	10.934	134.8	2.6E+07
1/4	$^{\bullet}CH_3$	+	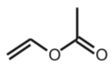	↔	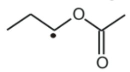	-74.4	-77.3	7.050	60.3	3.0E+05	11.088	134.7	3.7E+07
1/5	$^{\bullet}CH_3$	+	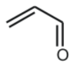	↔		-105.5	-82.4	6.816	42.0	5.2E+05	11.118	147.5	1.8E+07
1/6	$^{\bullet}CH_3$	+	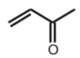	↔	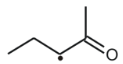	-101.9	-72.1	7.057	48.0	6.4E+05	10.821	149.9	8.1E+06
1/7	$^{\bullet}CH_3$	+	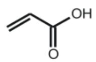	↔	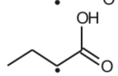	-87.6	-75.2	6.975	50.1	4.6E+05	10.902	137.7	2.0E+07
1/8	$^{\bullet}CH_3$	+	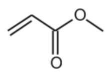	↔	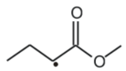	-87.6	-78.3	6.842	50.7	3.3E+05	10.931	138.3	2.1E+07

1/9	$^{\bullet}CH_3$	+	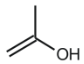	↔	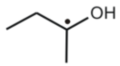	-66.5	-82.6	7.075	62.8	2.7E+05	11.389	129.3	1.0E+08
1/10	$^{\bullet}CH_3$	+	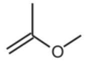	↔	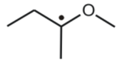	-80.3	-84.0	6.988	60.1	2.6E+05	11.377	140.4	5.2E+07
1/11	$^{\bullet}CH_3$	+	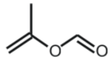	↔	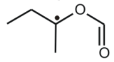	-74.4	-81.2	6.968	59.7	2.6E+05	11.208	134.1	5.1E+07
1/12	$^{\bullet}CH_3$	+	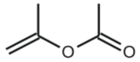	↔	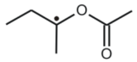	-71.1	-76.7	6.979	57.6	3.0E+05	10.983	128.7	4.2E+07
1/13	$^{\bullet}CH_3$	+	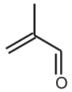	↔	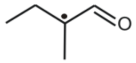	-104.3	-81.4	7.161	49.3	7.5E+05	11.415	153.6	2.5E+07
1/14	$^{\bullet}CH_3$	+	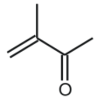	↔	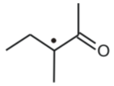	-102.2	-78.2	7.002	48.9	5.3E+05	11.088	151.1	1.4E+07
1/15	$^{\bullet}CH_3$	+	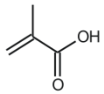	↔	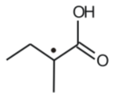	-97.0	-71.8	7.049	49.7	5.6E+05	10.801	146.7	9.4E+06
1/16	$^{\bullet}CH_3$	+	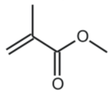	↔	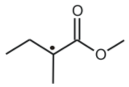	-97.5	-85.8	6.969	49.9	4.6E+05	11.453	147.4	4.0E+07
1/17	$^{\bullet}CH_3$	+	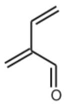	↔	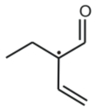	-146.7	-85.4	7.342	41.4	1.8E+06	11.804	188.1	7.8E+06
1/18	$^{\bullet}CH_3$	+	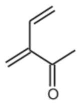	↔	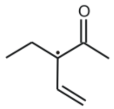	-146.1	-92.1	6.926	39.5	7.8E+05	11.737	185.6	7.8E+06
1/19	$^{\bullet}CH_3$	+	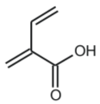	↔	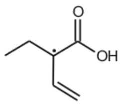	-142.6	-91.8	7.122	40.9	1.1E+06	11.916	183.5	1.3E+07
1/20	$^{\bullet}CH_3$	+	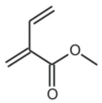	↔	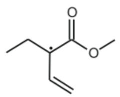	-138.7	-92.6	6.921	41.0	7.1E+05	11.756	179.7	1.2E+07
1/21	$^{\bullet}CH_3$	+	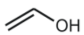	↔	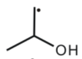	-48.2	-71.2	6.963	77.5	8.8E+04	10.684	125.7	2.5E+07
1/22	$^{\bullet}CH_3$	+	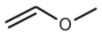	↔	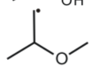	-49.6	-73.2	7.269	79.3	1.6E+05	11.093	128.9	5.4E+07
1/23	$^{\bullet}CH_3$	+	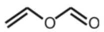	↔	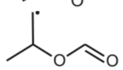	-68.7	-73.8	6.612	66.0	7.8E+04	10.469	134.7	9.0E+06

1/24	$^{\bullet}CH_3$	+	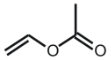	↔	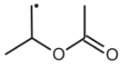	-67.7	-71.2	6.568	66.1	7.0E+04	10.285	133.8	6.2E+06
1/25	$^{\bullet}CH_3$	+	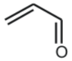	↔	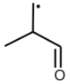	-62.6	-76.9	6.673	56.5	1.6E+05	10.692	119.1	3.8E+07
1/26	$^{\bullet}CH_3$	+	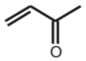	↔	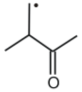	-61.3	-76.7	6.693	57.6	1.5E+05	10.699	118.9	4.0E+07
1/27	$^{\bullet}CH_3$	+	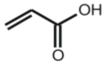	↔	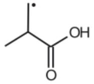	-57.8	-71.8	6.687	59.0	1.4E+05	10.440	116.8	2.5E+07
1/28	$^{\bullet}CH_3$	+	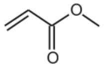	↔	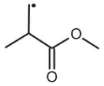	-59.0	-73.2	6.742	59.2	1.6E+05	10.567	118.2	3.0E+07
1/29	$^{\bullet}CH_3$	+	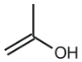	↔	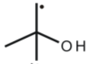	-39.3	-68.4	6.676	81.6	3.5E+04	10.250	120.9	1.2E+07
1/30	$^{\bullet}CH_3$	+	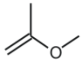	↔	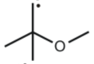	-37.7	-75.3	6.635	81.3	3.3E+04	10.568	119.0	2.9E+07
1/31	$^{\bullet}CH_3$	+	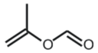	↔	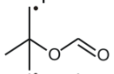	-66.6	-86.5	6.356	76.5	2.3E+04	10.874	143.1	1.4E+07
1/32	$^{\bullet}CH_3$	+	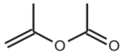	↔	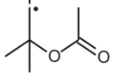	-65.5	-85.1	6.385	76.8	2.4E+04	10.829	142.3	1.3E+07
1/33	$^{\bullet}CH_3$	+	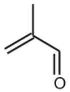	↔	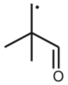	-46.4	-82.3	6.509	66.1	6.1E+04	10.810	112.5	7.5E+07
1/34	$^{\bullet}CH_3$	+	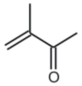	↔	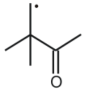	-49.6	-82.9	6.288	64.8	4.0E+04	10.621	114.4	4.3E+07
1/35	$^{\bullet}CH_3$	+	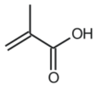	↔	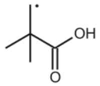	-51.3	-80.0	6.399	64.3	5.3E+04	10.578	115.6	3.6E+07
1/36	$^{\bullet}CH_3$	+	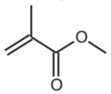	↔	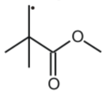	-52.4	-80.4	6.420	64.1	5.6E+04	10.620	116.5	3.8E+07

1/37	$^{\bullet}CH_3$ + 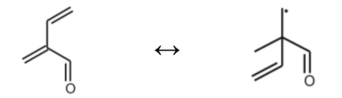	-38.5	-72.4	6.992	65.3	1.9E+05	10.776	103.8	1.2E+08
1/38	$^{\bullet}CH_3$ + 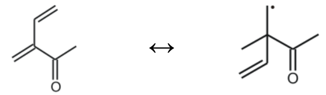	-47.7	-79.3	6.746	62.2	1.3E+05	10.890	109.9	1.1E+08
1/39	$^{\bullet}CH_3$ + 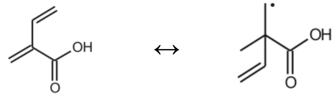	-43.5	-77.1	6.700	63.2	1.1E+05	10.725	106.7	8.7E+07
1/40	$^{\bullet}CH_3$ + 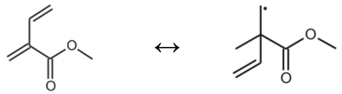	-40.9	-76.5	6.579	63.0	8.6E+04	10.573	103.9	7.3E+07
1/41		-48.6	-71.0	7.134	64.5	2.8E+05	10.842	113.1	7.8E+07
1/42	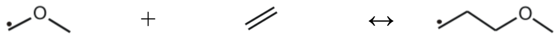	-43.4	-60.1	6.955	63.9	1.9E+05	10.094	107.3	2.0E+07
1/43		-63.9	-73.9	6.496	58.8	9.2E+04	10.355	122.7	1.4E+07
1/44	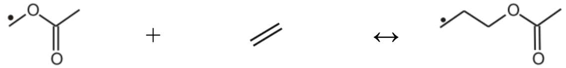	-62.5	-74.0	6.551	59.1	1.0E+05	10.416	121.6	1.7E+07
1/45	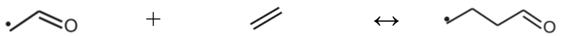	-27.4	-58.3	7.212	65.2	3.3E+05	10.260	92.6	7.0E+07
1/46	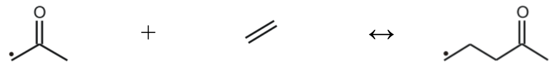	-31.9	-62.0	7.029	62.2	2.6E+05	10.270	94.1	6.5E+07
1/47	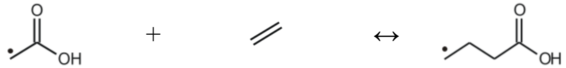	-45.8	-57.7	7.145	57.2	4.5E+05	10.158	103.0	3.0E+07
1/48		-44.3	-57.1	7.128	57.9	4.2E+05	10.109	102.2	2.8E+07
1/49		-44.1	-74.5	6.880	59.8	2.1E+05	10.773	103.9	1.1E+08
1/50		-40.8	-70.3	6.812	58.9	1.9E+05	10.482	99.7	7.6E+07
1/51		-58.6	-79.1	6.516	54.5	1.2E+05	10.650	113.1	5.0E+07
1/52		-58.0	-78.3	6.410	54.3	9.9E+04	10.498	112.3	3.7E+07
1/53		-9.9	-64.3	6.796	70.8	8.9E+04	10.157	80.7	1.1E+08
1/54	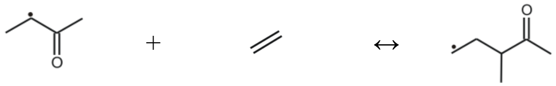	-11.4	-83.7	5.902	66.9	1.4E+04	10.273	78.3	1.7E+08

1/55	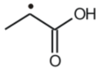	+		↔	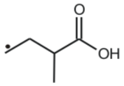	-26.9	-69.7	6.666	61.4	1.2E+05	10.309	88.3	1.0E+08
1/56	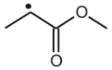	+		↔	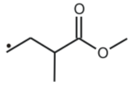	-27.8	-66.9	6.697	61.7	1.2E+05	10.194	89.5	7.2E+07
1/57	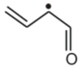	+		↔	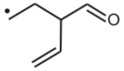	35.0	-55.7	7.002	96.3	3.1E+04	9.911	61.3	2.1E+08
1/58	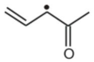	+		↔	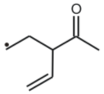	33.1	-62.5	6.801	88.8	3.1E+04	10.066	55.7	4.1E+08
1/59	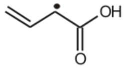	+		↔	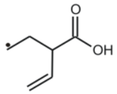	25.2	-50.9	6.940	87.6	4.5E+04	9.598	62.4	9.3E+07
1/60	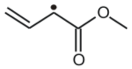	+		↔	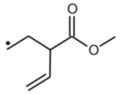	24.5	-48.2	6.931	87.4	4.5E+04	9.447	62.9	6.4E+07
1/61	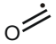	+		↔	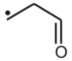	-37.7	-61.7	7.451	66.1	5.3E+05	10.676	103.8	9.3E+07
1/62	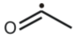	+		↔	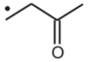	-35.0	-67.4	7.387	62.3	5.9E+05	10.907	97.3	2.4E+08
1/63	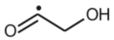	+		↔	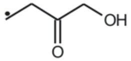	-50.1	-74.1	7.444	61.1	7.6E+05	11.314	111.2	2.8E+08
1/64	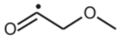	+		↔	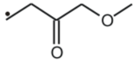	-36.0	-58.2	7.402	65.4	5.0E+05	10.440	101.4	6.2E+07
1/65	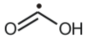	+		↔	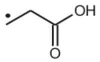	-82.0	-64.5	7.630	50.8	2.1E+06	11.001	132.8	3.6E+07
1/66	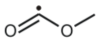	+		↔	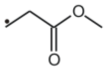	-79.1	-67.6	7.594	51.7	1.8E+06	11.123	130.8	5.2E+07

Table S7: Standard reaction enthalpies $\Delta_r H^o$ (kJ mol^{-1}), standard reaction entropies $\Delta_r S^o$ (J mol^{-1} K^{-1}), pre-exponential factors log*A* [log(m^3 mol^{-1} s^{-1})], activation energies E_a (kJ mol^{-1}) and rate coefficients *k* (m^3 mol^{-1} s^{-1}), at 2500 K for the training set of 66 carbon radical additions/*β*-scissions, from which the primary and secondary contributions are determined. [$k = \kappa A\ exp(-E_a/RT)$]. Arrhenius parameters do not include tunneling contributions.

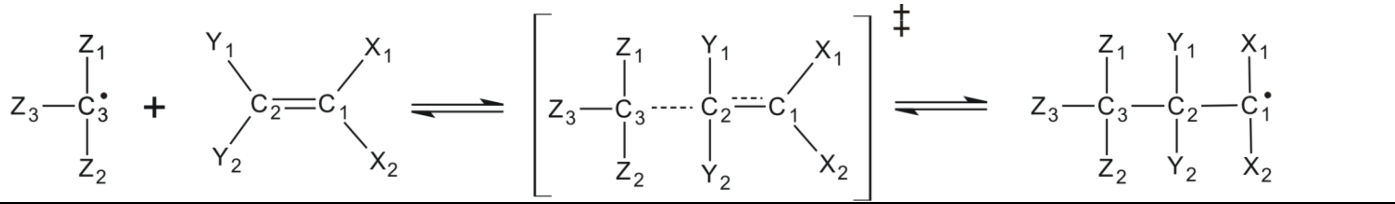

Reactions						addition					*β*-scission		
						$\Delta_r H^o$	$\Delta_r S^o$	log *A*	E_a	k_{for}	log *A*	E_a	k_{rev}
ref	$^{\bullet}CH_3$	+		↔		-54.2	-57.2	7.865	74.3	2.1E+06	10.853	128.5	1.5E+08
1/1	$^{\bullet}CH_3$	+	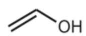	↔		-57.1	-75.3	7.455	78.0	6.7E+05	11.386	135.1	3.7E+08
1/2	$^{\bullet}CH_3$	+	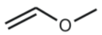	↔		-57.5	-67.6	8.076	80.8	2.5E+06	11.607	138.3	5.2E+08
1/3	$^{\bullet}CH_3$	+	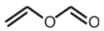	↔	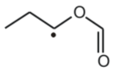	-64.6	-72.8	7.127	70.1	4.6E+05	10.932	134.7	1.3E+08
1/4	$^{\bullet}CH_3$	+	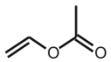	↔	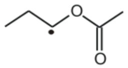	-64.0	-72.7	7.292	70.7	6.6E+05	11.087	134.7	1.9E+08
1/5	$^{\bullet}CH_3$	+	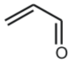	↔		-94.9	-77.6	7.059	52.4	9.2E+05	11.112	147.3	1.1E+08
1/6	$^{\bullet}CH_3$	+	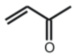	↔	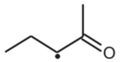	-91.4	-67.4	7.300	58.4	1.2E+06	10.821	149.8	4.9E+07
1/7	$^{\bullet}CH_3$	+	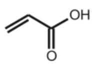	↔	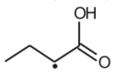	-76.8	-70.4	7.218	60.5	9.0E+05	10.893	137.3	1.1E+08
1/8	$^{\bullet}CH_3$	+	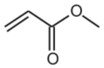	↔	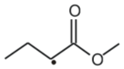	-76.8	-73.4	7.085	61.0	6.5E+05	10.921	137.8	1.1E+08
1/9	$^{\bullet}CH_3$	+	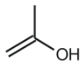	↔	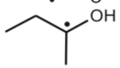	-56.1	-77.9	7.318	73.2	6.2E+05	11.387	129.3	4.9E+08
1/10	$^{\bullet}CH_3$	+	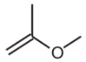	↔	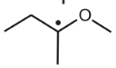	-69.7	-79.4	7.231	70.6	5.7E+05	11.377	140.3	2.8E+08
1/11	$^{\bullet}CH_3$	+	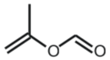	↔	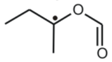	-64.0	-76.5	7.211	70.1	5.6E+05	11.208	134.1	2.5E+08

1/12	$^{\bullet}CH_3$	+	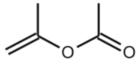	↔	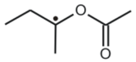	-60.7	-72.0	7.222	68.0	6.3E+05	10.983	128.7	2.0E+08
1/13	$^{\bullet}CH_3$	+	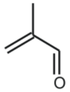	↔	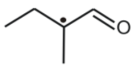	-93.9	-76.8	7.404	59.7	1.4E+06	11.416	153.6	1.6E+08
1/14	$^{\bullet}CH_3$	+	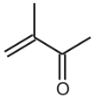	↔	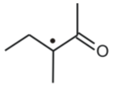	-91.6	-73.5	7.246	59.4	1.0E+06	11.087	151.0	8.6E+07
1/15	$^{\bullet}CH_3$	+	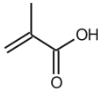	↔	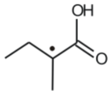	-86.5	-67.1	7.291	60.1	1.1E+06	10.798	146.6	5.5E+07
1/16	$^{\bullet}CH_3$	+	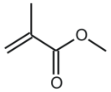	↔	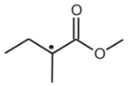	-87.0	-81.2	7.212	60.3	9.0E+05	11.452	147.3	2.4E+08
1/17	$^{\bullet}CH_3$	+	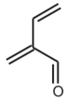	↔	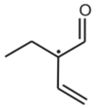	-136.3	-80.7	7.585	51.8	3.2E+06	11.803	188.1	7.5E+07
1/18	$^{\bullet}CH_3$	+	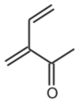	↔	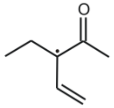	-135.7	-87.5	7.168	49.9	1.3E+06	11.737	185.6	7.2E+07
1/19	$^{\bullet}CH_3$	+	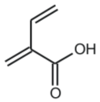	↔	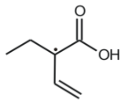	-132.2	-87.1	7.365	51.3	2.0E+06	11.917	183.5	1.2E+08
1/20	$^{\bullet}CH_3$	+	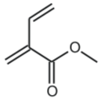	↔	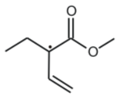	-127.9	-87.7	7.164	51.4	1.2E+06	11.746	179.3	1.0E+08
1/21	$^{\bullet}CH_3$	+	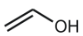	↔	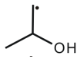	-37.5	-66.4	7.207	87.9	2.4E+05	10.677	125.4	1.1E+08
1/22	$^{\bullet}CH_3$	+	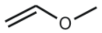	↔	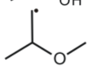	-38.8	-68.4	7.515	89.9	4.4E+05	11.090	128.7	2.5E+08
1/23	$^{\bullet}CH_3$	+	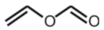	↔	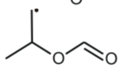	-58.0	-69.1	6.857	76.5	1.8E+05	10.464	134.5	4.5E+07

1/24	$^{\bullet}CH_3$	+	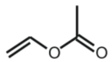	↔	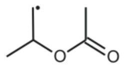	-57.1	-66.4	6.812	76.6	1.6E+05	10.283	133.7	3.1E+07
1/25	$^{\bullet}CH_3$	+	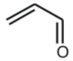	↔	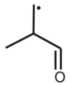	-52.2	-72.3	6.916	66.9	3.3E+05	10.691	119.1	1.6E+08
1/26	$^{\bullet}CH_3$	+	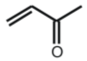	↔	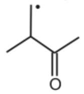	-50.8	-72.1	6.936	68.1	3.3E+05	10.700	118.9	1.6E+08
1/27	$^{\bullet}CH_3$	+	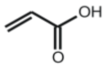	↔	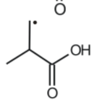	-47.2	-67.1	6.930	69.5	3.0E+05	10.436	116.7	1.0E+08
1/28	$^{\bullet}CH_3$	+	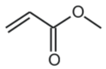	↔	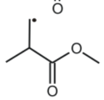	-48.6	-68.6	6.985	69.6	3.4E+05	10.567	118.2	1.3E+08
1/29	$^{\bullet}CH_3$	+	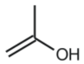	↔	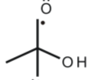	-28.5	-63.6	6.921	92.1	1.0E+05	10.242	120.6	5.3E+07
1/30	$^{\bullet}CH_3$	+	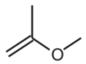	↔	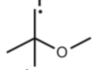	-27.1	-70.5	6.880	91.7	9.2E+04	10.563	118.8	1.2E+08
1/31	$^{\bullet}CH_3$	+	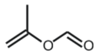	↔	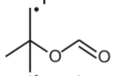	-56.0	-81.7	6.600	87.0	6.1E+04	10.870	143.0	7.7E+07
1/32	$^{\bullet}CH_3$	+	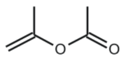	↔	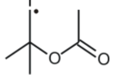	-54.9	-80.3	6.630	87.3	6.4E+04	10.826	142.2	7.2E+07
1/33	$^{\bullet}CH_3$	+	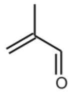	↔	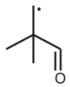	-36.0	-77.7	6.753	76.5	1.4E+05	10.810	112.5	2.9E+08
1/34	$^{\bullet}CH_3$	+	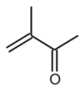	↔	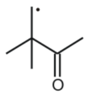	-39.1	-78.3	6.531	75.2	9.1E+04	10.619	114.3	1.7E+08
1/35	$^{\bullet}CH_3$	+	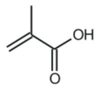	↔	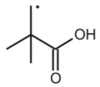	-40.8	-75.3	6.643	74.7	1.2E+05	10.575	115.5	1.5E+08
1/36	$^{\bullet}CH_3$	+	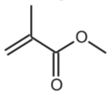	↔	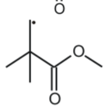	-41.9	-75.7	6.664	74.5	1.3E+05	10.618	116.4	1.5E+08
1/37	$^{\bullet}CH_3$	+	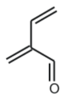	↔	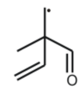	-27.9	-67.7	7.237	75.8	4.5E+05	10.774	103.7	4.0E+08
1/38	$^{\bullet}CH_3$	+	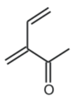	↔	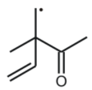	-37.1	-74.6	6.989	72.7	3.0E+05	10.888	109.8	3.9E+08

1/39	$^{\bullet}CH_3$	+	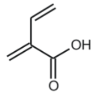	↔	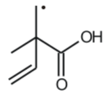	-32.8	-72.3	6.944	73.7	2.6E+05	10.722	106.5	3.1E+08
1/40	$^{\bullet}CH_3$	+	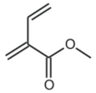	↔	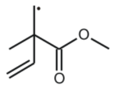	-30.0	-71.6	6.824	73.5	2.0E+05	10.565	103.5	2.5E+08
1/41	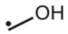	+		↔	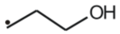	-37.7	-66.1	7.381	75.1	6.5E+05	10.835	112.8	3.0E+08
1/42	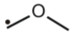	+		↔		-32.6	-55.3	7.200	74.4	4.4E+05	10.088	107.0	7.1E+07
1/43	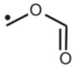	+		↔	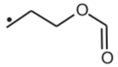	-53.1	-69.1	6.739	69.2	2.0E+05	10.348	122.3	6.2E+07
1/44	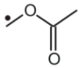	+		↔	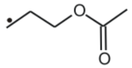	-51.9	-69.2	6.794	69.5	2.2E+05	10.409	121.4	7.5E+07
1/45	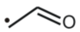	+		↔		-16.5	-53.5	7.457	75.6	7.6E+05	10.250	92.1	2.1E+08
1/46	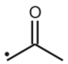	+		↔	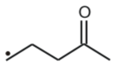	-21.0	-57.2	7.272	72.6	5.7E+05	10.259	93.6	2.0E+08
1/47	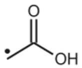	+		↔	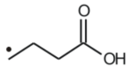	-35.0	-52.9	7.388	67.6	9.5E+05	10.150	102.6	1.0E+08
1/48	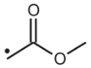	+		↔	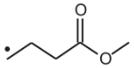	-33.6	-52.3	7.371	68.3	8.8E+05	10.101	101.9	9.3E+07
1/49	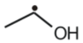	+		↔	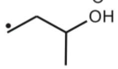	-33.3	-69.7	7.127	70.4	4.5E+05	10.767	103.7	4.0E+08
1/50	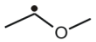	+		↔	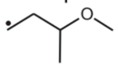	-30.0	-65.4	7.056	69.3	4.1E+05	10.473	99.3	2.5E+08
1/51	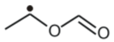	+		↔	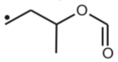	-47.8	-74.4	6.758	64.9	2.5E+05	10.642	112.7	1.9E+08
1/52	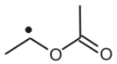	+		↔	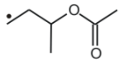	-47.2	-73.5	6.652	64.7	2.0E+05	10.489	111.9	1.4E+08
1/53	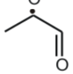	+		↔	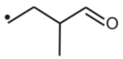	0.9	-59.5	7.041	81.3	2.2E+05	10.149	80.4	3.0E+08
1/54	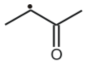	+		↔	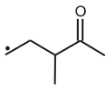	-0.5	-78.8	6.144	77.3	3.4E+04	10.262	77.8	4.3E+08

1/55	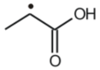	+		↔	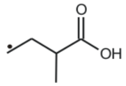	-16.2	-65.0	6.910	71.9	2.6E+05	10.303	88.1	2.9E+08
1/56	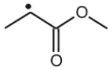	+		↔	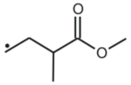	-17.2	-62.2	6.941	72.2	2.7E+05	10.190	89.4	2.1E+08
1/57	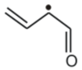	+		↔	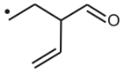	45.7	-50.9	7.246	106.8	1.0E+05	9.905	61.1	4.3E+08
1/58	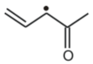	+		↔	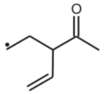	43.8	-57.7	7.049	99.4	9.4E+04	10.063	55.6	8.0E+08
1/59	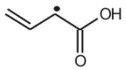	+		↔	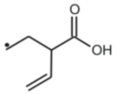	36.0	-46.1	7.186	98.2	1.4E+05	9.592	62.2	2.0E+08
1/60	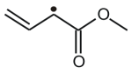	+		↔	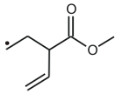	35.3	-43.3	7.178	98.0	1.4E+05	9.442	62.7	1.4E+08
1/61	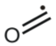	+		↔	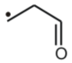	-24.3	-62.6	7.635	73.0	1.3E+06	10.907	97.3	7.6E+08
1/62	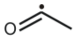	+		↔	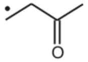	-39.4	-69.3	7.691	71.7	1.7E+06	11.312	111.1	1.0E+09
1/63	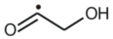	+		↔	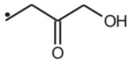	-25.2	-53.3	7.652	76.1	1.2E+06	10.437	101.3	2.1E+08
1/64	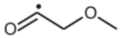	+		↔	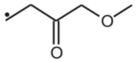	-71.5	-59.8	7.875	61.3	4.0E+06	11.001	132.8	1.7E+08
1/65	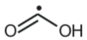	+		↔	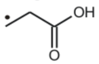	-68.5	-62.8	7.840	62.2	3.5E+06	11.121	130.7	2.5E+08
1/66	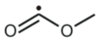	+		↔	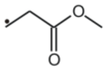	-68.4	-62.8	7.840	62.0	3.5E+06	11.121	130.4	2.5E+08

Table S8: Influence of the hindered rotation treatment around the formed/broken bond in products based on the averaged values for k_{HR} / k_{HO} at 300 and 1000 K for the carbon-centered radical additions to oxygenates and the *β*-scissions of oxygenates included in Table 6-1.

		k_{HR} / k_{HO}	
Set	**Reaction**	**300 K**	**1000 K**
1/	addition	1.08	0.71
	β-scission	1.17	0.64
2/	addition	1.18	0.96
	β-scission	1.17	0.83
3/	addition	2.06	2.32
	β-scission	0.96	0.80

Table S9: ΔGAV^os at 1500 K, 2000 K and 2500 K for carbon-centered radical additions to oxygenates and their reverse β-scissions of oxygenates. ($\tilde{A}$ in $m^3\ mol^{-1}\ s^{-1}$ and E_a in kJ mol^{-1}). Y_1, Y_2 and X_1, X_2 ligands correspond to O, CO, C, C_d or H whereas Z_1, Z_2 and Z_3 ligands can be O, O_d, CO, C, C_d or H. C_d and O_d refer to a double-bonded carbon or oxygen atom, respectively.

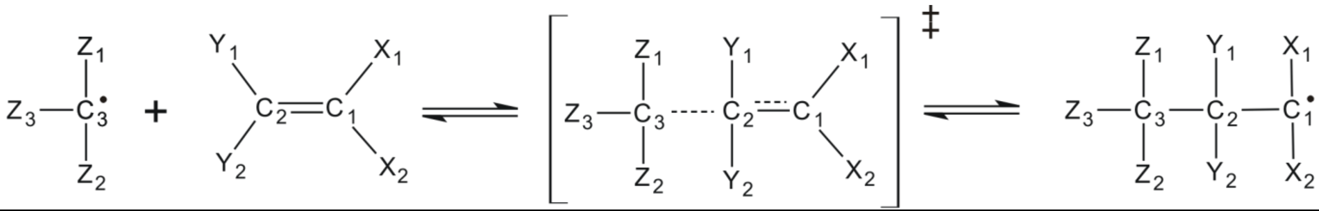

	addition						β-scission					
	1500 K		2000 K		2500 K		1500 K		2000 K		2500 K	
	$\log\tilde{A}$	E_a	$\log\tilde{A}$	E_a	$\log\tilde{A}$	E_a	$\log\tilde{A}$	E_a	$\log\tilde{A}$	E_a	$\log\tilde{A}$	E_a
Reference Reaction												
$^{\bullet}CH_3 + CH_2{=}CH_2$	6.406	53.5	6.719	63.9	6.962	74.3	10.559	128.8	10.556	128.7	10.552	128.5
	$\Delta GAV^o_{addition}$						**$\Delta GAV^o_{\beta\text{-scission}}$**					
	1500 K		2000 K		2500 K		1500 K		2000 K		2500 K	
Group	$\log\tilde{A}$	E_a	$\log\tilde{A}$	E_a	$\log\tilde{A}$	E_a	$\log\tilde{A}$	E_a	$\log\tilde{A}$	E_a	$\log\tilde{A}$	E_a
Primary Contributions												
C_1-(O)(H)	0.245	3.5	0.244	3.5	0.244	3.5	0.837	4.7	0.840	4.8	0.842	5.0
C_1-(CO)(H)	-0.005	-17.9	-0.006	-17.9	-0.006	-17.9	0.523	18.7	0.521	18.6	0.520	18.6
C_1-(C)(O)	0.003	-0.9	0.003	-0.9	0.003	-0.9	0.818	2.0	0.825	2.2	0.827	2.4
C_1-(C)(CO)	0.117	-16.2	0.116	-16.2	0.117	-16.1	0.760	24.7	0.767	25.0	0.771	25.2
C_1-(C_d)(CO)	0.148	-25.0	0.149	-24.9	0.149	-24.9	1.376	59.4	1.381	59.5	1.384	59.7
C_2-(O)(H)	-0.035	12.1	-0.030	12.2	-0.029	12.3	-0.081	-5.4	-0.088	-5.7	-0.091	-5.8
C_2-(CO)(H)	-0.216	-5.3	-0.216	-5.3	-0.215	-5.3	0.131	-11.9	0.137	-11.7	0.141	-11.4
C_2-(C)(O)	-0.373	18.9	-0.370	19.1	-0.369	19.1	-0.081	-4.8	-0.090	-5.1	-0.094	-5.2
C_2-(C)(CO)	-0.511	1.4	-0.510	1.5	-0.509	1.4	0.191	-15.3	0.195	-15.2	0.198	-15.0

C_2-(C_d)(CO)	-0.163	0.0	-0.160	0.1	-0.159	0.1	0.279	-23.9	0.278	-23.9	0.280	-23.8
C_3-(O)$(H)_2$	-0.257	0.4	-0.249	0.6	-0.245	0.8	0.171	-15.5	0.165	-15.7	0.163	-15.8
C_3-(CO)$(H)_2$	-0.096	2.1	-0.093	2.2	-0.093	2.2	-0.347	-33.1	-0.360	-33.4	-0.366	-33.7
C_3-(C)(O)(H)	-0.387	-4.4	-0.379	-4.1	-0.375	-3.9	0.349	-24.3	0.339	-24.7	0.335	-24.7
C_3-(C)(CO)(H)	-0.636	6.7	-0.631	6.8	-0.630	6.8	-0.240	-46.9	-0.251	-47.2	-0.255	-47.3
C_3-(C_d)(CO)(H)	-0.238	31.3	-0.228	31.6	-0.225	31.8	-0.721	-70.6	-0.729	-70.8	-0.731	-70.9
C_3-(O_d)(H)	0.119	1.8	0.130	2.2	0.135	2.4	0.107	-25.4	0.120	-24.9	0.129	-24.6
C_3-(O_d)(C)	0.051	-2.0	0.064	-1.6	0.069	-1.3	0.343	-31.6	0.348	-31.4	0.353	-31.2
C_3-(O_d)(O)	0.304	-13.2	0.309	-13.1	0.311	-13.0	0.442	4.0	0.445	4.1	0.449	4.3
Secondary Contributions												
O-(C_1)(C)	0.266	-0.1	0.267	0.0	0.267	0.1	0.104	7.2	0.104	7.2	0.105	7.1
O-(C_1)(CO)	-0.173	-5.9	-0.173	-5.9	-0.173	-5.9	-0.336	0.8	-0.335	0.9	-0.334	0.9
CO-(C_1)(C)	-0.110	1.3	-0.111	1.2	-0.111	1.3	-0.234	-1.0	-0.230	-0.9	-0.229	-0.9
CO-(C_1)(O)	-0.126	2.8	-0.127	2.8	-0.127	2.8	-0.147	-7.4	-0.152	-7.5	-0.156	-7.7
O-(C_2)(C)	0.132	0.8	0.133	0.8	0.134	0.8	0.357	0.5	0.363	0.7	0.367	0.8
O-(C_2)(CO)	-0.338	-8.2	-0.339	-8.2	-0.339	-8.2	0.140	14.9	0.147	15.2	0.151	15.4
CO-(C_2)(C)	-0.148	-1.0	-0.149	-1.1	-0.150	-1.1	-0.022	2.6	-0.023	2.6	-0.023	2.6
CO-(C_2)(O)	-0.137	-0.5	-0.137	-0.5	-0.137	-0.5	-0.171	1.3	-0.175	1.2	-0.178	1.0
O-(C_3)(C)	-0.120	-0.7	-0.123	-0.8	-0.126	-0.9	-0.518	-5.1	-0.519	-5.0	-0.520	-5.1
O-(C_3)(CO)	-0.507	-5.3	-0.514	-5.5	-0.518	-5.7	-0.327	8.9	-0.328	8.9	-0.329	8.8
CO-(C_3)(C)	-0.426	-4.8	-0.426	-4.8	-0.426	-4.8	0.093	-2.2	0.094	-2.2	0.093	-2.2
CO-(C_3)(O)	-0.134	-8.5	-0.136	-8.6	-0.136	-8.5	-0.194	6.5	-0.190	6.5	-0.189	6.6
C-($C_{3,d}$)(O)$(H)_2$	0.024	0.9	0.024	1.0	0.024	0.9	-0.035	9.3	-0.042	9.0	-0.045	8.9
O-($C_{3,d}$)(C)	-0.036	0.9	-0.035	0.9	-0.036	0.9	0.125	-1.9	0.122	-2.0	0.119	-2.1

Table S10: Rate coefficients ($m^3\ mol^{-1}\ s^{-1}$) in the temperature range 300 – 2500 K for the reactions presented in Table 6-1. Rate coefficients do not include tunneling contributions.

Reactions	300 K	400 K	500 K	600 K	700 K	800 K	900 K	1000 K	1200 K	1500 K	1800 K	2000 K	2200 K	2500 K
additions														
ref →	3.5E+00	7.3E+01	5.0E+02	2.0E+03	5.5E+03	1.2E+04	2.4E+04	4.2E+04	1.0E+05	2.8E+05	6.0E+05	9.0E+05	1.3E+06	2.1E+06
1 →	3.2E-01	9.5E+00	8.1E+01	3.6E+02	1.1E+03	2.7E+03	5.7E+03	1.0E+04	2.8E+04	8.1E+04	1.8E+05	2.8E+05	4.1E+05	6.7E+05
2 →	4.9E-01	1.8E+01	1.8E+02	9.0E+02	3.0E+03	7.7E+03	1.7E+04	3.2E+04	8.8E+04	2.7E+05	6.3E+05	9.9E+05	1.5E+06	2.5E+06
3 →	3.3E+00	4.6E+01	2.5E+02	8.2E+02	2.0E+03	4.2E+03	7.6E+03	1.3E+04	2.9E+04	7.2E+04	1.4E+05	2.1E+05	3.0E+05	4.6E+05
4 →	3.9E+00	5.7E+01	3.2E+02	1.1E+03	2.7E+03	5.7E+03	1.0E+04	1.7E+04	4.0E+04	1.0E+05	2.0E+05	3.0E+05	4.2E+05	6.6E+05
5 →	3.1E+03	7.7E+03	1.5E+04	2.4E+04	3.6E+04	5.1E+04	6.9E+04	9.0E+04	1.4E+05	2.5E+05	4.0E+05	5.2E+05	6.7E+05	9.2E+05
6 →	5.0E+02	2.2E+03	6.0E+03	1.2E+04	2.2E+04	3.6E+04	5.4E+04	7.6E+04	1.4E+05	2.7E+05	4.7E+05	6.4E+05	8.4E+05	1.2E+06
7 →	1.8E+02	9.8E+02	3.0E+03	6.8E+03	1.3E+04	2.2E+04	3.4E+04	4.9E+04	9.2E+04	1.9E+05	3.4E+05	4.6E+05	6.2E+05	9.0E+05
8 →	1.1E+02	6.1E+02	1.9E+03	4.5E+03	8.7E+03	1.5E+04	2.3E+04	3.4E+04	6.4E+04	1.3E+05	2.4E+05	3.3E+05	4.4E+05	6.5E+05
9 →	1.4E+00	2.7E+01	1.8E+02	6.8E+02	1.9E+03	4.1E+03	7.9E+03	1.4E+04	3.3E+04	8.7E+04	1.8E+05	2.7E+05	3.9E+05	6.2E+05
10 →	3.3E+00	5.0E+01	2.8E+02	9.5E+02	2.4E+03	5.0E+03	9.2E+03	1.5E+04	3.5E+04	8.8E+04	1.8E+05	2.6E+05	3.7E+05	5.7E+05
11 →	3.9E+00	5.5E+01	3.0E+02	1.0E+03	2.5E+03	5.1E+03	9.3E+03	1.5E+04	3.5E+04	8.7E+04	1.8E+05	2.6E+05	3.6E+05	5.6E+05
12 →	9.3E+00	1.1E+02	5.1E+02	1.6E+03	3.7E+03	7.2E+03	1.3E+04	2.0E+04	4.4E+04	1.1E+05	2.1E+05	3.0E+05	4.2E+05	6.3E+05
13 →	3.9E+02	1.9E+03	5.7E+03	1.2E+04	2.3E+04	3.8E+04	5.8E+04	8.4E+04	1.5E+05	3.1E+05	5.5E+05	7.5E+05	9.9E+05	1.4E+06
14 →	3.1E+02	1.5E+03	4.3E+03	9.2E+03	1.7E+04	2.8E+04	4.2E+04	6.1E+04	1.1E+05	2.2E+05	3.9E+05	5.3E+05	7.0E+05	1.0E+06
15 →	2.5E+02	1.3E+03	3.9E+03	8.8E+03	1.6E+04	2.7E+04	4.2E+04	6.1E+04	1.1E+05	2.3E+05	4.1E+05	5.6E+05	7.5E+05	1.1E+06
16 →	2.0E+02	1.0E+03	3.1E+03	7.0E+03	1.3E+04	2.2E+04	3.4E+04	5.0E+04	9.3E+04	1.9E+05	3.4E+05	4.6E+05	6.2E+05	9.0E+05
17 →	1.5E+04	3.3E+04	5.8E+04	9.2E+04	1.3E+05	1.9E+05	2.5E+05	3.3E+05	5.1E+05	8.9E+05	1.4E+06	1.8E+06	2.3E+06	3.2E+06
18 →	1.1E+04	2.1E+04	3.4E+04	5.0E+04	7.0E+04	9.5E+04	1.2E+05	1.6E+05	2.4E+05	4.0E+05	6.1E+05	7.8E+05	9.8E+05	1.3E+06
19 →	1.2E+04	2.4E+04	4.0E+04	6.2E+04	8.9E+04	1.2E+05	1.6E+05	2.1E+05	3.3E+05	5.6E+05	8.8E+05	1.1E+06	1.4E+06	2.0E+06
20 →	7.0E+03	1.4E+04	2.5E+04	3.8E+04	5.5E+04	7.6E+04	1.0E+05	1.3E+05	2.0E+05	3.5E+05	5.5E+05	7.1E+05	9.0E+05	1.2E+06
21 →	4.6E-03	3.2E-01	4.7E+00	3.0E+01	1.2E+02	3.6E+02	8.8E+02	1.8E+03	5.9E+03	2.1E+04	5.3E+04	8.8E+04	1.4E+05	2.4E+05
22 →	4.6E-03	3.8E-01	6.2E+00	4.3E+01	1.8E+02	5.6E+02	1.4E+03	3.0E+03	9.9E+03	3.6E+04	9.5E+04	1.6E+05	2.5E+05	4.4E+05
23 →	2.0E-01	4.5E+00	3.3E+01	1.3E+02	3.9E+02	9.1E+02	1.8E+03	3.2E+03	8.3E+03	2.3E+04	5.1E+04	7.8E+04	1.1E+05	1.8E+05
24 →	1.7E-01	3.9E+00	2.9E+01	1.2E+02	3.5E+02	8.1E+02	1.6E+03	2.9E+03	7.4E+03	2.1E+04	4.6E+04	7.0E+04	1.0E+05	1.6E+05
25 →	7.7E+00	7.6E+01	3.4E+02	9.7E+02	2.2E+03	4.2E+03	7.2E+03	1.1E+04	2.4E+04	5.7E+04	1.1E+05	1.6E+05	2.2E+05	3.3E+05
26 →	5.1E+00	5.7E+01	2.7E+02	8.1E+02	1.9E+03	3.7E+03	6.5E+03	1.0E+04	2.3E+04	5.5E+04	1.1E+05	1.5E+05	2.1E+05	3.3E+05
27 →	3.1E+00	3.8E+01	1.9E+02	6.1E+02	1.5E+03	3.0E+03	5.3E+03	8.8E+03	2.0E+04	4.8E+04	9.6E+04	1.4E+05	2.0E+05	3.0E+05
28 →	3.4E+00	4.2E+01	2.1E+02	6.8E+02	1.6E+03	3.3E+03	6.0E+03	9.8E+03	2.2E+04	5.4E+04	1.1E+05	1.6E+05	2.2E+05	3.4E+05
29 →	4.7E-04	4.9E-02	9.1E-01	6.9E+00	3.1E+01	1.0E+02	2.6E+02	5.8E+02	2.0E+03	7.8E+03	2.1E+04	3.5E+04	5.6E+04	1.0E+05
30 →	4.7E-04	4.9E-02	8.9E-01	6.7E+00	3.0E+01	9.7E+01	2.5E+02	5.5E+02	1.9E+03	7.3E+03	1.9E+04	3.3E+04	5.2E+04	9.2E+04
31 →	5.5E-06	1.7E-03	6.1E-02	7.2E-01	4.5E+00	1.8E+01	5.7E+01	1.4E+02	6.3E+02	3.0E+03	9.3E+03	1.7E+04	2.9E+04	5.5E+04
32 →	1.7E-03	1.1E-01	1.5E+00	9.2E+00	3.6E+01	1.1E+02	2.5E+02	5.2E+02	1.7E+03	5.8E+03	1.5E+04	2.4E+04	3.7E+04	6.4E+04

33 →	1.3E-01	3.2E+00	2.4E+01	1.0E+02	2.9E+02	6.9E+02	1.4E+03	2.5E+03	6.4E+03	1.8E+04	4.0E+04	6.1E+04	8.9E+04	1.4E+05
34 →	1.3E-01	2.7E+00	1.9E+01	7.7E+01	2.2E+02	5.0E+02	9.9E+02	1.8E+03	4.4E+03	1.2E+04	2.6E+04	4.0E+04	5.7E+04	9.1E+04
35 →	2.2E-01	4.3E+00	2.9E+01	1.1E+02	3.1E+02	7.1E+02	1.4E+03	2.4E+03	6.0E+03	1.6E+04	3.5E+04	5.3E+04	7.6E+04	1.2E+05
36 →	2.5E-01	4.8E+00	3.2E+01	1.2E+02	3.4E+02	7.6E+02	1.5E+03	2.6E+03	6.4E+03	1.7E+04	3.7E+04	5.6E+04	8.0E+04	1.3E+05
37 →	6.2E-01	1.3E+01	9.2E+01	3.7E+02	1.0E+03	2.4E+03	4.8E+03	8.4E+03	2.1E+04	5.9E+04	1.3E+05	1.9E+05	2.8E+05	4.5E+05
38 →	1.1E+00	1.7E+01	1.0E+02	3.7E+02	9.8E+02	2.1E+03	4.0E+03	6.9E+03	1.6E+04	4.3E+04	8.9E+04	1.3E+05	1.9E+05	3.0E+05
39 →	7.5E-01	1.3E+01	7.8E+01	2.9E+02	7.7E+02	1.7E+03	3.2E+03	5.5E+03	1.3E+04	3.6E+04	7.5E+04	1.1E+05	1.6E+05	2.6E+05
40 →	6.3E-01	1.0E+01	6.3E+01	2.3E+02	6.0E+02	1.3E+03	2.5E+03	4.3E+03	1.0E+04	2.8E+04	5.8E+04	8.6E+04	1.2E+05	2.0E+05
41 →	1.5E+00	2.6E+01	1.6E+02	6.2E+02	1.7E+03	3.8E+03	7.4E+03	1.3E+04	3.2E+04	8.7E+04	1.9E+05	2.8E+05	4.1E+05	6.5E+05
42 →	1.0E+00	1.9E+01	1.2E+02	4.5E+02	1.2E+03	2.7E+03	5.3E+03	9.2E+03	2.2E+04	6.1E+04	1.3E+05	1.9E+05	2.8E+05	4.4E+05
43 →	2.1E+00	2.6E+01	1.3E+02	4.1E+02	9.9E+02	2.0E+03	3.6E+03	5.8E+03	1.3E+04	3.2E+04	6.3E+04	9.2E+04	1.3E+05	2.0E+05
44 →	2.1E+00	2.7E+01	1.4E+02	4.4E+02	1.1E+03	2.2E+03	3.9E+03	6.4E+03	1.4E+04	3.5E+04	7.0E+04	1.0E+05	1.4E+05	2.2E+05
45 →	1.2E+00	2.4E+01	1.6E+02	6.3E+02	1.8E+03	4.1E+03	8.0E+03	1.4E+04	3.6E+04	9.9E+04	2.1E+05	3.3E+05	4.7E+05	7.6E+05
46 →	2.5E+00	3.7E+01	2.1E+02	7.4E+02	1.9E+03	4.1E+03	7.8E+03	1.3E+04	3.1E+04	8.2E+04	1.7E+05	2.6E+05	3.6E+05	5.7E+05
47 →	2.2E+01	2.0E+02	8.9E+02	2.6E+03	5.9E+03	1.1E+04	2.0E+04	3.2E+04	6.8E+04	1.6E+05	3.1E+05	4.5E+05	6.2E+05	9.5E+05
48 →	1.6E+01	1.6E+02	7.3E+02	2.2E+03	5.0E+03	9.9E+03	1.7E+04	2.8E+04	6.1E+04	1.5E+05	2.9E+05	4.2E+05	5.8E+05	8.8E+05
49 →	6.9E+00	6.6E+01	3.0E+02	9.1E+02	2.2E+03	4.3E+03	7.7E+03	1.3E+04	2.8E+04	7.1E+04	1.4E+05	2.1E+05	2.9E+05	4.5E+05
50 →	5.8E+00	6.2E+01	2.9E+02	8.8E+02	2.1E+03	4.2E+03	7.4E+03	1.2E+04	2.7E+04	6.5E+04	1.3E+05	1.9E+05	2.6E+05	4.1E+05
51 →	1.6E+01	1.1E+02	4.1E+02	1.1E+03	2.2E+03	4.0E+03	6.6E+03	1.0E+04	2.1E+04	4.7E+04	8.8E+04	1.2E+05	1.7E+05	2.5E+05
52 →	1.4E+01	9.4E+01	3.4E+02	8.6E+02	1.8E+03	3.3E+03	5.4E+03	8.2E+03	1.7E+04	3.7E+04	7.0E+04	9.9E+04	1.3E+05	2.0E+05
53 →	5.7E-02	1.8E+00	1.7E+01	8.0E+01	2.6E+02	6.7E+02	1.5E+03	2.8E+03	7.8E+03	2.4E+04	5.6E+04	8.9E+04	1.3E+05	2.2E+05
54 →	3.5E-02	7.5E-01	5.4E+00	2.2E+01	6.6E+01	1.6E+02	3.1E+02	5.7E+02	1.5E+03	4.2E+03	9.3E+03	1.4E+04	2.1E+04	3.4E+04
55 →	1.6E+00	2.1E+01	1.1E+02	3.8E+02	9.7E+02	2.0E+03	3.8E+03	6.3E+03	1.5E+04	3.8E+04	7.8E+04	1.2E+05	1.6E+05	2.6E+05
56 →	1.6E+00	2.1E+01	1.1E+02	3.9E+02	9.9E+02	2.1E+03	3.9E+03	6.6E+03	1.5E+04	4.0E+04	8.2E+04	1.2E+05	1.7E+05	2.7E+05
57 →	4.7E-06	1.6E-03	6.5E-02	8.4E-01	5.6E+00	2.4E+01	8.0E+01	2.1E+02	9.8E+02	5.1E+03	1.7E+04	3.1E+04	5.3E+04	1.0E+05
58 →	7.1E-05	1.1E-02	2.6E-01	2.5E+00	1.3E+01	4.8E+01	1.4E+02	3.3E+02	1.3E+03	5.8E+03	1.7E+04	3.1E+04	5.0E+04	9.4E+04
59 →	1.2E-04	1.9E-02	4.5E-01	4.1E+00	2.1E+01	7.7E+01	2.2E+02	5.2E+02	2.0E+03	8.8E+03	2.6E+04	4.5E+04	7.4E+04	1.4E+05
60 →	1.4E-04	2.0E-02	4.7E-01	4.2E+00	2.2E+01	7.9E+01	2.2E+02	5.2E+02	2.0E+03	8.8E+03	2.5E+04	4.5E+04	7.3E+04	1.4E+05
61 →	2.5E+00	4.2E+01	2.7E+02	1.0E+03	2.8E+03	6.4E+03	1.3E+04	2.2E+04	5.7E+04	1.6E+05	3.5E+05	5.3E+05	7.7E+05	1.3E+06
62 →	9.1E+00	1.1E+02	5.8E+02	1.9E+03	4.8E+03	1.0E+04	1.9E+04	3.1E+04	7.3E+04	1.9E+05	3.9E+05	5.9E+05	8.3E+05	1.3E+06
63 →	2.4E+01	2.4E+02	1.1E+03	3.4E+03	7.9E+03	1.6E+04	2.8E+04	4.6E+04	1.0E+05	2.6E+05	5.2E+05	7.6E+05	1.1E+06	1.7E+06
64 →	3.4E+00	5.1E+01	3.0E+02	1.1E+03	2.9E+03	6.5E+03	1.3E+04	2.2E+04	5.5E+04	1.5E+05	3.3E+05	5.0E+05	7.2E+05	1.2E+06
65 →	1.3E+03	5.7E+03	1.6E+04	3.3E+04	6.1E+04	1.0E+05	1.5E+05	2.2E+05	4.1E+05	8.6E+05	1.5E+06	2.1E+06	2.8E+06	4.0E+06

66 →	7.9E+02	3.7E+03	1.1E+04	2.4E+04	4.6E+04	7.7E+04	1.2E+05	1.8E+05	3.4E+05	7.1E+05	1.3E+06	1.8E+06	2.4E+06	3.5E+06
***β*-scissions**														
ref ←	6.0E-12	1.6E-06	3.1E-03	5.0E-01	1.9E+01	3.0E+02	2.5E+03	1.4E+04	1.8E+05	2.4E+06	1.3E+07	3.1E+07	6.3E+07	1.5E+08
1 ←	2.4E-12	1.0E-06	2.6E-03	5.1E-01	2.3E+01	3.9E+02	3.7E+03	2.2E+04	3.3E+05	4.9E+06	2.9E+07	7.3E+07	1.5E+08	3.7E+08
2 ←	1.1E-12	6.3E-07	2.0E-03	4.4E-01	2.1E+01	4.0E+02	3.9E+03	2.5E+04	3.9E+05	6.2E+06	3.9E+07	9.9E+07	2.1E+08	5.2E+08
3 ←	8.2E-13	3.6E-07	9.4E-04	1.9E-01	8.3E+00	1.4E+02	1.3E+03	8.1E+03	1.2E+05	1.8E+06	1.1E+07	2.6E+07	5.4E+07	1.3E+08
4 ←	1.4E-12	5.9E-07	1.5E-03	2.8E-01	1.2E+01	2.1E+02	2.0E+03	1.2E+04	1.7E+05	2.5E+06	1.5E+07	3.7E+07	7.8E+07	1.9E+08
5 ←	5.1E-15	9.3E-09	5.7E-05	2.0E-02	1.3E+00	3.1E+01	3.6E+02	2.6E+03	5.0E+04	9.6E+05	6.9E+06	1.8E+07	4.1E+07	1.1E+08
6 ←	1.9E-15	3.4E-09	2.1E-05	7.3E-03	4.9E-01	1.2E+01	1.4E+02	1.0E+03	2.0E+04	4.0E+05	3.0E+06	8.1E+06	1.8E+07	4.9E+07
7 ←	1.3E-13	9.6E-08	3.4E-04	8.2E-02	4.2E+00	8.0E+01	8.0E+02	5.1E+03	8.1E+04	1.3E+06	8.1E+06	2.0E+07	4.3E+07	1.1E+08
8 ←	1.1E-13	8.4E-08	3.1E-04	7.6E-02	4.0E+00	7.7E+01	7.8E+02	5.0E+03	8.1E+04	1.3E+06	8.3E+06	2.1E+07	4.5E+07	1.1E+08
9 ←	2.7E-11	6.1E-06	1.1E-02	1.7E+00	6.2E+01	9.5E+02	8.1E+03	4.5E+04	5.9E+05	7.8E+06	4.4E+07	1.0E+08	2.1E+08	4.9E+08
10 ←	3.3E-13	2.2E-07	7.5E-04	1.8E-01	9.1E+00	1.8E+02	1.8E+03	1.2E+04	1.9E+05	3.1E+06	2.0E+07	5.2E+07	1.1E+08	2.8E+08
11 ←	2.8E-12	9.9E-07	2.3E-03	4.3E-01	1.8E+01	3.1E+02	2.8E+03	1.7E+04	2.4E+05	3.5E+06	2.1E+07	5.1E+07	1.1E+08	2.5E+08
12 ←	1.5E-11	3.1E-06	5.2E-03	7.7E-01	2.8E+01	4.2E+02	3.5E+03	1.9E+04	2.5E+05	3.2E+06	1.8E+07	4.2E+07	8.5E+07	2.0E+08
13 ←	1.8E-15	4.6E-09	3.5E-05	1.4E-02	1.0E+00	2.7E+01	3.4E+02	2.6E+03	5.5E+04	1.2E+06	9.1E+06	2.5E+07	5.9E+07	1.6E+08
14 ←	1.9E-15	4.0E-09	2.7E-05	1.0E-02	7.2E-01	1.8E+01	2.2E+02	1.6E+03	3.3E+04	6.8E+05	5.1E+06	1.4E+07	3.2E+07	8.6E+07
15 ←	5.3E-15	7.4E-09	3.9E-05	1.3E-02	7.8E-01	1.8E+01	2.0E+02	1.4E+03	2.6E+04	5.0E+05	3.5E+06	9.4E+06	2.1E+07	5.5E+07
16 ←	1.9E-14	2.8E-08	1.5E-04	5.0E-02	3.2E+00	7.2E+01	8.3E+02	5.9E+03	1.1E+05	2.1E+06	1.5E+07	4.0E+07	9.0E+07	2.4E+08
17 ←	3.4E-21	2.9E-13	1.9E-08	3.1E-05	6.4E-03	3.5E-01	7.9E+00	9.7E+01	4.2E+03	1.8E+05	2.2E+06	7.8E+06	2.2E+07	7.5E+07
18 ←	8.7E-21	5.7E-13	3.1E-08	4.5E-05	8.6E-03	4.4E-01	9.6E+00	1.1E+02	4.6E+03	1.9E+05	2.2E+06	7.8E+06	2.1E+07	7.2E+07
19 ←	3.4E-20	1.7E-12	8.0E-08	1.1E-04	1.9E-02	9.3E-01	1.9E+01	2.2E+02	8.6E+03	3.4E+05	3.9E+06	1.3E+07	3.6E+07	1.2E+08
20 ←	5.0E-20	2.3E-12	9.9E-08	1.3E-04	2.1E-02	1.0E+00	2.1E+01	2.3E+02	8.5E+03	3.1E+05	3.5E+06	1.2E+07	3.1E+07	1.0E+08
21 ←	1.0E-11	2.3E-06	3.9E-03	5.8E-01	2.1E+01	3.1E+02	2.5E+03	1.3E+04	1.6E+05	2.0E+06	1.1E+07	2.5E+07	5.0E+07	1.1E+08
22 ←	9.3E-12	2.6E-06	5.1E-03	8.3E-01	3.2E+01	5.0E+02	4.2E+03	2.4E+04	3.1E+05	4.1E+06	2.3E+07	5.4E+07	1.1E+08	2.5E+08
23 ←	2.0E-13	1.0E-07	2.9E-04	6.1E-02	2.8E+00	4.9E+01	4.6E+02	2.8E+03	4.1E+04	6.1E+05	3.7E+06	9.0E+06	1.9E+07	4.5E+07
24 ←	2.2E-13	9.6E-08	2.5E-04	4.9E-02	2.2E+00	3.7E+01	3.4E+02	2.0E+03	2.9E+04	4.3E+05	2.6E+06	6.2E+06	1.3E+07	3.1E+07
25 ←	2.0E-10	2.1E-05	2.2E-02	2.4E+00	7.0E+01	8.7E+02	6.3E+03	3.0E+04	3.3E+05	3.5E+06	1.7E+07	3.8E+07	7.3E+07	1.6E+08
26 ←	2.4E-10	2.4E-05	2.5E-02	2.6E+00	7.5E+01	9.3E+02	6.6E+03	3.2E+04	3.4E+05	3.7E+06	1.8E+07	4.0E+07	7.6E+07	1.6E+08
27 ←	2.1E-10	1.9E-05	1.9E-02	2.0E+00	5.5E+01	6.7E+02	4.7E+03	2.2E+04	2.3E+05	2.4E+06	1.1E+07	2.5E+07	4.6E+07	1.0E+08
28 ←	2.2E-10	2.1E-05	2.1E-02	2.2E+00	6.1E+01	7.5E+02	5.3E+03	2.5E+04	2.7E+05	2.9E+06	1.4E+07	3.0E+07	5.8E+07	1.3E+08
29 ←	1.7E-11	2.8E-06	4.0E-03	5.1E-01	1.6E+01	2.2E+02	1.7E+03	8.6E+03	9.8E+04	1.1E+06	5.6E+06	1.2E+07	2.4E+07	5.3E+07
30 ←	1.0E-10	1.2E-05	1.5E-02	1.7E+00	5.0E+01	6.4E+02	4.6E+03	2.3E+04	2.5E+05	2.7E+06	1.3E+07	2.9E+07	5.5E+07	1.2E+08
31 ←	1.7E-14	2.0E-08	9.7E-05	2.8E-02	1.7E+00	3.5E+01	3.8E+02	2.6E+03	4.5E+04	7.9E+05	5.3E+06	1.4E+07	3.0E+07	7.7E+07
32 ←	2.3E-14	2.5E-08	1.1E-04	3.1E-02	1.7E+00	3.6E+01	3.9E+02	2.6E+03	4.4E+04	7.6E+05	5.1E+06	1.3E+07	2.8E+07	7.2E+07
33 ←	3.2E-09	1.8E-04	1.4E-01	1.2E+01	2.8E+02	3.1E+03	2.0E+04	8.8E+04	8.3E+05	7.9E+06	3.5E+07	7.5E+07	1.4E+08	2.9E+08
34 ←	8.4E-10	6.2E-05	5.4E-02	5.0E+00	1.3E+02	1.5E+03	9.9E+03	4.5E+04	4.5E+05	4.4E+06	2.0E+07	4.3E+07	8.1E+07	1.7E+08
35 ←	4.6E-10	3.8E-05	3.6E-02	3.5E+00	9.3E+01	1.1E+03	7.5E+03	3.5E+04	3.6E+05	3.6E+06	1.7E+07	3.6E+07	6.8E+07	1.5E+08

36 ←	3.7E-10	3.3E-05	3.2E-02	3.3E+00	8.9E+01	1.1E+03	7.4E+03	3.5E+04	3.6E+05	3.7E+06	1.8E+07	3.8E+07	7.2E+07	1.5E+08
37 ←	8.0E-08	2.1E-03	9.7E-01	5.9E+01	1.1E+03	1.0E+04	5.8E+04	2.3E+05	1.8E+06	1.5E+07	5.9E+07	1.2E+08	2.1E+08	4.0E+08
38 ←	9.5E-09	4.5E-04	2.9E-01	2.3E+01	5.2E+02	5.4E+03	3.3E+04	1.4E+05	1.3E+06	1.2E+07	5.1E+07	1.1E+08	1.9E+08	3.9E+08
39 ←	2.2E-08	7.7E-04	4.3E-01	2.9E+01	6.1E+02	5.9E+03	3.5E+04	1.4E+05	1.2E+06	1.0E+07	4.3E+07	8.7E+07	1.6E+08	3.1E+08
40 ←	2.9E-08	9.2E-04	4.8E-01	3.2E+01	6.3E+02	6.0E+03	3.4E+04	1.4E+05	1.1E+06	9.1E+06	3.7E+07	7.3E+07	1.3E+08	2.5E+08
41 ←	1.7E-09	1.2E-04	1.0E-01	9.6E+00	2.5E+02	2.8E+03	1.9E+04	8.5E+04	8.3E+05	8.0E+06	3.6E+07	7.8E+07	1.4E+08	3.0E+08
42 ←	3.3E-09	1.3E-04	8.0E-02	5.7E+00	1.2E+02	1.2E+03	7.4E+03	3.1E+04	2.7E+05	2.3E+06	9.6E+06	2.0E+07	3.5E+07	7.1E+07
43 ←	1.3E-11	2.4E-06	3.6E-03	4.7E-01	1.6E+01	2.2E+02	1.7E+03	8.8E+03	1.0E+05	1.2E+06	6.3E+06	1.4E+07	2.8E+07	6.2E+07
44 ←	2.2E-11	3.7E-06	5.2E-03	6.7E-01	2.2E+01	3.0E+02	2.3E+03	1.2E+04	1.3E+05	1.5E+06	7.7E+06	1.7E+07	3.4E+07	7.5E+07
45 ←	1.3E-06	1.4E-02	3.6E+00	1.5E+02	2.1E+03	1.6E+04	7.5E+04	2.6E+05	1.7E+06	1.1E+07	3.8E+07	7.0E+07	1.2E+08	2.1E+08
46 ←	7.0E-07	8.6E-03	2.5E+00	1.1E+02	1.7E+03	1.3E+04	6.3E+04	2.2E+05	1.5E+06	9.9E+06	3.5E+07	6.5E+07	1.1E+08	2.0E+08
47 ←	2.2E-08	5.6E-04	2.6E-01	1.5E+01	2.9E+02	2.7E+03	1.5E+04	6.0E+04	4.7E+05	3.8E+06	1.5E+07	3.0E+07	5.2E+07	1.0E+08
48 ←	2.3E-08	5.8E-04	2.6E-01	1.6E+01	3.0E+02	2.7E+03	1.5E+04	5.8E+04	4.6E+05	3.6E+06	1.4E+07	2.8E+07	4.8E+07	9.3E+07
49 ←	5.1E-08	1.5E-03	7.7E-01	5.0E+01	1.0E+03	9.4E+03	5.4E+04	2.2E+05	1.8E+06	1.4E+07	5.7E+07	1.1E+08	2.0E+08	4.0E+08
50 ←	9.3E-08	2.2E-03	9.7E-01	5.6E+01	1.0E+03	8.8E+03	4.8E+04	1.8E+05	1.4E+06	1.0E+07	3.9E+07	7.6E+07	1.3E+08	2.5E+08
51 ←	8.2E-10	6.8E-05	6.2E-02	5.9E+00	1.5E+02	1.8E+03	1.2E+04	5.5E+04	5.3E+05	5.2E+06	2.4E+07	5.0E+07	9.3E+07	1.9E+08
52 ←	8.0E-10	6.1E-05	5.3E-02	4.9E+00	1.2E+02	1.4E+03	9.3E+03	4.2E+04	4.0E+05	3.9E+06	1.7E+07	3.7E+07	6.8E+07	1.4E+08
53 ←	1.2E-04	3.8E-01	4.9E+01	1.3E+03	1.3E+04	7.5E+04	2.9E+05	8.7E+05	4.4E+06	2.2E+07	6.6E+07	1.1E+08	1.8E+08	3.0E+08
54 ←	3.7E-04	9.8E-01	1.1E+02	2.7E+03	2.6E+04	1.4E+05	5.3E+05	1.5E+06	7.3E+06	3.5E+07	1.0E+08	1.7E+08	2.6E+08	4.3E+08
55 ←	9.3E-06	5.9E-02	1.2E+01	4.1E+02	5.1E+03	3.4E+04	1.5E+05	5.0E+05	2.9E+06	1.7E+07	5.6E+07	1.0E+08	1.6E+08	2.9E+08
56 ←	4.3E-06	3.1E-02	6.7E+00	2.4E+02	3.2E+03	2.2E+04	9.9E+04	3.3E+05	2.0E+06	1.2E+07	4.0E+07	7.2E+07	1.2E+08	2.1E+08
57 ←	2.2E-01	8.7E+01	3.3E+03	3.8E+04	2.2E+05	8.1E+05	2.3E+06	5.1E+06	1.8E+07	6.0E+07	1.4E+08	2.1E+08	2.9E+08	4.3E+08
58 ←	3.0E+00	6.7E+02	1.8E+04	1.7E+05	8.1E+05	2.7E+06	6.8E+06	1.4E+07	4.4E+07	1.4E+08	2.8E+08	4.1E+08	5.6E+08	8.0E+08
59 ←	6.9E-02	3.1E+01	1.2E+03	1.5E+04	8.8E+04	3.4E+05	9.5E+05	2.2E+06	7.7E+06	2.7E+07	6.2E+07	9.3E+07	1.3E+08	2.0E+08
60 ←	4.0E-02	1.9E+01	7.9E+02	9.6E+03	5.8E+04	2.2E+05	6.3E+05	1.5E+06	5.2E+06	1.8E+07	4.2E+07	6.4E+07	9.0E+07	1.4E+08
61 ←	1.3E-07	2.6E-03	1.0E+00	5.6E+01	1.0E+03	8.9E+03	4.9E+04	1.9E+05	1.5E+06	1.2E+07	4.7E+07	9.3E+07	1.6E+08	3.2E+08
62 ←	1.9E-06	2.3E-02	7.0E+00	3.2E+02	4.9E+03	3.9E+04	1.9E+05	7.1E+05	4.9E+06	3.4E+07	1.2E+08	2.4E+08	4.0E+08	7.6E+08
63 ←	2.9E-08	1.2E-03	8.0E-01	6.1E+01	1.4E+03	1.4E+04	8.8E+04	3.8E+05	3.4E+06	3.1E+07	1.3E+08	2.8E+08	5.1E+08	1.0E+09
64 ←	8.9E-08	1.9E-03	7.6E-01	4.2E+01	7.6E+02	6.7E+03	3.6E+04	1.4E+05	1.1E+06	8.1E+06	3.2E+07	6.2E+07	1.1E+08	2.1E+08
65 ←	1.4E-12	6.6E-07	1.7E-03	3.3E-01	1.4E+01	2.4E+02	2.2E+03	1.3E+04	1.8E+05	2.5E+06	1.5E+07	3.6E+07	7.3E+07	1.7E+08
66 ←	3.6E-12	1.4E-06	3.4E-03	6.0E-01	2.5E+01	4.1E+02	3.6E+03	2.0E+04	2.8E+05	3.8E+06	2.2E+07	5.2E+07	1.1E+08	2.5E+08

Table S11: Applied symmetry numbers and corresponding reaction path degeneracy for the carbon-centered radical additions and their reverse *β*-scission reactions presented in Table 6-1. (σ_{ext}: external symmetry number, σ_{int}: internal symmetry number, n_{opt}: number of optical isomers, n_e: reaction path degeneracy or number of single events for the addition and the *β*-scission reaction).

Reaction	addition						β-scission						Reaction Path Degeneracy	
	reactant 1			reactant 2			reactant			transition state			addition	*β*-scission
	σ_{ext}	σ_{int}	n_{opt}	σ_{ext}	σ_{int}	n_{opt}	σ_{ext}	σ_{int}	n_{opt}	σ_{ext}	σ_{int}	n_{opt}	n_{efor}	n_{erev}
ref	6	1	1	4	1	1	1	6	1	1	3	1	8	2
1	6	1	1	1	1	1	1	3	1	1	3	2	4	2
2	6	1	1	1	3	1	1	9	1	1	9	2	4	2
3	6	1	1	1	1	1	1	3	1	1	3	2	4	2
4	6	1	1	1	3	1	1	9	1	1	9	2	4	2
5	6	1	1	1	1	1	1	3	1	1	3	2	4	2
6	6	1	1	1	3	1	1	9	1	1	9	2	4	2
7	6	1	1	1	1	1	1	3	1	1	3	2	4	2
8	6	1	1	1	3	1	1	9	1	1	9	2	4	2
9	6	1	1	1	3	1	1	9	1	1	9	2	4	2
10	6	1	1	1	9	1	1	27	1	1	27	2	4	2
11	6	1	1	1	3	1	1	9	1	1	9	2	4	2
12	6	1	1	1	9	1	1	27	1	1	27	2	4	2
13	6	1	1	1	3	1	1	9	1	1	9	2	4	2
14	6	1	1	1	9	1	1	27	1	1	27	2	4	2
15	6	1	1	1	3	1	1	9	1	1	9	2	4	2
16	6	1	1	1	9	1	1	27	1	1	27	2	4	2
17	6	1	1	1	1	1	1	3	1	1	3	2	4	2
18	6	1	1	1	3	1	1	9	1	1	9	2	4	2
19	6	1	1	1	1	1	1	3	1	1	3	2	4	2
20	6	1	1	1	3	1	1	9	1	1	9	2	4	2
21	6	1	1	1	1	1	1	3	1	1	3	2	4	2
22	6	1	1	1	3	1	1	9	1	1	9	2	4	2
23	6	1	1	1	1	1	1	3	1	1	3	2	4	2
24	6	1	1	1	3	1	1	9	1	1	9	2	4	2
25	6	1	1	1	1	1	1	3	1	1	3	2	4	2
26	6	1	1	1	3	1	1	9	1	1	9	2	4	2
27	6	1	1	1	1	1	1	3	1	1	3	2	4	2
28	6	1	1	1	3	1	1	9	1	1	9	2	4	2
29	6	1	1	1	3	1	1	9	1	1	9	2	4	2
30	6	1	1	1	9	1	1	27	1	1	27	2	4	2
31	6	1	1	1	3	1	1	9	1	1	9	2	4	2

32	6	1	1	1	9	1	1	27	1	1	27	2	4	2
33	6	1	1	1	3	1	1	9	1	1	9	2	4	2
34	6	1	1	1	9	1	1	27	1	1	27	2	4	2
35	6	1	1	1	3	1	1	9	1	1	9	2	4	2
36	6	1	1	1	9	1	1	27	1	1	27	2	4	2
37	6	1	1	1	1	1	1	3	1	1	3	2	4	2
38	6	1	1	1	3	1	1	9	1	1	9	2	4	2
39	6	1	1	1	1	1	1	3	1	1	3	2	4	2
40	6	1	1	1	3	1	1	9	1	1	9	2	4	2
41	1	1	1	4	1	1	1	1	1	1	1	2	8	2
42	1	3	1	4	1	1	1	3	1	1	3	2	8	2
43	1	1	1	4	1	1	1	1	1	1	1	2	8	2
44	1	3	1	4	1	1	1	3	1	1	3	2	8	2
45	1	1	1	4	1	1	1	1	1	1	1	2	8	2
46	1	3	1	4	1	1	1	3	1	1	3	2	8	2
47	1	2	1	4	1	1	1	2	1	1	1	1	8	2
48	1	3	1	4	1	1	1	3	1	1	3	2	8	2
49	1	3	1	4	1	1	1	3	1	1	3	2	8	2
50	1	9	1	4	1	1	1	9	1	1	9	2	8	2
51	1	3	1	4	1	1	1	3	1	1	3	2	8	2
52	1	9	1	4	1	1	1	9	1	1	9	2	8	2
53	1	3	1	4	1	1	1	3	1	1	3	2	8	2
54	1	9	1	4	1	1	1	9	1	1	9	2	8	2
55	1	3	1	4	1	1	1	3	1	1	3	2	8	2
56	1	9	1	4	1	1	1	9	1	1	9	2	8	2
57	1	1	1	4	1	1	1	1	1	1	1	2	8	2
58	1	3	1	4	1	1	1	3	1	1	3	2	8	2
59	1	1	1	4	1	1	1	1	1	1	1	2	8	2
60	1	3	1	4	1	1	1	3	1	1	3	2	8	2
61	1	1	1	4	1	1	1	1	1	1	1	2	8	2
62	1	3	1	4	1	1	1	3	1	1	3	2	8	2
63	1	1	1	4	1	1	1	1	1	1	1	2	8	2
64	1	3	1	4	1	1	1	3	1	1	3	2	8	2
65	1	1	1	4	1	1	1	1	1	1	1	2	8	2
66	1	3	1	4	1	1	1	3	1	1	3	2	8	2

Table S12: Arrhenius parameters for the reference reaction (carbon-centered radical addition of methyl radical to ethene and the reverse β-scission of 1-propyl radical into methyl and ethene in temperature range from 300 to 2500 K). (Temperature T (K), single-event pre-exponential factor $\log\tilde{A}$ [$\log(m^3\ mol^{-1}\ s^{-1})$], activation energy E_a (kJ mol^{-1})).

	addition		β-scission	
T	$\log\tilde{A}$	E_a	$\log\tilde{A}$	E_a
300	4.882	30.5	10.184	125.1
400	5.075	31.8	10.313	125.9
500	5.265	33.4	10.400	126.7
600	5.439	35.2	10.458	127.3
700	5.593	37.1	10.496	127.8
800	5.731	39.1	10.521	128.1
900	5.855	41.1	10.537	128.4
1000	5.968	43.1	10.547	128.5
1100	6.070	45.2	10.553	128.7
1200	6.164	47.2	10.556	128.7
1300	6.250	49.3	10.558	128.8
1400	6.331	51.4	10.559	128.8
1500	6.406	53.5	10.559	128.8
1600	6.476	55.5	10.558	128.8
1700	6.542	57.6	10.558	128.8
1800	6.604	59.7	10.557	128.8
1900	6.663	61.8	10.556	128.7
2000	6.719	63.9	10.556	128.7
2100	6.772	65.9	10.555	128.7
2200	6.823	68.0	10.554	128.6
2300	6.871	70.1	10.553	128.6
2400	6.917	72.2	10.553	128.6
2500	6.962	74.3	10.552	128.5

Table S13: Average deviation for the comparison between GA predicted and AI calculated values for the reactions included in Table 6-1 using (a) only primary contributions and (b) primary along with secondary contributions at 300 K, 600 K and 1000 K. (MAD: mean absolute deviation, RMS: root mean square deviation, MAX: maximum deviation). Single-event pre-exponential factors, $\log\tilde{A}$ [$\log(m^3\ mol^{-1}\ s^{-1})$], and activation energies, E_a ($kJ\ mol^{-1}$).

	300 K				**600 K**				**1000 K**			
	addition		***β*-scission**		**addition**		***β*-scission**		**addition**		***β*-scission**	
Only primary contributions included												
	$\log\tilde{A}$	E_a	$\log\tilde{A}$	E_a	$\log\tilde{A}$	E_a	$\log\tilde{A}$	E_a	$\log\tilde{A}$	E_a	$\log\tilde{A}$	E_a
MAD	0.127	2.1	0.140	3.5	0.131	2.2	0.148	3.5	0.133	2.2	0.149	3.6
RMS	0.173	2.7	0.182	4.4	0.181	2.8	0.192	4.5	0.184	2.9	0.194	4.5
MAX	0.621	6.9	0.457	12.1	0.618	6.9	0.451	12.4	0.615	7.0	0.446	12.6
Primary and secondary contributions included												
	$\log\tilde{A}$	E_a	$\log\tilde{A}$	E_a	$\log\tilde{A}$	E_a	$\log\tilde{A}$	E_a	$\log\tilde{A}$	E_a	$\log\tilde{A}$	E_a
MAD	0.082	1.0	0.101	1.4	0.083	1.0	0.105	1.5	0.083	1.0	0.107	1.5
RMS	0.110	1.3	0.138	1.9	0.114	1.3	0.144	2.0	0.115	1.3	0.147	2.1
MAX	0.330	3.9	0.373	4.9	0.356	4.0	0.404	5.0	0.360	4.0	0.417	5.1

Table S14: Standard reaction enthalpies $\Delta_r H^o$ (kJ mol^{-1}), standard reaction entropies $\Delta_r S^o$ (J mol^{-1} K^{-1}), pre-exponential factors log*A* [log(m^3 mol^{-1} s^{-1})], activation energies E_a (kJ mol^{-1}) and rate coefficients *k* (m^3 mol^{-1} s^{-1}), at 300 K for the 24 reactions of the ab initio validation set. [$k = \kappa A\, exp(-E_a/RT)$]. Arrhenius parameters do not include tunneling contributions.

	Reactions	addition					β-scission		
		$\Delta_r H^o$	$\Delta_r S^o$	log *A*	E_a	κk_{for}	log *A*	E_a	κk_{rev}
2/1	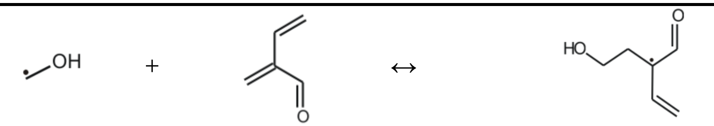	-168.3	-140.3	4.018	-4.0	4.7E+04	11.348	164.3	5.2E-18
2/2	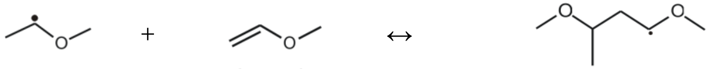	-80.4	-124.1	4.480	28.1	4.5E-01	10.961	108.5	1.4E-08
2/3	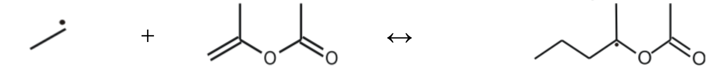	-98.4	-122.7	3.822	20.3	2.4E+00	10.233	118.7	4.5E-11
2/4		-96.0	-126.5	3.515	26.2	1.1E-01	10.125	122.2	9.4E-12
2/5	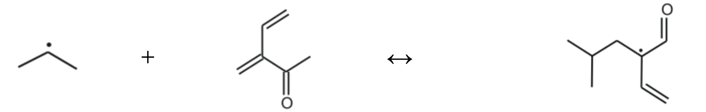	-170.7	-148.9	3.820	-5.9	6.6E+04	11.598	164.8	8.0E-18
2/6	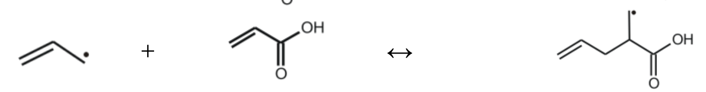	-24.4	-108.4	4.205	46.8	1.5E-04	9.870	71.2	4.0E-03
2/7		-135.9	-117.1	4.553	7.3	2.0E+03	10.671	143.2	6.1E-15
2/8		-85.7	-114.3	4.654	29.2	4.5E-01	10.625	114.9	5.1E-10
2/9		-79.6	-124.7	4.042	29.4	9.6E-02	10.558	109.0	4.6E-09
2/10	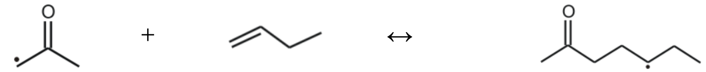	-70.7	-107.2	3.750	21.0	1.4E+00	9.350	91.7	2.9E-07
2/11	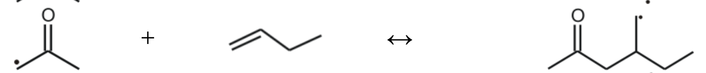	-66.0	-125.9	3.276	24.7	1.1E-01	9.850	90.7	1.4E-06
2/12	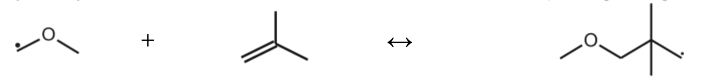	-76.2	-130.2	3.517	33.6	5.6E-03	10.317	109.8	1.9E-09

2/13	$^{\bullet}CH_3$	+	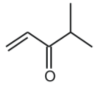	↔	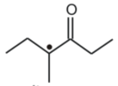	-129.5	-100.5	5.058	15.7	2.5E+02	10.306	145.2	1.2E-15
2/14	$^{\bullet}CH_3$	+	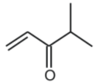	↔	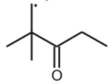	-81.6	-116.7	4.406	30.4	1.6E-01	10.503	112.0	1.3E-09
2/15		+	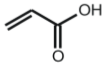	↔	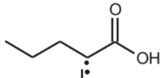	-115.7	-125.5	3.706	9.9	1.0E+02	10.260	125.6	2.7E-12
2/16		+	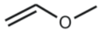	↔	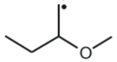	-78.0	-129.0	3.958	40.2	1.2E-03	10.698	118.2	1.8E-10
2/17	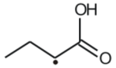	+		↔	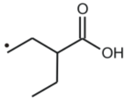	-66.7	-111.0	4.317	22.0	3.6E+00	10.117	88.7	5.7E-06
2/18	$^{\bullet}CH_3$	+	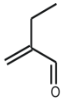	↔	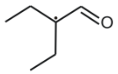	-130.7	-105.8	5.104	15.9	2.5E+02	10.630	146.6	1.4E-15
2/19	$^{\bullet}CH_3$	+	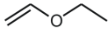	↔	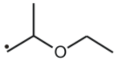	-81.8	-104.5	5.352	44.0	6.5E-03	10.809	125.8	1.1E-11
2/20	$^{\bullet}CH_3$	+	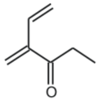	↔	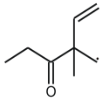	-81.0	-113.1	4.874	27.4	1.5E+00	10.783	108.4	1.0E-08
2/21	$^{\bullet}CH_3$	+	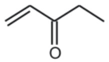	↔	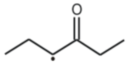	-128.4	-99.3	5.079	14.9	3.5E+02	10.266	143.3	2.3E-15
2/22	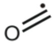	+	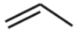	↔	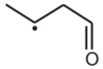	-72.1	-94.6	4.662	24.1	3.3E+00	9.605	96.2	8.4E-08
2/23	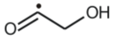	+	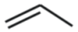	↔	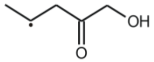	-87.3	-119.1	4.745	21.4	1.1E+01	10.968	108.7	1.3E-08
2/24	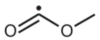	+	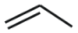	↔	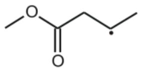	-115.7	-102.7	4.869	11.1	9.1E+02	10.233	126.8	1.6E-12

Table S15: Standard reaction enthalpies $\Delta_r H^o$ (kJ mol^{-1}), standard reaction entropies $\Delta_r S^o$ (J mol^{-1} K^{-1}), pre-exponential factors log$A$ [log(m^3 mol^{-1} s^{-1})], activation energies E_a (kJ mol^{-1}) and rate coefficients k (m^3 mol^{-1} s^{-1}), at 600 K for the 24 reactions of the ab initio validation set. [$k = \kappa A\ exp(-E_a/RT)$]. Arrhenius parameters do not include tunneling contributions.

	Reactions	addition					β-scission		
		$\Delta_r H^o$	$\Delta_r S^o$	log A	E_a	κk_{for}	log A	E_a	κk_{rev}
2/1	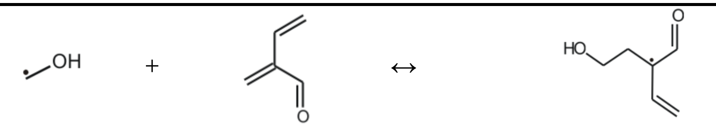	-163.4	-129.3	5.021	4.1	4.5E+04	11.773	167.5	1.5E-03
2/2	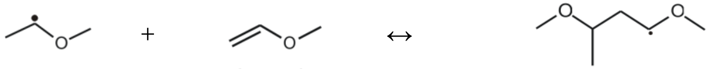	-74.9	-111.2	5.330	35.0	2.0E+02	11.138	109.9	3.9E+01
2/3	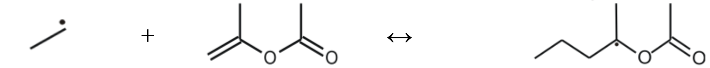	-95.7	-116.6	4.445	25.4	1.8E+02	10.536	121.1	1.0E+00
2/4	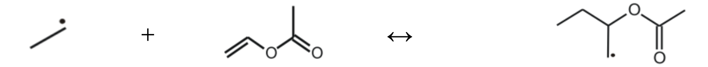	-91.3	-115.7	4.244	32.2	2.9E+01	10.286	123.5	3.7E-01
2/5	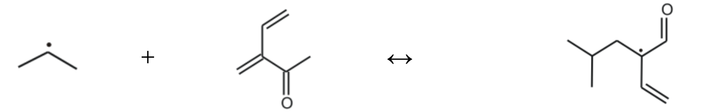	-166.5	-139.6	4.504	-0.2	3.3E+04	11.795	166.3	2.1E-03
2/6	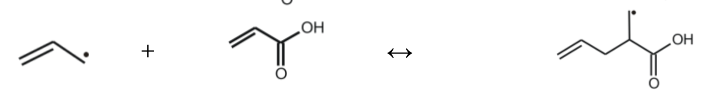	-18.1	-93.6	5.038	53.6	2.5E+00	9.928	71.7	5.3E+03
2/7		-131.6	-107.2	5.312	13.5	1.4E+04	10.913	145.1	2.0E-02
2/8		-81.3	-104.1	5.362	35.0	2.2E+02	10.801	116.3	5.0E+00
2/9		-74.6	-113.5	4.929	36.7	5.7E+01	10.856	111.3	1.6E+01
2/10	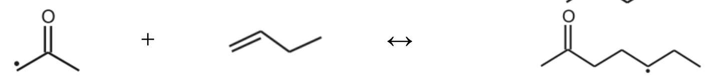	-66.1	-96.6	4.560	27.6	1.5E+02	9.607	93.7	2.9E+01
2/11	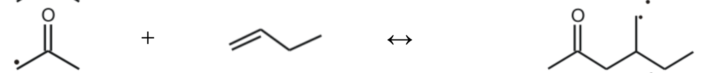	-60.0	-112.0	4.267	32.8	2.7E+01	10.116	92.8	1.1E+02
2/12	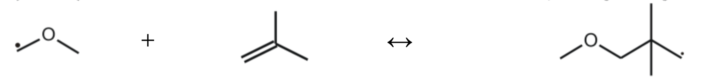	-70.7	-117.5	4.333	40.3	7.0E+00	10.471	111.0	6.8E+00

2/13	$^{\bullet}CH_3$	+	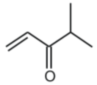	↔	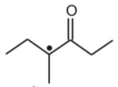	-128.3	-98.0	5.614	20.3	7.2E+03	10.731	148.6	6.5E-03
2/14	$^{\bullet}CH_3$	+	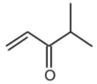	↔	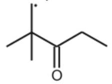	-77.9	-108.5	5.026	35.6	8.9E+01	10.695	113.5	7.0E+00
2/15		+	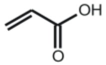	↔	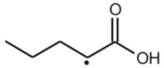	-112.6	-118.5	4.334	15.1	1.1E+03	10.523	127.7	2.6E-01
2/16		+	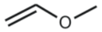	↔	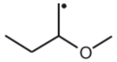	-72.8	-117.0	4.732	46.5	5.2E+00	10.844	119.3	3.1E+00
2/17	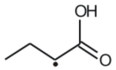	+		↔	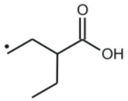	-61.1	-98.0	5.110	28.5	4.4E+02	10.228	89.6	2.9E+02
2/18	$^{\bullet}CH_3$	+	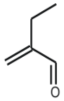	↔	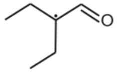	-129.6	-103.6	5.661	20.5	7.7E+03	11.071	150.1	1.0E-02
2/19	$^{\bullet}CH_3$	+	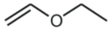	↔	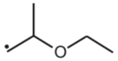	-78.5	-97.0	5.983	49.2	5.3E+01	11.050	127.7	9.4E-01
2/20	$^{\bullet}CH_3$	+	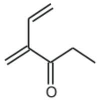	↔	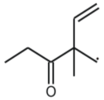	-77.0	-104.2	5.512	32.7	4.8E+02	10.956	109.7	2.7E+01
2/21	$^{\bullet}CH_3$	+	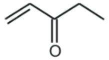	↔	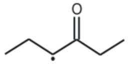	-127.1	-96.6	5.646	19.6	8.9E+03	10.690	146.7	8.6E-03
2/22	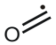	+	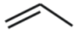	↔	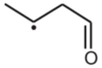	-67.8	-85.0	5.498	31.0	6.5E+02	9.936	98.8	2.2E+01
2/23	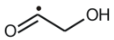	+	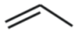	↔	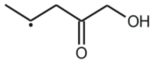	-82.2	-107.5	5.549	28.0	1.3E+03	11.166	110.2	3.8E+01
2/24	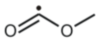	+	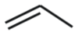	↔	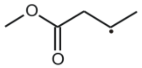	-110.4	-90.4	5.676	17.7	1.4E+04	10.396	128.1	1.8E-01

Table S16: Standard reaction enthalpies $\Delta_r H^o$ (kJ mol^{-1}), standard reaction entropies $\Delta_r S^o$ (J mol^{-1} K^{-1}), pre-exponential factors log$A$ [log(m^3 mol^{-1} s^{-1})], activation energies E_a (kJ mol^{-1}) and rate coefficients k (m^3 mol^{-1} s^{-1}), at 1000 K for the 24 reactions of the ab initio validation set. [$k = \kappa A\ exp(-E_a/RT)$]. Arrhenius parameters do not include tunneling contributions.

Reactions						addition					β-scission		
						$\Delta_r H^o$	$\Delta_r S^o$	**log *A***	E_a	κk_{for}	**log *A***	E_a	κk_{rev}
2/1	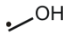	+	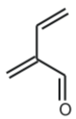	↔	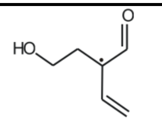	-154.6	-118.0	5.651	13.5	8.8E+04	11.815	168.1	1.1E+03
2/2	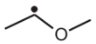	+	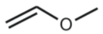	↔	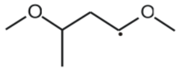	-66.3	-100.1	5.910	43.6	4.3E+03	11.140	109.9	2.6E+05
2/3		+	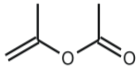	↔	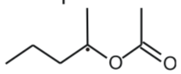	-89.1	-108.2	4.973	33.3	1.7E+03	10.627	122.4	1.8E+04
2/4		+	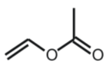	↔	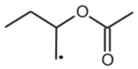	-83.2	-105.4	4.808	40.7	4.9E+02	10.315	123.9	7.2E+03
2/5		+	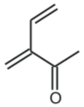	↔	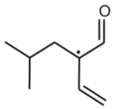	-158.9	-129.8	5.056	8.0	4.3E+04	11.837	166.9	1.3E+03
2/6	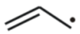	+	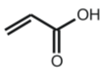	↔	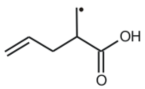	-9.4	-82.5	5.627	62.4	2.4E+02	9.937	71.8	1.6E+06
2/7	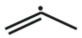	+	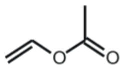	↔	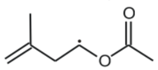	-124.2	-97.9	5.881	22.0	5.4E+04	10.993	146.2	2.3E+03
2/8	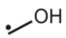	+	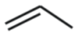	↔	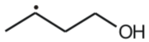	-73.2	-93.8	5.923	43.4	4.6E+03	10.823	116.6	5.5E+04
2/9	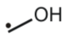	+	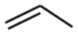	↔	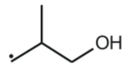	-65.8	-102.2	5.545	45.8	1.4E+03	10.884	111.6	1.2E+05
2/10	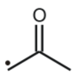	+	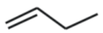	↔	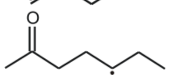	-58.6	-87.0	5.118	35.9	1.8E+03	9.665	94.5	5.5E+04
2/11	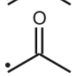	+	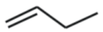	↔	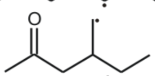	-51.3	-100.7	4.902	42.2	5.1E+02	10.162	93.5	2.0E+05
2/12	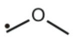	+	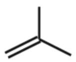	↔	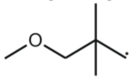	-61.5	-105.6	4.935	49.2	2.3E+02	10.450	110.7	4.8E+04

2/13	$^{\bullet}CH_3$	+	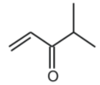	↔	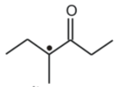	-122.4	-90.6	6.134	28.1	4.7E+04	10.867	150.5	1.0E+03
2/14	$^{\bullet}CH_3$	+	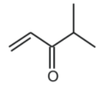	↔	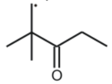	-70.6	-99.2	5.566	43.7	2.0E+03	10.750	114.3	6.2E+04
2/15		+	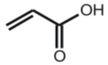	↔	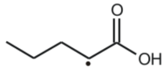	-105.6	-109.7	4.870	23.2	4.6E+03	10.601	128.8	7.5E+03
2/16		+	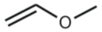	↔	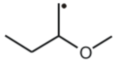	-64.3	-106.2	5.310	55.1	2.8E+02	10.855	119.4	4.3E+04
2/17	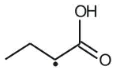	+		↔	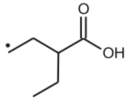	-52.3	-86.8	5.689	37.1	5.7E+03	10.222	89.4	3.6E+05
2/18	$^{\bullet}CH_3$	+	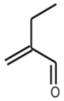	↔	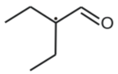	-123.9	-96.4	6.182	28.3	5.1E+04	11.219	152.2	1.9E+03
2/19	$^{\bullet}CH_3$	+	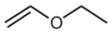	↔	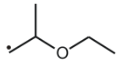	-71.1	-87.7	6.533	57.5	3.5E+03	11.116	128.6	2.6E+04
2/20	$^{\bullet}CH_3$	+	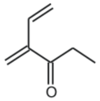	↔	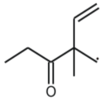	-68.7	-93.6	6.057	40.9	8.5E+03	10.947	109.6	1.7E+05
2/21	$^{\bullet}CH_3$	+	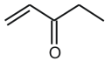	↔	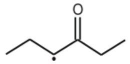	-121.1	-89.1	6.171	27.5	5.5E+04	10.826	148.6	1.2E+03
2/22	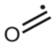	+	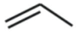	↔	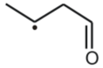	-60.4	-75.4	6.117	40.2	1.1E+04	10.057	100.6	6.5E+04
2/23	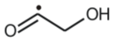	+	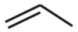	↔	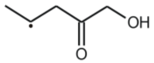	-74.4	-97.5	6.138	36.8	1.7E+04	11.231	111.2	2.7E+05
2/24	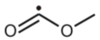	+	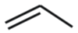	↔	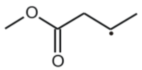	-102.4	-80.1	6.268	26.5	7.7E+04	10.453	128.9	5.3E+03

Table S17: Comparison between group additive (GA) predicted and ab initio (AI) calculated kinetic parameters at 600 K for the ab initio validation set of 24 reactions. ($\Delta\log A = \log A_{GA} - \log A_{AI}$ in $\log(m^3\ mol^{-1}\ s^{-1})$, $\Delta E_a = E_{a,GA} - E_{a,AI}$ in kJ mol^{-1}). [MAD: mean absolute deviation, RMS: root mean square deviation, MAX: maximum deviation, <ρ>: factor of deviation between two values taken from equation (6-4)].

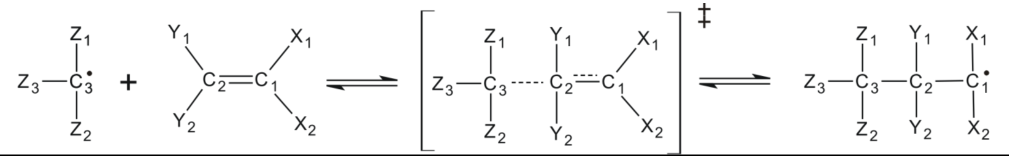

	Reactions					addition			β-scission			
						Δlog *A*	**ΔE_a**	**k_{GA}/k_{AI}**	**Δlog *A***	**ΔE_a**	**k_{GA}/k_{AI}**	$\frac{K^{eq}_{GA}}{K^{eq}_{AI}}$
2/1	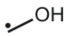	+	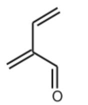	↔	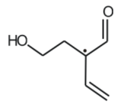	0.227	5.2	0.6	0.248	3.9	0.8	0.75
2/2	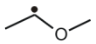	+	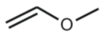	↔	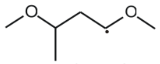	0.041	-2.4	1.7	0.182	1.5	1.1	1.60
2/3		+	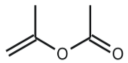	↔	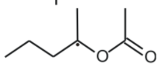	0.152	1.1	1.1	0.237	-0.3	1.7	0.62
2/4		+	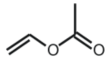	↔	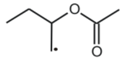	0.104	4.2	0.5	0.159	5.6	0.4	1.19
2/5		+	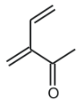	↔	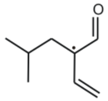	-0.121	4.4	0.3	-0.213	1.2	0.5	0.66
2/6	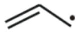	+	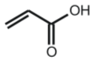	↔	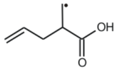	0.065	2.3	0.7	-0.117	4.1	0.3	2.25
2/7	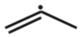	+	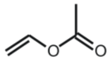	↔	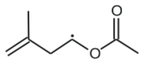	0.069	2.8	0.7	0.087	2.1	0.8	0.84
2/8	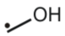	+	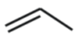	↔	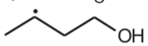	-0.251	-2.0	0.8	-0.033	-4.4	2.1	0.38
2/9	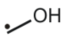	+	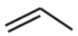	↔	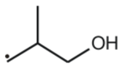	-0.141	3.9	0.3	-0.091	1.6	0.6	0.57
2/10	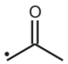	+	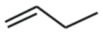	↔	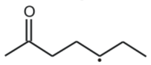	0.306	2.7	1.1	0.482	-0.7	3.4	0.34
2/11	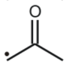	+		↔	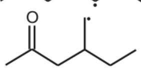	0.276	5.1	0.6	-0.030	1.2	0.7	0.92

2/12	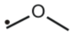	+	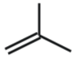	↔	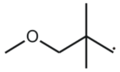	0.470	4.2	1.2	-0.717	-2.9	0.3	3.80
2/13	$^{\bullet}CH_3$	+	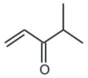	↔	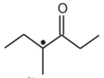	0.143	0.3	1.3	0.162	0.9	1.2	1.09
2/14	$^{\bullet}CH_3$	+	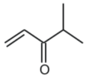	↔	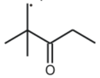	0.044	-0.2	1.1	-0.028	1.7	0.6	1.74
2/15		+	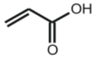	↔	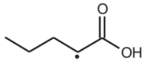	0.285	2.9	1.1	0.246	3.5	0.8	1.27
2/16		+	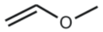	↔	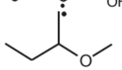	0.085	-1.2	1.5	-0.163	-4.4	1.5	0.95
2/17	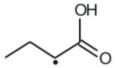	+		↔	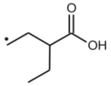	0.100	3.9	0.6	-0.085	-0.8	0.9	0.61
2/18	$^{\bullet}CH_3$	+	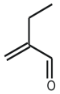	↔	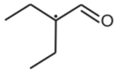	0.204	-1.3	2.0	0.079	0.7	1.0	2.03
2/19	$^{\bullet}CH_3$	+	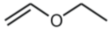	↔	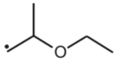	-0.304	-2.3	0.8	-0.598	-4.6	0.6	1.29
2/20	$^{\bullet}CH_3$	+	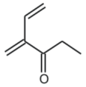	↔	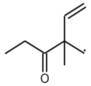	-0.108	1.0	0.6	-0.173	-2.6	1.1	0.57
2/21	$^{\bullet}CH_3$	+	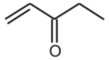	↔	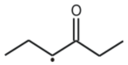	-0.012	-0.8	1.1	0.032	-2.1	1.6	0.70
2/22	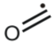	+	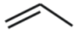	↔	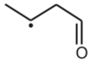	-0.079	2.3	0.5	0.645	1.0	3.5	0.15
2/23	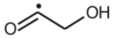	+	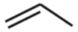	↔	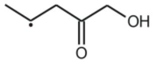	-0.155	1.9	0.5	-0.283	-6.5	1.9	0.25
2/24	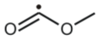	+	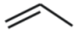	↔	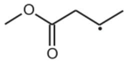	-0.058	2.7	0.5	0.749	1.4	4.1	0.12
					MAD	0.158	2.5		0.243	2.5		
					RMS	0.197	3.0		0.296	2.8		
					MAX	0.470	5.2		0.749	6.5		
					<*ρ*>			1.7			1.8	

Table S18: Comparison between group additive (GA) predicted and ab initio (AI) calculated kinetic parameters at 1000 K for the ab initio validation set of 24 reactions. ($\Delta\log A = \log A_{GA} - \log A_{AI}$ in $\log(m^3\ mol^{-1}\ s^{-1})$, $\Delta E_a = E_{a,GA} - E_{a,AI}$ in kJ mol^{-1}). [MAD: mean absolute deviation, RMS: root mean square deviation, MAX: maximum deviation, $<\rho>$: factor of deviation between two values taken from equation (6-4)].

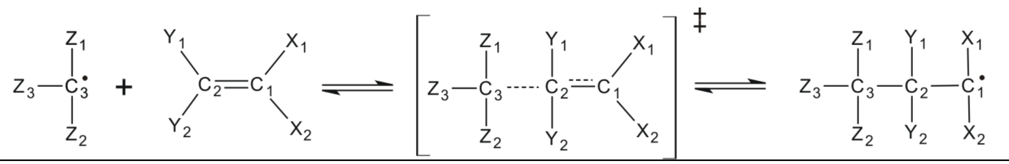

	Reactions	addition $\Delta\log A$	addition ΔE_a	addition k_{GA}/k_{AI}	β-scission $\Delta\log A$	β-scission ΔE_a	β-scission k_{GA}/k_{AI}	$\frac{K_{GA}^{eq}}{K_{AI}^{eq}}$
2/1	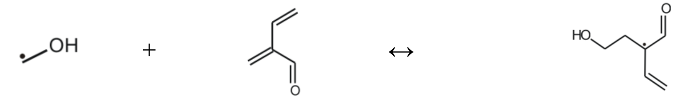	0.187	4.7	0.9	0.288	4.5	1.1	0.79
2/2		0.045	-2.3	1.4	0.205	1.8	1.3	1.15
2/3	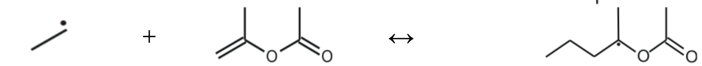	0.149	1.1	1.2	0.237	-0.3	1.7	0.70
2/4		0.099	4.1	0.7	0.150	5.5	0.7	1.05
2/5	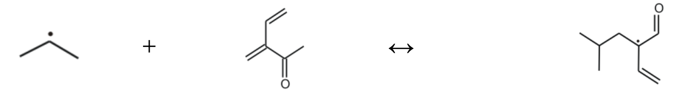	-0.107	4.7	0.4	-0.215	1.2	0.5	0.85
2/6	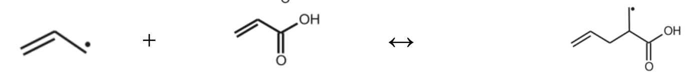	0.070	2.3	0.9	-0.096	4.5	0.5	1.92
2/7		0.076	2.9	0.8	0.086	2.2	0.9	0.89
2/8		-0.226	-1.7	0.7	0.000	-3.9	1.6	0.46
2/9		-0.168	3.6	0.4	-0.107	1.5	0.6	0.68
2/10		0.324	2.9	1.5	0.444	-1.2	3.1	0.46
2/11		0.220	4.3	1.0	-0.099	0.2	0.8	1.29
2/12		0.431	3.7	1.7	-0.735	-3.1	0.3	6.54

2/13	$^{\bullet}CH_3$	+	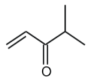	↔	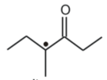	0.144	0.3	1.3	0.180	1.1	1.3	1.02
2/14	$^{\bullet}CH_3$	+	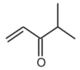	↔	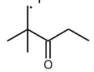	0.041	-0.2	1.1	-0.031	1.7	0.7	1.48
2/15		+	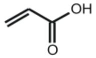	↔	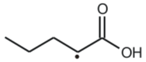	0.288	2.8	1.4	0.194	2.8	1.1	1.24
2/16		+	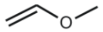	↔	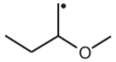	0.066	-1.4	1.3	-0.167	-4.3	1.1	1.20
2/17	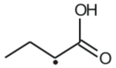	+		↔	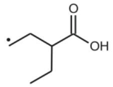	0.099	3.9	0.8	-0.080	-0.6	0.9	0.87
2/18	$^{\bullet}CH_3$	+	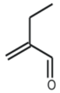	↔	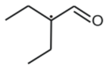	0.205	-1.2	1.9	0.069	0.6	1.1	1.72
2/19	$^{\bullet}CH_3$	+	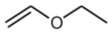	↔	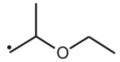	-0.307	-2.4	0.6	-0.628	-5.0	0.4	1.54
2/20	$^{\bullet}CH_3$	+	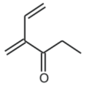	↔	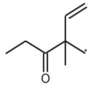	-0.105	1.1	0.7	-0.130	-2.0	0.9	0.74
2/21	$^{\bullet}CH_3$	+	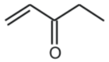	↔	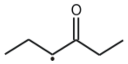	-0.014	-0.8	1.1	0.007	-2.5	1.4	0.78
2/22	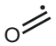	+	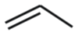	↔	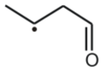	-0.059	2.6	0.6	0.657	1.2	3.8	0.16
2/23	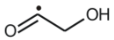	+	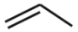	↔	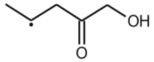	-0.111	2.4	0.6	-0.272	-6.4	1.1	0.51
2/24	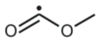	+	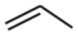	↔	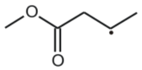	-0.049	2.8	0.6	0.751	1.5	4.6	0.14
					MAD	0.150	2.5		0.243	2.5		
					RMS	0.188	2.9		0.300	2.0		
					MAX	0.431	4.7		0.751	6.4		
					<ρ>			1.5			1.7	

Table S19: Applied symmetry numbers and corresponding reaction path degeneracy for carbon radical additions and their reverse *β*-scission reactions of the ab initio validation set included in Table S14. (σ_{ext}: external symmetry number, σ_{int}: internal symmetry number, n_{opt}: number of optical isomers, n_e: reaction path degeneracy or number of single events for the addition and the *β*-scission reaction).

Reaction	**addition**						***β*-scission**						**Reaction Path Degeneracy**	
	reactant 1			**reactant 2**			**reactant**			**transition state**			**addition**	**β-scission**
	σ_{ext}	σ_{int}	n_{opt}	σ_{ext}	σ_{int}	n_{opt}	σ_{ext}	σ_{int}	n_{opt}	σ_{ext}	σ_{int}	n_{opt}	n_{efor}	n_{erev}
1	1	1	1	1	1	1	1	1	1	1	1	2	2	2
2	1	9	1	1	3	1	1	27	1	1	27	2	2	2
3	1	6	1	1	9	1	1	27	1	1	27	2	4	2
4	1	6	1	1	3	1	1	9	1	1	9	2	4	2
5	1	9	1	1	3	1	1	27	1	1	27	2	2	2
6	2	1	1	1	1	1	1	1	1	1	1	2	4	2
7	1	3	1	1	3	1	1	9	1	1	9	2	2	2
8	1	1	1	1	3	1	1	3	1	1	3	2	2	2
9	1	1	1	1	3	1	1	3	1	1	3	2	2	2
10	1	6	1	1	3	1	1	9	1	1	18	2	2	1
11	1	6	1	1	3	1	1	9	1	1	18	2	2	1
12	1	6	1	1	9	1	1	27	1	1	27	2	4	2
13	6	1	1	1	9	1	1	27	1	1	27	2	4	2
14	6	1	1	1	9	1	1	27	1	1	27	2	4	2
15	1	6	1	1	1	1	1	3	1	1	3	2	4	2
16	1	6	1	1	3	1	1	9	1	1	9	2	4	2
17	1	3	1	4	1	1	1	3	1	1	3	2	8	2
18	6	1	1	1	3	1	1	9	1	1	9	2	4	2
19	6	1	1	1	3	1	1	9	1	1	9	2	4	2
20	6	1	1	1	3	1	1	9	1	1	9	2	4	2
21	6	1	1	1	3	1	1	9	1	1	9	2	4	2
22	1	1	1	1	3	1	1	3	1	1	3	2	2	2
23	1	1	1	1	3	1	1	3	1	1	3	2	2	2
24	1	3	1	1	3	1	1	9	1	1	9	2	2	2

1.4 Transition State Geometries

Geometries of the transition states for all reactions considered in this work

Geometries (Å), HO frequencies (cm^{-1}) in the transition state, rotational barrier in (kJ mol^{-1}), fitted Fourier coefficients for the 1D HR treatment (kJ mol^{-1}), substituted frequency (cm^{-1}) and reduced moment of inertia (amu $bohr^2$)

Notation for Fourier coefficients

cos = C_1, C_2, C_3, (C_4, C_5)
sin = D_1, D_2, D_3, (D_4, D_5)

Indicates that the potential energy profile for rotation can be approximated by the Fourier expansion:

$$V(\phi)=\sum_{i=1}^{5}\frac{1}{2}C_i(1-\cos(i\phi))+\sum_{i=1}^{5}D_i\sin(i\phi)$$

In the following pages for every reaction the two reactants and the product of the carbon radical addition and the particular geometry of the transition state are mentioned.

TRAINING SET OF REACTIONS

Reference Reaction

methyl/ethene/1-propyl
C -1.162726 -1.181242 0.000000
C 0.000000 0.805307 0.000000
C 1.335576 0.553859 0.000000
H -2.176925 -0.798104 0.000000
H -0.809457 -1.627553 0.920833
H -0.809457 -1.627553 -0.920833
H -0.506481 1.079880 -0.917909
H -0.506481 1.079880 0.917909
H 1.885851 0.412951 0.923465
H 1.885851 0.412951 -0.923465
ImagFreq 446i
Internal rotation:
cos -0.00 -0.00 1.91
barrier 1.91
symmetry 3
Im,red 10.16
freq 99.3 (from rotation profile)

Reaction 1/1

methyl/ethenol/1-hydroxy-propyl
C 0.849360 0.373873 0.358547
O 1.626804 -0.579708 -0.240684
C -0.250204 0.867760 -0.273154
C -2.046811 -0.515031 0.083407
H -0.352864 0.722472 -1.340866
H -0.751655 1.721337 0.160641
H -2.804109 -0.042089 -0.532294
H -2.188121 -0.443328 1.155311
H -1.640669 -1.449052 -0.284900
H 2.318637 -0.853300 0.366906
H 1.090281 0.622010 1.387878
ImagFreq 482i
Internal rotation:
cos -0.00 -0.00 1.75
barrier 1.76
symmetry 3
Im,red 11.36
freq 97.5 (from rotation profile)

Reaction 1/2

methyl/methoxy-ethene/1-methoxy-propyl
C 0.194649 0.587640 0.319302
O 1.070056 -0.080621 -0.479109
C -1.032997 0.951587 -0.145483
C -2.505694 -0.807561 0.066655
H -1.209414 0.966562 -1.213002
H -1.641595 1.601128 0.467530
H -3.394106 -0.397921 -0.401399
H -2.549021 -0.945330 1.140425
H -1.969970 -1.564082 -0.493240
H 0.484733 0.701739 1.360902
C 2.311325 -0.423952 0.122960
H 2.164169 -1.068845 0.997467
H 2.882764 -0.966079 -0.628955
H 2.868296 0.471508 0.422543
ImagFreq 479i
Internal rotation:
cos -0.01 -0.01 1.71
barrier 1.72
symmetry 3
Im,red 11.74
freq 92.2 (from rotation profile)

Reaction 1/3

methyl/1-ethenyl-formate/1-formyloxy-propyl
C -0.152607 0.604859 0.304839
O 0.664708 0.134707 -0.710721
C -1.428563 0.954088 0.002794
C -2.779366 -0.906725 0.088415
H -1.712465 1.107910 -1.029894
H -2.014336 1.455317 0.760554
H -3.731452 -0.464323 -0.181525
H -2.661450 -1.214835 1.119689
H -2.299887 -1.524967 -0.659946
H 0.275536 0.564122 1.295832
C 1.911763 -0.295347 -0.389932
O 2.388931 -0.315158 0.707173
H 2.407580 -0.620862 -1.313022
ImagFreq 476i
Internal rotation:
cos -0.00 -0.00 1.71
barrier 1.71
symmetry 3
Im,red 11.92
freq 92.1 (from rotation profile)

Reaction 1/4

methyl/1-ethenyl-acetate/1-acetyloxy-propyl
C 0.690708 -0.736172 -0.327347
O -0.322562 0.195796 -0.449016
C 1.922070 -0.431469 -0.811765
C 3.113019 0.728489 0.774729
H 2.038456 0.395275 -1.500135
H 2.664936 -1.216027 -0.847215
H 4.039166 0.900279 0.237975
H 3.149494 0.014543 1.588071
H 2.465964 1.585557 0.913207
H 0.436996 -1.617311 0.244248
C -1.537846 -0.082985 0.122605
O -1.768947 -1.091447 0.731927
C -2.500390 1.043884 -0.137446
H -3.451330 0.824024 0.342663
H -2.092195 1.981291 0.246638
H -2.644788 1.167102 -1.213382
ImagFreq 479i
Internal rotation:
cos -0.00 -0.00 1.70
barrier 1.70
symmetry 3
Im,red 12.04
freq 81.0 (from rotation profile)

Reaction 1/5

methyl/prop-2-enal/1-oxobutan-2-yl
C -0.280564 0.589910 -0.373865
C 0.884148 0.947527 0.241775
C 2.452244 -0.785409 -0.093424
H 0.987903 0.829561 1.315380
H 1.584751 1.619671 -0.236206
H 3.287918 -0.345520 0.436938
H 2.491443 -0.789107 -1.174511
H 1.928470 -1.601258 0.386381
H -0.459703 0.805157 -1.422639
C -1.331185 -0.134179 0.331176
O -2.382660 -0.484398 -0.167477
H -1.107356 -0.350414 1.400501
ImagFreq 411i
Internal rotation:
cos -0.00 -0.00 1.27
barrier 1.27
symmetry 3
Im,red 11.81
freq 90.0 (from rotation profile)

Reaction 1/6

methyl/but-3-en-2-one/2-methylpent-1-en-3-yl
C 0.038672 -0.889642 -0.166317
C 1.217571 -0.648347 -0.804001
C 2.651018 0.421000 0.758824
H 1.311426 0.244738 -1.409349
H 1.943089 -1.437455 -0.954549
H 3.536635 0.497445 0.140461
H 2.658846 -0.304966 1.560700
H 2.041273 1.305359 0.881091
H -0.134436 -1.837523 0.334603
C -1.017977 0.140086 -0.094386
O -0.852077 1.265344 -0.537826
C -2.323925 -0.266878 0.564972
H -3.024069 0.566644 0.535849
H -2.759109 -1.132027 0.054384
H -2.149194 -0.562284 1.604870
ImagFreq 395i
Internal rotation:
cos 0.03 0.03 2.18
barrier 2.21
symmetry 3
Im,red 12.08
freq 101.3 (from rotation profile)

Reaction 1/7

methyl/prop-2-enoic-acid/1-carboxypropyl
C 0.027431 -0.903997 -0.125277
C 1.181490 -0.633508 -0.793652
C 2.622329 0.484763 0.692994
H 1.232624 0.243679 -1.426307
H 1.923004 -1.406566 -0.947317
H 3.484819 0.579044 0.044800
H 2.678462 -0.232701 1.500699
H 2.005041 1.360517 0.839197
H -0.122450 -1.833215 0.410508
C -1.045482 0.094671 -0.058764
O -1.009586 1.212782 -0.525463
O -2.132002 -0.375640 0.611015
H -2.783399 0.340535 0.602203
ImagFreq 402i
Internal rotation:

cos 0.02 0.02 2.12
barrier 2.14
symmetry 3
Im,red 12.05
freq 98.3 (from rotation profile)

Reaction 1/8

methyl/methylprop-2-enoate/1-methoxy-1-oxobutan-2-yl
C 0.610531 0.966752 0.026021
C 1.798517 0.708128 0.637762
C 3.008937 -0.754335 -0.745669
H 1.842270 -0.055264 1.404343
H 2.604871 1.429028 0.601748
H 3.919877 -0.818214 -0.163281
H 3.042716 -0.187056 -1.666275
H 2.320174 -1.586351 -0.692982
H 0.480195 1.805764 -0.646386
C -0.536482 0.067791 0.211553
O -0.538101 -0.956559 0.860500
O -1.627741 0.527605 -0.451105
C -2.808882 -0.279152 -0.328878
H -3.571099 0.226740 -0.917789
H -2.629983 -1.284490 -0.714655
H -3.118012 -0.353640 0.715377
ImagFreq 409i
Internal rotation:
cos 0.02 0.02 2.15
barrier 2.17
symmetry 3
Im,red 12.13
freq 110.1 (from rotation profile)

Reaction 1/9

methyl/prop-1-en-2-ol/2-hydroxybutan-2-yl
C 0.621455 0.075550 0.214077
O 1.103114 1.230912 -0.343536
C -0.543468 0.034121 0.931485
C -2.330703 -0.176387 -0.468478
H -0.956582 0.951695 1.336925
H -0.788410 -0.869403 1.471809
H -3.159375 -0.089085 0.226277
H -2.176741 -1.158566 -0.899810
H -2.187279 0.660068 -1.143118
H 0.547014 1.967321 -0.066131
C 1.419238 -1.111598 -0.209645
H 1.052773 -2.021102 0.266406
H 1.369950 -1.240943 -1.297518
H 2.474605 -0.977396 0.048815
ImagFreq 479i
Internal rotation:
cos -0.00 -0.00 1.52
barrier 1.52
symmetry 3
Im,red 11.74
freq 82.8 (from rotation profile)

Reaction 1/10

methyl/2-methoxyprop-1-ene/2-methoxybutan-2-yl
C 0.126815 0.410808 -0.368834
O 0.988812 -0.633899 -0.595119
C -1.133447 0.295588 -0.886669
C -2.545199 -0.688391 0.639359
H -1.330087 -0.500318 -1.592565
H -1.756713 1.176610 -0.951173
H -3.471063 -0.704805 0.074737
H -2.511116 -0.003127 1.478304
H -2.056075 -1.644376 0.782344
C 2.001575 -0.912615 0.364642
H 1.572292 -1.169206 1.339996
H 2.546547 -1.773971 -0.019699
H 2.700544 -0.078621 0.485552
C 0.593154 1.577387 0.448012
H 0.790291 1.309513 1.493112
H 1.517367 2.007035 0.044484
H -0.169865 2.355800 0.446799
ImagFreq 459i
Internal rotation:
cos -0.00 -0.00 1.74
barrier 1.74
symmetry 3
Im,red 11.94
freq 100.7 (from rotation profile)

Reaction 1/11

methyl/prop-1-ene-2-yl-formate/2-formyloxybutan-2-yl
C 0.192524 0.308117 0.198913
O -0.532253 -0.782626 -0.324114
C 1.260225 -0.013257 0.978712
C 3.052415 -0.508455 -0.366606
H 1.315247 -0.998335 1.421629
H 1.804226 0.782609 1.468268
H 3.783274 -0.792767 0.381719
H 3.221558 0.433351 -0.874093
H 2.627790 -1.308300 -0.959900
C -1.882235 -0.806234 -0.244630
O -2.584117 0.007867 0.281067
H -2.232783 -1.717819 -0.748396
C -0.121242 1.653619 -0.365472
H 0.599556 2.387318 -0.002193
H -0.071278 1.633159 -1.461094
H -1.126747 1.976119 -0.087069
ImagFreq 486i
Internal rotation:
cos 0.00 0.00 1.82
barrier 1.82
symmetry 3

Im,red 11.93
freq 99.4 (from rotation profile)

Reaction 1/12

methyl/prop-1-ene-2-yl-acetate/2-acetyloxybutan-2-yl
C -0.703923 0.799808 -0.339584
O 0.609356 0.457938 -0.717196
C -1.722827 0.155362 -0.970952
C -2.310497 -1.697821 0.229711
H -1.501829 -0.444504 -1.843625
H -2.725170 0.552863 -0.887592
H -2.763516 -2.305106 -0.545997
H -2.986521 -1.266485 0.958223
H -1.345867 -2.012918 0.604945
C 1.388222 -0.253902 0.149646
O 1.002966 -0.674797 1.207520
C 2.774032 -0.424741 -0.417531
H 3.360567 -1.057648 0.244743
H 2.719129 -0.866310 -1.414515
H 3.252747 0.552160 -0.519122
C -0.819769 1.813370 0.747634
H -1.859883 2.116172 0.876758
H -0.454029 1.410947 1.697841
H -0.225634 2.703255 0.512207
ImagFreq 488i
Internal rotation:
cos -0.01 -0.01 1.16
sin 0.00 0.00 0.23
barrier 1.25
symmetry 3
Im,red 12.11
freq 71.5 (from rotation profile)

Reaction 1/13

methyl/2-methylprop-2-enal/2-formylbutan-2-yl
C -0.209778 0.275932 0.339692
C 0.978620 0.041292 0.977027
C 2.598128 -0.471682 -0.672669
H 1.152119 -0.913992 1.460290
H 1.616514 0.859557 1.286801
H 3.451807 -0.606365 -0.019973
H 2.556625 0.436549 -1.259175
H 2.153121 -1.359648 -1.101408
C -1.138204 -0.843857 0.158316
O -2.215835 -0.758669 -0.398401
H -0.791380 -1.811654 0.582422
C -0.603889 1.604340 -0.233402
H 0.106145 2.387387 0.037997
H -0.666449 1.551460 -1.325667
H -1.601077 1.889906 0.112139
ImagFreq 419i
Internal rotation:
cos 0.00 0.00 1.29
barrier 1.29
symmetry 3
Im,red 12.04
freq 76.0 (from rotation profile)

Reaction 1/14

methyl/3-methylbut-3-en-2-one/3-methyl-2-oxopentan-3-yl
C 0.046474 0.538894 0.347559
C 1.114429 -0.062191 0.959164
C 2.663124 -0.677619 -0.713302
H 1.062213 -1.087167 1.301372
H 1.896726 0.543118 1.401075
H 3.418381 -1.121124 -0.076098
H 2.874370 0.298691 -1.128927
H 2.063604 -1.349083 -1.313730
C -1.149710 -0.228029 -0.076548
O -2.073037 0.342619 -0.637465
C -1.225720 -1.723306 0.196609
H -2.164874 -2.096320 -0.208823
H -0.392907 -2.257685 -0.269098
H -1.190518 -1.931265 1.269869
C 0.041293 2.003813 0.014301
H -0.844744 2.492046 0.428734
H 0.934026 2.501751 0.397069
H -0.011325 2.156712 -1.068425
ImagFreq 428i
Internal rotation:
cos 0.00 0.00 1.22
barrier 1.22
symmetry 3
Im,red 12.11
freq 77.2 (from rotation profile)

Reaction 1/15

methyl/2-methylprop-2-enoic-acid/2-carboxybutan-2-yl
C 0.008043 0.562406 0.325589
C 1.122223 0.088166 0.958713
C 2.646092 -0.611670 -0.697657
H 1.136355 -0.915129 1.359868
H 1.861619 0.781867 1.340091
H 3.470808 -0.890537 -0.053424
H 2.749928 0.297462 -1.275085
H 2.052986 -1.409746 -1.123040
C -1.102233 -0.338196 -0.036230
O -2.133384 0.021090 -0.562920
O -0.878158 -1.646876 0.271683
H -1.677460 -2.119330 -0.000762
C -0.154229 1.993920 -0.096890
H -1.086833 2.411007 0.292631
H 0.679878 2.602875 0.255522
H -0.214331 2.080064 -1.187056
ImagFreq 418i
Internal rotation:
cos 0.02 0.02 1.91
barrier 1.93
symmetry 3
Im,red 12.14
freq 87.0 (from rotation profile)

Reaction 1/16

methyl/methyl-2-methylprop-2-enoate/1-methoxy-2-methyl-1-oxobutan-2-yl
C 0.709298 0.618649 0.328505
C 1.409110 -0.370879 0.959711
C 2.319415 -1.776491 -0.694659
H 0.891801 -1.226150 1.370086
H 2.406396 -0.171034 1.332647
H 2.880986 -2.445310 -0.054044
H 2.880659 -1.063048 -1.283512
H 1.390832 -2.145098 -1.108735
C -0.716486 0.449489 -0.023644
O -1.393227 1.309705 -0.546186
O -1.208776 -0.775960 0.293547
C -2.596616 -0.978619 -0.011996
H -2.817509 -1.998744 0.295563
H -3.219709 -0.269995 0.536706
H -2.778495 -0.852157 -1.080695
C 1.330829 1.913980 -0.108105
H 2.361025 1.992294 0.243380
H 1.326013 2.005925 -1.199607
H 0.760721 2.766574 0.270447
ImagFreq 423i
Internal rotation:
cos 0.02 0.02 1.93
barrier 1.94
symmetry 3
Im,red 12.20
freq 0.0 (from rotation profile)

Reaction 1/17

methyl/2-methylidenebut-3-enal/3-formylpent-1-en-3-yl
C -0.264018 -0.042553 0.366709
C 0.859690 -0.475570 1.017691
C 2.511442 -1.075968 -0.723544
H 0.901977 -1.487216 1.403757
H 1.603807 0.213231 1.393936
H 3.362059 -1.257832 -0.079407
H 2.463658 -0.139129 -1.261080
H 2.001888 -1.930327 -1.147269
C -1.320737 -1.042088 0.103880
O -2.378056 -0.809179 -0.441844
H -1.080578 -2.066881 0.461148
C -0.506418 1.316509 -0.106900
H -1.496434 1.464720 -0.526955
C 0.357845 2.339002 -0.083470
H 1.366043 2.247216 0.307035
H 0.075207 3.313654 -0.462609
ImagFreq 361i
Internal rotation:
cos -0.00 -0.00 0.97 F
barrier 0.99
symmetry 3
Im,red 12.23
freq 85.8 (from HO analysis)

Reaction 1/18

methyl/2-methylidenepent-4-en-2-one/3-acetylpent-1-en-3-yl
C -0.075943 -0.257407 0.323755
C -0.602005 0.839625 0.954810
C -1.558739 2.284823 -0.792367
H 0.025775 1.654300 1.285557
H -1.593986 0.806173 1.386053
H -2.034173 3.016656 -0.151961
H -2.175829 1.521248 -1.245110
H -0.656497 2.577057 -1.312158
C 1.369468 -0.299523 -0.062516
O 1.843226 -1.290676 -0.590281
C -0.859612 -1.439924 -0.030643
H -0.268039 -2.256882 -0.429040
C -2.188094 -1.581397 0.069260
H -2.839892 -0.795232 0.436115
H -2.669309 -2.507229 -0.222202
C 2.253591 0.905130 0.220722
H 3.244497 0.700309 -0.180750
H 1.854939 1.813578 -0.238611
H 2.334713 1.087461 1.296233
ImagFreq 383i
Internal rotation:
cos 0.00 0.00 1.00
barrier 1.03
symmetry 3
Im,red 12.25
freq 0.0 (from rotation profile)

Reaction 1/19

methyl/2-methylidenebut-3-enoic-acid/3-carboxypent-1-en-3-yl
C -0.074976 -0.261980 0.331922
C -0.656502 0.792642 0.979291
C -1.532788 2.295818 -0.775256
H -0.054924 1.616708 1.331514
H -1.659847 0.709906 1.375951
H -2.072378 2.988125 -0.142052
H -2.096050 1.554338 -1.324680
H -0.572527 2.602256 -1.165615
C 1.365161 -0.208184 -0.029575
O 1.991000 -1.118415 -0.524544
C -0.769022 -1.482968 -0.069304
H -0.119766 -2.254820 -0.468217
C -2.088222 -1.707874 -0.005912
H -2.794143 -0.970096 0.360599
H -2.503735 -2.654753 -0.328129
O 1.950773 0.987214 0.248148
H 2.877275 0.893210 -0.015205
ImagFreq 363i
Internal rotation:

cos 0.01 0.01 1.43
barrier 1.45
symmetry 3
Im,red 12.29
freq 99.1 (from rotation profile)

Reaction 1/20

methyl/methyl-2-methylidenebut-3-enoate/3-methoxycarbonylpent-1-en-3-yl
C -0.560103 -0.268982 0.335673
C -0.899381 0.888158 0.980844
C -1.400935 2.546371 -0.772728
H -0.131930 1.553536 1.345649
H -1.900227 1.029393 1.367232
H -1.777085 3.343922 -0.145096
H -2.111850 1.950863 -1.328480
H -0.394332 2.631246 -1.157275
C 0.861654 -0.546321 -0.012842
O 1.259261 -1.581002 -0.500868
C -1.507848 -1.300504 -0.077376
H -1.045221 -2.195321 -0.479400
C -2.844726 -1.226590 -0.020376
H -3.370828 -0.353336 0.350500
H -3.458836 -2.054846 -0.352091
O 1.687758 0.488012 0.274211
C 3.076672 0.268122 -0.020311
H 3.463787 -0.571787 0.558996
H 3.215628 0.058592 -1.082093
H 3.582737 1.190139 0.258009
ImagFreq 373i
Internal rotation:
cos 0.01 0.01 1.47
barrier 1.49
symmetry 3
Im,red 12.32
freq 86.3 (from rotation profile)

Reaction 1/21

methyl/ethenol/2-hydroxypropyl
C 0.981953 -1.125247 -0.120952
C 0.405263 -0.000437 0.399260
C -1.758570 -0.187393 -0.110884
H 0.122002 0.026811 1.448326
H -2.175494 0.656591 0.432844
H -2.068344 -1.164594 0.241182
H -1.692916 -0.068571 -1.185671
H 0.892350 -2.069508 0.397125
H 1.450594 -1.101910 -1.096259
O 0.698417 1.214726 -0.178887
H 0.112598 1.881836 0.189003
ImagFreq 561i
Internal rotation:
cos 0.01 0.01 3.70
barrier 3.70
symmetry 3
Im,red 11.43
freq 131.2 (from rotation profile)

Reaction 1/22

methyl/methoxy-ethene/2-methoxypropyl
C -1.467693 -1.167595 -0.017304
C -0.365001 -0.437513 0.347378
C -1.013374 1.657506 -0.103882
H -0.222623 -0.139488 1.384308
H -0.265205 2.278343 0.380109
H -2.008655 1.718253 0.320582
H -0.965623 1.618927 -1.185827
H -2.345688 -1.169240 0.612666
H -1.512750 -1.647896 -0.985831
O 0.779992 -0.575594 -0.388035
C 1.915058 0.123721 0.097437
H 1.786400 1.207737 0.007747
H 2.121440 -0.129185 1.144951
H 2.758830 -0.189418 -0.516200
ImagFreq 560i
Internal rotation:
cos -0.02 -0.02 2.58
barrier 2.59
symmetry 3
Im,red 11.78
freq 107.6 (from rotation profile)

Reaction 1/23

methyl/1-ethenyl-formate/2-formyloxypropyl
C 1.899435 -0.978776 -0.219436
C 0.692378 -0.363628 -0.356863
C 0.991550 1.772771 0.264686
H 0.312698 0.007231 -1.298573
H 0.022237 2.170666 -0.011961
H 1.835622 2.095694 -0.332516
H 1.179014 1.625460 1.321281
H 2.667381 -0.822276 -0.964076
H 2.143019 -1.536394 0.675123
O -0.304883 -0.728230 0.561962
C -1.573753 -0.339474 0.311602
O -1.945480 0.307531 -0.625330
H -2.214728 -0.720150 1.117735
ImagFreq 562i
Internal rotation:
cos 0.00 0.00 4.29
barrier 4.30
symmetry 3
Im,red 12.01
freq 129.9 (from rotation profile)

Reaction 1/24

methyl/1-ethenyl-acetate/2-acetyloxypropyl
C 2.137218 -1.222069 -0.163165
C 1.109250 -0.358639 -0.397025
C 1.638835 1.540602 0.668109
H 1.014570 0.227392 -1.300583
H 0.826827 2.163907 0.312224
H 2.628583 1.779814 0.298174
H 1.581188 1.196293 1.693547

H 3.065011 -1.108322 -0.706322
H 2.083130 -1.952537 0.633176
O -0.108309 -0.643830 0.230435
C -1.218413 0.033444 -0.181851
O -1.210200 0.865237 -1.049836
C -2.421182 -0.411241 0.607191
H -2.533358 -1.495307 0.541730
H -2.282704 -0.159750 1.661519
H -3.309431 0.084668 0.222180
ImagFreq 563i
Internal rotation:
cos 0.01 0.01 4.33
barrier 4.34
symmetry 3
Im,red 12.07
freq 135.9 (from rotation profile)

Reaction 1/25

methyl/prop-2-enal/2-formylpropyl
C 0.152199 1.653988 -0.231837
C 0.210463 0.533362 0.554420
C 1.729490 -0.945229 -0.287775
H 0.776569 0.548270 1.480702
H 1.710467 -1.761801 0.425448
H 2.593575 -0.294335 -0.255426
H 1.297384 -1.136037 -1.261510
H 0.808968 2.498947 -0.068289
H -0.535577 1.690710 -1.068053
C -0.838051 -0.519474 0.448116
O -1.670938 -0.574886 -0.425666
H -0.808491 -1.282551 1.254909
ImagFreq 445i
Internal rotation:
cos -0.02 -0.02 2.78
barrier 2.80
symmetry 3
Im,red 11.84
freq 124.3 (from rotation profile)

Reaction 1/26

methyl/but-3-en-2-one/2-methyl-3-oxobutyl
C 1.530836 -1.220645 -0.359565
C 0.609552 -0.243178 -0.625991
C 1.255945 1.661066 0.442073
H 0.645670 0.278038 -1.577524
H 0.510270 2.392926 0.152166
H 2.237715 1.772941 0.000000
H 1.217276 1.303299 1.462468
H 2.418803 -1.345857 -0.966574
H 1.403904 -1.856059 0.508621
C -0.712898 -0.257930 0.088786
O -0.862781 -0.835642 1.144381
C -1.863732 0.446860 -0.605784
H -2.171702 -0.144812 -1.475099
H -2.706770 0.534613 0.078258
H -1.571138 1.433018 -0.974476
ImagFreq 464i
Internal rotation:
cos -0.01 -0.01 2.19
barrier 2.22
symmetry 3
Im,red 11.98
freq 80.3 (from rotation profile)

Reaction 1/27

methyl/prop-2-enoic-acid/2-carboxypropyl
C 1.446124 -1.310394 -0.236282
C 0.620379 -0.277476 -0.587842
C 1.270810 1.610719 0.493409
H 0.753153 0.238868 -1.530289
H 0.565412 2.322598 0.082363
H 2.294060 1.676427 0.146400
H 1.124034 1.307806 1.522256
H 2.380065 -1.484309 -0.755128
H 1.202367 -1.937056 0.612653
C -0.745560 -0.214005 0.000882
O -1.125201 -0.809386 0.979075
O -1.556450 0.612859 -0.708551
H -2.416404 0.594820 -0.263448
ImagFreq 477i
Internal rotation:
cos -0.02 -0.02 3.24
barrier 3.26
symmetry 3
Im,red 12.03
freq 121.6 (from rotation profile)

Reaction 1/28

methyl/methylprop-2-enoate/3-methoxy-2-methyl-3-oxopropyl
C 2.095439 -1.069183 -0.304121
C 1.091503 -0.188828 -0.603102
C 1.469890 1.764553 0.485456
H 1.094371 0.353978 -1.540080
H 0.654617 2.363438 0.097963
H 2.462938 1.994211 0.120708
H 1.393825 1.433966 1.513481
H 3.024423 -1.072301 -0.859901
H 1.996671 -1.738948 0.541097
C -0.243102 -0.371527 0.036673
O -0.468126 -1.034290 1.020293
O -1.199496 0.306802 -0.639524
C -2.530565 0.193082 -0.108097
H -2.855482 -0.848582 -0.107686
H -2.570439 0.575787 0.913157
H -3.158936 0.789769 -0.765749
ImagFreq 480i
Internal rotation:

cos -0.02 -0.02 3.35
barrier 3.36
symmetry 3
Im,red 12.11
freq 110.9 (from rotation profile)

Reaction 1/29

methyl/prop-1-en-2-ol/2-hydroxy-2-methylpropyl
C 0.394730 -1.020737 1.081108
C 0.349244 -0.107700 0.047239
C -1.843169 0.194753 -0.064498
H -1.849679 0.790581 -0.970404
H -2.132100 0.707447 0.846743
H -2.232551 -0.812147 -0.168961
H 0.310823 -0.687967 2.106101
H 0.338161 -2.087280 0.892299
O 0.584865 -0.496206 -1.255597
H 0.469491 -1.450148 -1.319845
C 0.741686 1.336857 0.238128
H 0.292421 1.970438 -0.526958
H 0.440112 1.695877 1.222216
H 1.829454 1.423810 0.151722
ImagFreq 597i
Internal rotation:
cos -0.03 -0.03 3.62
barrier 3.64
symmetry 3
Im,red 11.68
freq 115.2 (from rotation profile)

Reaction 1/30

methyl/2-methoxyprop-1-ene/2-methoxy-2-methylpropyl
C 0.184367 -0.316709 1.516686
C 0.284750 -0.339510 0.137833
C 0.993551 1.718557 -0.207948
H 0.949768 1.702716 -1.291417
H 1.986918 1.756285 0.225859
H 0.260604 2.353338 0.277412
H 1.079144 -0.454491 2.107723
H -0.707441 0.006371 2.033691
O -0.812934 -0.337068 -0.693282
C -2.056133 0.079757 -0.153563
H -2.409609 -0.612607 0.618998
H -1.992055 1.088576 0.269880
H -2.760535 0.082648 -0.984469
C 1.424608 -1.056337 -0.549825
H 2.354422 -0.933361 0.006054
H 1.192254 -2.124047 -0.611667
H 1.563140 -0.683436 -1.564902
ImagFreq 590i
Internal rotation:
cos -0.05 -0.05 3.24
barrier 3.26
symmetry 3
Im,red 11.82
freq 92.9 (from rotation profile)

Reaction 1/31

methyl/prop-1-ene-2-yl-formate/2-formyloxy-2-methylpropyl
C 0.474478 -0.186018 1.562953
C 0.657362 -0.300300 0.207928
C 0.693848 1.845419 -0.451250
H 0.724598 1.692970 -1.524580
H 1.599902 2.227346 0.004260
H -0.238655 2.211209 -0.042033
H 1.348316 -0.036763 2.184160
H -0.501817 -0.089897 2.008772
O -0.381799 -0.748666 -0.652983
C -1.678913 -0.423350 -0.487617
O -2.158027 0.275445 0.358583
H -2.246619 -0.916558 -1.290057
C 1.973123 -0.729325 -0.392845
H 2.802443 -0.312745 0.179768
H 2.048943 -1.821089 -0.369826
H 2.062112 -0.407264 -1.430283
ImagFreq 601i
Internal rotation:
cos -0.05 -0.05 4.87
barrier 4.90
symmetry 3
Im,red 12.03
freq 133.7 (from rotation profile)

Reaction 1/32

methyl/prop-1-ene-2-yl-acetate/2-acetyloxy-2-methylpropyl
C 1.238356 -0.703498 -1.335054
C 1.006191 0.205026 -0.332418
C 1.312036 -1.044122 1.506497
H 1.020957 -0.316207 2.256064
H 2.366121 -1.293151 1.467880
H 0.621033 -1.857761 1.329941
H 2.263391 -0.877570 -1.636451
H 0.466567 -1.350658 -1.717559
O -0.293092 0.687430 -0.037734
C -1.413230 -0.083453 -0.083472
O -1.437099 -1.254236 -0.353418
C -2.616976 0.755088 0.270860
H -2.519150 1.129904 1.292392
H -2.678929 1.621529 -0.390798
H -3.515989 0.148929 0.182894
C 1.990975 1.301183 -0.003872
H 3.013020 0.935953 -0.110315
H 1.849039 2.140763 -0.691956
H 1.851360 1.671373 1.011878
ImagFreq 602i
Internal rotation:
cos -0.07 -0.07 4.79
barrier 4.82
symmetry 3
Im,red 12.07
freq 138.4 (from rotation profile)

Reaction 1/33

methyl/2-methylprop-2-enal/2-formyl-2-methylpropyl
C -1.294485 -0.640711 -1.100507
C -0.343087 -0.357722 -0.143585
C -0.703965 1.795670 0.407947
H 0.132310 1.987178 1.069812
H -1.671809 1.657817 0.873944
H -0.704407 2.326648 -0.536513
H -2.233313 -1.117570 -0.846391
H -1.155131 -0.335330 -2.132061
C 1.009374 0.030582 -0.641151
O 2.030363 -0.075084 -0.004652
H 1.016312 0.422777 -1.681618
C -0.401649 -0.977285 1.234796
H -0.030338 -2.005847 1.192279
H 0.231229 -0.437470 1.938427
H -1.424884 -1.000744 1.614340
ImagFreq 482i
Internal rotation:
cos -0.02 -0.02 3.87
barrier 3.88
symmetry 3
Im,red 11.93
freq 118.9 (from rotation profile)

Reaction 1/34

methyl/3-methylbut-3-en-2-one/22-dimethyl-3-oxobutyl
C 0.758346 -1.250648 -1.112118
C 0.554549 -0.092539 -0.392384
C 0.856739 -0.691712 1.763594
H 0.513871 0.199386 2.275999
H 1.928294 -0.841125 1.718912
H 0.259772 -1.586134 1.893884
H 1.732949 -1.481104 -1.526588
H -0.013168 -1.999535 -1.233380
C -0.853108 0.363750 -0.087826
O -1.075866 1.533003 0.152044
C -1.988882 -0.645865 -0.131097
H -1.736823 -1.585245 0.364037
H -2.863313 -0.199378 0.340124
H -2.234035 -0.875352 -1.172867
C 1.587016 1.015935 -0.448370
H 2.597385 0.603219 -0.477404
H 1.436509 1.616264 -1.350795
H 1.497534 1.691450 0.400928
ImagFreq 488i
Internal rotation:
cos -0.01 -0.01 3.65
barrier 3.66
symmetry 3
Im,red 11.99
freq 130.3 (from rotation profile)

Reaction 1/35

methyl/2-methylprop-2-enoic-acid/2-carboxy-2-methylpropyl
C 0.894293 -1.045207 -1.218607
C 0.556804 -0.004421 -0.382215
C 0.826348 -0.822779 1.704940
H 0.432775 -0.009106 2.303280
H 1.902518 -0.943395 1.700600
H 0.237197 -1.730028 1.670235
H 1.904229 -1.138583 -1.600298
H 0.186337 -1.825947 -1.458863
C -0.889484 0.259694 -0.100168
O -1.337260 1.331515 0.230992
O -1.682184 -0.830940 -0.259553
H -2.582787 -0.533200 -0.066971
C 1.452603 1.212255 -0.266200
H 2.503028 0.916630 -0.290969
H 1.268866 1.891714 -1.103997
H 1.260005 1.770069 0.648975
ImagFreq 506i
Internal rotation:
cos -0.03 -0.03 4.42
barrier 4.43
symmetry 3
Im,red 12.05
freq 137.0 (from rotation profile)

Reaction 1/36

methyl/methyl-2-methylprop-2-enoate/3-methoxy-22-dimethyl-3-oxopropyl
C 1.167474 -1.092258 -1.255434
C 0.968165 -0.043763 -0.385676
C 1.142315 -0.962219 1.668630
H 0.849967 -0.129626 2.298365
H 2.195824 -1.213073 1.658649
H 0.447517 -1.789416 1.603334
H 2.157712 -1.307291 -1.639885
H 0.362935 -1.764762 -1.517732
C -0.433042 0.406176 -0.089656
O -0.723200 1.524630 0.264698
O -1.350937 -0.570693 -0.267238
C -2.714045 -0.190185 -0.017391
H -2.836882 0.142899 1.014498
H -3.017316 0.615785 -0.687535
H -3.304526 -1.084811 -0.203298
C 2.017758 1.038948 -0.234382
H 3.019680 0.607218 -0.271411
H 1.927232 1.763333 -1.049605
H 1.899199 1.588056 0.698389
ImagFreq 507i
Internal rotation:
cos -0.03 -0.03 4.55
barrier 4.56
symmetry 3
Im,red 12.10

freq 117.5 (from rotation profile)

Reaction 1/37

methyl/2-methylidenebut-3-enal/3-methyl-3-2-oxoethylbut-1-en-4-yl
C -0.381712 1.199264 -1.278169
C -0.022095 0.202046 -0.387952
C 0.479707 1.246424 1.530268
H 0.745941 0.407008 2.161241
H -0.496151 1.685257 1.691737
H 1.279458 1.931250 1.272247
H -1.414055 1.453971 -1.476749
H 0.378885 1.795041 -1.770085
C 1.406634 -0.246345 -0.451650
O 1.819527 -1.308831 -0.055255
H 2.086776 0.494981 -0.923727
C -0.982385 -0.775897 0.176462
H -0.506481 -1.639763 0.629973
C -2.311239 -0.683962 0.165358
H -2.840104 0.155995 -0.272883
H -2.923941 -1.462268 0.604375
ImagFreq 474i
Internal rotation:
cos -0.02 -0.02 4.44
barrier 4.48
symmetry 3
Im,red 12.02
freq 138.1 (from rotation profile)

Reaction 1/38

methyl/2-methylidenepent-4-en-2-one/2-ethenyl-2-methyl-4-oxopentyl
C -0.359556 1.489842 -0.839961
C -0.264559 0.254193 -0.223960
C -0.032286 0.700866 1.966938
H 0.085716 -0.296567 2.372780
H -0.995696 1.171859 2.111366
H 0.832839 1.351158 2.021956
H -1.319795 1.951359 -1.030982
H 0.515594 2.074414 -1.086058
C 1.069327 -0.471746 -0.213859
O 1.123658 -1.666049 -0.006735
C -1.445717 -0.633961 -0.060471
H -1.211890 -1.592993 0.387558
C -2.699637 -0.370186 -0.424602
H -2.995245 0.556360 -0.905038
H -3.486999 -1.095059 -0.254924
C 2.336892 0.315187 -0.503359
H 3.191850 -0.311163 -0.253740
H 2.381705 0.562089 -1.568590
H 2.385877 1.251766 0.055192
ImagFreq 484i
Internal rotation:
cos -0.08 -0.08 3.77
barrier 3.81
symmetry 3
Im,red 12.06
freq 120.8 (from rotation profile)

Reaction 1/39

methyl/2-methylidenebut-3-enoic-acid/3-carboxymethyl-3-methylbut-1-en-4-yl
C 0.390120 -1.415540 -0.962919
C 0.259435 -0.238707 -0.248185
C -0.047029 -0.870195 1.888473
H -0.179181 0.083161 2.386448
H 0.902258 -1.367382 2.038427
H -0.922687 -1.501337 1.802634
H 1.363602 -1.847364 -1.155130
H -0.480308 -1.967683 -1.284949
C -1.080041 0.441562 -0.221559
O -1.260461 1.606667 0.038805
C 1.401691 0.672497 0.019913
H 1.125084 1.590477 0.526273
C 2.675250 0.467304 -0.312164
H 3.013432 -0.416515 -0.841867
H 3.434112 1.198860 -0.062095
O -2.107694 -0.390095 -0.526509
H -2.907622 0.153679 -0.489465
ImagFreq 496i
Internal rotation:
cos -0.07 -0.07 4.73
barrier 4.76
symmetry 3
Im,red 12.11
freq 139.7 (from rotation profile)

Reaction 1/40

methyl/methyl-2-methylidenebut-3-enoate/3-2-methoxy-2-oxoethyl-3-methylbut-1-en-4-yl
C -0.792669 1.320443 -1.085659
C -0.666926 0.227492 -0.248634
C -0.546424 1.091081 1.824457
H -0.383780 0.204593 2.426259
H -1.533186 1.532941 1.870119
H 0.289794 1.771482 1.723205
H -1.766906 1.697849 -1.368250
H 0.077771 1.868967 -1.413435
C 0.691645 -0.398320 -0.065996
O 0.878055 -1.525050 0.328205
C -1.794156 -0.696926 0.039089
H -1.537490 -1.516845 0.700264
C -3.031227 -0.613536 -0.448153
H -3.342095 0.161073 -1.140584
H -3.784232 -1.340194 -0.167539
O 1.699081 0.440344 -0.392155
C 3.023660 -0.102040 -0.255277
H 3.215396 -0.389274 0.779771
H 3.147280 -0.977342 -0.894616
H 3.696946 0.695237 -0.562560
ImagFreq 499i
Internal rotation:
cos -0.07 -0.07 4.82
barrier 4.85

symmetry 3
Im,red 12.15
freq 45.9 (from rotation profile)

Reaction 1/41

hydroxy-methyl/ethene/3-hydroxy-propyl
C -1.083501 0.581504 0.243782
C 1.103282 0.629242 -0.261912
C 1.664662 -0.551541 0.134876
H -1.503758 1.408931 -0.317596
H -0.989010 0.713253 1.320633
O -1.549995 -0.621720 -0.200694
H 0.855673 0.783901 -1.306290
H 1.259649 1.530855 0.321605
H 2.078963 -0.678790 1.129015
H 1.671172 -1.420160 -0.514030
H -1.079392 -1.319452 0.271735
ImagFreq 454i
Internal rotation:
cos 3.32 3.27 2.23
sin -1.68 0.60 -0.25
barrier 7.54
symmetry 1
Im,red 30.76
freq 80.6 (from rotation profile)

Reaction 1/42

methoxy-methyl/ethene/3-methoxypropyl
C -0.422770 -1.056677 0.345842
C 1.653563 -0.450484 -0.240205
C 1.970843 0.839303 0.084672
H -0.411153 -0.838244 1.414257
H -0.367429 -2.101594 0.057052
O -1.345520 -0.386901 -0.397333
H 2.041831 -1.267581 0.360313
H 1.410562 -0.702574 -1.266753
H 1.767561 1.659928 -0.594015
H 2.375928 1.097345 1.056777
C -1.665013 0.917029 0.074466
H -2.437732 1.310184 -0.585155
H -2.048805 0.874647 1.101723
H -0.786339 1.568078 0.045808
ImagFreq 440i
Internal rotation:
cos 2.27 0.32 1.62
sin 1.17 -0.43 0.17
barrier 4.33
symmetry 1
Im,red 43.99
freq 50.8 (from rotation profile)

Reaction 1/43

methanoyl-oxyl-methyl/ethene/3-formyloxypropyl
C -0.070002 0.843628 0.586127
C -1.625519 -0.331033 -0.537711
C -2.822149 -0.293942 0.114969
O 1.036643 0.944823 -0.246555
H 0.058457 0.205568 1.450789
H -0.547138 1.806526 0.697684
H -1.456066 0.300949 -1.402819
H -0.989717 -1.205764 -0.461214
H -3.069960 -1.017082 0.883597
H -3.541965 0.496871 -0.063965
C 1.894344 -0.104119 -0.293080
O 1.786392 -1.121511 0.330130
H 2.702065 0.139230 -0.994501
ImagFreq 453i
Internal rotation:
cos 0.64 2.06 2.34
sin 0.41 -0.08 -0.28
barrier 4.73
symmetry 1
Im,red 56.74
freq 53.9 (from rotation profile)

Reaction 1/44

acetyloxymethyl/ethene/3-acetyloxypropyl
C 0.607961 -0.704965 -0.813543
C 2.034313 0.200690 0.670805
C 3.307419 0.210326 0.181765
O -0.604466 -0.881039 -0.165428
H 1.071264 -1.660526 -1.014828
H 0.619558 0.066129 -1.572977
H 1.436941 1.105137 0.654416
H 1.734120 -0.549559 1.394453
H 3.975826 -0.631835 0.321869
H 3.674824 1.031444 -0.423209
C -1.443802 0.196941 -0.073280
O -1.176429 1.278761 -0.523990
C -2.708437 -0.183424 0.648370
H -2.470433 -0.604672 1.627341
H -3.338115 0.696407 0.760580
H -3.241548 -0.951717 0.083004
ImagFreq 449i
Internal rotation:
cos 1.01 2.12 2.39
barrier 5.13
symmetry 1
Im,red 61.96
freq 52.5 (from rotation profile)

Reaction 1/45

2-oxo-ethyl/ethene/4-oxobutyl
C -0.305482 0.900396 -0.205955
C 1.245898 -0.571826 0.292243
C 2.435060 -0.055559 -0.146081
C -1.479013 0.236362 0.322100

H -0.168396 0.876865 -1.280162
H 0.086921 1.760822 0.323505
H 1.022224 -0.570083 1.353259
H 0.724019 -1.319149 -0.293897
H 2.760588 -0.181564 -1.172295
H 3.054980 0.561743 0.493948
O -2.139882 -0.584584 -0.296211
H -1.740051 0.491796 1.371488
ImagFreq 482i
Internal rotation:
cos 5.92 -2.08 4.88
barrier 10.83
symmetry 1
Im,red 50.81
freq 66.7 (from rotation profile)

Reaction 1/46

2-oxo-propyl/ethene/4-oxopentyl
C -0.067873 -0.055586 0.948966
C -1.610490 0.012303 -0.627921
C -2.822404 0.149202 -0.009184
C 1.141865 -0.195634 0.143446
H -0.429810 -0.955067 1.430019
H -0.271384 0.882795 1.452030
H -1.168236 0.866530 -1.128634
H -1.278957 -0.958282 -0.977456
H -3.366304 -0.711520 0.362833
H -3.245953 1.125132 0.198931
O 1.511743 -1.289411 -0.265795
C 1.914124 1.072993 -0.192034
H 2.636024 0.859842 -0.979499
H 1.247225 1.881270 -0.505983
H 2.452124 1.424920 0.694483
ImagFreq 483i
Internal rotation:
cos 3.95 -1.98 4.80
sin 1.45 -0.18 -0.39
barrier 9.21
symmetry 1
Im,red 58.60
freq 56.1 (from rotation profile)

Reaction 1/47

carboxymethyl/ethene/3-carboxypropyl
C -0.032215 -0.163964 0.964281
C -1.576336 0.058141 -0.623619
C -2.801849 0.034668 -0.020131
C 1.168281 -0.132040 0.143228
H -0.316257 -1.133237 1.347131
H -0.274614 0.706683 1.557371
H -1.143269 1.001212 -0.936690
H -1.202425 -0.824447 -1.129743
H -3.323947 -0.897461 0.163246
H -3.263502 0.939421 0.358579
O 1.719915 -1.096079 -0.346597
O 1.604813 1.142399 -0.088327
H 2.378896 1.056440 -0.663057
ImagFreq 467i
Internal rotation:
cos 2.80 -0.98 4.73
barrier 7.53
symmetry 1
Im,red 57.15
freq 62.5 (from rotation profile)

Reaction 1/48

2-methoxy-2-oxo-ethyl/ethene/4-methoxy-4-oxobutyl
C 0.621903 0.592532 0.899302
C 1.938926 -0.404253 -0.590007
C 3.214038 -0.398972 -0.099010
C -0.653511 0.527150 0.197494
H 1.097227 1.562455 0.923774
H 0.782943 -0.072343 1.736408
H 1.341338 -1.307006 -0.536613
H 1.645101 0.312526 -1.348201
H 3.883961 0.435045 -0.274286
H 3.577020 -1.194405 0.541870
O -1.084879 1.369407 -0.563383
O -1.304330 -0.644131 0.449824
C -2.556381 -0.809104 -0.232418
H -2.416668 -0.764445 -1.314224
H -2.925321 -1.788469 0.065590
H -3.261778 -0.029682 0.061980
ImagFreq 474i
Internal rotation:
cos 2.95 -0.90 4.85
barrier 7.80
symmetry 1
Im,red 63.18
freq 57.9 (from rotation profile)

Reaction 1/49

1-hydroxyethyl/ethene/3-hydroxybutyl
C 0.732240 0.130567 0.411192
C -1.199626 -0.851841 -0.126450
C -2.209476 0.062112 -0.000910
H 0.553321 0.118347 1.487389
O 0.659682 1.361373 -0.183859
H -0.804798 -1.085706 -1.109756
H -1.068740 -1.623966 0.625333
H -2.750207 0.188857 0.930555
H -2.482152 0.719189 -0.819321
H -0.169724 1.773670 0.092228
C 1.846837 -0.709038 -0.113738
H 1.795137 -0.777454 -1.203975
H 2.825303 -0.278122 0.140936
H 1.804555 -1.716601 0.306927
ImagFreq 413i
Internal rotation:
cos 3.90 4.56 3.13
barrier 8.95
symmetry 1
Im,red 51.09

freq 75.7 (from rotation profile)

Reaction 1/50

1-methoxy-ethyl/ethene/3-methoxybutyl
C 0.280660 0.489585 0.334722
C -1.283732 -0.962702 -0.317477
C -2.530708 -0.635755 0.142035
H 0.313226 0.228113 1.394563
O 1.422822 0.185568 -0.360006
H -1.003749 -0.743752 -1.342748
H -0.753785 -1.793704 0.136453
H -2.897112 -0.998290 1.095966
H -3.167789 0.059452 -0.392764
C 2.171167 -0.916495 0.134351
H 3.077212 -0.977363 -0.467423
H 2.443562 -0.765234 1.186397
H 1.613127 -1.853826 0.040362
C -0.267550 1.830234 -0.027086
H -1.249983 1.969547 0.428077
H 0.392986 2.638372 0.314049
H -0.369291 1.922941 -1.112160
ImagFreq 420i
Internal rotation:
cos 1.19 0.33 2.09
barrier 3.55
symmetry 1
Im,red 56.63
freq 46.6 (from rotation profile)

Reaction 1/51

1-formyloxyethyl/ethene/3-formyloxybutyl
C -0.069882 0.638245 -0.327349
C -1.317235 -1.033894 0.463481
C -2.559232 -1.053619 -0.102904
H 0.131711 0.223387 -1.308130
O 1.048297 0.640049 0.511667
H -0.559388 -1.735056 0.132584
H -1.183084 -0.634822 1.463813
H -3.383115 -0.485496 0.314028
H -2.751251 -1.588123 -1.026391
C -0.865015 1.890505 -0.200554
H -1.100106 2.104354 0.845627
H -0.318786 2.754235 -0.602829
H -1.800535 1.789957 -0.754112
C 2.034916 -0.257114 0.277093
O 2.052184 -1.067375 -0.605992
H 2.819389 -0.114567 1.031403
ImagFreq 453i
Internal rotation:
cos 1.18 2.62 2.76
sin -1.14 0.26 0.62
barrier 6.72
symmetry 1
Im,red 61.91
freq 57.3 (from rotation profile)

Reaction 1/52

1-acetyloxyethyl/ethene/3-acetyloxybutyl
C 0.558087 0.644720 0.415060
C 1.664778 -1.043465 -0.535003
C 2.976981 -1.075452 -0.158631
H 0.504638 0.237833 1.418180
O -0.671917 0.655166 -0.242886
H 0.956197 -1.732627 -0.089652
H 1.389369 -0.650028 -1.508362
H 3.736735 -0.519949 -0.696881
H 3.297081 -1.604863 0.731740
C 1.339532 1.886396 0.158693
H 1.411022 2.092813 -0.912807
H 0.874079 2.759606 0.635611
H 2.348986 1.775633 0.559415
C -1.632646 -0.233374 0.153408
O -1.477598 -1.021110 1.048900
C -2.873860 -0.071176 -0.683470
H -3.239355 0.956015 -0.618497
H -2.642695 -0.269589 -1.732680
H -3.637173 -0.763179 -0.334530
ImagFreq 446i
Internal rotation:
cos 1.53 2.66 2.81
sin -1.38 0.27 0.64
barrier 7.17
symmetry 1
Im,red 65.33
freq 63.2 (from rotation profile)

Reaction 1/53

1-oxo-prop-2-yl/ethene/3-formylbutyl
C -0.269005 0.336798 0.628107
C 1.302171 -0.857221 -0.268800
C 2.489084 -0.190310 -0.092451
C -1.358832 -0.604137 0.407886
H 0.148483 0.336232 1.630936
H 1.100772 -1.738228 0.331036
H 0.807964 -0.831341 -1.233696
H 2.816413 0.574830 -0.786505
H 3.100051 -0.347058 0.789201
O -2.128461 -0.554087 -0.538720
H -1.437619 -1.423787 1.153424
C -0.270967 1.636368 -0.118307
H 0.711672 2.111628 -0.103604
H -0.591624 1.488519 -1.151075
H -0.983129 2.332924 0.341443
ImagFreq 508i
Internal rotation:
cos 5.22 -1.93 6.07
barrier 11.29
symmetry 1

Im,red 58.71
freq 69.4 (from rotation profile)

Reaction 1/54

3-oxo-but-2-yl/ethene/3-methyl-4-oxopentyl
C 0.189071 0.638276 -0.607833
C -1.721872 0.424267 0.406453
C -2.370808 -0.753680 0.133453
C 0.965464 -0.420406 0.053670
H -0.170955 0.415449 -1.608224
H -1.243544 0.561826 1.369832
H -2.058042 1.331592 -0.082717
H -3.016571 -0.856426 -0.731359
H -2.215113 -1.639950 0.737451
O 1.612557 -0.195963 1.068748
C 0.918488 -1.806069 -0.564002
H 1.366328 -2.526243 0.120066
H -0.109647 -2.098153 -0.797441
H 1.479065 -1.812659 -1.504733
C 0.539463 2.065679 -0.310713
H -0.253645 2.755846 -0.608765
H 0.758044 2.194107 0.750457
H 1.444785 2.353913 -0.860721
ImagFreq 504i
Internal rotation:
cos 1.72 1.25 5.04
sin -2.35 -0.59 1.15
barrier 9.54
symmetry 1
Im,red 63.40
freq 56.3 (from rotation profile)

Reaction 1/55

2-methylbut-1-en-3-yl/ethene/3-carboxybutyl
C -0.021474 0.438553 -0.593669
C -1.401021 -0.881192 0.487421
C -2.682180 -0.596898 0.094695
C 1.218411 -0.067848 -0.007268
H -0.252573 0.057336 -1.581268
H -0.902559 -1.762181 0.099700
H -1.043656 -0.524252 1.447534
H -3.271140 0.166372 0.589883
H -3.126891 -1.074932 -0.770864
O 1.811655 0.421901 0.932250
O 1.641060 -1.222862 -0.601296
H 2.437684 -1.492087 -0.121788
C -0.429008 1.841200 -0.269953
H -1.480018 2.012661 -0.510729
H -0.256511 2.064555 0.784447
H 0.165580 2.557323 -0.851907
ImagFreq 491i
Internal rotation:
cos 2.87 -0.49 5.87
barrier 8.77
symmetry 1
Im,red 63.18
freq 63.5 (from rotation profile)

Reaction 1/56

1-methoxy-1-oxo-prop-2-yl/ethene/4-methoxy-3-methyl-4-oxobutyl
C -0.571207 0.524294 -0.596716
C -1.532811 -1.125538 0.483565
C -2.842382 -1.213629 0.092364
C 0.759806 0.403169 0.002957
H -0.671878 0.086519 -1.582840
H -0.807584 -1.831534 0.095523
H -1.288620 -0.681191 1.442641
H -3.621414 -0.644588 0.586313
H -3.135690 -1.798931 -0.771892
O 1.167906 1.045311 0.949746
O 1.496617 -0.570324 -0.600923
C 2.805189 -0.782674 -0.049658
H 2.740785 -1.069859 1.001569
H 3.244148 -1.585273 -0.638900
H 3.408393 0.123598 -0.129197
C -1.367083 1.753589 -0.289791
H -0.995609 2.606533 -0.872777
H -2.420717 1.616265 -0.541386
H -1.277074 2.023302 0.764034
ImagFreq 494i
Internal rotation:
cos 3.03 -0.36 6.00
barrier 9.08
symmetry 1
Im,red 67.09
freq 60.8 (from rotation profile)

Reaction 1/57

1-oxo-but-3-en-2-yl/ethene/3-formylpent-1-en-5-yl
C 0.262468 0.045970 0.502474
C -1.097966 -1.083840 -0.565717
C -2.334116 -1.166535 0.063321
C -0.438865 1.340764 0.441536
H 0.158516 -0.488294 1.442882
H -1.018627 -0.495983 -1.474427
H -0.447220 -1.950583 -0.535044
H -2.525794 -1.907739 0.830568
H -3.114185 -0.438126 -0.123687
O -0.178651 2.233028 -0.338918
H -1.282110 1.442762 1.157052
C 1.526479 -0.092331 -0.196248
H 1.693003 0.614850 -1.003734
C 2.457805 -1.016479 0.087214
H 2.326730 -1.731497 0.893931
H 3.384067 -1.074915 -0.471674
ImagFreq 581i
Internal rotation:
cos 6.62 -1.30 7.35
sin -1.44 -1.28 1.40
barrier 14.31
symmetry 1
Im,red 67.85
freq 69.5 (from rotation profile)

Reaction 1/58

4-oxopent-1-en-3-yl/ethene/3-acetylpent-1-en-5-yl
C -0.410811 -0.114316 0.383150
C 0.070213 1.687144 -0.526662
C 1.246764 2.243511 -0.048397
C 0.737283 -0.948303 -0.061216
H -0.380489 0.223518 1.415327
H 0.066671 1.263616 -1.525528
H -0.869818 2.129806 -0.217399
H 1.254756 2.872716 0.834406
H 2.206629 2.003546 -0.490525
O 0.734587 -1.515930 -1.139985
C -1.720513 -0.432302 -0.152207
H -1.715830 -0.970348 -1.095907
C -2.886381 -0.103856 0.428255
H -2.925326 0.430378 1.372903
H -3.835159 -0.372124 -0.020764
C 1.916818 -1.040950 0.886332
H 2.748668 -1.539865 0.390469
H 2.221972 -0.046501 1.225906
H 1.630996 -1.612867 1.775460
ImagFreq 582i
Internal rotation:
cos 8.49 -1.30 7.28
barrier 15.98
symmetry 1
Im,red 70.38
freq 64.6 (from rotation profile)

Reaction 1/59

3-carboxyprop-1-en-3-yl/ethene/3-carboxypent-1-en-5-yl
C 0.418001 -0.086868 -0.397712
C -0.178968 1.670638 0.560791
C -1.381909 2.137968 0.061601
C -0.699930 -0.971878 -0.023736
H 0.389058 0.282339 -1.416065
H -0.162036 1.231058 1.552595
H 0.736055 2.175264 0.272370
H -1.419837 2.760532 -0.824765
H -2.329801 1.808307 0.469119
O -0.767410 -1.642392 0.983199
C 1.715830 -0.382887 0.170661
H 1.703407 -0.965738 1.087340
C 2.886294 0.029054 -0.345418
H 2.934336 0.609385 -1.261690
H 3.828405 -0.215293 0.129842
O -1.711012 -0.927482 -0.930995
H -2.408114 -1.503022 -0.583493
ImagFreq 579i
Internal rotation:
cos 6.53 -2.23 7.39
barrier 14.02
symmetry 1
Im,red 71.74
freq 57.7 (from rotation profile)

Reaction 1/60

4-methoxy-4-oxobut-1-en-3-yl/ethene/3-methoxycarbonylpent-1-en-5-yl
C 0.733548 -0.162851 -0.376374
C 0.864285 1.736617 0.485894
C -0.155030 2.561987 0.046477
C -0.590124 -0.585599 0.124114
H 0.752047 0.144928 -1.415244
H 0.830398 1.363809 1.504163
H 1.862348 1.883127 0.088803
H -0.071724 3.115394 -0.881661
H -1.111148 2.599466 0.554436
O -0.800352 -1.123851 1.189543
C 1.890184 -0.866102 0.134529
H 1.750584 -1.364481 1.089750
C 3.086558 -0.913759 -0.476806
H 3.258839 -0.430328 -1.433519
H 3.921068 -1.449420 -0.041011
O -1.573931 -0.256056 -0.746948
C -2.908416 -0.579915 -0.323747
H -3.151679 -0.068983 0.609536
H -3.559344 -0.240816 -1.126778
H -3.013162 -1.655702 -0.173757
ImagFreq 581i
Internal rotation:
cos 6.50 -2.32 7.58
barrier 14.12
symmetry 1
Im,red 74.19
freq 0.0 (from rotation profile)

Reaction 1/61

carbonyl/ethene/3-oxopropyl
C -0.999593 0.019944 0.484724
C 1.001049 0.692867 -0.064246
C 1.639242 -0.507766 -0.104233
H 0.617715 1.148310 -0.969854
H 1.132078 1.360294 0.780299
H 2.145972 -0.911800 0.764935
H 1.614506 -1.130948 -0.990678
O -1.810886 -0.134380 -0.358935
H -0.867370 -0.621090 1.389312
ImagFreq 429i
Internal rotation:
cos 7.39 1.13 5.50
sin 4.35 -1.71 -1.35
barrier 13.46
symmetry 1
Im,red 34.35
freq 105.4 (from rotation profile)

Reaction 1/62

acetyl/ethene/3-oxobutyl
C 0.848439 -0.173051 0.017670
C -1.308452 -0.726449 0.155266
C -2.150813 0.314148 -0.121223
H -1.112722 -1.489147 -0.590479
H -1.152929 -1.043373 1.181618
H -2.496967 0.986782 0.655390
H -2.456428 0.540786 -1.136447
O 1.635019 -1.047902 -0.094051
C 1.078910 1.312348 0.031865
H 2.123960 1.551800 -0.180227
H 0.411644 1.779552 -0.695103
H 0.794786 1.694844 1.016196
ImagFreq 352i
Internal rotation:
cos 7.59 -2.68 -0.12
barrier 8.63
symmetry 1
Im,red 44.17
freq 30.2 (from HO analysis)

Reaction 1/63

hydroxyacetyl/ethene/4-hydroxy-3-oxobutyl
C -0.262269 0.564597 -0.050617
C 1.967372 0.473966 -0.098709
C 2.454896 -0.790293 0.081359
H 1.949259 0.916755 -1.088924
H 1.972944 1.186157 0.719450
H 2.640110 -1.190351 1.071706
H 2.622066 -1.458392 -0.755772
O -0.820479 1.606470 0.024452
C -0.906018 -0.805059 0.034971
H -0.501871 -1.427471 -0.766835
H -0.543568 -1.233072 0.983815
O -2.308958 -0.788813 -0.067226
H -2.627331 0.005854 0.376727
ImagFreq 345i
Internal rotation:
cos 6.77 -3.30 0.71
barrier 8.24
symmetry 1
Im,red 44.63
freq 27.1 (from HO analysis)

Reaction 1/64

methoxyacetyl/ethene/4-methoxy-3-oxobutyl
C -0.726907 0.945450 -0.178619
C -1.647595 -1.632234 0.571421
C -1.610116 -1.011165 -0.641231
H -0.812184 -2.226757 0.922501
H -2.479885 -1.495535 1.252429
H -2.496128 -0.528399 -1.037616
H -0.834371 -1.257613 -1.354954
O -1.454078 1.839458 0.099526
C 0.719178 0.816563 0.278857
H 1.217254 1.765505 0.025075
H 0.722513 0.716477 1.376132
O 1.333210 -0.279429 -0.349151
C 2.685050 -0.444215 0.038911
H 3.290580 0.433903 -0.225005
H 2.775564 -0.621265 1.119758
H 3.065943 -1.312938 -0.497356
ImagFreq 406i
Internal rotation:
cos 0.30 10.70 0.32
barrier 12.72
symmetry 1
Im,red 82.96
freq 97.3 (from rotation profile)

Reaction 1/65

hydroxycarbonyl/ethene/2-carboxyethyl
C 0.841917 -0.105104 0.000240
C -1.328070 -0.778250 0.001576
C -2.137903 0.316130 -0.001349
H -1.136085 -1.327850 -0.913032
H -1.136565 -1.323225 0.919056
H -2.442747 0.796490 0.920923
H -2.442338 0.791847 -0.926163
O 1.760165 -0.858487 -0.001088
O 0.876160 1.228307 0.000674
H 1.811469 1.507519 -0.000268
ImagFreq 348i
Internal rotation:
cos 2.31 -1.97 0.35
barrier 3.36
symmetry 1
Im,red 44.64
freq 26.5 (from HO analysis)

Reaction 1/66

methoxycarbonyl/ethene/3-methoxy-3-oxopropyl
C 0.278641 0.543784 -0.001339
C -2.000032 0.466125 -0.005598
C -2.417735 -0.827897 0.005221
H -1.990936 1.054208 0.905108
H -1.987951 1.037621 -0.926795
H -2.552255 -1.386879 -0.913434
H -2.555403 -1.370356 0.933278
O 0.880231 1.571415 0.004119
O 0.751626 -0.691826 -0.003753
C 2.204826 -0.815541 0.000689
H 2.614537 -0.345733 0.895246
H 2.402473 -1.884145 -0.001947
H 2.620480 -0.340253 -0.888216
ImagFreq 326i
Internal rotation:
cos 2.33 -1.77 0.29
barrier 3.17
symmetry 1
Im,red 45.49
freq 8.3 (from HO analysis)

VALIDATION SET OF REACTIONS

Reaction 2/1

hydroxy-methyl/2-methylidenebut-3-enal/3-formyl-5-hydroxypent-1-en-3-yl
C -0.612096 0.070053 0.565203
C 0.286598 -0.322391 1.518597
C 2.206378 -0.884005 0.015573
H 0.177264 -1.289734 1.996053
H 0.953730 0.377593 2.003869
H 2.449873 -1.897135 0.306001
H 2.810124 -0.062125 0.387447
C -1.642299 -0.895875 0.145049
O -2.495716 -0.685363 -0.692684
H -1.595204 -1.872568 0.672987
C -0.575205 1.342107 -0.148024
H -1.408463 1.487355 -0.829299
C 0.377678 2.285681 -0.067134
H 1.231523 2.201795 0.597863
H 0.309287 3.196413 -0.649862
O 1.671267 -0.794435 -1.215614
H 1.421131 0.123366 -1.394253
ImagFreq 260i
Internal rotation:
cos 3.58 6.87 5.17
barrier 12.43
symmetry 1
Im,red 79.28
freq 85.6 (from rotation profile)

Reaction 2/2

1-methoxy-ethyl/methoxy-ethene/13-dimethoxybutyl
C 1.160489 -1.044854 0.171200
O 1.984935 0.036196 0.325959
C 0.087134 -1.221735 1.001979
C -1.717262 -0.138385 0.195125
H 0.074971 -0.694284 1.948809
H -0.410178 -2.183127 0.983065
H -2.227273 0.049077 1.145127
H 1.340260 -1.661275 -0.704627
C 2.918905 0.240875 -0.724458
H 2.409375 0.447672 -1.672973
H 3.523262 1.102979 -0.444636
H 3.573505 -0.630537 -0.847242
O -1.297462 0.995843 -0.449553
C -0.795358 2.021220 0.397606
H -1.519287 2.267466 1.185662
H 0.154535 1.722109 0.848970
H -0.639325 2.898869 -0.229885
C -2.356396 -1.107292 -0.747128
H -2.681186 -2.005163 -0.216174
H -3.232654 -0.667516 -1.242682
H -1.650851 -1.401554 -1.530604
ImagFreq 456i
Internal rotation:
cos 1.95 2.59 1.79
sin 0.73 1.15 0.04
barrier 6.34
symmetry 1
Im,red 226.48
freq 48.8 (from HO analysis)

Reaction 2/3

ethyl/prop-1-ene-2-yl-acetate/2-acetyloxypentan-2-yl
C -0.165666 1.121123 -0.223037
O 1.085124 0.593439 -0.603614
C -1.193948 0.967572 -1.104756
C -2.319239 -0.968159 -0.769560
H -0.972728 0.657415 -2.117745
H -2.088702 1.558521 -0.957905
H -3.177771 -0.725993 -1.390930
H -1.611277 -1.644400 -1.239115
C 1.621595 -0.438547 0.107284
O 1.065756 -0.990525 1.020260
C 2.996031 -0.771677 -0.414523
H 3.364892 -1.665677 0.083492
H 2.962872 -0.923235 -1.495000
H 3.673080 0.064362 -0.222326
C -0.209849 1.802956 1.103331
H -1.178389 2.283142 1.249703
H -0.040629 1.099884 1.924086
H 0.568226 2.573289 1.163183
C -2.543423 -1.135541 0.700793
H -3.130909 -0.312323 1.119463
H -3.095918 -2.062208 0.917055
H -1.592800 -1.192454 1.235681
ImagFreq 483i
Internal rotation:
cos 0.66 1.35 2.23
sin 0.05 0.65 0.70
barrier 4.47
symmetry 1
Im,red 103.60
freq 84.8 (from rotation profile)

Reaction 2/4

ethyl/1-ethenyl-acetate/2-acetyloxybutyl
C 1.512797 1.821926 -0.404236
C 0.618815 1.030397 0.255671
C 1.669945 -0.870885 0.758813
H 0.395418 1.131997 1.308597
H 0.853680 -1.305538 1.328125
H 2.476119 -0.478362 1.371473
H 2.285286 2.334132 0.152545
H 1.533487 1.863211 -1.485119

O -0.443536 0.519500 -0.505764
C -1.514201 -0.004239 0.154578
O -1.598702 -0.064758 1.352889
C -2.545858 -0.494743 -0.827472
H -2.740657 0.264165 -1.586850
H -2.168042 -1.383642 -1.339559
H -3.460230 -0.745684 -0.294097
C 2.045153 -1.519283 -0.536277
H 1.170935 -1.679991 -1.173822
H 2.764684 -0.914244 -1.094475
H 2.507317 -2.503022 -0.370278
ImagFreq 548i
Internal rotation:
cos 0.72 1.55 3.64
sin 1.44 -1.09 -0.03
barrier 6.22
symmetry 1
Im,red 96.08
freq 52.7 (from rotation profile)

Reaction 2/5

propan-2-yl/2-methylidenebut-3-enal/3-formylhex-1-en-3-yl
C -0.977973 0.050856 0.446360
C 0.019972 0.067051 1.388289
C 2.155789 -0.391674 0.292429
H 0.179364 -0.807923 2.007805
H 0.451051 0.991792 1.748192
H 2.620985 -0.596392 1.253392
C -1.645713 -1.238485 0.189900
O -2.528142 -1.420894 -0.624869
H -1.281810 -2.075895 0.824215
C -1.430541 1.192101 -0.342946
H -2.211251 0.944492 -1.055983
C -1.000027 2.458276 -0.259016
H -0.231749 2.773267 0.439129
H -1.419175 3.229524 -0.894033
C 2.509890 0.906517 -0.357500
H 3.470697 0.821475 -0.890927
H 1.762120 1.201265 -1.099680
H 2.618139 1.716917 0.367183
C 1.853622 -1.573017 -0.569445
H 2.753259 -1.891531 -1.119177
H 1.510179 -2.432190 0.011191
H 1.093209 -1.337389 -1.320789
ImagFreq 321i
Internal rotation:
cos 1.65 -0.17 0.52
barrier 2.19
symmetry 1
Im,red 203.77
freq 27.6 (from HO analysis)

Reaction 2/6

allyl/prop-2-enoic-acid/2-carboxypent-1-en-5-yl
C -2.121526 -1.257641 0.099166
C -1.087298 -0.559293 -0.500505
C 0.741951 -1.442100 0.154624
H -0.883848 -0.716718 -1.553355
H 0.534657 -2.392787 -0.321591
H 0.520167 -1.406235 1.215385
H -2.522018 -2.159044 -0.346726
H -2.488786 -0.955887 1.072046
C -0.790299 0.810887 -0.001760
O -0.946803 1.201814 1.129824
O -0.292595 1.597689 -0.984910
H -0.079592 2.447581 -0.571369
C 1.875933 -0.694387 -0.310161
H 2.189972 -0.861900 -1.338080
C 2.546053 0.218407 0.426967
H 2.268601 0.427563 1.454868
H 3.387142 0.766177 0.019522
ImagFreq 567i
Internal rotation:
cos 4.96 -1.84 6.47
barrier 11.60
symmetry 1
Im,red 143.80
freq 43.5 (from rotation profile)

Reaction 2/7

1-ethenyl-acetate/prop-1-en-2-yl/4-acetyloxy-2-methylbut-1-en-4-yl
C -0.178995 -1.052748 0.298250
O -1.089996 -0.355660 -0.475902
C 1.013135 -1.398245 -0.244239
C 2.575784 0.290742 -0.008828
H 1.160221 -1.334799 -1.314251
H 1.658990 -2.060543 0.314565
H -0.474514 -1.204070 1.326448
C -2.264303 0.049521 0.105124
O -2.539281 -0.152044 1.256502
C -3.120919 0.762621 -0.905794
H -4.054749 1.065805 -0.437647
H -2.593494 1.638633 -1.290343
H -3.321837 0.104509 -1.754044
C 3.798711 -0.100266 -0.283442
H 4.036213 -1.119168 -0.577738
H 4.643581 0.591645 -0.228503
C 1.950395 1.561718 0.402279
H 1.210630 1.891792 -0.334003
H 1.425097 1.451736 1.356402
H 2.701222 2.356038 0.514220
ImagFreq 386i
Internal rotation:
cos 1.01 1.07 0.10
sin 0.18 0.06 0.01
barrier 1.81
symmetry 1
Im,red 159.50
freq 20.9 (from HO analysis)

Reaction 2/8

hydroxy-methyl/propene/4-hydroxybutan-2-yl
C -1.586345 0.207401 0.592348
C 0.310124 1.090615 -0.219365
C 1.172346 0.085511 -0.564125
H -2.245565 1.064591 0.677524
H -1.203936 -0.208611 1.523754
O -2.036508 -0.680794 -0.348262
H -0.264078 1.591442 -0.990309
H 0.483961 1.663756 0.687343
H 1.093500 -0.353065 -1.556492
H -1.390349 -1.391794 -0.425966
C 2.179374 -0.524302 0.364515
H 1.965320 -1.580963 0.575139
H 3.187708 -0.498647 -0.066242
H 2.212512 0.004300 1.321107
ImagFreq 473i
Internal rotation:
cos 2.04 1.75 2.14
sin -1.09 0.47 -0.40
barrier 4.88
symmetry 1
Im,red 54.66
freq 55.9 (from rotation profile)

Reaction 2/9

hydroxy-methyl/propene/3-hydroxy-2-methylpropyl
C 1.103683 -0.810146 0.122371
C -0.797169 0.214434 -0.426268
C -0.698941 1.467606 0.120745
H 1.166202 -1.638296 -0.576091
H 0.835582 -1.054385 1.150080
O 2.116610 0.084742 -0.065724
H -0.518999 0.106400 -1.471975
H -1.114048 1.691504 1.098688
H -0.161912 2.263240 -0.382458
H 1.954223 0.842866 0.509781
C -1.771782 -0.814132 0.099190
H -1.446653 -1.837212 -0.108806
H -1.908186 -0.713581 1.179637
H -2.753835 -0.685047 -0.369295
ImagFreq 479i
Internal rotation:
cos 2.23 5.62 5.02
sin -1.96 1.30 -0.59
barrier 11.20
symmetry 1
Im,red 48.46
freq 88.9 (from rotation profile)

Reaction 2/10

2-oxo-propyl/1-butene/6-oxoheptan-3-yl
C -1.234616 0.803632 -0.963095
C 0.380807 1.740234 0.211476
C 1.563235 1.099410 -0.059608
C -1.582793 -0.402056 -0.225395
H -0.688967 0.663269 -1.887212
H -1.906528 1.654748 -0.923150
H 0.174661 2.694483 -0.259273
H -0.113350 1.572556 1.162922
H 2.133736 1.420318 -0.929900
O -1.018124 -1.473189 -0.425865
C -2.674009 -0.286267 0.831867
H -2.662569 -1.174336 1.462871
H -2.549865 0.609806 1.447123
H -3.653317 -0.211654 0.347503
C 2.106439 -0.076585 0.688299
H 3.049729 0.222587 1.168373
H 1.420629 -0.352963 1.494907
C 2.375367 -1.296212 -0.212446
H 3.072998 -1.043226 -1.016909
H 1.444107 -1.652567 -0.655050
H 2.817148 -2.110455 0.368133
ImagFreq 461i
Internal rotation:
cos 2.53 6.64 2.60
sin -3.11 -0.39 2.25
barrier 14.87
symmetry 1
Im,red 266.92
freq 34.2 (from rotation profile)

Reaction 2/11

2-oxo-propyl/1-butene/2-ethyl-4-oxopentyl
C -0.927249 0.794159 -0.836219
C 0.971409 0.647851 0.247370
C 1.516904 1.895343 0.040386
C -1.729099 -0.246001 -0.203168
H -0.512017 0.562500 -1.809039
H -1.190719 1.830782 -0.662136
H 0.464280 0.488687 1.196921
H 2.176972 2.084520 -0.799901
H 1.234565 2.746844 0.648489
O -1.640819 -1.423839 -0.536770
C -2.665616 0.178334 0.920420
H -3.011617 -0.704512 1.456819
H -2.177999 0.869465 1.614170
H -3.533005 0.699721 0.502206
C 1.559946 -0.597190 -0.380302
H 0.770763 -1.328980 -0.567767
H 1.995386 -0.336870 -1.351338
C 2.637208 -1.228977 0.516538
H 2.224148 -1.509395 1.490064
H 3.466498 -0.538284 0.691074
H 3.038286 -2.134874 0.054457

ImagFreq 489i
Internal rotation:
cos 8.57 2.62 5.05
sin 1.93 0.40 -2.07
barrier 14.30
symmetry 1
Im,red 175.04
freq 45.8 (from rotation profile)

Reaction 2/12

methoxy-methyl/2-methylprop-1-ene/3-methoxy-22-dimethylpropyl
C 0.697029 -0.914300 -0.523060
C -1.117016 0.245873 0.056691
C -0.743182 1.571176 -0.013188
H 0.808998 -0.626930 -1.569412
H 0.315306 -1.912606 -0.332101
O 1.749018 -0.628276 0.293801
H -0.309830 2.079340 0.841021
H -0.804956 2.127500 -0.942219
C 2.539430 0.485222 -0.106395
H 3.337680 0.585635 0.628285
H 2.976004 0.312155 -1.098343
H 1.939901 1.399891 -0.129669
C -2.006993 -0.320279 -1.034832
H -1.902592 -1.404677 -1.132780
H -3.059429 -0.118202 -0.802096
H -1.790690 0.135153 -2.004326
C -1.285094 -0.386806 1.427742
H -2.221114 -0.047525 1.886476
H -1.323779 -1.477488 1.372022
H -0.462694 -0.111350 2.090982
ImagFreq 485i
Internal rotation:
cos 6.54 -0.93 3.32
sin -1.99 2.07 -0.81
barrier 11.44
symmetry 1
Im,red 126.27
freq 54.7 (from rotation profile)

Reaction 2/13

methyl/2-methylpent-1-en-3-one/3-methyl-4-oxohexan-3-yl
C 0.752608 0.580853 0.346910
C 1.450348 -0.428419 0.955708
C 2.459516 -1.735967 -0.731372
H 0.948992 -1.303230 1.347369
H 2.443394 -0.239971 1.345728
H 2.933246 -2.476843 -0.099061
H 3.096418 -0.985955 -1.181285
H 1.590862 -2.047512 -1.296199
C -0.681508 0.448082 -0.012246
O -1.251527 1.367665 -0.580473
C -1.436730 -0.833533 0.339356
H -0.909429 -1.684363 -0.108072
H -1.374061 -0.986117 1.423249
C 1.412523 1.870180 -0.053885
H 0.873325 2.726709 0.359408
H 2.450078 1.906050 0.283296
H 1.390112 1.998202 -1.140889
C -2.895351 -0.809200 -0.112018
H -2.969265 -0.685687 -1.194066
H -3.398023 -1.739123 0.165513
H -3.431869 0.024541 0.344077
ImagFreq 428i
Internal rotation:
cos 0.00 0.00 1.24
barrier 1.24
symmetry 3
Im,red 12.18
freq 0.0 (from rotation profile)

Reaction 2/14

methyl/2-methylpent-1-en-3-one/22-dimethyl-3-oxopentyl
C 1.286946 -1.289119 -1.030005
C 1.027258 -0.109693 -0.364435
C 1.141482 -0.649392 1.825129
H 0.774554 0.262242 2.281615
H 2.210248 -0.816808 1.873295
H 0.520186 -1.530218 1.932971
H 2.294489 -1.535146 -1.345087
H 0.526665 -2.040042 -1.199223
C -0.397371 0.369319 -0.196006
O -0.618681 1.544713 0.016137
C -1.543815 -0.628282 -0.341046
H -1.298418 -1.551148 0.192695
H -1.594434 -0.905313 -1.401652
C 2.071746 0.989714 -0.359979
H 3.076784 0.568520 -0.293435
H 2.004063 1.567859 -1.286689
H 1.917288 1.687310 0.461526
C -2.886631 -0.066087 0.121603
H -3.122321 0.859005 -0.405659
H -3.687483 -0.786875 -0.060362
H -2.869866 0.164149 1.189348
ImagFreq 493i
Internal rotation:
cos -0.01 -0.01 3.65
barrier 3.67
symmetry 3
Im,red 12.05
freq 123.7 (from rotation profile)

Reaction 2/15

ethyl/prop-2-enoic-acid/1-carboxybutyl
C -0.471440 1.026763 -0.364705
C 0.584750 1.434203 0.394458
C 2.455376 0.137518 -0.126675
H 0.660642 1.084398 1.416531
H 1.141934 2.323190 0.128953
H 3.001944 0.419377 0.767732
H 2.742631 0.671926 -1.026306

H -0.677249 1.452554 -1.339061
C -1.351492 -0.046689 0.100375
O -1.230462 -0.679517 1.129218
O -2.371343 -0.280538 -0.771268
H -2.898576 -0.991429 -0.379194
C 1.987069 -1.272275 -0.259130
H 1.485292 -1.621805 0.645843
H 1.295708 -1.388348 -1.097621
H 2.836531 -1.946543 -0.446408
ImagFreq 379i
Internal rotation:
cos 2.17 0.29 1.17
sin 0.19 0.03 0.78
barrier 4.13
symmetry 1
Im,red 70.50
freq 89.8 (from rotation profile)

Reaction 2/16

ethyl/methoxy-ethene/2-methoxybutyl
C 0.086329 1.977104 -0.172279
C -0.439199 0.812087 0.329189
C 1.352205 -0.426697 0.779112
H -0.714096 0.741825 1.379840
H 0.907706 -1.192800 1.411886
H 1.949852 0.289496 1.335010
H 0.552685 2.688409 0.494630
H 0.145188 2.140658 -1.240155
O -1.157967 0.008165 -0.520769
C -1.817242 -1.092051 0.085078
H -1.103339 -1.839106 0.449911
H -2.452710 -0.766345 0.917967
H -2.443786 -1.542208 -0.684183
C 1.878328 -0.871694 -0.551100
H 1.098678 -1.356007 -1.146899
H 2.261389 -0.027364 -1.129739
H 2.699642 -1.594371 -0.442112
ImagFreq 559i
Internal rotation:
cos 1.78 2.45 2.67
sin -0.87 1.34 -0.22
barrier 5.48
symmetry 1
Im,red 80.98
freq 62.1 (from rotation profile)

Reaction 2/17

1-carboxypropyl/ethene/3-carboxypentyl
C 0.008973 0.175307 -0.419403
C -1.957959 -0.461880 0.320588
C -2.886629 0.486321 -0.017967
C 0.768135 -0.986032 0.042979
H -0.254895 0.161779 -1.471294
H -1.897421 -1.382660 -0.247984
H -1.595481 -0.515896 1.341597
H -3.094878 1.331946 0.627088
H -3.394048 0.463120 -0.975803
O 1.416325 -1.048621 1.068567
O 0.637912 -2.060734 -0.789623
H 1.143886 -2.777108 -0.379806
C 0.299906 1.506003 0.209482
H -0.535339 2.184834 0.014396
H 0.378516 1.380133 1.292811
C 1.603752 2.135846 -0.317578
H 2.463343 1.505130 -0.081279
H 1.567988 2.275479 -1.401852
H 1.767361 3.114702 0.141976
ImagFreq 474i
Internal rotation:
cos 2.67 -0.55 5.62
barrier 8.31
symmetry 1
Im,red 64.27
freq 60.9 (from rotation profile)

Reaction 2/18

methyl/2-methylidenebutanal/3-formylpentan-3-yl
C -0.066909 -0.308493 0.530561
C 1.210478 -0.617121 0.917896
C 2.725998 0.064138 -0.765060
H 1.572918 -1.634429 0.817823
H 1.752442 0.019983 1.605769
H 3.625920 -0.355502 -0.332566
H 2.603941 1.137873 -0.714755
H 2.300895 -0.443172 -1.620712
C -0.837539 -1.332851 -0.182102
O -1.985367 -1.196429 -0.561531
H -0.296095 -2.289641 -0.350710
C -0.718357 1.025873 0.779258
H -1.724550 0.846973 1.171542
H -0.158464 1.565596 1.548828
C -0.841230 1.896622 -0.485570
H 0.140158 2.119749 -0.912249
H -1.440361 1.389086 -1.242821
H -1.328516 2.845909 -0.247794
ImagFreq 421i
Internal rotation:
cos 0.00 0.00 1.29
barrier 1.30
symmetry 3
Im,red 12.13
freq 64.5 (from rotation profile)

Reaction 2/19

methyl/ethenyl-ethyl-ether/2-ethoxypropyl
C -1.913018 -1.255433 -0.131313
C -0.925214 -0.443063 0.366383
C -1.669808 1.593319 -0.183947

H -0.942547 -0.136156 1.410090
H -1.038116 2.267990 0.386319
H -2.713609 1.580498 0.107500
H -1.479313 1.558569 -1.250183
H -2.864513 -1.320830 0.376840
H -1.794460 -1.739015 -1.092000
O 0.312632 -0.491440 -0.212506
C 1.339457 0.266033 0.427596
H 1.103397 1.335075 0.365986
H 1.391175 -0.008969 1.489857
C 2.650897 -0.038220 -0.270990
H 3.465728 0.525419 0.190817
H 2.882955 -1.103288 -0.205100
H 2.594368 0.236410 -1.326457
ImagFreq 563i
Internal rotation:
cos -0.03 -0.03 2.53
barrier 2.54
symmetry 3
Im,red 11.92
freq 122.7 (from rotation profile)

Reaction 2/20

methyl/4-methylidenehex-5-en-3-one/2-ethenyl-2-methyl-3-oxopentyl
C -0.895662 1.480791 -0.857613
C -0.718278 0.264837 -0.221074
C -0.587415 0.765836 1.968536
H -0.405867 -0.212517 2.396667
H -1.586905 1.165594 2.078801
H 0.224791 1.480472 2.031556
H -1.885619 1.862571 -1.071963
H -0.065302 2.130952 -1.093204
C 0.667231 -0.357724 -0.159182
O 0.800816 -1.537257 0.094137
C -1.831790 -0.709813 -0.073275
H -1.544277 -1.631262 0.419933
C -3.084197 -0.562116 -0.502531
H -3.429324 0.318829 -1.033007
H -3.818470 -1.341986 -0.338521
C 1.883606 0.516303 -0.453349
H 1.842101 0.779249 -1.517691
H 1.794241 1.463449 0.087470
C 3.206843 -0.174980 -0.130389
H 3.282830 -0.401607 0.935355
H 3.294204 -1.118919 -0.669465
H 4.049039 0.464430 -0.405765
ImagFreq 486i
Internal rotation:
cos -0.09 -0.09 3.77
barrier 3.81
symmetry 3
Im,red 12.10
freq 27.1 (from rotation profile)

Reaction 2/21

methyl/3-methylidenepent-1-ene/4-oxohexan-3-yl
C -0.679686 0.974725 -0.047517
C -1.864569 0.696099 -0.658643
C -3.062133 -0.772065 0.768518
H -1.897044 -0.091318 -1.401531
H -2.682909 1.404413 -0.639691
H -3.971434 -0.857109 0.186682
H -3.100983 -0.188759 1.678702
H -2.352123 -1.585844 0.718372
H -0.581345 1.842369 0.598283
C 0.491491 0.088559 -0.203056
O 0.428030 -0.961155 -0.823783
C 1.786274 0.551119 0.455800
H 2.013974 1.556496 0.078049
H 1.584429 0.687579 1.526608
C 2.960574 -0.397192 0.236710
H 3.176011 -0.511336 -0.827446
H 3.859146 -0.023338 0.733574
H 2.736333 -1.391383 0.627782
ImagFreq 398i
Internal rotation:
cos 0.03 0.03 2.15
barrier 2.18
symmetry 3
Im,red 12.16
freq 106.9 (from rotation profile)

Reaction 2/22

carbonyl/propene/4-oxobutan-2-yl
C -1.533360 0.228531 0.309939
C 0.277645 1.162884 -0.433387
C 1.164958 0.453778 0.317325
H 0.057236 0.869204 -1.453944
H 0.018667 2.180484 -0.164678
H 1.469826 0.851721 1.282762
O -1.893885 -0.783588 -0.188416
H -1.533382 0.441816 1.406959
C 1.693787 -0.896239 -0.051026
H 2.789925 -0.896481 -0.069809
H 1.395463 -1.656920 0.680862
H 1.335170 -1.214850 -1.031927
ImagFreq 418i
Internal rotation:
cos 1.96 12.00 -0.50
barrier 14.22
symmetry 1
Im,red 32.25
freq 71.5 (from rotation profile)

Reaction 2/23

hydroxyacetyl/propene/5-hydroxy-4-oxopentan-2-yl
C 0.688057 0.151439 0.601436
C -1.283878 -0.797735 0.901771
C -1.929808 -0.635369 -0.292137

H -0.900978 -1.772203 1.184675
H -1.471221 -0.109313 1.718804
H -1.860930 -1.425007 -1.037125
O 0.757657 1.335773 0.677403
C 1.644739 -0.715186 -0.208956
H 1.969909 -1.554708 0.412421
H 1.044963 -1.127604 -1.033957
O 2.782880 -0.020178 -0.662324
H 2.536033 0.909392 -0.741878
C -2.642783 0.615626 -0.698169
H -2.138963 1.111854 -1.538103
H -3.663407 0.399522 -1.034693
H -2.697672 1.330656 0.125564
ImagFreq 386i
Internal rotation:
cos 1.08 4.22 0.10
sin 1.72 0.48 -0.77
barrier 7.31
symmetry 1
Im,red 123.70
freq 40.5 (from HO analysis)

Reaction 2/24

methoxycarbonyl/propene/4-methoxy-4-oxobutan-2-yl
C 0.856158 0.627382 -0.067299
C -1.328163 1.198088 0.073130
C -2.043983 0.119083 0.506106
H -1.071007 1.999882 0.754974
H -1.316665 1.460281 -0.980101
H -2.160237 -0.032969 1.576427
O 1.733895 1.411992 -0.250495
O 0.957529 -0.684063 0.118436
C 2.310134 -1.225594 0.090769
H 2.913204 -0.760166 0.870912
H 2.198709 -2.291669 0.270855
H 2.765160 -1.041617 -0.883019
C -2.578007 -0.954698 -0.386505
H -2.048406 -1.901604 -0.221363
H -3.638116 -1.149751 -0.187756
H -2.470866 -0.691382 -1.441669
ImagFreq 351i
Internal rotation:
cos 1.62 -1.25 0.19
barrier 2.93
symmetry 1
Im,red 94.52
freq 22.8 (from HO analysis)

Appendix F

Appendix F for Chapter 7

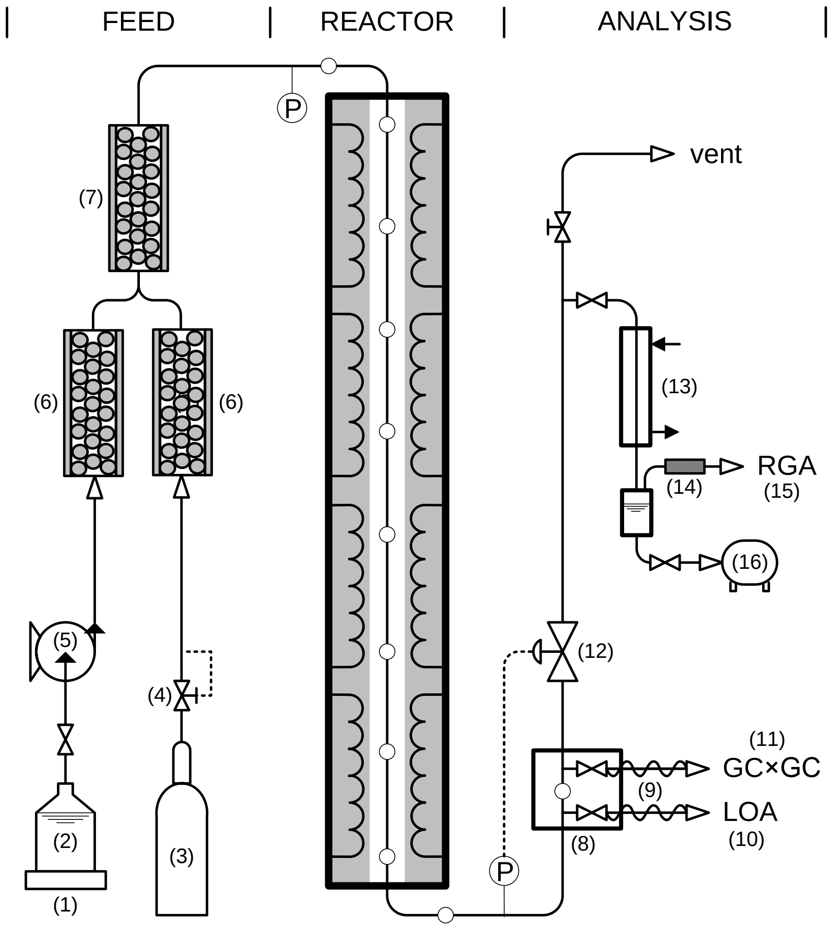

Figure S1: Schematic representation of the experimental pyrolysis set-up (Pyl SP, Schietekat CM, Van Geem KM, Reyniers M-F, Vercammen J, Beens J, Marin GB. Rapeseed oil methyl ester pyrolysis: On-line product analysis using comprehensive two-dimensional gas chromatography. J Chromatogr A. 2011;1218(21):3217-23), indicating the most important process gas temperature (○) and pressure measurements (P) (1: electronic balance, 2: liquid feed reservoir (methyl butanoate), 3: gaseous diluent/internal standard (N_2), 4: coriolis mass flow controller, 5: peristaltic pump, 6: evaporator/heater, 7: mixer, 8: heated sampling oven, 9: heated transfer lines, 10: Light Oxygenates Analyzer, 11: GC×GC-FID/(TOF-MS), 12: outlet pressure restriction valve, 13: water cooled heat exchanger, 14: dehydrator, 15: Refinery Gas Analyzer, 16: condensate drum).

Table S1: Arrhenius parameters for the modified Arrhenius equation, $k(T) = AT^{n} \exp(-E_a/RT)$, for bond scission reactions from the work of Huynh and Violi (JOC 73: 94-101, 2008) and Ali and Violi (JOC 78: 5898-5908, 2013) used in this study for describing the corresponding reaction families. (A in $cm^3\ mol^{-1}\ s^{-1}$, E_a in $kJ\ mol^{-1}$).

	Reactions					A	n	E_a
1	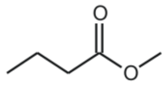	↔	$^{\bullet}CH_3$	+	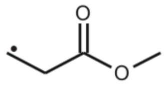	3.62E+14	0	334.7
2	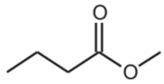	↔		+	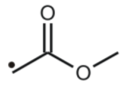	1.13E+15	0	325.1
3	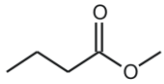	↔		+	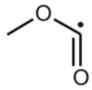	3.92E+15	0	366.5
4	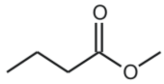	↔	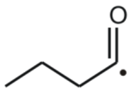	+	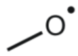	6.09E+14	0	387.0
5	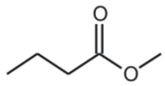	↔	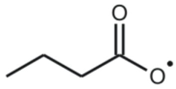	+	$^{\bullet}CH_3$	1.46E+15	0	349.8
6	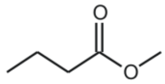	↔	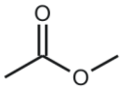	+		5.91E+13	0	416.7
7	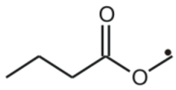	↔	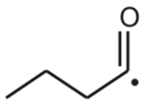	+	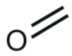	1.64E+14	0	153.6
8	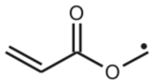	↔	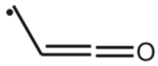	+	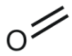	8.62E+12	0	125.5
9	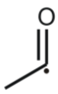	↔	$^{\bullet}CH_3$	+	CO	3.77E+14	0	71.4
10	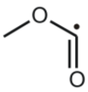	↔	$^{\bullet}CH_3$	+	CO_2	1.06E+14	0	66.5
11	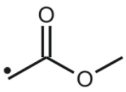	↔		+	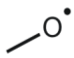	1.21E+14	0	206.1

Table S2: Arrhenius parameters for the modified Arrhenius equation, k(T) = AT^n exp($-E_a/RT$) for the hydrogen abstraction reactions from Bennadji et al. (Int. J. Chem. Kin. 43: 204-218, 2011) included in the MB pyrolysis reaction mechanism developed in this work. (A in $cm^3\ mol^{-1}\ s^{-1}$, E_a in $kJ\ mol^{-1}$).

	Reactions							A	n	E_a
1	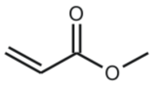	+	$^{\bullet}CH_3$	↔	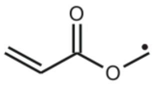	+	CH_4	3.00E+12	0	38.5
2	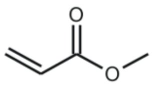	+	$^{\bullet}O$	↔	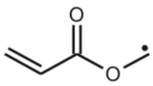	+	$^{\bullet}OH$	5.10E+13	0	32.8
3	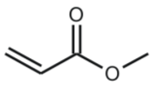	+	$^{\bullet}OH$	↔	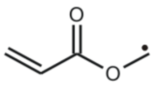	+	H_2O	2.70E+12	0	1.9
4	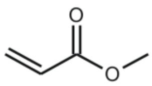	+	$HOO^{\bullet}$	↔	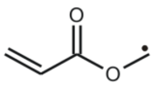	+	HOOH	6.00E+11	0	71.1
5	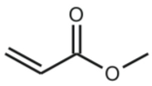	+	$HC^{\bullet}=O$	↔	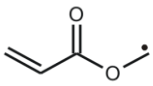	+	$H_2C=O$	3.16E+12	0	77.4
6	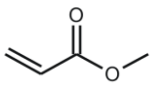	+	$^{\bullet}CH_2OH$	↔	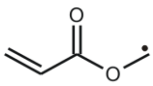	+	CH_3OH	7.01E+10	0	58.6
7	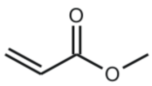	+	$CH_3O^{\bullet}$	↔	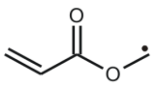	+	CH_3OH	1.60E+11	0	30.5
8	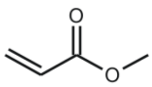	+	$CH_3OO^{\bullet}$	↔	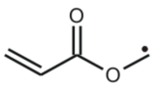	+	CH_3OOH	6.00E+12	0	83.7
9	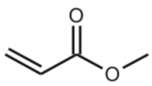	+	$^{\bullet}CH_2CH_3$	↔	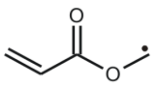	+	CH_3CH_3	3.00E+11	0	56.5

Table S3: Summary of methyl butanoate conversion and measured product yields at selected process conditions (temperature range 1013-1053 ^oC).

Dilution 0.6 mol_{N2}/mol_{MB}									
Conditions									
MB flow rate [g/h]	257	257	257	257	257	257	257	257	257
N2 Dilution flow rate [g/h]	40	40	40	40	40	40	40	40	40
T-setting [°C]	**1013**	**1013**	**1013**	**1033**	**1033**	**1033**	**1053**	**1053**	**1053**
T-profile reactor [°C]									
T at 0 mm (inlet)	566.4	567.8	568.0	566.2	566.2	566.9	568.5	568.5	568.5
T at 190 mm	1021.0	1020.0	1013.6	1035.0	1033.2	1033.6	1056.2	1054.3	1052.9
T at 380 mm	1043.6	1041.5	1037.1	1059.9	1061.1	1061.8	1084.9	1084.4	1084.0
T at 480 mm	1014.1	1013.8	1013.2	1032.5	1032.9	1033.2	1053.6	1053.2	1053.2
T at 670 mm	1004.9	1004.9	1003.7	1023.5	1024.0	1024.0	1044.3	1043.8	1043.8
T at 860 mm	1014.5	1014.1	1013.2	1032.9	1032.9	1033.2	1053.8	1053.2	1053.2
T at 1050 mm	1020.0	1020.3	1019.4	1039.2	1039.4	1039.7	1060.8	1060.1	1060.1
T at 1240 mm	1014.5	1014.8	1014.5	1033.6	1033.6	1033.4	1054.1	1053.2	1053.2
T at 1430 mm	822.4	823.9	826.6	834.9	837.9	838.1	851.8	854.0	855.8
T at 1475 mm (outlet)	721.2	721.9	721.7	722.6	721.7	721.9	722.1	721.2	722.6
P reactor [MPa]	0.17	0.17	0.17	0.17	0.17	0.17	0.17	0.17	0.17
Conversion of MB [%]	**64.3**	**64.5**	**64.4**	**77.5**	**77.4**	**77.4**	**86.3**	**86.3**	**86.3**
Yields [wt%]									
H_2	0.29	0.34	0.32	0.38	0.38	0.39	0.48	0.49	0.49

CO_2	11.26	11.19	11.18	12.83	12.68	12.64	14.58	14.58	14.55
CH_4	10.53	10.47	10.49	13.24	13.25	13.27	15.10	15.10	15.10
CO	14.87	14.94	14.49	19.09	19.41	19.37	23.41	23.34	23.24
C_2H_6	1.45	1.47	1.41	1.92	2.02	2.01	2.32	2.29	2.23
C_2H_4	8.10	8.12	8.11	11.07	11.06	11.07	13.20	13.26	13.34
C_3H_8	0.27	0.26	0.26	0.30	0.30	0.31	0.32	0.31	0.31
C_3H_6	6.38	6.32	6.62	7.49	7.21	7.31	7.04	7.12	7.19
C_4H_8	0.42	0.45	0.47	0.61	0.58	0.59	0.58	0.60	0.61
C_4H_6	0.23	0.26	0.26	0.48	0.51	0.51	0.78	0.78	0.78
CH_2O	3.17	3.38	3.53	3.61	3.60	3.56	2.87	2.79	2.89
H_2O	0.69	0.68	0.68	0.68	0.64	0.65	0.76	0.76	0.73
CH_3OH	0.41	0.41	0.36	0.54	0.54	0.47	0.62	0.62	0.59
Methyl Acetate	0.29	0.29	0.29	0.26	0.26	0.26	0.39	0.39	0.39
Methyl Propenoate	5.09	5.06	5.07	3.81	3.81	3.82	2.42	2.42	2.42
Methyl Propanoate	0.22	0.21	0.22	0.13	0.13	0.13	0.08	0.08	0.08
C>5 chains	0.64	0.65	0.66	1.00	1.01	1.01	1.33	1.34	1.34
MB	35.69	35.48	35.56	22.53	22.56	22.60	13.68	13.68	13.68
Total	**100.0**	**100.0**	**100.0**	**100.0**	**100.0**	**100.0**	**100.0**	**100.0**	**100.0**

Table S4: Summary of methyl butanoate conversion and measured product yields at selected process conditions (temperature range 1073-1113 ^oC).

	Dilution 0.6 mol_{N2}/mol_{MB}								
Conditions									
MB flow rate [g/h]	257	257	257	257	257	257	257	257	257
N2 Dilution flow rate [g/h]	40	40	40	40	40	40	40	40	40
T-setting [°C]	**1073**	**1073**	**1073**	**1093**	**1093**	**1093**	**1113**	**1113**	**1113**
T-profile reactor [°C]									
T at 0 mm (inlet)	569.9	569.7	569.7	570.8	571.3	571.8	573.2	572.2	572.0
T at 190 mm	1072.7	1072.9	1071.8	1093.2	1090.8	1092.2	1112.2	1112.7	1113.4
T at 380 mm	1106.3	1106.6	1106.3	1129.9	1128.4	1129.4	1153.2	1154.1	1154.8
T at 480 mm	1073.4	1073.2	1072.9	1093.2	1092.9	1093.2	1113.2	1113.4	1113.6
T at 670 mm	1063.6	1063.6	1063.4	1083.3	1083.0	1083.3	1102.6	1103.0	1103.0
T at 860 mm	1073.2	1073.2	1073.2	1093.2	1093.2	1093.2	1113.2	1113.2	1113.6
T at 1050 mm	1080.7	1080.7	1080.7	1101.4	1100.4	1100.9	1121.4	1121.4	1121.9
T at 1240 mm	1073.2	1073.4	1073.4	1094.6	1092.9	1093.2	1113.6	1113.4	1114.1
T at 1430 mm	870.5	871.4	873.4	891.6	891.8	893.6	909.3	910.2	911.4
T at 1475 mm (outlet)	722.4	721.5	722.1	722.4	722.4	721.2	721.7	721.7	721.9
P reactor [MPa]	0.17	0.17	0.17	0.17	0.17	0.17	0.17	0.17	0.17
Conversion of MB [%]	**92.4**	**92.3**	**92.3**	**96.9**	**96.9**	**96.9**	**99.1**	**99.1**	**99.1**
Yields [wt%]									
H_2	0.57	0.59	0.60	0.70	0.70	0.70	0.81	0.81	0.81

CO_2	15.83	15.81	15.73	16.75	16.65	16.58	17.16	17.15	17.09
CH_4	16.48	16.54	16.57	17.79	17.77	17.83	18.58	18.64	18.70
CO	26.30	26.67	26.86	29.30	29.24	29.35	30.82	30.87	30.93
C_2H_6	2.43	2.41	2.38	2.39	2.39	2.40	2.20	2.21	2.21
C_2H_4	14.91	15.13	15.25	16.64	16.65	16.70	17.61	17.55	17.66
C_3H_8	0.31	0.29	0.28	0.25	0.25	0.25	0.18	0.18	0.18
C_3H_6	6.61	6.10	5.80	4.86	4.94	4.83	3.53	3.51	3.41
C_4H_8	0.57	0.48	0.44	0.31	0.32	0.31	0.16	0.16	0.15
C_4H_6	0.92	1.08	1.05	1.27	1.29	1.29	1.29	1.32	1.32
CH_2O	1.95	1.83	2.02	1.16	1.13	1.18	0.77	0.66	0.63
H_2O	0.82	0.75	0.68	0.79	0.78	0.79	0.69	0.74	0.75
CH_3OH	0.71	0.66	0.63	0.61	0.72	0.64	0.59	0.57	0.53
Methyl Acetate	0.63	0.63	0.64	0.83	0.83	0.83	1.02	1.02	1.02
Methyl Propenoate	1.45	1.45	1.45	0.65	0.65	0.65	0.23	0.23	0.23
Methyl Propanoate	0.06	0.06	0.06	0.03	0.03	0.03	0.01	0.01	0.01
C>5 chains	1.80	1.83	1.84	2.57	2.56	2.56	3.44	3.44	3.45
MB	7.62	7.65	7.67	3.06	3.06	3.07	0.90	0.91	0.91
Total	**100.0**	**100.0**	**100.0**	**100.0**	**100.0**	**100.0**	**100.0**	**100.0**	**100.0**

Table S5: Comparison between simulated bench-scale reactor product yields (wt %) and experimental data at different set-up temperature settings (1033−1113 K).

	T-setting 1033 K		T-setting 1053 K		T-setting 1073 K		T-setting 1093 K		T-setting 1113 K	
	Simulated	**Exp**	**Simulated**	**Exp**	**Simulated**	**Exp**	**Simulated**	**Exp**	**Simulated**	**Exp**
CO_2	13.46	12.83	15.77	14.58	17.57	15.83	18.09	16.75	19.04	17.16
CH_4	11.03	13.24	12.60	15.10	13.93	16.48	14.02	17.79	15.03	18.58
CO	8.54	19.09	11.35	23.41	14.24	26.30	16.11	29.30	19.29	30.82
C_2H_6	0.35	1.92	0.43	2.32	0.50	2.43	1.04	2.39	1.11	2.20
C_2H_4	9.79	11.07	12.19	13.20	14.41	14.91	15.83	16.64	17.94	17.61
C_3H_6	8.19	7.49	8.57	7.04	8.43	6.61	7.83	4.86	6.84	3.53
CH_2O	3.13	3.61	3.12	2.87	2.83	1.95	2.59	1.16	1.90	0.77
Methyl Propenoate C3:1	10.45	3.81	7.86	2.42	5.30	1.45	3.76	0.65	1.86	0.23
C>5 chains	9.76	4.42	11.36	5.39	12.40	6.42	13.36	7.40	13.37	8.20
MB	25.30	22.53	16.75	13.68	10.39	7.62	7.37	3.06	3.62	0.90
Conversion of MB [%]	74.70	77.47	83.25	86.32	89.61	92.38	92.63	96.94	96.38	99.10
Total	100.0	100.0	100.0	100.0	100.0	100.0	100.0	100.0	100.0	100.0

Glossary

Ab initio	Latin term for "from first principles". It refers to the fact that the results are obtained by applying the established laws of nature without assumptions or experimental input. Ab initio methods determine the energy of a system by solving the Schrödinger equation.
Arrhenius activation energy	The coefficient E_a catching the temperature dependency of the rate coefficient $k = A \exp(-E_a/RT)$ with A the temperature independent pre-exponential factor
Arrhenius pre-exponential factor	See Arrhenius activation energy.
Basis set	Set of functions used to project the molecular orbitals onto ab initio calculations.

Bond dissociation energy	The bond dissociation energy (BDE) is the enthalpy change for an homolytic bond scission.
Density Functional Theory	Density Functional Theory (DFT) is a computational method that derives properties of the molecule based on a determination of the electron density of the molecule. Unlike the wave function, which is not a physical reality but a mathematical construction, electron density is a physical characteristic of all molecules.
Dividing surface	Surface dividing the reactant region from the product region in the phase space. The dividing surface is perpendicular to the reaction coordinate.
Electron Correlation	The interaction between electrons of a quantum system.
Elementary Reaction	A chemical reaction in which one or more species react to products in a single step and with a single transition state.
Enthalpy	The enthalpy H is a thermodynamic quantity and is calculated from the internal energy U as $H = U + pV$, with p the pressure and V the volume of the system.
Entropy	The entropy S is a thermodynamic property that is related to the disorder of the system. A system with a larger number of states that can be occupied, will therefore have a higher entropy.
Gibbs free energy	The Gibbs free energy is a thermodynamic quantity that is calculated

	as $G = H - TS$ with H the enthalpy, T the temperature and S the entropy.
Group additivity method	A group additivity method is a technique that allows to predict properties from molecular structures. For example, within Benson's group additivity method a property can be written as a sum of contributions arising from its constituent groups.
Group contribution method	See group additivity method.
Harmonic oscillator approximation	Model to describe internal modes in molecules. The harmonic oscillator (HO) approximation deals well with vibrations but lacks accuracy when describing low-frequency vibrational motions such as internal rotations.
Hindered rotor treatment	Alternative to the harmonic oscillator approximation for the treatment of internal rotations. The 1-D hindered rotor treatment involves determination of the potential energy profile for internal rotation and solving the Schrödinger equation for this motion to obtain the energy levels.
Hyperconjugation	The favorable interaction of a filled or partially filled orbital, typically a σ orbital, with a nearby empty orbital.
Internal Energy	The internal energy U is the total energy contained by a thermodynamic system. It has two major contributions, i.e. the

	kinetic energy and potential energy.
Level of theory	A level of theory is an approach to solve the Schrödinger equation. In general there are two degrees of freedom: 1) the treatment of electron correlation and 2) the basis set.
Number of single events	The number of energetically equivalent paths that reactants can follow to be converted into products.
Partition function	The partition function encodes the statistical properties of a system. For a canonical ensemble, the partition function is the Boltzmann sum over the different microstates the system can occupy.
Pyrolysis	The uncatalyzed decomposition of organic components resulting from exposure to high temperature, in the absence of molecular oxygen.
Reaction family	A class of reactions that are characterized by the same pattern of electronic/atomic rearrangement steps.
Reaction path degeneracy	See number of single events
Resonance effect	The effect (on reaction rates, etc.) attributed to a substituent due to overlap of its p- or π-orbitals with the p- or π-orbitals of the rest of the molecular entity.

Scaling factor	Empirical factor that is used to improve the agreement between experimental and calculated frequencies.
Single-event microkinetic model	A kinetic model that describes processes using only elementary reactions.
Single-event pre-exponential factor	The pre-exponential factor excluding the number of single events of the reaction.
Spin-orbit coupling	Interaction of a particle spin with its motion.
Spin contamination	The artificial mixing of states with different electronic spin-states. Spin contamination results from the fact that during unrestricted calculations the alpha and beta orbitals are allowed to differ from each other. As a result the wave function is no longer an eigenfunction of the total spin operator $<S^2>$.
Spin projection methods	Method to remove spin contamination in cases the wave function is not an eigenfunction of the total spin $<S^2>$.
Standard enthalpy of formation	The standard enthalpy of formation is the change of enthalpy that accompanies the formation of one mole of a substance in its standard state from its constituent elements in their standard state.
Steam cracking	A petrochemical process in which saturated compounds (hydrocarbons, oxygenates) are converted into small unsaturated compounds by exposure to high temperature in the presence of

	steam.
Transition state	The transition state of an elementary reaction is that set of states in which an assembly of atoms, when randomly placed there, would have equal probability to form the reactants or products of that elementary reaction.
Transition state structure	Saddle point on the potential energy surface along the minimum energy path. A normal mode analysis on the TS structure yields one imaginary frequency.
Transition state theory	Theory that allows to calculate rate coefficients assuming quasi-equilibrium between the reactant and transition state.
Tunneling coefficient	The tunneling coefficient is a correction factor to the rate coefficient accounting for quantum effects, mainly tunneling of particles through the reaction barrier.
Variational transition state theory	Refinement of the transition state theory. In this theory the location of the dividing surface varies along the reaction coordinate which minimizes the reaction rate.
Zero-point vibrational energy	The zero-point vibrational energy is the ground state energy of the vibrations and is calculated from the harmonic frequencies obtained from a normal mode analysis.

List of Publications

Journal Papers

1. Paraskevas P.D.; M.K. Sabbe; M.F. Reyniers; N.G. Papayannakos; G.B. Marin, Group Additive Values for the Gas Phase Standard Enthalpy of Formation, Entropy and Heat Capacity of Oxygenates. *Chemistry - A European Journal* **2013**, *19*, 16431-16452.

2. Paraskevas P.D.; M.K. Sabbe; M.F. Reyniers; N.G. Papayannakos; G.B. Marin, Kinetic Modeling of α-Hydrogen Abstractions from Unsaturated and Saturated Oxygenate Compounds by Carbon-Centered Radicals. *Chem Phys Chem* **2014**, 15, 1849-1866.

3. Paraskevas P.D.; M.K. Sabbe; M.F. Reyniers; N.G. Papayannakos; G.B. Marin, Kinetic Modeling of α-Hydrogen Abstractions from Unsaturated and Saturated Oxygenate Compounds by Hydrogen Atom. *J Phys Chem A*, **2014**, 118, 9296-9309.

4. Paraskevas P.D.; M.K. Sabbe; M.F. Reyniers; N.G. Papayannakos; G.B. Marin, Group Additive Kinetics for Hydrogen Transfer Between Oxygenates, *J Phys Chem A*, **2015**, 119, 6961-6980.

Oral Presentations

1. Paraskevas P.D.; M.K. Sabbe; M.F. Reyniers; N.G. Papayannakos; G.B. Marin, Group additivity for the thermochemistry and H-abstraction kinetics of oxygenates, **2013**, 8th International Conference on Chemical Kinetics (ICCK), 8-12 July, Seville, Spain.

Poster Presentations

1. Paraskevas P.D.; M.K. Sabbe; M.F. Reyniers; N.G. Papayannakos; G.B. Marin, Steam Cracking of Renewable Feedestock: Ab Initio Based Modeling of Thermochemistry, **2011**, 21st Panhellenic Chemistry Conference, 9-12 December, Thessaloniki, Greece.